

C-H BORYLATION:  
A ROUTE TO NOVEL  
PYRENES AND PERYLENES  
AND THE INVESTIGATION OF THEIR EXCITED  
STATES AND  
REDOX PROPERTIES

Dissertation zur Erlangung des naturwissenschaftlichen Doktorgrades  
der Julius-Maximilians-Universität Würzburg

vorgelegt von

**Julia Merz**  
aus Soest

Würzburg 2019





Eingereicht bei der Fakultät für Chemie und Pharmazie am

---

Gutachter der schriftlichen Arbeit

1. Gutachter: Prof. Dr. Dr. h. c. Todd B. Marder
2. Gutachter: Prof. Dr. Ingo Fischer

Prüfer des öffentlichen Promotionskolloquiums

1. Prüfer: Prof. Dr. Dr. h. c. Todd B. Marder
2. Prüfer: Prof. Dr. Ingo Fischer
3. Prüfer:

Datum des öffentlichen Promotionskolloquiums

---

Doktorurkunde ausgehändigt am

---



*Für meine Familie*



*The more I learn,  
the more I realize how much I don't know.*

Albert Einstein

Die Experimente zur vorliegenden Arbeit wurden in der Zeit von August 2015 bis Mai 2019 am Institut für Anorganische Chemie der Julius-Maximilians-Universität Würzburg unter der Aufsicht von Prof. Dr. Dr. h. c. Todd B. Marder durchgeführt.

## Acknowledgements

First of all, thank you **Prof. Dr. Dr. h. c. Todd B. Marder** for the chance to do my PhD in your group. I am very thankful for the scientific freedom that I had all four years and the enormous trust you had in me right from the beginning when I came to Würzburg. Thank you for always having a “minute” to talk about science, life, future plans and also for all the good laughs. You gave me so many opportunities to meet interesting people from around the world and I learned so much from you. It was a great pleasure to be part of the Marder family, and I will never forget the house parties with Anne. Thank you for also supporting me to attend numerous conferences such as IC3EM in Lisbon, IMEBORON in Hongkong and the many meetings in Germany.

Furthermore, I want to thank **Prof. Dr. Andreas Steffen** for always having a sympathetic ear for me. Thank you for all your advice about science and life! You taught me so much especially about photophysics and DFT/TD-DFT calculations. I am also very thankful for the coffee breaks and discussions we had.

Thank you, **Prof. Dr. Ingo Fischer**, for being my second supervisor. I really appreciate that you always had an open door for me.

Thank you, **Prof. Dr. Christoph Lambert**, for giving me the opportunity to do several spectroelectrochemical, transient absorption and cyclic voltammetry measurements in your group. I am very grateful for your advices, explanations and discussions during these four years. Thank you, **Michael Moos**, for introducing me to spectroelectrochemical and cyclic voltammetry measurements. Thank you for all your help during the measurements and the discussions afterwards! It was always a great time to work with you and I will never forget the many laughs we had! Thank you, **David Mims**, for performing transient absorption measurements for me. It was nice to cooperate with you! Furthermore, thank you, **Dr. Stefan Riese** and **Dr. Julian Schäfer**, for the discussions we had.

Furthermore, thank you **Prof. Dr. Holger Braunschweig** for the possibility to perform numerous cyclic voltammetry measurements. I am very grateful for **Dr. Ivo Krummenacher** for always finding time to perform the measurements for me and discuss the results with me.

I would also like to thank my cooperation partner **Dr. Gerard P. McGlacken** from Cork in Ireland for the quinolone derivatives that you provided. Thank you, **Rachel M. Shanahan**, **Leticia M. Pardo** and especially **Aobha Hickey** for the great cooperation. Thank you **Aobha**

for the great time! It was a pleasure to work with you and a lot of fun! Thank you also for introducing some Irish culture to us!

Most important of all, I want to thank the whole **Marder group**! Without all of you I would not have been able to accomplish the research resulting in this thesis. Thank you, **Dr. Alexandra Friedrich**, for solving several crystal structures for me and for writing the X-ray part in my papers! A big thank you to **Dr. Rüdiger Bertermann** for all special NMR measurements and help. You always had a sympathetic ear for me! Thank you, **Dr. Daniel Sieh**, for solving several crystal structures for me and proofreading my papers. Thank you for the discussions we had and thank you for your help you offered me at any time! It was nice to share lab 122/121 with you. Thank you, **Dr. Stefan Wagner** for the countless GC-MS repairs and discussions on mass spectra. Thank you, **Dr. Jörn Nitsch**, for the DFT/TD-calculations you performed for me and thank you for proofreading my papers.

A special thank you goes to the **materials subgroup**! I will never forget our subgroup meetings with the obligatory dinner afterwards at the Greek restaurant. It was a pleasure to work with you guys and so many of you became good friends to me! Thank you, **Dr. Ji Lei**, for introducing me to pyrene chemistry and all your synthetic advice! Thank you for all the discussions and the laughs! Thank you, **Dr. Stefanie Griesbeck**, for our discussions and advices and for the runs we had together! Moreover, thank you for being such a good friend! Thank you, **Florian Rauch**, for the discussions and advices and the great time! Thank you for being my travel buddy in Hongkong and Lisbon. **Matthias Ferger**, thank you so much for being such a good friend and listening to all my problems! Thank you for all your advice and encouragement at any time! It was a lot of fun in Lisbon with you! Thank you, **Jiang He**, for the compounds you gave me and thank you for the discussions! It was always fun to have a beer with you and talk about everything possible! Thank you, **Sarina Berger**, for the great time we had and thank you for organizing so much for the group! Especially thank you for watching Loki =). **Johannes Krebs**, thank you for the great time in the lab 122/121! You were a great lab mate and it was fun to discuss synthetic strategies and calculations with you! Thank you also **Dr. Jian Zhao**, **Dr. Xiangqing Jia** and **Zhu Whu**.

Furthermore, I am very grateful for my students **Julian Fink**, **Christine Heinz**, **Robin Bissert**, **Johannes Ackermann**, **Maximilian Dietz**, **Maximilian Kirchner**, **Haopeng Gao**, **Yvonne Vonhausen**, **Roland Graf**, **Frederik Wöber**, **Lena Dietrich** and **Tom Parsons**. It was a

pleasure to work with all of you and I had a lot of fun in our lab! Thank you all for the effort and the many, many, many laughs we had and for the beer or apple ciders we shared in the evenings!

Thank you, **Jan Maier**, for the great time and discussions! You are a great friend to me! Thank you for organizing so many gaming events and thank you for the great photos of my compounds and of my wedding =). Thank you also for babysitting Loki! Thank you, **Florian Kerner**, **Yaming Tian**, **Wenbo Ming** and **Dr. Xiaoning** for organizing so much in our group!

I am thankful for **AK Steffen**, especially **Benjamin Hupp**, for organizing so much in our group! **Benni**, you always found time for discussions and advice even when you were very busy and did not let me notice it!

I owe my deepest gratitude to **Sabine Lorenzen**! You provided so many compounds for me and helped me with so many synthetic questions. Thank you for everything **Sabine**! I am also very grateful to **Christioph Mahler**, for the synthesis of compounds and for the tons of HRMS measurements that you performed for me! Thank you for your help and advice all the time! **Christoph** and **Sabine**, you both also helped me so much with SPS solvents, waste, moving to the new building and several other tasks you did for the group! Thank you also to **Hildegard Holzinger** for all the chemicals and consumables that you ordered for me and the group.

Furthermore, I am very thankful for **Bianca Putz**, **Stefanie Ziegler** and especially **Maria Eckhardt** and **Cornelia Walter**. You helped me so much in so many ways such as last minute contracts or travels. **Maria**, thank you for organizing so much for the group and thank you for all your advice concerning my future and my curriculum vitae.

Thank you, **Marie-Luise Schäfer** for all the NMR measurements you performed for me and thank you, **Sabine Timmroth** and **Liselotte Michels**, for the numerous elemental analysis measurements. Thank you, **Alfred Schertzer**, for the gas supply and dry ice! A big thank you to the workshop team **Alois Ruf**, **Wolfgang Obert**, **Frank Förtsch**, **Michael Ramold**, **Manfred Reinhart**. Thank you, **Bernhard Werner** and **Berthold Fertig** for the repairing my Schlenk line and broken glassware so many times.

I want to thank all of the people from the **Inorganic Institute** for making my time here really enjoyable.

Last but not least, I want to thank my **family** and **friends**. I am very grateful for my girls here in Würzburg: **Nico, Juli, Ulli, Andrea** and **Steffi**! Thank you for your support and encouragement and the great times we had exercising (thank you Ulli for being my running trainer and half marathon buddy), relaxing in the sauna, eating cheese cake / sushi or Afghan or drinking wine together. I am also very grateful for my friends at home! Thank you **Judith, Amin, Linda** and **Angelika**! You guys always supported and encouraged me! Thank you for all the great times we have had and will have in the future! I am very grateful for my brothers **Christian** and **Kevin** for being so great. I really love you both! Ich möchte auch meinen **Eltern** ganz herzlich danken! Danke, dass ihr mich immer so sehr unterstützt und stets an meiner Seite steht! Ich danke euch für all eure Ermutigungen ohne euch wäre ich nicht der Mensch der ich jetzt bin! Danke auch **Katharina**, dass du die beste Schwiegermutter bist, die man sich nur wünschen kann! Danke für all deine Unterstützung und Ermutigung! **Viktor**, ich hätte nie gedacht, dass ich meinen Ehemann im Chemiestudium mal finden werde! Du hast mich während meines Studiums und meiner Promotion unendlich unterstützt, aufgemuntert und motiviert! Du bist mein bester Freund und freue mich schon auf unseren nächsten gemeinsamen Zukunftsschritt vor allem mit dem kleinen **Loki**, der echt der beste Buddy beim Schreiben für mich war!

## List of Publications

The publications listed below are partly reproduced in this dissertation with permission from the Royal Society of Chemistry and Wiley-VCH. The table itemizes at which position in this work the paper have been reproduced.

Publication	Position
J. Merz, J. Fink, A. Friedrich, I. Krummenacher, H. H. Al Mamari, S. Lorenzen, M. Haehnel, A. Eichhorn, M. Moos, M. Holzapfel, H. Braunschweig, C. Lambert, A. Steffen, L. Ji and T. B. Marder, <i>Chem. Eur. J.</i> , <b>2017</b> , <i>23</i> , <b>13164 -13180</b> .	Chapter 1
J. Merz, A. Steffen, J. Nitsch, J. Fink, C. B. Schürger, A. Friedrich, I. Krummenacher, H. Braunschweig, M. Moos, D. Mims, C. Lambert and T. B. Marder, <i>Chem. Sci.</i> <b>2019</b> , <i>submitted</i> .	Chapter 2

And in the following theses (under supervision of Julia Merz):

Novel Donor-Acceptor Pyrene Derivatives, M. Dietz, Bachelor Thesis, Julius-Maximilians-Universität Würzburg, **2017**.

Further publication:

T. Sick, J. M. Rotter, S. Reuter, S. Kandambeth, N. N. Bach, M. Döblinger, J. Merz, T. B. Marder, T. Bein, D. D. Medina, *J. Am. Chem. Soc.* **2019**, *submitted*.



## List of Abbreviations

A	acceptor
Å	Ångström (1 Å = 10 <sup>-10</sup> m)
Abs	absorption
APCI	atmospheric-pressure chemical ionization
ASAP	atmospheric solids analysis probe
bpy	2,2'-bipyridine
br	broad
CI	configuration interaction
CQ	quadrupole coupling constant
COD	1,5-cyclooctadiene
COE	cyclooctene
CT	charge transfer
D	donor
d	doublet
dba	dibenzylidene acetone
DFT	density functional theory
DME	ethylene glycol dimethyl ether
DMF	dimethylformamide
DMSO	dimethyl sulfoxide
DNA	deoxyribonucleic acid
dtbpy	4,4'-di- <i>tert</i> -butyl-2,2-dipyridyl
Em	emission
eq	equivalents
FTIR	fourier-transform infrared spectroscopy
HCl	hydrochloric acid
HOMO	highest occupied molecular orbital
HPLC	high-pressure liquid chromatography

<i>i</i>	iso
ICT	intramolecular charge
IRF	instrument response transfer
IV-CT	intervalence charge transfer
$k_r$	radiative decay function
$k_{nr}$	non-radiative decay rate
LE	locally excited
LIFDI	liquid injection field description ionization
LUMO	lowest unoccupied molecular orbital
m	multiplet
MAS	magic-angle spinning
MeCN	acetonitrile
mes	mesityl, 2,4,6-trimethylbenzene
MS	mass spectrometry
MTBE	methyl <i>tert</i> -butyl ether
NIR	near-infrared
NMR	nuclear magnetic resonance
OFET	organic field-effect transistor
OLED	organic light emitting diode
OPV	organic photovoltaic cells
PAH	polycyclic aromatic hydrocarbons
PBu <sub>3</sub>	tributylphosphine
PCM	polarizable continuum model
PCy <sub>3</sub>	tricyclohexylphosphine
pin	pinacolato
PMe <sub>3</sub>	trimethylphosphine
PPh <sub>3</sub>	triphenylphosphine
P( <i>t</i> Bu) <sub>3</sub>	tri- <i>tert</i> -butylphosphine
q	quartet

---

ROS	reactive oxygen species
r.t.	room temperature
S	singlet
s	singlet
SMAP	silicon-constrained monodentate alkyl-phosphine
sPhos	2-dicyclohexylphosphino-2',6'-dimethoxybiphenyl
T	triplet
t	triplet
<i>t</i>	<i>tert</i>
TCSPC	time-correlated single-photoncounting
TD-DFT	time-dependent density functional theory
THF	tetrahydrofuran
THP	4,5,9,10-tetrahydropyrene
TICT	twisted intramolecular charge transfer
TLC	thin-layer chromatography
TPD	<i>N,N'</i> -diphenyl- <i>N,N'</i> -bis(3-methylphenyl)-(1,1'-biphenyl)-4,4'-diamine
UV	ultraviolet
Vis	visible
xPhos	2-Dicyclohexylphosphino-2',4',6'-triisopropylbiphenyl



## Table of Contents

1 Pyrene MO Shuffle Controlling Excited State and Redox Properties by Changing the Nature of the Frontier Orbitals _____	- 1 -
1.1 Introduction _____	- 1 -
1.2 Results and Discussion _____	- 8 -
1.2.1 Synthesis _____	- 8 -
1.2.2 Crystal Structure Analysis _____	- 11 -
1.2.2 Photophysical Properties _____	- 18 -
1.2.3 Redox Properties _____	- 23 -
1.2.4 Spectroelectrochemistry _____	- 26 -
1.2.5 DFT and TD-DFT calculations _____	- 28 -
1.3 Conclusions _____	- 33 -
2 Synthesis, Photophysical and Electronic Properties of Tetra-Donor- or Acceptor-Substituted <i>ortho</i> -Perylenes Displaying Four Reversible Oxidations or Reductions _____	- 39 -
2.1 Introduction _____	- 39 -
2.2 Results and Discussion _____	- 44 -
2.2.1 Synthesis _____	- 44 -
2.2.2 Crystal Structure Analysis _____	- 46 -
2.2.3 Photophysical Properties _____	- 49 -
2.2.4 Reactivity with Oxygen _____	- 54 -
2.2.5 Redox Properties _____	- 55 -
2.2.6 Spectroelectrochemistry _____	- 57 -
2.2.7 DFT and TD-DFT Calculations _____	- 59 -
2.3 Conclusions _____	- 64 -
3 Synthesis, Photophysical and Electronic Properties of Novel Red to NIR Emitting Donor-Acceptor Pyrene Derivatives _____	- 69 -

---

3.1 Introduction	- 69 -
3.2 Results and Discussion	- 74 -
3.2.1 Synthesis	- 74 -
3.2.2 Crystal Structure Analysis	- 78 -
3.2.3 Photophysical and redox properties	- 84 -
3.2.5 Redox Properties	- 86 -
3.2.6 Spectroelectrochemistry	- 88 -
3.2.7 DFT and TD-DFT calculations	- 89 -
3.3 Conclusions	- 92 -
4 Iridium Catalyzed C–H Borylation of 4-Quinolones	- 97 -
4.1 Introduction to C–H Activation	- 97 -
4.1.1 Overview of the Development of the [Ir(OMe)COD] <sub>2</sub> /dtbpy Catalytic System	- 100 -
4.1.2 Mechanism of the [Ir(OMe)COD] <sub>2</sub> /dtbpy Catalyzed Arene C–H Borylation	- 105 -
4.1.3 Directed <i>Ortho</i> Borylation	- 107 -
4.1.4 Borylation of Heteroarenes – the Interplay of Steric and Electronic Effects	- III -
4.1.4.1 Borylation of Heteroaromatic Compounds Catalyzed by the [Ir(OMe)COD] <sub>2</sub> /dtbpy System	- III -
4.1.4.2 Borylation of Heteroaromatic Compounds Catalyzed by the [Ir(OMe)COD] <sub>2</sub> /Si-SMAP System	- 116 -
4.2 Introduction to 4-Quinolones	- 118 -
4.2.1 The Importance of the Quinolone Motif	- 118 -
4.2.2 Current Methodology for the Synthesis of 7-Substituted Quinolones	- 121 -
4.3 Results and Discussion	- 122 -
4.3.1 C–H Borylation of 4-Quinolones Catalyzed by the Ir/dtbpy System	- 122 -
4.3.2 C–H borylation of 4-Quinolones Catalyzed by the Ir/Si-SMAP System	- 132 -
4.4 Conclusions	- 135 -

---

5 Summary / Zusammenfassung	- 139 -
5.1 Summary	- 139 -
5.1.1 Chapter 1	- 139 -
5.1.2 Chapter 2	- 141 -
5.1.3 Chapter 3	- 143 -
5.1.4 Chapter 4	- 145 -
5.2 Zusammenfassung	- 147 -
5.2.1 Kapitel 1	- 147 -
5.2.2 Kapitel 2	- 149 -
5.2.3 Kapitel 3	- 151 -
5.2.4 Kapitel 4	- 152 -
6 Experimental	- 157 -
6.1 General Information	- 157 -
6.2 Cyclic Voltammetry	- 158 -
6.3 Single Crystal X-Ray Diffraction	- 158 -
6.4 General Photophysical Measurements	- 159 -
6.5 Fluorescence Quantum Yield Measurements	- 159 -
6.6 Fluorescence Lifetime Measurements	- 159 -
6.7 Transient Absorption Measurements	- 160 -
6.8 Spectroelectrochemical Measurements	- 160 -
6.9 Theoretical Studies	- 161 -
6.10 Synthesis	- 162 -
6.11 X-Ray	- 197 -
6.12 DFT and TD-DFT Calculations	- 215 -
7 References	- 225 -
8 Appendix	- 251 -

---

Permission of Wiley-VCH \_\_\_\_\_ - 325 -

Affidavit \_\_\_\_\_ - 331 -

Eidesstaatliche Erklärung \_\_\_\_\_ - 331 -





# Chapter 1

Pyrene MO Shuffle

Controlling Excited State

and

Redox Properties

by Changing the Nature of the

Frontier Orbitals



# 1 Pyrene MO Shuffle Controlling Excited State and Redox Properties by Changing the Nature of the Frontier Orbitals

*The following section is slightly modified and reproduced from ref. [1] with permission from Wiley-VCH.*

## 1.1 Introduction

The polycyclic aromatic hydrocarbon (PAH) pyrene (Figure 1-1) is among the most widely studied chromophores with applications in a wide range of scientific fields due to its interesting properties including excimer and exciplex formation, a high fluorescence quantum yield and an exceptionally long-lived singlet excited state.<sup>[2,3]</sup> In addition to its photophysical properties, its high chemical stability and charge-carrier mobility have led to its broad range of applications. Pyrene derivatives have already been used in organic light emitting diodes (OLEDs), organic field-effect transistors (OFETs) and organic photovoltaic cells (OPVs).<sup>[2,4,5]</sup> In addition, they are used in applications such as sensing of temperature,<sup>[6]</sup> pressure<sup>[7]</sup> or pH,<sup>[8]</sup> or to detect guest molecules such as O<sub>2</sub> or NH<sub>3</sub>,<sup>[9-11]</sup> organic molecules<sup>[12-14]</sup> or metals.<sup>[2,15-18]</sup> Its remarkably long fluorescence lifetime of 354 ns, compared to other PAHs, makes pyrene exceptionally well suited for further applications such as the determination of cellular oxygen concentrations in biological systems.<sup>[19,20]</sup>

Clearly, it is of fundamental importance to understand how to modulate the electronic and photophysical properties of pyrene depending on the specific desired application. Typically, this modulation is achieved in conjugated  $\pi$ -systems by substitution with donors (D) and/or acceptors (A), which can strongly influence the frontier orbital levels. For example, materials with high HOMO energies are especially useful for hole transport, and the D- $\pi$ -D compound *N,N'*-diphenyl-*N,N'*-bis(3-methylphenyl)-(1,1'-biphenyl)-4,4'-diamine (TPD) is commonly used for this purpose. On the other hand, materials with a low LUMO energy, such as mes<sub>2</sub>B-(C<sub>4</sub>H<sub>2</sub>S)<sub>n</sub>-Bmes<sub>2</sub> (n = 2, 3), are suitable for use as electron transport materials.<sup>[21]</sup> Typical  $\pi$ -donors that have been employed include amines<sup>[22]</sup> containing a lone pair on N, whereas diarylboryl groups, such as B(mes)<sub>2</sub> (mes = 2,4,6-Me<sub>3</sub>C<sub>6</sub>H<sub>2</sub>), containing an empty p<sub>z</sub>-orbital on B are well known to be strong  $\pi$ -acceptors in conjugated  $\pi$ -systems.<sup>[23-30]</sup>

However, introducing any desired substitution pattern with the greatest variability of donors and/or acceptors at pyrene can become synthetically quite challenging, as both the HOMO and LUMO of pyrene have a nodal plane which lies perpendicular to the molecule and passes through the 2- and 7-positions (Figure 1-1).<sup>[31,32]</sup> Consequently, these positions are difficult to functionalize directly *via* typical aromatic substitution chemistry and, until recently, circuitous routes were the only ones available for 2- or 2,7-substituted pyrenes. Thus, most pyrene derivatives are functionalized at one or more of the 1-,3-,6-, and 8-positions, as these are the sites of maximum contributions of the HOMO (and LUMO) and consequently those at which electrophilic (and nucleophilic) substitution take place.<sup>[2,31-36]</sup>

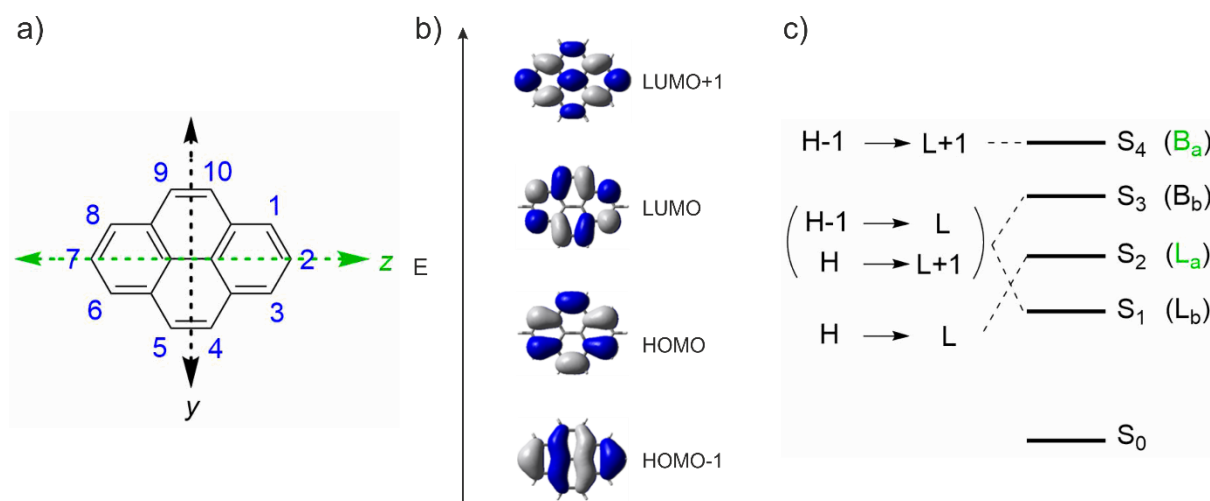


**Figure 1-1.** a) Atom numbering system in pyrene with principle Cartesian coordinate system used for pyrene; b) the four frontier orbitals of pyrene; c) optical transitions of pyrene.

Even though the 1,3,6- and 8-positions are relatively easy to derivatize, the preparation of unsymmetrically substituted pyrene derivatives containing both donors and acceptors remains challenging.<sup>[37-39]</sup> Such D- $\pi$ -A compounds, which exhibit charge-transfer (CT) excited states, are of considerable interest as they typically exhibit a narrowed energy gap, give rise to strong solvatochromism, environment-influenced photophysics, and even the possibility for energy or electron transfer.<sup>[38]</sup> However, only a few examples of D/A-substituted pyrenes have been reported, of which the photophysical properties already indicate their potential for applications. Song reported<sup>[39]</sup> a D- $\pi$ -A pyrene derivative with a diphenylamine moiety at the 2-position and a thienyl acrylic acid acceptor at the 7-position (Chart 1-1, 1-A).

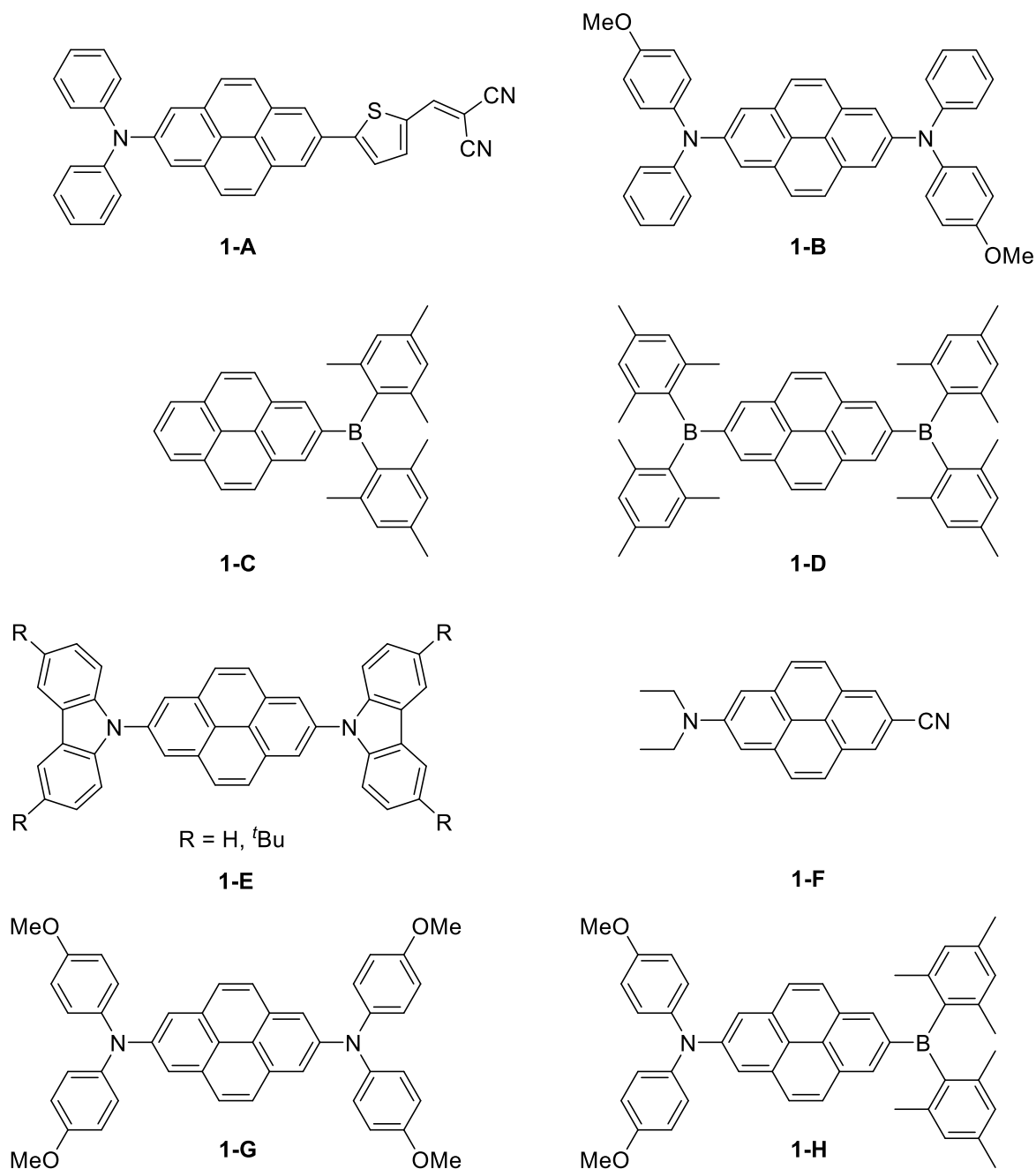


**Chart 1-1.** Schematic overview of some important 2- and 2,7-pyrene derivatives.

Even though they do not list their absorption and emission maxima, the apparent Stokes shift<sup>[40]</sup> is estimated from their reported spectrum, to be ca. 4 500-5 400  $\text{cm}^{-1}$ . Müllen and co-workers developed D- $\pi$ -A systems at the K-region of pyrene (carbons 4,5,9,10) and showed that, in comparison to their symmetric D- $\pi$ -D or A- $\pi$ -A systems, the unsymmetrically functionalized ones have significantly narrower HOMO-LUMO gaps and, along with compound 1-A, among

the largest apparent Stokes shifts ( $5\,400\text{ cm}^{-1}$ ) for D- $\pi$ -A pyrenes reported.<sup>[38,39,41]</sup> Niko, Konishi and co-workers synthesized D- $\pi$ -A pyrene systems with donors and acceptors at the 1-,3-,6- and 8-positions, which displayed strong solvatochromism with emissions into the red region and high quantum yields ( $\phi > 0.75$ ), but they also demonstrated the synthetic difficulty to obtain, selectively, one D- $\pi$ -A pyrene derivative at these positions.<sup>[37]</sup>

It was therefore of interest to develop a facile route to unsymmetric pyrene derivatives, and to examine their optical and electronic properties. Marder and co-workers reported<sup>[32,42]</sup> a general and selective method to synthesize 2- and 2,7-substituted pyrene derivatives by a sterically controlled Ir-catalyzed C-H borylation reaction.<sup>[43,44]</sup> As a result of the exceptionally broad range of synthetic possibilities available from arylboronate esters,<sup>[45]</sup> 2-monosubstituted and both symmetric and unsymmetric 2,7-disubstituted pyrenes became readily accessible for the first time.<sup>[32,43,45-63]</sup> A few examples are presented (Chart I-1) of both D-pyrene-D (**I-B**),<sup>[46]</sup> A-pyrene-A (**I-D**),<sup>[63]</sup> and D-pyrene-A (**I-F**),<sup>[47]</sup> compounds prepared *via* 2-Bpin-7-bromopyrene, using the approach reported by Marder and co-workers, which serves as a valuable intermediate for the synthesis of 2,7-disubstituted pyrenes containing two different substituents.<sup>[47]</sup> Others have reported a few examples using either Marder and co-workers' methodology or more conventional, longer synthetic strategies (**I-A**, **I-E**, **I-G**, **I-H**).<sup>[39,64-67]</sup>

Pyrene's lowest-lying singlet excited state observed in the absorption spectrum at 372 nm ( $\epsilon = 510\text{ M}^{-1}\text{ cm}^{-1}$ ) is the result of a configuration interaction (CI) between HOMO-1 $\rightarrow$ LUMO and HOMO $\rightarrow$ LUMO+1, where the respective transition dipole moments  $\mathbf{M}$  of these two contributions cancel each other and, consequently, the  $S_1\leftarrow S_0$  electronic excitation is transition dipole forbidden.<sup>[31]</sup> This transition is polarized along the short 'y' axis of pyrene (Figure I-1) and, according to the Platt nomenclature, is called  $L_b$ . As the  $S_1\leftarrow S_0$  transition is forbidden, fluorescence from  $S_1$  is also forbidden and, therefore, the  $S_1$  state is long-lived, borrowing some intensity from  $S_2$  by vibrational coupling. The long 'z' axis polarized HOMO $\rightarrow$ LUMO (Platt:  $L_a$ )  $S_2\leftarrow S_0$  transition at 334 nm ( $\epsilon = 55\,000\text{ M}^{-1}\text{ cm}^{-1}$ ) is allowed. The higher electronic transition  $S_3\leftarrow S_0$  at 272 nm<sup>[68]</sup> ( $\epsilon = 54\,000\text{ M}^{-1}\text{ cm}^{-1}$ ) is also the result of a CI between HOMO-1 $\rightarrow$ LUMO and HOMO $\rightarrow$ LUMO+1, but with the respective  $\mathbf{M}$  enhancing each other. Consequently, this short axis polarized transition is allowed and is called  $B_b$  according to Platt, while the fully allowed  $S_4\leftarrow S_0$  transition at 243 nm ( $\epsilon = 88\,000\text{ M}^{-1}\text{ cm}^{-1}$ ) is long axis polarized and called  $B_a$ .<sup>[69,70]</sup>

Substitution at the “traditional” 1,3,6,8-positions of pyrene significantly influences the  $S_1 \leftarrow S_0$  transition.<sup>[2,31,34,35]</sup> These derivatives usually have short fluorescence lifetimes in the range of 2-3 ns and, consequently, do not retain pyrene’s exceptionally long-lived singlet excited state.<sup>[31]</sup> The influence of substituents at the 2,7-positions is typically less pronounced than that for 1-substituted derivatives,<sup>[31]</sup> but bathochromic shifts in the lowest lying  $S_1 \leftarrow S_0$  transition of 900-5500  $\text{cm}^{-1}$  with respect to pyrene were reported for some closed-shell 2,7-derivatives,<sup>[31]</sup> along with an increase of “allowedness,” with  $\epsilon$  values of 600-7000  $\text{M}^{-1} \text{cm}^{-1}$  compared to  $\epsilon = 510 \text{ M}^{-1} \text{cm}^{-1}$  for pyrene. Long fluorescence lifetimes for 2,7-substituted derivatives of tens to several hundreds of ns have also been reported.<sup>[31]</sup>

Triarylboranes have attracted much interest for use in optoelectronic materials,<sup>[23-30,71,72]</sup> as the vacant  $p_z$  orbital on a three-coordinate boron center readily interacts with an adjacent  $\pi$ -system. Bulky groups, such as mesityl, sterically protect the empty  $p$ -orbital from nucleophilic attack providing air- and moisture stable products. Mixing of the  $B_{3u}$  LUMO+1 of pyrene with the empty  $p_z$  orbital of the boron atom of a 2- $B\text{mes}_2$  fragment switches the energetic order of LUMO+1 and LUMO by strongly stabilizing the pyrene LUMO+1.<sup>[31]</sup> Therefore, Marder and co-workers prepared and structurally characterized the 2,7-bis( $B\text{mes}_2$ )pyrene derivative **I-D** and its singly and doubly reduced species.<sup>[63]</sup> Their DFT calculations revealed the reversal of the LUMO+1 and LUMO levels with respect to those of pyrene, with  $B\text{mes}_2$  groups at either the 2-position<sup>[31,46]</sup> or at both the 2- and 7-positions.<sup>[63]</sup> Electrochemical and structural investigations revealed very strong electron delocalization between the two boron centers *via* the 2- and 7-positions of the pyrene bridge.<sup>[63]</sup> Thus, the studies of compounds **I-B** and **I-F** (as for **I-E** and **I-G**), showed that amine donors reverse the order of HOMO-1 and HOMO, and  $B\text{mes}_2$  acceptors (**I-C** and **I-D**) reverse the order of LUMO and LUMO+1, which leads to interesting photophysical properties such as strong emission shifts, and Stokes shifts that were not reached in other compounds. Therefore, in this chapter, the effect of even stronger amine donors in both D- $\pi$ -D and D- $\pi$ -A pyrene systems are examined and the electronic coupling between the 2- and 7-positions is investigated.

The combination of diarylboryl  $\pi$ -acceptors and  $\pi$ -donors is well known to provide compounds with useful linear and nonlinear optical properties.<sup>[23-25,64,73,74,75]</sup> Very common amine donors used in dyes are diarylamino, diethylamino, dimethylamino or carbazolyl moieties.<sup>[65,76]</sup> Diarylamines, for example, are known to be among the strongest electron donors.<sup>[22]</sup> In

comparison to other amine donors, they offer outstanding electron donating abilities, high stability, flexibility and are, moreover, easy to synthesize. Nevertheless, a significant drawback can be energy loss due to the rotational motion of the phenyl rings which can result in a reduction in luminescence efficiency.<sup>[77,78]</sup> In addition, the possibility of rotation around the N-C( $\pi$ ) bond can lead to twisted intramolecular charge transfer (TICT) excited states (*vide infra*). Thus, an amine donor moiety on the 2- and 2,7-positions of pyrene is developed that would provide better conjugation over the pyrene linker in combination with a B(mes)<sub>2</sub> acceptor at the 7-position to achieve a new class of D- $\pi$ -A and D- $\pi$ -D pyrene derivative with unparalleled photophysical properties for 2,7-pyrenes (Chart 1-2). The compound 1,1,7,7-tetramethyljulolidine is known to be one of the strongest donors, and the julolidine moiety has been thoroughly studied since its discovery in 1892 by Pinkus,<sup>[79]</sup> and is used in a wide range of dyes.<sup>[74,80,81]</sup> Its nitrogen lone pair is conformationally restricted to remain parallel to the aromatic system,<sup>[82]</sup> in this case, the pyrene linker, in both the ground and excited states.

Therefore, Jul<sub>2</sub>Pyr (**1-4**) as well as the biphenyl analogue 4,4'-bis(1,1,7,7-tetramethyljulolidine) (**1-14**) is synthesized and the electronic communication through both the rigid pyrene and rotationally flexible biphenyl  $\pi$ -bridges (Chart 1-2) is studied. Very recently, Ito and co-workers isolated and characterized 2,7-bis(dianisylamino)pyrene **1-G**, (analogue of **1-B**<sup>[31,46]</sup>) and its mono- and dication, related to the 2,7-bis(Bmes<sub>2</sub>)pyrene **1-D** and its mono- and dianion reported by Marder and co-workers.<sup>[83]</sup> They analyzed the electronic structures of all three oxidation states and also concluded that the switch in the energetic order of the HOMO-1 and HOMO leads to a large electronic coupling ( $V = 2\ 608\ \text{cm}^{-1}$ ) through the pyrene bridge. Hence, the D- $\pi$ -A system, **II**, is also synthesized to explore the fundamental properties of a compound containing a strong donor and acceptor at the 2- and 7-positions, respectively, of pyrene.

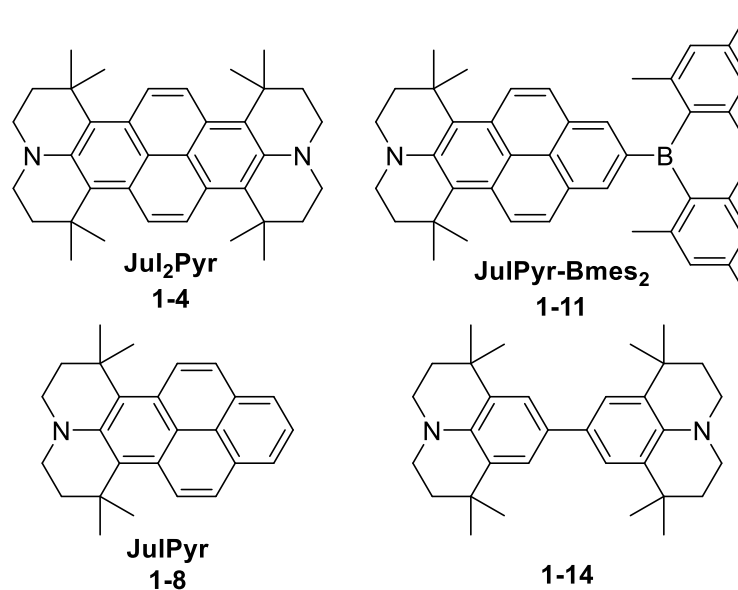


**Chart 1-2.** Molecular structures of **1-4**, **1-8**, **1-11** and **1-14**.

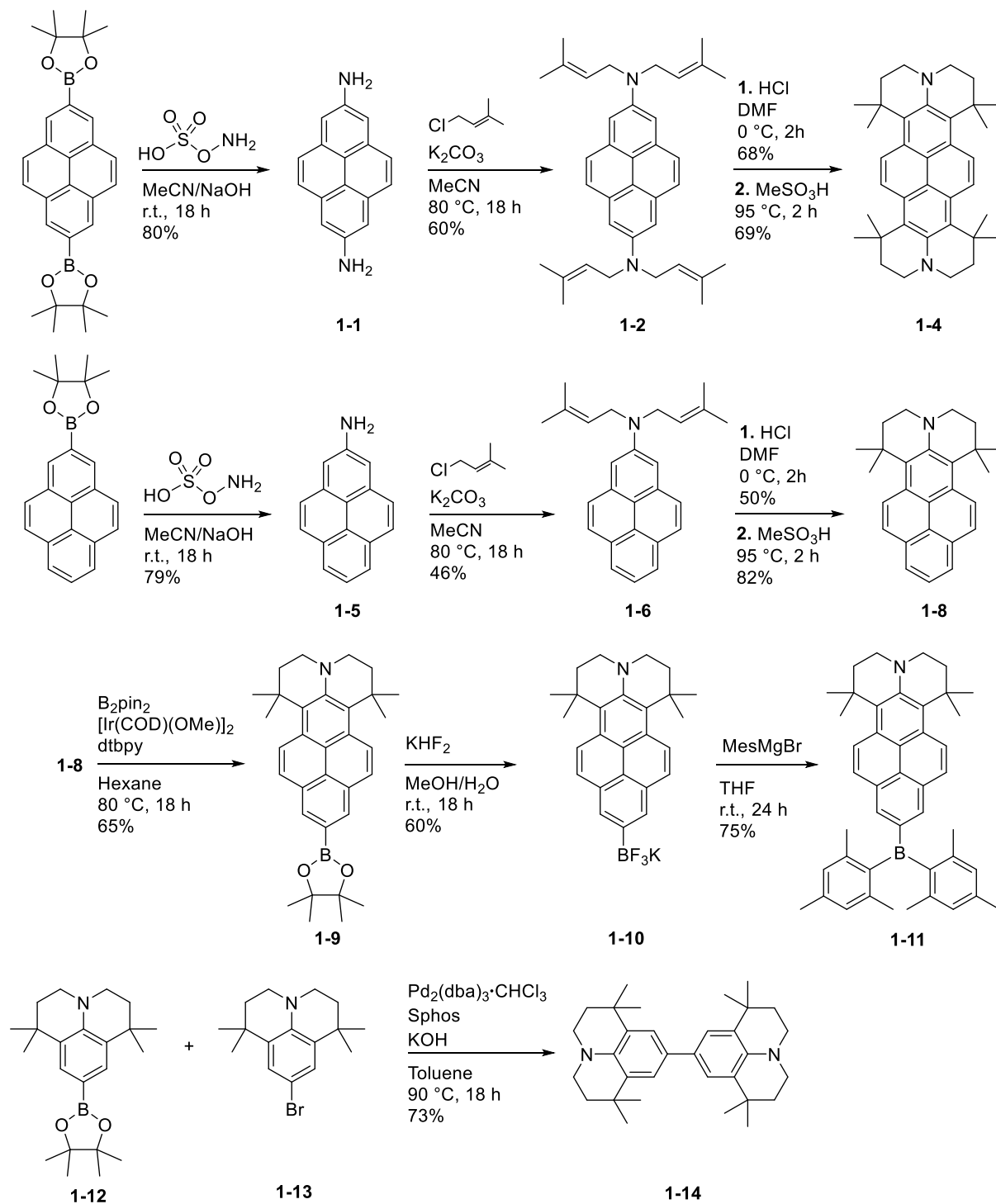
While this work was in progress, Ito and co-workers reported the occurrence of a TICT state in the D- $\pi$ -A compound **I-H**, bearing dianisylamino donors, leading to strong solvatochromism.<sup>[67]</sup> However, the reported apparent Stokes shifts and excited state assignments in the absorption spectra are incorrect, as will be demonstrated in the discussion (*vide infra*). It is worth mentioning that an additional benefit of introducing the julolidine-like donor moiety into these compounds is that it prevents the formation of such TICT states, and thus allows the study of the photophysical and electronic influence of the donor moiety on the pyrene system without further complication by solvent-dependent population of additional types of excited states.

## 1.2 Results and Discussion

### 1.2.1 Synthesis

The procedures used to synthesize the four key compounds are summarized in Scheme I-1. Compounds **1-4** and **1-8** were obtained starting from the high yielding syntheses of 2,7-bis(Bpin)pyrene (95%) and 2-(Bpin)pyrene (65%), respectively,<sup>[32,42,46]</sup> both of which are useful entry points for the synthesis of 2-, and 2,7-substituted pyrene derivatives. Aminations to give the key intermediates 2-amino (**1-5**) and 2,7-di(amino)pyrene (**1-1**) were achieved in high yields using the metal-free method reported by McCubbin and co-workers.<sup>[84]</sup> These primary amines can serve as very convenient precursors for a variety of new 2- and 2,7-substituted pyrene derivatives. The synthesis of 2-(amino)pyrene has before been reported by Bolton in 1964,<sup>[85]</sup> using an indirect route *via* the reduction of pyrene to 4,5,9,10-tetrahydropyrene (THP), nitration at the 2-position, re-aromatization and reduction to 2-(amino)pyrene with an overall yield of ca. 25%. In addition to the low yield, this route suffers from the fact that the synthesis of THP involves high pressures of H<sub>2</sub> and long reaction times,<sup>[86,87]</sup> large amounts of catalyst<sup>[88]</sup> and prior purification of the commercial pyrene with RANEY® nickel.<sup>[34,87-89]</sup> This new synthetic route *via* the initial iridium-catalyzed C–H borylation consists of only two steps, with overall yields of 51% for **1-5** and 76% for **1-1**, starting from commercial pyrene. The amine moieties were alkylated with 1-chloro-3-methylbutene in the presence of the base, K<sub>2</sub>CO<sub>3</sub>. The alkylation reaction was complete after 48 h and gave the desired products as a bright yellow solid (**1-2**, 46%) or as a yellow oil (**1-6**, 60%). Adding aqueous HCl to DMF suspensions of the alkylated compounds **1-2** and **1-6** enabled the synthesis of their respective ammonium salts in 50% (**1-3**) and 68% (**1-7**) yields, which were used to synthesize the tetramethyljulolidine moieties. Thus, the corresponding salt was stirred with methanesulfonic acid at 95 °C for 2 h to achieve the ring closure in 69% (**4**) and 82% (**8**) yield, respectively, giving bright yellow solid products. The mono-substituted pyrene (**8**) was further functionalized by Ir-catalyzed C–H borylation<sup>[32,43]</sup> at the 7-position in 65% yield. Compound **1-9** was transformed into its potassium trifluoroborate salt under an ambient atmosphere in a methanol/water mixture in 60% yield after 18 h. The potassium organotrifluoroborate **1-10** reacts with the Grignard reagent mesMgBr, giving the final compound **1-11** in 75% yield. This methodology for the preparation of triarylboranes provides very efficient access to new boron-containing  $\pi$ -conjugated materials in high yields, few steps and with a broad reaction scope. Furthermore, the organotrifluoroborate intermediates are air

and moisture stable, easy to handle and purify.<sup>[90,91]</sup> Marder and co-workers previously demonstrated the utility of the reaction of aryllithium reagents with aryl trifluoroborates to obtain boroles.<sup>[92]</sup> Wagner *et al.* also showed that aryltrifluoroborates can serve as versatile starting materials for the synthesis of triarylboranes.<sup>[93,94]</sup> The biphenyl analogue of **1-4** was synthesized by Suzuki-Miyaura cross-coupling of **1-12**<sup>[74]</sup> with Br-tetramethyljulolidine **1-13** to obtain **1-14**. All products were fully characterized by multinuclear NMR spectroscopy, high resolution mass spectrometry and elemental analysis.



**Scheme 1-1.** Synthesis of the compounds **1-1** to **1-14** (excluding the ammonium salts **1-3** and **1-7**).

### 1.2.2 Crystal Structure Analysis

The final compounds **1-4**, **1-8**, **1-II** and **1-14** and the precursors **1-1**, **1-6** and **1-9** were investigated by single-crystal X-ray diffraction to analyze their crystal and molecular structures, and to investigate further the influence of the donors and acceptors on structural parameters. The molecular structures are presented in Figure 1-2 and their crystal packing is depicted in Figures 1-3 to 1-5. Selected bond lengths and angles are listed in Tables 1-1 and plotted in Figure 1-6. While the biphenyl unit of the pyrene moiety exhibits typical aromatic C–C bond lengths ranging from 1.383(4) to 1.429(3) Å (bonds **a**, **b**, **f**, **g**, **i**, and **j** in Figure 1-6), bond **d** (1.350(3) Å on average in all compounds studied) is more typical of a C=C double bond, indicating that the pyrene core obeys Clar's sextet rule<sup>[95]</sup>, *i.e.*, it can be viewed as a biphenyl unit constrained to be planar by two –CH=CH– groups. This has also recently been observed for 2-(Bmes<sub>2</sub>)pyrene **1-C** and 2,7-bis(Bmes<sub>2</sub>)pyrene **1-D** (Chart 1-1) by Marder and co-workers.<sup>[63]</sup> A comparison of the average bond distances **a** and **b** in the unsymmetrically substituted pyrene derivatives **1-8**, **1-9**, and **1-II**, ranging between 1.426(3)-1.428(6) Å and 1.412(3)-1.414(3) Å, respectively, with those of the bonds **f** (1.395(3)-1.397(3) Å) and **g** (1.383(4)-1.398(3) Å), show that the julolidine-type moiety has a significant influence on the bonds of the arene ring to which it is connected. Consequently, the symmetrical Jul<sub>2</sub>Pyr **1-4** also shows longer bond distances for **f** and **g**, whereas the precursor compounds **1-1** and **1-6** exhibit shorter bond lengths for **a**, **b**, **f** and **g** of 1.385(2)-1.408(3) Å (Figure 1-6). The above-mentioned increased bond lengths in **1-4**, **1-8**, **1-9** and **1-II** are of similar magnitude to those of bonds **i** and **j** of the biphenyl unit in the rigid inner part of the pyrene core, which hardly vary in the series of compounds. Hence, the more constrained bonding environment of the arene rings enforced by the julolidine-type moieties seems to be the reason for the bond lengthening. Interestingly, the julolidine-type donor also effects the central bond **h**, which links the two phenyl rings, by increasing the bond length from 1.424(3) and 1.421(2) Å in **1-1** and **1-6**, respectively, to 1.434(3)-1.436(3) Å in **1-8**, **1-9**, and **1-II**, which contain one julolidine moiety, to 1.449(2) Å in **1-4** containing two julolidine moieties (Figures 1-6). However, the average central bond (1.490(3) Å) linking the two phenyl rings in the biphenyl compound **1-14** is significantly longer than the corresponding central C7–C7' bond in the pyrene analogue (**1-4**).

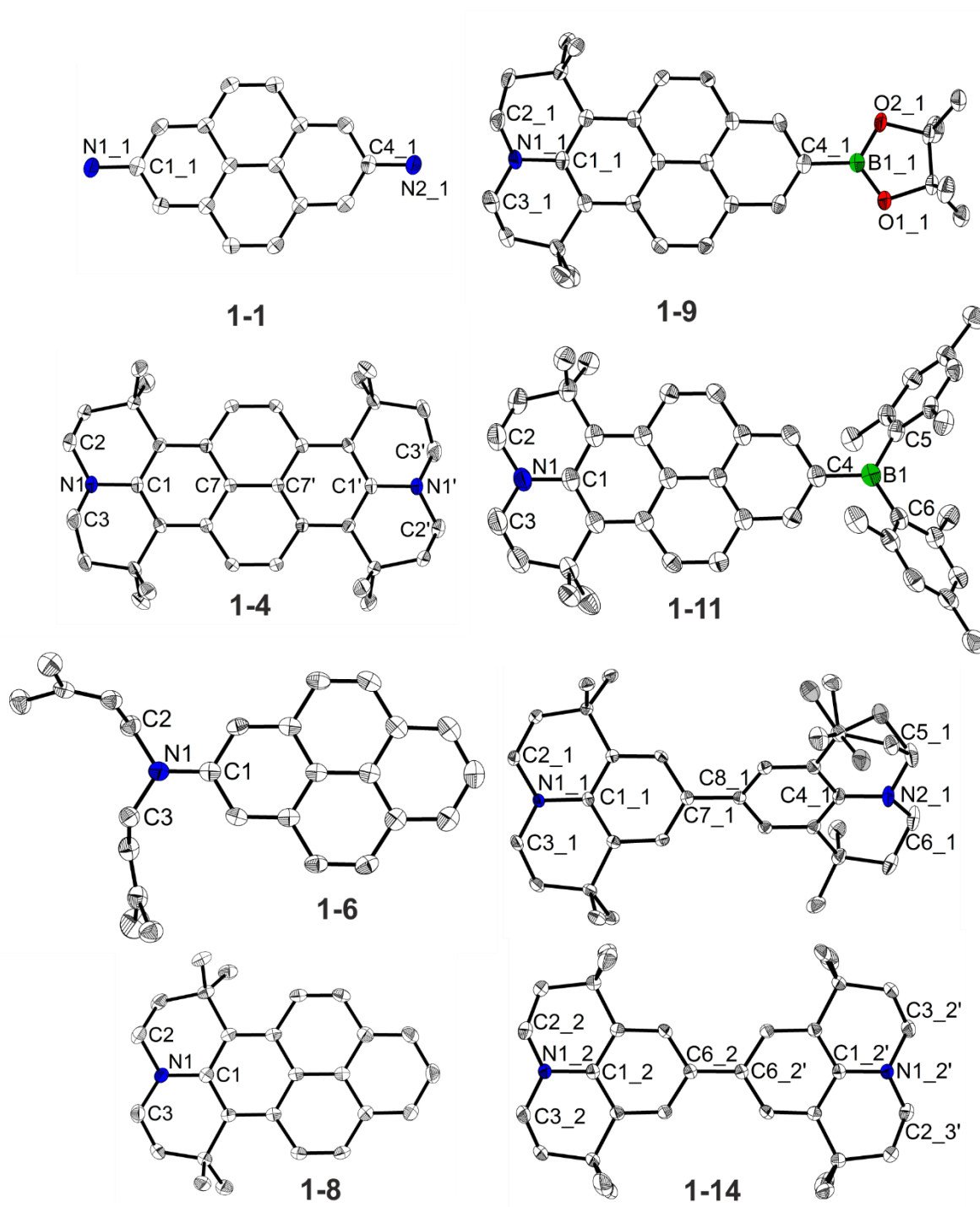


**Figure 1-2.** Molecular structures of 1-1, 1-4, 1-6, 1-8, 1-9, 1-11 and 1-14 obtained from single-crystal X-ray diffraction. Hydrogen atoms are omitted for clarity. Element color: carbon (white), nitrogen (blue), boron (green), oxygen (red). Atomic displacement ellipsoids shown at the 50% probability level. Disordered carbon atoms are shown in grey in molecule 1 of compound 1-14.

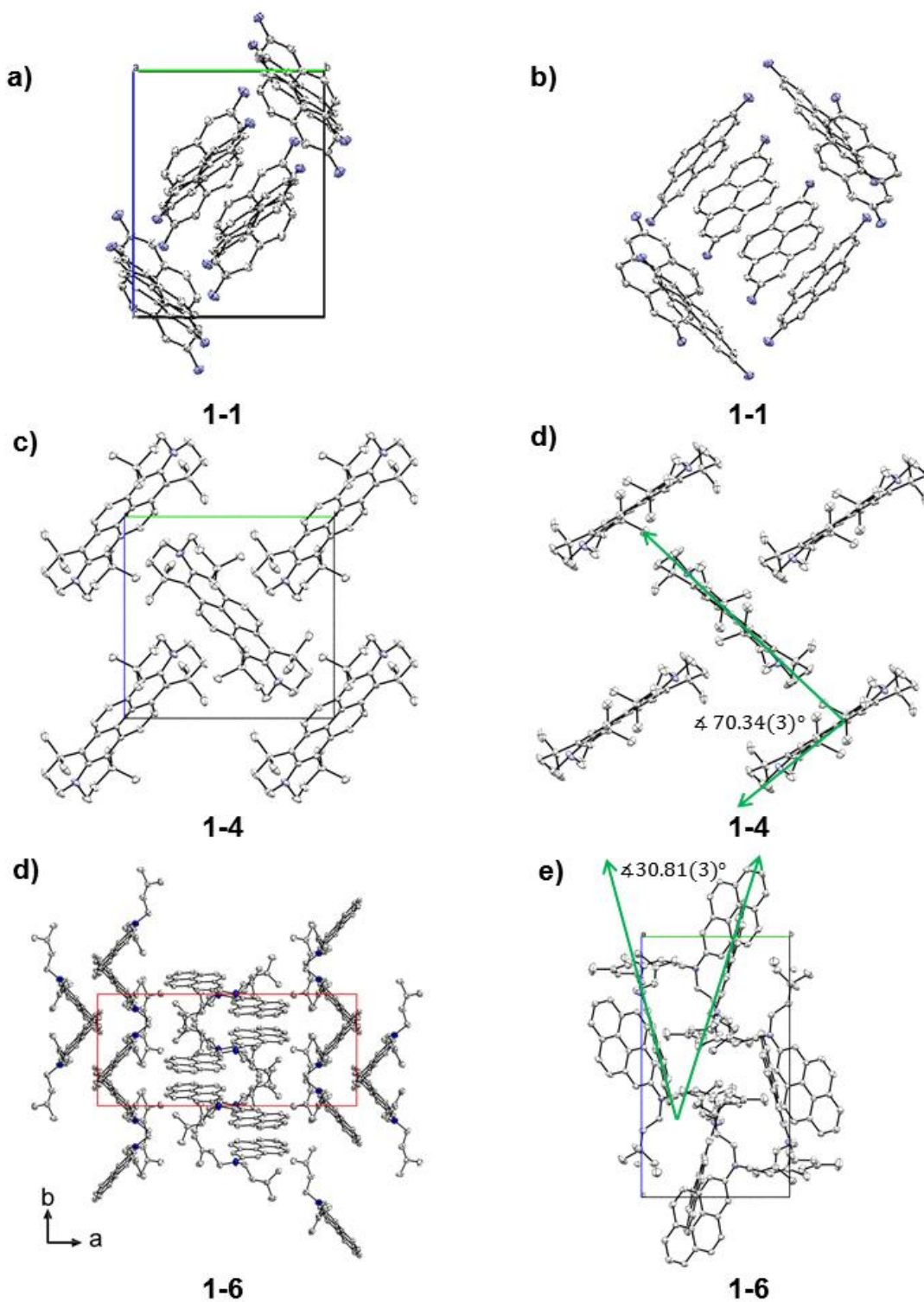


**Figure 1-3.** Crystal packing of 1-1, 1-4, 1-6, obtained from single-crystal X-ray diffraction. Hydrogen atoms are omitted for clarity. Element color: carbon (white), nitrogen (blue), boron (green), oxygen (red). Atomic displacement ellipsoids shown at the 50% probability level.

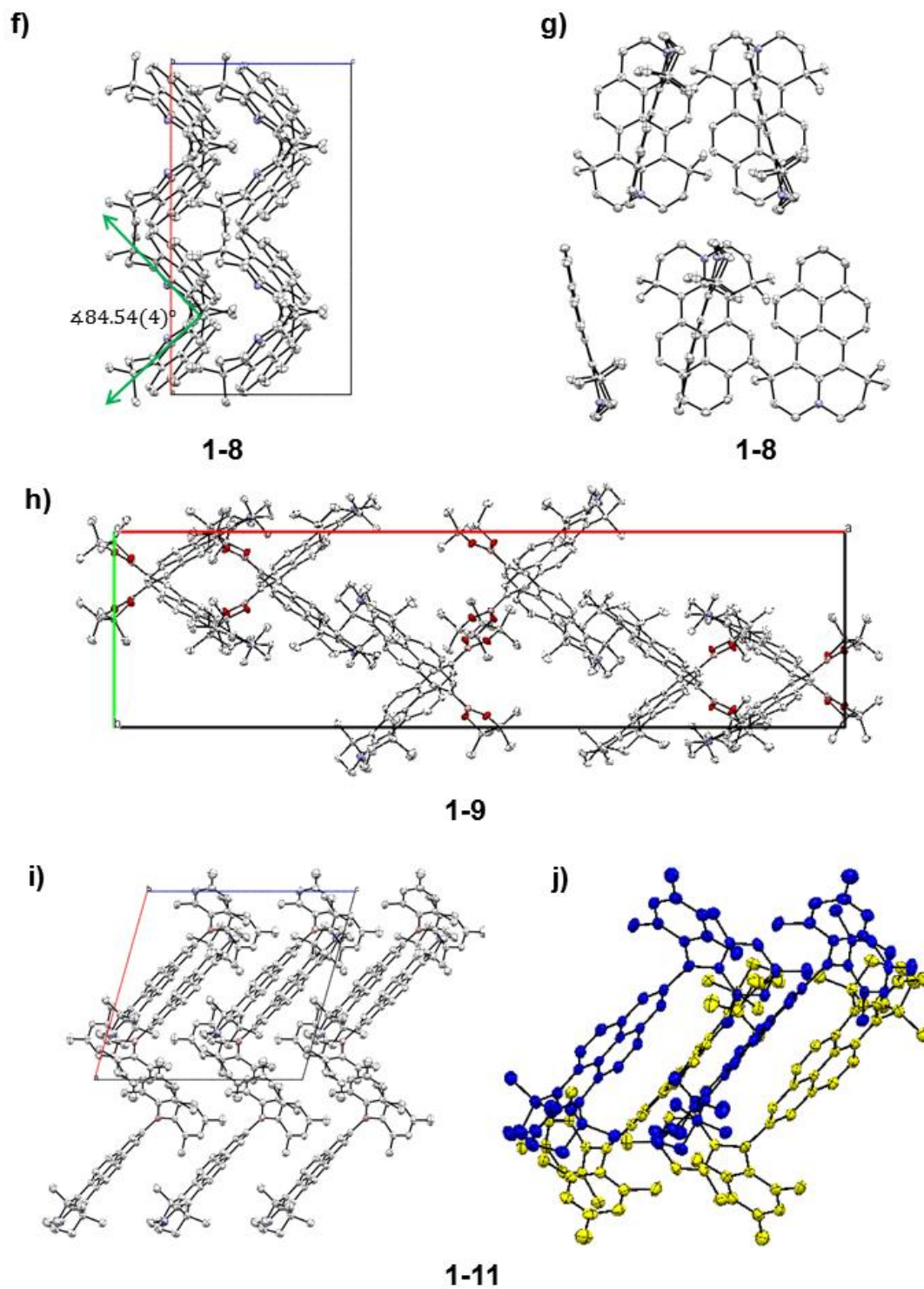


**Figure 1-4.** Crystal packing of 1-8, 1-9, 1-11, obtained from single-crystal X-ray diffraction. Hydrogen atoms are omitted for clarity. Element color: carbon (white), nitrogen (blue), boron (green), oxygen (red). Atomic displacement ellipsoids shown at the 50% probability level.

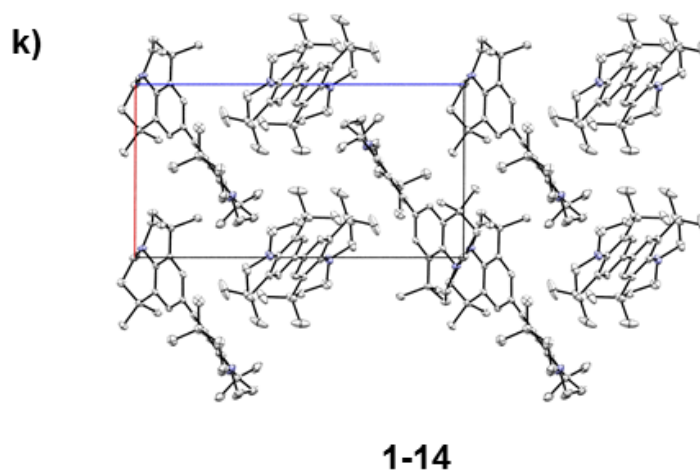


**Figure 1-5.** Crystal packing of **1-14**, obtained from single-crystal X-ray diffraction. Hydrogen atoms are omitted for clarity. Element color: carbon (white) and nitrogen (blue). Atomic displacement ellipsoids shown at the 50% probability level.

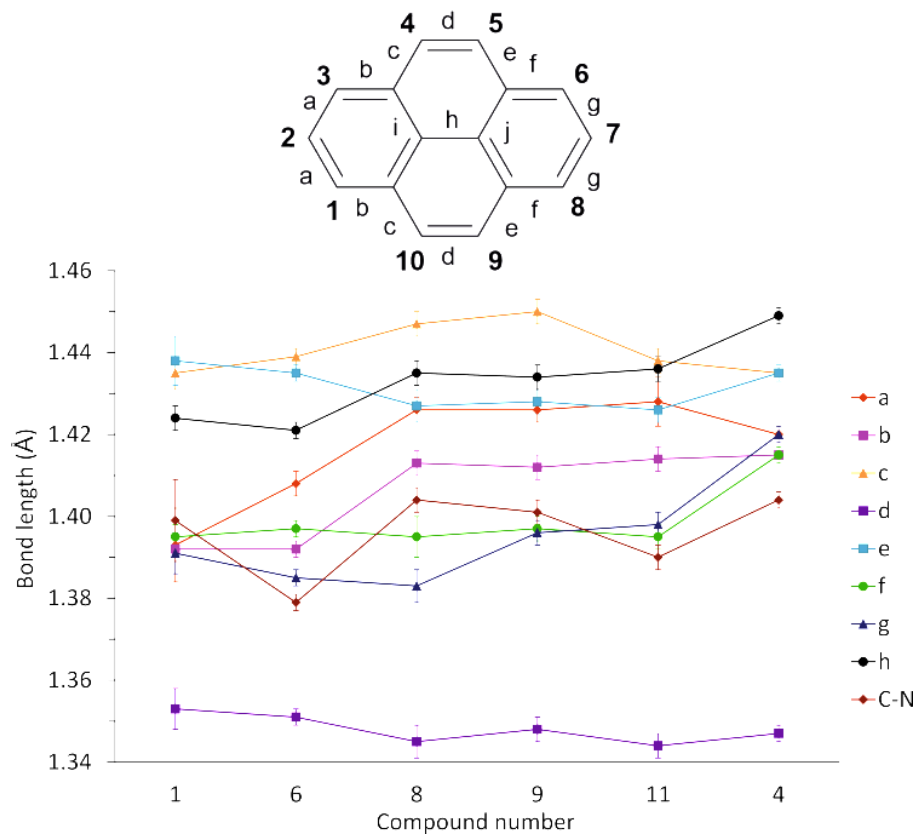


**Figure 1-6.** Comparison of the average bond lengths (Å) of compounds **1**, **4**, **6**, **8**, **9** and **11**. Top: numbering scheme of the bonds of the pyrene core.

As is usually observed for aromatic amines, the N–C(pyrene) bond length is significantly shorter than the other N–C bonds of the amine moieties. The N–C(pyrene) bond length is very similar in **1-1**, **1-4**, **1-8**, **1-9**, and **1-14** with an average length of 1.403(3) Å. Slightly and significantly shorter N–C bonds are observed in **1-II** (1.391(3) Å) and **1-6** (1.379(2) Å), respectively (Table 1-1). In contrast, the N–C(pyrene) bond length of 1-(dimesitylboryl)-6-(di-4-anisylamino)pyrene, a positional isomer of **1-H** (Chart 1-1) (1.442(4) Å), wherein the functional groups are located at the 1,6-positions, is significantly longer.<sup>[67]</sup> The sum of the C–N–C angles involving the julolidine moiety is similar in compounds **1-4**, **1-8**, and **1-9** (350(1)° on average), slightly larger in **1-II** (355.7(6)°), and varying between about 344° and 350° in **1-14** (Table 1-1). These sums imply slightly pyramidalized nitrogen atoms. In contrast, the nitrogen atoms in **1-6** have a nearly ideal trigonal planar configuration, with the sum of the C–N–C angles being 360.0(4)°. The dihedral angle between the NC<sub>3</sub> and pyrene planes is fairly small and varies between 9.2° and 21.3° in all these compounds (Table 1-1). For example, the dihedral angle in 2,7-bis(dianisylamino)pyrene **1-G** of 31° is significantly larger.<sup>[83]</sup> The B–C(pyrene) bond lengths of compounds **1-9** (1.555(3) Å) and **1-II** (1.562(4) Å) are typical for trigonal coordinated boron bonded to an aromatic carbon. Similar lengths are also observed for the B–C(mes) bonds in compound **1-II**. The boron atoms in **1-9** and **1-II** have a nearly perfect trigonal planar configuration, with the sum of the three C–B–C, C–B–O and O–B–O angles, respectively, being 360.0(6)°. The dihedral angle between the BC<sub>3</sub> and pyrene planes is 25.41(11)° in **1-II** (Table 1-1), which is smaller than that of 2-(Bmes<sub>2</sub>)pyrene **1-C** (36.32(6)°) and 2,7-bis(Bmes<sub>2</sub>)pyrene **1-D** (31.7(1)°), respectively.<sup>[63]</sup> The crystal structure of **1-14** contains two symmetry-independent molecules in the unit cell. In one of the molecules, the two julolidine moieties are twisted with respect to one another with a dihedral angle of 43.97(4)°, which is close to the typical equilibrium angle of biphenyl (44.4°<sup>[96]</sup>), while the other molecule lies on an inversion center and is planar (Figure 1-2).

The compounds **1-4**, **1-8**, **1-9**, and **1-14** crystalize in a herringbone-type packing, while those of **1-6** and **1-II** do not show obvious  $\pi$ - $\pi$ -interactions due to the steric demand of the respective donor and acceptor substituents. Furthermore, in compound **1-1** the herringbone is made up of sandwich-like diads with both edge-to-face and offset face-to-face interactions of  $\pi$ - $\pi$  stacked molecules that have an interplanar distance of  $X = 3.32$ - $3.39$  Å. The herringbones in compound **1-4** on the other hand, are arranged with edge-to-face stacking. The interplanar angle is 70.34(3)° and in compound **1-8** 84.54(4)° between the pyrene moieties.

**Table 1-1.** Selected bond lengths (Å) and angles (°) of 1-1, 1-4, 1-6, 1-8, 1-9, 1-11 and 1-14.

	1-1 <sup>[a]</sup>	1-4	1-6 <sup>[a]</sup>	1-8	1-9 <sup>[b]</sup>	1-11	1-14(1)	1-14(2)
N1-C1	1.396(3) 1.383(3)	1.4044(16)	1.379(2) 1.380(2)	1.404(3)	1.398(3) 1.403(3) 1.402(3)	1.391(3)	1.4116(17)	1.4050(17)
N2-C4	1.409(3) 1.409(3)	-	-	-	-	-	1.4048(18)	-
B1-C4	-	-	-	-	1.552(3) 1.557(3) 1.557(3)	1.562(3)	-	-
∠ NC <sub>3</sub> -pyrene	-	19.79(9)	12.00(5) 9.17(9)	11.41(14)	19.70(15) 15.99(12) 21.32(8)	10.78(16)	14.00(8) 9.45(10)	12.76(11)
Sum ∠ CNC	-	349.4(3)	360.0(4) 360.0(4)	350.7(5)	351.8(6) 350.0(6) 350.0(6)	355.7(6)	343.8(3) 350.4(4)	347.9(4)
∠ BCE <sub>2</sub> -pyrene	-	-	-	-	3.05(12) 4.45(11) 5.83(10)	25.41(11)		
Sum ∠ (C,E)B(C,E)	-	-	-	-	360.0(6) 360.0(6) 360.0(6)	359.9(6)		

[a] Two independent molecules in the unit cell. [b] Three independent molecules in the unit cell.

## 1.2.2 Photophysical Properties

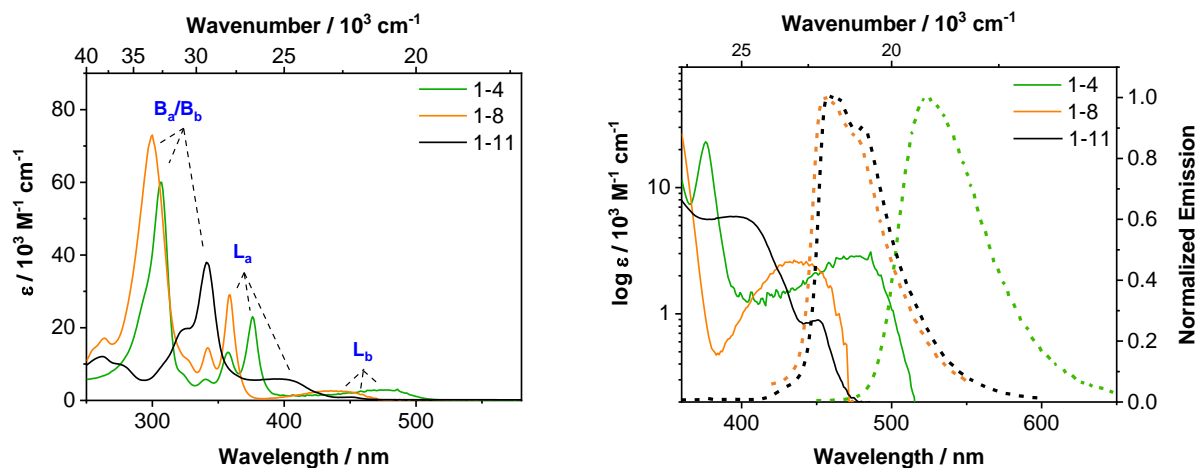


**Figure 1-7.** Left: Absorption spectra of **1-4** (green), **1-8** (orange) and **1-11** (black) recorded in hexane at room temperature. Right: Absorption (logarithmic scale, solid lines) and emission (linear scale, dashed lines) spectra of **1-4** (green), **1-8** (orange) and **1-11** (black) recorded in hexane at room temperature.

The absorption spectra of the D- and D/A-substituted compounds **1-4**, **1-8**, **1-9** and **1-11** are generally very similar to that of pyrene, in that the  $S_1 \leftarrow S_0$  absorption, which is attributed to the short-axis-polarized and transition dipole-forbidden  $L_b$  transition, is comparably weak<sup>[31,69,70]</sup> with extinction coefficients of  $\epsilon = 900\text{-}3\,300 \text{ M}^{-1} \text{ cm}^{-1}$  (Figure 1-7 and Table 1-2). This band shifts bathochromically in the order **1-8** < **1-9** < **1-11** < **1-4**, leading, in the case of **1-4** with  $\lambda_{\text{max}}(\text{abs}) = 475 \text{ nm}$ , to the lowest energy absorption reported so far for 2- and 2,7-substituted pyrene derivatives. In addition, the  $L_b$  band is unusually broad with no vibrational progression, covering a range of up to ca.  $6\,000 \text{ cm}^{-1}$ , indicative of a more pronounced CT character.

It is interesting to observe that, in comparison to pyrene, a much stronger bathochromic shift of the  $S_1 \leftarrow S_0$  absorption is caused by the julolidine donors in **1-4** and **1-8** than by the acceptor units in previously published 2-(Bmes<sub>2</sub>)pyrene and 2,7-bis(Bmes<sub>2</sub>)pyrene, showing  $\lambda_{\text{max}}(\text{abs}) = 413$  and  $444 \text{ nm}$ , respectively. Bearing in mind that the first singlet excited state in pyrene is due to a combination of HOMO  $\rightarrow$  LUMO+1 and HOMO-1  $\rightarrow$  LUMO transitions, the donor substituents appear to exert a more destabilizing effect on the occupied frontier orbitals than the acceptor Bmes<sub>2</sub> stabilizes the empty ones (*vide infra*). This also explains why **1-4** exhibits the  $L_b$  band at lower energy than the D/A-system **1-11** ( $\lambda_{\text{max}}(\text{abs}) = 475$  vs.  $450 \text{ nm}$ ). Interestingly, the  $\lambda_{\text{max}}$  of the allowed transition  $L_a$ , which is long-axis-polarized and tentatively assigned as  $S_2 \leftarrow S_0$ , and the overlapping  $B_b$  and  $B_a$  bands of very high extinction coefficients are much more

influenced by the CT character in **1-II** than in the pure donor-substituted pyrene derivatives **1-4** and **1-8** (Figure 1-7, left), leading to more pronounced bathochromic shifts and lower extinction coefficients  $\epsilon$  for **1-II**. The additional Bpin moiety in **1-9** has no significant influence on the photophysical properties compared to those of **1-8**, as the oxygen substituents at the boron atom decrease its  $\pi$ -acceptor properties.<sup>[97]</sup>

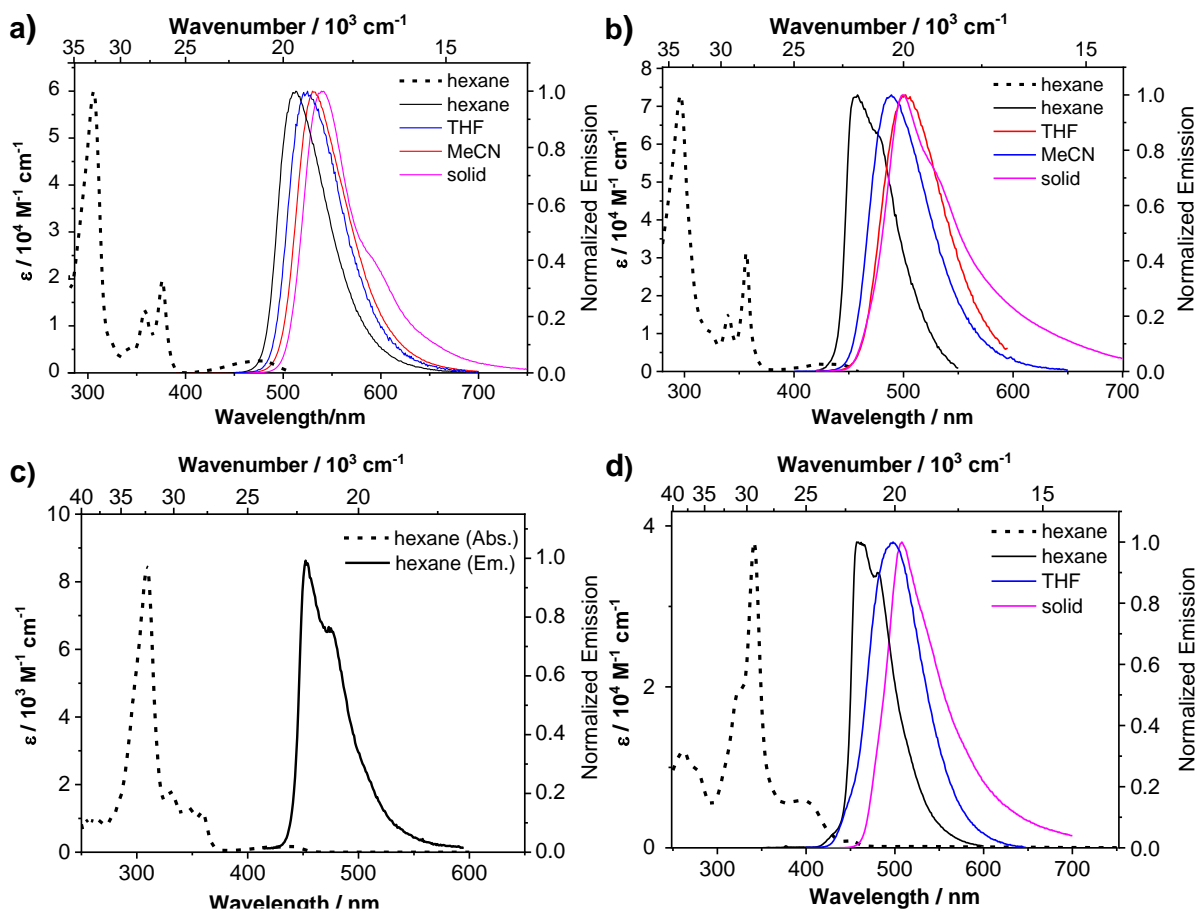


**Figure 1-8.** UV-visible absorption (dashed line) in hexane and emission spectra (solid line) of the compounds a) **1-4**, b) **1-8**, c) **1-9** and d) **1-11** in three different solvents (due to low solubility only in two solvents for compound **1-11**) and in the solid state (emission only) (compound **1-9** only in hexane).

Pyrene derivatives **1-4**, **1-8** and **1-II** show intense fluorescence in the blue to green region of the electromagnetic spectrum in solution as well as in the solid state, with quantum yields  $\phi$  of up to 0.61 (Figure 1-7, right and Table 1-2). All compounds exhibit significant solvatochromism, which is most pronounced for **1-II**, and the weak vibrational progression observed in hexane vanishes with increasing polarity of the solvent (Figure 1-8), confirming the CT nature of the lowest energy excited state. The photophysical properties of the pyrene derivatives **1-4** and **1-8**

with the exceptionally strong julolidine-type donor, and of the D/A compound **I-II** with the very strong acceptor Bmes<sub>2</sub>, are highly unusual in many regards. Green emission with  $\lambda_{\max}(\text{em}) = 503\text{-}540\text{ nm}$  has previously not been achieved with 2- or 2,7-substituted pyrene derivatives, which normally emit in the blue region ( $\lambda_{\max}(\text{em}) = 370\text{-}480\text{ nm}$ ).<sup>[2,31,46,47,50,63,65]</sup>

Surprisingly, the emission of D/D-compound **I-4** is significantly red-shifted compared to that of the D/A-compound **I-II**, and exhibits one of the largest apparent Stokes shifts yet observed for 2,7-substituted pyrene derivatives. Normally one would expect larger bathochromic and Stokes shifts for a donor-acceptor system such as **I-II**. The second donor moiety apparently destabilizes the ground state S<sub>0</sub> more strongly than the additional acceptor Bmes<sub>2</sub> stabilizes the singlet excited state S<sub>1</sub>, explaining the differences in the absorption and emission energies of **I-4**, **I-8** and **I-II**. Furthermore, the radiative rate constants of **I-4** in THF ( $k_r = 4.2 \cdot 10^7\text{ s}^{-1}$ ) and of **I-II** in the solid state ( $k_r = 7.1 \cdot 10^7\text{ s}^{-1}$ ) are among the highest reported so far for 2- and 2,7-substituted pyrene derivatives,<sup>[32,43,45-63]</sup> approaching values of pyrenes substituted at the non-nodal-plane positions with regard to HOMO and LUMO (*vide supra*).<sup>[32,43,46-63]</sup> However, for all compounds, the non-radiative decay rates  $k_{nr}$  in solution of  $2.1\text{-}7.1 \cdot 10^7\text{ s}^{-1}$  are greatly enhanced in the solid state by up to one order of magnitude ( $k_{nr} = 16\text{-}53 \cdot 10^7\text{ s}^{-1}$ ), which leads to decreased quantum yields. Ito and co-workers have reported apparent Stokes shifts of the D- $\pi$ -A compound **I-H** ranging from  $3\,292\text{ cm}^{-1}$  in hexane ( $\lambda_{\max}(\text{em}) = 458\text{ nm}$ ) to  $8\,649\text{ cm}^{-1}$  in acetone ( $\lambda_{\max}(\text{em}) = 600\text{ nm}$ ).<sup>[67]</sup> However, these very high values are the result of an incorrect excited state assignment. The authors conclude that the observed intense absorption band at  $400\text{ nm}$  ( $\epsilon = 26\,200\text{ M}^{-1}\text{ cm}^{-1}$ ) is the S<sub>1</sub>←S<sub>0</sub> transition, which would then be more allowed than S<sub>1</sub>←S<sub>0</sub> for the isomeric 1,6-D- $\pi$ -A-substituted pyrene analogue **I-I** ( $\epsilon_{463} = 18\,500\text{ M}^{-1}\text{ cm}^{-1}$ ), and much more allowed than in **I-II** (*vide supra*). However, the radiative rate constant of **I-H** ( $k_r = 0.9 \cdot 10^7\text{ s}^{-1}$ ) is smaller by a factor of 10 than found for **I-I** ( $k_r = 11.5 \cdot 10^7\text{ s}^{-1}$ ), and by a factor of two compared to **I-II** ( $k_r = 1.7 \cdot 10^7\text{ s}^{-1}$ ), and is thus typical for a forbidden transition (the Strickler-Berg relation<sup>[98]</sup>). Consequently, the observed absorption band centered around  $400\text{ nm}$  must be the S<sub>2</sub>←S<sub>0</sub> transition, *i.e.* the L<sub>a</sub> band, while the actual S<sub>1</sub>←S<sub>0</sub> (L<sub>b</sub>) transition of very low oscillator strength occurs between ca.  $440\text{-}480\text{ nm}$ , similar to the D- $\pi$ -A compound **I-II**, and fully in line with the very long pure radiative lifetime of 110 ns reported by the authors. Actually, their theoretical results obtained with the CAM-B3LYP functional are also in line with their experimental lifetime data, *i.e.* a forbidden S<sub>1</sub>←S<sub>0</sub> transition, but due to a better agreement of the excited state energies obtained with the B3LYP functional, which is known to produce the wrong excited state

ordering,<sup>[31]</sup> the authors were apparently misled. Unfortunately, no excitation or absorption spectra at high concentrations were reported, which would have allowed direct observation of the forbidden  $L_b$  band. Nonetheless, larger apparent Stokes shifts would be expected to arise from TICT excited states, which are possible in the Ito systems but not in the pyrene derivatives presented in this chapter.

**Table 1-2.** Selected photophysical data of pyrene (**P**) and its derivatives **1-4**, **1-8**, **1-9** and **1-11** recorded under argon at room temperature.

Cpd.	medium	$\lambda_{\text{abs}} / \text{nm} (\epsilon / 10^3 \text{ M}^{-1} \text{ cm}^{-1})$	$\lambda_{\text{em}} / \text{nm}^{[a]}$	Apparent Stokes shift / $\text{cm}^{-1}$	$\phi$	$\tau / \text{ns}^{[b]}$	$\tau_0 / \text{ns}^{[c]}$	$k_r / 10^7 \text{ s}^{-1}$	$k_{\text{nr}} / 10^7 \text{ s}^{-1}$
<b>P</b>	hexane	362 (0.6), 338 (69)	372	700	0.64	354	553	0.2	0.1
<b>1-4</b>	hexane	475 (3.3), 376 (26), 307 (60)	511	1 500	0.37	10	27	3.7	6.3
	THF	481, 379, 310	525	1 700	0.44	9.6 (87), 15 (13)	24	4.2	5.3
	MeCN	487, 378, 310	532	1 700	0.22	7.2 (48), 11 (52)	42	2.4	8.5
	solid	-	540	-	0.04	1.3 (78), 3.6 (22)	45	2.2	53
<b>1-8</b>	hexane	433 (2.8), 357 (32), 300 (73)	460	1 400	0.61	16 (88), 29 (12)	30	3.4	2.1
	THF	432, 359, 298	489	2 700	0.40	12	30	3.4	5.1
	MeCN	441, 358, 300	503	2 800	0.23	9.4 (92), 19 (8)	47	2.1	7.1
	solid	-	501	-	0.14	2.3 (48), 6.0 (40), 16 (12)	39	2.5	16
<b>1-9</b>	hexane	440 (2.4), 360 (15), 309 (85)	454	700	0.36	12	33	3.0	5.3
<b>1-11</b>	hexane	450 (0.9), 400 (6.1), 341 (38)	464	700	0.37	18 (87), 35 (13)	59	1.7	2.9
	THF	462, 405, 346	497	1 600	0.30	8.3 (88), 21 (12)	40	2.5	5.8
	solid	-	509	-	0.17	2.0 (84), 4.5 (16)	14	7.1	35

[a] Excited at the respective  $\lambda_{\text{abs}}(\text{max})$  of  $S_0 \rightarrow S_1$  and  $S_0 \rightarrow S_2$ . [b] Pre-exponential factors  $B_n$  scaled to 100 and given in parentheses. [c] For multi-exponential decays the pure radiative lifetime  $\tau_0 = \tau / \phi$  has been approximated by using the experimental average lifetime  $\tau = \sum \tau_n B_n / \sum B_n$ , with  $B_n$  being the pre-exponential factors of the respective lifetime component  $\tau_n$ .

### 1.2.3 Redox Properties

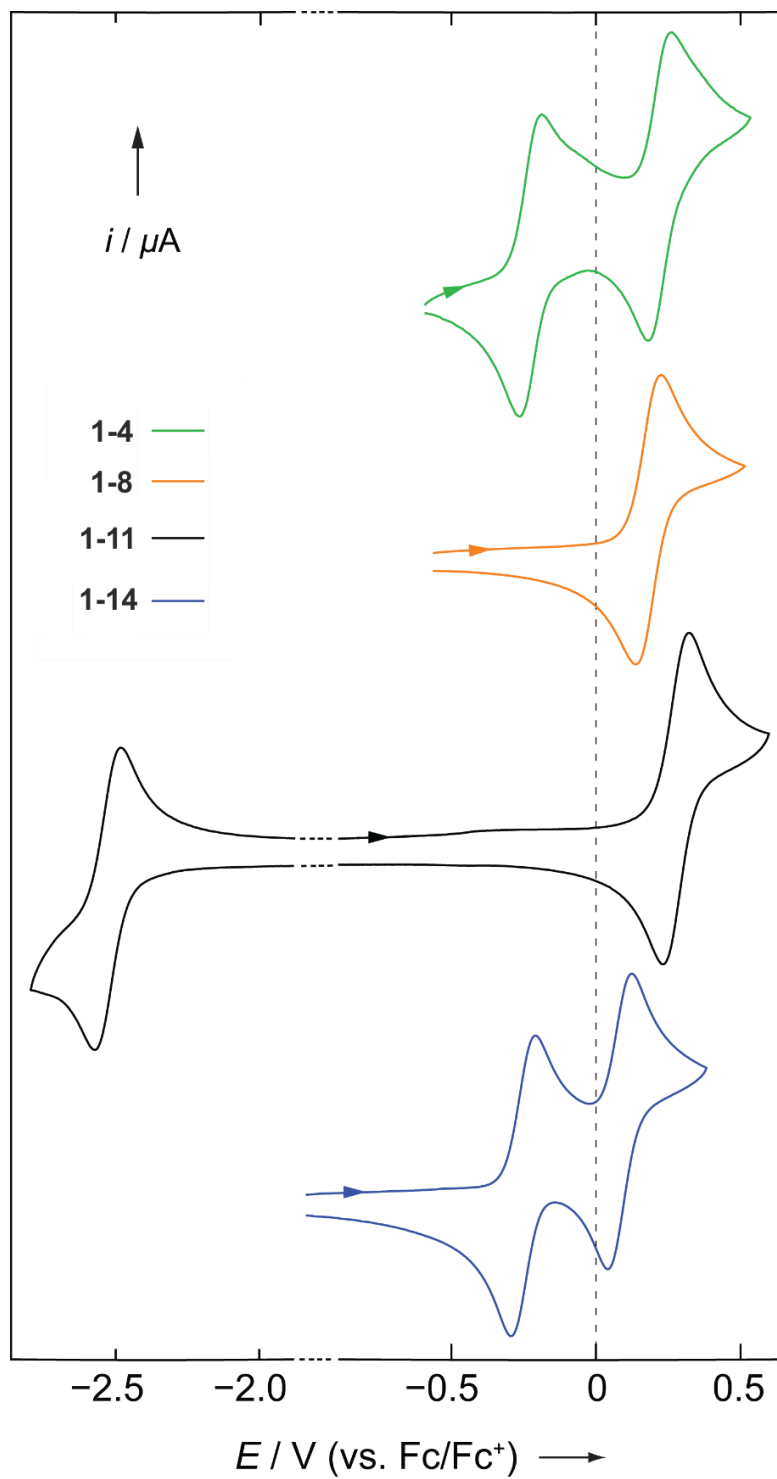


**Figure 1-9.** Cyclic voltammograms of **1-4** (green), **1-8** (orange), and **1-14** (blue) in  $\text{CH}_2\text{Cl}_2/0.1 \text{ M}$   $[\text{n-Bu}_4\text{N}][\text{PF}_6]$ , and of **1-11** (black) in  $\text{THF}/0.1 \text{ M}$   $[\text{n-Bu}_4\text{N}][\text{PF}_6]$  relative to the  $\text{Fc}/\text{Fc}^+$  couple.

The cyclic voltammetry measurements show that, due to the Bmes<sub>2</sub> moiety, **1-II** is the only compound in this series, which can be reduced reversibly, with reduction occurring at  $E_{1/2} = -2.51$  V in THF (Figure 1-9 and Table 1-3), similar to **1-H** ( $E_{1/2} = -2.46$  V). However, **1-4**, **1-8** (both in CH<sub>2</sub>Cl<sub>2</sub>) and **1-II** (in THF) are reversibly oxidizable, which is important to obtain stable hole transport materials to minimize decomposition reactions that may occur in a device.<sup>[99]</sup> The same is true for the bis(julolidine) compound **1-14**, which was also studied in CH<sub>2</sub>Cl<sub>2</sub> for comparison. The oxidation potential of the D/A-compound **1-II** ( $E_{1/2}(\text{ox}) = 0.29$  V), which is very similar to that of **1-H** ( $E_{1/2}(\text{ox}) = 0.26$  V), and also that of the JulPyr **1-8** ( $E_{1/2}(\text{ox}) = 0.20$  V) are significantly higher than that of Jul<sub>2</sub>Pyr **1-4** ( $E_{1/2}(\text{ox})^1 = -0.18$  V), implying that the HOMO in **1-4** is greatly destabilized by the second donor. This is in stark contrast to the findings of Zhong *et al.*, who studied the influence of one to four amino substituents in the 1,3,6,8-positions of pyrene on the  $E_{1/2}(\text{ox})^1$  values.<sup>[100]</sup>

**Table 1-3.** Cyclic voltammetry results for compounds **1-4**, **1-8** and **1-14** measured in CH<sub>2</sub>Cl<sub>2</sub>/0.1 M [*n*-Bu<sub>4</sub>N][PF<sub>6</sub>], and of **1-11** in THF/0.1 M [*n*-Bu<sub>4</sub>N][PF<sub>6</sub>] relative to the Fc/Fc<sup>+</sup> couple.

Cpd	$E_{1/2}(\text{red}) / \text{V}$	$E_{1/2}(\text{ox})^1 / \text{V}$	$E_{1/2}(\text{ox})^1 / \text{V}$	$\Delta E / \text{mV}$
<b>1-4</b>	-	-0.18	+0.26	440
<b>1-8</b>	-	+0.20	-	-
<b>1-II</b>	-2.51	+0.29	-	-
<b>1-14</b>	-	-0.23	+0.11	340

According to their experiments,  $E_{1/2}(\text{ox})^1$  of the 1-monoamino-substituted pyrene differs from that of the 1,3-diamino-substituted pyrene by only 0.11 V, and from that of the 1,3,6,8-tetraamino-substituted pyrene by 0.28 V. In addition, the HOMO energy difference upon going from one to four amino groups in that study is not as large as it is for the compounds **1-4** and **1-8**, which underlines the much stronger destabilizing effect on the HOMO of the donor-substituents at the 2,7-positions compared to diarylamino groups at the 1,3,6,8-positions. The D- $\pi$ -D compounds **1-4** and **1-14**, unlike the mono-donor substituted compounds, display a second reversible one-electron oxidation at +0.26 V and +0.11 V, respectively, and a remarkably large potential splitting  $\Delta E$  (440 mV) for this type of compound (Table 1-3).<sup>[63,65,66,83]</sup> In addition, **1-4**<sup>+</sup> is very stable with respect to disproportionation to the dication **1-4**<sup>2+</sup> and neutral **1-4**, as

evidenced by a high comproportionation constant  $K_c = 2.7 \cdot 10^{7[101]}$  for the reverse process, which is larger than that of the previously reported radical anion of 2,7-bis(Bmes<sub>2</sub>)pyrene ( $K_c = 5.6 \cdot 10^4$ ).<sup>[63]</sup> The biphenyl monocation compound **1-14**<sup>+</sup> has a smaller comproportionation constant ( $K_c = 5.0 \cdot 10^5$ ) compared to that of **1-4**<sup>+</sup>.<sup>[101]</sup> A different trend was found in previous reports on related systems.<sup>[65,66,83]</sup> For example, the very small  $\Delta E = 104$  mV of 2,7-bis(carbazole)pyrene is similar to that of the biphenyl-bridged analogue ( $\Delta E = 76$  mV). Ito and co-workers reported 2,7-bis(dianisylamino)pyrene **1-G** to have an  $\Delta E$  of 240 mV and for the biphenyl-bridged analogue 300 mV.<sup>[83]</sup>

Even though electrochemical measurements, such as cyclic voltammetry, are often used for comparison of the strength of electronic coupling, it is noteworthy that  $\Delta E$  can be influenced by several factors. For example, ion pairing between the mono- and dication of interest and the counterion from the electrolyte plays an important role, as it influences the ease of adding/removing electrons to/from the system. Moreover,  $\Delta E$  reflects properties of M vs. M<sup>+</sup> and M<sup>+</sup> vs. M<sup>2+</sup>,<sup>[102]</sup> while the electronic coupling is only attributed to M<sup>+</sup>.<sup>[99,103]</sup> The  $\Delta E$  value is only a qualitative, but not a quantitative measure of the ground-state delocalization of a mixed-valent system.<sup>[104]</sup> Winter *et al.* showed, for several examples, that the  $\Delta E$  and the true electronic couplings are not related to each other. Sáveant and co-workers pointed out that systems, especially those containing a fully  $\pi$ -conjugated bridge which actively participates in the redox processes, tend to have smaller  $\Delta E$  and rather larger electronic couplings. The small magnitude of  $\Delta E$  is often a result of an increased solvation energy that stabilizes the doubly oxidized form with respect to the mixed-valent state, which sometimes even leads to a potential inversion.<sup>[104,105]</sup>

### 1.2.4 Spectroelectrochemistry

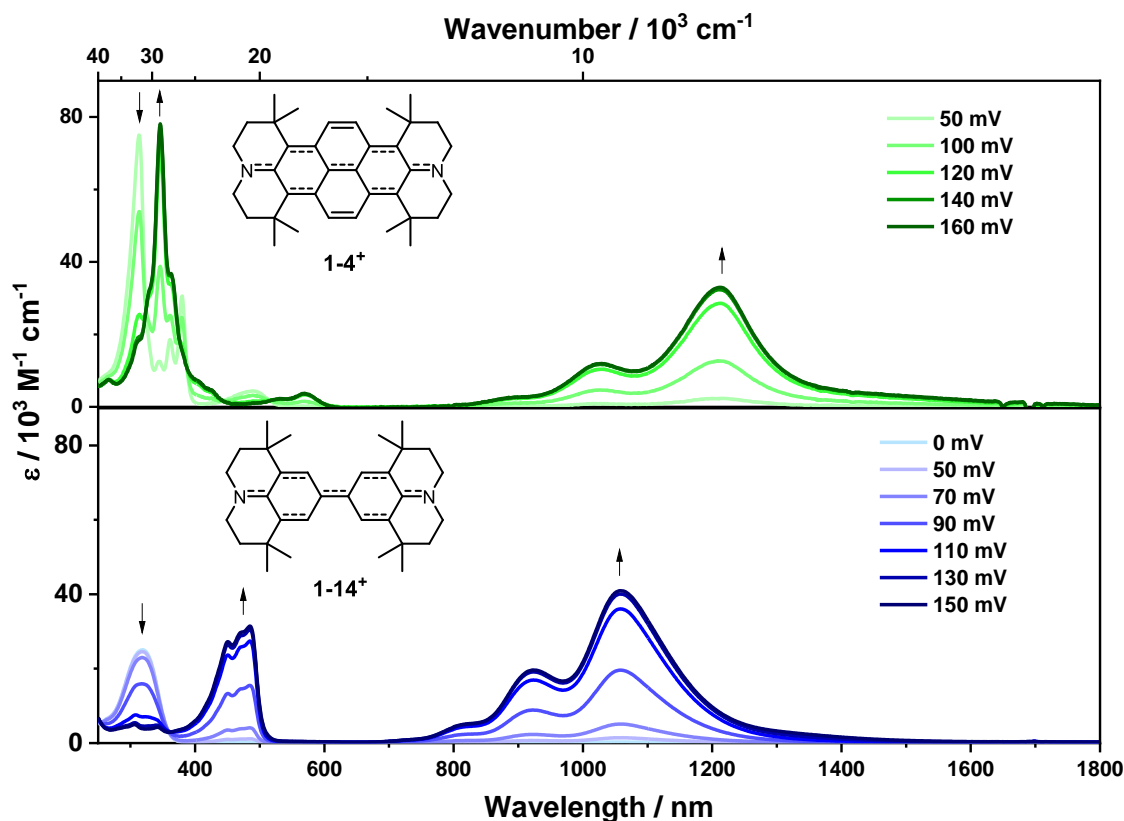


**Figure 1-10.** Spectroelectrochemical measurements of the stepwise oxidation processes in  $\text{CH}_2\text{Cl}_2/0.1 \text{ M } [n\text{-Bu}_4\text{N}][\text{PF}_6]$ . The absorption spectra of **1-4<sup>+</sup>** and of **1-14<sup>+</sup>** are given as the solid dark green and solid dark blue lines, respectively.

Thus, in order to quantify the electronic coupling between the 2,7-substituents in **1-4**, UV/vis/NIR spectroelectrochemical measurements in  $\text{CH}_2\text{Cl}_2$  were conducted. As previous reports have used biphenyl analogues for comparison of the electronic coupling between the substituents in pyrene, the spectroelectrochemical behavior of **1-14** was also studied. The optical spectra of the monoradical cations of both compounds, depicted in Figure 1-10, show intense absorptions ( $8\,250 \text{ cm}^{-1}$ ,  $\epsilon = 33\,000 \text{ M}^{-1} \text{ cm}^{-1}$  for **1-4<sup>+</sup>**;  $9\,400 \text{ cm}^{-1}$ ,  $\epsilon = 41\,000 \text{ M}^{-1} \text{ cm}^{-1}$  for **1-14<sup>+</sup>**) in the NIR, with well-defined vibrational fine structures. These features indicate a delocalized (Robin-Day-class-III) mixed valence structure of the radical cations.<sup>[106-109]</sup> Indeed, TD-DFT computations with a specially adjusted functional (BLYP with 35% exact HF exchange<sup>[110]</sup>) reveal for both radical cations a vanishing permanent dipole moment for the ground state and the excited states. In this case, the electronic coupling between the localized (= diabatic) mixed

valence states can readily be evaluated by eq. (1) from half the energy of the intervalence charge transfer band.<sup>[106-109]</sup>

$$V = \frac{\tilde{\nu}_{max}}{2} \quad (1)$$

This yields  $V = 4\,130\text{ cm}^{-1}$  for **1-4**<sup>+</sup> and  $4\,710\text{ cm}^{-1}$  for **1-14**<sup>+</sup>, which compares favorably with the values obtained from TD-DFT computations of  $V = 3\,706\text{ cm}^{-1}$  (**1-4**<sup>+</sup>) and  $V = 5\,178\text{ cm}^{-1}$  (**1-14**<sup>+</sup>) for half of the IV-CT excitation energy ( $\beta$ -HOMO $\rightarrow\beta$ -LUMO). The orbitals involved in this excitation show the expected phase behavior for a MV excitation with a large contribution of the nitrogen atom coefficients (Figure 1-11). However, unlike for **1-14**<sup>+</sup> where the DFT calculations predict the IV-CT excitation to be the lowest energy excitation, the quantum chemical calculations suggest that there is an even lower band for **1-4**<sup>+</sup> at  $6\,097\text{ cm}^{-1}$  (1 639 nm). This band is symmetry forbidden ( $\beta$ -HOMO-1 $\rightarrow\beta$ -LUMO) but could be visible due to vibronic coupling effects. Indeed, such a band is observed in the spectra as a weak shoulder at the low energy side of the more intense IV-CT band. A deconvolution of the reduced spectra of **1-4**<sup>+</sup> with Gaussian functions disclosed this band to be at  $7\,330\text{ cm}^{-1}$  (1 379 nm).

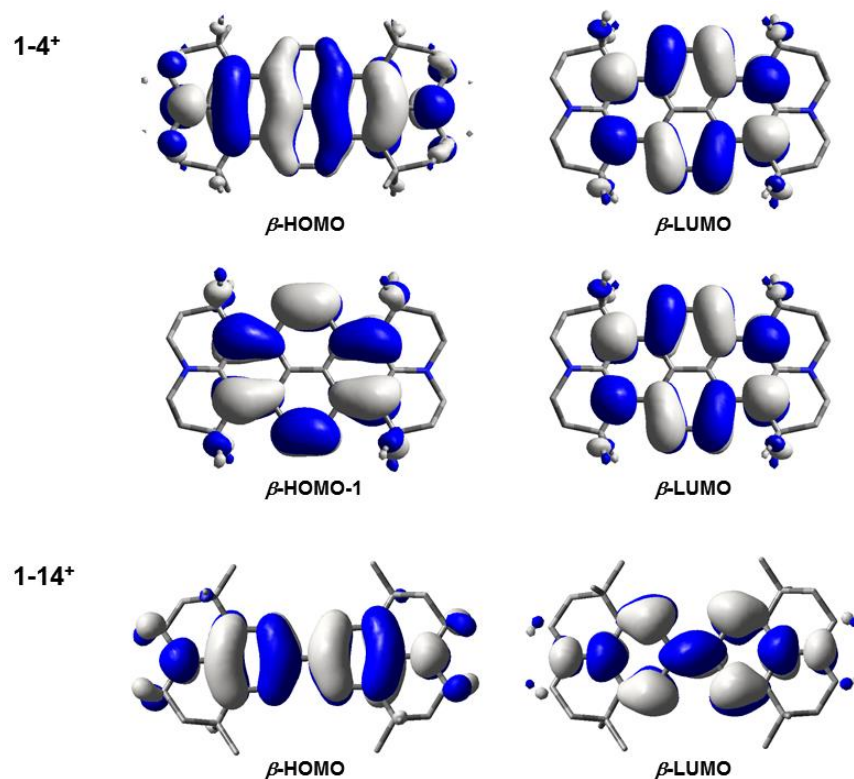


**Figure 1-11.** Depiction of the orbitals that are responsible for the lowest energy absorption (IV-CT band) of the derivatives **1-4**<sup>+</sup> and **1-14**<sup>+</sup>. For compound **1-4**<sup>+</sup> the orbitals that are responsible for the second lowest energy band are also depicted.

### 1.2.5 DFT and TD-DFT calculations

The photophysical studies showed that the bis(donor)-substituted pyrene derivative **1-4** experiences a stronger bathochromic shift of the emission compared to pyrene itself than the donor-acceptor compound **1-II**, an observation which is counterintuitive. The other observed trends mentioned above, are rationalized by DFT and TD-DFT studies of the compounds **1-4**, **1-8**, **1-II** and **1-14**. The ground state structures were first optimized in the gas-phase at the B3LYP/6-31 G(d) level of theory. Previous studies<sup>[31]</sup> have shown that range-separated hybrid functionals are necessary to obtain a reliable picture of the nature and relative energetic ordering of the excited states in pyrenes. Thus, the CAM-B3LYP functional was used for the subsequent TD-DFT calculations.

The  $S_1 \leftarrow S_0$  transition of pyrene is described as a nearly 50:50 weighted configuration interaction of HOMO-1  $\rightarrow$  LUMO and HOMO  $\rightarrow$  LUMO+1. Consequently, these four key frontier molecular orbitals are the focus of this study, which are shown in Figure 1-8 for pyrene and compounds **1-4**, **1-8** and **1-II**. The nitrogen  $2p_z$  orbitals, *i.e.* the *N*-lone pairs of the julolidine-type moieties, mix very well with the  $b_{2g}$ -symmetrical HOMO-1 of the pyrene core. This leads to a drastic destabilization of that orbital by ca. 1.30 eV in mono-substituted **1-8** and **1-II**, and an even more pronounced effect of 2.47 eV in **1-4**, which consequently switches the order of the HOMO and HOMO-1 orbitals. In fact, the influence of the two donors in **1-4** leads to the highest energy HOMO reported for a 2,7-disubstituted pyrene derivative.<sup>[47,63,65,66,83]</sup> The difference of the HOMO energy of 1.16 eV between the bis(donor)- and mono(donor)-substituted compounds **1-4** and **1-8** is relatively large compared to that of analogous compounds. Even substitution with donors at the 1,3,6,8-positions does not lead to such a strong destabilizing influence on the HOMO.<sup>[100]</sup> Consequently, the HOMO-LUMO gap of the doubly-substituted pyrene **1-4** is smaller than that of the mono-substituted pyrene **1-8**. Furthermore, the HOMO of **1-4** and **1-8** is fully delocalized over the  $\pi$ -bridge and the donor moieties, which is different than that in previously reported pyrene derivatives with carbazole<sup>[65,66]</sup> and dianisylamine<sup>[83]</sup> substituents at the 2,7-positions, wherein the HOMO is localized at the donor. This finding is reflected in the strong bathochromic shift, the high  $\Delta E$ , and the enormous electronic coupling (*vide supra*). The addition of the Bmes<sub>2</sub> acceptor leads to another frontier orbital shuffling by lowering the LUMO+1 energy by 0.81 eV in the D- $\pi$ -A compound **1-II** compared to that of the pyrene LUMO+1, and by 1.21 eV compared to **1-8**, while the julolidine slightly destabilizes the former pyrene LUMO by 0.18 eV.<sup>[63]</sup> Such a drastic influence of donors and acceptors at the 2- and 7-

positions of pyrene on the frontier orbitals is very rare.<sup>[39]</sup> However, the influence of the second donor on the HOMO is larger than the influence of the acceptor on the LUMO, which leads to a narrower HOMO-LUMO gap for **1-4** (2.51 eV) compared to **1-II** (3.45 eV), highlighting the donor strength of julolidine. Comparing the pyrene- and biphenyl-bridged compounds **1-4** and **1-14** (**1-14**: HOMO = -4.62 eV, LUMO = -0.27 eV), the LUMO of the latter is destabilized by 1.23 eV due to the lower degree of conjugation of the biphenyl unit compared to the pyrene core. Hence, **1-14** has a larger HOMO-LUMO gap than **1-4**. The TD-DFT calculations show that the pyrene-like nature of the transitions is generally maintained in these compounds (Figure 1-8 and Table 1-4), thus leading to a very similar behavior. However, the orbital shuffle obtained by introduction of the julolidine and Bmes<sub>2</sub> moieties changes the respective contributions of the orbital transitions to the electronic excitation, and thus increases the transition dipole moment for the absorption to S<sub>1</sub> and consequently also for the emission from S<sub>1</sub>, according to the Strickler-Berg relation.<sup>[98]</sup> In addition, the CT nature of the excited states is greatly increased compared to those in pyrene, and thus large bathochromic shifts and significant solvatochromism are also observed.

Specifically, the S<sub>1</sub>←S<sub>0</sub> excitations in the donor-substituted pyrene compounds **1-4** and **1-8** are predominantly symmetry-forbidden HOMO→LUMO transitions with only a small admixture of HOMO-1→LUMO+1 (Table 1-4). As a consequence, although still being characterized as an L<sub>b</sub> transition, the oscillator strengths (**1-4**:  $f = 0.088$ , **1-8**:  $f = 0.053$ ) are slightly higher than those for previously reported 2,7-pyrenes. This matches well with the comparatively large extinction coefficients that were measured for this transition (Table 1-2), and the observation of the highest radiative rate constants  $k_r$  for the fluorescence of 2,7-substituted pyrene derivatives. The S<sub>1</sub> state in **1-4** and **1-8** is further characterized by a CT from the donor-substituents to the pyrene core (Figure 1-11), which gives rise to the observed bathochromic shift of that absorption band compared to pyrene, and the much greater Stokes shift (pyrene: 740 cm<sup>-1</sup>). A pronounced solvatochromism also results from the CT nature of the lowest excited singlet state, which is much larger for the JulPyr **1-8** than for Jul<sub>2</sub>Pyr **1-4** as a result of either stronger CT or due to larger geometrical reorganization in the S<sub>1</sub> state. The highest oscillator strengths of 1.519 and 1.149 for **1-4** (S<sub>4</sub>←S<sub>0</sub>) and **1-8** (S<sub>5</sub>←S<sub>0</sub>), respectively, were found for the symmetry-allowed B<sub>a</sub> transition, which is a configuration interaction (CI) dominated by HOMO→LUMO+1 with an admixture of HOMO-1→LUMO (Table 1-4).

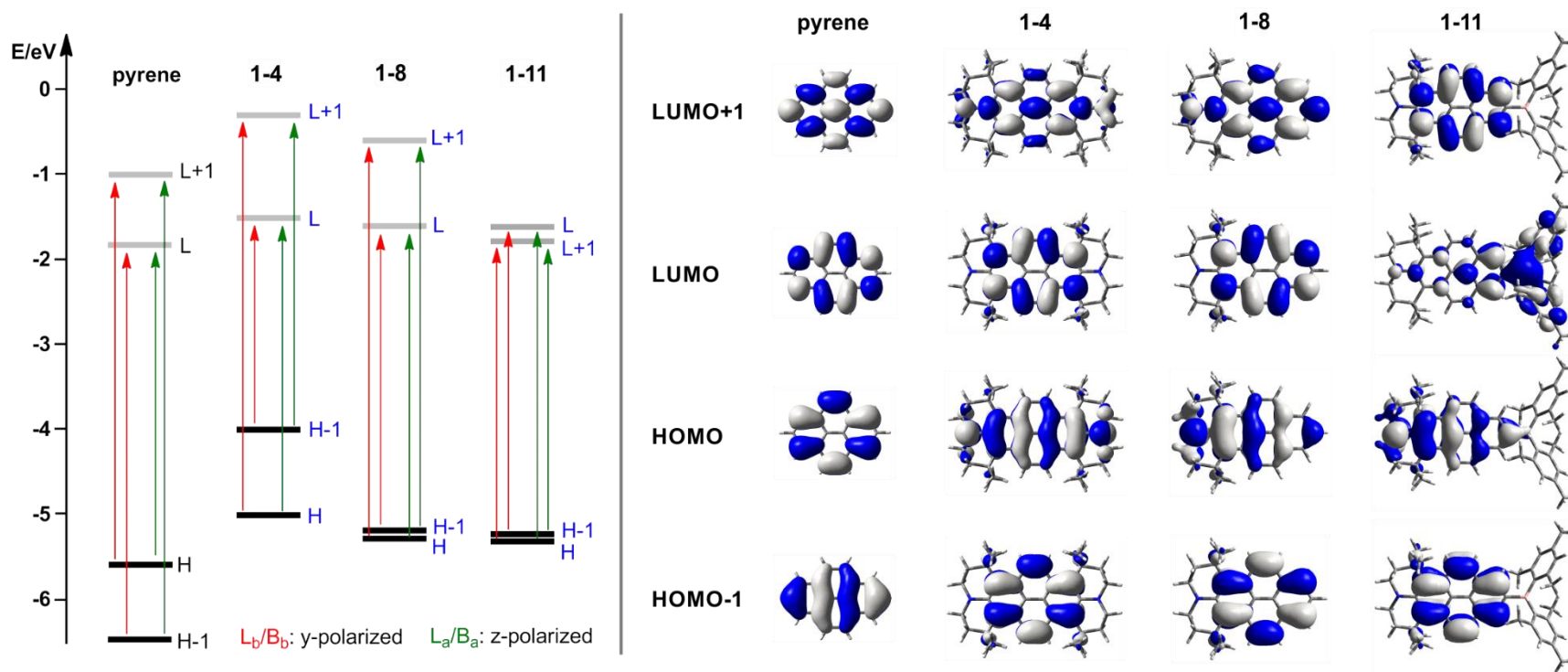


**Figure 1-11.** Left: molecular orbital diagram of pyrene, **1-4**, **1-8** and **1-11** including the transitions involved in the four experimentally observed major absorptions  $L_b/B_b$  (short axis y-polarized) and  $L_a/B_a$  (long axis z-polarized). To make comparison easier, the orbitals in **1-4**, **1-8** and **1-11** in blue are labelled according to their pyrene-like nature (H-1, H, L, L+1). Right: depiction of the HOMO-1, HOMO, LUMO and LUMO+1 of pyrene, **1-4**, **1-8**, and **1-11**.

**Table 1-4.** TD-DFT results (CAM-B3LYP/6-31 G(d)) for the observed major absorption bands of pyrene (**P**), **1-4**, **1-8** and **1-11** and TD-DFT results (ublyp/svp) for the observed major absorption bands of **1-4<sup>+</sup>** and **1-14<sup>+</sup>**.

S <sub>n</sub>	Cpd	E / eV (nm)	f	Configuration <sup>a</sup>	Pol. <sup>b</sup>
S <sub>1</sub>	<b>P</b>	3.99 (311)	0.000	H-1→L (0.49), H→L+1 (0.50)	y (L <sub>b</sub> )
S <sub>2</sub>		4.02 (309)	0.323	H→L (0.67), H-1→L+1 (-0.23)	z (L <sub>a</sub> )
S <sub>3</sub>		4.90 (253)	0.000	H-2→L (0.21), H→L+2 (0.67)	-
S <sub>4</sub>		5.10 (243)	0.000	H-2→L (0.66), H→L+2 (-0.19)	-
S <sub>5</sub>		5.11 (243)	0.414	H-1→L (0.50), H→L+1 (-0.49)	y (B <sub>b</sub> )
S <sub>7</sub>		5.78 (214)	0.969	H→L (0.22), H-1→L+1 (0.65)	z (B <sub>a</sub> )
S <sub>1</sub>	<b>1-8</b>	3.46 (358)	0.053	H-1→L+1 (0.25), H→L (0.65)	y (L <sub>b</sub> )
S <sub>2</sub>		3.80 (326)	0.303	H-1→L (0.66), H→L+1 (-0.24)	z (L <sub>a</sub> )
S <sub>3</sub>		4.58 (271)	0.121	H-1→L+1 (0.55), H→L (-0.22)	y (B <sub>b</sub> )
S <sub>4</sub>		4.83 (257)	0.002	H-2→L (-0.42), H-1→L+1 (0.52)	z
S <sub>5</sub>		4.93 (251)	1.149	H-1→L (0.24), H→L+1 (0.64)	z (B <sub>a</sub> )
S <sub>1</sub>	<b>1-4</b>	3.16 (392)	0.088	H-1→L+1 (0.19), H→L (0.67)	y (L <sub>b</sub> )
S <sub>2</sub>		3.62 (343)	0.425	H-1→L (0.67), H→L+1 (-0.21)	z (L <sub>a</sub> )
S <sub>3</sub>		4.15 (298)	0.000	H-2→L (0.65)	-
S <sub>4</sub>		4.74 (262)	1.519	H-1→L (0.21), H→L+1 (0.65)	z (B <sub>a</sub> )
S <sub>5</sub>		4.77 (260)	0.249	H-1→L+1 (0.66), H→L (-0.20)	y (B <sub>b</sub> )
S <sub>1</sub>	<b>1-11</b>	3.37 (368)	0.008	H-1→L (-0.42), H→L+1 (0.52)	y (L <sub>b</sub> )
S <sub>2</sub>		3.67 (338)	0.020	H-1→L+1 (-0.54), H→L (0.40)	z (L <sub>a</sub> )
S <sub>3</sub>		3.90 (318)	0.122	H-1→L (0.52), H→L+1 (0.43)	y (B <sub>b</sub> )
S <sub>4</sub>		4.08 (304)	1.589	H-1→L+1 (-0.38), H→L (0.41)	z (B <sub>a</sub> )
S <sub>5</sub>		4.10 (302)	0.137	H-2→L (0.67), H-2→L+2 (-0.13)	y
S <sub>1</sub>	<b>1-4<sup>+</sup></b>	0.76 (1640)	0.000	<i>β</i> -H-1→ <i>β</i> -L (0.99)	-
S <sub>2</sub>		0.92 (1349)	0.421	<i>β</i> -H→ <i>β</i> -L (0.92)	-
S <sub>3</sub>		2.05 (606)	0.008	<i>α</i> -H-1→ <i>α</i> -L (0.42), <i>β</i> -H-1→ <i>β</i> -L (0.35)	-
S <sub>4</sub>		2.67 (466)	0.019	<i>β</i> -H-2→ <i>β</i> -L (0.86)	-
S <sub>5</sub>		2.72 (456)	0.037	<i>α</i> -H→ <i>α</i> -L (0.50), <i>β</i> -H-3→ <i>β</i> -L (0.44)	-
S <sub>1</sub>	<b>1-14<sup>+</sup></b>	1.28 (966)	0.631	<i>β</i> -H→ <i>β</i> -L (0.96)	-
S <sub>2</sub>		2.42 (512)	0.003	<i>β</i> -H-1→ <i>β</i> -L (0.96)	-
S <sub>3</sub>		2.58 (481)	0.000	<i>β</i> -H-2→ <i>β</i> -L (0.95)	-
S <sub>4</sub>		3.09 (402)	0.666	<i>α</i> -H→ <i>α</i> -L (0.83)	-
S <sub>5</sub>		3.24 (382)	0.000	<i>β</i> -H-3→ <i>β</i> -L (0.74)	-

<sup>a</sup>CI coefficients are given in parentheses. For L<sub>b</sub>/B<sub>b</sub> and L<sub>a</sub>/B<sub>a</sub> absorptions, only the transitions involving the frontier orbitals depicted in Figure 1-11 are listed and are given in the order that match the nature of the respective transitions in pyrene (**P**).

<sup>b</sup>Polarization direction. Nomenclature of the respective absorption according to Platt is given in parentheses.

Similar to pyrene and the donor-substituted derivatives **1-4** and **1-8**, the  $S_1 \leftarrow S_0$  transition of **1-11** is also of  $L_b$  type and a result of a configuration interaction between  $HOMO \rightarrow LUMO+1$  and  $HOMO-1 \rightarrow LUMO$ . Effectively, a large CT from the julolidine donor to the Bmes<sub>2</sub> acceptor occurs, leading to much lower oscillator strength of 0.008 in agreement with the observed lowest extinction coefficient of  $\epsilon = 2\ 100\ M^{-1}\ cm^{-1}$  (Table 1-2). The low oscillator strength is also in line with the observed radiative rate constants  $k_r$  of **1-11**, which are the smallest among this series of pyrene derivatives. Another consequence of the large CT character of the  $S_1$  state is the observed solvatochromism. The higher lying excited states are also influenced, as shown by the loss of vibrational fine structure of the  $L_a$  and  $B_b$  bands, and their bathochromic shift compared to **1-4** and **1-8**.

### 1.3 Conclusions

The synthesis and structural characterization of pyrene derivatives substituted at the 2- and 2,7-positions is presented with a julolidine-type moiety as a very strong donor, giving D- $\pi$  and D- $\pi$ -D systems, and with Bmes<sub>2</sub> as a very strong acceptor, leading to a D- $\pi$ -A system. The synthesis of the latter is particularly intriguing, as unsymmetrically substituted pyrene derivatives are rare. Both donor and acceptor substituents greatly influence the photophysical properties of the pyrene core, leading to several remarkable observations for 2,7-substituted pyrene derivatives. All compounds studied here exhibit very unusual low-energy S<sub>1</sub>←S<sub>0</sub> absorptions, reaching an unprecedented shift to  $\lambda_{\text{max}}(\text{abs}) = 475 \text{ nm}$  for the 2,7-bis(donor) pyrene derivative **1-4**. The charge transfer character of the excited state S<sub>1</sub> in **1-4**, which is indicated by the observed solvatochromism, gives rise to a very large apparent Stokes shift and emission in the green region of the electromagnetic spectrum in hexane, whereas all other previously reported pyrene derivatives substituted at the 2,7-positions show blue luminescence. Very high fluorescence rate constants have also been achieved, with the D/D- and D/A-substituted **1-4** and **1-II** exhibiting  $k_f$  values in THF and in the solid state which are among the highest reported thus far for 2,7-substituted pyrene derivatives, with lifetimes approaching those observed for 1-substituted pyrenes. Cyclic voltammetry studies reveal reversible one- and two-electron-oxidations for the mono- and disubstituted julolidine pyrenes **1-8** and **1-4**, respectively. The D/A-compound **1-II** can be reversibly oxidized as well as reduced. Spectroelectrochemical measurements suggest strong coupling between the substituents at the 2,7-positions of pyrene in **1-4**, which is unexpected as the HOMO and LUMO of pyrene itself both have a nodal plane passing through these positions.

According to the theoretical studies, the mentioned properties are a result of the very strong julolidine-type donor and the very strong Bmes<sub>2</sub> acceptor coupling well to the pyrene HOMO-1 and LUMO+1, respectively. Destabilization of the former and stabilization of the latter lead to an orbital shuffle between HOMO and HOMO-1, and LUMO and LUMO+1 of pyrene, respectively. Consequently, the S<sub>1</sub> state, which for pyrene is described as a configurational interaction between HOMO→LUMO+1 and HOMO-1→LUMO, changes its nature sufficiently enough to gain higher oscillator strength, and the photophysical and electrochemical properties are then greatly influenced by the substituents.

Thus, by judicious choice of substituents in the 2,7-positions of pyrene, the frontier orbital order of pyrene can be modified, giving enhanced control over the nature and properties of the excited states and the redox potentials, and allowing the design of new luminescent materials.





## Chapter 2

Synthesis, Photophysical and  
Electronic Properties of  
Tetra-Donor- or Acceptor-  
Substituted *ortho*-Perylenes  
Displaying Four Reversible  
Oxidations or Reductions



## 2 Synthesis, Photophysical and Electronic Properties of Tetra-Donor- or Acceptor-Substituted *ortho*-Perylenes Displaying Four Reversible Oxidations or Reductions

### 2.1 Introduction

Polycyclic aromatic hydrocarbons (PAHs) show very different and unusual properties compared to small aromatic compounds as a result of their extended  $\pi$ -conjugation. Their narrower HOMO-LUMO gaps lead to long-wavelength absorptions and emissions. Furthermore, PAHs such as perylene have lower oxidation and/or reduction potentials, higher mechanical strengths and stronger  $\pi$ - $\pi$ -interactions.<sup>[111]</sup> Perylene diimides (PDIs) have attracted much interest for use as dyes, pigments<sup>[112]</sup> and semiconductors<sup>[113]</sup> in diverse applications.<sup>[114,115]</sup> They exhibit high chemical, thermal and photochemical stability, strong absorption and fluorescence and unique self-assembly behavior, which facilitates charge mobility.<sup>[116,117]</sup> In addition, their high electron affinity makes PDIs promising candidates for electronic materials such as organic field effect transistors and solar cells.<sup>[115,116,118]</sup>

The perylene core has twelve positions and can be considered as two naphthalene moieties conjoined at the 1 and 8 positions (Figure 2-1).<sup>[119]</sup> Diamagnetic susceptibility studies indicate that the central ring of perylene fails to display fully aromatic character as the naphthalene units dominate the perylene structure.<sup>[119,120]</sup> Furthermore, Nucleus-Independent Chemical Shift (NICS) calculations indicate that the central ring is non-aromatic<sup>[121]</sup> and X-ray structural data demonstrates that the C-C bonds joining the two naphthalene units are relatively long compared to typical aromatic C-C bonds. For the  $\beta$  polymorph of perylene, a C6a-C6b (or C12a-C12b) bond length of 1.474(1) Å was reported at 130 K from single-crystal X-ray diffraction data,<sup>[122]</sup> while a bond length of 1.467(4) Å was reported at 200 K by Botoshansky *et al.*<sup>[123]</sup> For the  $\alpha$  polymorph of perylene, C6a-C6b (or C12a-C12b) bond lengths were reported to be in the range of 1.462-1.480 Å.<sup>[123-125]</sup> These distances are typical of C( $sp^2$ )-C( $sp^2$ ) single bonds.<sup>[126-128]</sup>

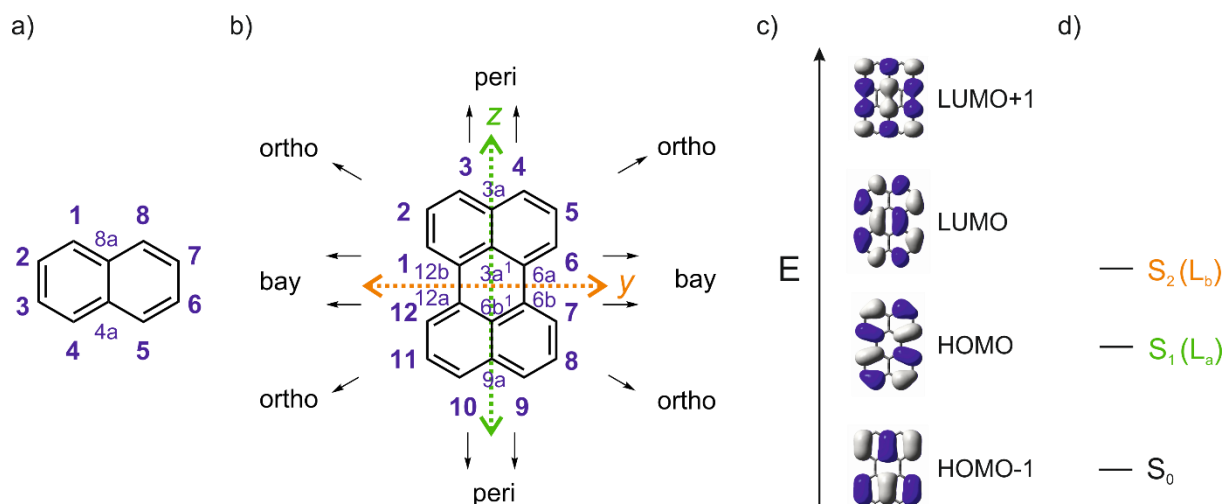


**Figure 2-1.** a) Atom numbering system in naphthalene; b) atom numbering system with principle Cartesian coordinate system used for perylene; c) the four frontier orbitals of perylene; and d) low energy optical transitions of perylene with the Platt nomenclature.<sup>[129]</sup>

This combination of two connected naphthalene units leads to particular photophysical properties. Substituting naphthalene at its 1 and 8 positions leads to a modulation of its  $L_a$  transition in such a way that in perylene the  $S_1 \leftarrow S_0$  transition is polarized along the z-axis ( $L_a$ ) and not along the y-axis ( $L_b$ ) as in naphthalene. Perylene's lowest-lying singlet excited state, observed in the absorption spectrum at 440 nm ( $\epsilon = 34\,000\text{ M}^{-1}\text{ cm}^{-1}$  in toluene), consists of four vibrational sub-bands with a  $1\,400\text{ cm}^{-1}$  interval and is assigned to a symmetry allowed HOMO  $\rightarrow$  LUMO transition.<sup>[130,131]</sup> The y-axis-polarized ( $L_b$ )  $S_2 \leftarrow S_0$  transition at 253 nm ( $\epsilon = 52\,000\text{ M}^{-1}\text{ cm}^{-1}$  in hexane) is energetically well separated from  $S_1$  by  $16\,800\text{ cm}^{-1}$ . As the  $S_1 \leftarrow S_0$  transition is allowed, emission from  $S_1$  is also ( $\lambda_{\text{max}}(\text{em}) = 444\text{ nm}$  in toluene) allowed and, therefore, the intrinsic lifetime ( $\tau_0$ ) of 5.5 ns is quite short, and fluorescence is strong with a quantum yield near unity.<sup>[131]</sup> **PDI-A's** (Figure 2-2) lowest energy z-axis-polarized ( $L_a$ ) absorption is observed at 526 nm in chloroform, and is stronger than perylene's with  $\epsilon = 88\,000\text{ M}^{-1}\text{ cm}^{-1}$ .<sup>[116,132]</sup> This compound emits in the yellow-green region at 533 nm in chloroform with  $\tau_0 = 4\text{ ns}$ .

As perylenes play an important role in electronic materials, their electronic properties have been studied by several groups.<sup>[133,134]</sup> Cyclic voltammetry measurements show that unsubstituted perylene can be reversibly reduced to its radical anion at -1.27 V and dianion at -1.76 V vs.  $\text{Fc}/\text{Fc}^+$  (DMF/MeCN) and reversibly oxidized at +1.25 V vs.  $\text{Fc}/\text{Fc}^+$  (Table 2-1).<sup>[113,134,135]</sup> PDIs are a class

of compounds that are very easy to reduce, with **PDI-A** having a reduction potential of -0.98 V vs. Fc/Fc<sup>+</sup>. Further substitution can give rise to even stronger oxidants.<sup>[116]</sup>

**Table 2-1.** Redox properties of perylene and PDI

	$E_{1/2}$ (red) <sup>1</sup> / V	$E_{1/2}$ (red) <sup>2</sup> / V	$E_{1/2}$ (ox) / V
<b>perylene</b>	-1.27 vs. Fc/Fc <sup>+</sup> (MeCN) <sup>[113]</sup>	-1.76 vs. Fc/Fc <sup>+</sup> (DMF) <sup>[113]</sup>	+1.25 vs. Fc/Fc <sup>+</sup> (MeCN) <sup>[113]</sup>
	-1.67 vs. SCE (DMF/MeCN) <sup>[134,135]</sup>	-2.21 vs. SCE (DMF) <sup>[133]</sup> -2.17 vs. SCE (THF) <sup>[133]</sup>	+1.09 vs. NHE (DMF or MeCN) <sup>[134]</sup> +0.85 vs. SCE (MeCN) <sup>[136]</sup>
	-1.63 vs. SCE (THF) <sup>[133]</sup>		
<b>PDI-A</b>	-0.98 vs. Fc/Fc <sup>+</sup> (MeCN) <sup>[137]</sup>	-1.21 vs. Fc/Fc <sup>+</sup> (MeCN) <sup>[137]</sup>	+1.21 vs. Fc/Fc <sup>+</sup> (MeCN) <sup>[137]</sup>
	-1.38 vs. SCE <sup>[113]</sup>	-1.61 vs. SCE <sup>[113]</sup>	+0.81 vs. SCE <sup>[113]</sup>

However, perylene derivatives without carboxyimide groups at the *peri* positions are much less well studied due to difficulties in functionalizing the perylene core directly.<sup>[32,138,139]</sup> One method to functionalize perylene directly is *via* Ir-catalyzed C–H borylation, which was reported by Marder and co-workers in 2005.<sup>[32]</sup> As a result of the very crowded nature of the active five-coordinate Ir(III)-catalyst, borylation of C–H bonds *ortho* to a substituent or ring junction is inhibited.<sup>[43]</sup> Therefore, it is possible to borylate the 2,5,8,11- positions of perylene selectively, providing a useful entry point for the synthesis of diverse *ortho* substituted perylene derivatives.<sup>[45,46]</sup> In 2011, Shinokubo and co-workers<sup>[140]</sup> employed a modified Ir-catalyzed borylation reaction with an *ortho* directing ligand, which enabled the functionalization of the four *ortho* positions of PDI's with heteroaryl, OMe and OH moieties for the first time. They observed a slight blue-shift in the absorption (from 525 to 512 nm) and emission (from 533 to 516 nm) spectra through the introduction of OH groups, which is caused by an intramolecular hydrogen bonding interaction between the carbonyl and hydroxy groups. The OMe moieties on the other hand, cause a small red shift in the absorption (from 525 to 538 nm) and emission (from 533 to 549 nm) spectra. In 2012, a Suzuki-Miyaura cross-coupling was reported by Ikeda *et al.* using 2,5,8,11-tetra(Bpin)perylene to give a porphyrin-perylene-porphyrin triad,<sup>[141]</sup> and in 2016 Tran *et al.* reported Suzuki-Miyaura coupling of our 2,5,8,11-tetra(Bpin)perylene to give

microporous coordination polymers.<sup>[142]</sup> However, there are no reports so far, of only *ortho* heteroatom substituted perylenes. Thus, investigations of the effect of substituents on the 2,5,8,11-positions of the perylene core are still lacking. In 2017, Zeng and co-workers<sup>[139]</sup> prepared *ortho* and *bay* octa-substituted perylene derivatives by an indirect method, namely oxidative radical-radical coupling of two naphthene units followed by reduction. They synthesized 2,5,8,11-tetrabromo-1,6,7,12-tetra-*n*-butoxyperylenes and showed the versatility of that derivative by performing Suzuki-Miyaura coupling reactions and nucleophilic substitution reactions with copper cyanide or sodium methoxide to place cyano or methoxy moieties at the *ortho* positions. However, the *n*-butoxy substituents at the *bay* positions lead to a twisted core, which influences the properties of these perylene derivatives. In 2017, Hariharan, Shaijumon and co-workers demonstrated, with a twisted PDI, that the energy levels of the reduced species are altered and a single plateau discharge profile can be achieved, which is crucial for rechargeable battery electrodes.<sup>[143]</sup> To investigate the influence of substitution only at the *ortho* positions on the perylene core, we prepared an *ortho* perylene derivative with four donors (D) and one with four acceptors (A), due to their strong influence on the frontier orbital levels.

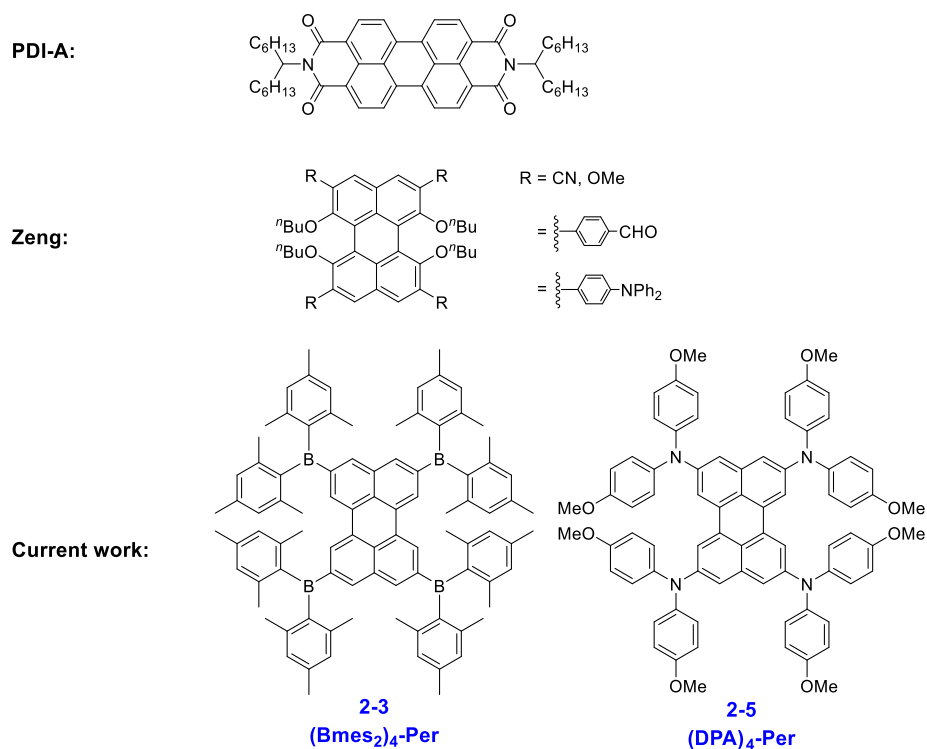


**Figure 2-2.** Examples of known perylene derivatives <sup>[116,139]</sup> and the two target perylene derivatives of this work.

Materials with high HOMO energies, such as the compound *N,N'*-diphenyl-*N,N'*-bis(3-methylphenyl)-(1,1'-biphenyl)-4,4'-diamine (TPD), are especially useful for hole transport.<sup>[144-150]</sup> Common  $\pi$ -donors that have been used in dyes to boost HOMO energies include amines, with a lone pair on the nitrogen, such as diarylamino, diethylamino, dimethylamino or carbazolyl moieties.<sup>[22]</sup> Diarylamines are among the strongest  $\pi$ -electron donors and have been employed in diverse applications,<sup>[151-163]</sup> due to their outstanding physical, photochemical and electrochemical properties. Furthermore, they are easy to synthesize and handle.<sup>[164]</sup> A methoxy group at the position *para* to the nitrogen not only increases the electron donating strength of diarylamines, but enables reversible oxidations.<sup>[103,164]</sup> In contrast, materials with low LUMO energies, such as  $\text{mes}_2\text{B}-(\text{C}_4\text{H}_2\text{S})_n\text{-Bmes}_2$  ( $n = 2, 3$ ;  $\text{mes} = 2,4,6\text{-Me}_3\text{C}_6\text{H}_2$ ), are useful for electron transport.<sup>[165]</sup> Diarylboryl groups have attracted much interest for use in optoelectronic materials, as the vacant  $p_z$ -orbital of the three-coordinate boron serves as a strong  $\pi$ -acceptor, interacting with an adjacent  $\pi$ -system.<sup>[23-25,27,29,30,71,72,166,167]</sup> This conjugation provides the electron-deficient character that gives rise to useful photophysical properties.<sup>[168]</sup> For example, attaching a  $\text{Bmes}_2$  moiety to the 2- and 2,7-positions of pyrene leads to a switch of the energetic order of the LUMO+1 and LUMO orbitals, which is a consequence of the mixing of the empty  $p_z$ -orbital with the pyrene  $\text{B}_{3u}$  LUMO+1 the orbital that leads to strong stabilization of the LUMO+1 such that it drops below the LUMO in energy.<sup>[31,47,63]</sup> Kinetic stabilization by bulky groups, such as mesityl or 2,4,6-( $\text{CF}_3$ )<sub>3</sub> $\text{C}_6\text{H}_2$  (Fmes), sterically protects the empty  $p_z$ -orbital from nucleophilic attacks leading to air- and moisture stable materials.<sup>[24,25,169,170]</sup> Incorporation of the boron into a rigid and planar structure is an alternative method to provide increased stability *via* structural constraints.<sup>[171]</sup>

With the above issues in mind, the motivation of this work was to use the Ir-catalyzed C-H borylation reaction<sup>[32]</sup> to prepare new compounds in order to study the effect of strong  $\pi$ -donors and -acceptors at the 2,5,8,11-positions of perylene. Hence, the photophysical and electrochemical properties of the target compounds **(Bmes<sub>2</sub>)<sub>4</sub>-Per** and **(DPA)<sub>4</sub>-Per** were examined experimentally and theoretically.

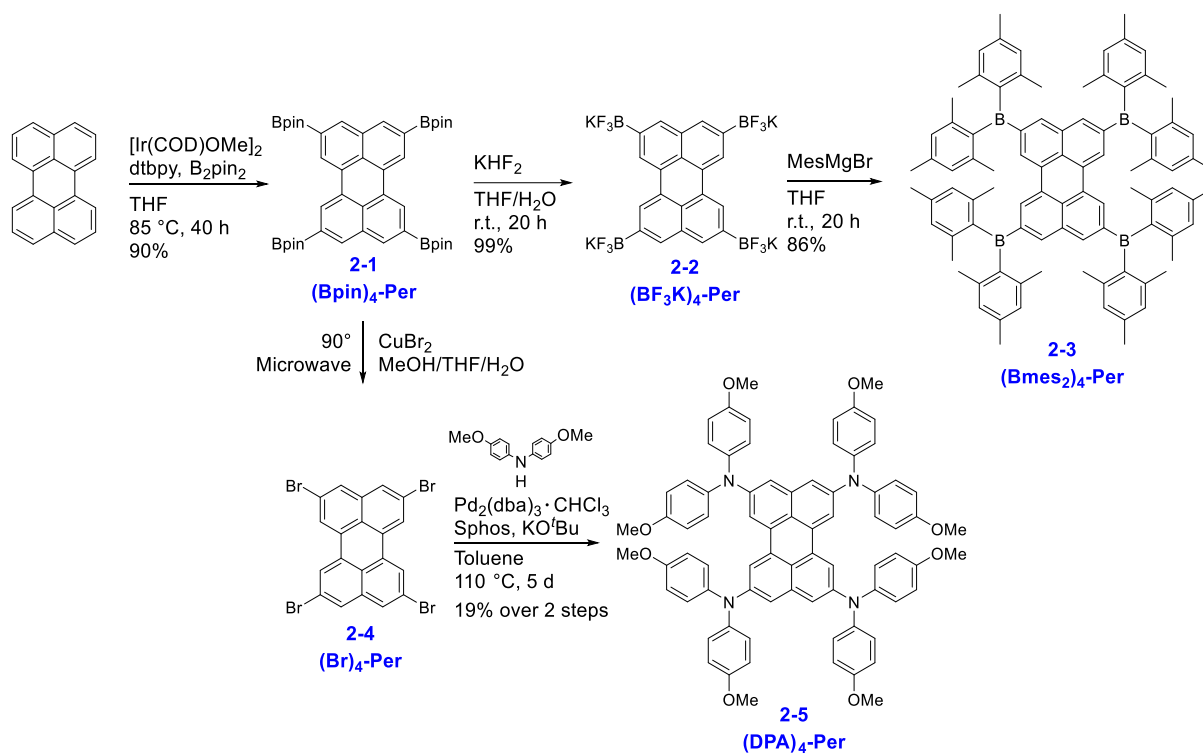
## 2.2 Results and Discussion

### 2.2.1 Synthesis

The synthesis of the compounds **(Bmes<sub>2</sub>)<sub>4</sub>-Per** and **(DPA)<sub>4</sub>-Per** is summarized in Scheme 2-1. The starting point of our approach is the high yielding Ir-catalyzed borylation of perylene, which was previously reported by Marder and co-workers in 2005, providing **(Bpin)<sub>4</sub>-Per** in 90% yield.<sup>[32]</sup> This synthesis is very convenient, as it can be run on a multigram scale and the tetraborylated product does not need further purification, such as column chromatography, because the product crystallizes directly from the reaction solution. Suzuki-Miyaura cross-couplings with **(Bpin)<sub>4</sub>-Per** have been reported before.<sup>[141,142]</sup> Here, on the other hand, this precursor was transformed into its potassium trifluoroborate salt **(BF<sub>3</sub>K)<sub>4</sub>-Per**. The synthesis was carried out in air in a THF/water mixture giving a yield of 99%. Potassium trifluoroborate salts are air- and moisture stable, and easy to handle and purify.<sup>[90,172]</sup> Furthermore, they can function as carbon nucleophiles and are important intermediates in diverse synthetic reactions.<sup>[173]</sup> However, they can also serve as boron electrophiles. Thus, **(BF<sub>3</sub>K)<sub>4</sub>-Per** reacts with the Grignard reagent *mes*MgBr to give **(Bmes<sub>2</sub>)<sub>4</sub>-Per** in 86% yield. Marder and co-workers previously demonstrated the utility of this approach to derivatize pyrene with a (Bmes<sub>2</sub>) moiety.<sup>[1]</sup> Additionally, boroles were prepared from aryl trifluoroborates and aryllithium reagents.<sup>[170]</sup> The utility of a BF<sub>3</sub>K salt as a boron electrophile for the synthesis of triarylboranes has also been demonstrated by Wagner and co-workers using aryllithium instead of Grignard reagents.<sup>[93,94]</sup>

The precursor **(Bpin)<sub>4</sub>-Per** can also be transformed into the corresponding halogenated **(Br)<sub>4</sub>-Per** by a halodeboration.<sup>[174,175]</sup> Thus, **(Bpin)<sub>4</sub>-Per** and CuBr<sub>2</sub> were suspended in a mixture of THF/MeOH/H<sub>2</sub>O (1:1:1) and the reaction mixture was irradiated in a microwave reactor at 90 °C for 20 h. Performing this reaction in an oil bath instead of a microwave reactor results in a mixture of **(Br)<sub>3</sub>-Per** and **(Br)<sub>4</sub>-Per** as some protodeborylation occurs. Bromodeborylation of the C–Bpin bond is especially useful as it converts a carbon nucleophile into a carbon electrophile in one easy step. Thus, the **(Br)<sub>4</sub>-Per** building block is a further useful intermediate that can serve in numerous types of coupling reactions including a Buchwald-Hartwig amination, which was performed to obtain **(DPA)<sub>4</sub>-Per**. The fourfold amination of **(Br)<sub>4</sub>-Per**, using Pd<sub>2</sub>(dba)<sub>3</sub>·CHCl<sub>3</sub> as the catalyst precursor and *s*Phos as the ligand, was achieved in an overall yield of 19% in two steps starting from **(Bpin)<sub>4</sub>-Per**. **(DPA)<sub>4</sub>-Per** exhibits very good

solubility in common organic solvents. The new products 2-2 to 2-5 were fully characterized by multinuclear NMR spectroscopy, high-resolution mass spectrometry, and elemental analysis.



**Scheme 2-1.** Synthesis of the compounds **(Bpin)<sub>4</sub>-Per**, **(BF<sub>3</sub>K)<sub>4</sub>-Per**, **(Bmes<sub>2</sub>)<sub>4</sub>-Per**, **(Br)<sub>4</sub>-Per** and **(DPA)<sub>4</sub>-Per**.

## 2.2.2 Crystal Structure Analysis

The solid-state structure of **(DPA)<sub>4</sub>-Per** was determined *via* single-crystal X-ray diffraction. The molecule shows inversion symmetry. In **(DPA)<sub>4</sub>-Per**, the individual bond lengths are similar to those of perylene (Table 2-2).<sup>[127]</sup> The naphthalene units of the perylene moiety exhibit typical aromatic C–C bond lengths ranging from 1.371(3) to 1.426(3) Å (Figure 2-3a and Table 2-2). The **b** and **f** bonds (1.371(3)–1.380(3) Å) are considerably shorter than the **a**, **c**, **d**, and **e** bonds (1.412(3)–1.426(3) Å) which is also observed in naphthalene and perylene.<sup>[128]</sup> The length of the C11–C13 bond (Figure 2-3a, bond **g**, Table 2-2) connecting the naphthalene units in **(DPA)<sub>4</sub>-Per** is 1.470(2) Å at 100 K (Figure 2-3). This is in the same range as the related bond distances reported for the two polymorphs of perylene (1.462–1.480 Å)<sup>[122–125,127,176]</sup> and, hence, resembles a C(*sp*<sup>2</sup>)-C(*sp*<sup>2</sup>) single bond.<sup>[126–128]</sup>

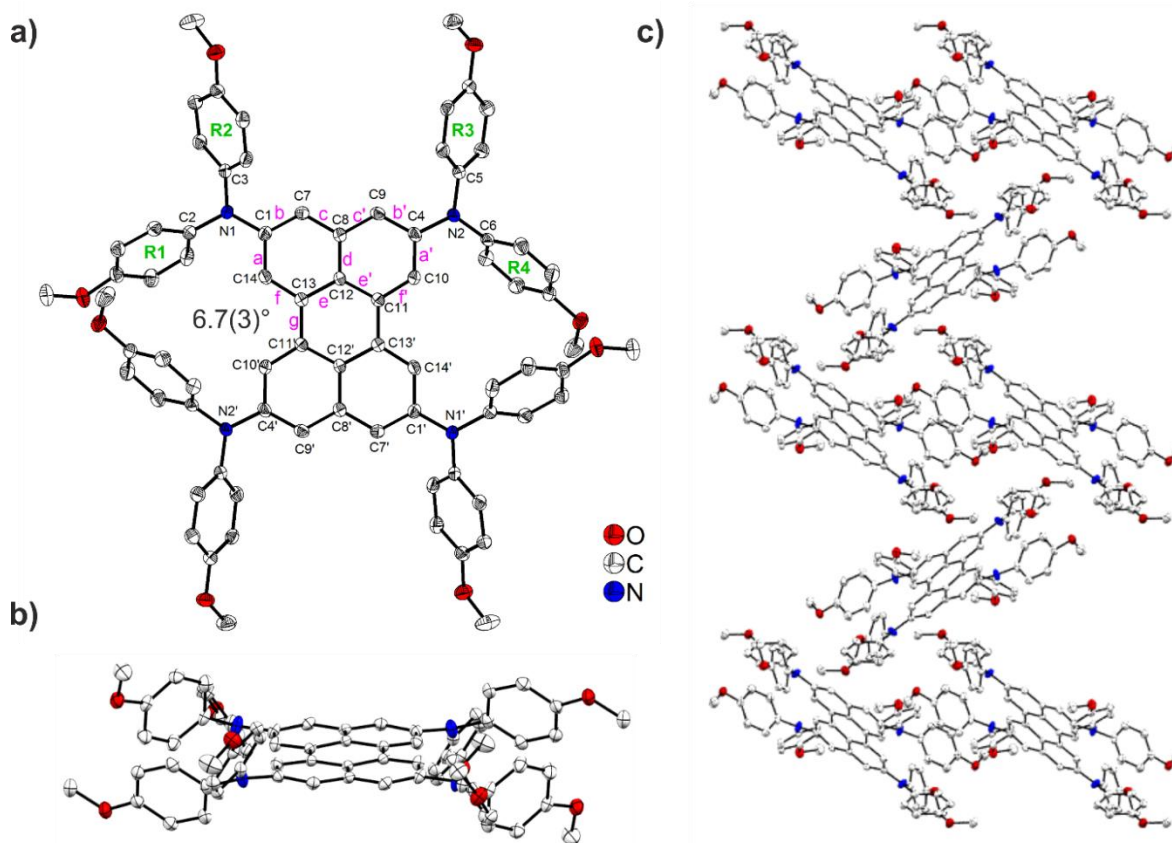


**Figure 2-3.** Molecular structure of **(DPA)<sub>4</sub>-Per**: a) top view; b) side view; and c) packing of **(DPA)<sub>4</sub>-Per** molecules. Hydrogen atoms are omitted for clarity. Element color: carbon (white), nitrogen (blue), oxygen (red). Atomic displacement ellipsoids are shown at the 50% probability level.

**Table 2-2.** Selected bond lengths (Å) and angles (°) of **(DPA)<sub>4</sub>-Per** compared to perylene. Bonds are labelled according to the scheme in Figure 2-3.

	<b>(DPA)<sub>4</sub>-Per</b>	<b><i>β</i>-perylene<sup>[127]</sup></b>
a, a'	1.412(3), 1.412(3)	1.407(1), 1.409(1)
b, b'	1.372(3), 1.378(3)	1.370(1), 1.371(1)
c, c'	1.412(3), 1.416(3)	1.417(1), 1.418(1)
d	1.426(3)	1.429(1)
e, e'	1.424(3), 1.422(2)	1.430(1), 1.429(1)
f, f'	1.380(3), 1.371(3)	1.389(1), 1.387(1)
g	1.479(2)	1.474(1)
NI-C1	1.406(2)	
NI-C2	1.429(2)	
NI-C3	1.422(2)	
N2-C4	1.399(2)	
N2-C5	1.413(2)	
N2-C6	1.432(2)	
∠ NIC <sub>3</sub> -R1	42.90(8)	
∠ NIC <sub>3</sub> -R2	43.99(9)	
∠ N2C <sub>3</sub> -R3	44.15(7)	
∠ N2C <sub>3</sub> -R4	66.00(9)	
Sum ∠ CNIC	359.8(2)	
Sum ∠ CN2C	359.2(2)	

The perylene core of **(DPA)<sub>4</sub>-Per** is only slightly twisted with a small C10–C11–C13–C14 dihedral angle of 6.7(3)° (Figure 2-3a-b). Crystal structures of perylene and *peri*-substituted perylenes in general show nearly planar perylene cores. For example, dihedral angles in the range 0.1–1.8° were reported for  $\beta$ - and  $\alpha$ -peryene.<sup>[123–125,127,176,177]</sup> This shows that the substitution of the sterically demanding DPA moieties at the four *ortho* positions does not significantly affect the planarity of the perylene core. The nitrogen atoms are virtually trigonal planar with the sum of the angles around N1 being 359.8(2)° and N2 being 359.2(2)°, respectively. The interplanar angles between the terminal phenyl rings bonded to nitrogen and the NC<sub>3</sub> planes are 42.9–44.2° for R1, R2, and R3, and 66.0° for R4 (Figure 2-3a, Table 2-2). In contrast, the crystal structures of most of the perylene compounds containing *bay* substituents show a strong twist between the naphthalene units of the core due to steric repulsion created by the *bay* moieties.<sup>[139,178]</sup> For example, dihedral angles of 30.7–34.3° between the two naphthalene units have been reported for *bay*- and *ortho*-octasubstituted perylenes by Zeng and co-workers.<sup>[139]</sup> The packing of the **(DPA)<sub>4</sub>-Per** molecules in the crystal structure is determined by the large steric demand of the amine moieties. There is no  $\pi$ - $\pi$  stacking interaction present. Between the methoxy groups of the R1 and R4' phenyl rings, and their inversion-symmetric groups, intramolecular C–H...O interactions exist (Table 2-2). Intermolecular C–H...C, C–H... $\pi$ , and C–H...O interactions are present between methoxy groups, phenyl rings, and the perylene core. They are listed in detail in Table 2-2. A Hirshfeld surface analysis was performed in order to quantify the nature and type of intermolecular interactions.<sup>[179]</sup> Fingerprint analysis and its breakdown to the individual relative contributions,<sup>[180]</sup> shows a major contribution from H...H interactions (59%), followed by a significant amount from C...H (29%) and O...H (10%) interactions, and minor contribution of O...C interactions (1%). Only very weak contributions (< 1%) from C...C, O...O, and N...H interactions are observed.

### 2.2.3 Photophysical Properties

The absorption spectra of **(Br)<sub>4</sub>-Per** and **(Bpin)<sub>4</sub>-Per** are generally very similar to that of perylene (Figure 2-4). Their  $S_1 \leftarrow S_0$  transition, which is z-axis polarized ( $L_a$ ) and basically attributed to a HOMO  $\rightarrow$  LUMO transition, is allowed with extinction coefficients of 28 000-32 000  $M^{-1} cm^{-1}$  (perylene: 34 000  $M^{-1} cm^{-1}$ ). Furthermore, this band has a well-defined vibronic fine structure with an interval of 1 400  $cm^{-1}$  between the sub-bands as in perylene. However, it is slightly bathochromically shifted (310  $cm^{-1}$  for **(Bpin)<sub>4</sub>-Per** and 360  $cm^{-1}$  **(Br)<sub>4</sub>-Per**) with respect to the parent perylene. Thus, the  $S_1 \leftarrow S_0$  transition in these derivatives is a pure  $\pi \rightarrow \pi^*$  transition. As observed previously on pyrene,<sup>[1]</sup> the Bpin moieties barely influence the photophysical properties of perylene, as oxygen substituents at the boron atom decreases its  $\pi$ -acceptor properties.<sup>[97]</sup> Bromo substituents are only weak  $\pi$ -donors; therefore, these two derivatives show hardly any CT character. This is consistent with the observed absorption properties reported for bromo-substituted PDI's.<sup>[181]</sup> It is interesting to observe that, in comparison with the 2,5,8,11-tetrabromo-1,6,7,12-tetra-*n*-butoxyperylene reported by Zeng and co-workers,<sup>[139]</sup> the  $S_1 \leftarrow S_0$  transition of **(Br)<sub>4</sub>-Per** is narrower, structurally better defined and, furthermore, slightly more allowed.<sup>[182]</sup> This indicates some influence of the donating *bay* substituents on the absorption properties. However, there are no previous reports on perylene derivatives substituted only at the *ortho* positions for comparison. Stronger  $\pi$ -accepting moieties, such as Bmes<sub>2</sub>, at the *ortho* positions leads to a pronounced influence on the  $S_1 \leftarrow S_0$  transition. Hence, the lowest energy band in **(Bmes<sub>2</sub>)<sub>4</sub>-Per** is much broader and is strongly bathochromically shifted (1 220  $cm^{-1}$ ) with respect to the  $L_a$  band of perylene which indicates a stabilization of the unoccupied orbitals of this derivative in comparison to those of perylene (*vide supra*).

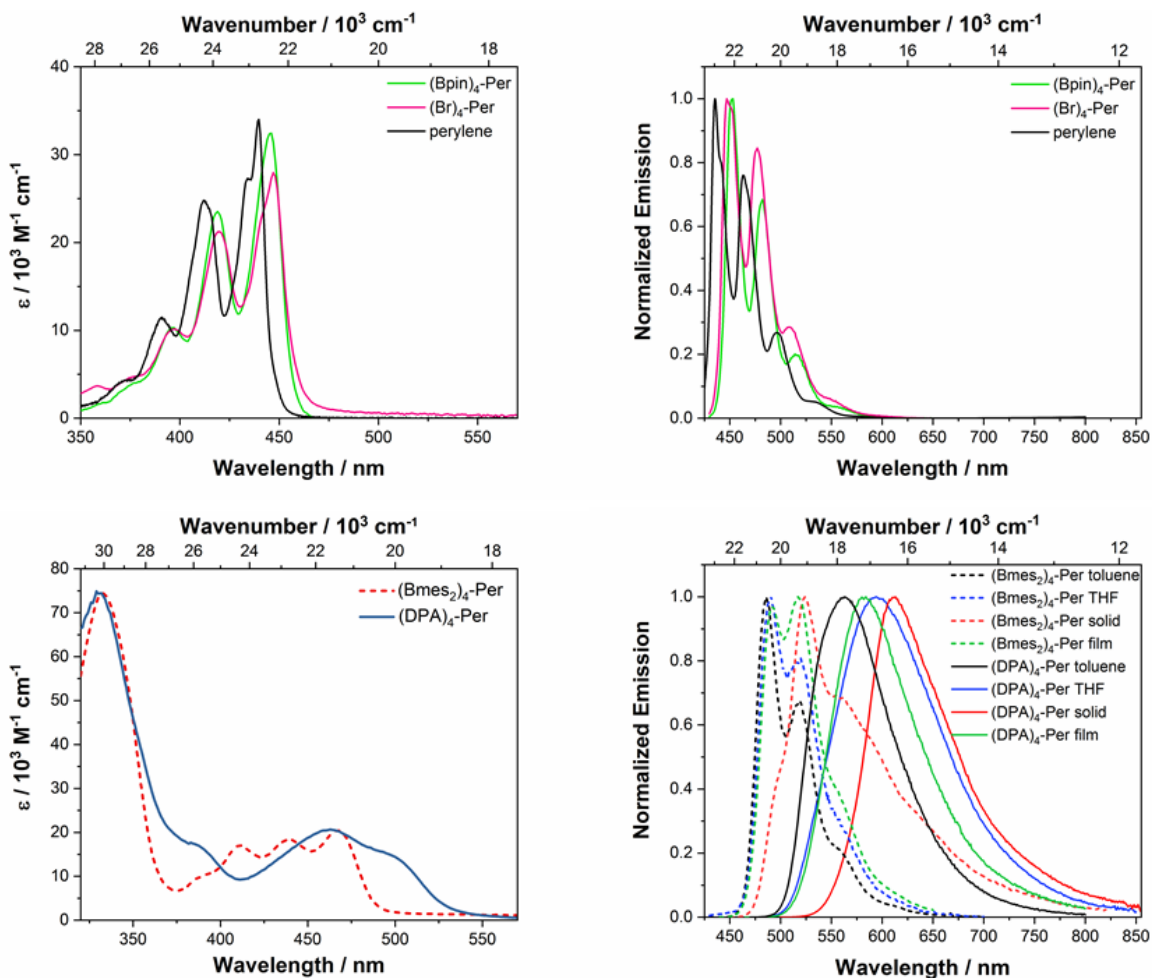


Figure 2-4. Absorption (left) and emission (right) spectra of **(Br)<sub>4</sub>-Per** and **(Bpin)<sub>4</sub>-Per** (top) and **(Bmes<sub>2</sub>)<sub>4</sub>-Per** and **(DPA)<sub>4</sub>-Per** (bottom) recorded in toluene if not otherwise noted.

**Table 2-3.** Selected photophysical data of perylene and its derivatives **(Bpin)<sub>4</sub>-Per**, **(Br)<sub>4</sub>-Per**, **(Bmes<sub>2</sub>)<sub>4</sub>-Per** and **(DPA)<sub>4</sub>-Per** recorded under argon at room temperature if not otherwise noted.

cpd	medium	$\lambda_{abs} / \text{nm}$ ( $\epsilon / 10^3 \text{ M}^{-1} \text{ cm}^{-1}$ )	$\lambda_{em} / \text{nm}^a)$	Apparent Stokes <sup>[40]</sup> shift / $\text{cm}^{-1}$	$\tau / \text{ns}^b)$	$\tau_{avg} / \text{ns}^c)$	$\Phi$	$\tau_0 / \text{ns}$	$k_{nr} / 10^7 \text{ s}^{-1}$	$k_r / 10^7 \text{ s}^{-1}$
<b>Perylene<sup>d)</sup></b>	toluene	440 (34)	444	4	4.0	-	0.95	4.0	1.3	24
<b>(Bpin)<sub>4</sub>-Per</b>	toluene	446 (32), 419 (24), 397 (10)	453	350	4.9	-	0.58	8.0	8.6	12
<b>(Br)<sub>4</sub>-Per</b>	toluene	447 (28), 420 (21), 397 (10)	453	300	4.7	-	0.55	9.0	9.6	12
<b>(Bmes<sub>2</sub>)<sub>4</sub>-Per</b>	toluene	465 (20), 440 (18), 412 (17), 333 (74)	489	1060	6.6	-	0.43	15	8.6	6.5
	THF	466, 441, 412, 335	489	1010	8.6	-	0.41	21	6.7	4.8
	solid	-	525	-	0.9 (87), 3.6 (13)	1.2	0.04	31	79	3.2
<b>(DPA)<sub>4</sub>-Per</b>	film	-	490, 517	-	7.3 (87), 13 (13)	8.0	0.36	22	8.0	4.5
	toluene	499 (15), 463 (20), 386 (17), 331 (74)	569	2470	12	-	0.26	46	6.2	2.2
	toluene <sup>e)</sup>	-	569	-	4.6	-	0.09	51	20	2.0
	THF	501, 459, 383, 327	593	3100	8.5	-	0.09	94	11	1.1
	solid	-	612	-	2.5 (67), 6.4 (33)	3.8	0.07	54	26	1.9
	film	-	580	-	12 (86), 20 (14)	13	0.14	92	6.7	1.1

**a)** Excited at the respective  $\lambda_{abs}$  (max) of  $S_1 \leftarrow S_0$ . **b)** Pre-exponential factors  $B_n$  scaled to 100 and given in parentheses. **c)** For multi-exponential decays the pure radiative lifetime  $\tau_0 = \tau / \Phi$  has been approximated by using the experimental average lifetime  $\tau = \sum \tau_n B_n / \sum B_n$  with  $B_n$  being the pre-exponential factors of the respective lifetime component  $\tau_n$ . **d)** from Brites and co-workers.<sup>[183]</sup> **e)** In an O<sub>2</sub>-saturated solution. **f)** PMMA film doped with 1% of the respective perylene derivative.

Furthermore, this transition is much less allowed with an extinction coefficient of  $20\,000\text{ M}^{-1}\text{ cm}^{-1}$ . However, this band still possesses a vibronic fine structure, but the modes have rather similar intensity. In comparison to the acceptor version reported by Zeng and co-workers<sup>[139]</sup> (2,5,8,11-tetracyano-1,6,7,12-tetra-*n*-butoxyperylene) ( $\lambda_{\text{max}}(\text{abs}) = 454\text{ nm}$ ) the absorption of **(Bmes<sub>2</sub>)<sub>4</sub>-Per** is further bathochromically shifted ( $\lambda_{\text{max}}(\text{abs}) = 465\text{ nm}$ ), which indicates a stronger stabilization of the unoccupied orbitals in our derivative. Marder and co-workers have previously shown<sup>[31,46,47,63]</sup> that CN is a less effective  $\pi$ -acceptor than Bmes<sub>2</sub> when attached to pyrene. The influence on the S<sub>1</sub>←S<sub>0</sub> transition is even more pronounced in **(DPA)<sub>4</sub>-Per** as it does not have any vibrational progression. Its L<sub>a</sub> band is broader and more strongly bathochromically shifted with respect to the L<sub>a</sub> band of perylene ( $2\,690\text{ cm}^{-1}$ ) than for **(Bmes<sub>2</sub>)<sub>4</sub>-Per**. Hence, the donor DPA substituents exert a larger destabilizing effect on the occupied frontier orbitals than the acceptor Bmes<sub>2</sub> stabilizes the empty ones. This observation is similar to 2,7-pyrene derivatives.<sup>[1]</sup> Both target derivatives, **(Bmes<sub>2</sub>)<sub>4</sub>-Per** and **(DPA)<sub>4</sub>-Per** have the lowest energy absorptions reported so far for *ortho* substituted perylene derivatives.

All derivatives show intense fluorescence in the blue to orange region of the electromagnetic spectrum with quantum yields  $\phi$  of up to 0.58 (Figure 2-4, Table 2-3). The emission spectra of **(Br)<sub>4</sub>-Per** and **(Bpin)<sub>4</sub>-Per** are very similar to that of perylene, in that the apparent Stokes shifts<sup>[40]</sup> are very small ( $300\text{-}350\text{ cm}^{-1}$ ) and the band shape is a mirror image of its respective S<sub>1</sub>←S<sub>0</sub> absorption. The radiative rate constants of both **(Br)<sub>4</sub>-Per** and **(Bpin)<sub>4</sub>-Per** are the same order of magnitude ( $k_r = 12 \cdot 10^7\text{ s}^{-1}$ ) as that of perylene. Thus, their excited state structures are presumably very similar to those in the ground state. It is interesting to note that 2,5,8,11-tetrabromo-1,6,7,12-tetra-*n*-butoxyperylene displays a broad emission without vibronic fine structure and a significantly larger apparent Stokes shift of  $2\,120\text{ cm}^{-1}$ , indicating modest geometry changes in its excited state. Furthermore, its emission quantum yield of  $\phi = 0.30$  is only half that of **(Br)<sub>4</sub>-Per** ( $\phi = 0.58$ ) but, as Zheng and co-workers did not report lifetimes or radiative decay rates, a full comparison is not possible. The differences observed must be a result of the *bay* substituents that lead to a twisted core.<sup>[184]</sup> The significant influence of *bay* substituents on the photophysical properties of PDI's such as enhanced non-radiative decay was already reported by several groups.<sup>[116,178,181,185]</sup> Nevertheless, for PAHs with heavy atoms such as Br, the emissions we measured are intense, and no phosphorescence was detected at 77 K. However, Dreeskamp and Koch already reported<sup>[186,187]</sup> that the bromination of perylene at its *peri* position (*i.e.* 3-bromoperylene) does not lead to a quenching of the fluorescence by intersystem crossing (ISC) from S<sub>1</sub> *via* spin-orbit coupling. They found that the energy gap between the S<sub>1</sub> and T<sub>1</sub> of 3-bromoperylene is not small enough for ISC to compete with fluorescence. Furthermore, Hariharan and co-workers demonstrated that the bromination of

PDIs also fails to promote ISC and, even in dibromoethane solutions, no effect of the external heavy atoms on ISC was observed.<sup>[188]</sup>

The emission of **(Bmes<sub>2</sub>)<sub>4</sub>-Per**, with  $\lambda_{\max}(\text{em}) = 489 \text{ nm}$ , is bathochromically shifted by  $2\,073 \text{ cm}^{-1}$  in comparison to that of perylene and thus has a larger apparent Stokes shift of  $1\,055 \text{ cm}^{-1}$ . Its intense emission (quantum yield  $\Phi = 0.43$ ) shows vibronic fine structure in toluene, which does not vanish in THF. Furthermore, this derivative shows no solvatochromism which indicates the absence of CT character. In the solid state, a green emission with  $\lambda_{\max}(\text{em}) = 525 \text{ nm}$  is observed, but the non-radiative decay rate  $k_{nr}$  is greatly enhanced by more than one order of magnitude ( $k_{nr} = 79 \cdot 10^7 \text{ s}^{-1}$ ), which leads to a decreased quantum yield. However, emission in the solid state is rather uncommon for perylene derivatives. The fluorescence of PDIs, for instance, is quenched in the solid state on account of H-type aggregation due to  $\pi$ - $\pi$  interactions.<sup>[189]</sup> The emission of the donor-substituted derivative **(DPA)<sub>4</sub>-Per** is further bathochromically shifted ( $\lambda_{\max}(\text{em}) = 569 \text{ nm}$ ), shows no vibronic fine structure and is very broad. Furthermore, it exhibits significant solvatochromism, confirming a pronounced CT character. The large apparent Stokes shift ( $3\,100 \text{ cm}^{-1}$  in THF) is untypical for perylenes, as PDIs usually have very small apparent Stokes shifts. However, a large apparent Stokes shift helps to reduce self-quenching and thus to avoid measurement errors.<sup>[131]</sup> The excited state of **(DPA)<sub>4</sub>-Per** has an intrinsic lifetime of  $\tau_0 = 46 \text{ ns}$  and is thus significantly longer lived than perylene ( $\tau_0 = 4 \text{ ns}$ ) and is highly stabilized in a polar environment, as in THF  $\tau_0 = 94 \text{ ns}$ . The radiative decay rates  $k_r$  of the target compounds **(DPA)<sub>4</sub>-Per** ( $k_r = 2.2 \cdot 10^7 \text{ s}^{-1}$ ) and **(Bmes<sub>2</sub>)<sub>4</sub>-Per** ( $k_r = 6.5 \cdot 10^7 \text{ s}^{-1}$ ) are one order of magnitude slower than of perylene ( $k_r = 24 \cdot 10^7 \text{ s}^{-1}$ ) which is in full agreement with the Strickler-Berg relationship<sup>[98]</sup> as the  $S_1 \leftarrow S_0$  transition of these derivatives is also less allowed. The **(DPA)<sub>4</sub>-Per** derivative has the slowest radiative decay which is also in full agreement with the Strickler-Berg relationship<sup>[98]</sup> as its emission is further bathochromically shifted. Interestingly, substituting one DPA moiety at a *peri* position of perylene results in two emissions at  $\lambda_{\max}(\text{em}) = 530 \text{ nm}$  and  $630 \text{ nm}$ , respectively, while further studies showed<sup>[183]</sup> that the dual emission results from two excited state rotamers with different angular distribution. However, emission from the *peri*-substituted derivative proceeds significantly faster with radiative decay rates of  $k_r = 8.8 \cdot 10^7 \text{ s}^{-1}$ .<sup>[183]</sup> Hence, substituents at the *ortho* positions have a distinctly different influence on the excited state properties than substituents at the *peri* positions.

### 2.2.4 Reactivity with Oxygen

In 1974, Dreeskamp, Koch and co-workers showed that the rate of ISC from the fluorescent singlet to a triplet state can be increased in perylene by an intermolecular energy transfer to halogenated-naphthalene.<sup>[186,187,190]</sup> This precedence was a motivation to take a closer look at these presented perylene systems as the fluorescence quantum yield of **(DPA)<sub>4</sub>-Per** is particularly low ( $\phi = 0.26$ ) compared to perylene and triplet sensitizers are of great interest with many applications in phosphorescent materials,<sup>[191-193]</sup> phosphorescent bioimaging,<sup>[191,193,194]</sup> chemosensors,<sup>[191,193,195]</sup> photoinitiated polymerization,<sup>[193,196]</sup> photocatalysis,<sup>[193,197-200]</sup> triplet-triplet annihilation based upconversion,<sup>[193,201]</sup> and oncological or antibacterial photodynamic therapy.<sup>[193,202]</sup> There are a few reports on triplet states of PDIs and these make use of bimolecular triplet sensitization,<sup>[203]</sup> incorporation of sulfur<sup>[204]</sup> or heavy metals such as Ir,<sup>[188,205,206]</sup> Pt,<sup>[207]</sup> Pd,<sup>[206,208]</sup> or Ru.<sup>[206]</sup> Flamigni and co-workers demonstrated<sup>[209]</sup> that unsymmetrical substitution of PDIs is an alternative method to access triplet states. Furthermore, in 2016, Hariharan and co-workers reported<sup>[188]</sup> that, through heavy atom substitution combined with a twisted-core structure of PDIs, triplet states of PDIs become accessible. One indication for an enhanced ISC rate is energy transfer from the triplet state of a compound formed upon photoexcitation to ground state oxygen ( $^3\Sigma_g^-$ ). This leads to the generation of singlet oxygen ( $^1\Delta_g$ ), which can be detected by its luminescence at 1272 nm. Accordingly, upon excitation of an O<sub>2</sub>-saturated toluene solution of **(DPA)<sub>4</sub>-Per**, an emission at 1272 nm was detected.

Compared to the standard, perinaphthenone, for which the quantum yield of  $^1\Delta_g$  production is close to unity,<sup>[210]</sup> **(DPA)<sub>4</sub>-Per** sensitizes  $^1\Delta_g$  with a quantum yield of 0.60. On the other hand, the derivative **(Bmes<sub>2</sub>)<sub>4</sub>-Per** does not sensitize  $^1\Delta_g$  to any measurable extent. However, as the singlet excited state of **(DPA)<sub>4</sub>-Per** is long-lived ( $\tau = 12$  ns,  $\phi = 0.26$ ) and quenched in an O<sub>2</sub>-saturated solution ( $\tau = 4.6$  ns,  $\phi = 0.09$ ), it is reasonable that the formation of  $^1\Delta_g$  is not only a product of its triplet state but also of the singlet excited state.<sup>[211,212]</sup> McLean and co-workers reported that perylene sensitizes  $^1\Delta_g$  with a quantum yield of 0.65 in an oxygen-saturated benzene solution even though formation of its triplet state has a vanishing quantum yield, thus, implying  $^1\Delta_g$  sensitization from its excited singlet state only.<sup>[212,213]</sup> However, as for **(DPA)<sub>4</sub>-Per** the yield of sensitized  $^1\Delta_g$  is larger than the fluorescence quantum yield, a significant part must be sensitized from its triplet state. To confirm this, we performed transient absorption measurements on **(DPA)<sub>4</sub>-Per** in order to investigate a possible triplet state. Indeed, excited state absorption in the range 400-710 nm was observed revealing a long-lived excited state with a lifetime of 500  $\mu$ s, which is completely quenched in an O<sub>2</sub>-equilibrated solution.

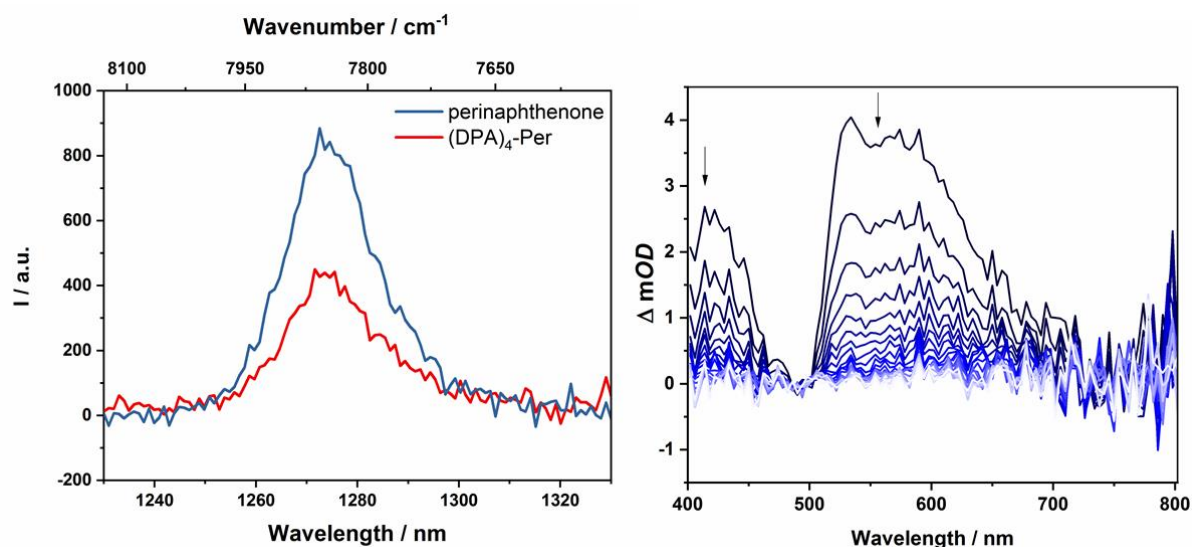


**Figure 2-5.** Singlet oxygen luminescence from optically matched toluene solutions of **(DPA)<sub>4</sub>-Per** and the standard perinaphthenone; excitation at 340 nm (left); nanosecond transient absorption spectrum of **(DPA)<sub>4</sub>-Per** in a degassed DMF solution (right) at intervals of 169.9  $\mu$ s.

## 2.2.5 Redox Properties

Cyclic voltammetry studies on **(Bmes)<sub>2</sub>-Per** revealed four reversible reductions occurring at -2.04 V, -2.45V, -2.79 V and -2.98 V with respect to Fc/Fc<sup>+</sup> (in THF) to its anion, dianion, trianion and tetraanion, respectively, as shown in Figure 2-6 and Table 2-4. The first reduction is anodically shifted by 0.15 V while the second, third and fourth reductions are cathodically shifted by 0.26 V, 0.6 V and 0.79 V, respectively, compared to the first reduction of perylene.<sup>[133]</sup> The fourth reduction is cathodically shifted by 0.25 V compared to the second reduction of perylene. However, **(Bmes)<sub>2</sub>-Per** shows stability towards very high reduction potentials with the advantage that it has a high electron capacity, as up to four electrons can be stored. This intriguing property is interesting for applications including molecular switches,<sup>[214,215]</sup> receptors,<sup>[215,216]</sup> photoactive dyads<sup>[217]</sup> or photocatalysis.<sup>[199,218]</sup>

The donor-substituted counterpart, **(DPA)<sub>4</sub>-Per**, can be oxidized up to five times according to cyclic voltammetry studies in CH<sub>2</sub>Cl<sub>2</sub>/0.1 M [*n*-Bu<sub>4</sub>N][PF<sub>6</sub>]. The first two oxidations are well separated, but the second, third and fourth oxidations are very close to one another and hard to quantify. Therefore, we performed square-wave voltammetry measurements which are known to be more sensitive than cyclic voltammetry.<sup>[219]</sup> The first two oxidations are again well separated occurring at 0.13 V and 0.31 V, the third oxidation occurs at 0.41 V and the larger signal intensity of the latter indicates a fourth oxidation within this area. A further oxidation at 0.98 V occurs which is possibly due to the methoxy moieties. We performed a further cyclic voltammetry study using the weakly coordinating anion (WCA)-containing electrolyte [*n*-Bu<sub>4</sub>N][Al(OC(CF<sub>3</sub>)<sub>3</sub>)<sub>4</sub>].<sup>[220]</sup> WCAs are known to separate charged species in electrochemical

studies better and thus give a larger potential splitting.<sup>[221]</sup> Thus, four clear, reversible oxidations at 0.040 V, 0.24 V, 0.41 V and 0.51 V to the cation, dication, trication and tetracation, respectively, of **(DPA)<sub>4</sub>-Per** were observed, whereas the fifth oxidation is not reversible in this electrolyte.

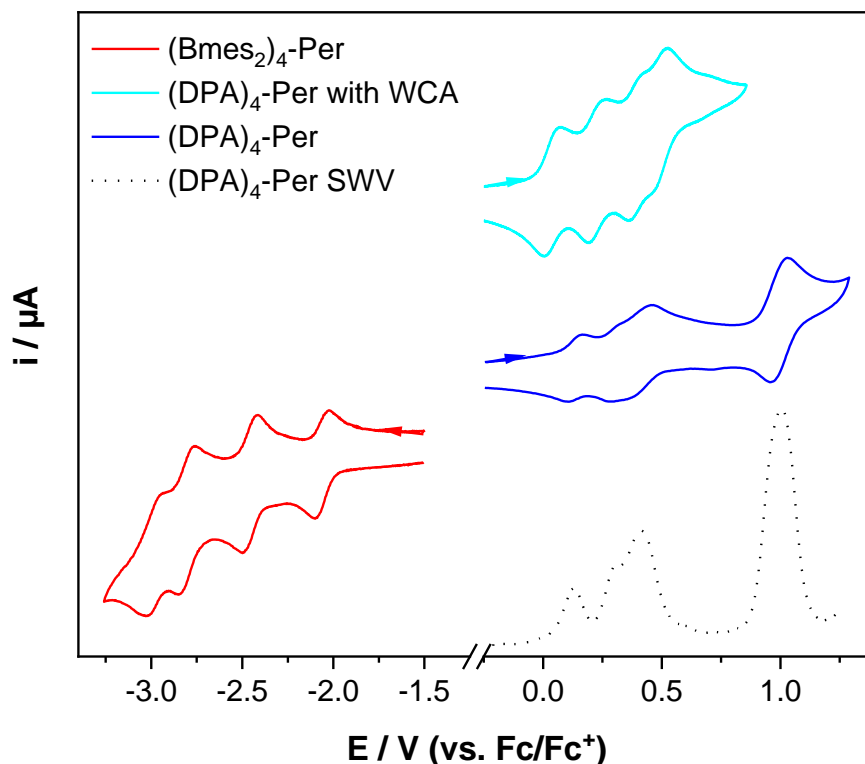


**Figure 2-6.** Cyclic voltammograms of **(Bmes<sub>2</sub>)<sub>4</sub>-Per** in THF/0.1 M [*n*-Bu<sub>4</sub>N][PF<sub>6</sub>] at 500 mV/s (red) and **(DPA)<sub>4</sub>-Per** in CH<sub>2</sub>Cl<sub>2</sub>/0.1 M [*n*-Bu<sub>4</sub>N][PF<sub>6</sub>] (blue), and CH<sub>2</sub>Cl<sub>2</sub>/0.1 M [Al(O(CF<sub>3</sub>)<sub>3</sub>)<sub>4</sub>][*n*-Bu<sub>4</sub>N] (cyan), respectively, at 250 mV / s, and a square wave voltammogram (dashed line) of **(DPA)<sub>4</sub>-Per** in CH<sub>2</sub>Cl<sub>2</sub>/0.1 M [*n*-Bu<sub>4</sub>N][PF<sub>6</sub>].

**Table 2-4.** Cyclic voltammetry results for **(Bmes<sub>2</sub>)<sub>4</sub>-Per** in THF/0.1 M [*n*-Bu<sub>4</sub>N][PF<sub>6</sub>] and **(DPA)<sub>4</sub>-Per** in CH<sub>2</sub>Cl<sub>2</sub>/0.1 M [*n*-Bu<sub>4</sub>N][PF<sub>6</sub>] relative to the Fc/Fc<sup>+</sup> couple if not otherwise noted.

	$E_{1/2} / \text{V}$							
	(red) <sup>1</sup>	(red) <sup>2</sup>	(red) <sup>3</sup>	(red) <sup>4</sup>	(ox) <sup>1</sup>	(ox) <sup>2</sup>	(ox) <sup>3</sup>	(ox) <sup>4</sup>
<b>(Bmes<sub>2</sub>)<sub>4</sub>-Per</b>	-2.04	-2.45	-2.79	-2.98	-	-	-	-
<b>(DPA)<sub>4</sub>-Per</b>	-	-	-	-	0.13	0.31	0.41	0.98
<b>(DPA)<sub>4</sub>-Per with WAC<sup>a</sup></b>	-	-	-	-	0.040	0.24	0.41	0.51

a) Measured in CH<sub>2</sub>Cl<sub>2</sub>/0.1 M [*n*-Bu<sub>4</sub>N][Al(OC(CF<sub>3</sub>)<sub>3</sub>)<sub>4</sub>] relative to the Fc/Fc<sup>+</sup> couple.

These numerous reductions and oxidations of the two derivatives are remarkable for perylenes, because PDIs only possess up to two reductions or oxidations and a fourfold reduction has only been reported for bi(PDI)s.<sup>[222]</sup> PAHs that can be reduced or oxidized multiple times are rare, with the typical example being fullerenes.<sup>[223]</sup> A recent report by Oki *et al.* indicated that a pyrrole-fused azacoronene analogue could be reversibly oxidized four times, which was also observed for hexapyrrolohexaazacoronenes.<sup>[224]</sup> Nevertheless, the *bay* and *ortho* octa-substituted perylenes reported by Zeng and co-workers<sup>[139]</sup> show only a maximum of two oxidations at 0.42 V and 0.72 V in CH<sub>2</sub>Cl<sub>2</sub>/0.1 M [*n*-Bu<sub>4</sub>N][PF<sub>6</sub>] for the derivative with four methoxy moieties at the *ortho* positions (2,5,8,11-tetramethoxy-1,6,7,12-tetra-*n*-butoxyperylene vs. Fc/Fc<sup>+</sup>). These oxidations are significantly shifted to higher potentials compared to (DPA)<sub>4</sub>-Per. Hence, the donor substituted perylene derivative is among the most electron-rich perylenes reported to date, and the HOMO of (DPA)<sub>4</sub>-Per must be strongly destabilized, which is unique for perylenes as they usually have very poor electron-donating abilities.<sup>[225]</sup> The compound 2,5,8,11-tetracyano-1,6,7,12-tetra-*n*-butoxyperylene has only one irreversible reduction at -1.63 V in CH<sub>2</sub>Cl<sub>2</sub>/0.1 M [*n*-Bu<sub>4</sub>N][PF<sub>6</sub>]. Thus, Bmes<sub>2</sub> as an acceptor at the *ortho* positions of perylene enables the possibility of multiple reductions, in contrast to the cyano acceptor.<sup>[139]</sup>

### 2.2.6 Spectroelectrochemistry

To investigate the properties of the cation, dication, trication and tetracation of (DPA)<sub>4</sub>-Per UV/Vis/NIR spectrochemical measurements were performed in CH<sub>2</sub>Cl<sub>2</sub>/0.1 M [*n*-Bu<sub>4</sub>N][Al(OC(CF<sub>3</sub>)<sub>3</sub>)<sub>4</sub>]. However, due to the small redox-potential separations, it was not possible to generate exclusively each charged species. Nevertheless, the monocation can be observed as the “nearly pure” radical cation without further deconvolution and is depicted in Figure 2-7. Upon oxidation to the mono-cation a very broad and symmetric transition appears between 2 400 and 8 000 cm<sup>-1</sup> with a maximum at  $\tilde{\nu}_{max}^{IVCT} = 3\ 813\ \text{cm}^{-1}$  (2 622 nm,  $\epsilon = 9\ 900\ \text{M}^{-1}\ \text{cm}^{-1}$ ) in the NIR. The transition at ca. 1 100 nm appears at higher oxidation potentials and thus belongs to the dication.

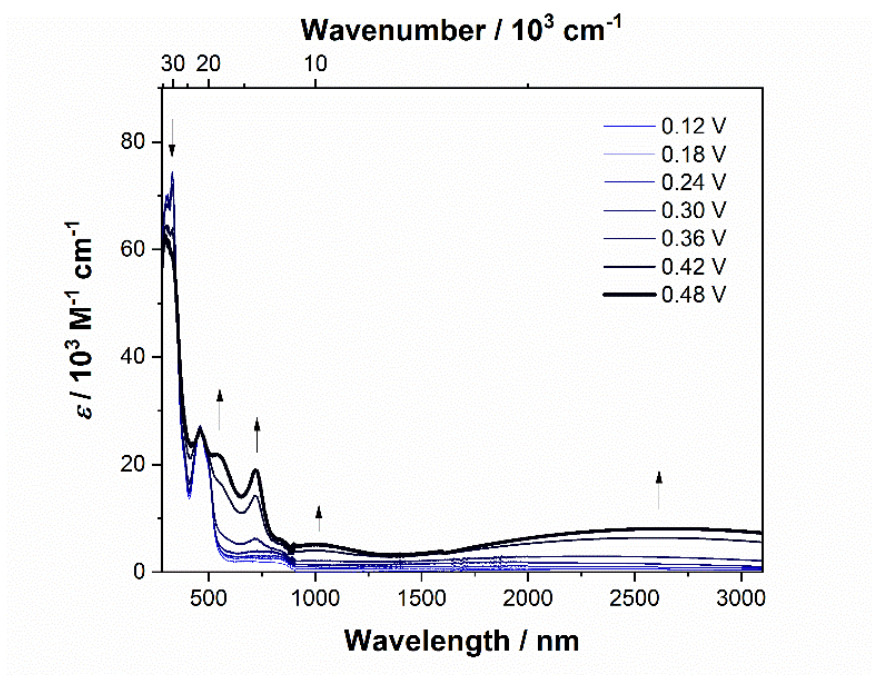


**Figure 2-7.** Spectroelectrochemical measurements of the stepwise oxidation process of **(DPA)<sub>4</sub>-Per** in CH<sub>2</sub>Cl<sub>2</sub>/0.1 M [*n*-Bu<sub>4</sub>N][Al(OC(CF<sub>3</sub>)<sub>3</sub>)<sub>4</sub>]. The absorption spectrum of **(DPA)<sub>4</sub>-Per<sup>+</sup>** is shown as a solid black line.

The analysis of this intervalence charge-transfer band (IV-CT) according to the Mulliken-Hush theory is straight forward as DFT calculations (see below) reveal a vanishing dipole moment difference between ground and excited state upon excitation. Thus, the radical cation is a delocalized Robin-Day-class-III mixed valence (MV) compound and the electronic coupling between the two diabatic redox states can be evaluated as one half of the energy of the absorption maximum.<sup>[99,106-109]</sup>

$$V = \frac{\tilde{\nu}_{max}^{IVCT}}{2} \quad (1)$$

In this way the electronic coupling  $V$  was evaluated to be 1807 cm<sup>-1</sup> as half of the IV-CT excitation energy ( $\beta$ -HOMO  $\rightarrow$   $\beta$ -LUMO). This result is fully in line with the TD-DFT computations of the mono-cation as the orbitals involved in the excitation show the expected phase behavior for a Robin-Day-class-III compound (Figure 2-8). Unfortunately, it was not possible to evaluate the electronic coupling within the trication, because the redox-potential separations between the dication, trication and tetracation are too close to each other. Furthermore, **(Bmes<sub>2</sub>)<sub>4</sub>-Per** could not be studied by spectroelectrochemical measurements, as the absorption spectrum of the neutral species cannot be reproduced in intensity after the reductions.

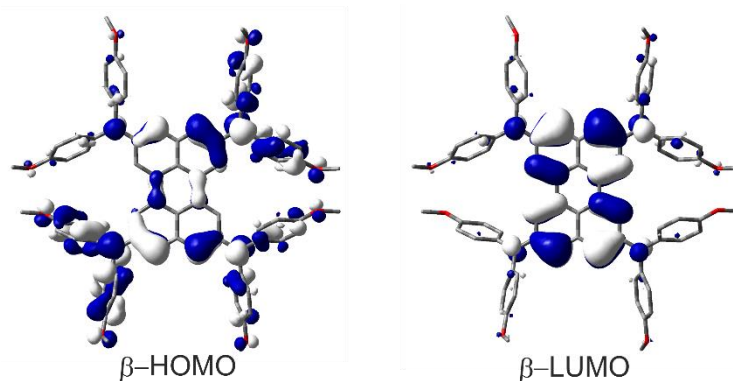


**Figure 2-8.** Depiction of the  $\beta$ -HOMO and  $\beta$ -LUMO orbitals that are responsible for the lowest energy absorption (IV-CT band) of  $(\text{DPA})_4\text{-Per}^+$ .

### 2.2.7 DFT and TD-DFT Calculations

To rationalize the observed trends and properties, DFT and TD-DFT studies were performed on perylene,  $(\text{DPA})_4\text{-Per}$ , and  $(\text{Bmes}_2)_4\text{-Per}$ . The ground-states were optimized in the gas-phase at the B3LYP/6-31G (d,p) level of theory. Previous studies<sup>[31,226]</sup> have shown that range-separated hybrid functionals are necessary to obtain a reliable picture of the nature and relative energetic ordering of the excited states. Therefore, the CAM-B3LYP functional was employed for the subsequent TD-DFT calculations for the perylene derivatives.

Perylene has a large HOMO-LUMO gap (3.05 eV) and its HOMO-1/HOMO and LUMO/LUMO+1 orbitals are well separated. Adding four Bmes<sub>2</sub> moieties to the *ortho* positions of perylene ( $(\text{Bmes}_2)_4\text{-Per}$ ) leads to a 0.20 eV stabilization of the LUMO orbital, which is a combination of the empty  $p_z$  orbitals of the boron atoms of the Bmes<sub>2</sub> fragments and the perylene LUMO resulting in larger orbital coefficients at the *ortho* positions compared to the parent perylene (Figure 2-9).

Perylene's LUMO+1, LUMO+3 and LUMO+4 orbitals mix even stronger with the Bmes<sub>2</sub> fragments, which leads to an increased stabilization of their energies by 1.35 eV, 1.54 eV and 1.58 eV, respectively. Hence, these three orbitals above the LUMO, are all greatly stabilized in  $(\text{Bmes}_2)_4\text{-Per}$  and are close in energy. This is a plausible explanation for the four electron reductions of this compound that were observed within the cyclic voltammetry studies. The stabilization of the LUMO furthermore explains the observed bathochromic shift of the  $S_1 \leftarrow S_0$  transition, which consists of a pure HOMO  $\rightarrow$  LUMO transition. This contrasts strongly with 2,5,8,11-tetracyano-1,6,7,12-tetra-*n*-butoxyperylene, which shows that the cyano group does not mix as efficiently with the perylene LUMO and Marder and co-workers already made this observation in a closely related pyrene derivative.<sup>[47,139]</sup> This is reflected in the photophysical

behavior, as the  $S_1 \leftarrow S_0$  transition of 2,5,8,11-tetracyano-1,6,7,12-tetra-*n*-butoxyperylene is not as bathochromically shifted as that of **(Bmes<sub>2</sub>)<sub>4</sub>-Per**. Nevertheless, this comparison should be treated with caution as the *bay* substituents certainly have some influence (*vide supra*). However, the calculations show that the LUMO is mainly distributed over the four boron centers and the perylene core while the mesityl moieties do not contribute to this orbital (Figure 2-9). Even though there is some contribution of the Bmes<sub>2</sub> fragments to the LUMO and LUMO+1 to LUMO+3 orbitals of **(Bmes<sub>2</sub>)<sub>4</sub>-Per**, these orbitals generally resemble those in unsubstituted perylene. Therefore, the HOMO→LUMO transition of **(Bmes<sub>2</sub>)<sub>4</sub>-Per** does not have much CT character, and is predominantly a local excited state (LE), which agrees with our photophysical studies, as the emission spectra of **(Bmes<sub>2</sub>)<sub>4</sub>-Per** does not show solvatochromism. The HOMO is not influenced by the Bmes<sub>2</sub> fragments and thus does not change much in energy. However, 16 orbitals, which are based on the mesityl fragments only, *i.e.*, are not affected by the perylene core or boron atoms, and form the HOMO-1 to HOMO-16 (Figure 2-9, grey) of **(Bmes<sub>2</sub>)<sub>4</sub>-Per**. The former HOMO-1 through HOMO-4 are not altered by the Bmes<sub>2</sub> groups and now form the HOMO-17 to HOMO-20 (Figure 2-9, black, blue, cyan and green).

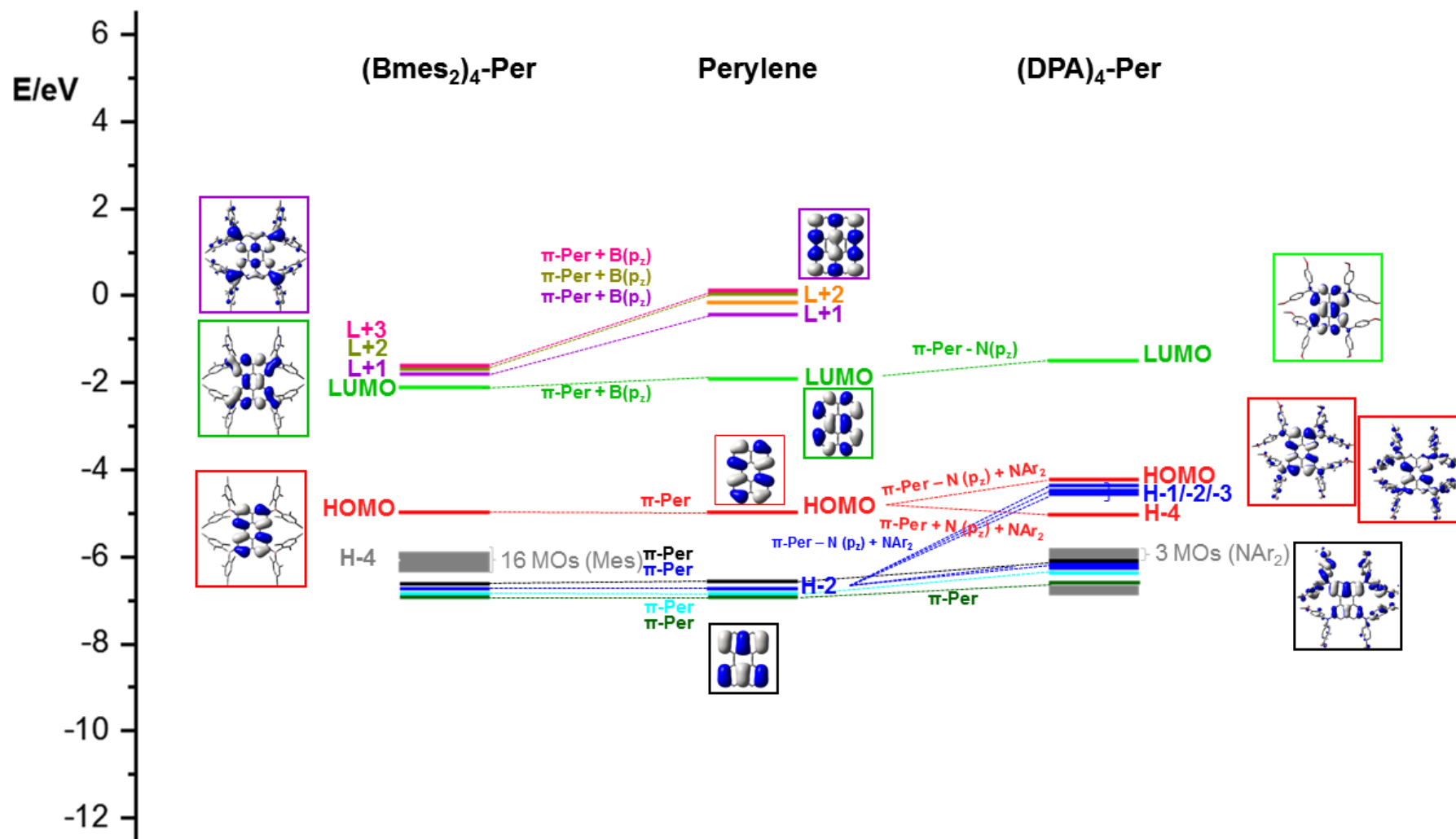


**Figure 2-9.** Frontier MO-diagram (B3LYP/6-31 G(d,p)) and depiction of **B(mes<sub>2</sub>)<sub>4</sub>-Per** (left), **perylene** (middle) and **(DPA)<sub>4</sub>-Per** (right) showing the relation between the frontier orbitals of perylene and its acceptor and donor substituted derivatives. The key frontier molecular orbitals are shown in color-coded boxes.

In contrast, adding four amine donor moieties to the *ortho* positions of the perylene core destabilizes the occupied orbitals much more than the virtual ones. The nitrogen  $p_z$  orbitals of the DPA moieties mix very well with the occupied orbitals of the perylene core, but the  $\pi$ -orbitals of the methoxy phenyl rings also contribute significantly. The mixing of the perylene HOMO with  $N(p_z)$  and  $NAr_2$  orbitals leads to two new perylene-like HOMO orbitals in **(DPA)<sub>4</sub>-Per** (HOMO and HOMO-4) (Figure 2-9, red). The new HOMO of **(DPA)<sub>4</sub>-Per** is strongly destabilized by 0.73 eV while HOMO-4 is slightly stabilized in comparison to the HOMO of perylene. In a similar manner, for HOMO-2 of perylene, two new sets are formed in **(DPA)<sub>4</sub>-Per** (Figure 2-9, blue). One set (HOMO-1 through HOMO-3) is strongly destabilized by ca. 0.79 eV and the second by ca. 0.59 eV (HOMO-9 and HOMO-10). Perylene's HOMO-1 to HOMO-3 and HOMO-4 orbitals (Figure 2-9, black, cyan and green), on the other hand, are less destabilized in **(DPA)<sub>4</sub>-Per**. These results agree with our observed photophysical properties. The strong destabilizing effect of the HOMO in **(DPA)<sub>4</sub>-Per** explains the strong bathochromic shift of the  $S_1 \leftarrow S_0$  transition and as the HOMO of **(DPA)<sub>4</sub>-Per** is also distributed over the four amine moieties and displays a pronounced CT character, this is reflected in the broad and structureless absorption and emission spectra as well as the solvatochromic behavior. Thus, the effect of the DPA groups on the occupied orbitals of the perylene is more pronounced than is the case of the **Bmes<sub>2</sub>** moieties, where only the unoccupied orbitals were affected. Furthermore, the observed electrochemical behavior is consistent with these calculations, as the influence on the occupied orbitals results in four orbitals that are very close in energy and around the HOMO of **(DPA)<sub>4</sub>-Per**, thus, removing four electrons successively from the system is possible.

TD-DFT calculations show that the nature of both  $S_1 \leftarrow S_0$  transition in **(DPA)<sub>4</sub>-Per** and **(Bmes<sub>2</sub>)<sub>4</sub>-Per** remain HOMO  $\rightarrow$  LUMO in character as in perylene. Thus, these transitions can best be described for the **(Bmes<sub>2</sub>)<sub>4</sub>-Per** derivative as an LE transition with a small CT contribution whereas there is an increased CT contribution for the **(DPA)<sub>4</sub>-Per** derivative. This is in accordance with the slightly lower oscillator strengths for the **(DPA)<sub>4</sub>-Per** derivative ( $f = 0.367$  for **(Bmes<sub>2</sub>)<sub>4</sub>-Per**; and  $f = 0.318$  for **(DPA)<sub>4</sub>-Per**) and lower extinction coefficients ( $\epsilon = 20\,000\text{ M}^{-1}\text{ cm}^{-1}$  for **(Bmes<sub>2</sub>)<sub>4</sub>-Per** and  $\epsilon = 15\,000\text{ M}^{-1}\text{ cm}^{-1}$  for **(DPA)<sub>4</sub>-Per**). However, the red shift of both  $\lambda_{\text{max}}(\text{abs})$  and  $\lambda_{\text{max}}(\text{em})$  as well as the larger apparent Stokes shift, agrees well with increasing CT admixture for the **(DPA)<sub>4</sub>-Per** compound as does the observed solvatochromism, which also results from the CT nature of the lowest excited singlet state, which is not observed for **(Bmes<sub>2</sub>)<sub>4</sub>-Per**.

**Table 2-5.** TD-DFT results (CAM-B3LYP/6-31G (d,p)) for the five vertical transitions of **perylene**, **(Bmes)<sub>2</sub>**<sup>4-</sup>**Per** and **(DPA)<sub>4</sub>**<sup>-</sup>**Per**.

	FC- S <sub>n</sub>	E/eV (E /nm)	f	Configuration (major contributions > 10%)
<b>Perylene</b>	S <sub>1</sub>	3.21 (387)	0.446	H→L (99%)
	S <sub>2</sub>	4.06 (305)	0.000	H→L+1 (58%), H-1→L (33%)
	S <sub>3</sub>	4.34 (285)	0.004	H-2→L (52%), H→L+3 (38%)
	S <sub>4</sub>	4.45 (278)	0.000	H→L+2 (42%), H-4→L (24%), H-1→L (23%)
	S <sub>5</sub>	4.88 (254)	0.000	H→L+2 (52%), H-4→L (30%), H→L+1 (13%)
<b>(Bmes)<sub>2</sub></b> <sup>4-</sup>	S <sub>1</sub>	3.03 (410)	0.367	H→L (96%)
<b>Per</b>	S <sub>2</sub>	3.21 (386)	0.000	H→L+1 (87%)
	S <sub>3</sub>	3.54 (350)	0.212	H→L+3 (79%)
	S <sub>4</sub>	3.64 (340)	0.000	H→L+2 (92%)
	S <sub>5</sub>	4.01 (310)	0.055	H-4→L+1 (21%), H-2→L (20%), H-1→L+2 (21%), H-3→L+3 (16%)
<b>(DPA)<sub>4</sub></b> <sup>-</sup>	S <sub>1</sub>	3.00 (413)	0.318	H→L (91%)
<b>Per</b>	S <sub>2</sub>	3.11 (398)	0.017	H-1→L (76%)
	S <sub>3</sub>	3.30 (376)	0.281	H-2→L (74%)
	S <sub>4</sub>	3.48 (356)	0.005	H-3→L (77%)
	S <sub>5</sub>	3.92 (316)	0.294	H-4→L (78%)

## 2.3 Conclusions

Novel *ortho*-tetrasubstituted perylenes were synthesized with a strong DPA donor or a strong Bmes<sub>2</sub> acceptor, which represent the first examples of perylenes substituted only at the *ortho* positions with donors or acceptors. The synthesis of these two systems required two new intermediates (**Br**)<sub>4</sub>-**Per** and (**BF<sub>3</sub>K**)-**Per**, which could potentially be used for the synthesis of many new *ortho*-perylene derivatives. The donor and the acceptor substituents significantly influence the frontier orbitals which leads to interesting and potentially useful properties. Cyclic voltammetry and square wave voltammetry experiments reveal up to four reversible reductions for the acceptor derivative (**Bmes<sub>2</sub>**)<sub>4</sub>-**Per** and four reversible oxidations for the donor derivative (**DPA**)<sub>4</sub>-**Per**, which is unprecedented for perylenes and has only been observed previously for bi(PDI)s. Spectroelectrochemical measurements suggest a strong electronic coupling between the amine moieties through the perylene bridge, which can be categorized as a typical Robin-Day-class-III system. (**DPA**)<sub>4</sub>-**Per** reached an unparalleled bathochromic shift of its S<sub>1</sub>←S<sub>0</sub> transition ( $\lambda_{\text{max}}(\text{abs}) = 499 \text{ nm}$ ) and emission ( $\lambda_{\text{max}}(\text{em}) = 593 \text{ nm}$ ) for *ortho*-substituted perylenes which do not have carboxyimide moieties at the *peri*-positions. Both derivatives have unusually long intrinsic singlet lifetimes with that of (**DPA**)<sub>4</sub>-**Per** being 94 ns. Transient absorption measurements reveal an additional excited state with a 500  $\mu\text{s}$  lifetime which effectively sensitizes singlet oxygen. This presumed triplet state could prove useful in organophotocatalysis.<sup>[193,197-200]</sup> Theoretical studies show that the acceptor Bmes<sub>2</sub> couples well with the unoccupied orbitals, which leads to a strong stabilization of the LUMO to LUMO+4 orbitals. However, while the nature of the S<sub>1</sub> state is maintained, the HOMO→LUMO transition is less allowed in comparison to the one in perylene. Hence, the radiative decay rates decrease resulting in a longer-lived singlet excited state. The donor DPA also mixes very well with the occupied orbitals, strongly destabilizing the HOMO to HOMO-4 levels. In contrast to the former derivative, its CT character gives rise to a less allowed S<sub>1</sub>←S<sub>0</sub> transition which results in the slowest radiative decay reported so far for perylenes. Furthermore, it possesses the strongest bathochromic shift observed for *ortho*-perylene and a large apparent Stokes shift.

This synthetic procedure has the potential to produce a wide variety of *ortho*-perylene derivatives with a broad range of properties as required for diverse applications. As one can anticipate that alternative donors and acceptors could result in typical  $\pi$ -stacking interactions, which are inhibited in these current compounds.





# Chapter 3

Synthesis, Photophysical  
and Electronic Properties  
of Novel Red to NIR Emitting  
Donor-Acceptor  
Pyrene Derivatives



## 3 Synthesis, Photophysical and Electronic Properties of Novel Red to NIR Emitting Donor-Acceptor Pyrene Derivatives

### 3.1 Introduction

The polycyclic aromatic hydrocarbon (PAH) pyrene is among the most widely studied chromophores and possesses some unique properties together with excimer and exciplex formation, such as intense blue emission and an exceptionally long-lived excited singlet state.<sup>[2]</sup> In addition to its photophysical properties, it has high chemical stability and charge-carrier mobility. Therefore, pyrene derivatives have been used in a broad range of applications in diverse scientific fields such as organic light emitting diodes (OLEDs), organic field-effect transistors (OFETs) and organic photovoltaic cells (OPVs).<sup>[2,4,5]</sup> Furthermore, they have been used for sensing of temperature,<sup>[6]</sup> pressure<sup>[7]</sup> or pH,<sup>[8]</sup> or to detect guest molecules such as O<sub>2</sub> or NH<sub>3</sub>,<sup>[9-11]</sup> organic molecules<sup>[12-14]</sup> or metals.<sup>[2,15-18]</sup> Its monomer and excimer fluorescence have also been used to characterize macromolecules<sup>[227]</sup> or polymeric systems.<sup>[228]</sup> Its remarkably long fluorescence lifetime of 354 ns, compared to other PAHs, makes pyrene exceptionally well suited for further applications such as the determination of cellular oxygen concentrations in biological systems.<sup>[19,20]</sup>

To adjust the required properties, electron donors and/or acceptors are often introduced onto a PAH core as they strongly modulate the frontier orbitals. Moreover, substituting PAHs with donors and acceptors gives derivatives with properties such as a permanent dipole moment, charge transfer (CT) excited states, strong solvatochromism, environmentally-influenced photophysics, the possibility for energy or electron transfer and narrowed energy gaps.<sup>[1,38]</sup> Furthermore, these chromophores can absorb and emit in the near-infrared region (NIR), which is in demand for applications such as bioimaging and cell recognition, as NIR light penetrates deeper into biological tissues, is less damaging than visible or UV light, and gives minimum interference from background autofluorescence by biomolecules.<sup>[229]</sup> In general, materials with high HOMO energies, such as the compound *N,N'*-diphenyl-*N,N'*-bis(3-methylphenyl)-(1,1'-biphenyl)-4,4'-diamine (TPD), are especially useful for hole transport.<sup>[144-150]</sup> Common  $\pi$ -donors that have been used in dyes to boost HOMO energies include amines, with a lone pair on the nitrogen, such as diarylamino, diethylamino, dimethylamino or carbazolyl moieties.<sup>[22]</sup> Diarylamines are among the strongest  $\pi$ -electron donors and have been employed in diverse

applications,<sup>[151-163]</sup> due to their outstanding physical, photochemical and electrochemical properties. Moreover, they are easy to synthesize and handle.<sup>[164]</sup> A methoxy group at the position *para* to the nitrogen not only increases the electron donating strength of diarylamines, but enables reversible oxidations.<sup>[103,164]</sup> Nevertheless, a significant drawback can be energy loss due to the rotational motion of the phenyl rings which can result in a reduction in luminescence efficiency.<sup>[77,78]</sup> In addition, the possibility of rotation around the N-C( $\pi$ ) bond can lead to twisted intramolecular charge transfer (TICT) excited states.<sup>[1]</sup> The compound 1,1,7,7-tetramethyl-julolidine is known to be an even stronger  $\pi$ -donor than diarylamines. The julolidine moiety has been thoroughly studied since its discovery in 1892 by Pinkus,<sup>[79]</sup> and is used in a wide range of dyes.<sup>[1,74,80,81]</sup> Its nitrogen lone pair is conformationally restricted to remain parallel to the aromatic system,<sup>[82]</sup> in our case, the pyrene moiety, in both the ground and excited states, and our previous studies revealed a significantly enhanced electron donating effect on the pyrene core compared to diarylamines.<sup>[1]</sup>

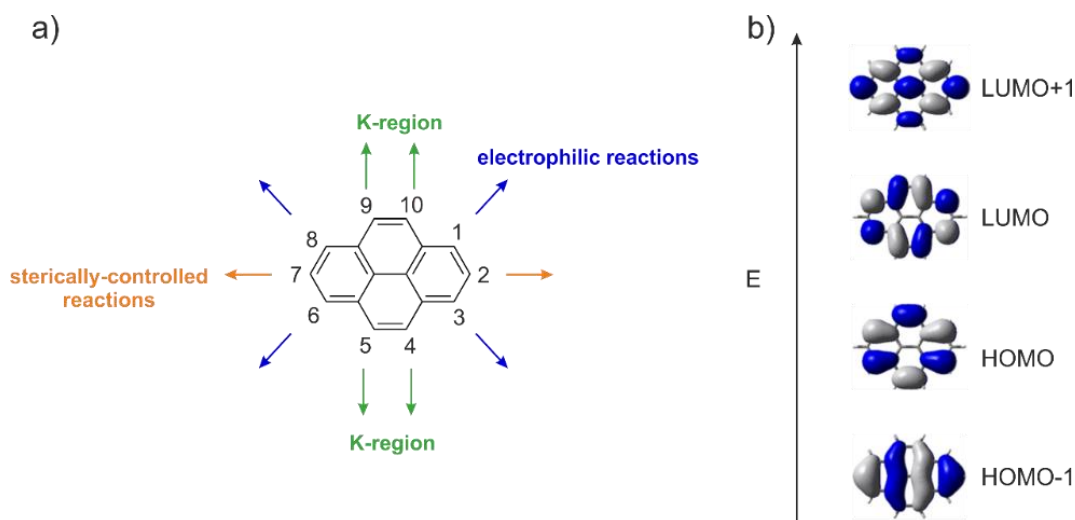
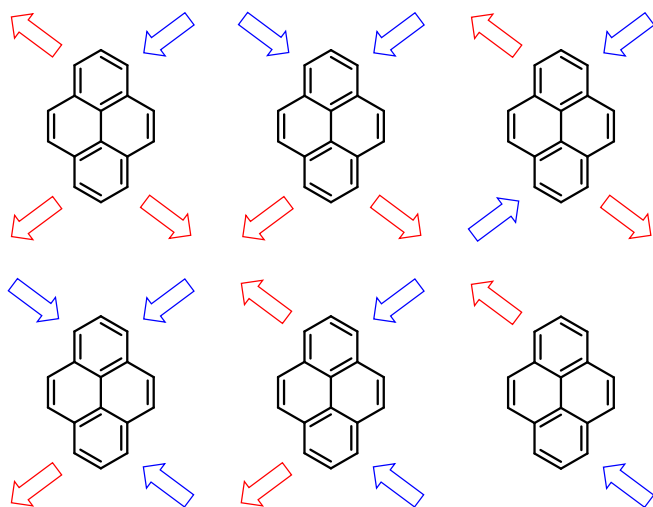


**Figure 3-1.** a) Atom numbering system in pyrene with the three sets of chemically inequivalent sites; b) the four frontier orbitals of pyrene.

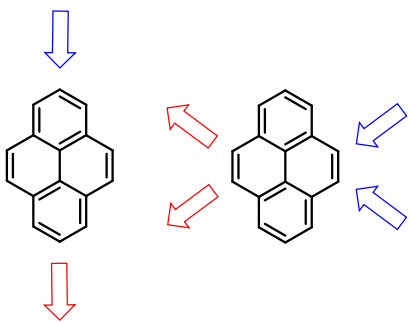
Pyrene exhibits 10 peripheral reactive sites, which can be classified into three sets of chemically inequivalent sites (Figure 3-1, a)). Thus, the position of substitution is very important and typically, the easily accessible positions 1,3,6 and 8 are functionalized by electrophilic substitution reactions as the HOMO has its largest coefficients at these positions (Figure 3-1, b)).<sup>[2,34,35]</sup> Indeed, the pyrene LUMO also has a nodal plane through carbons 2 and 7. Therefore,  $\pi$ -orbitals of substituents at the 1,3,6,8-positions mix very efficiently with pyrene's

HOMO/LUMO orbitals. However, unsymmetrical substitution at these positions is rather challenging due to the numerous possible isomers (Scheme 3-1). Niko, Konishi and co-workers synthesized D- $\pi$ -A pyrene systems with donors and acceptors at the 1,3,6- and 8-positions, which displayed strong solvatochromism with emissions into the red region (557-648 nm, in MeOH) and high quantum yields ( $\phi > 0.75$ ).<sup>[37]</sup>

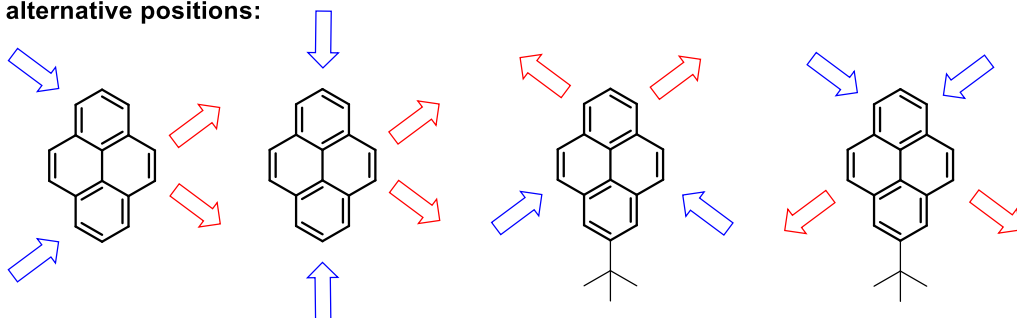
**D/A at 1,3,6,8-positions:**



**D/A at 2,7-positions or at K-region:**



**alternative positions:**



**Scheme 3-1.** Schematic representation of reported D/A-pyrene patterns. Blue arrow = D, Red Arrow = A.

Substituents at the 2,7-positions do not interact with the HOMO/LUMO orbitals of pyrene as they lie on the nodal plane (Figure 3-1, b)). However, they can interact strongly with the HOMO-1 and LUMO+1 of pyrene that have nonzero contributions at these positions. We previously reported that the photophysical properties of pyrenes with substituents at the 2-position significantly differ from those with substituents at the 1-position.<sup>[31]</sup> Moreover, previous studies demonstrated that strong  $\pi$ -donors/acceptors are able to switch the energetic ordering of its HOMO/HOMO-1 and LUMO/LUMO+1, which results in greatly influenced photophysical and redox properties of these derivatives.<sup>[1,47,63,67,83]</sup> Unsymmetrical substitution at these positions is straightforward *via* iridium-catalyzed C–H borylation, and the introduction of julolidine-like donors to the 2,7-positions (**3-I**, Scheme 3-1) even resulted in an unusual green luminescence.<sup>[1,39,47,63,67,83]</sup>

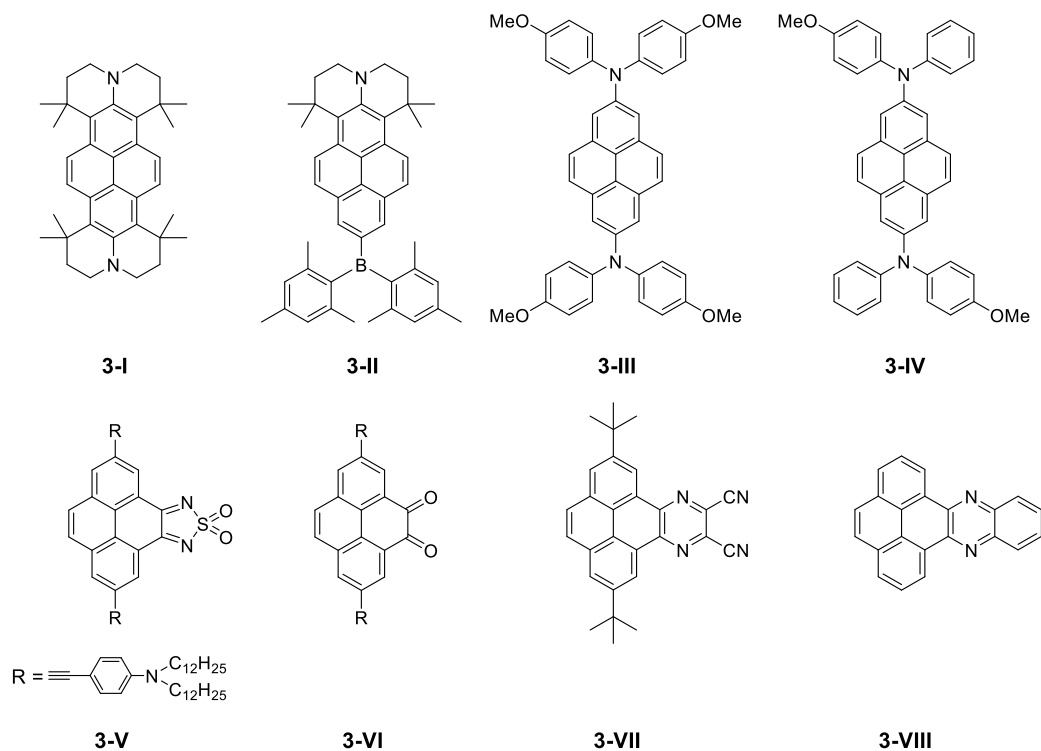
The K-region (positions 4,5,9,10) has large HOMO/LUMO as well as HOMO-1/LUMO+1 contributions. Ottonelli and co-workers showed<sup>[33]</sup> that the contribution of HOMO/LUMO increases in the following order: 2,7 < 4,5,9,10 < 1,3,6,8, while the HOMO-1/LUMO+1 contribution increases in the following order 4,5,9,10 < 1,3,6,8 < 2,7. The K-region possesses alkene-like rather than aromatic character. Hence, reagents such as osmium tetroxide, which are known to react with alkene double bonds, selectively react with pyrene at the 4,5,9,10-positions. Müllen and co-workers reported a protocol for the usymmetric substitution of these sites and presented a few examples with up to orange light emission (613 nm in THF) (Scheme 3-1).<sup>[38,41]</sup>

There are also reports on pyrenes that have donor and acceptor moieties on alternative positions, besides the typical three categories (*vide supra*). Hu and co-workers developed unsymmetric pyrenes with donors at the 1,3-positions and acceptors at the 5,9-positions that emit in the blue-green region (Scheme 3-1).<sup>[230]</sup> Sutherland and co-workers combined the 2,7- and 1,8-positions with the K-region (**3-V** and **3-VI**, Scheme 3-2), respectively, and obtained an  $S_1 \leftarrow S_0$  absorbance up to 900 nm, as it was their objective to obtain strongly redshifted absorptions with high molar absorptivities. However, their derivatives are not emissive and thus studies are missing on the influence on the excited state properties and how additional K-region moieties influence 2,7-substituted pyrenes.<sup>[56,231]</sup>

In previous reports Marder and co-workers showed that the influence of a second amine donor at the 2,7-positions on the occupied orbitals is larger than that of a cyano or even Bmes<sub>2</sub> acceptor

on the unoccupied orbitals and thus the D- $\pi$ -D derivative (**3-I**, Scheme 3-2) emits further redshifted than the D- $\pi$ -A compound (**3-II**, Scheme 3-2). Thus, the motivation of this project was to utilize the two julolidine-like donors at the 2,7-positions and add additional acceptors to the pyrene core to obtain a new class of D- $\pi$ -A pyrene derivative with unparalleled photophysical properties such as red to NIR emission and interesting redox behavior. Moreover, it is of great interest to see how much more the  $S_1$  state can be influenced by the additional acceptors at the K-region.

As the acceptor unit *n*-azaacenes fused to the K-region of pyrene were chosen that were reported by Mateo-Alonso and co-workers and which possess strong  $\pi$ -accepting properties (**3-VII** and **3-VIII**, Scheme 3-2). *N*-azaacenes have attracted much attention for their outstanding electronic properties and application in organic electronic devices and as anion radicals.<sup>[232]</sup> In particular, pyrene-fused azaacenes are even more stable than their *n*-azaacene analogues and emit strongly in the blue to green region of the electromagnetic spectrum.<sup>[233,234]</sup>



**Scheme 3-2.** Schematic overview of some reported pyrene derivatives that possess either the same acceptor or similar donor moieties as the derivatives **3-6**, **3-7** or **3-8**.

**Table 3-1.** Selected optical and electrochemical properties of the pyrene derivatives **3-I** to **3-VIII**.

	$\lambda_{abs}$ / nm	$\lambda_{em}$ / nm	$E_{1/2}$ (red) / V <sup>a)</sup>	$E_{1/2}$ (ox) <sup>1</sup> / V <sup>a)</sup>	$E_{1/2}$ (ox) <sup>2</sup> / V <sup>a)</sup>
<b>3-I</b> <sup>[1]</sup>	475 (hexane) 481 (THF)	511 (hexane) 525 (THF)	-	-0.18 (CH <sub>2</sub> Cl <sub>2</sub> )	+0.26 (CH <sub>2</sub> Cl <sub>2</sub> )
<b>3-II</b> <sup>[1]</sup>	450 (hexane) 462 (THF)	464 (hexane) 497 (THF)	-2.51 (THF)	+0.29 (THF)	
<b>3-III</b> <sup>[83]</sup>	-	-	-	+0.14 (CH <sub>2</sub> Cl <sub>2</sub> )	+0.38 (CH <sub>2</sub> Cl <sub>2</sub> )
<b>3-IV</b> <sup>[31]</sup>	453 (toluene)	482 (toluene)	-	-	-
<b>3-V</b> <sup>[231]</sup>	630 (CHCl <sub>3</sub> )	-	-0.67 (CHCl <sub>3</sub> )	+0.39 (CHCl <sub>3</sub> )	-
<b>3-VI</b> <sup>[56]</sup>	575 (CHCl <sub>3</sub> )	-	-1.04 (CHCl <sub>3</sub> )	+0.33 (CHCl <sub>3</sub> )	-
<b>3-VII</b> <sup>[235]</sup>	455 (CH <sub>2</sub> Cl <sub>2</sub> )	538 (CH <sub>2</sub> Cl <sub>2</sub> )	-1.43 (THF)	-	-
<b>3-VIII</b> <sup>[236]</sup>	435 (CH <sub>2</sub> Cl <sub>2</sub> )	471 (CH <sub>2</sub> Cl <sub>2</sub> )	-	-	-

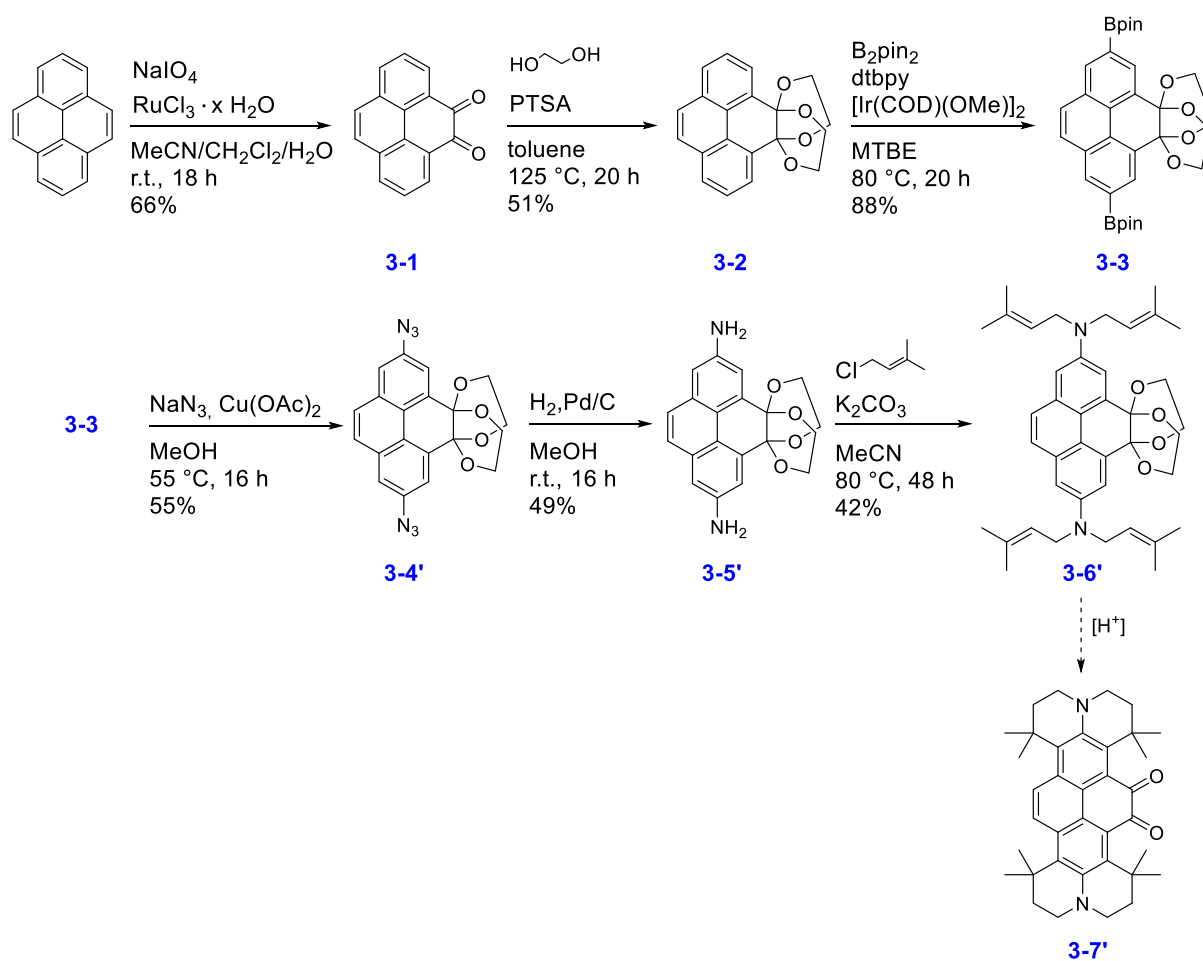
a) Redox potentials were measured with the addition of 0.1 M [*n*-Bu<sub>4</sub>N][PF<sub>6</sub>] and are referenced vs. the Fc/Fc<sup>+</sup> couple.

## 3.2 Results and Discussion

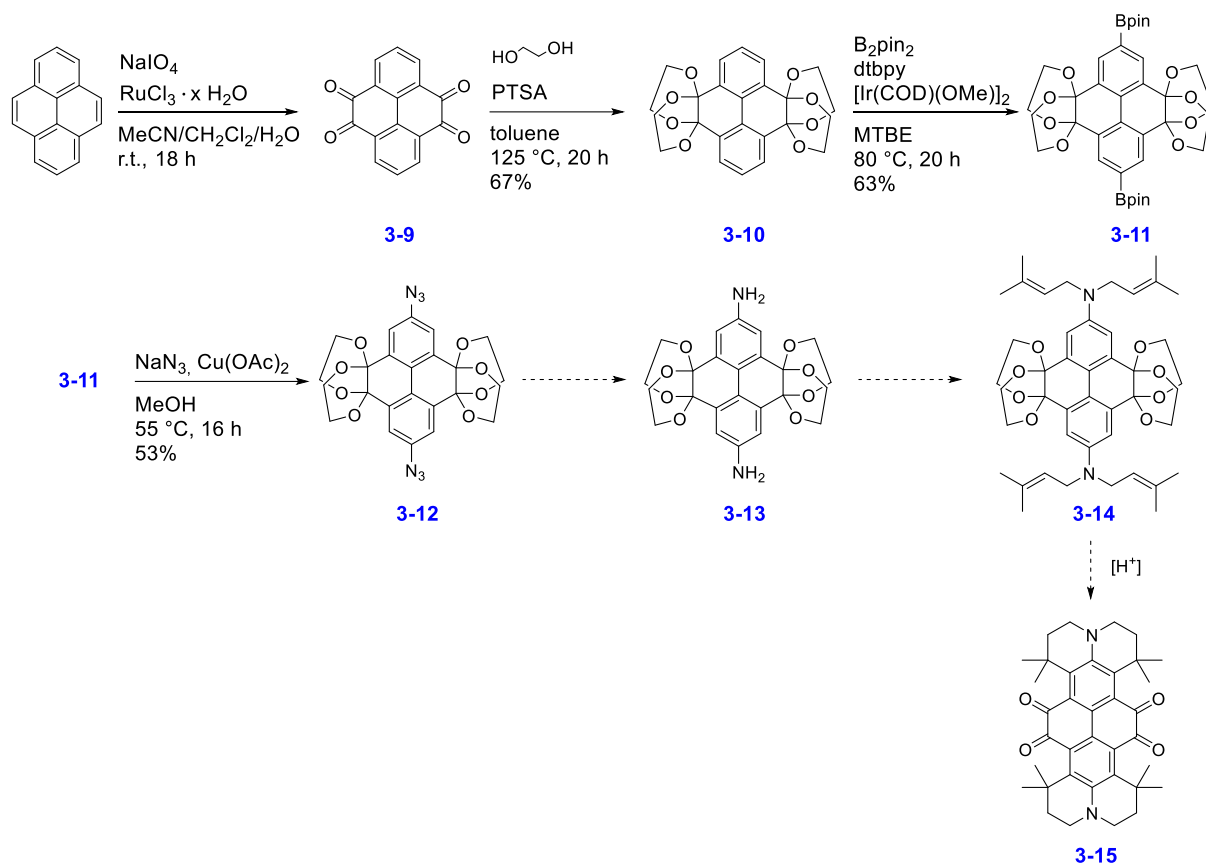
### 3.2.1 Synthesis

The procedures used to synthesize the three key compounds are summarized in Schemes 3-3 and 3-5. At the beginning of this project, we aimed for derivative **3-7'** (Scheme 3-3) and its analogue with ketone moieties at all four K-region positions (Scheme 3-4). The selective RuO<sub>4</sub>-catalyzed oxidation of pyrene at its 4- and 5-positions is the starting point for the synthesis route and gives the dione **3-I**. This one-step reaction was reported by Harris and co-workers in 2005 as an alternative to the toxic OsO<sub>4</sub>-catalyzed oxidation of pyrene.<sup>[237,238]</sup> In this regard, RuO<sub>4</sub> is generated *in situ* from RuCl<sub>3</sub>·3H<sub>2</sub>O and NaIO<sub>4</sub>. The oxidation takes place in a solvent mixture of MeCN, CH<sub>2</sub>Cl<sub>2</sub> and H<sub>2</sub>O (1:1:1.25). The addition of MeCN to the RuO<sub>4</sub>-catalyzed oxidation was already reported by Sharpless in 1981 to improve greatly the effectiveness of the reaction. However, this reaction procedure suffers from several disadvantages. Thus, the reaction can only be performed on a small scale and, furthermore, there are various side products such as dialdehydes or acids that complicate the workup and reduce the yield, which Nowicka *et al.* identified in detail.<sup>[239]</sup> Bodwell and co-workers recently introduced an improved RuO<sub>4</sub>-

catalyzed oxidation procedure to obtain **3-1**, which is scalable and eases the workup. This method includes the additive *N*-methylimidazole and the solvent MeCN is replaced by THF.<sup>[240]</sup> In order to perform the Ir-catalyzed C-H borylation, the ketone groups had to be protected as a diketal to prevent unwanted reactions with the Ir-catalyst. The lack of reactivity of oxidized pyrene in other metal-catalyzed reactions has been reported before.<sup>[241,242]</sup> Compound **3-2** was easily obtained by refluxing **3-1** in toluene with excess of ethylene glycol and the addition of *p*-toluenesulfonic acid for 20 h. The C-H borylation was performed according to our reported procedure<sup>[32]</sup> and takes place at the 2,7-positions selectively providing **3-3**.



**Scheme 3-3.** Synthesis of the derivatives **3-1** to **3-3** and **3-4'** to **3-7'**.

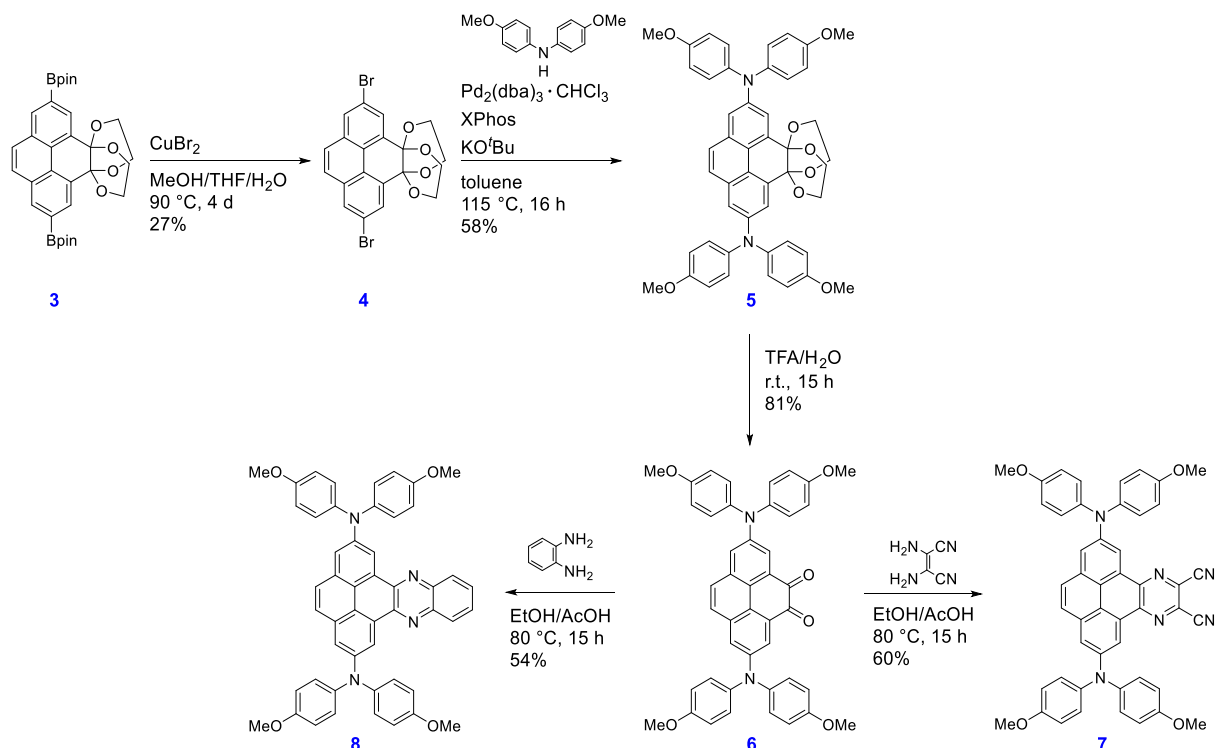


**Scheme 3-4.** Synthesis of the derivatives 3-9 to 3-14.

The Bpin moieties were further converted to azide moieties according to the report of Chang and co-workers.<sup>[243]</sup> They converted arylboronic acids to arylazides in MeOH by using 1.50 eq  $\text{NaN}_3$  as the azide source and 5 mol% of  $\text{Cu}(\text{OAc})_2$  as the catalyst. Subsequent reduction of the azido species **3-4'** with Pd/C and  $\text{H}_2$  gas gave the corresponding primary amine **3-5'**. Therefore, the reaction mixture was stirred at room temperature until reaction monitoring by IR spectroscopy confirmed the complete disappearance of azide moieties (in the region  $2000\text{--}2270\text{ cm}^{-1}$ ) and the appearance of primary amine bands at  $3450\text{ cm}^{-1}$ ,  $3363\text{ cm}^{-1}$  and  $1620\text{ cm}^{-1}$  (Appendix, Figure 8-77). The amine moieties were alkylated in MeCN with 1-chloro-3-methylbutene in the presence of the base  $\text{K}_2\text{CO}_3$ , according to the synthesis of our previous reported derivative **3-I**.<sup>[1]</sup> The alkylation reaction was complete after 48 h and gave the desired product **3-6'** as a bright yellow solid (42%). Unfortunately, the final step in order to obtain the desired derivative **3-7'** could not be achieved. The aim of the last step was to obtain a ring closure and simultaneously deprotect the acetal groups in order to regenerate the two ketone moieties

at the K-region back. However, in diverse acids, the acetal protecting groups were removed first, which most likely generated a pyrene core which was too deactivated to permit the ring closure to take place. Therefore, we changed our julolidine-like donor moiety to a diarylamine moiety. The new synthesis route is depicted in Scheme 3-5. In this final route, compound **3-3** was further transformed into the corresponding dibromo species **3-4** by a bromodeboronation reaction.<sup>[174,175]</sup>

Thus, **3-3** and  $\text{CuBr}_2$  were suspended in a mixture of THF/MeOH/ $\text{H}_2\text{O}$  (1:1:1) and the reaction mixture was stirred at 90 °C for 4 d. The Buchwald-Hartwig amination, which we performed to obtain **3-5** from **3-4** using  $\text{Pd}_2(\text{dba})_3 \cdot \text{CHCl}_3$  as the catalyst precursor and xPhos as the ligand, was achieved in a yield of 58%. The deprotection of **3-5** in a trifluoroacetic acid and water mixture (6:1) is straightforward, and compound **3-6** was obtained in 81% yield. The cyclocondensation reactions between dione **3-6** and 2,3-diaminomaleonitrile to give **3-7** or benzene-1,2-diamine to give **3-8** were performed in an ethanol/acetic acid mixture (1:1) at 80 °C for 15 h according to the procedure of Mateo-Alonso and co-workers.<sup>[233,241,244]</sup>



**Scheme 3-5.** Synthesis of the derivatives **3-3** to **3-8**.

### 3.2.2 Crystal Structure Analysis

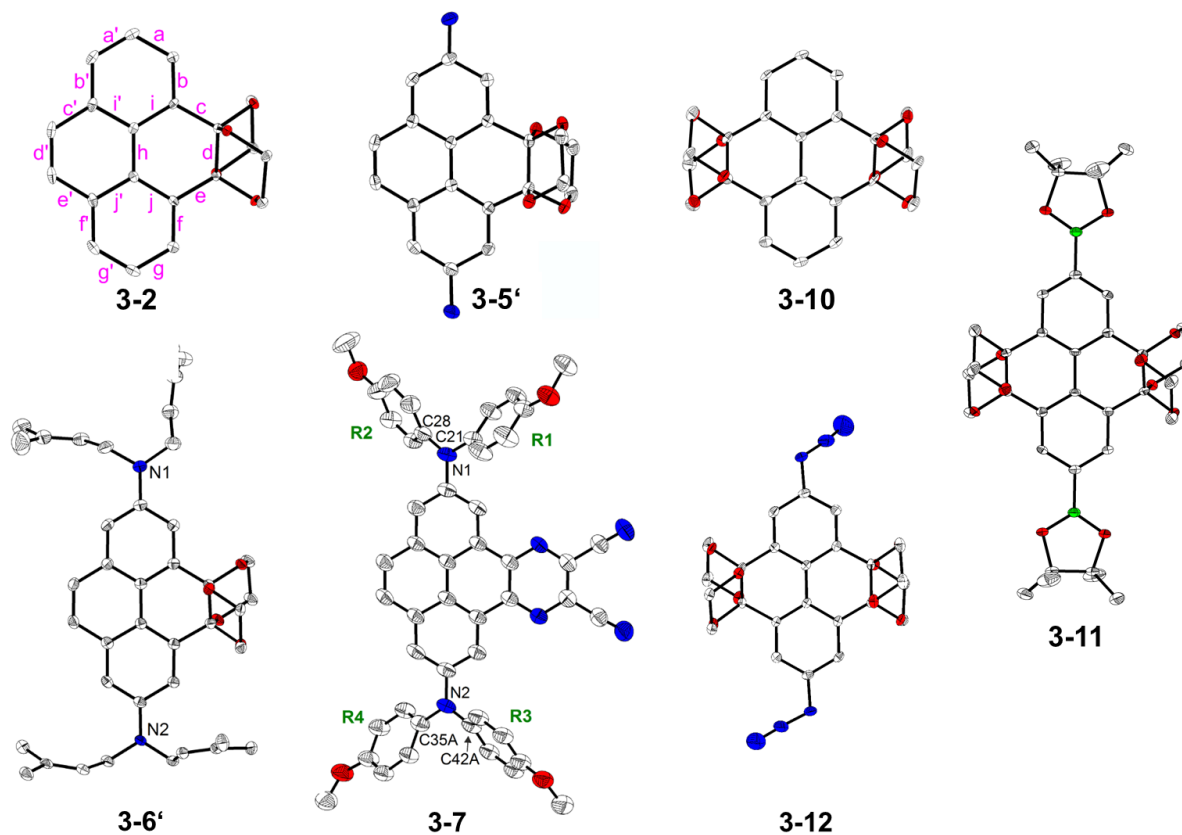


**Figure 3-2.** Solid-state molecular structures of compounds **3-2**, **3-5'**, **3-6'**, **3-7**, **3-10**, **3-11** and **3-12** as determined by single-crystal X-ray diffraction at 100 K. Hydrogen atoms, solvent molecules, and disordered parts of lower occupancies are omitted for clarity. Atomic displacement ellipsoids are shown at the 50% probability level. Element color: carbon (white), nitrogen (blue), oxygen (red) and boron (green). Representative bond labeling is shown on compound **3-2**. Aryl rings are labeled R1 to R4 in **3-7**.

The solid-state crystal structures of compounds **3-2**, **3-5'**, **3-6'**, **3-7**, **3-10**, **3-11** and **3-12** were determined *via* single-crystal X-ray diffraction (Figure 3-2). In compound **3-7**, the biphenyl unit of the pyrene moiety exhibits typical aromatic C–C bond lengths ranging from 1.391(4) to 1.418(3) Å (bonds **a**, **b**, **f**, **g**, **i**, and **j** and their symmetrical equivalents, Figure 3-2 and Table 3-2), as is also observed in pyrene. The **c'** and **e'** bonds on the unsubstituted site of the pyrene moiety are slightly longer (1.444(3) and 1.431(4) Å), and the **d'** bond (1.355(3) Å) is more typical of a C=C double bond, indicating that this site of the pyrene core obeys Clar's sextet.<sup>[245]</sup> This means that it can be viewed as a biphenyl unit constrained to be planar by a –CH=CH– group. This has also recently been observed for many other 2-, and 2,7-substituted pyrenes by Marder and co-workers.<sup>[1,47,63]</sup> Similar bond lengths have also been reported for both sides of the pyrene moiety of 2,7-Bis(dianisylamino)pyrene,<sup>[83]</sup> the azaacene-free analogue of our compound **3-7**. However, in **3-7** the **c**, **d**, and **e** bonds on the 4,5-azaacene-substituted side of the pyrene moiety are all longer than the equivalent bonds on the unsubstituted side, the **d** bond (1.426(3) Å) being shorter than the **c** and **e** bonds (1.451(3) and 1.453(3) Å) (Table S2). Hence, the substitution of the azaacene moiety on the 4,5-positions has a bond-lengthening effect, and the **d** bond can no longer be compared with a C=C double bond but rather has aromatic character. Interestingly, the azaacene-moiety also effects the central bond **h**, which links the two phenyl rings and is slightly longer (1.435(3) Å) than in the azaacene-free analogue compound (1.416(2) Å).<sup>[83]</sup>

A similar, even more pronounced effect is observed in the asymmetric compounds with acetals substituted on the 4,5-positions of pyrene, *i.e.* compounds **3-2**, **3-5'**, and **3-6'**. While the unsubstituted side of the pyrene core still shows bond distances similar to those of pyrene or compound **3-7**, the 4,5-substituted side shows long bond distances for the **c**, **d**, and **e** bonds (1.515(2)–1.555(3) Å), which are typical of C–C single bonds, indicating the loss of aromaticity and, hence, of the pyrene core character (Table 3-2). The central **h** bond is also further elongated (1.440(3)–1.447(3) Å) with respect to **3-7**. The symmetric compounds with acetals substituted on the 4,5,9,10-positions of pyrene, *i.e.* compounds **3-10**, **3-11** and **3-12** show elongated bond length as well. Thus, the **c**, **d**, **d'**, **e** and **h** bonds are elongated (Table 3-3), which indicates an even greater loss of aromaticity compared to the asymmetric derivatives **3-2**, **3-5'**, and **3-6'**. As is usually observed for aromatic amines, in compound **3-7** the N–C(pyrene) bond lengths are significantly shorter (1.406(3) and 1.415(3) Å) than the other N–C bonds of the amine moieties (1.422(3) – 1.435(2) Å). Similar distances were also reported for the azaacene-free pyrene with amines substituted at the 2- and 7- positions.<sup>[83]</sup> The nitrogen atoms have a nearly ideal trigonal

planar configuration with the sum of the C–N–C angles being between 359.0(6) and 360.0(3)°. The interplanar angles between the NC<sub>3</sub> and pyrene planes (37.45(10) for N1 and 32.3(2)–33.2(4)° for the disordered groups bonded to N2) are in a similar range as those between NC<sub>3</sub> and the terminal phenyl rings (35.2(4)–47.5(2)°) (Table 3-2). Again, this is in agreement with the NC<sub>3</sub>–pyrene angle (31°) which was reported for the analogous azaacene-free 2,7-substituted pyrene compound.<sup>[83]</sup> The phenylmethoxy groups R3 and R4 of **3-7** are strongly disordered and show a higher degree of rotational freedom than the groups R1 and R2. Indeed, the interplanar angles between the NC<sub>3</sub> and the terminal ring vary between 38.2(4) and 47.5(2)° for the disordered parts of R3 and between 35.2(4) and 39.0(6)° for those of R4. In addition, important intermolecular interactions involving the phenylmethoxy groups are only present for the R1 and R2 groups but are not observed for the R3 and R4 groups (Table 3-3).

**Table 3-2.** Selected bond lengths (Å) and angles (°) of compounds 3-2, 3-5', 3-6', and 3-7. Bonds of the pyrene moiety and of aryl rings are labelled according to the labelling in Figure 3-2.

	3-2	3-5'	3-6' <sup>a</sup>	3-7 <sup>b</sup>
a, a'	1.400(2), 1.373(3)	1.413(4), 1.380(4)	1.420(3), 1.395(3)	1.396(4), 1.392(3)
b, b'	1.379(2), 1.407(3)	1.375(4), 1.403(4)	1.377(3), 1.406(3)	1.400(3), 1.398(3)
c, c'	1.515(2), 1.436(3)	1.521(4), 1.441(4)	1.522(3), 1.440(3)	1.451(3), 1.444(3)
d, d'	1.552(3), 1.346(4)	1.549(4), 1.341(4)	1.555(3), 1.363(3)	1.426(3), 1.355(3)
e, e'	= c, c'	1.518(3), 1.445(4)	1.517(3), 1.436(3)	1.453(3), 1.431(4)
f, f'	= b, b'	1.374(3), 1.404(3)	1.382(3), 1.407(3)	1.392(3), 1.406(3)
g, g'	= a, a'	1.413(4), 1.385(4)	1.415(3), 1.393(3)	1.397(3), 1.391(4)
h	1.447(3)	1.440(3)	1.442(3)	1.435(3)
i, i'	1.407(2), 1.415(2)	1.409(3), 1.414(3)	1.411(3), 1.411(3)	1.418(3), 1.417(3)
j, j'	= i, i'	1.402(3), 1.418(3)	1.414(3), 1.409(3)	1.418(3), 1.417(3)
N1-C <sub>pyrene</sub>		1.398(4)	1.399(3)	1.406(3)
N1-C (R1)			1.460(4)	1.427(3)
N1-C (R2)			1.477(3)	1.422(3)
N2-C <sub>pyrene</sub>		1.387(4)	1.386(3)	1.415(3)
N2-C (R3)			1.460(3)	1.429(3)
N2-C (R4)			1.457(3)	1.435(2)
∠ NIC <sub>3</sub> -pyrene			13.23(17)	37.45(10)
∠ NIC <sub>3</sub> -R1				46.21(13)
∠ NIC <sub>3</sub> -R2				38.02(12)
∠ N2C <sub>3</sub> -pyrene			15.54(13)	32.3(2) / 32.7(4) / 33.2(4)
∠ N2C <sub>3</sub> -R3				47.5(2) / 38.7(4) / 38.2(4)
∠ N2C <sub>3</sub> -R4				35.5(3) / 35.2(4) / 39.0(6)
Sum ∠ CNIC			357.7(2)	359.8(2)
Sum ∠ CN2C			359.5(2)	360.0(3) / 360.0(5) / 359.0(6)

<sup>a</sup> The alkyl chains bonded to the N1 nitrogen atom are disordered. Only the distances and angles for the major part (89% occupancy) are given here. <sup>b</sup> The phenylmethoxy groups bonded to the N2 nitrogen atom are strongly disordered. Due to similar occupancies of the three parts, different values for the distances and angles are given.

**Table 3-3.** Selected bond lengths (Å) and angles (°) of compounds **3-10**, **3-11**, and **3-12**. Bonds of the pyrene moiety are labelled according to the labelling in Figure 3-2.

	<b>3-10</b>	<b>3-11</b>	<b>3-12</b>
a, a'	1.380(4), 1.392(4)	1.392(4), 1.396(4)	1.397(3), 1.393(3)
b, b'	1.399(4), 1.385(4)	1.381(3), 1.396(3)	1.386(3), 1.389(3)
c, c'	1.520(4), 1.523(4)	1.510(4) 2x	1.518(3), 1.517(3)
d, d'	1.544(4), 1.544(4)	1.548(3) 2x	1.547(3), 1.553(3)
e, e'	1.523(4), 1.523(4)	= c, c'	1.519(3), 1.524(3)
f, f'	1.391(4), 1.394(4)	= b, b'	1.386(3), 1.392(3)
g, g'	1.389(4), 1.375(4)	= a, a'	1.389(4), 1.397(3)
h	1.473(4)	1.474(4)	1.466(3)
i, i'	1.401(4), 1.401(4)	1.400(3), 1.400(4)	1.395(3), 1.406(3)
j, j'	1.400(4), 1.398(4)	= i, i'	1.407(3), 1.397(3)
N1/BI-C <sub>pyrene</sub>		1.557(4)	1.404(3)
N2-C <sub>pyrene</sub>			1.407(3)

In the crystal structure of **3-7**, the molecules form  $\pi\cdots\pi$ -stacked dimers related by inversion symmetry. Hence, a  $\pi$ -stacking interaction with an interplanar separation of ca. 3.41–3.47 Å is present between the pyrene core and the azaacene group. Dimers are arranged edge-to-face in a sandwich-herringbone packing, which is typically observed for pyrene itself and its derivatives (Figure 3-3).<sup>[42,246]</sup> Parallel and inverted molecules that are offset along the *a* axis exhibit C...C intermolecular interactions between their CN end groups. The molecular packing is further determined by the large steric demand of the amine moieties and the presence of tetrahydrofuran solvent molecules in the crystal lattice.

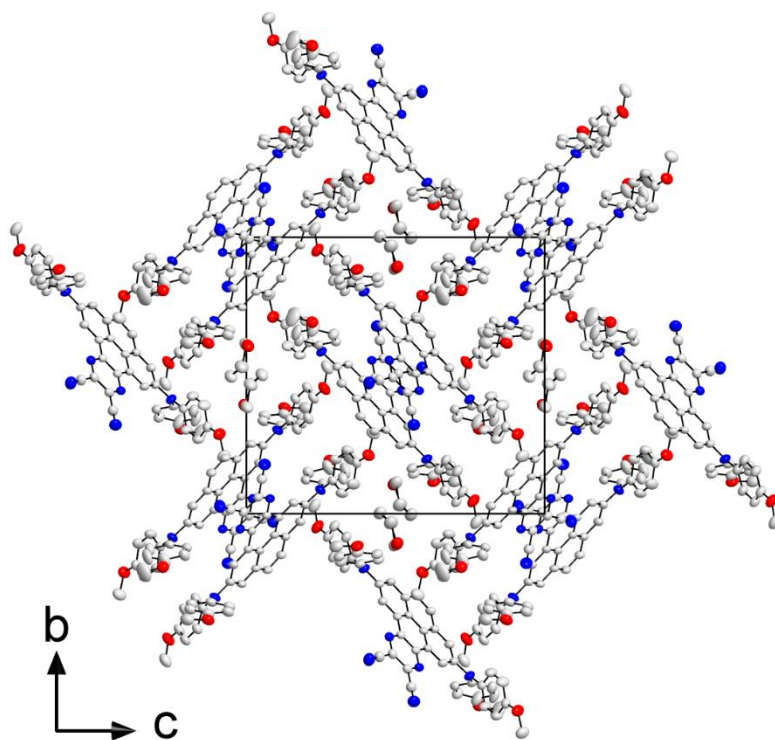


**Figure 3-3.** Crystal structure of compound **3-7** projected along the  $a$  axis, at 100 K. Hydrogen atoms and disordered parts of lower occupancies are omitted for clarity. Compound **3-7** crystallizes in a sandwich-herringbone packing wherein the herringbone is made up of sandwich-like diads with both edge-to-face and offset face-to-face interactions of  $\pi$ - $\pi$  stacked molecules that have an interplanar distance of  $X = 3.41$ - $3.47$  Å. Atomic displacement ellipsoids are shown at the 50% probability level. Element color: carbon (white), nitrogen (blue), oxygen (red).

### 3.2.3 Photophysical and redox properties

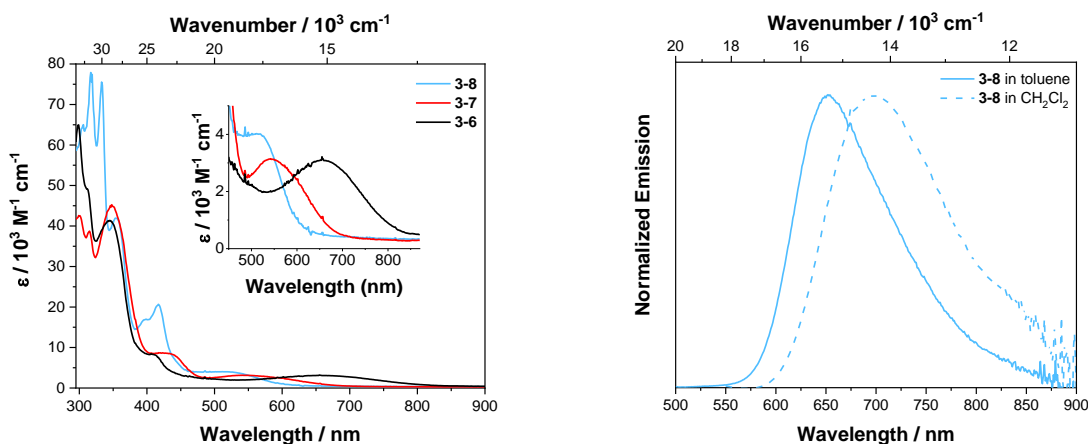


**Figure 3-4.** Absorption (left) of **3-6**, **3-7** and **3-8** recorded in toluene and emission (right) spectrum of **8** recorded in toluene and CH<sub>2</sub>Cl<sub>2</sub>.

The absorption spectra of derivatives **3-6**, **3-7** and **3-8** are depicted in Figure 3-4 and are generally similar to that of pyrene, in that the S<sub>1</sub>←S<sub>0</sub> absorption, which is a transition-dipole forbidden L<sub>b</sub> transition, is comparably weak with extinction coefficients of  $\epsilon = 2\,700\text{--}4\,000\text{ M}^{-1}\text{ cm}^{-1}$ . However, for 2,7-substituted pyrenes, these are the largest extinction coefficients reported so far. Thus, the acceptor moieties at the K-region increase the allowedness of this transition. Furthermore, the S<sub>1</sub>←S<sub>0</sub> absorption is strongly bathochromic shifted in the order **3-8** < **3-7** < **3-6**, and remarkably broad, covering a range of  $6\,000\text{ cm}^{-1}$ , with no vibrational progression, providing an indication of strong charge transfer (CT) character. In particular, dione **6** has a very pronounced bathochromic shift with  $\lambda_{\text{max}}(\text{abs}) = 658\text{ nm}$ , which is significantly stronger compared to the analogue dione **3-VI** reported by Sutherland and co-workers (Scheme 3-2).<sup>[56]</sup> However, the donor moieties in their derivative are further separated from the pyrene core by alkyne and phenyl spacers.<sup>[247]</sup> Hence, the donating ability through the 2,7-positions is reduced and, as a result, a weaker CT character is obtained. Thus, derivative **3-VI** has a smaller bathochromic shift with  $\lambda_{\text{max}}(\text{abs}) = 575\text{ nm}$  compared to derivative **3-6**. It is interesting to observe that the substituents at the 2,7-positions in these derivatives have such a significant effect on the S<sub>1</sub>←S<sub>0</sub> absorption, which is unusual. The CT character of these derivatives is even more evident when comparing them to their analogues without the donor moieties at the 2,7-positions. Mateo-Alonso and co-workers reported<sup>[235]</sup> that  $\lambda_{\text{max}}(\text{abs}) = 455\text{ nm}$  for **3-VII**, the analogue of our derivative **3-7**, which demonstrates that the resulting CT character introduced *via* the additional

donors cause a bathochromic shift of 3 500 cm<sup>-1</sup> of the S<sub>1</sub>←S<sub>0</sub> absorption in our systems. Compound **VIII**, the analogue of our derivative **3-8**, has λ<sub>max</sub> (abs) = 435 nm according to Sahoo *et al.* Hence, the CT character introduced through the additional donors at the 2,7-positions shifts the S<sub>1</sub>←S<sub>0</sub> absorption by 3 700 cm<sup>-1</sup>.

**Table 3-4.** Selected photophysical data of the derivatives **3-6**, **3-7** and **3-8** recorded under argon at room temperature.

cpd	medium	λ <sub>abs</sub> /nm (ε /10 <sup>3</sup> M <sup>-1</sup> cm <sup>-1</sup> )	λ <sub>em</sub> <sup>a)</sup> /nm	Apparent Stokes <sup>[40]</sup> shift /cm <sup>-1</sup>	τ <sup>b)</sup> /ns	φ	τ <sub>0</sub> /ns	k <sub>r</sub> /10 <sup>7</sup> s <sup>-1</sup>	k <sub>nr</sub> /10 <sup>7</sup> s <sup>-1</sup>
<b>3-6</b>	toluene	658 (2.7), 408 (7.0), 344 (41), 299 (31) 542 (3.1), 427	-	-	-	-	-	-	-
<b>3-7</b>	toluene	(8.5), 348 (48), 300 (42) 519 (4.0), 417 (21),	-	-	-	-	-	-	-
<b>3-8</b>	toluene	399 (17), 354 (42), 333 (76), 317 (78)	652	3 930	32.3	0.31	104	1.0	2.1
<b>3-8</b>	CH <sub>2</sub> Cl <sub>2</sub>	521, 416, 397, 352, 332, 316	700	4 908	8.8	0.03	293	0.3	11.0
<b>3-8</b>	solid	-	679	-	-	<0.01	-	-	-

a) Excited at the respective λ<sub>max</sub> (abs) of S<sub>1</sub>←S<sub>0</sub>.

Compounds **3-6** and **3-7** are not emissive; however, **3-8** emits in the red to NIR region of the electromagnetic spectrum with λ<sub>max</sub> (em) = 652 nm in toluene, which is intriguing for pyrenes as they usually emit in the blue region and, to the best of our knowledge, such a red-shifted emission has not been reported before for monomeric pyrenes. Even pyrene-fused azaacenes reported previously do not have such a red-shifted emission.<sup>[244]</sup> Furthermore, compound **3-8** exhibits significant solvatochromism, as the emission shifts bathochromically with increasing solvent polarity from toluene to CH<sub>2</sub>Cl<sub>2</sub> by 1 051 cm<sup>-1</sup> (48 nm), confirming the CT nature of the lowest energy excited state and a large change in dipole moment between ground and excited state. The large CT nature of the excited state becomes more evident when comparing the emission of **3-8** with previously reported analogues that only possess a donor or acceptor moiety. Derivative **3-VIII** emits in the blue region with λ<sub>max</sub> (em) = 471 nm and compound **3-IV** (unfortunately, there is no report of an emission of compound **3-III**) emits in the green region

with  $\lambda_{\max}(\text{em}) = 520 \text{ nm}$  (both in  $\text{CH}_2\text{Cl}_2$ ) while we observe a  $\lambda_{\max}(\text{em}) = 700 \text{ nm}$  for **3-8** in  $\text{CH}_2\text{Cl}_2$ .<sup>[83,236]</sup> Nevertheless, the non-radiative decay rates are significantly increased in  $\text{CH}_2\text{Cl}_2$  ( $k_{nr} = 11 \cdot 10^7 \text{ s}^{-1}$ ), which is fully in line with the energy gap law as the reorganization energy is enhanced in polar solvents.<sup>[248]</sup> Therefore, the quantum yield is strongly decreased in the polar solvent. The apparent Stokes shifts are very large for pyrenes with values ranging from 3 900 to 4 900  $\text{cm}^{-1}$  and are much larger compared to pyrenes that have D/A groups at the 2,7- or 1,3,6,8-positions only.<sup>[1,31,37,47]</sup> However, the pyrene derivatives reported by Müllen and co-workers that have D/A moieties at the K-region exhibit even larger Stokes shifts ranging from 4 500 to 5 400  $\text{cm}^{-1}$ .<sup>[38]</sup> Interestingly the radiative decay rates are rather slow ( $k_r = 0.3\text{-}1.0 \cdot 10^7 \text{ s}^{-1}$ ), which is a result of the strong CT character. However, such slow radiative rate constants are also typical for forbidden transitions (Strickler-Berg relation) and, thus, the lifetimes remain quite long ( $\tau_0 = 104\text{-}293 \text{ ns}$ ) in this derivative, which is a typical property of 2,7-substituted pyrenes.<sup>[31]</sup> There are not many reports on lifetimes of K-region substituted pyrenes, but they are typically in the range of ( $\tau_0 = 13\text{-}16 \text{ ns}$ ), which we recently reported.<sup>[249]</sup> Müllen and co-workers do not give lifetimes for their K-region D/A derivatives; however, the  $S_1 \leftarrow S_0$  absorptions are significantly more allowed with  $\epsilon > 7\,000 \text{ M}^{-1} \text{ cm}^{-1}$  and therefore, shorter lifetimes than for 2,7-substituted pyrenes can be assumed.<sup>[38,250]</sup> Compared to compound **3-8**, derivative **3-7** has a more pronounced CT nature, hence its energy gap is even smaller and, thus, it is possible that the non-radiative decay rates are largely increased, so that fluorescence becomes too weak to detect.

### 3.2.5 Redox Properties

In order to determine the impact of the acceptor groups on the K-region in combination with the donors at the 2,7-positions, cyclic voltammetry was performed. The cyclic voltammograms are shown in Figure 3 and the respective reduction and oxidation potentials are given in Table 3-3. All derivatives exhibit one reversible reduction, whereas compound **3-6** has the lowest reduction potential with  $E_{1/2} = -1.13 \text{ V}$  and **3-8** the highest with  $E_{1/2} = -1.84 \text{ V}$  vs.  $\text{Fc}/\text{Fc}^+$ . Hence, the accepting strength of our derivatives is quite strong and decreases in the order **3-6** > **3-7** > **3-8**. Furthermore, all three derivatives can be reversibly oxidized twice, whereas derivative **3-8** is the easiest to be oxidized with  $E_{1/2} = 0.17$  and  $0.39 \text{ V}$ , and derivatives **3-6** and **3-7** have equal oxidation potentials of  $E_{1/2} = 0.28$  and  $0.45 \text{ V}$  vs.  $\text{Fc}/\text{Fc}^+$ . Hence, our derivatives possess quite strong donors and the donating strength in **3-8** is only minimally influenced by the additional acceptor as compound **3-III** has oxidation potentials of  $E_{1/2} = 0.14$  and  $0.38 \text{ V}$  vs.  $\text{Fc}/\text{Fc}^+$ . A similar trend is observed in our derivative **3-6**, as the reduction potential is comparable to the analogous

derivative **3-VI**, which was reported by Sutherland<sup>[56]</sup> (Table 3-1). Consequently, the different donating abilities at the 2,7-positions do not influence the accepting effect of acceptors at the K-region. This observation is also in line with the reduction potential of our derivative **3-7**, which is very similar to that of compound **3-VII** in THF which has no donors at the 2,7-positions (Table 3-1).

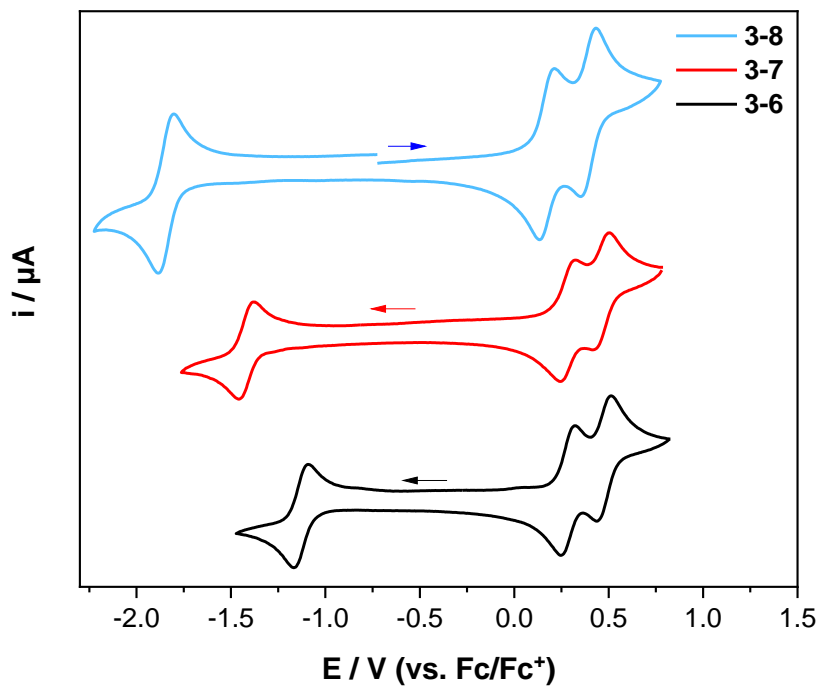


**Figure 3-5.** Cyclic voltammograms of **3-6**, **3-7** and **3-8** in  $\text{CH}_2\text{Cl}_2/0.1 \text{ M } [n\text{-Bu}_4\text{N}][\text{PF}_6]$  250 mV/s.

**Table 3-3.** Cyclic voltammetry results for **3-6**, **3-7** and **3-8** in  $\text{CH}_2\text{Cl}_2/0.1 \text{ M } [n\text{-Bu}_4\text{N}][\text{PF}_6]$  relative to the  $\text{Fc}/\text{Fc}^+$  couple.

cpd	$E_{1/2}(\text{red}) / \text{V}$	$E_{1/2}(\text{ox})^1 / \text{V}$	$E_{1/2}(\text{ox})^2 / \text{V}$
<b>3-6</b>	-1.13	0.28	0.47
<b>3-7</b>	-1.42	0.28	0.45
<b>3-8</b>	-1.84	0.17	0.39

### 3.2.6 Spectroelectrochemistry

To gain further information about the electronic structure of the corresponding  $3-7^+$ ,  $3-7^{2+}$  and  $3-8^+$ ,  $3-8^{2+}$  derivatives, we performed UV/vis/NIR spectroelectrochemical measurements in  $\text{CH}_2\text{Cl}_2/0.1 \text{ M } [n\text{-Bu}_4\text{N}][\text{PF}_6]$ .

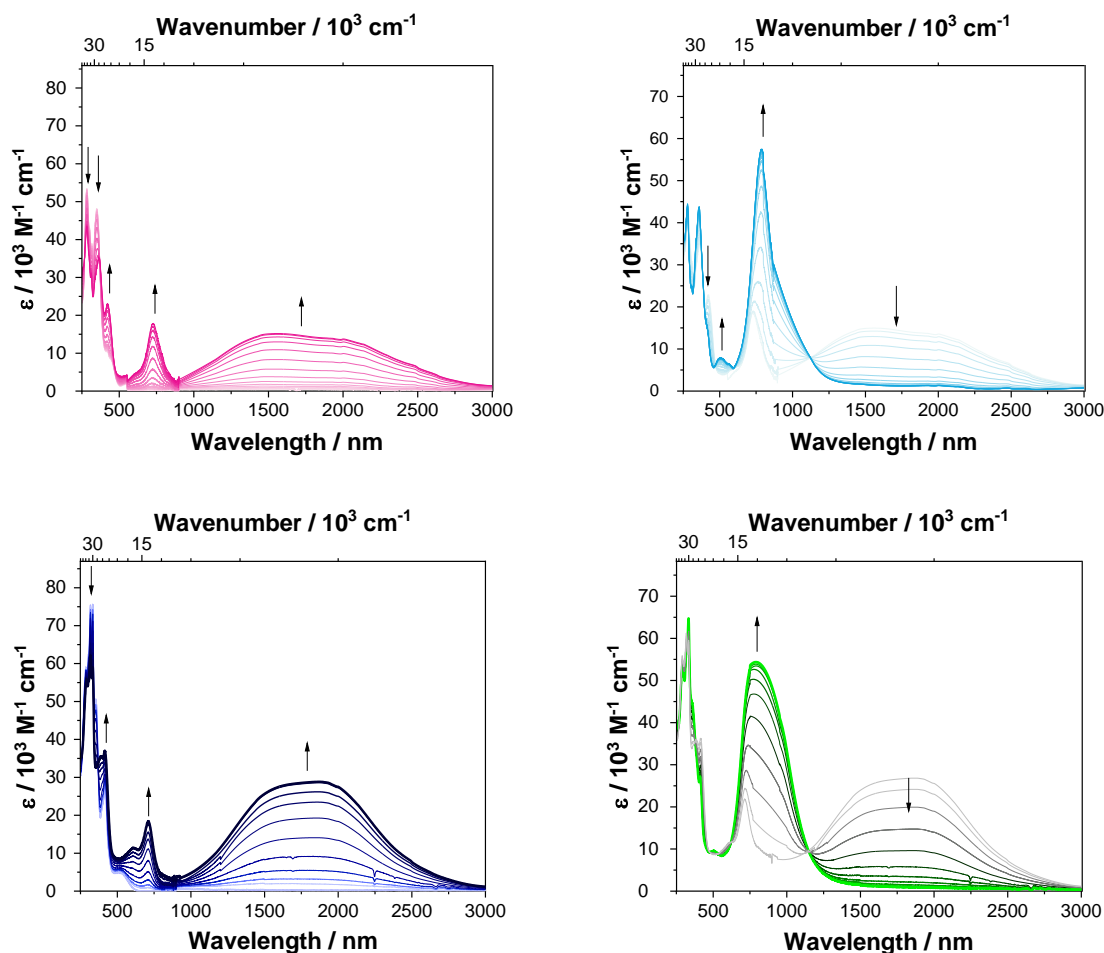


**Figure 3-4.** Spectroelectrochemical measurements of the stepwise oxidation process of  $3-7$  and  $3-8$  in  $\text{CH}_2\text{Cl}_2/0.1 \text{ M } [n\text{-Bu}_4\text{N}][\text{PF}_6]$ . Top left: absorption spectrum of  $3-7^+$  (magenta); top right: of  $3-7^{2+}$  (cyan); bottom left: of  $3-8^+$  (dark blue) and bottom right: of  $3-8^{2+}$  (green).

Upon oxidation to the respective monocations  $3-7^+$  and  $3-8^+$  a band rises in the near infrared that is very broad, covering a range of ca.  $7\,000 \text{ cm}^{-1}$ . This lowest energy band has a maximum at  $\tilde{\nu}_{max}^{IVCT} = 6\,400 \text{ cm}^{-1}$  ( $1\,563 \text{ nm}$ ,  $\epsilon = 15\,160 \text{ M}^{-1} \text{ cm}^{-1}$ ) for  $3-7^+$  and  $\tilde{\nu}_{max}^{IVCT} = 5\,350 \text{ cm}^{-1}$  ( $1\,869 \text{ nm}$ ,  $\epsilon = 28\,830 \text{ M}^{-1} \text{ cm}^{-1}$ ) for  $3-8^+$  and shows some asymmetry in its shape (Figure S1). The absorption spectra of the monocations  $3-7^+$  and  $3-8^+$  are very similar to that of compound  $3\text{-III}^+$ , which was

reported by Ito and co-workers, which lowest energy band has a maximum at  $5\,260\text{ cm}^{-1}$  (1 900 nm) and is also slightly asymmetric.<sup>[83]</sup>

Furthermore, both spectra show a band rising at 727 nm ( $13\,800\text{ cm}^{-1}$ ) and 415-421 nm ( $24\,000\text{ cm}^{-1}$ ) while the bands at 320-350 nm ( $29\,000\text{--}31\,000\text{ cm}^{-1}$ ) decrease, which is also very similar to the observations made for the oxidation to the monocation of compound **3-III**.<sup>[83]</sup> Upon further oxidation to the respective dications, the IV-CT band decreases and an intense band at 790-792 nm ( $12\,660\text{--}12\,630\text{ cm}^{-1}$ ) rises (**3-7**<sup>2+</sup>:  $\epsilon_{max} = 57\,000\text{ M}^{-1}\text{ cm}^{-1}$ , **3-8**<sup>2+</sup>:  $\epsilon_{max} = 54\,000\text{ M}^{-1}\text{ cm}^{-1}$ ) which is caused by a localized  $\pi\text{-}\pi^*$  excitation of the triarylamine radical cation.

### 3.2.7 DFT and TD-DFT calculations

To rationalize the observed trends and properties we performed DFT and TD-DFT calculations. The ground state structures were first optimized in the gas-phase at the B3LYP/6-31 G(d) level of theory. Previous studies<sup>[31]</sup> have shown that range-separated hybrid functionals are necessary to obtain a reliable picture of the nature and relative energetic ordering of the excited states in pyrenes. We have thus used the CAM-B3LYP functional for the subsequent TD-DFT calculations.

The nitrogen  $2p_z$  orbitals in both pyrene derivatives **3-7** and **3-8** mix very efficiently with the HOMO-1 of the pyrene core. This leads to a drastic destabilization of the HOMO-1 (black, Figure 3-6) by ca. 1.51 eV in **3-7** and 1.82 eV in **3-8**, which consequently switches the order of the HOMO and HOMO-1 orbitals. The pyrene-like HOMO (black, Figure 3-6), on the other hand, mixes with the acceptor unit at the K-region. Hence, the pyrene bridge and the acceptor unit are fully delocalized and thus, this orbital is stabilized by ca. 0.54 eV in **3-7** and 0.08 eV in **3-8**. A new orbital (blue, Figure 3-6) of non-bonding character with large coefficients at the nitrogens of the dianisylamine donors is energetically positioned between the pyrene-like HOMO and HOMO-1 orbitals, which was also observed for derivative **3-IX**. The LUMOs of both **3-7** and **3-8** are greatly delocalized over the acceptor units and the pyrene bridge. Hence, these orbitals are considerably stabilized, with the LUMO of **3-7** stabilized by 1.08 eV, and of **3-8** by 0.52 eV compared to the one in pyrene. This pronounced stabilization of the LUMOs in **3-7** and **3-8** is reflected in our cyclic voltammetry studies by the remarkably low reduction potentials of -1.42 V and -1.84 V vs. Fc/Fc<sup>+</sup>, respectively. The pyrene LUMO and LUMO+1-like orbitals (grey, Figure 3-6) are not significantly effected in **3-7** and **3-8**. The pyrene LUMO-like still delocalized over the acceptor

unit and the pyrene core, while the pyrene LUMO+1-like orbital is delocalized over the dianisylamine donors and the pyrene core.

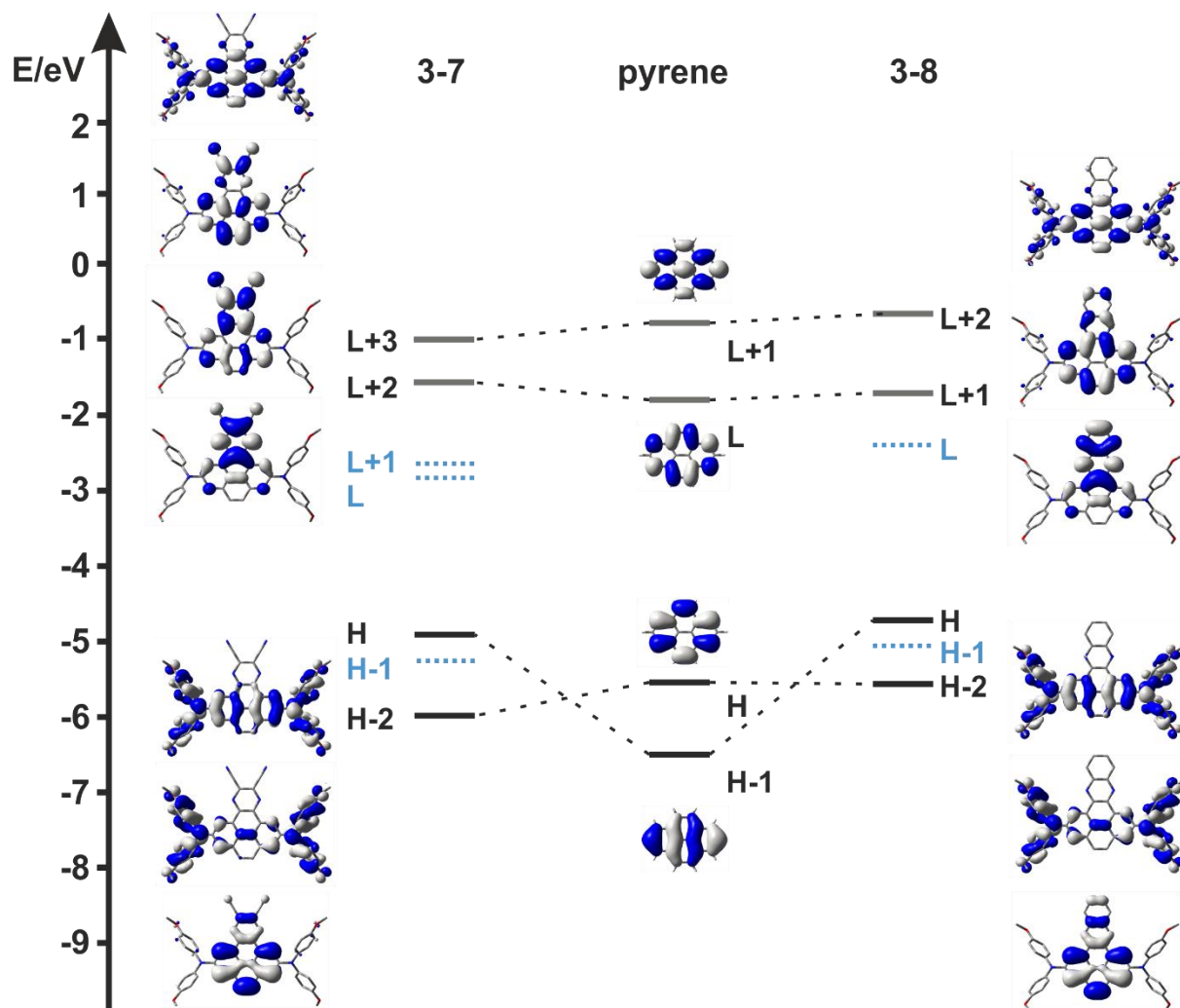


Figure 3-6. Molecular orbital diagram with orbital depictions of pyrene, 3-7 and 3-8.

The TD-DFT calculations show that the nature of the  $S_1 \leftarrow S_0$  transition changed in such a way that it is no longer a nearly 50:50 weighted configuration interaction of HOMO-1  $\rightarrow$  LUMO and HOMO  $\rightarrow$  LUMO+1 as in pyrene anymore (Table 3-5). In the pyrene derivatives 3-7 and 3-8, the  $S_1 \leftarrow S_0$  transitions are nearly pure HOMO  $\rightarrow$  LUMO transitions, which have a strong CT nature (Figure 3-6). Therefore, this transition is strongly bathochromically shifted and has low oscillator strengths in the order 3-7 > 3-8, which matches well with the absorption maxima and

extinction coefficients that were measured for this band (**3-7**:  $\lambda_{\max}(\text{abs}) = 542 \text{ nm}$ ,  $\epsilon = 3\,100 \text{ M}^{-1} \text{ cm}^{-1}$  and **3-8**:  $\lambda_{\max}(\text{abs}) = 519 \text{ nm}$ ,  $\epsilon = 4\,000 \text{ M}^{-1} \text{ cm}^{-1}$ ).

**Table 3-5.** TD-DFT results (CAM-B3LYP/6-31 G(d)) for the five vertical transitions of pyrene, **3-7** and **3-8**.

	FC-S <sub>n</sub>	E / eV (E / nm)	f	Configuration (major contribution > 10%)
<b>pyrene</b>	S <sub>1</sub>	3.99 (311)	0.000	H-1→L (49%), H→L+1 (50%)
	S <sub>2</sub>	4.02 (309)	0.323	H→L (67%), H-1→L+1 (23%)
	S <sub>3</sub>	4.90 (253)	0.000	H-2→L (21%), H→L+2 (67%)
	S <sub>4</sub>	5.10 (243)	0.000	H-2→L (66%), H→L+2 (19%)
	S <sub>5</sub>	5.11 (243)	0.414	H-1→L (50%), H→L+1 (49%)
<b>7</b>	S <sub>1</sub>	2.69 (461)	0.071	H→L (90%)
	S <sub>2</sub>	2.76 (449)	0.047	H→L+1 (84%)
	S <sub>3</sub>	3.40 (365)	0.059	H-1→L (66%), H-2→L (18%)
	S <sub>4</sub>	3.43 (361)	0.005	H-1→L+1 (79%)
	S <sub>5</sub>	3.57 (348)	0.167	H-2→L (72%), H-1→L (20%)
<b>8</b>	S <sub>1</sub>	2.93 (423)	0.120	H→L (90%)
	S <sub>2</sub>	3.19 (398)	0.006	H→L+1 (66%), H-2→L (12%)
	S <sub>3</sub>	3.63 (342)	0.390	H-2→L (75%), H→L+1 (15%)
	S <sub>4</sub>	3.64 (341)	0.002	H-8→L (90%)
	S <sub>5</sub>	3.76 (330)	0.000	H-1→L (82%)

### 3.3 Conclusions

New D- $\pi$ -A pyrene derivatives that have diarylamine donor moieties at the 2,7-positions, respectively, and an acceptor group at the K-region were synthesized and characterized. Although it was not possible to synthesize a D- $\pi$ -A derivative with julolidine-like donors at the 2,7-positions (as a follow-up of chapter 1), new pyrenes with an outstandingly strong CT character were achieved. Hence, the influence of the diarylamine donors through the 2,7-positions in combination with the acceptors through the K-region is remarkably strong.

Thus, all three target D- $\pi$ -A pyrene derivatives possess very unusual low-energy  $S_1 \leftarrow S_0$  absorptions of up to 800 nm, and, moreover, compound **3-8** emits at  $\lambda_{\max}(\text{em}) = 700$  nm in  $\text{CH}_2\text{Cl}_2$ , which is the strongest bathochromically shifted emission reported so far for monomeric pyrenes. This is remarkable in many regards, for one, pyrenes usually emit in the blue region and a strong influence on the  $S_0$  and  $S_1$  state in these derivatives is achieved through the donors at the 2,7-positions although there is a nodal plane usually passing through these positions. Furthermore, the intrinsic lifetimes remain rather long ( $\tau_0 = 104\text{-}293$  ns), which is a typical property of 2,7-substituted pyrenes, whereas the excited states of K-region substituted pyrenes live only ca.  $\tau_0 = 13\text{-}16$  ns.

Cyclic voltammetry studies reveal two reversible one-electron oxidations and one reversible reduction for all three derivatives **3-6**, **3-7** and **3-8**, with very low potentials showing the unique donating and accepting properties of these derivatives. Spectroelectrochemical measurements of the monocations of the derivatives **3-7** and **3-8** show a strong IV-CT band rising between 1 000-3 000 nm ( $10\ 000\text{-}3\ 300\ \text{cm}^{-1}$ ) that is similar to the band observed in compound **3-III**<sup>+</sup>. Thus, the acceptors at the K-region effect the properties of the monocation only to a small extend.

According to the performed DFT calculations all these properties are a result of the strong donors and acceptors that couple very well with the pyrene core. The nitrogen  $2p_z$  orbitals mix very well with the HOMO-1 of the pyrene core. This leads to a drastic destabilization of that orbital and consequently the order of the HOMO and HOMO-1 orbitals is switched. Therefore, the HOMO in these D- $\pi$ -A pyrene derivatives is fully delocalized over the bridge and there is no nodal plane going through the 2,7-positions. Furthermore, the TD-DFT calculations show that the nature of the  $S_1 \leftarrow S_0$  transition changed in such a way that it is no longer a nearly 50:50

---

weighted configuration interaction of HOMO-1→LUMO and HOMO→LUMO+1 as in pyrene anymore, but a nearly pure HOMO→LUMO transition with strong CT character.



**Chapter 4**  
Iridium-Catalyzed  
C–H  
Borylation of  
4-Quinolones



## 4 Iridium Catalyzed C–H Borylation of 4-Quinolones

### 4.1 Introduction to C–H Activation

The direct functionalization of unreactive hydrocarbons on aryl (but also alkyl and alkenyl) moieties gives access to a huge range of organic molecules, and several groups have made progress toward selective conversions of aryl C–H bonds to C–C, C=C, C–O, C–N, and C–X (X = F, Cl, Br, and I) bonds among others.<sup>[43,251]</sup> The number of methods for C–H bond functionalization increased dramatically in the last few decades as these conversions give new options for efficient strategies for fine chemical synthesis and are consequently of great importance particularly for the chemical industry.<sup>[252]</sup> However, the catalytic conversion of C–H bonds to C–B bonds is a relatively recent development in synthetic chemistry. Aryl boronates, especially aryl boronic acids and – esters, are an important class of compounds that have been applied as synthetic intermediates extensively due to the fact that they can be converted to diverse functional groups (Figure 4-1).<sup>[45,253]</sup> Great advances in the development of novel methodologies towards aryl boronates have been made particularly since the report of the palladium-catalyzed cross-coupling reaction with aryl halides by Suzuki and Miyaura in 1979.<sup>[254]</sup> Moreover, compared to other organometallic carbon nucleophiles, aryl boronates are most frequently used as they possess low toxicity, are easy to handle and have a high functional group compatibility.<sup>[45]</sup> Organoboron derivatives also find considerable use in biological and medical fields, *i.e.* as receptors and sensors for carbohydrates and other small molecules,<sup>[45]</sup> as <sup>10</sup>B carriers for neutron capture therapy or as drugs themselves.<sup>[255]</sup>

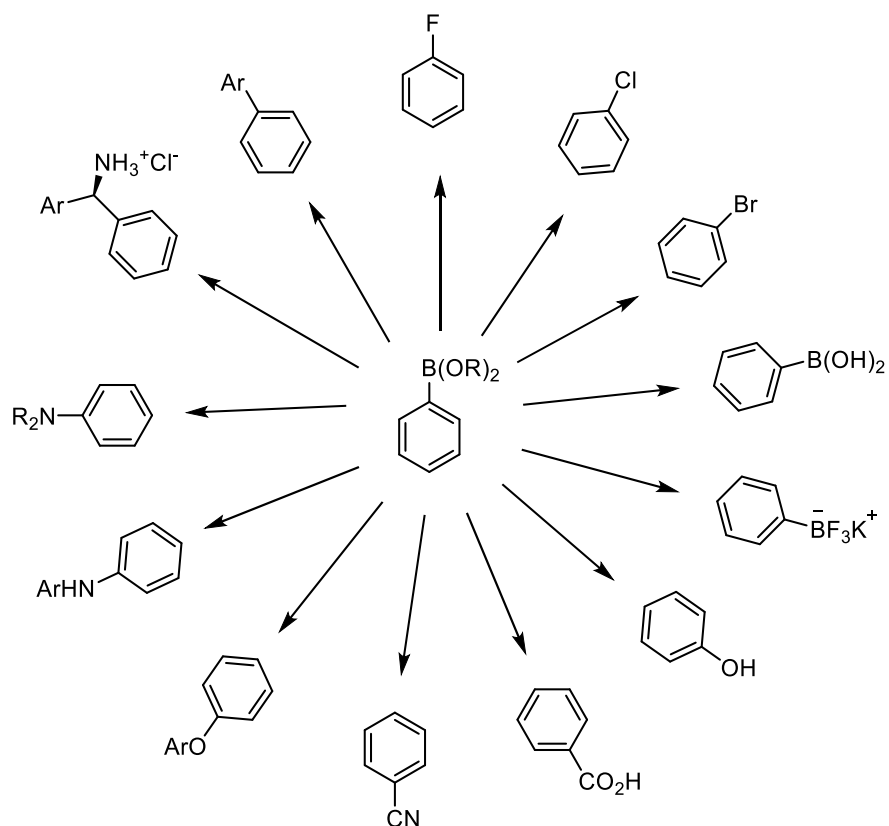
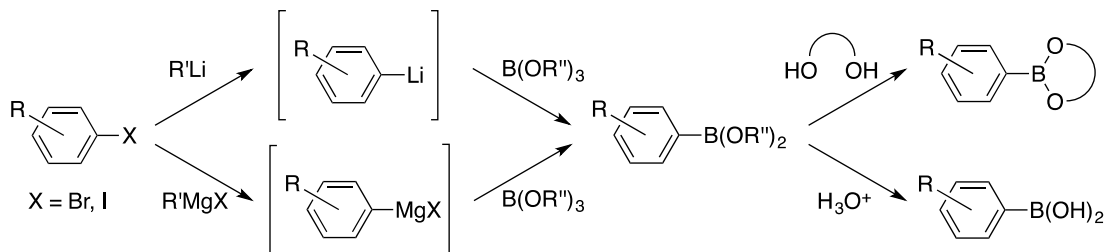


**Figure 4-1.** Overview of the reactions of organoboron compounds.<sup>[45]</sup>

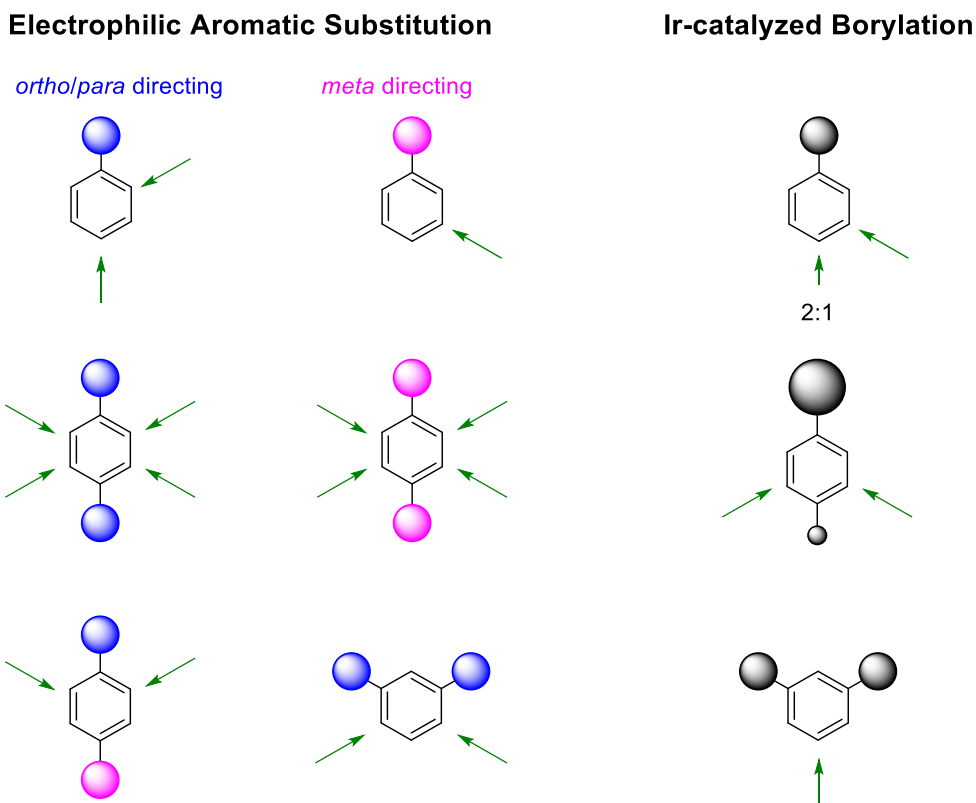
The classic way to synthesize aryl boronates involves the reaction of air- and water-sensitive organometallic intermediates, such as lithium or Grignard reagents, with a borate ester at low temperatures. This method is quite efficient for simple boron compounds. The conversion to the final boronic acid or ester is accomplished by the addition of either an acid (hydrolysis) or a diol (transesterification), respectively (Scheme 4-1).<sup>[43,45]</sup>



**Scheme 4-1.** Classic syntheses of aryl boronate esters and acids.<sup>[43]</sup>

A more recently developed method is based on transition metal-catalyzed coupling reactions of aryl halides (C-X) with mono- or diboron reagents, *i.e.* pinacolborane (H-Bpin) and bis(pinacolato)diboron (B<sub>2</sub>pin<sub>2</sub>).<sup>[256]</sup> Thus, various palladium-,<sup>[256]</sup> nickel-,<sup>[257]</sup> zinc-,<sup>[258]</sup> copper-<sup>[259]</sup> and cobalt-based<sup>[260]</sup> catalysts for C-X borylation reactions have been reported.<sup>[261]</sup> However, since their synthesis is still often based on using a halogenated precursor, the availability of aryl boronates is linked to the availability of the adequately substituted aryl halides.

The direct C-H borylation of aromatic substrates found increasing attraction as this transformation can be performed in a single preparative step, thus it is more economic, efficient, mild and elegant compared to the classic methods. These direct borylation methods granted the path to novel classes of organoboron compounds without relying on the accessibility of aryl halides. However, not only the utility of the products but also the unique selectivity of this reaction is advantageous, which is sterically controlled while the regioselectivity in traditional aromatic substitutions is determined by electronic effects.<sup>[32,43]</sup> Moreover, electrophilic aromatic substitution reactions are dependent on the substituents as there are two classes: *ortho-/para*-directors and *meta*-directors. Thus, substituted benzenes usually do not give well-defined regiochemical products especially with *ortho-/para*-directors (Scheme 4-2). Furthermore, aryls with electron-deficient substituents are deactivated towards electrophilic aromatic substitution reactions. Disubstituted aryls, in particular 1,4-disubstituted aryls, are challenging as *ortho-/para*-directors and *meta*-directors give both low regioselectivity.<sup>[262]</sup> Thus, *meta* functionalization of 1,3-disubstituted aryls with electron-donating substituents or halogens is impossible *via* electrophilic aromatic substitution.<sup>[263]</sup> Maleczka, Smith and co-workers among others showed how versatile this unique regioselectivity of C-H borylations is by reporting on a one-pot unified route to *meta*-substituted phenols that have *ortho-/para*-directing groups at the 1- and 3-positions.<sup>[264]</sup> The traditional synthesis of *e.g.* 3-bromo-5-chloro-phenol consisted of 10 steps starting from TNT (2,4,6-trinitrotoluene).<sup>[264,265]</sup> Hence, the Ir-catalyzed C-H borylation offers an alternative selectivity, which significantly eases and reduces the synthesis routes to diverse aryls.

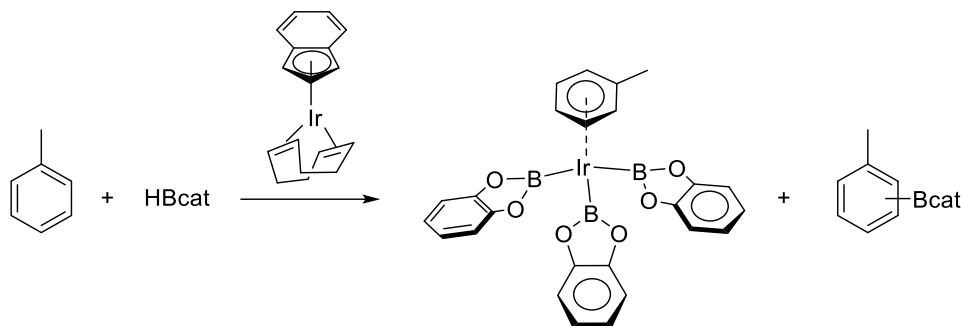


**Scheme 4-2.** Schematic overview of the regiochemical trend in electrophilic aromatic substitution and Ir-catalyzed borylation reactions of some substituted aryls.

Several catalytic C–H borylation methodologies have been developed for aryls in the last few years one of those methods is the iridium-catalyzed C–H borylation. This method has been used earlier in this thesis to selectively borylate pyrene and perylene and the following pages provide a more detailed overview of the mechanism and applicability of this method.

#### 4.1.1 Overview of the Development of the $[\text{Ir}(\text{OMe})\text{COD}]_2/\text{dtbpy}$ Catalytic System

In 1993, Marder and co-workers reported the first synthesis of a trisboryl iridium complex and noted that during the reaction of excess H–Bcat (cat = 1,2- $\text{O}_2\text{C}_6\text{H}_4$ ) and  $[(\eta^5\text{-indeny})\text{Ir}(\text{COD})]$  (COD = 1,5-cyclooctadiene) in aryl solvents (aryl =  $\text{C}_6\text{H}_6$ ,  $\text{C}_6\text{D}_6$ ,  $\text{C}_6\text{H}_5\text{Me}$  and 1,3,5- $\text{C}_6\text{H}_3\text{Me}_3$ ) the respective trisboryl compounds  $[(\eta^6\text{-aryl})\text{Ir}(\text{Bcat})_3]$  were formed, but interestingly, small amounts of borylated aryls were also detected by GC-MS. They recognized two isomers of tolylboronate esters as side products arising from the borylation of the toluene solvent and included this results in their supporting information (Scheme 4-3).<sup>[266]</sup>

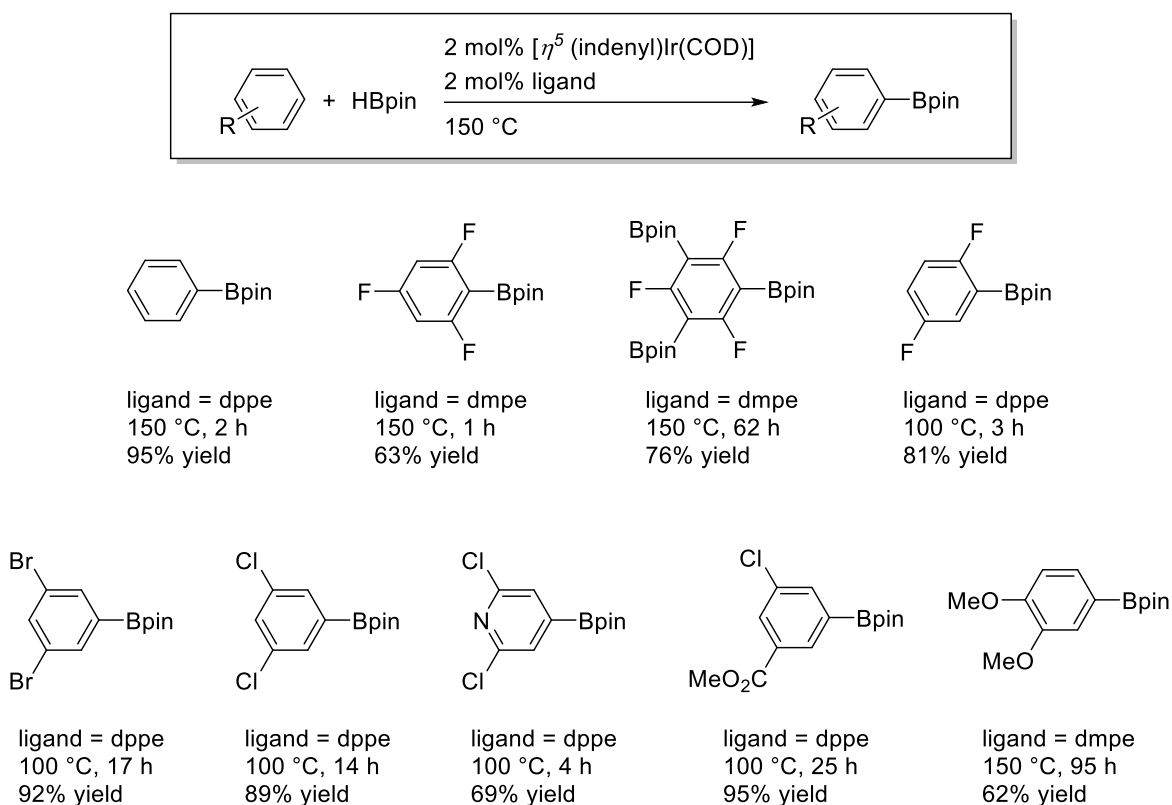


**Scheme 4-3.** First observed Ir-catalyzed C–H borylation by Marder and co-workers.<sup>[266]</sup>

In 1999, Smith and Iverson showed that 17 mol% of  $\text{Cp}^*\text{Ir}(\text{PMe}_3)(\text{H})(\text{Bpin})$  catalyzes the borylation of deuterated benzene at 150 °C with 5 eq HBpin to form  $\text{C}_6\text{H}_5\text{Bpin}$  in 53% yield.<sup>[267]</sup> The scope of this reaction was further investigated by the same group and they found out that the precatalyst  $[\text{Cp}^*\text{Ir}(\text{PMe}_3)(\text{H})(\text{Bpin})]$  can borylate a range of mono- and disubstituted aryls.<sup>[268]</sup> *Ortho* borylation with this catalytic system is hardly observed while the *para/meta* positions are statistically distributed (ca. 1:2) in mono-substituted derivatives. However, 1,3-disubstituted aryls are exclusively borylated at their *meta* position providing 1,3,5-trisubstituted aryls.<sup>[268]</sup> Interestingly, the yields and the reaction rates appeared to be higher with electron-deficient than with electron-rich compounds.<sup>[268,269]</sup> Compared to Hartwig's rhodium based precatalyst  $[\text{Cp}^*\text{Rh}(\eta^5\text{-C}_6\text{Me}_6)]$  or Marder's rhodium based precatalyst  $[[\text{RhCl}(\text{P}i\text{Pr}_3)_2(\text{N}_2)]]$ , the iridium based precatalyst was more selective towards aryl C–H activation. However, the turnover numbers (TONs) were too low.<sup>[268,269,270]</sup>

Further investigations revealed that iridium systems containing phosphine or nitrogen based ligands catalyze the C–H borylation of aryls with much higher rates and higher yields compared to the first systems with  $\text{Cp}^*$  ligands that also required elevated temperatures ranging from 150–200 °C.<sup>[262,271]</sup> Smith and co-workers used the observations made by Marder and co-workers in 1993 and developed an analogous trisboryl Ir-complex,  $[\eta^6\text{-C}_6\text{Me}_6\text{Ir}(\text{Bpin})_3]$  and  $[\eta^5\text{-(indenyl)Ir}(\text{COD})]$ .<sup>[272]</sup> In combination with the phosphine-containing ligands  $\text{PMe}_3$ , dppe (1,2-bis(diphenylphosphino)ethane) or dmpe (1,2-bis(dimethylphosphino)ethane) and the boron source HBpin they were able to obtain increased activity and TONs (up to 4500) for the borylation of diverse aryls. Numerous different aryls that are electron-deficient or electron-rich reacted with HBpin in the presence of  $[\eta^5\text{-(indenyl)Ir}(\text{COD})]$  and dppe or dmpe regardless whether the aryls possessed halogens, alkoxides, esters or were heteroaromatic compounds

(Scheme 4-4). The reaction of benzene with HBpin catalyzed by  $[\eta^6\text{-(C}_6\text{Me}_6\text{)Ir(Bpin)}_3]$  and  $\text{PMe}_3$  at 150 °C afforded the monoborylated product in 98% yield after 15 h. With the precatalyst  $[\eta^5\text{-(indenyl)Ir(COD)}]$  and the ligand  $\text{PMe}_3$  a yield of 88% for the same reaction could be obtained after 18 h, while the combination of  $[\eta^5\text{-(indenyl)Ir(COD)}]$  and the ligand dppe yielded even 95% borylated benzene after only 2 h.<sup>[272]</sup> Among others, it was also possible to obtain a threefold borylation of 1,3,5-trifluorobenzene by using 4 equivalents of HBpin and a longer reaction time.<sup>[272]</sup>

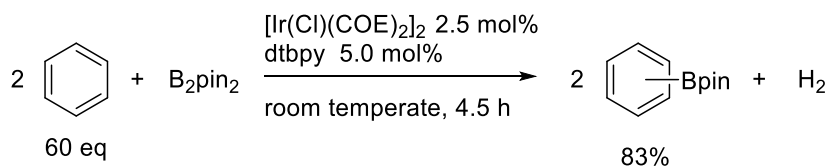


**Scheme 4-4.** Some examples of borylated aryls reported by Smith and co-workers with HBpin and combination of the precatalyst  $[\eta^5\text{-(indenyl)Ir(COD)}]$  and the ligand dppe (1,2-bis(diphenylphosphino)ethane) or dmpe (1,2-bis(dimethylphosphino)ethane).<sup>[272]</sup>

Meanwhile in 2002, Ishiyama, Miyaura, Hartwig and co-workers focused on Ir-catalyzed C–H borylation systems that are based on nitrogen-containing ligands, which seemed to be even more effective than those that are based on phosphine-containing ligands.<sup>[43,262]</sup> They used the commercially available iridium(I) precatalyst  $[\text{Ir}(\text{Cl})\text{COD}]_2$  in combination with bpy (2,2'-bipyridine) or dtbpy (4,4'-di-*tert*-butyl-2,2'-bipyridine) as the ligands and  $\text{B}_2\text{pin}_2$  as the boron source and were able to obtain effective borylations of mono- and disubstituted aryls at 80 °C in

high yields and a maximum of even 8000 TONs. The products of monosubstituted aryls gave regioisomeric mixtures of *meta* and *para* borylation in statistical ratios (ca. 2:1) as was reported for the iridium-phosphine system (*vide supra*). Borylation *ortho* to a substituent was not observed so that 1,2- and 1,4-disubstituted aryls (with two identical substituents) provided only one product and the yields were lower for the latter systems due to steric hindrance.<sup>[262]</sup> In addition, there is a small electronic effect that directs the C–H borylation to the more electron-deficient carbon if the steric effects allow it.<sup>[273]</sup> Furthermore, they also noticed that electron-deficient aryls undergo borylation reactions more effective than electron-rich aryls (*vide supra*). In order to investigate this further, they made three different equimolar mixtures (1) of trifluorobenzene and toluene, (2) trifluorobenzene and anisole and (3) of toluene and anisole and afforded the corresponding arylboronate esters in ratios of 90:10 for (1), 85:15 for (2) and 40:60 for (3). Consequently, the borylation of electron-deficient aryls must occur faster than of electron-rich aryls.

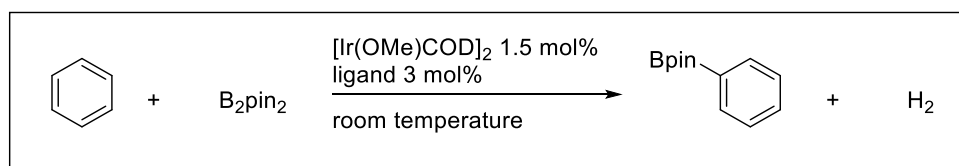
The analysis of the early stages of the reaction between benzene-*d*<sub>6</sub> and the catalytic system B<sub>2</sub>pin<sub>2</sub>, [Ir(Cl)COD]<sub>2</sub> and bpy revealed an induction period in which COD was reduced to COE-*d*<sub>2</sub>, which Marder and co-workers noted in 1993 already.<sup>[262,266]</sup> Therefore, the authors developed the precatalyst [Ir(Cl)COE]<sub>2</sub> to skip this induction period, which enabled the borylation of benzene even at room temperature in only 4.5 h (Scheme 4-5). In addition, they used the ligand dtbpy instead of bpy as the *tert*-butyl moieties make the catalyst more soluble and protect the ligand from borylation. This was the first example of a metal catalyzed borylation of aryls that occurred at room temperature.



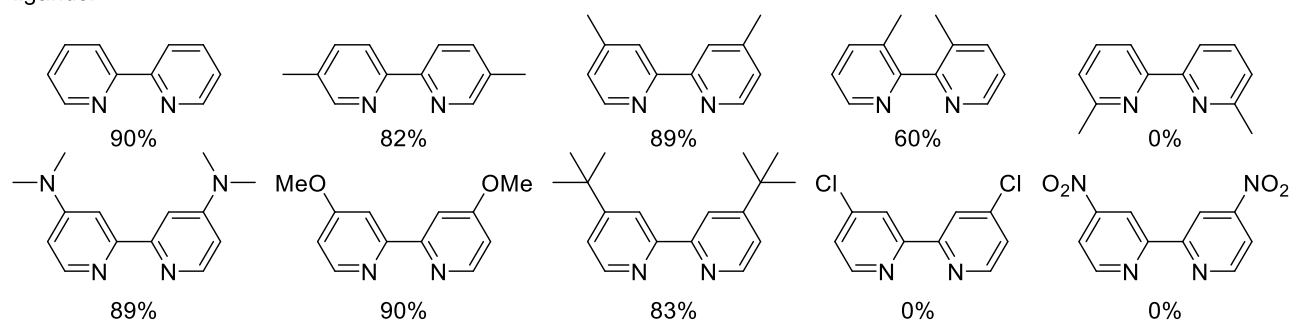
**Scheme 4-5.** First reported Ir-catalyzed room temperature borylation of aryls.<sup>[274]</sup>

Further optimization studies showed that a greater effect on the catalyst activity could be achieved by varying the anionic ligands of the precatalyst.<sup>[274]</sup> Thus, different [Ir(X)COD]<sub>2</sub> complexes (X = Cl, BF<sub>4</sub>, OH, OPh, OMe, OAc) were combined with the ligands bpy and B<sub>2</sub>pin<sub>2</sub> to borylate benzene at room temperature. The conclusion of this study was that strongly basic

and nucleophilic anions such as OMe, OH or OPh enhanced the facile formation of Ir(III) tris(boryl) complex, which is the key intermediate in the catalytic borylation of aryls (*vide infra*). Furthermore, diverse bpy ligands were investigated to probe the electronic and steric effects of the ligand on the borylation (Scheme 4-6).<sup>[274]</sup>



ligands:



**Scheme 4-6.** Borylation of aryls at room temperature with  $\text{B}_2\text{pin}_2$  catalyzed by the combination of  $[\text{Ir}(\text{OMe})\text{COD}]_2$  and 2,2'-bipyridine ligands.<sup>[274]</sup>

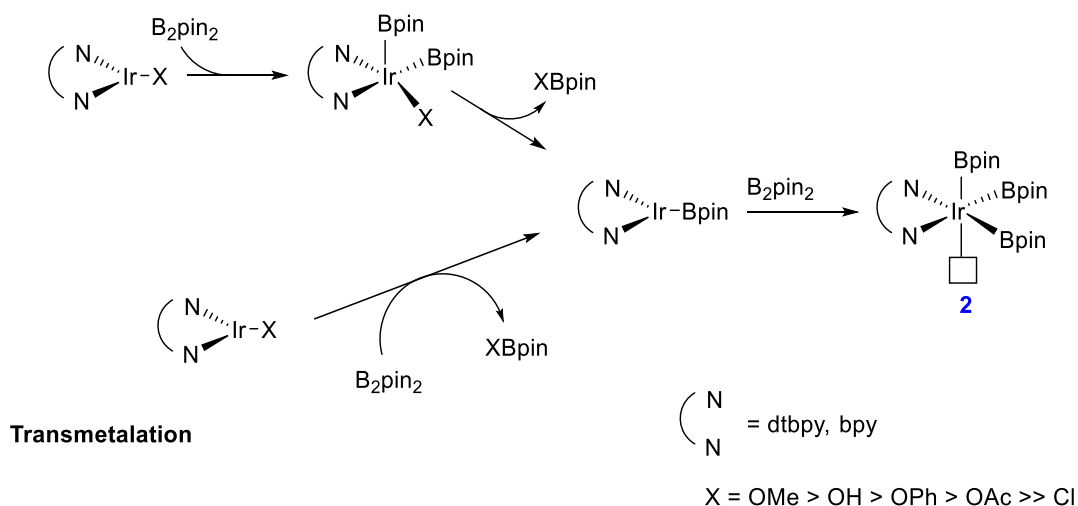
The yields show that there is not a large difference between 4,4'- and 5,5'-dimethyl-2,2'-bipyridine at room temperature.<sup>[274]</sup> However, 3,3'-dimethyl-2,2'-bipyridine was significantly less effective and consequently gave moderate yields. Thus, a coplanar arrangement of the two pyridine rings is favored. The 6,6'-dimethyl-2,2'-bipyridine derivative on the other hand, inhibited the borylation of benzene completely. Therefore, it was suggested that the methyl groups in this derivative prevent the ligand from binding tightly to the iridium center.<sup>[43,274]</sup> Furthermore, electron-rich ligands containing  $\text{NMe}_2$  or OMe groups revealed superiority over electron-poor ligands that contain Cl or  $\text{NO}_2$  groups. Nevertheless, formed iridium complexes of the bpy, *tert*-butyl,  $\text{NMe}_2$  and OMe ligands gave comparable yields.

Ishiyama, Miyaura and co-workers presented borylation reactions in inert (non-aromatic) solvents, which is desirable for solid or expensive substrates.<sup>[274]</sup> They concluded that reactions were faster in non-polar solvents such as hexane, while they were slow in coordinating solvents such as DME or DMF.

### 4.1.2 Mechanism of the $[\text{Ir}(\text{OMe})\text{COD}]_2/\text{dtbpy}$ Catalyzed Arene C–H Borylation

Several experimental and theoretical investigations were performed to obtain details about the catalytic cycle of the Ir-catalyzed C–H borylation of arenes.<sup>[262,275,276]</sup> Early mechanistic studies indicated that an Ir(III) trisboryl complex<sup>[266]</sup> could be an intermediate in the catalytic borylation of aryls.<sup>[262,272,275]</sup> Hence, Ishiyama, Miyaura, Hartwig and co-workers synthesized  $[\text{Ir}(\text{dtbpy})(\text{COE})(\text{Bpin})_3]$  and found that dissolving this complex in benzene- $d_6$  generated borylated benzene (80% yield) within minutes at room temperature.<sup>[262]</sup> Thus,  $[\text{Ir}(\text{dtbpy})(\text{COE})(\text{Bpin})_3]$  is competent to be an active intermediate in the catalytic cycle or in equilibrium with a species in the cycle. Their results are related to what was already reported by Marder and co-workers in 1993.<sup>[266]</sup> The proposed catalytic cycle for the Ir-catalyzed C–H borylation of arenes is shown in Scheme 4-8. The combination of  $[\text{Ir}(\text{OMe})\text{COD}]_2$ , dtbpy and  $\text{B}_2\text{pin}_2$  leads to the formation of the Ir(III) trisboryl complex **1**, which was also isolated and characterized by X-ray analysis.<sup>[262]</sup> The active catalyst complex **2** can be formed either by oxidative addition of  $\text{B}_2\text{pin}_2$  to the Ir(I) precatalyst followed by reductive elimination sequence or by transmetalation (Scheme 4-7).<sup>[274]</sup>

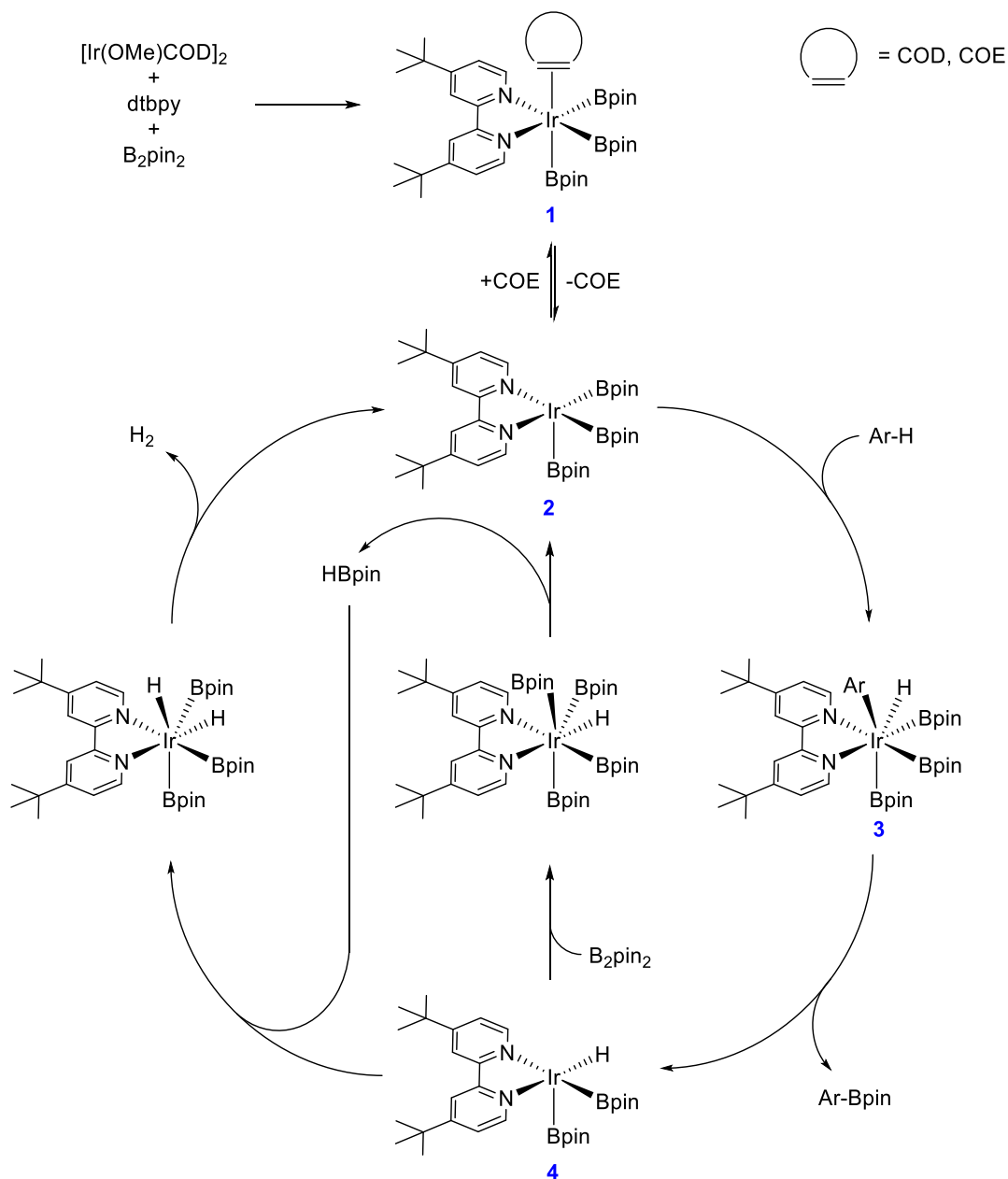
#### Oxidative Addition / Reductive Elimination



**Scheme 4-7.** Proposed formation of a Ir(III) trisboryl complex *via* a Ir(I) monoboryl complex.<sup>[274]</sup>

In both pathways, the reductive elimination of X–Bpin is favored with X = OMe due to the higher bond energy of the resulting B–O bond than that of B–Cl. Hence, the most effective precatalyst is  $[\text{Ir}(\text{OMe})\text{COD}]_2$  (*vide supra*).<sup>[274]</sup> In addition, the COD ligand is reduced to COE, which can

reversibly dissociate to form the unsaturated Ir(III) trisboryl complex **2**. Further studies by Hartwig and co-workers showed that the initial induction period, which was observed during the reaction of benzene with  $B_2pin_2$ , could be prevented through the addition of HBpin for the initiation of the reaction and thus, much faster reactions of  $B_2pin_2$  with 1,2-dichlorobenzene were obtained.<sup>[275]</sup>



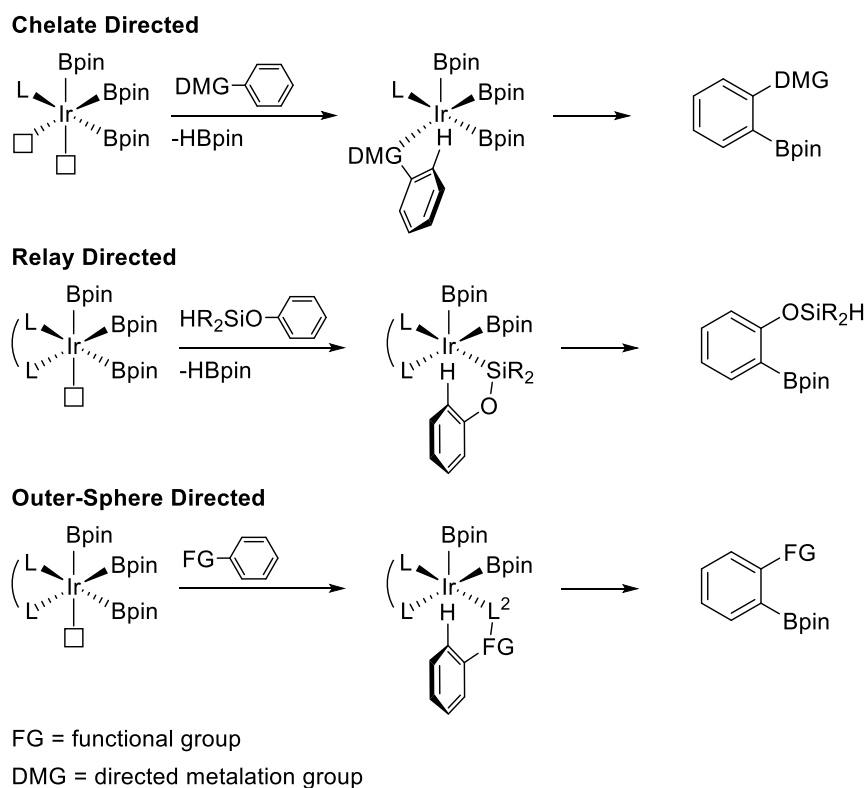
**Scheme 4-8.** Proposed catalytic cycle for the Ir-catalyzed C-H borylation.<sup>[276]</sup>

The unsaturated 16 e<sup>-</sup> Ir(III) trisboryl complex **2** then undergoes C–H activation of the arene even though the Ir(I) monoboryl complex (Scheme 4-7) was initially also considered to be the active catalyst.<sup>[275]</sup> Interestingly, theoretical studies by Sakaki and co-workers show that the Ir(III) trisboryl complex **2** species is easily formed (under these catalytic reaction conditions), while the Ir(I) monoboryl complex cannot exist as a stable species as it is more readily converted to the Ir(III) trisboryl complex **2** than it reacts with an arene.<sup>[276]</sup> That complex **2** reacts with an arene C–H bond, is fully in line with the NMR studies performed by Boller *et al.*<sup>[275]</sup> The activation of the arene by complex **2** leads to the formation of the Ir(V) intermediate **3** (Scheme 4-8). This process likely occurs by the coordination and subsequent oxidative addition of an arene C–H bond, consistent with DFT calculations of Sakaki and co-workers.<sup>[275,276]</sup> This step is selectivity determining due to the steric hindrance of the ligand dtbpy as well as its electron donation to the Ir-center and is the turnover-limiting step in this catalytic cycle.<sup>[277]</sup> The oxidative addition is favored if the arene is electron-deficient, which fits to the observed trend as such compounds show faster borylation.<sup>[43]</sup> Furthermore, Marder and co-workers observed that the ligand dtbpy remains complexed to the iridium throughout the catalytic cycle otherwise it would be borylated as well.<sup>[278]</sup> Following the oxidative addition to complex **3**, reductive elimination occurs generating the arene boronate ester. The resulting [Ir(Bpin)<sub>2</sub>(dtbpy)(H)] complex **4** reacts with another B<sub>2</sub>pin<sub>2</sub> moiety to regenerate the active catalyst. The resulting HBpin can also convert the [Ir(Bpin)<sub>2</sub>(dtbpy)(H)] complex **4** back to complex **2** by releasing H<sub>2</sub> as the sole byproduct.<sup>[275]</sup>

### 4.1.3 Directed *Ortho* Borylation

The regioselectivity of the Ir-catalyzed C–H borylation of arenes is mainly sterically controlled as the active catalyst species has only one vacant coordination site. However, in order to enable an alternation of this regioselectivity in this type of reaction different strategies have been developed (Scheme 4-9). The first reports relied on a chelate-directed mechanism, which involves the modification of the ligand.<sup>[279,280]</sup> One example was demonstrated by Sawamura and co-workers who developed a new ligand that was found to be, in combination with [Ir(OMe)COD]<sub>2</sub> and B<sub>2</sub>pin<sub>2</sub>, very effective for the synthesis of diverse *ortho* borylated arenes.<sup>[280,281,282]</sup> The reaction of B<sub>2</sub>pin<sub>2</sub> with a series of arenes containing directing groups such as ester, amide, sulfonate, acetal, alkoxymethyl, and chloro groups catalyzed by the combination of [Ir(OMe)COD]<sub>2</sub> and the silica-supported monodentate, electron-rich, caged, and compact phosphine ligand SMAP (silicon-constrained monodentate alkyl-phosphine) resulted in *ortho*-

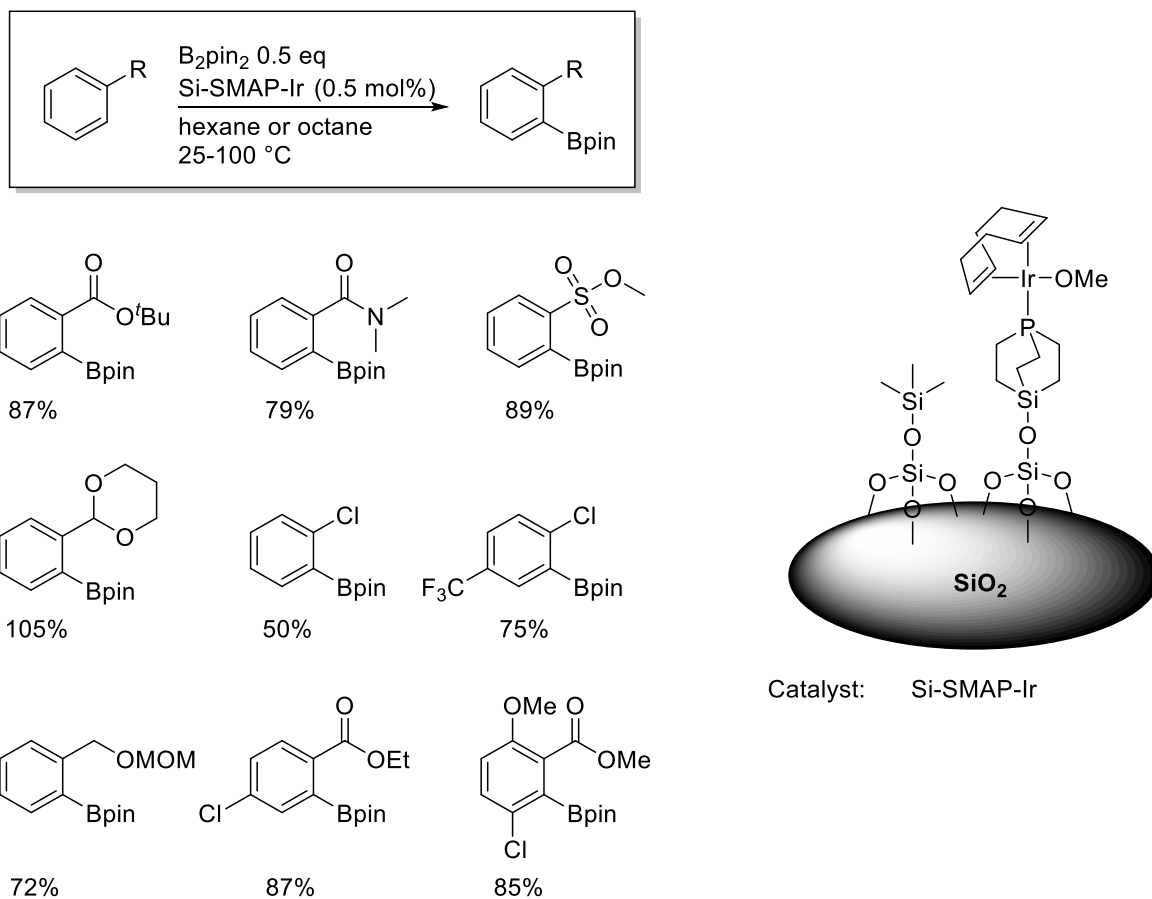
borylation under mild conditions (Scheme 4-10). Their Si-SMAP ligand contains phosphorus and silicon atoms at each bridgehead of a bicyclo[2.2.2]octane framework (Scheme 4-10).



**Scheme 4-9.** Strategies for *ortho*-directed C–H borylation.<sup>[279]</sup>

This results in a very small steric demand around the phosphorus center, which is comparable to  $\text{PMe}_3$  (trimethylphosphine) and projects the phosphorus-lone pair and the Si-substituent in diametrically opposite directions. Furthermore, DFT calculations showed that the electron donating ability of this ligand is comparable with  $\text{PMe}_3$ .<sup>[281,283]</sup> Such a rigid trialkylphosphine ligand is very unique in the literature and it provides selectively monophosphine-metal complexes such as the Ir/Si-SMAP catalyst in this case.<sup>[280,281]</sup> The methyl ester, *tert*-butyl ester, *N,N*-dimethylamide and sulfonate groups direct the borylation *via* coordination to the second vacant coordination site in the Ir *via* their  $\text{sp}^2$  oxygen atoms. MOM-protected hydroxymethyl groups (methoxymethyl) and acetal on the other hand, direct the borylation *via* their  $\text{sp}^3$  oxygen atoms.<sup>[280]</sup> Interestingly, even chlorine can direct the borylation to the *ortho* position of the substrate. However, the selectivity is slightly decreased 92:8 (*ortho*: [*meta+para*]). Even highly functionalized substrates such as methyl-2-methoxy-5-chlorobenzoate afford the respective

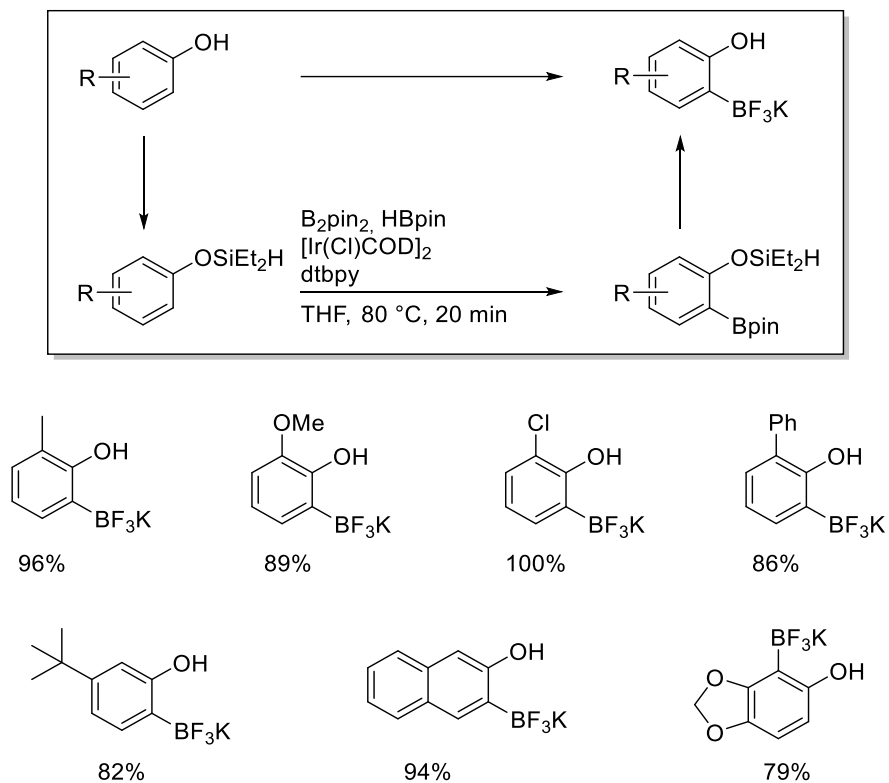
boronic ester in excellent regioselectivity and yield (Scheme 4-10). It is noteworthy that the immobilization of this ligand seems to be crucial for this reaction as no reaction was observed under the same conditions with other phosphines such as 4-CF<sub>3</sub>-Ph-SMAP, Ph<sub>3</sub>P, (*t*-Bu)<sub>3</sub>P, Cy<sub>3</sub>P, and Me<sub>3</sub>P (using 1:1 or 1:2 Ir/P ratios).<sup>[280]</sup> The immobilization site-isolates the monophosphine-coordinated Ir species.



**Scheme 4-10.** *Ortho*-directed borylation of arenes with  $B_2pin_2$  catalyzed by Silica-SMAP-Ir. The isolated yield is calculated based on  $B_2pin_2$  (using a 2:1 substrate- $B_2pin_2$  ratio).<sup>[280]</sup>

A second strategy to Ir-catalyzed arene boronic esters is based on the relay-directed mechanism in which a substrate binds to a vacant metal site reversibly by a  $\sigma$ -bond metathesis (Scheme 4-9).<sup>[284]</sup> In 2008, Hartwig and Boebel showed that Ir-catalyzed arene borylation is directed *ortho* to a hydrosilylmethyl, siloxide or silylamine substituent (Scheme 4-11).<sup>[285]</sup> The mechanism of this directed reaction has not been studied in detail, however, NMR investigations indicate that the hydrosilyl group triggers C–H cleavage at the *ortho* position (Scheme 4-9). Therefore, a temporary coordination of Si to the Ir-center would take place. The authors suggest an Ir

bisboryl monosilyl complex formation, which would allow linkage of the *ortho* C–H bond of the arene to the Ir-center as well.<sup>[285]</sup> The B–C bond formation from this species generates an *ortho*-borylated arylsilyl complex and reductive elimination of the silane would release the borylated formed product. Another equivalent of B<sub>2</sub>pin<sub>2</sub> would regenerate the active Ir(III) trisboryl complex **2**.



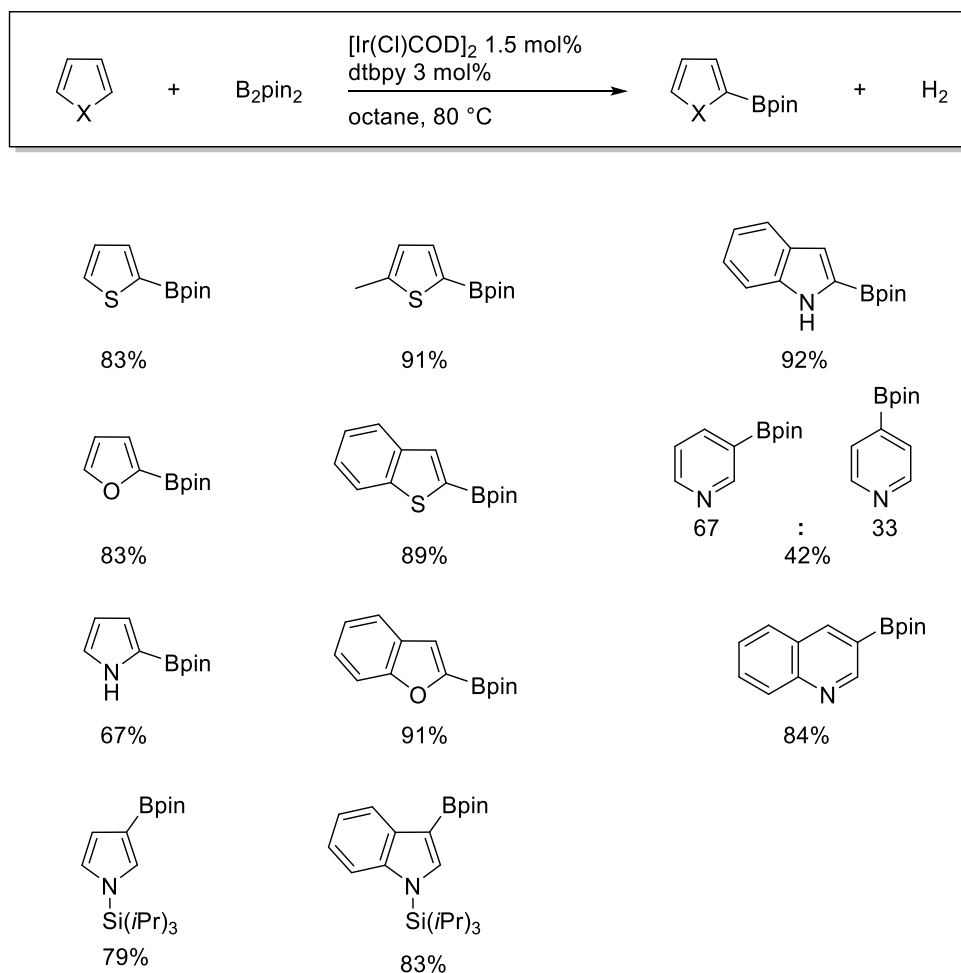
**Scheme 4-11.** One-pot *ortho* directed borylation of phenols.<sup>[285]</sup>

Furthermore, later studies demonstrated that *ortho*-directed Ir-catalyzed C–H borylations can proceed through so called “outer-sphere” mechanisms according to Taube’s definition (Scheme 4-9).<sup>[286]</sup> Examples of such reactions include Lewis acid-base,<sup>[287]</sup> hydrogen bonding<sup>[284,288]</sup> and electrostatic interactions.<sup>[289]</sup>

## 4.1.4 Borylation of Heteroarenes – the Interplay of Steric and Electronic Effects

### 4.1.4.1 Borylation of Heteroaromatic Compounds Catalyzed by the [Ir(OMe)COD]2/dtbpy System

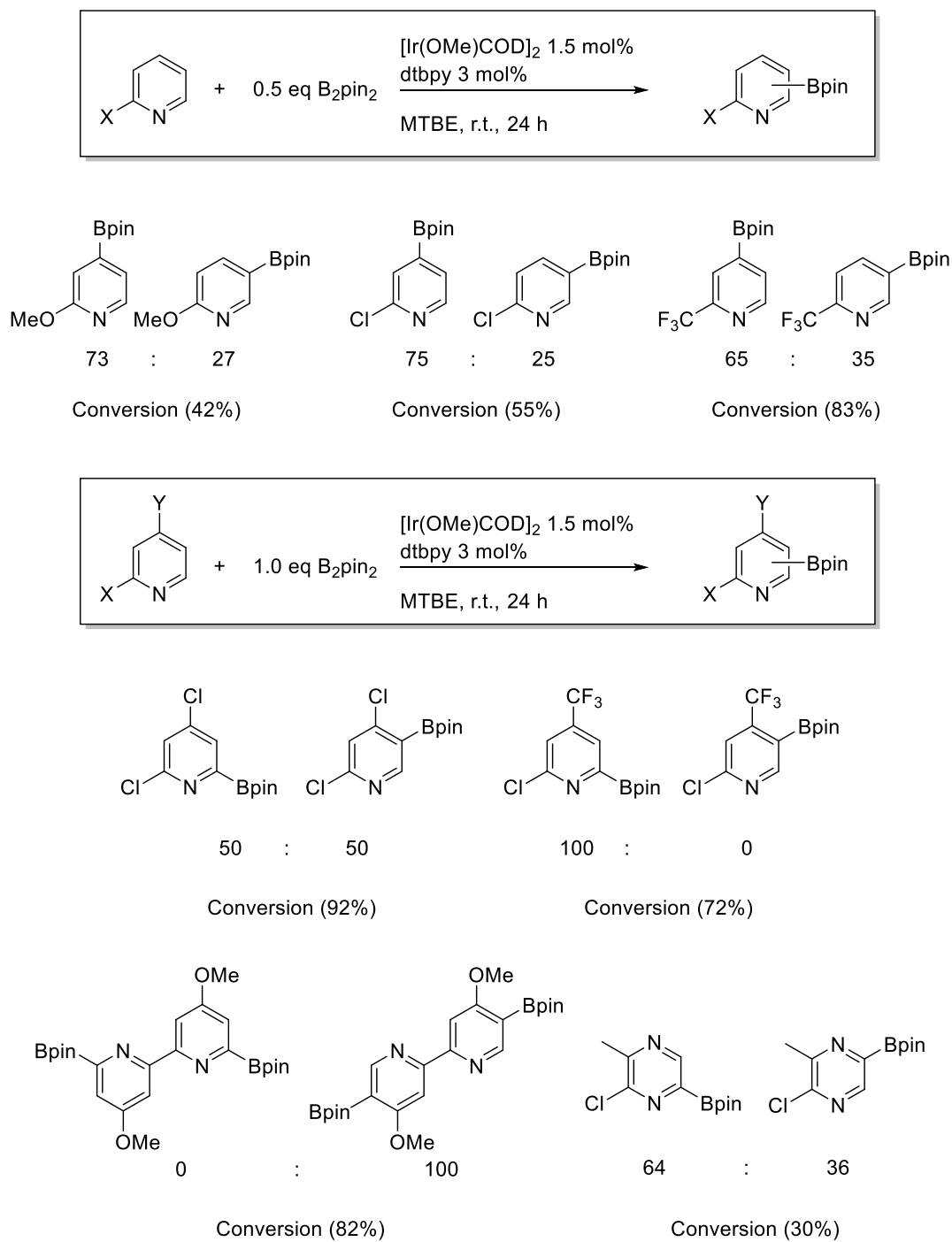
The scope of the Ir-catalyzed C–H borylation expanded enormously since the isolation of the first Ir(III) trisboryl complex in 1993.<sup>[266]</sup> Heteroaromatic compounds are of great interest as these structures are important motifs in pharmaceuticals, bioactive natural compounds and functional organic materials. The methodology of the Ir/dtbpy-catalyzed C–H borylation appeared to be effective for a wide range of substrates including five-membered heteroaromatic compounds such as thiophene, furan and pyrroles and six-membered heteroaromatic compounds such as pyridine.<sup>[43,278,290,291]</sup>



Scheme 4-12. Ir-catalyzed borylation of heteroaromatic compounds. The reaction of pyridine and quinoline was carried out at 100 °C.<sup>[291]</sup>

The five-membered heteroaromatic compounds produce exclusively products that are borylated alpha to the heteroatom, in the presence of  $[\text{Ir}(\text{Cl})\text{COD}]_2$  and dtbpy (Scheme 4-12).<sup>[291]</sup> Nevertheless, the regioselectivity of those five-membered heteroaromatics can be altered by adding steric hindrance to the system. Thus, pyrrole and indole undergo borylation selectively at the 3-position when the nitrogen bears a large protecting group such as tri(isopropyl)silyl (Scheme 4-12).<sup>[291]</sup>

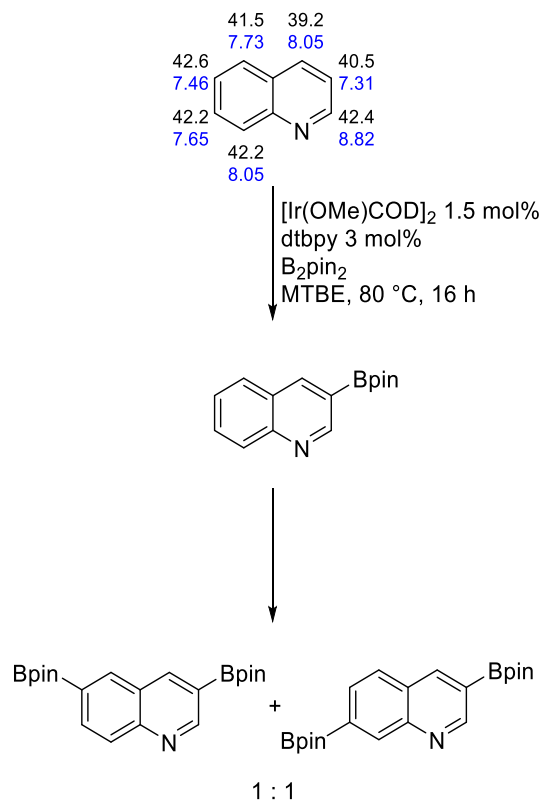
Borylation of six-membered heteroaromatic compounds on the contrary, occurred not alpha to the heteroatom, but rather forms a statistical mixture of borylation products at the 3- and 4-positions (Scheme 4-13). Furthermore, the yield was comparably low even at 100 °C (Scheme 4-13). Quinoline yields only the 3-borylated product due to the ring junction next to the 4-position. Marder, Steel and co-workers later demonstrated that the borylation reaction of pyridines is inhibited by the Lewis basic azinyl nitrogen, as its lone pair binds to the vacant site of the Ir(III) trisboryl complex hindering the C-H activation step. Thus, substituting the neighboring 2-position inhibits N-coordination to Ir and leads to higher borylation yields (Scheme 4-13).<sup>[292]</sup> Moreover, decreasing the basicity of pyridines, through substituents with a negative inductive effect, increases the yield of the borylation. This is a result of the reduced electronic repulsion between the nitrogen lone pair and the developing negative charge on the alpha position during the C-H activation step. Thus, even twofold-borylation at room temperature occurs with substituents at the 2-position in the order  $\text{H} < \text{OMe} < \text{Cl} < \text{CF}_3$ .



**Scheme 4-13.** Ir-catalyzed borylation of pyridines and pyrazine (which was borylated with 2.5 mol% of  $[\text{Ir}(\text{OMe})\text{COD}]_2$  and 5 mol% dtbpy).<sup>[292]</sup>

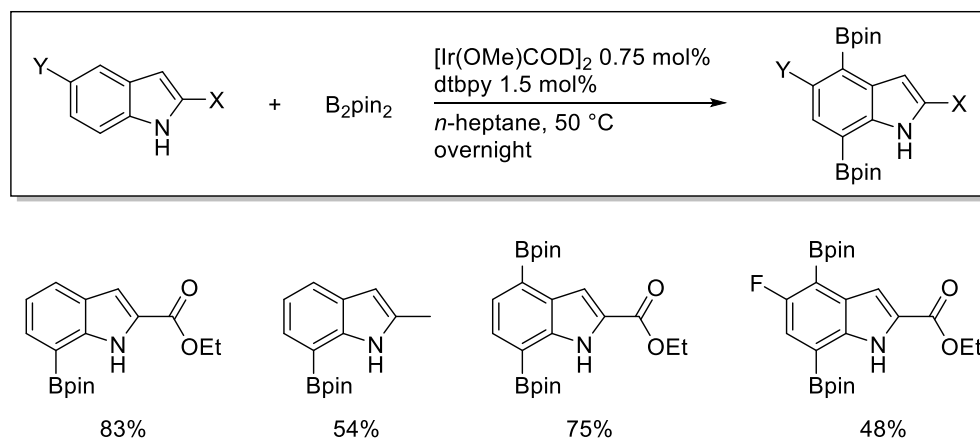
This electronic effect is nicely exemplified in the borylation of 2-chloro-3-methyl-pyrazine (Scheme 4-13) where the reaction occurs preferably alpha to the less basic nitrogen. Borylation of disubstituted pyridines occurs preferably at the least sterically hindered position even when the effect of the nitrogen lone pair on the 2-position is reduced. Thus, in the case of 2,4-dichloropyridine a 50:50 mixture of 5- and 6-borylated pyridines is obtained. On the other hand, borylation of 2-chloro-4-trifluoromethyl-pyridine yields exclusively the 6-borylated product as the large steric demand of the CF<sub>3</sub> moiety predominates over electronic effects.

In another study, Marder, Steel and co-workers presented the borylation of quinolines, which shows an intriguing selectivity. Furthermore, the authors presented a protocol for estimating the preferred site of borylation, which is useful for related derivatives (*vide infra*).<sup>[273]</sup> The heterocyclic ring in quinoline is the more reactive one and thus borylation occurs selectively at the 3-position and not at the carbocyclic ring (Scheme 4-14). However, with an excess of B<sub>2</sub>pin<sub>2</sub>, a second Bpin moiety can be introduced into the quinoline scaffold, which occurs at the carbocyclic ring.<sup>[293]</sup> Borylation occurs generally at the least sterically demanding site and at the most acidic C-H bond.<sup>[273,294]</sup> On this basis, Marder, Steel and co-workers observed a good correlation between NMR shift patterns and the preferred site of borylation.<sup>[273]</sup> Thus, the most deshielded protons in the <sup>1</sup>H NMR spectrum are most likely to be borylated if steric effects are considered (Scheme 4-14).



**Scheme 4-14.** Borylation of quinoline with calculated  $pK_a$  values (black) and  $^1\text{H}$  NMR chemical shifts in  $\text{CDCl}_3$ <sup>[295]</sup> (blue).

Interestingly, in 2-substituted indoles the 7-position is exclusively borylated even though less sterically hindered positions are available.<sup>[296]</sup> Diborylation is also possible when more  $\text{B}_2\text{pin}_2$  is employed (Scheme 4-15).

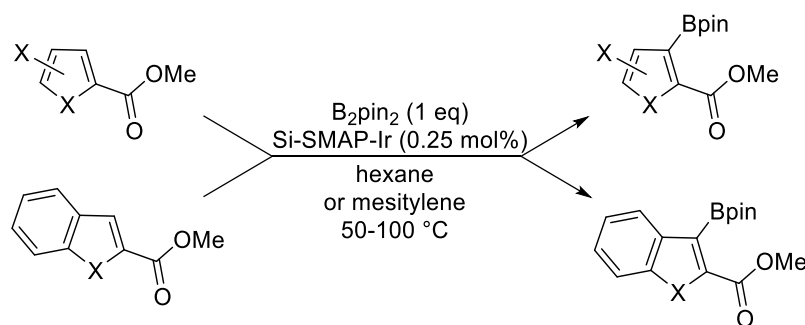


**Scheme 4-15.** Ir-catalyzed borylation of indoles with 0.7 eq of  $\text{B}_2\text{pin}_2$  for monoborylation and 2.5 eq  $\text{B}_2\text{pin}_2$  for diborylation (1.2 eq of  $\text{B}_2\text{pin}_2$  for the fluorinated species).<sup>[300]</sup>

Tse and co-workers assume an *ortho*-directing effect that leads to this unique observed selectivity. Remarkably, the borylation of heteroaromatic compounds is compatible with diverse functional groups such as halides, alkoxides, nitriles, and esters.<sup>[296]</sup>

#### 4.1.4.2 Borylation of Heteroaromatic Compounds Catalyzed by the [Ir(OMe)COD]<sub>2</sub>/Si-SMAP System

The regioselectivity of the Ir-catalyzed borylation of arenes with the ligand Si-SMAP differs from the Ir-catalyzed borylation with the ligand dtbpy (*vide supra*). In 2010, Sawamura demonstrated the site-selective borylation catalyzed by Ir/Si-SMAP of thiophenes, pyrroles, furans, benzothiophenes, benzofurans and indole derivatives that possess a 2-methoxycarbonyl directing group (Scheme 4-16).<sup>[297]</sup>

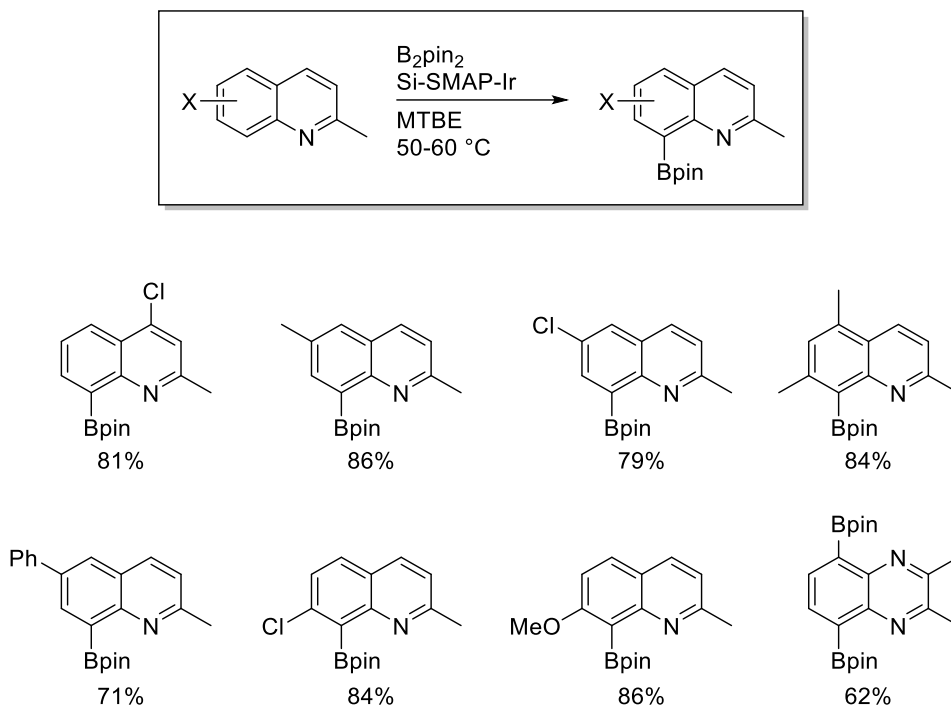


**Scheme 4-16.** Ir/Si-SMAP-catalyzed borylation of five-membered heteroaromatic compounds.<sup>[297]</sup>

The observed borylation regioselectivity of the five-membered heteroaromatic compounds catalyzed by the Ir/Si-SMAP-system contrasts with that seen with the Ir/dtbpy system. The borylation does not occur selectively alpha to the heteroatom as is observed with the latter system, but at the 3-position, which is adjacent to the ester group.<sup>[297]</sup> Interestingly, this selectivity is also observed in 2-substituted indole so that the borylation takes place on the heterocyclic ring whereas with the Ir/dtbpy system borylation occurred at the 7-position (*vide supra*).<sup>[296]</sup>

Steel, Marder, Sawamura and co-workers investigated the Ir/Si-SMAP-catalyzed borylation of quinoline, a 6-membered heteroaromatic compound, which occurs selectively at the 8-position.<sup>[298]</sup> Thus, this system gives a complementary regioselectivity to the borylation of quinolines catalyzed by the Ir/dtbpy system, which occurs preferentially at the 3-position (*vide supra*). Direct functionalization at the 8-position of quinoline is much desired as other routes

require multiple steps.<sup>[298,299]</sup> The reaction of quinoline with  $B_2pin_2$  catalyzed by the Ir/Si-SMAP system proceeded with 94% consumption of quinoline. However, not only was 8-(Bpin)-quinoline detected, but also small amounts of reduced products such as 1,2,3,4-tetrahydroquinoline. This could be inhibited by the addition of a methyl group at the 2-position of the quinoline framework, which then gave exclusively borylation at the 8-position and no reduced side product.



**Scheme 4-17.** Ir/Si-SMAP-catalyzed borylation of quinolines with isolated yields.<sup>[298]</sup>

Remarkably, the ring nitrogen is enough to direct the borylation *via* coordination to the Ir-center.<sup>[298]</sup> Thus, in contrast to previous reports, no additional coordination-based directing moiety is required for the borylation of quinoline.<sup>[280,297]</sup> It is noteworthy that the borylation of quinolines was not successful with other phosphine ligands such as  $PMe_3$ ,  $PBu_3$ ,  $PCy_3$ ,  $P^tBu_3$ ,  $PPh_3$ ,  $xPhos$  or the silica-supported TRIP. Hence, the SMAP structure and its immobilization on a solid surface is essential for this reaction.<sup>[298]</sup> Additional functional groups at the ring are tolerated and even substituents such as Cl or MeO at the 7-position that add steric hindrance do not inhibit the borylation (Scheme 4-II). The scope of this reaction can even be expanded and the reaction of 2,3-dimethylquinoxaline with 2.2 eq of  $B_2pin_2$  afforded 5,8-diborylated product (Scheme 4-17).

## 4.2 Introduction to 4-Quinolones

As the C–H borylation of 4-quinolones was studied, in cooperation with the research group of Dr. Gerard P. McGlacken from Cork in Ireland, a small introduction for this structural motif is provided below.

### 4.2.1 The Importance of the Quinolone Motif

The molecule quinolone, structurally derived from quinoline, was discovered in the early 1960s and since then has been the center of interest particularly for medical applications.<sup>[300]</sup> Quinolones possess numerous favorable properties such as antiallergenic, anticancer and antimicrobial activities.<sup>[301,302]</sup> Moreover, they offer excellent bioavailability after oral administration, good tissue penetrability and relatively low incidence of adverse effects and thus have found considerable use in many synthetic drugs to treat *e.g.* urinary, systemic and respiratory tract infections.<sup>[300,303]</sup> Quinolones are natural occurring compounds with varying substitution patterns (Scheme 4-18), which have profound medicinal properties or provided inspiration for the design of synthetic quinolones.<sup>[304]</sup> Several antibiotics were developed in the last decades that are derived from the quinolone motif such as grepafloxacin, flumequine, norfloxacin or sitafloxacin whereas nalidixic acid was the first one (Scheme 4-18).<sup>[301,305]</sup> Several chemical modifications that enhance biological and pharmacological activities were introduced and structure-activity relationship studies gave essential understanding for the modulation of this structure.<sup>[306]</sup>

#### Positions 1, 3, 4:

Substituents at the nitrogen are part of the enzyme-DNA binding complex.<sup>[307]</sup> Cyclopropyl or 2,4-difluorophenyl moieties are by far the optimal substituents for this site.<sup>[308]</sup> The 3-carboxylate and the 4-carbonyl groups are essential to mediate binding to the DNA gyrase complex.<sup>[308]</sup> Furthermore, their chelating ability enables transportation into the bacterial cell.

#### Position 2:

This site has proximity to the DNA gyrase binding site. Thus, substituents here are generally deleterious and hydrogen is the best substituent for this site.<sup>[308]</sup>

#### Position 5:

Substituents at the 5-position affect the planar configuration of the quinolone scaffold and can thus affect the overall activity.<sup>[307]</sup> However, small substituents such as amino, hydroxyl or

methyl groups can significantly increase *in vitro* activity against gram-positive bacteria. Halogens or a methoxy group, on the other hand, tend to reduce the activity of the drug.

**Position 6:**

In particular fluoroquinolones represent a large class of these type of antibiotics as a fluoro moiety at the 6-position provides a greatly broadened spectrum of activity against gram-negative and gram-positive pathogens.<sup>[303]</sup> Moreover, they have a > 10-fold increase in gyrase inhibition and up to a 100-fold improvement in minimum inhibitory concentration.<sup>[300]</sup>

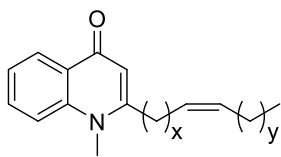
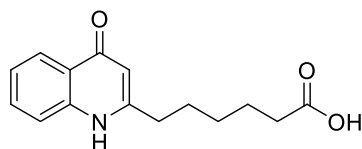
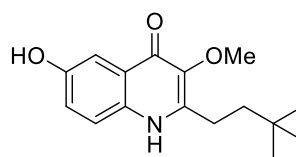
**Position 7:**

Substituents at this site are very important as they directly interact with DNA gyrase or topoisomerase IV.<sup>[307]</sup> Bulky groups have been found to increase anti-anaerobic activity. The drugs moxifloxacin and trovafloxacin have among the largest groups at this position.<sup>[307]</sup> Furthermore, substitution with a nitrogen heterocycle is seen to vastly improve potency.

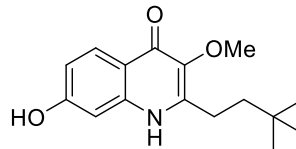
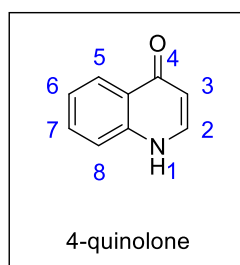
**Position 8:**

Similar to substituents at the 5-position, substituents at position 8 can affect the overall configuration of the molecule.<sup>[307,308]</sup> Thus, the target affinity can be altered by changing drug access to the enzyme or DNA binding sites. Certain groups such as halogens or COMe can expand the antibacterial spectrum to include activity against anaerobes.<sup>[308]</sup> Furthermore, the *in vitro* activity against gram-positive cocci can be increased through substituents such as halogens, methyl as well as methoxy. Nevertheless, larger groups tend to diminish activities against both gram-positive and gram-negative bacteria.<sup>[307]</sup>

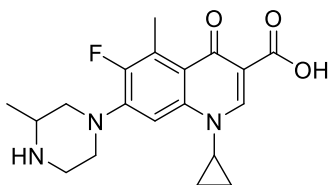
## Natural quinolones

Evocarpine  
 $x = 7, y = 3$ 

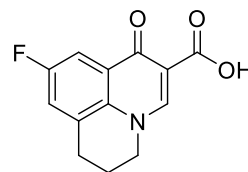
Malatyamine

isolated from *Spathelia excelsa*

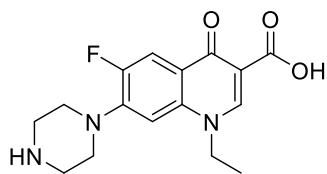
## Synthetic quinolone antibiotics



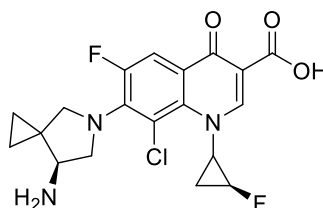
grepafloxacin



flumequine



norfloxacin

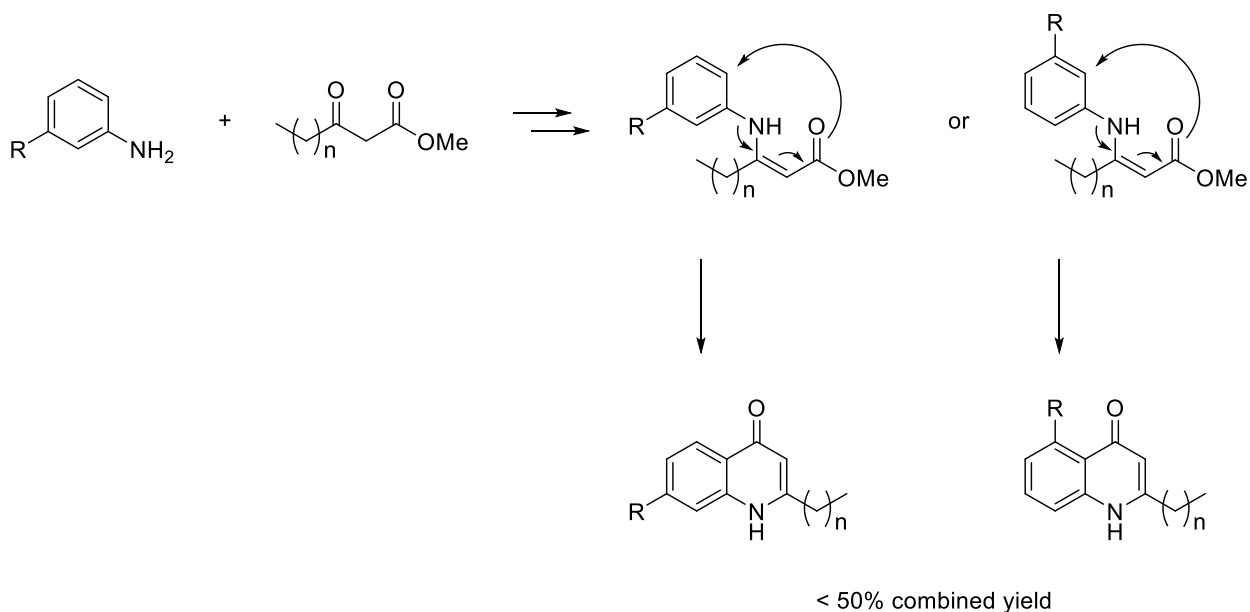


sitafloxacin

Scheme 4-18. Some natural and synthetic 4-quinolines and its numbering scheme.

### 4.2.2 Current Methodology for the Synthesis of 7-Substituted Quinolones

As quinolones are very useful substrates, diverse methods have been developed for the synthesis including Conrad-Limpach,<sup>[309]</sup> Niementowski,<sup>[310]</sup> or Camps cyclization.<sup>[311-313]</sup> However, in particular, accessing the C7 position requires cumbersome preassembly of the functional group as two possible isomers are formed from the *meta*-substituted aniline according to the Conrad-Limpach synthesis route (Scheme 4-19). Furthermore, the synthesis becomes very complex when higher substituted quinolones are desired especially as these methods usually require harsh reaction conditions.<sup>[61-64]</sup>



**Scheme 4-19.** Current used methodology towards 7-substituted quinolones.<sup>[311-313]</sup>

Zhu and co-workers previously described a Co(III)-catalyzed enaminone-directed C–H amidation method to access also 7-substituted quinolones.<sup>[313]</sup> However, their method also requires the prefunctionalization of the 7-position and is only suitable for quinolones without further functional moieties at the 2- or 3-positions.

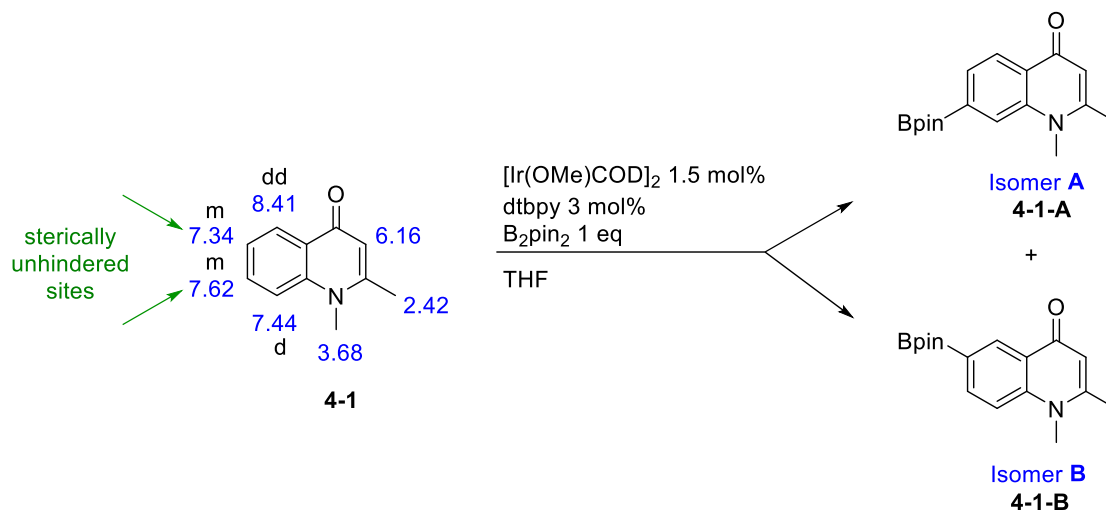
To overcome the problem of preassembly of the functional group at the 7-position, a direct C–H activation of the 7-position is highly desirable as current yields are poor, the synthesis routes require multiple steps and moreover, prefunctionalized starting materials are necessary.

## 4.3 Results and Discussion

### 4.3.1 C–H Borylation of 4-Quinolones Catalyzed by the Ir/dtbpy System

The Ir-catalyzed C–H borylation represents a convenient method for late-stage functionalization of aromatic compounds (*vide supra*). It is thus a very attractive possibility particularly for advanced synthetic intermediates with complex functionality to introduce a specific moiety.

The C–H bond borylation of a series of 4-quinolones with  $B_2pin_2$  catalyzed by  $[Ir(OMe)COD]_2$  and the ligand dtbpy was carried out to study the regioselectivity of the reaction. As the borylation with this catalytic system occurs preferably at the least steric hindered position (*vide supra*), positions 6 and 7 of the 2-substituted quinolones are possible borylation sites from the steric point of view. However, electronic effects are not negligible, particularly with heteroaromatic compounds (*vide supra*). As Marder and co-workers observed a good correlation between  $^1H$  NMR shift patterns and the most acidic C–H bond in quinolines, the  $^1H$  NMR shifts of quinolone **4-1**<sup>[314]</sup> were considered here as well (Scheme 4-20).

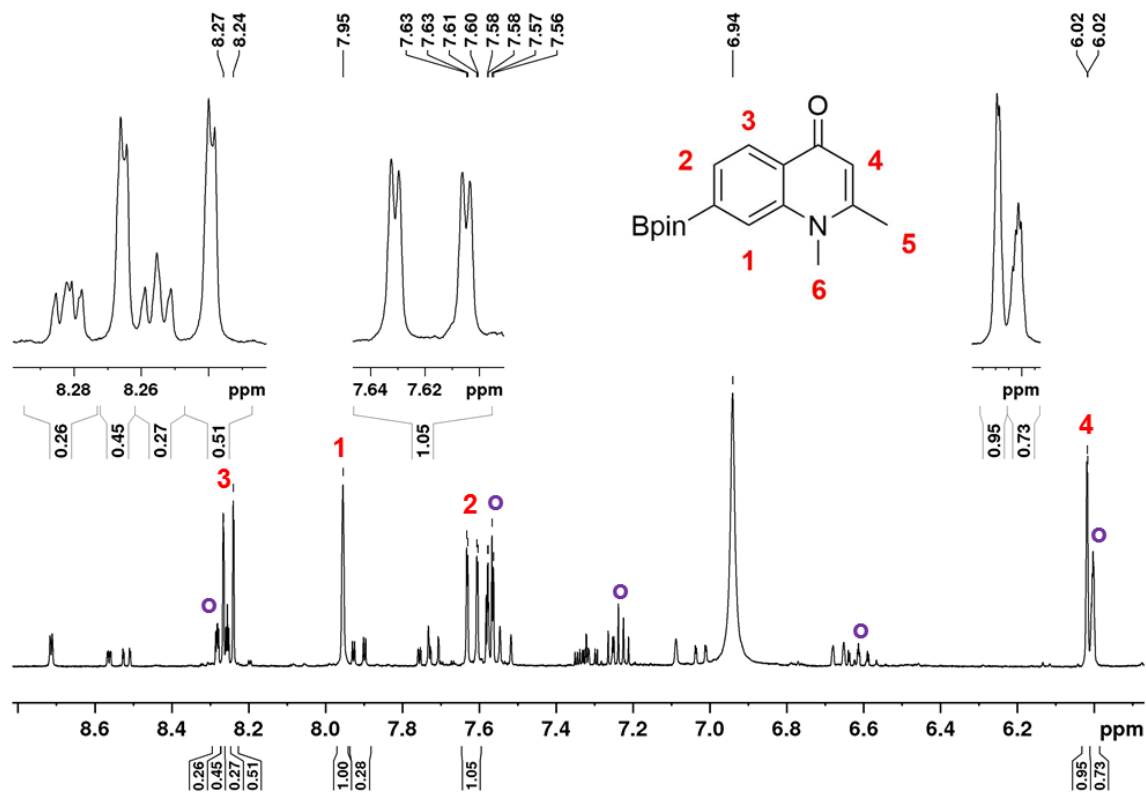


**Scheme 4-20.** Ir/dtbpy-catalyzed borylation of quinolone **4-1** with  $B_2pin_2$  in THF. The  $^1H$  chemical shifts (blue) measured in  $CDCl_3$  are listed for each proton of **4-1**.

The heterocyclic ring is sterically blocked for the borylation and, in addition, this ring has no aromatic character, which is clearly seen from the  $^1H$  NMR shifts. Hence, only the carbocyclic ring is available for borylation with this catalytic system. Positions 5 and 8 are adjacent to a ring junction and are therefore also not favorable for borylation. Thus, the sterically unhindered sites 6 and 7 are possible borylation sites. From the electronic point of view, the 7-position should be

avored as this proton is more acidic than the proton at 6. The carbonyl group possesses a negative mesomeric effect (-M), which was already observed by Marder, Steel and co-workers to lead to enhanced *para* selectivity. The amine moiety on the other hand has a positive mesomeric (+M) and negative inductive (-I) effect, which leads to *meta* selectivity. Hence, the favored selectivity for position 7 over 6 here should be higher compared to quinolines. This trend is also indicated by the chemical shifts, as proton 7 shows a more deshielded character than proton 6 (Scheme 4-20).

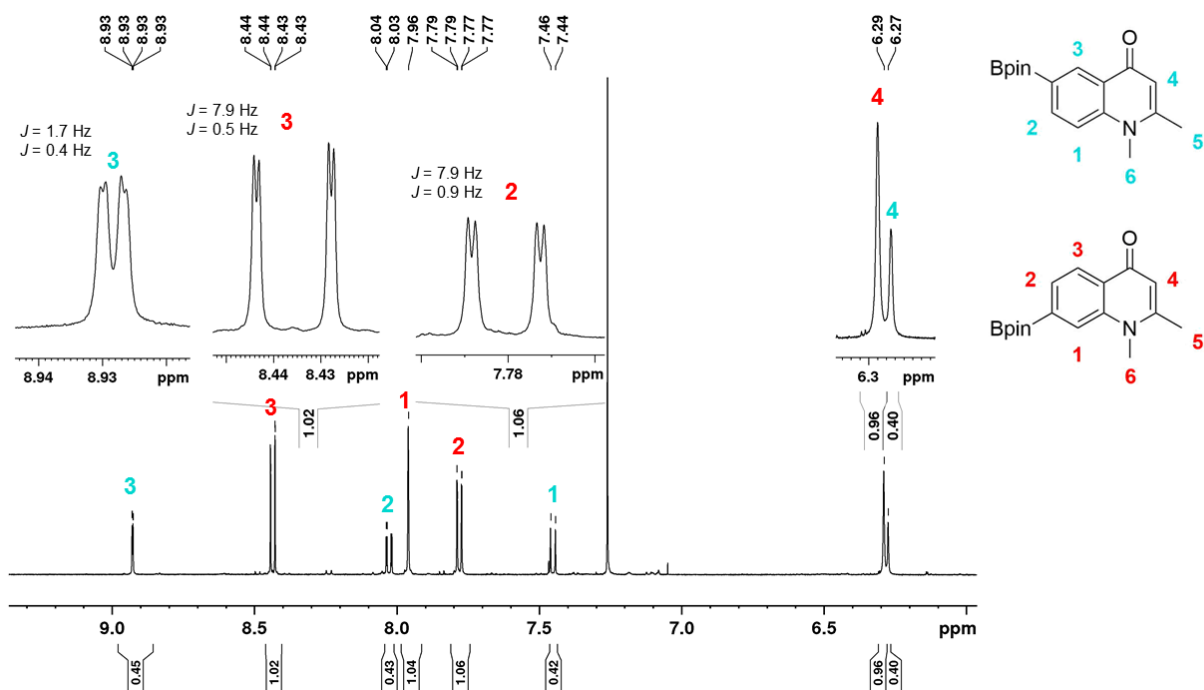
The initial test borylation with 1 eq of B<sub>2</sub>pin<sub>2</sub> catalyzed by [Ir(OMe)COD]<sub>2</sub> and dtbpy was performed in THF-*d*<sub>8</sub> at room temperature to obtain a slower reaction and thus a higher regioselectivity. Unfortunately, quinolone **4-1** was not soluble in hexane or MTBE, which are non-coordinating solvents.<sup>[315]</sup> However, the <sup>1</sup>H NMR spectra of the crude reaction mixture showed the borylation proceeded with high selectivity at the 7-position (Scheme 4-20). The successful monoborylation was also confirmed by HRMS and GC-MS. However, after 10 days the starting material was still not completely consumed (purple circle, Scheme 4-20). This contrasts to the borylation of quinoline, which converted completely within 24 h (*vide supra*).<sup>[273]</sup> Furthermore, as expected, 2-methyl-quinoline demonstrated less regioselectivity than observed with quinolone **4-1**.



**Scheme 4-20.**  $^1\text{H}$  NMR spectrum of quinolone **4-1** measured in  $\text{THF-}d_8$  at 300 MHz. Starting material signals are marked with a purple circle.

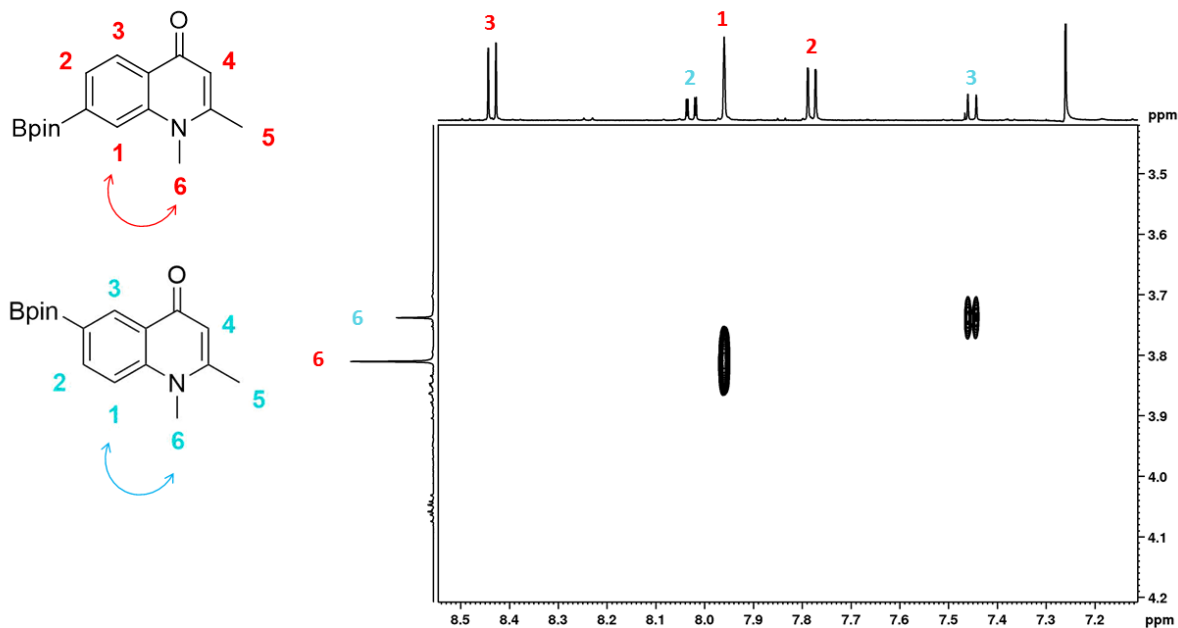
Other isomers such as presumably isomer B (**4-I-B**) were also formed (Scheme 4-19). However, the ratio **4-I-A** vs. other isomers is very low (1:0.28), thus a clear identification was difficult particularly with the remaining starting material.

Performing the same reaction at elevated temperatures ( $80\text{ }^\circ\text{C}$ ) resulted in a full conversion within 24 h (Scheme 4-21). The elevated temperature however, led to a reduced regioselectivity of this reaction, as expected. Hence, other isomers were concentrated enough in the crude reaction mixture to be analyzed by NMR spectroscopy. As predicted beforehand, the borylation also occurs at the 6-position of quinolone **4-1** thus, giving a ratio of 1 : 0.4 (**4-I-A** : **4-I-B**) at elevated temperatures according to NMR spectroscopy (Scheme 4-21).



**Scheme 4-21.**  $^1\text{H}$  NMR spectrum of crude quinolone **4-1** measured in  $\text{CDCl}_3$  at 500 MHz.

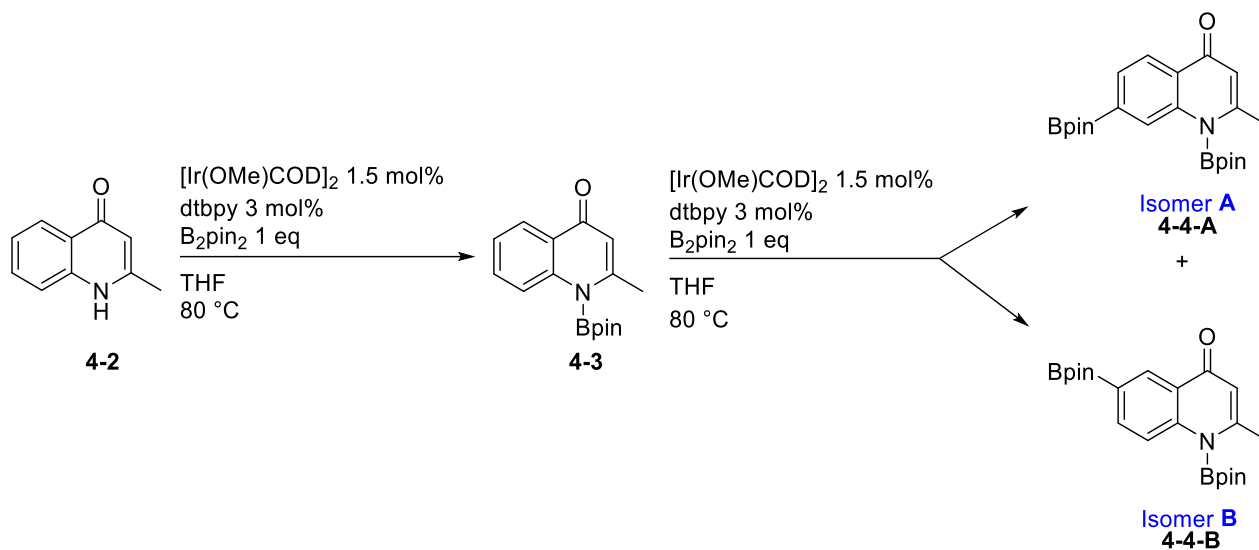
A NOESY experiment confirmed that the major component is isomer A (red, Scheme 4-22). The methyl group at the nitrogen with the highest intensity (at 3.81 ppm) couples to the neighboring aromatic proton at 7.96 ppm (1, Scheme 4-22) that is a singlet. Consequently, the signals with the highest intensity must belong to isomer A (**4-1-A**). On the other hand, the methyl group at the nitrogen (at 3.74 ppm) couples with a doublet at 7.45 ppm. Consequently, the signals with lower intensity must belong to isomer B (**4-1-B**).



**Scheme 4-22.** NOESY spectrum in  $\text{CDCl}_3$  at 500 MHz.

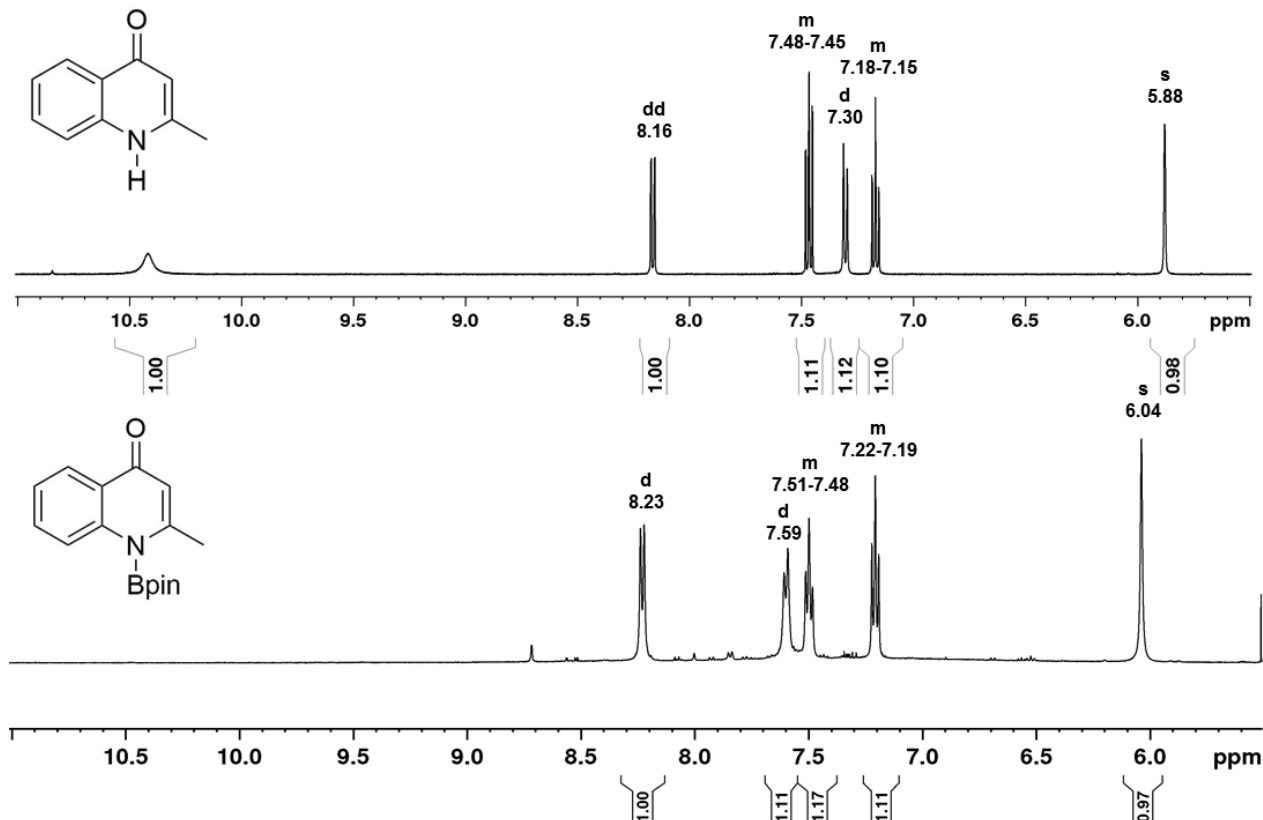
However, flash column chromatography or Kugelrohr distillation are not sufficient enough to separate these two isomers. HPLC or other separation methods are probably necessary.

If the nitrogen is not protected, in the quinolone motif, then borylation occurs first at the nitrogen because its proton is the most acidic (Scheme 4-23).



**Scheme 4-23.** Ir/dtbpy-catalyzed borylation of quinolone **4-2** with  $\text{B}_2\text{pin}_2$  in THF.

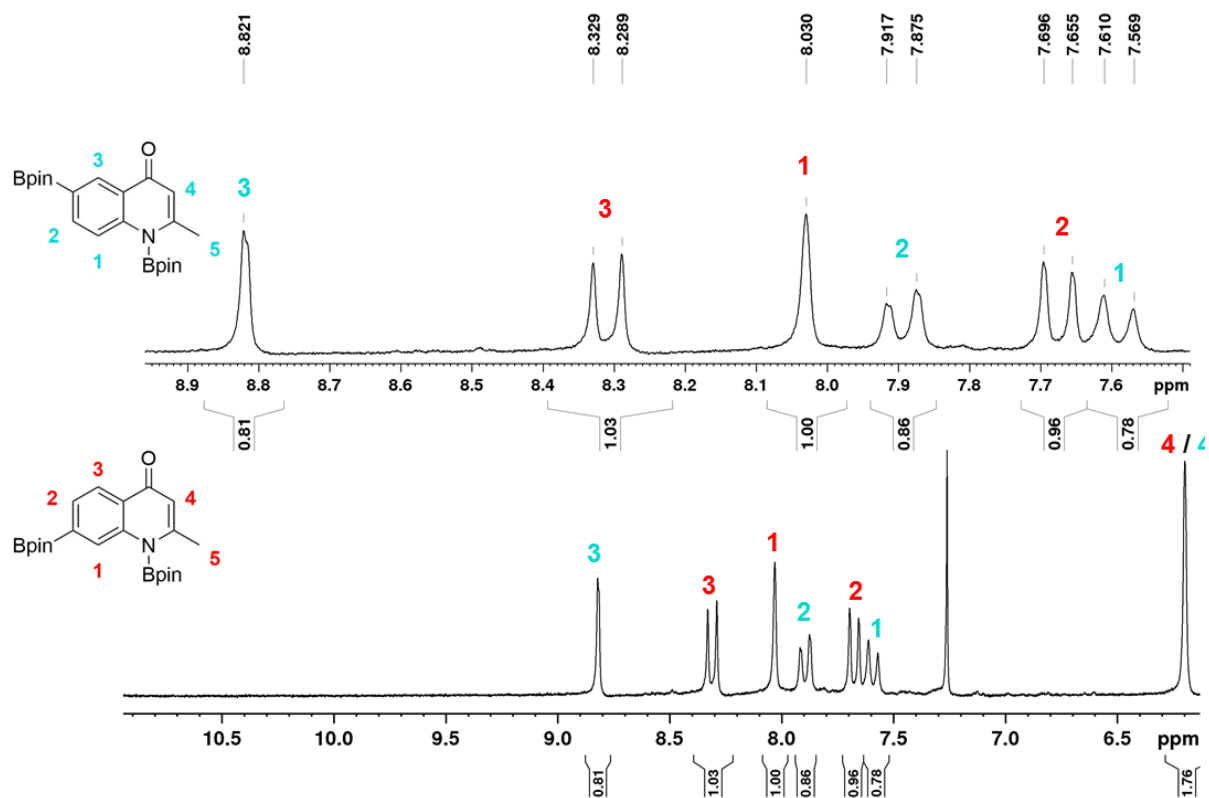
Thus, the  $^1\text{H}$  NMR spectrum of the crude reaction mixture of **4-3** still shows all 4 protons of the carboxylic ring (7.19–8.23 ppm) and the proton of the heteroring at 6.04 ppm (Scheme 4-24). All of them are slightly shifted downfield compared to the starting material, which indicates that the Bpin moiety withdraws some electron density. However, the proton of the NH group, which occurred at 10.42 ppm in the starting material is not observed. In addition, the  $^{11}\text{B}$  shift at 34.7 ppm confirms a Bpin moiety within this compound and the HRMS ( $[\text{M}-\text{H}]^+ = 285.1644$ ) also proves the monoborylation of quinolone **4-2**.



**Scheme 4-24.** <sup>1</sup>H NMR spectrum of the starting material (top) and crude product of **4-3** (bottom) in THF-*d*<sub>8</sub> at 500 MHz.

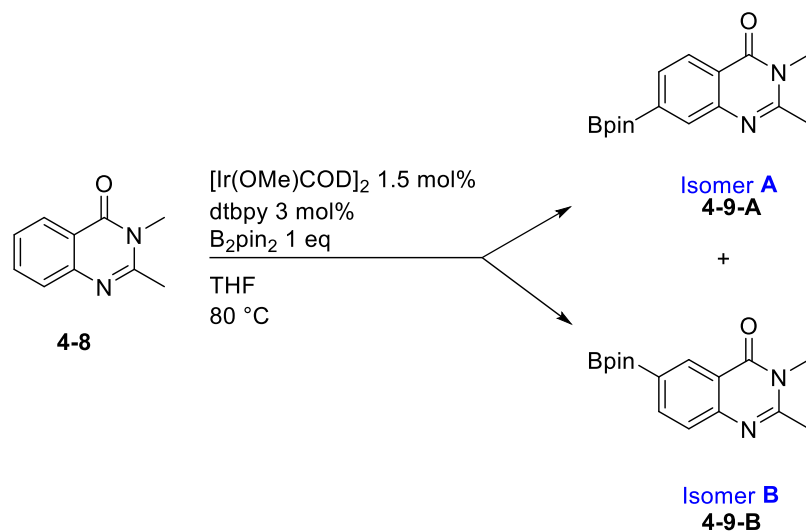
Nevertheless, the addition of 2 eq of B<sub>2</sub>pin<sub>2</sub> leads to a two-fold borylation, which proceeds even slightly faster as all protons gained acidic character because of the Bpin moiety at the nitrogen. However, this also leads to a reduced selectivity as the sterically unhindered positions 6 and 7 become more similar from the electronic point of view. The 7-position is still preferred for the Ir-catalyzed borylation, however only slightly more than the 6-position as the ratio of the two resulting borylated isomers is ca. 1:0.8 (**4-4-A** : **4-4-B**) according to the <sup>1</sup>H NMR spectrum (Scheme 4-25). Compared to quinolone **4-1** that has a N-methyl instead of a NH moiety, the borylation selectivity at the carboxylic ring is reduced by a factor of ca. 2. Therefore, the first Bpin moiety at the amine moiety greatly influences the electronic properties of the quinolone. The Bpin moiety is weakly π-accepting (-M). Consequently, it competes against the electronic effect of the amine moiety on the carboxylic ring, which results in a reduced regioselectivity of the borylation. Nevertheless, this result demonstrates that the NH moiety in quinolones can be protected by one Bpin group and a second equivalent can be used to obtain borylation at the

carboxylic ring. This is a very convenient method to obtain diverse NH functionalized quinolones.



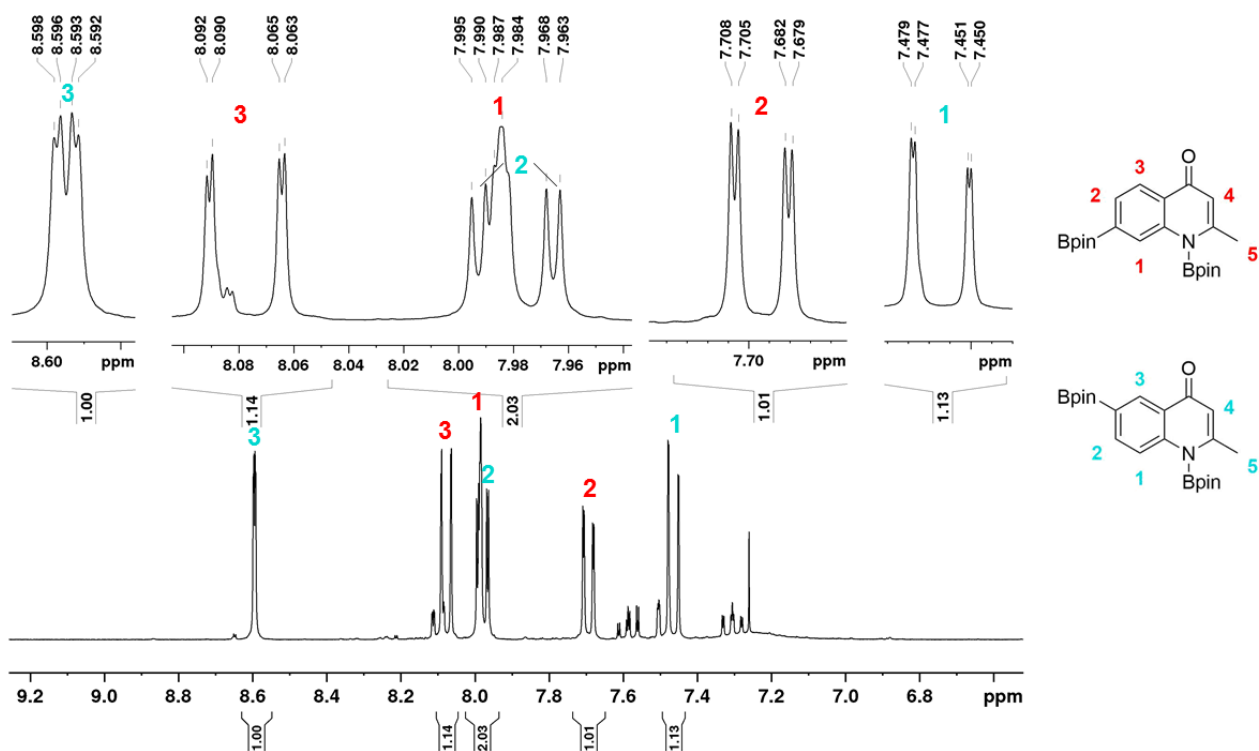
Scheme 4-25.  $^1\text{H}$  NMR spectrum of the crude product of 4-4 in  $\text{CDCl}_3$  at 200 MHz.

These observations and trends can be applied to other quinolones. Hence, the borylation method is also compatible with additional functional groups such as amines that are incorporated into the quinoline framework (Scheme 4-26). The borylation of quinolone 4-8 yields two borylated products as the positions 6 and 7 are the only steric unhindered sites that are available. However, the electronic properties are altered as the amine moiety donates electrons. Therefore, the carbonyl group is not as electron deficient and thus the *para* position (position 7) is not as strongly acidic.



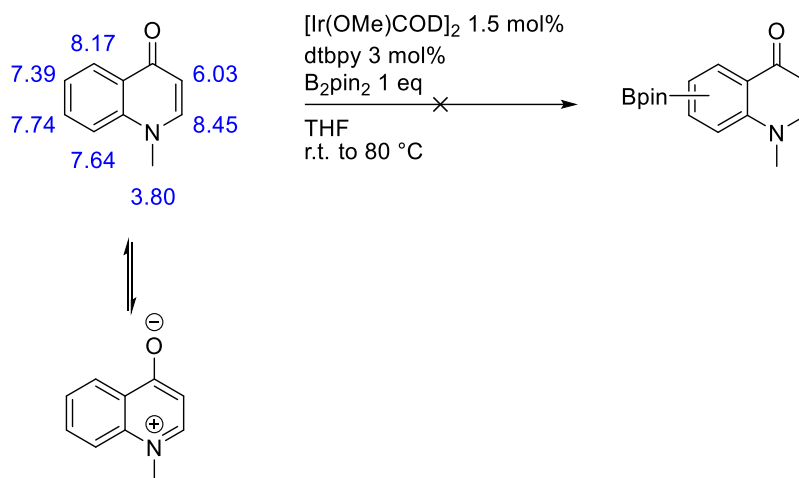
**Scheme 4-26.** Ir/dtbp-catalyzed borylation of quinolone **4-8** with  $\text{B}_2\text{pin}_2$  in THF.

As expected, the  $^1\text{H}$  NMR spectrum demonstrates that the addition of an amine moiety to the 3-position of the quinolone motif decreases the regioselectivity of the borylation reaction (Scheme 4-27). Hence, the ratio of the two isomers A and B is ca. 1:1. Thus, the 7-position is not electronically favored in this quinolone. A quinolone with an electron deficient moiety at the 3-position would be an interesting candidate for the Ir-catalyzed borylation.



**Scheme 4-27.**  $^1\text{H}$  NMR spectrum of the crude product of 4-9 in  $\text{CDCl}_3$  at 200 MHz.

However, it is intriguing that if the 2-position of the quinolone is unsubstituted, the borylation does not proceed at all (Scheme 4-28).

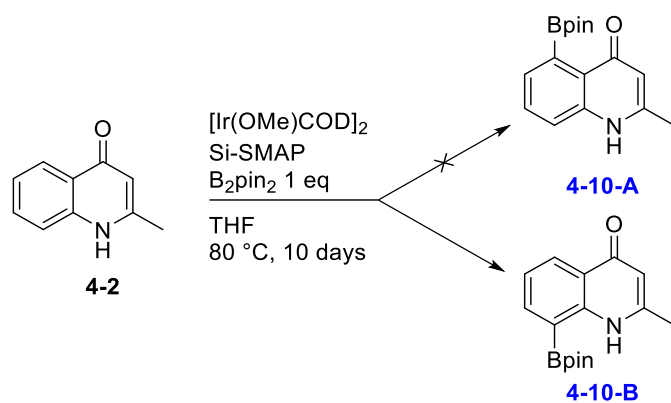


**Scheme 4-28.** Ir/dtbpY-catalyzed borylation of a quinolone with  $\text{B}_2\text{pin}_2$  in THF. The  $^1\text{H}$  chemical shifts (blue) measured in  $\text{DMSO}-d_6$  are listed for each proton.<sup>[316]</sup>

This might be a result of the tautomerization of the quinolone, which becomes increasingly favored if the 2-position is unsubstituted. Thus, a dipolar product is formed with increased aromaticity. This tautomer-product may bind to the vacant site of the Ir-catalyst and block the C–H activation.

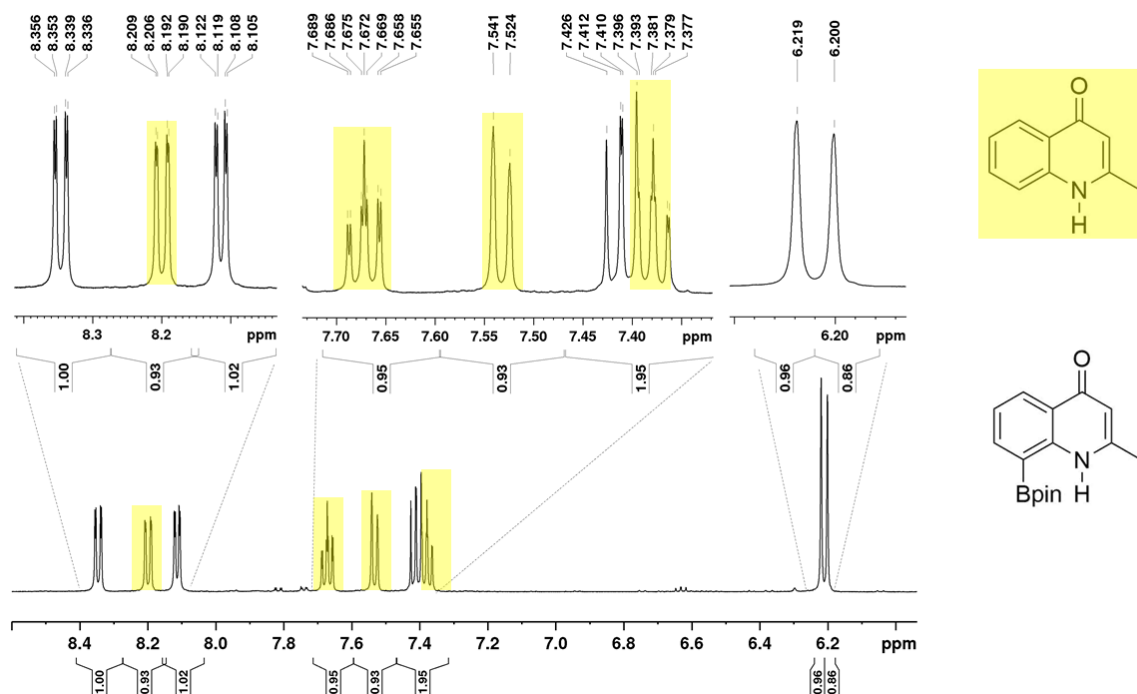
### 4.3.2 C–H borylation of 4-Quinolones Catalyzed by the Ir/Si-SMAP System

The C–H borylation catalyzed by  $[\text{Ir}(\text{OMe})\text{COD}]_2$  and the ligand Si-SMAP occurs *ortho* to a directing group and is thus not controlled by steric effects (*vide infra*). Motivated by the intriguing regioselectivity obtained for the borylation of quinolines with the Ir/Si-SMAP system, we investigated the borylation of quinolone **4-2** as well with this system (Scheme 4-29). In quinolone **4-2**, the NH moiety and/or the carbonyl group could act as a directing group for the borylation (Scheme 4-29). Thus, two isomers **4-10a** and **4-10b** are possible products of this reaction.



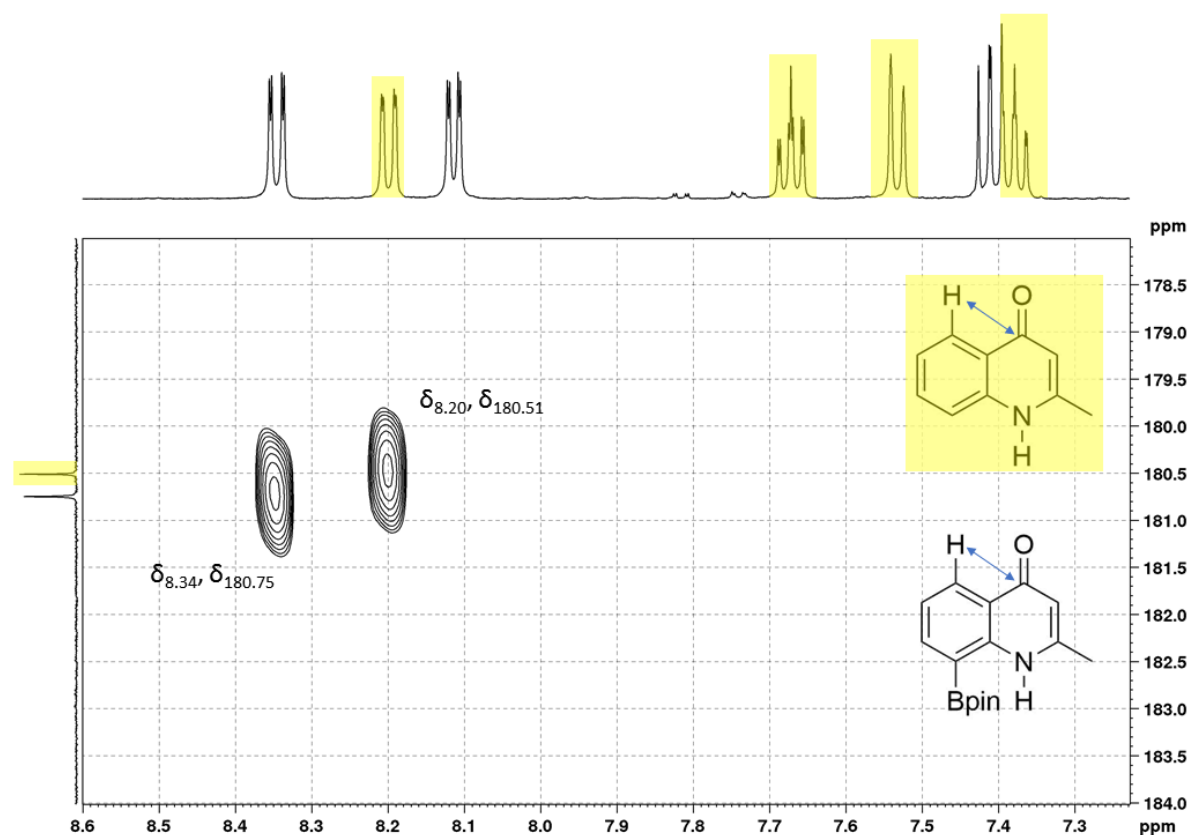
**Scheme 4-29.** Ir/Si-SMAP-catalyzed borylation of quinolone **4-2** with  $\text{B}_2\text{pin}_2$  in THF.

After 10 days, 50% of the starting material **4-2** was consumed (yellow, Scheme 4-30) and one product formed (Scheme 4-21). The  $^1\text{H}$  NMR measurement shows three new aromatic peaks and that is a doublet of doublets at 8.34 ppm, a doublet of doublets at 8.11 ppm and two doublets at 7.42 and 7.40 ppm whereas no singlet was detected. This combination and number of multiplicities is only possible if the borylation takes place next to the NH or next to the carbonyl group (Scheme 4-30).



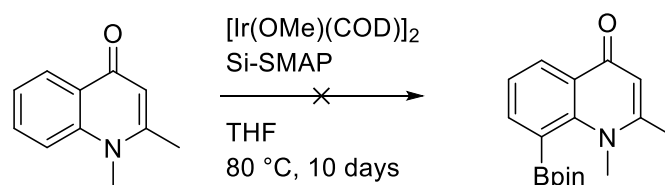
**Scheme 4-30.**  $^1\text{H}$  NMR spectrum of the crude reaction mixture of **4-10** in  $\text{CD}_3\text{OD}$  at 500 MHz.

In order to identify the obtained product,  $^{13}\text{C}$  and  $^{13}\text{C}$ ,  $^1\text{H}$  HMBC and HSQC measurements were performed. The  $^{13}\text{C}$ ,  $^1\text{H}$  HMBC spectrum clearly shows a cross peak between the proton *ortho* to the carbonyl group at 8.34 ppm and the carbonyl carbon at 180.75 ppm (Scheme 4-31). Therefore, the Bpin group must be located at the 8-position (next to the NH moiety) and thus only isomer **4-10b** was formed. Interestingly, the carbonyl moiety does not act as directing group in this reaction at all. However, the reaction did not run to completion after 10 days, which contrasts to the borylation of quinolines (*vide supra*). As quinolines do not possess a carbonyl group, this functionality might be a reason for the incomplete reaction.



**Scheme 4-31.**  $^{13}\text{C}$ ,  $^1\text{H}$  HMBC NMR spectrum of the crude reaction mixture of **4-10** in  $\text{CD}_3\text{OD}$  at 500 MHz.

To confirm that only the NH group can direct the borylation, a follow up experiment with the Ir/Si-SMAP system was performed with quinolone **4-1** (Scheme 4-32). The nitrogen is protected by a methyl group in this compound; thus, this moiety should not be able to direct the borylation. After 10 days no product formation was detected even at elevated temperatures. Thus, without the NH moiety in the quinolone framework, which can direct the borylation, the reaction does not proceed. Furthermore, the ketone moiety in the quinolone framework cannot direct the borylation, which is surprising as other carbonyls such as 2-methoxycarbonyl served as an excellent directing group in many cases (*vide supra*).



**Scheme 32.** Ir/Si-SMAP-catalyzed borylation of quinolone **4-1** with  $\text{B}_2\text{pin}_2$  in THF.

## 4.4 Conclusions

The Ir-catalyzed C–H borylation of quinolones is a convenient method to introduce functional groups at the 7-position of a quinolone. Classical procedures require functionalization of this site at the first synthesis step. Thus, the routes to the desired quinolones become complex and long especially if further functionalities at other positions are necessary. The Ir-catalyzed borylation allows the direct borylation of quinolones. Thus, later stage functionalization is possible and higher functionalized quinolones are also compatible with this mild reaction conditions. The borylations occurred with high regioselectivities and some insights into factors governing selectivity are given. The borylation with the Si-SMAP ligand gave another regioselectivity than that obtained with the dtbpy ligand. The 8-position is favored, as the borylation is directed via the NH moiety at the 1-position, whereas no other isomer is formed. The results and trends are in good agreement with previous observations made by Marder, Steel and Sawamura on quinolines.



# **Chapter 5**

## Summary



## 5 Summary / Zusammenfassung

### 5.1 Summary

#### 5.1.1 Chapter 1

Pyrene is a polycyclic aromatic hydrocarbon (PAH) that has very interesting photophysical properties which make it suitable for a broad range of applications. The 2,7-positions of pyrene are situated on nodal planes in both the HOMO and LUMO. Hence, electrophilic reactions take place at the 1-, 3-, 6-, and 8-positions. Marder and co-workers previously demonstrated a selective method to substitute directly the 2,7-positions by an iridium-catalyzed C-H borylation. In this manner they were able to develop a large library of diverse 2- and 2,7-substituted pyrene derivatives. The goal of this project was to develop novel pyrene derivatives substituted at the 2- and 2,7-positions, with very strong donors or/and acceptors, to achieve unprecedented properties and to provide a deeper understanding of how to control the excited states and redox properties. For that reason, a julolidine-type moiety was chosen as a very strong donor, giving D- $\pi$  (**1-8**) and D- $\pi$ -D (**1-4**) systems and, with Bmes<sub>2</sub> as a very strong acceptor, D- $\pi$ -A (**1-11**) system.

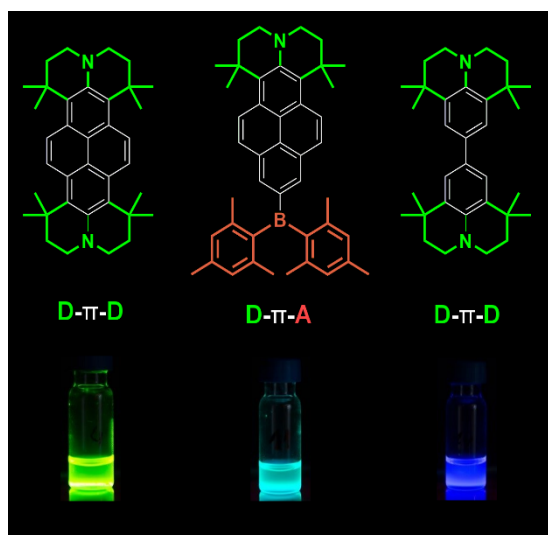


**Figure 5-1.** Three target 2- and 2,7-derivatives of this project with their emission in hexane solutions.

These compounds exhibit unusual photophysical properties such as emission in the green region of the electromagnetic spectrum in hexane, whereas all other previously reported pyrene derivatives substituted at the 2,7-positions show blue luminescence. Interestingly, the D- $\pi$ -D

pyrene derivative emits further in the red region than the D- $\pi$ -A pyrene derivative. Consequently, the second donor moiety apparently destabilizes the ground state  $S_0$  more strongly than the additional acceptor Bmes<sub>2</sub> stabilizes the singlet excited state  $S_1$ . Furthermore, spectroelectrochemical measurements suggest very strong coupling between the substituents at the 2,7-positions of pyrene in the D- $\pi$ -D system. The analogous biphenyl compound **1-14** was synthesized and oxidized to compare the electron delocalization over the pyrene and biphenyl bridge. Evaluation of the rising IV-CT band in the NIR of the monocation species of both D- $\pi$ -D systems reveals that these compounds can be categorized as typical delocalized Robin-Day-class III derivatives, whereas the electronic coupling is a little stronger in the biphenyl derivative.

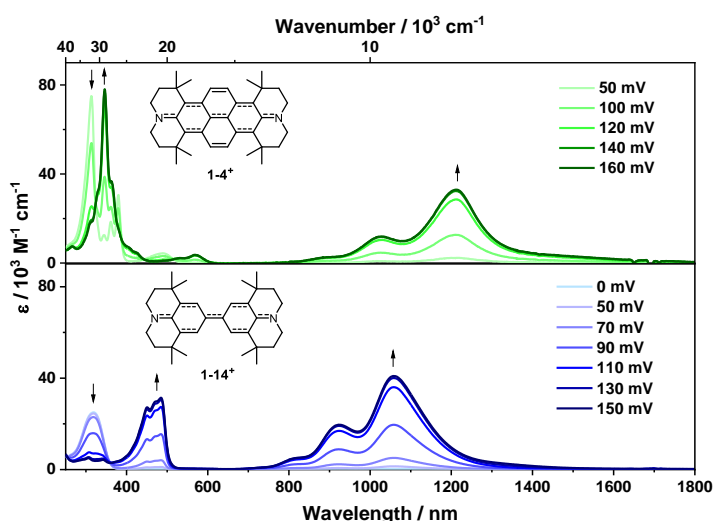


**Figure 5-2.** Spectroelectrochemical measurements of the stepwise oxidation processes in  $\text{CH}_2\text{Cl}_2/0.1 \text{ M } [n\text{-Bu}_4\text{N}][\text{PF}_6]$ . The absorption spectra of **1-4**<sup>+</sup> and of **1-14**<sup>+</sup> are given as the solid dark green and solid dark blue lines, respectively.

Theoretical studies show that these properties result from the very strong julolidine-type donor and Bmes<sub>2</sub> acceptor coupling efficiently to the pyrene HOMO-1 and LUMO+1, respectively. Destabilization of the former and stabilization of the latter lead to an orbital shuffle between HOMO and HOMO-1, and LUMO and LUMO+1 of pyrene. Consequently, the  $S_1$  state changes its nature sufficiently enough to gain higher oscillator strength, and the photophysical and electrochemical properties are then greatly influenced by the substituents.

### 5.1.2 Chapter 2

The polycyclic aromatic hydrocarbon perylene, especially perylene diimide, has received considerable attention in recent years and has found use in numerous applications such as dyes, pigments and semiconductors. Nevertheless, it is of fundamental importance to understand how to modulate the electronic and photophysical properties of perylene depending on the specific desired application. Perylenes without carboxyimide groups at the *peri* positions are much less well studied due to the difficulties in functionalizing the perylene core directly. In particular, only *ortho* heteroatom substituted perylenes have not been reported thus far (exception: (Bpin)<sub>4</sub>-Per was already reported by Marder and co-workers). Thus, the effect of substituents on the *ortho* positions of the perylene core has not been investigated.

Two perylene derivatives were synthesized that bear four strong diphenylamine donor or strong Bmes<sub>2</sub> acceptor moieties at the *ortho* positions. These compounds represent the first examples of perylenes substituted only at the *ortho* positions with donors or acceptors.

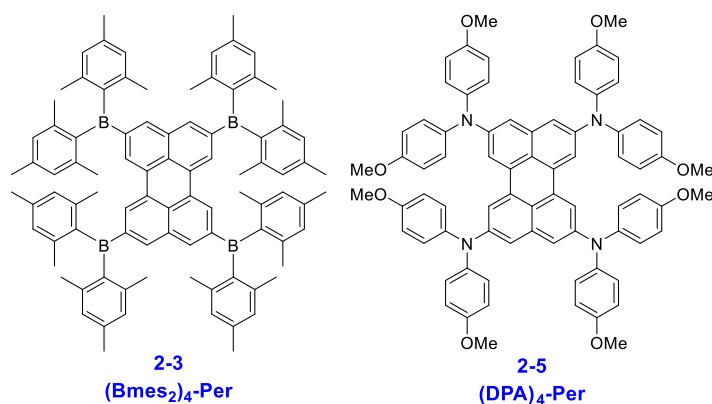
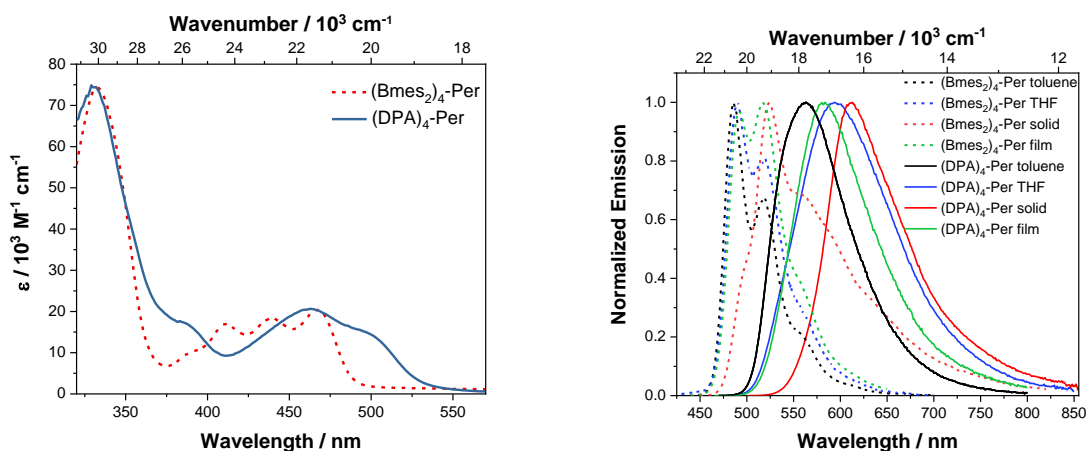


Figure 5-3. Two target derivatives.

The investigations show that the photophysical and electronic properties of these derivatives are unique and different compared to the well-studied perylene diimides. Thus, up to four reversible reductions or oxidations are possible, which is unprecedented for monomeric perylenes. Moreover, these derivatives show stability towards very high potentials. Spectroelectrochemical investigations revealed absorptions up to 3000 nm of the monocation of our donor-substituted perylene and that it can be classified as a fully delocalized Robin-Day-class III compound. Furthermore, the photophysical properties of these two *ortho*-substituted derivatives are unusual compared to reported perylenes on many regards. Thus, large Stokes

shifts are obtained, and the singlet excited state of our derivatives lives remarkably long with intrinsic lifetimes of up to 94 ns.



**Figure 5-4.** Absorption (left) and emission (right) spectra  $(Bmes_2)_4\text{-Per}$  and  $(DPA)_4\text{-Per}$  recorded in toluene if not otherwise noted.

Transient absorption measurements revealed a further excited state with a 500  $\mu\text{s}$  lifetime, which efficiently sensitizes singlet oxygen. In addition, these two derivatives are emissive in the solid state as the four large substituents block  $\pi\text{-}\pi$  interactions. X-ray analysis of the amine-substituted derivative shows a nearly planar perylene core. Hence, neither the used amine nor the triarylborane substituents at the *ortho* positions influence the planarity of the perylene core, which is different from *bay* substituted perylenes.

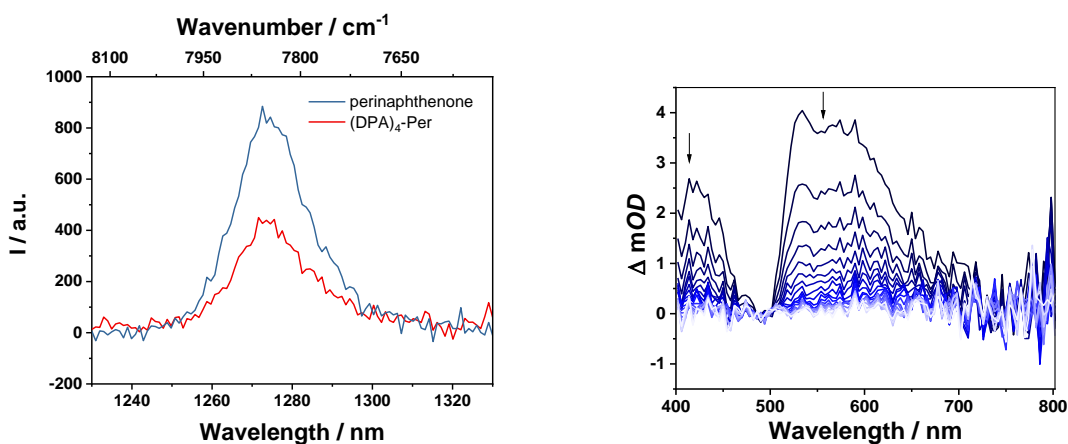


**Figure 5-5.** Singlet oxygen luminescence from optically matched toluene solutions of  $(DPA)_4\text{-Per}$  and the standard perinaphthenone; excitation at 340 nm (left); nanosecond transient absorption spectrum of  $(DPA)_4\text{-Per}$  in a degassed DMF solution (right) at intervals of 169.9  $\mu\text{s}$ .

### 5.1.3 Chapter 3

As the D- $\pi$ -D pyrene derivative (**1-4**) showed very unusual properties such as green luminescence and a strongly redshifted  $S_1 \leftarrow S_0$  absorption, further derivatives were synthesized with additional acceptor moieties at the K-region of pyrene. Unfortunately, it was not possible to synthesize a derivative with the two julolidine-like donors at the 2,7-positions and additional acceptor moieties. However, changing the julolidine-like donor to a diphenyl amine donor allowed the successful synthesis of three new target derivatives.

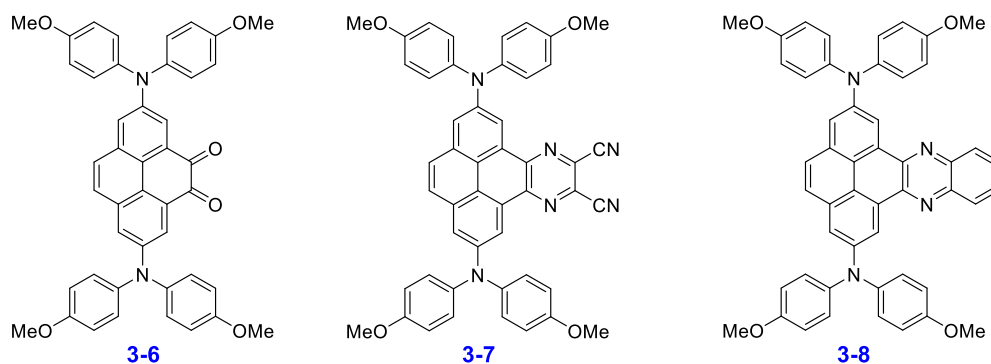
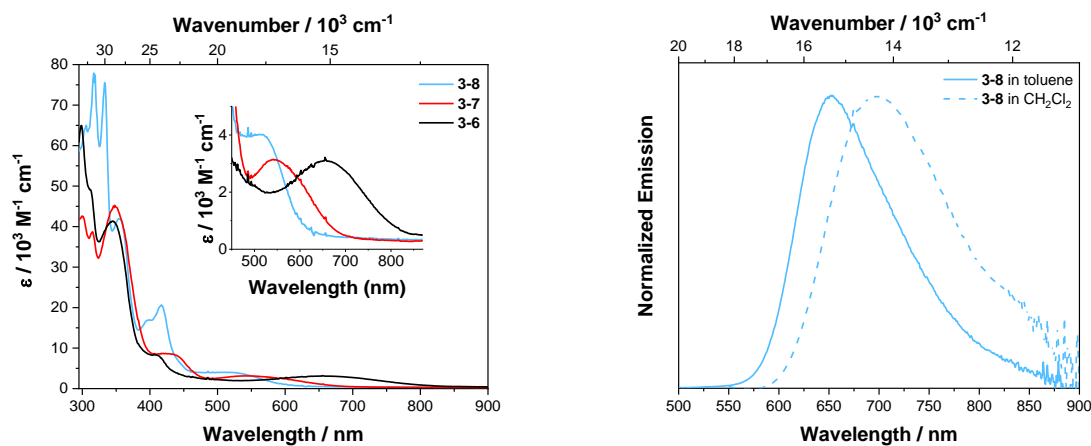


Figure 5-6. Three target K-region substituted derivatives.

X-ray analysis of compound **3-7** shows that the introduction of the acceptors at the K-region results in an enhanced aromatic character of the former K-region bonds. Thus, this bond is no longer a C=C double bond but rather has aromatic character.

All three target derivatives exhibit strong bathochromically shifted absorption maxima (519-658 nm), which is a result of the outstanding charge transfer character introduced into the D- $\pi$ -D pyrene system through the additional acceptor moiety at the K-region. Compound **3-8** is emissive in the red to NIR region with an emission maximum at 700 nm in  $\text{CH}_2\text{Cl}_2$ . Its excited state lives unusual long for K-region substituted pyrenes; however, such a lifetime is rather typical for 2,7-substituted pyrene derivatives.



**Figure 5-7.** Absorption (left) of **3-6**, **3-7** and **3-8** recorded in toluene and emission (right) spectrum of **8** recorded in toluene and  $\text{CH}_2\text{Cl}_2$ .

Electrochemical studies revealed that all three derivatives possess very low and reversible reduction and oxidation potentials, which is a result of the strong donor and acceptor groups.

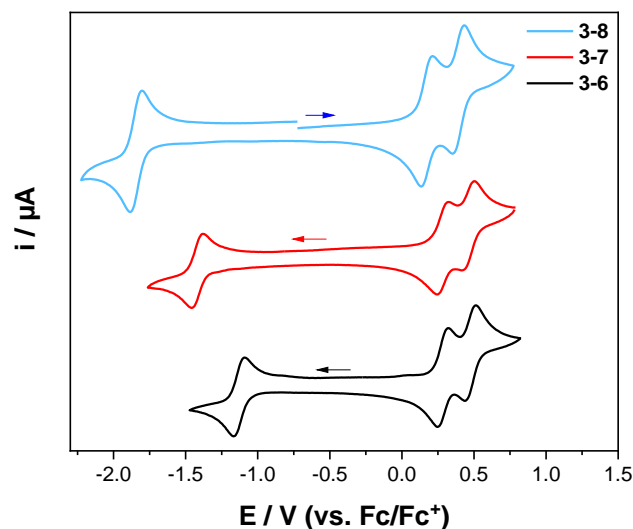


**Figure 5-8.** Cyclic voltammograms of **3-6**, **3-7** and **3-8** in  $\text{CH}_2\text{Cl}_2/0.1 \text{ M } [n\text{-Bu}_4\text{N}][\text{PF}_6]$  250 mV/s.

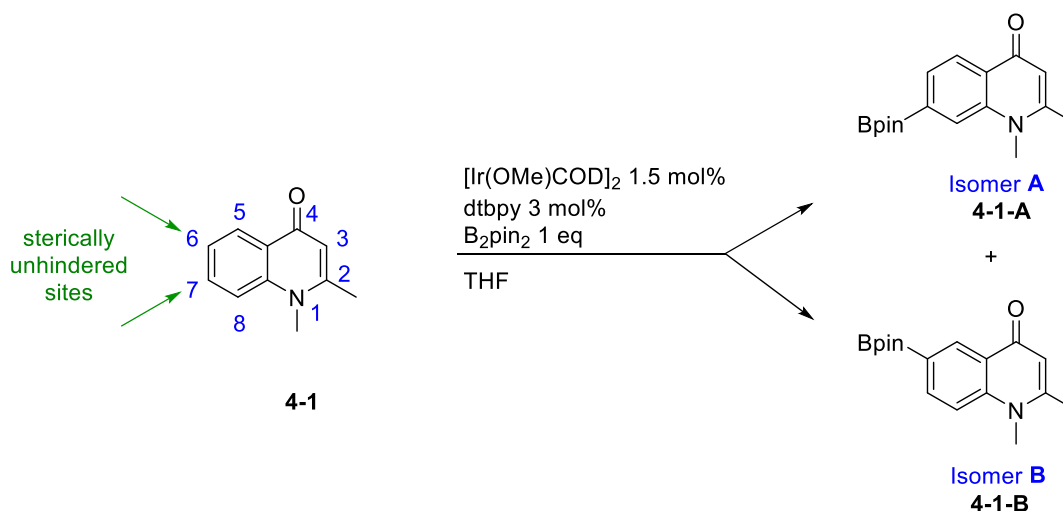
DFT and TD-DFT calculations show strong intramolecular charge transfer character of the  $S_1 \leftarrow S_0$  transition that has mainly  $\text{HOMO} \rightarrow \text{LUMO}$  character in both pyrene derivatives **3-7** and **3-8**.

### 5.1.4 Chapter 4

Compounds based on 4-quinolones are of great interest particularly for medical applications. However, even though these quinolones demonstrated important properties, the synthesis of 4-quinolones that bear substituents at the 6- or 7-positions remain challenging.

In a cooperation with Dr. Gerard P. McGlacken at University College Cork in Ireland, different quinolones were borylated using an iridium catalyst system to study the electronic and steric effect of the substrates. It was possible to demonstrate that the Ir-catalyzed borylation with the dtbpy ligand allows the direct borylation of various 4-quinolones at the 6- and 7-positions. Thus, later stage functionalization is possible with this method and more highly functionalized quinolones are also compatible with this mild reaction conditions.

The borylation usually occurred at the least sterically hindered positions, which are the 6- and the 7-positions.

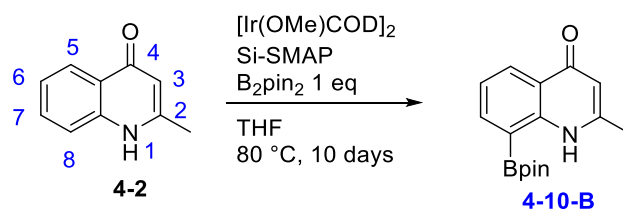


**Scheme 5-1.** Ir/dtbpy-catalyzed borylation of quinolone **4-1** with  $\text{B}_2\text{pin}_2$  in THF.

However, some electronic effects play an important role and, consequently, the most acidic C–H moiety was borylated with higher selectivity. Thus, in the case of quinolone **4-1**, the 7-position was preferably borylated.

In a further investigation, borylation of 4-quinolones using the Si-SMAP ligand combined with the Ir-catalyst allowed regioselective C–H borylation at the 8-position (Scheme 5-6). Hence, the selectivity with this ligand is different to the one with the dtbpy ligand as the regioselectivity is

governed by directing groups rather than steric effects. Thus, borylation with the Si-SMAP ligand always occurs *peri* to the 1-NH directing group. In addition, NMR experiments also showed that the ketone moiety at the 4-position cannot direct the borylation. Thus, if the NH moiety is protected by a methyl group the borylation does not occur.



**Scheme 5-2.** Ir/Si-SMAP-catalyzed borylation of quinolone **4-2** with  $B_2pin_2$  in THF.

## 5.2 Zusammenfassung

### 5.2.1 Kapitel 1

Pyren ist ein polycyclischer aromatischer Kohlenwasserstoff (PAK) mit sehr interessanten photophysikalischen Eigenschaften, der sich daher für ein breites Anwendungsspektrum eignet. Die 2,7-Positionen von Pyren befinden sich sowohl im HOMO als auch im LUMO auf Knotenebenen. Daher finden elektrophile Reaktionen an den 1-, 3-, 6- und 8-Positionen statt. Marder und Mitarbeiter demonstrierten zuvor eine selektive Methode, um die 2,7-Positionen direkt durch eine Iridium-katalysierte C–H Borylierung zu funktionalisieren. Auf diese Weise konnten sie eine große Bibliothek verschiedener 2- und 2,7-substituierter Pyrenderivate erstellen. Das Ziel dieses Projekts war die Entwicklung neuer Pyrenderivate, die an den 2- und 2,7-Positionen substituiert sind und sehr starke Donoren oder / und Akzeptoren aufweisen, um beispiellose Eigenschaften zu erzielen und ein tiefgreifenderes Verständnis für die Steuerung der angeregten Zustände und Redoxzustände zu erhalten. Aus diesem Grund wurde die Julolidin-Einheit als sehr starker Donor gewählt um D- $\pi$  (**1-8**) und D- $\pi$ -D (**1-4**) -Systeme zu entwickeln und mit Bmes<sub>2</sub> als sehr starker Akzeptor wurde ein D- $\pi$ -A (**1-II**) System entwickelt.

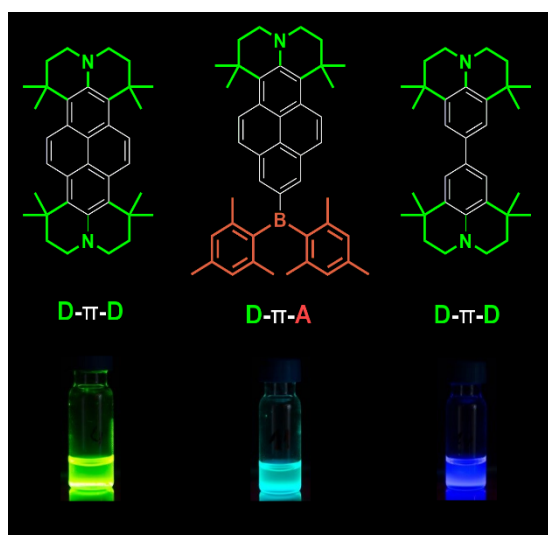


**Abbildung 5-6.** Drei Zielderivate dieses Projekts mit ihrer Emission in einer Hexanlösung.

Diese Verbindungen zeigen ungewöhnliche photophysikalische Eigenschaften wie die Emission im grünen Bereich des elektromagnetischen Spektrums in Hexan, während alle anderen zuvor beschriebenen Pyrenderivate, die an den 2,7-Positionen substituiert sind, blaue Lumineszenz

zeigen. Interessanterweise emittiert das D- $\pi$ -D-Pyrenderivat weiter bathochrom verschoben als das D- $\pi$ -A-Pyrenderivat. Folglich destabilisiert die zweite Donoreinheit den Grundzustand  $S_0$  offensichtlich stärker als der zusätzliche Akzeptor Bmes<sub>2</sub> den angeregten Singulettzustand  $S_1$ . Darüber hinaus legen spektroelektrochemische Messungen eine unerwartet starke Kopplung zwischen den Substituenten an den 2,7-Positionen von Pyren im D- $\pi$ -D-System nahe. Weiterhin wurde die analoge Verbindung **1-14** synthetisiert und oxidiert, um die Elektronendelokalisierung über die Pyren- und Biphenylbrücke zu vergleichen. Die Auswertung der wachsenden IV-CT Bande im NIR der Monokationspezies beider D- $\pi$ -D-Systeme zeigt, dass diese Verbindungen als typische delokalisierte Robin-Day-Klasse-III-Derivate eingestuft werden können, wobei die elektronische Kopplung im Biphenylderivat etwas stärker ist.

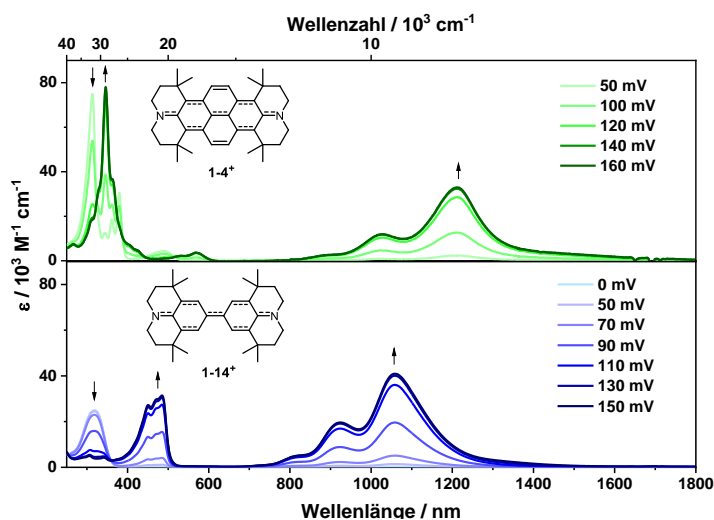


**Abbildung 5-7.** Spektroelektrochemische Messungen der schrittweisen Oxidationsprozesse in  $\text{CH}_2\text{Cl}_2$  / 0.1 M [n-Bu<sub>4</sub>N] [PF<sub>6</sub>]. Die Absorptionsspektren von **1-4**<sup>+</sup> und **1-14**<sup>+</sup> sind als durchgezogene dunkelgrüne bzw. durchgezogene dunkelblaue Linien angegeben.

Theoretische Studien zeigen, dass diese Eigenschaften aus der sehr starken Kopplung zwischen dem Julolidin-Donor und Bmes<sub>2</sub>-Akzeptor mit dem Pyren HOMO-1 bzw. LUMO + 1 resultieren. Die Destabilisierung des Ersteren und die Stabilisierung des Letzteren führen zu einem Orbital-Shuffle zwischen HOMO und HOMO-1 und LUMO und LUMO+1 von Pyren. Folglich ändert der  $S_1$ -Zustand seinen Charakter ausreichend, um eine höhere Oszillatorstärke zu erzielen. Die photophysikalischen und elektrochemischen Eigenschaften werden damit stark von den Substituenten beeinflusst.

## 5.2.2 Kapitel 2

Der polycyclische aromatische Kohlenwasserstoff Perylen, insbesondere Perylendiimid, erlangte in den letzten Jahren beträchtliche Aufmerksamkeit und fand Verwendung in zahlreichen Anwendungen wie Farbstoffen, Pigmenten oder Halbleitern. Dennoch ist es von grundlegender Bedeutung zu verstehen, wie die elektronischen und photophysikalischen Eigenschaften von Perylen in Abhängigkeit von der spezifischen gewünschten Anwendung moduliert werden können. Perylene ohne Carboxyimidgruppen an den Peripositionen sind aufgrund der Schwierigkeiten bei der direkten Funktionalisierung des Perylenkerns bislang kaum untersucht worden. Ziel dieses Projektes war es den bisher unbekanntem Einfluss von Substituenten auf die *ortho*-Positionen des Perylenkerns zu untersuchen.

Es wurden zwei Perylenderivate synthetisiert, die an den *ortho*-Positionen vier starke Diphenylamin-Donor oder vier starke Bmes<sub>2</sub>-Akzeptor-Einheiten aufweisen. Diese Verbindungen stellen die ersten Beispiele für Perylene dar, die nur an den *ortho*-Positionen mit Donoren oder Akzeptoren substituiert sind.

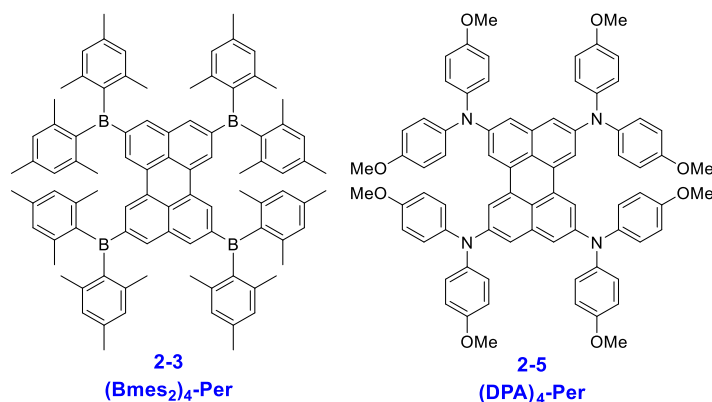
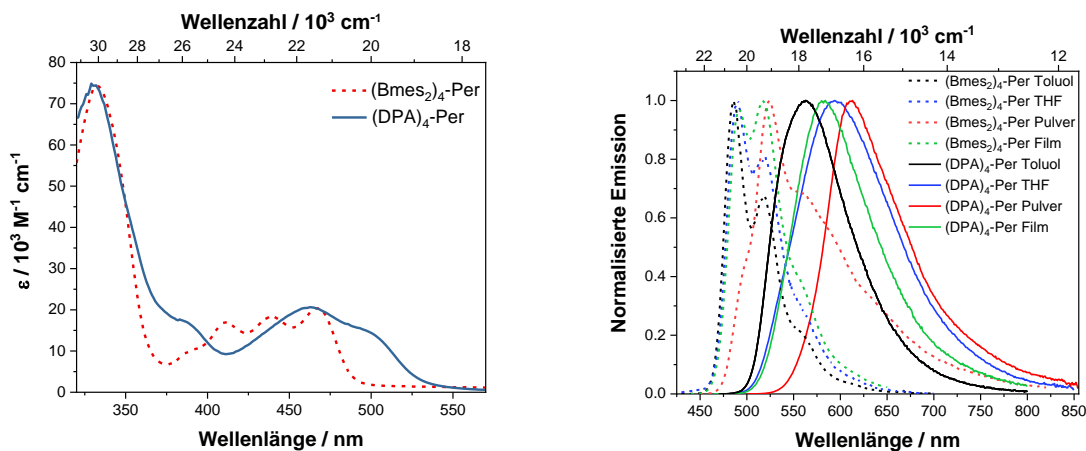


Abbildung 5-8. Die zwei Zielverbindungen.

Die Untersuchungen zeigen, dass die photophysikalischen und elektronischen Eigenschaften dieser Derivate im Vergleich zu den gut untersuchten Perylendiimiden einzigartig sind. Somit sind bis zu vier reversible Reduktionen oder Oxidationen dieser Verbindungen möglich, was für monomere Perylene bisher beispiellos ist. Darüber hinaus zeigen diese Derivate Stabilität gegenüber sehr hohen Potentialen. Spektroelektrochemische Untersuchungen zeigten Absorptionen des Monokations des donorsubstituierten Perylens von bis zu 3000 nm. Des Weiteren kann es als vollständig delokalisierte Robin-Day-Klasse-III-Verbindung klassifiziert

werden. Darüber hinaus sind die photophysikalischen Eigenschaften dieser beiden *ortho*-substituierten Derivate in vielerlei Hinsicht ungewöhnlich im Vergleich zu den bekannten Perylenen. Durch Substitution an den *ortho*-Positionen werden große Stokes-Verschiebungen erhalten und der Singulett-angeregte Zustand unserer Derivate ist mit intrinsischen Lebensdauern von bis zu 94 ns bemerkenswert lang.



**Abbildung 5-4.** Absorptions- (links) (in Toluol) und Emissionsspektren (rechts) von **(Bmes<sub>2</sub>)<sub>4</sub>-Per** und **(DPA)<sub>4</sub>-Per**.

Transiente Absorptionsmessungen ergaben einen weiteren angeregten Zustand mit einer Lebensdauer von 500  $\mu$ s, der Singulett-sauerstoff sensibilisiert. Außerdem emittieren diese beiden Derivate im festen Zustand, da die vier großen Substituenten  $\pi$ - $\pi$ -Wechselwirkungen blockieren. Die Röntgenstrukturanalyse des aminsubstituierten Derivats zeigt einen nahezu planaren Perylenkern. Daher beeinflussen weder die verwendeten Amin- noch Triarylboransubstituenten an den *ortho*-Positionen die Planarität des Perylenkerns, was sich von den *bay*-substituierten Perylenen unterscheidet.

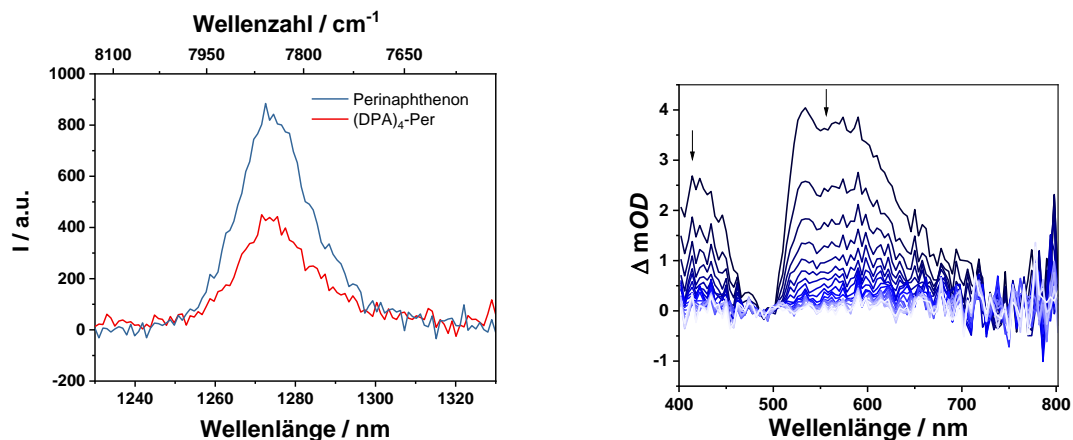


**Abbildung 5-5.** Singulett-Sauerstoff-Lumineszenz aus optisch abgestimmten Toluollösungen von **(DPA)<sub>4</sub>-Per** und dem Standard-Perinaphthenon; Anregung bei 340 nm (links); Transiente Nanosekunden-Absorptionsspektrum von **(DPA)<sub>4</sub>-Per** in einer entgasteten DMF-Lösung (rechts) gemessen in Intervallen von 169,9  $\mu$ s.

### 5.2.3 Kapitel 3

Da das D- $\pi$ -D-Pyrenderivat (**1-4**) sehr ungewöhnliche Eigenschaften wie grüne Lumineszenz und eine stark rotverschobene  $S_1 \leftarrow S_0$ -Absorption aufwies, wurden weitere Derivate mit zusätzlichen Akzeptoreinheiten in der K-Region von Pyren synthetisiert. Leider war es synthetisch nicht möglich, ein Derivat mit Julolidin-Typ Donoren an den 2,7-Positionen und zusätzlichen Akzeptoreinheiten zu erhalten. Der Wechsel vom Julolidin-Typ Donor zum Diphenylamin-Donor ermöglichte jedoch die erfolgreiche Synthese von drei neuen Zielerivaten.

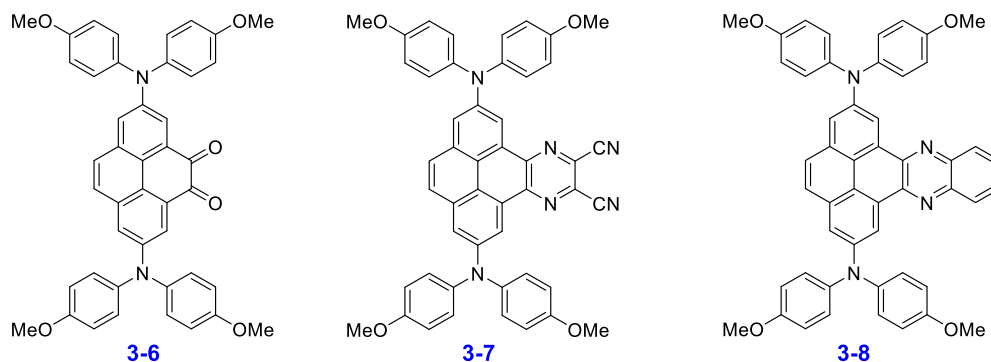


**Abbildung 5-9.** Die drei Zielerivate.

Die Röntgenstrukturanalyse von Verbindung **3-7** zeigt, dass die Einführung der Akzeptoren in der K-Region zu einem verstärkten aromatischen Charakter der früheren K-Region-Bindungen führt. Somit ist diese Bindung nicht mehr mit einer C=C-Doppelbindung zu vergleichen, sondern hat eher aromatischen Charakter.

Alle drei Zielderivate weisen starke bathochrom verschobene Absorptionsmaxima (519-658 nm) auf, was auf den hervorragenden Ladungstransfercharakter zurückzuführen ist, der durch die zusätzliche Akzeptoreinheit in der K-Region in das D- $\pi$ -D-Pyrensystem eingeführt wurde. Die Verbindung **3-8** emittiert im Rot-NIR-Bereich mit einem Emissionsmaximum bei 700 nm in CH<sub>2</sub>Cl<sub>2</sub>. Der angeregte Zustand ist ungewöhnlich langlebig für K-substituierte Pyrene, diese sind jedoch typisch für 2,7-substituierte Pyrenderivate.

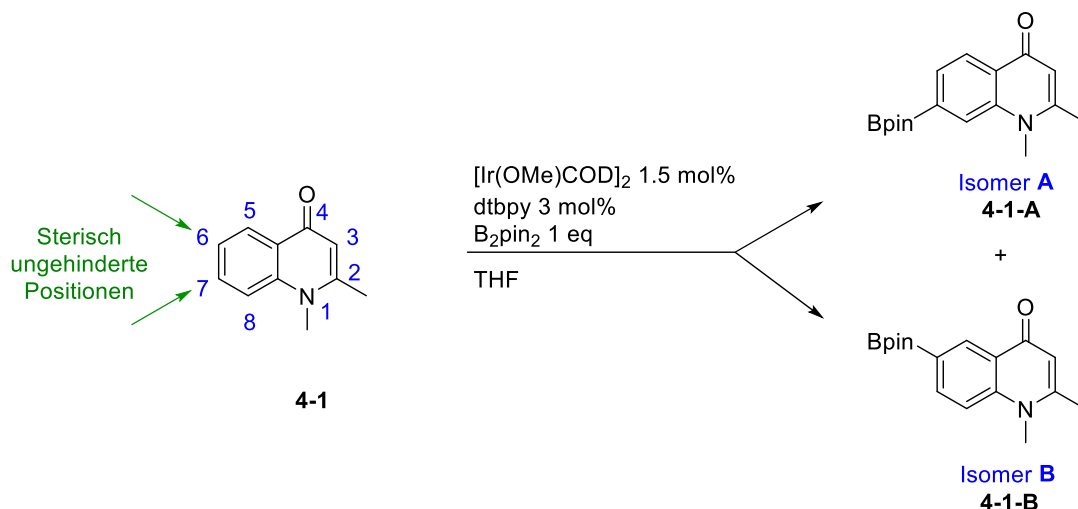
Elektrochemische Untersuchungen ergaben, dass alle drei Derivate sehr niedrige und reversible Reduktions- und Oxidationspotentiale besitzen, was auf die starken Donor- und Akzeptorgruppen zurückzuführen ist.

#### **5.2.4 Kapitel 4**

Verbindungen auf der Basis von 4-Quinolonen sind insbesondere für medizinische Anwendungen von großem Interesse. Obwohl diese Quinolone wichtige Eigenschaften aufwiesen, bleibt die Synthese von 4-Quinolonen mit Substituenten in 6- oder 7-Stellung eine Herausforderung.

In Zusammenarbeit mit Dr. Gerard P. McGlacken vom University College Cork in Irland wurden verschiedene Quinolone mittels eines Iridium-Katalysatorsystems boryliert, um die elektronische und sterische Kontrolle der Substrate zu untersuchen. Es konnte gezeigt werden, dass die Ir-katalysierte Borylierung mit dem dtbpy-Liganden die direkte Borylierung verschiedener 4-Quinolone in 6- und 7-Position ermöglicht. Somit ist mit dieser Methode eine spätere Funktionalisierung möglich, und höher funktionalisierte Quinolone sind mit diesen milden Reaktionsbedingungen auch kompatibel.

Die Borylierung trat, wie erwartet, an den am wenigsten sterisch gehinderten Positionen auf, nämlich an der 6- und der 7-Position.



**Schema 5-1.** Ir/dtbpy-katalysierte Borylierung von Quinolon **4-1** mit  $\text{B}_2\text{pin}_2$  in THF.

Einige elektronische Effekte spielen jedoch eine wichtige Rolle, weshalb die azideste C–H Position mit höherer Selektivität boryliert wurde. So wurde im Fall von Quinolon **4-1** die 7-Position vorzugsweise boryliert.

In einer weiteren Untersuchung ermöglichte die Borylierung von 4-Quinolonen mit dem Si-SMAP-Liganden in Kombination mit dem Ir-Katalysator eine regioselektive C–H Borylierung an der 8-Position (Schema 5-6). Daher unterscheidet sich die Selektivität mit diesem Liganden von der mit dem dtbpy-Liganden. Die Regioselektivität wird mit dem Si-SMAP Liganden eher durch dirigierende Gruppen als durch sterische Effekte bestimmt. Daher erfolgt die Borylierung mit dem Si-SMAP-Liganden immer *peri* zur 1-NH dirigierenden Gruppe. Zusätzlich zeigten NMR-Experimente auch, dass die Ketongruppe an der 4-Position die Borylierung nicht dirigieren kann. Wenn also die NH-Einheit durch eine Methylgruppe geschützt ist, findet keine Borylierung statt.



# **Chapter 6**

## Experimental



## 6 Experimental

### 6.1 General Information

Unless otherwise noted, the following conditions apply. Reactions were performed using standard Schlenk or glovebox (Innovative Technology Inc.) techniques under an atmosphere of argon. Only oven-dried glassware was used. Solvents used for the synthesis were HPLC grade, further treated to remove trace water using a commercial solvent purification system and deoxygenated using the freeze-pump-thaw method.

The catalyst  $[\text{Ir}(\text{OMe})\text{COD}]_2$ ,<sup>[317]</sup>  $\text{Pd}_2(\text{dba})_3 \cdot \text{CHCl}_3$ ,<sup>[318]</sup> and the starting materials 2,7-(Bpin)pyrene,<sup>[32,46]</sup> 2-(Bpin)pyrene,<sup>[32,46]</sup> 4-Bpin-tetramethyljulolidine,<sup>[74]</sup> pyrene-4,5-dione<sup>[237,240,319,320]</sup> and pyrene-4,5,9,10-tetraone<sup>[237]</sup> were prepared according to literature procedures. All other starting materials were purchased from commercial sources and used as received.

Microwave-heating was performed in a Biotage® Initiator+ reactor. The reactions were set up in standard microwave tubes 20 mL, which were sealed with crimp caps. Reaction progress was monitored using thin layer chromatography (TLC) plates pre-coated with a layer of silica (Polygram® Sil G/UV254) with fluorescent indicator UV254 from Macherey-Nagel. Column chromatography was performed using either Silica Gel 60 (40-63 microns) or  $\text{Al}_2\text{O}_3$  as the stationary phase and the solvent system indicated. Automated flash column chromatography was performed using a Biotage® Isolera Four system with silica gel (Biotage SNAP cartridge KP-Sil 50 g, KP-Sil 100 g or KP-NH II g obtained from Biotage) as the stationary phase and the solvent system indicated. Solvents were generally removed *in vacuo* using a rotary evaporator at a maximum temperature of 50 °C.

The  $^1\text{H}$ ,  $^{13}\text{C}\{^1\text{H}\}$ ,  $^{11}\text{B}\{^1\text{H}\}$ ,  $^{19}\text{F}$ ,  $^{15}\text{N}$  HMBC NMR spectra were recorded at ambient temperature in  $\text{CDCl}_3$ ,  $\text{CD}_2\text{Cl}_2$ ,  $\text{DMSO}-d_6$ , benzene- $d_6$ , THF- $d_8$ ,  $\text{CD}_3\text{OD}$  solutions either on a Bruker Avance I HD 500 ( $^1\text{H}$ , 500 MHz;  $^{13}\text{C}$ , 125 MHz;  $^{11}\text{B}$ , 160 MHz,  $^{19}\text{F}$ , 470 MHz) or Bruker Avance III HD 300 ( $^1\text{H}$ , 300 MHz;  $^{13}\text{C}$ , 75 MHz;  $^{11}\text{B}$ , 96 MHz) spectrometer.  $^1\text{H}$  NMR and  $^{13}\text{C}$  spectra are referenced to the residual protonated solvent  $\text{CDCl}_3$  ( $^1\text{H}$ ,  $\delta = 7.26$ ),  $\text{CD}_2\text{Cl}_2$  ( $^1\text{H}$ ,  $\delta = 5.32$ ),  $\text{DMSO}-d_6$  ( $^1\text{H}$ ,  $\delta = 2.50$ ), benzene- $d_6$  ( $^1\text{H}$ ,  $\delta = 7.16$ ), THF- $d_8$  ( $^1\text{H}$ ,  $\delta = 1.72$ ) or  $\text{CD}_3\text{OD}$  ( $^1\text{H}$ ,  $\delta = 3.31$ ).  $^{13}\text{C}$  NMR spectra were broad-band proton decoupled  $^{13}\text{C}\{^1\text{H}\}$ .  $^{11}\text{B}\{^1\text{H}\}$  NMR signals were referenced to external  $\text{BF}_3 \cdot \text{OEt}_2$

and  $^{15}\text{N}$  HMBC signals were referenced to  $\text{MeNO}_2 + 10\% \text{CDCl}_3$ . Chemical shifts are listed in parts per million (ppm) and coupling constants in Hertz (Hz). The solid-state magic-angle spinning (MAS) NMR spectra were recorded using a Bruker DSX-400 spectrometer operating at 128 MHz for  $^{11}\text{B}$  and 100 MHz for  $^{13}\text{C}$  with a 4 mm rotor (o. d.). Chemical shifts were calibrated externally using adamantane (38.48 ppm). Isotropic chemical shifts were estimated by simulating the observed spectrum using the Solid Line Shape Analysis 2.2.4 (SOLA) module in Bruker TopSpin 3.5. The second order quadrupolar powder patterns were simulated to extract the isotropic chemical shifts ( $\delta_{\text{iso}}$ ), the quadrupolar constants ( $C_q$ ) and the asymmetry parameters ( $\eta_{\text{Quad}}$ ).

HRMS were recorded using a Thermo Scientific Exactive Plus Orbitrap MS system with either an Atmospheric Sample Analysis Probe (ASAP) or by Electrospray Ionization (ESI). Elemental analyses were performed on an Elementar vario MICRO cube elemental analyzer.

## 6.2 Cyclic Voltammetry

Cyclic voltammetry experiments were performed using a Gamry Instruments Reference 600 potentiostat. A standard three-electrode cell configuration was employed using a platinum disk working electrode, a platinum wire counter electrode, and a silver wire, separated by a Vycor tip, serving as the reference electrode. Formal redox potentials are referenced to the ferrocene/ferrocenium ( $[\text{Cp}_2\text{Fe}]^{+/0}$ ) redox couple by using decamethylferrocene ( $[\text{Cp}^*_2\text{Fe}]$ ;  $E_{1/2} = -0.427 \text{ V}$  in THF and  $E_{1/2} = -0.532 \text{ V}$  in  $\text{CH}_2\text{Cl}_2$ ) as an internal standard. Tetra-*n*-butylammonium hexafluorophosphate ( $[\text{n-Bu}_4\text{N}][\text{PF}_6]$ ) or  $[\text{n-Bu}_4\text{N}][\text{Al}(\text{OC}(\text{CF}_3)_3)_4]$  were employed as supporting electrolytes. Compensation for resistive losses (*iR* drop) was employed for all measurements.

## 6.3 Single Crystal X-Ray Diffraction

A crystal suitable for single-crystal X-ray diffraction was selected, coated in perfluoropolyether oil, and mounted on a MiTeGen sample holder. Diffraction data were collected on a Bruker X8 Apex II 4-circle diffractometer with a CCD area detector using Mo-K $\alpha$  radiation generated by a Nonius FR591 rotating anode and monochromated by graphite. The crystal was cooled using an Oxford Cryostreams low-temperature device. Data were collected at 100 K. The images were processed and corrected for Lorentz-polarization effects and absorption as implemented in the Bruker software packages. The structure was solved using the intrinsic phasing method

(SHELXT)<sup>[321]</sup> and Fourier expansion technique. All non-hydrogen atoms were refined in anisotropic approximation, with hydrogen atoms ‘riding’ in idealized positions, by full-matrix least squares against  $F^2$  of all data, using SHELXL<sup>[322]</sup> software. Diamond<sup>[323]</sup> software was used for graphical representation. Other structural information was extracted using Mercury<sup>[324]</sup> and OLEX2<sup>[325]</sup> software. Full structural information has been deposited with Cambridge Structural Database. CCDC-1542751 to 1542757, CCDC-1881912, CCDC-1917153 to 1917159.

## 6.4 General Photophysical Measurements

All photophysical measurements were carried out under an argon atmosphere. All solution state measurements were performed in standard quartz cuvettes (1 cm x 1 cm cross section). UV/Vis absorption spectra were recorded using an Agilent 1100 diode array UV/Vis spectrophotometer. Excitation, emission, lifetime and quantum yield measurements were recorded using an Edinburgh Instruments FLSP920 spectrometer equipped with a 450 W Xenon arc lamp, double monochromators for the excitation and emission pathways, and a red-sensitive photomultiplier (PMT-R928P) and a near-IR PMT as detectors. The measurements were made in right-angle geometry mode and all spectra were fully corrected for the spectral response of the instrument. All solutions used in photophysical measurements had a concentration lower than  $10^{-5}$  M.

## 6.5 Fluorescence Quantum Yield Measurements

Fluorescence quantum yields of the samples were measured using a calibrated integrating sphere (150 mm inner diameter) from Edinburgh Instruments combined with the FLSP920 spectrometer described above. For solution-state measurements, the longest wavelength absorption maximum of the compound in the respective solvent was chosen for the excitation. In order to avoid self-absorption, the emission spectra were measured with dilute samples (*ca.* 0.1 OD at the excitation wavelength).

## 6.6 Fluorescence Lifetime Measurements

Lifetime measurements were conducted using the time-correlated single-photon counting method (TCSPC) on the FLSP920 spectrometer equipped with a high-speed photomultiplier tube positioned after a single emission monochromator. Measurements were made in right-angle geometry mode, and the emission was collected through a polarizer set to the magic angle. Solutions were excited with either a 315 (pulse width 932.5 ps), 376 (pulse width 72.6 ps) or a

472 nm (pulse width 90.6 ps) pulsed diode laser at repetition rates of 1-5 MHz and were recorded at emission maxima. Decays were recorded to 10 000 counts in the peak channel with a record length of at least 1 000 channels. The band-pass of the monochromator was adjusted to give a signal count rate of <20 KHz. Iterative reconvolution of the IRF with one decay function and nonlinear least-squares analysis were used to analyze the data. The quality of all decay fits was judged to be satisfactory, based on the calculated values of the reduced  $\chi^2$  and Durbin-Watson parameters and visual inspection of the weighted and autocorrelated residuals.

## 6.7 Transient Absorption Measurements

Transient absorption spectra were measured with an Edinburgh LP920 laser flash spectrometer equipped with a EKSPLA NT340 Nd:YAG laser with integrated optical parametric oscillator, a 450 W Xe flash lamp, a Hamamatsu R955 photomultiplier and a Tektronix TD3012B oscilloscope for detection of the spectra. The transient maps were obtained by measuring decay profiles in 4 nm steps between *ca.* 25 000  $\text{cm}^{-1}$  (400 nm) and 14 085  $\text{cm}^{-1}$  (710 nm). The instrument response (*ca.* 8 ns) of the set-up was determined by measuring the scattered light using a LUDOX AS-30 colloidal silica suspension in water. Decay curves were fitted with the tailfit function of the spectrometer software. The quality of all decay fits was judged to be satisfactory, based on the calculated values of the reduced  $\chi^2$  and Durbin-Watson parameters and visual inspection of the weighted and autocorrelated residuals. All solvents were spectroscopic grade and were used without further purification. The sample solutions in the quartz cuvettes were carefully degassed by bubbling argon through the solutions. The samples were excited with *ca.* 3-6 ns laser pulses at 10 Hz repetition rate. Measurements were performed at pulse energies of 1.2 mJ (excitation at 460 and 550 nm). The stability of the samples was verified by recording the steady-state absorption spectra before and after the time-resolved measurements.

## 6.8 Spectroelectrochemical Measurements

Spectroelectrochemical experiments in reflection mode were performed using an Agilent Cary 5000 spectrometer in combination with a designed sample compartment consisting of a cylindrical PTFE cell with an Infrasil® wedge window with an angle of 0.5° and an adjustable three-in-one electrode (6 mm platinum disc working electrode, 1 mm platinum counter electrode and pseudo reference electrode). The potentials were adjusted with a Gamry 600

potentiostat and all experiments were measured at room temperature under an argon atmosphere.

## 6.9 Theoretical Studies

All calculations (DFT and TD-DFT) were carried out with the program package Gaussian 09 (Rev. E.01)<sup>[326]</sup> and were performed on a parallel cluster system. GaussView 5.0.9 was used to visualize the results, to measure calculated structural parameters, and to plot orbital surfaces (isovalue:  $\pm 0.02 [e a_0^{-3}]^{1/2}$ ). The ground-state geometries were optimized using the B3LYP functional<sup>[327]</sup> in combination with the 6-31G (d) or 6-31 G (d,p) basis set.<sup>[328]</sup> The optimized geometries were confirmed to be local minima by performing frequency calculations and obtaining only positive (real) frequencies. Based on these optimized structures, the lowest-energy gas-phase vertical transitions were calculated (singlets, 10 states) by TD-DFT, using the Coulomb-attenuated functional CAM-B3LYP<sup>[329]</sup> in combination with the 6-31 G (d,p) or 6-31 G (d) basis set. The calculations of the monocations were performed at the density functional level, using UBLYP with 35% exact-exchange admixture, the SVP basis set and a polarizable continuum model accounting for solvent effects. The time dependent (TD-DFT) calculations were done at the same level of theory.<sup>[110,330]</sup>

## 6.10 Synthesis

### 2,7-Diaminopyrene (1-1)

To a Schlenk flask, 2,7-bis(Bpin)pyrene (4.60 mmol, 2.09 g) and hydroxylamine-*O*-sulfonic acid (HSA) (13.8 mmol, 1.65 g) were added followed by MeCN (25 mL) and NaOH (1.00 M, 25.0 mL). The biphasic mixture was stirred at r.t. for 18 h. The precipitated solid was collected by centrifugation. The liquid phase was removed and the solid washed with water, MeCN and hexane by putting the centrifuge tube into an ultrasonic bath for 15 min. The title compound was obtained as a bright yellow powder (0.86 g, 80%).

$^1\text{H NMR}$  (500 MHz, THF-*d*<sub>8</sub>, r.t., ppm):  $\delta$  = 7.66 (s, 4 H), 7.28 (s, 4 H), 4.73 (br, 4 H, NH<sub>2</sub>).

$^{13}\text{C}\{^1\text{H}\}$  NMR (125 MHz, THF-*d*<sub>8</sub>, r.t., ppm):  $\delta$  = 146.3, 131.8, 127.1, 119.6, 111.7.

$^{15}\text{N NMR}$  (300 MHz, THF-*d*<sub>8</sub>, r.t., ppm):  $\delta$  = -327.5.

**HRMS** (ASAP<sup>+</sup>): *m/z* found: 233.1069 [M+H]<sup>+</sup>; calcd. for [C<sub>16</sub>H<sub>12</sub>N<sub>2</sub>+H]<sup>+</sup> 233.1073 (| $\Delta$ | = 1.72 ppm).

**Elem. anal. calcd.** (%) for C<sub>16</sub>H<sub>12</sub>N<sub>2</sub> C 82.73, H 5.21, N 12.06; found: C 82.62, H 5.33, N 12.19.

***N, N, N, N*-Tetrakis(3-methylbut-2-enyl)pyrene-2,7-diamine (1-2)**

In a round-bottom flask fitted with a reflux condenser **1-1** (3.30 mmol, 0.77 g), K<sub>2</sub>CO<sub>3</sub> (6.60 mmol, 0.91 g), molecular sieves (4 Å, 0.50 g), 1-chloro-3-methylbut-2-ene (14.5 mmol, 1.52 g) were dissolved in MeCN (100 mL). The reaction mixture was heated to 80 °C for 48 h. After cooling to r.t. and removing the solvent, the crude product was passed through a pad of alumina with the eluent CH<sub>2</sub>Cl<sub>2</sub>/hexane 1:3. Recrystallization from toluene afforded the title compound as bright yellow needles (0.99 g, 60%).

<sup>1</sup>H NMR (300 MHz, CDCl<sub>3</sub>, r.t., ppm): δ = 7.80 (s, 4 H), 7.45 (s, 4 H), 5.38-5.34 (m, 4 H), 4.09 (d, *J* = 7 Hz, 8 H), 1.80 (s, 12 H), 1.76 (s, 12 H).

<sup>13</sup>C{<sup>1</sup>H} NMR (75 MHz, CDCl<sub>3</sub>, r.t., ppm): δ = 146.8, 134.5, 131.1, 127.3, 122.0, 118.4, 110.8, 48.9, 26.0, 18.2.

<sup>15</sup>N NMR (300 MHz, CDCl<sub>3</sub>, r.t., ppm): δ = -313.5.

**HRMS** (ASAP<sup>+</sup>): *m/z* found 504.3490 [M+H]<sup>+</sup>; calcd. for [C<sub>36</sub>H<sub>44</sub>N<sub>2</sub>] 504.3499 (|Δ| = 1.78 ppm).

**Elem. anal. calcd.** (%) for C<sub>36</sub>H<sub>44</sub>N<sub>2</sub> C 85.66, H 8.79, N 5.55; found: C 85.75, H 8.79, N 5.41.

***N, N, N, N*-Tetrakis(3-methylbut-2-enyl)pyrene-2,7-diammonium chloride (1-3)**

Compound **1-2** (0.15 mmol, 76.0 mg) was suspended in DMF (2 mL) and cooled to 0 °C (ice bath). Concentrated HCl (37%) was added dropwise to the mixture until it became a clear solution. Then, the ice bath was removed, and the solution was stirred for 1 h. The precipitating salt was collected by filtration to give the title compound as white powder (52 mg, 68%).

<sup>1</sup>H NMR (500 MHz, CDCl<sub>3</sub>, r.t., ppm): δ = 14.62 (br, 2 H), 8.59 (s, 4 H), 8.22 (s, 4 H), 5.57-5.53 (m, 4 H), 4.27 (d, *J* = 6 Hz, 8 H), 1.63 (s, 12 H), 1.55 (s, 12 H).

<sup>13</sup>C{<sup>1</sup>H} NMR (125 MHz, CDCl<sub>3</sub>, r.t., ppm): δ = 143.7, 137.4, 132.0, 128.8, 123.7, 119.6, 113.0, 55.5, 25.9, 18.4.

HRMS (HESI<sup>+</sup>): *m/z* found 505.35767 [M+H]<sup>+</sup>; calcd. for [M+H]<sup>+</sup> 505.35773 (|Δ| = 1.19 ppm).

**Jul<sub>2</sub>Pyr (1-4)**

Compound **1-3** (0.10 mmol, 51.0 mg) was added into a 100 mL round bottom flask and MeSO<sub>3</sub>H (1.00 mL) was added dropwise which immediately turned the reaction mixture purple. The mixture was stirred at r. t. for 10 min and heated to 95 °C for 2 h. After cooling the reaction mixture to r. t., the pH value was adjusted to 8 with NH<sub>4</sub>OH (25%). The purple solution turned orange and was extracted with toluene (3 x 50 mL) and washed with water (3 x 50 mL) and the organic layer was separated, dried over Na<sub>2</sub>SO<sub>4</sub> and filtrated. The filtrate was passed through a pad of silica with toluene as the eluent. After removing the solvent under reduced pressure, the title compound was obtained as a bright yellow-orange powder in 69% yield.

<sup>1</sup>H-NMR (500 MHz, benzene-*d*<sub>6</sub>, r.t., ppm): δ = 8.54 (s, 4 H), 3.00-2.98 (m, 8 H), 1.89-1.88 (m, 8 H), 1.79 (s, 24 H).

<sup>13</sup>C{<sup>1</sup>H} NMR (125 MHz, benzene-*d*<sub>6</sub>, r.t., ppm): δ = 141.6, 127.5, 125.4, 124.2, 122.7, 47.8, 44.2, 34.4, 32.5.

<sup>15</sup>N NMR (300 MHz, CDCl<sub>3</sub>, r.t., ppm): -309.3; HRMS (ASAP<sup>+</sup>): *m/z* found 505.35676 [M+H]<sup>+</sup> calcd. for [M+H]<sup>+</sup> 505.35773 (|Δ| = 1.92 ppm).

**Elem. anal. calcd.** (%) for C<sub>36</sub>H<sub>44</sub>N<sub>2</sub> C 85.66, H 8.79, N 5.55; found: C 85.25, H 9.03, N 5.29.

**2-Aminopyrene (1-5)**

2-Bpin-pyrene (980 mg, 2.99 mmol) and HSA (1.36 g, 12.0 mmol) were dissolved in MeCN (25 mL) and NaOH (1.00 M, 20.0 mL) in a Schlenk flask. The reaction mixture was stirred at r.t. for 48 h. The suspension was diluted with water (50 mL) and extracted with EtOAc (3 x 40 mL). The combined organic fractions were washed with H<sub>2</sub>O (20 mL), dried over Na<sub>2</sub>SO<sub>4</sub> and the solvent was removed under reduced pressure. Purification of the brown residue by column chromatography (silica, hexane/CH<sub>2</sub>Cl<sub>2</sub>/NEt<sub>3</sub> 1:1:0 to 0:1:0.1) and subsequent recrystallization from toluene gave the title compound as tan metallic plates (510 mg, 79%).

The spectral data match those reported previously.<sup>[331]</sup>

**<sup>1</sup>H-NMR** (300 MHz, CDCl<sub>3</sub>, r.t., ppm):  $\delta$  = 8.09 (d,  $J$  = 8 Hz, 2 H), 7.99 (d,  $J$  = 9 Hz, 2 H), 7.89-7.84 (m, 3 H), 7.48 (s, 2 H), 4.13 (br, 2 H).

**HRMS** (ASAP<sup>+</sup>):  $m/z$  found 218.0961 [M+H]<sup>+</sup>; calcd. for [M+H]<sup>+</sup> 218.0959 ( $|\Delta|$  = 1.38 ppm).

***N,N*-Bis(3-methylbut-2-en-1-yl)pyrene-2-amine (1-6)**

In a Young's tube, **1-5** (300 mg, 1.38 mmol), K<sub>2</sub>CO<sub>3</sub> (477 mg, 3.45 mmol), molecular sieves (4 Å, 0.50 g), 1-chloro-3-methylbut-2-ene (390 μL, 3.45 mmol) were suspended in MeCN (20 mL). The tube was sealed and heated to 80 °C in an oil bath for 48 h. After cooling to r.t., the precipitate was collected by filtration and washed with CH<sub>2</sub>Cl<sub>2</sub> (50 mL). The filtrate was washed with H<sub>2</sub>O (20 mL), dried over Na<sub>2</sub>SO<sub>4</sub> and the solvent was removed under reduced pressure. The brown residue was passed through a pad of alumina with hexane/CH<sub>2</sub>Cl<sub>2</sub> (3:1) as the eluent. The solvents were removed under reduced pressure. Purification of the yellow residue by column chromatography (silica, cyclohexane/CH<sub>2</sub>Cl<sub>2</sub> 3:1) gave the title compound as a yellow oil (224 mg, 46%), that crystallized at r.t. after 14 d.

<sup>1</sup>H NMR (300 MHz, CDCl<sub>3</sub>, r.t., ppm): δ = 8.07 (d, *J* = 8 Hz, 2 H), 7.97 (d, *J* = 9 Hz, 2 H), 7.90 (d, *J* = 9 Hz, 2 H), 7.81-7.86 (t, *J* = 8 Hz, 1 H), 7.51 (s, 2 H), 5.34-5.39 (m, 2 H), 4.14 (br d, *J* = 6 Hz, 4 H), 1.82 (s, 6 H), 1.78 (s, 6 H).

<sup>13</sup>C{<sup>1</sup>H} NMR (75 MHz, CDCl<sub>3</sub>, r.t., ppm): δ = 147.9, 134.8, 132.6, 129.9, 127.6, 127.2, 125.1, 125.0, 124.1, 121.7, 111.8, 110.1, 48.8, 26.0, 18.2.

HRMS (ASAP<sup>+</sup>): *m/z* found: 355.2245 [M+H]<sup>+</sup>; calcd. for [M+H]<sup>+</sup> 355.2250 (|Δ| = 1.41 ppm).

Elem. anal. calcd. (%) for C<sub>26</sub>H<sub>27</sub>N C 88.34, H 7.70, N 3.96; found: C 88.05, H 7.82, N 3.85.

***N,N*-Bis(3-methylbut-2-en-1-yl)pyrene-2-ammonium chloride (1-7)**

In a round-bottom flask **1-6** (1.20 g, 3.39 mmol) was dissolved in DMF (4 mL) and cooled to 0 °C by an ice bath. To this solution, concentrated HCl (37%) (0.60 mL) was added dropwise and the mixture was stirred at 0 °C for 2 h. The precipitate was collected by filtration and washed with THF (3 x 5 mL), affording the title compound as a white solid (656 mg, 50%).

<sup>1</sup>H NMR (500 MHz, CDCl<sub>3</sub>, r.t., ppm): δ = 14.39 (br s, 1 H), 8.46 (s, 2 H), 8.27 (d, *J* = 8 Hz, 2 H), 8.18 (d, *J* = 9 Hz, 2 H), 8.07-8.12 (m, 3 H), 5.56-5.60 (m, 2 H), 4.24-4.29 (m, 4 H), 1.60 (s, 6 H), 1.50 (s, 6 H).

<sup>13</sup>C{<sup>1</sup>H} NMR (126 MHz, CDCl<sub>3</sub>, r.t., ppm): δ = 143.5, 136.4, 132.1, 131.2, 129.5, 127.1, 127.0, 126.3, 124.6, 124.0, 118.4, 113.3, 55.7, 26.0, 18.4.

<sup>15</sup>N NMR (500 MHz, CDCl<sub>3</sub>, r.t., ppm): δ = -307.8.

HRMS (ESI<sup>+</sup>): *m/z* found: 355.22456 [M-Cl]<sup>+</sup>; calcd. for [C<sub>26</sub>H<sub>28</sub>N]<sup>+</sup> 355.22498 (|Δ| = 1.18 ppm).

Elem. anal. calcd. (%) for C<sub>26</sub>H<sub>28</sub>ClN C 80.29, H 7.00, N 3.60; found: C 80.34, H 7.35, N 3.84.

**JulPyr (1-8)**

To a Schlenk flask containing **1-7** (217 mg, 614  $\mu\text{mol}$ ), degassed  $\text{MeSO}_3\text{H}$  (3.00 mL) was added slowly. The solution immediately turned purple and the mixture was stirred at r.t. for 10 min and then heated at 95  $^\circ\text{C}$  in an oil bath for 2.5 h. After cooling to 0  $^\circ\text{C}$ , the pH was raised to 8 by using  $\text{NH}_4\text{OH}$  (25%). The yellow suspension was extracted with toluene (40 mL). The organic fraction was washed successively with  $\text{H}_2\text{O}$  (10 mL), saturated aqueous  $\text{NH}_4\text{Cl}$  (10 mL), brine (10 mL) and  $\text{H}_2\text{O}$  (10 mL) and dried over  $\text{Na}_2\text{SO}_4$ . After removal of the solvent under reduced pressure, the residue was passed through a plug of silica with toluene as the eluent. The solvent was removed under reduced pressure to give the title compound as a yellow solid (177 mg, 82%).

$^1\text{H}$  NMR (300 MHz, benzene- $d_6$ , r.t., ppm):  $\delta$  = 8.56 (d,  $J$  = 10 Hz, 2 H), 7.93 (d,  $J$  = 8 Hz, 2 H), 7.82 (d,  $J$  = 10 Hz, 2 H), 7.68-7.73 (m, 1 H), 2.91-2.95 (m, 4 H), 1.80-1.84 (m, 4 H), 1.71 (s, 12 H);

$^{13}\text{C}\{^1\text{H}\}$  NMR (75 MHz, benzene- $d_6$ , r.t., ppm):  $\delta$  = 143.0, 129.7, 129.6, 126.4, 126.4, 125.8, 125.8, 125.1, 124.3, 121.1, 47.7, 43.9, 34.4, 32.2.

$^{15}\text{N}$  NMR (300 MHz, benzene- $d_6$ , r.t., ppm): -306.8.

HRMS (ASAP<sup>+</sup>):  $m/z$  found: 355.2244  $[\text{M}+\text{H}]^+$ ; calcd. for  $[\text{C}_{26}\text{H}_{27}\text{N}+\text{H}]^+$  355.2250 ( $|\Delta|$  = 1.69 ppm).

Elem. anal. calcd. (%) for  $\text{C}_{26}\text{H}_{27}\text{N}$  C 88.34, H 7.70, N 3.96; found: C 88.46, H 7.83, N 3.72.

**JulPyr-Bpin (1-9)**

In an argon-filled glovebox, **1-8** (2.19 g, 6.20 mmol), B<sub>2</sub>pin<sub>2</sub> (1.57 g, 6.18 mmol), [Ir(OMe)COD]<sub>2</sub> (61.6 mg, 92.9 μmol), dtbpy (49.9 mg, 186 μmol, 3.00 mol%) and hexane (100 mL) were added to a Young's tube. The tube was sealed, taken out of the glovebox and heated at 85 °C in an oil bath for 18 h. After cooling to r.t., the solvent was removed under reduced pressure. Purification of the residue by column chromatography (silica, hexane/CH<sub>2</sub>Cl<sub>2</sub> 1:1) gave the title compound as a yellow solid (1.87 g, 65%).

<sup>1</sup>H NMR (500 MHz, benzene-*d*<sub>6</sub>, r.t., ppm): δ = 8.96 (s, 2 H), 8.48 (d, *J* = 10 Hz, 2 H), 7.91 (d, *J* = 10 Hz, 2 H), 2.89-2.92 (m, 4 H), 1.77-1.79 (m, 4 H), 1.66 (s, 12 H), 1.25 (s, 12 H).

<sup>13</sup>C{<sup>1</sup>H} NMR (126 MHz, benzene-*d*<sub>6</sub>, r.t., ppm): δ = 143.4, 132.2, 130.2, 129.1, 128.4, 128.2, 126.3, 126.3, 125.6, 121.0, 83.8, 47.7, 43.9, 34.3, 32.1, 25.2.

<sup>11</sup>B{<sup>1</sup>H} NMR (160 MHz, benzene-*d*<sub>6</sub>, r.t., ppm): δ = 33.3.

<sup>15</sup>NNMR (500 MHz, benzene-*d*<sub>6</sub>, r.t., ppm): δ = -306.1.

HRMS (ASAP<sup>+</sup>): *m/z* found: 480.3067 [M+H]<sup>+</sup>; calcd. for [C<sub>32</sub>H<sub>38</sub>BNO<sub>2</sub>+H]<sup>+</sup> 480.3068 (|Δ| = 0.21 ppm).

Elem. anal. calcd. (%) for C<sub>32</sub>H<sub>38</sub>BNO<sub>2</sub> C 80.16, H 7.99, N 2.92; found: C 80.04, H 8.18, N 2.97.

**JulPyr-trifluoroborate potassium salt (1-10)**

In a round-bottom flask **1-9** (250 mg, 521  $\mu\text{mol}$ ) was dissolved in MeOH (200 mL). To this solution  $\text{KHF}_2$  (122 mg, 1.56 mmol) in  $\text{H}_2\text{O}$  (2 mL) was added and the mixture was stirred vigorously at r.t. for 20 h. The solvent was removed *in vacuo* and the residue was extracted with hot acetone (3 x 50 mL). The organic fractions were combined and the solvent was removed under reduced pressure. The green residue was purified by recrystallization from ethanol to give the title compound as a green solid (143 mg, 60%).

$^1\text{H}$  NMR (500 MHz,  $\text{DMSO-}d_6$ , r.t., ppm):  $\delta$  = 8.35 (d,  $J$  = 10 Hz, 2 H), 8.02 (s, 2 H), 7.85 (d,  $J$  = 10 Hz, 2 H), 3.23-3.25 (m, 4 H), 1.95-1.97 (m, 4 H), 1.75 (s, 12 H).

$^{13}\text{C}\{^1\text{H}\}$  NMR (126 MHz,  $\text{DMSO-}d_6$ , r.t., ppm):  $\delta$  = 141.9, 129.0, 128.1, 126.9, 125.9, 124.1, 124.1, 123.7, 119.8, 46.9, 43.1, 33.8, 31.6 (one C not observed, likely that attached to B).

$^{11}\text{B}\{^1\text{H}\}$  NMR (160 MHz,  $\text{DMSO-}d_6$ , r.t., ppm):  $\delta$  = 3.8.

$^{19}\text{F}\{^1\text{H}\}$  NMR (470 MHz,  $\text{DMSO-}d_6$ , r.t., ppm):  $\delta$  = -138.0.

HRMS (ESI):  $m/z$  found: 420.2116 [M-K] $^-$ ; calcd. for  $[\text{C}_{26}\text{H}_{26}\text{BF}_3\text{N}]^-$  420.2110 ( $|\Delta|$  = 1.43 ppm)

**JulPyr-Bmes<sub>2</sub> (1-11)**

To a Schlenk flask, **1-10** (212 mg, 461  $\mu\text{mol}$ ) and THF (15 mL) followed by mesMgBr (1.40 M in THF, 0.72 mL, 1.01 mmol) were added to the reaction mixture and the suspension was kept stirring at r.t. for 24 h. The mixture was diluted with H<sub>2</sub>O and extracted with EtOAc (3 x 15 mL). After removing the solvents *in vacuo*, the crude product was purified by column chromatography (silica, cyclohexane/EtOAc 25:1). After removing all remaining solvents under reduced pressure, the title compound was obtained as bright yellow powder (208 mg, 75%).

<sup>1</sup>H NMR (500 MHz, THF-*d*<sub>8</sub>, r.t., ppm):  $\delta$  = 8.49 (d, *J* = 8 Hz, 2 H), 8.10 (s, 2 H), 7.81 (d, *J* = 8 Hz, 2 H), 6.84 (s, 4 H), 3.32-3.30 (m, 4 H), 2.30 (s, 6 H), 1.99 (m, 16 H), 1.77 (s, 12 H).

<sup>13</sup>C{<sup>1</sup>H} NMR (126 MHz, THF-*d*<sub>8</sub>, r.t., ppm):  $\delta$  = 144.0, 143.0, 141.7, 141.5, 139.0, 133.2, 130.5, 129.3, 128.9, 128.6, 126.6, 126.5, 125.8, 120.5, 48.0, 44.0, 34.7, 32.0, 24.0, 21.4.

<sup>15</sup>N NMR (300 MHz, THF-*d*<sub>8</sub>, r.t., ppm): -305.0.

<sup>11</sup>B SSNMR (128 MHz, r.t., ppm)  $\delta$  = 74.3.

HRMS (ASAP<sup>+</sup>): *m/z* found: 601.3871 [M+H]<sup>+</sup>; calcd. for [M+H]<sup>+</sup> 601.3874 ( $|\Delta|$  = 0.50 ppm).

**9-Bromo-tetramethyljulolidine (1-B)**

Tetramethyljulolidine (1.00 g, 4.40 mmol) was dissolved in MeCN (20 mL) in a Schlenk flask and cooled to 0 °C in an ice bath. NBS (0.82 g, 4.58 mmol) was dissolved in MeCN and added dropwise. The solution immediately turned dark and GC-MS results indicated that the reaction was finished within the first 5 min. The mixture was washed with sodium thiosulfate (3 x 10 mL), H<sub>2</sub>O (3 x 10 mL) and extracted with EtOAc (3 x 15 mL). The combined organic layers were dried over Na<sub>2</sub>SO<sub>4</sub> and solvents were removed under reduced pressure. The crude product was passed through a pad of silica with toluene. After removing all remaining solvents under reduced pressure the title compound was obtained as a colorless oil (1.25 g, 92%).

<sup>1</sup>H NMR (500 MHz, DMSO-*d*<sub>6</sub>, r.t., ppm): δ = 7.03 (s, 2 H), 3.12-3.08 (m, 4H), 1.68-1.64 (m, 4 H), 1.19 (s, 12 H).

<sup>13</sup>C{<sup>1</sup>H} NMR (126 MHz, DMSO-*d*<sub>6</sub>, r.t., ppm): δ = 139.6, 132.5, 126.1, 106.7, 45.9, 36.0, 32.1, 30.9.

<sup>15</sup>N NMR (300 MHz, DMSO-*d*<sub>6</sub>, r.t., ppm): δ = -313.3.

HRMS (ASAP<sup>+</sup>): *m/z* found: 308.0999 [M+H]<sup>+</sup>; calcd. for [M+H]<sup>+</sup> 308.1008 (|Δ| = 2.92 ppm).

Elem. anal. calcd. (%) for C<sub>16</sub>H<sub>22</sub>BrN C 62.34, H 7.19, N 4.54; found: C 62.45, H 7.19, N 4.39.

**Bis(1,1,7,7-tetramethyl)julolidine (1-14)**

In an argon-filled glovebox, **1-13** (1.00 mmol, 308 mg), 4-Bpin-tetramethyljulolidine (1.00 mmol, 355 mg), KOH (5.00 mmol, 280 mg), Pd<sub>2</sub>(dba)<sub>3</sub> (0.01 mmol, 10.0 mg), sPhos (0.02 mmol, 8.00 mg, 2.00 mol%) and toluene 20.0 mL were added to a microwave vial. The tube was sealed, taken out of the glovebox and 1 mL of degassed distilled H<sub>2</sub>O was added *via* syringe through the septum to the mixture. Then, the reaction was heated to 100 °C for 24 h in the microwave. After cooling to room temperature, water (20 mL) was added, and the mixture was extracted with toluene (3 x 50 mL). The organic layer was dried over Na<sub>2</sub>SO<sub>4</sub>, and passed through a pad of silica with toluene. The solvents were removed under reduced pressure and the product was obtained as white crystals after recrystallization from hexane (333 mg, 73%).

<sup>1</sup>H NMR (300 MHz, benzene-*d*<sub>6</sub>, r.t., ppm): δ = 7.52 (s, 4 H), 2.95-2.93 (m, 8 H), 1.69-1.67 (m, 8 H), 1.31 (s, 24 H).

<sup>13</sup>C{<sup>1</sup>H} NMR (126 MHz, benzene-*d*<sub>6</sub>, r.t., ppm): δ = 139.8, 132.1, 131.2, 123.5, 47.4, 37.9, 32.7, 32.0.

<sup>15</sup>N NMR (300 MHz, DMSO-*d*<sub>6</sub>, r.t., ppm): δ = -315.7.

HRMS (ASAP<sup>+</sup>): *m/z* found: 457.3564 [M+H]<sup>+</sup>; calcd. for [M+H]<sup>+</sup> 457.3577 (|Δ| = 2.80 ppm);

Elem. anal. calcd. (%) for C<sub>32</sub>H<sub>45</sub>N<sub>2</sub> C 84.16, H 9.71, N 6.13; found: C 84.02, H 9.85, N 5.94.

**(Bpin)<sub>4</sub>-Per (2-1)**

In an argon-filled glovebox, perylene (1.00 g, 3.96 mmol), B<sub>2</sub>pin<sub>2</sub> (5.03 g, 19.8 mmol), [Ir(OMe)COD]<sub>2</sub> (78.8 mg, 119 μmol), dtbpy (63.8 mg, 238 μmol) and THF (100 mL) were added to a Schlenk flask. The mixture was refluxed at 85 °C in an oil bath for 40 h. After cooling to room temperature, the solvent was removed under reduced pressure. The residue was washed with cyclohexane (2 x 20 mL) and MeOH (2 x 20 mL) to give **2-1** as a yellow solid (2.69 g, 90%). The spectral data matched those reported previously.<sup>[32]</sup>

<sup>1</sup>H NMR (300 MHz, CDCl<sub>3</sub>, r.t., ppm): δ = 8.63 (s, 4H), 8.25 (s, 4H), 1.43 (s, 48H).

<sup>13</sup>C{<sup>1</sup>H} NMR (75 MHz, CDCl<sub>3</sub>, r.t., ppm): δ = 137.1, 133.4, 132.1, 130.5, 126.8 (br), 126.2, 84.2, 25.1.

<sup>11</sup>B{<sup>1</sup>H} NMR (96 MHz, CDCl<sub>3</sub>, r.t., ppm): δ = 34.2.

HRMS (ASAP<sup>+</sup>): *m/z* calcd. for [M+H]<sup>+</sup> 757.4420; found: [M+H]<sup>+</sup> 757.4422 (|Δ| = 0.26 ppm).

Elem. anal. calcd. (%) for C<sub>44</sub>H<sub>56</sub>B<sub>4</sub>O<sub>8</sub> C 69.89, H 7.47; found: C 69.69, H 7.35.

**(BF<sub>3</sub>K)<sub>4</sub>-Per (2-2)**

In a round-bottom flask (Bpin)<sub>4</sub>-Per (2-1) (378 mg, 500 μmol) was dissolved in THF (30 mL). To this solution KHF<sub>2</sub> (469 mg, 6.00 mmol) in H<sub>2</sub>O (3 mL) was added and the mixture was stirred vigorously at room temperature for 20 h. The solvent was removed under reduced pressure and the residue was washed with hot acetone (2 x 40 mL), hot EtOH (2 x 40 mL) and hot MeOH (40 mL) to give the product of 2-2 as a green solid (335 mg, 99%).

<sup>1</sup>H NMR (500 MHz, DMSO-*d*<sub>6</sub>, r.t., ppm): δ = 8.11 (s, 4H), 7.40 (s, 4H).

<sup>13</sup>C{<sup>1</sup>H} NMR (125 MHz, DMSO-*d*<sub>6</sub>, r.t., ppm): δ = 133.8, 129.0, 128.9, 126.8, 122.2 (one C not observed, likely that attached to B).

<sup>11</sup>B{<sup>1</sup>H} NMR (160 MHz, DMSO-*d*<sub>6</sub>, r.t., ppm): δ = 3.9.

<sup>19</sup>F{<sup>1</sup>H} NMR (470 MHz, DMSO-*d*<sub>6</sub>, r.t., ppm): δ = -138.7.

**(Bmes<sub>2</sub>)<sub>4</sub>-Per (2-3)**

Under an argon atmosphere, (BF<sub>3</sub>K)-Per (2-2) (1.00 g, 1.48 mmol) and degassed THF (20 mL) were added to a Schlenk flask. The suspension was treated with mesMgBr (0.9 M in THF, 13.6 mmol, 15.1 mL) and the reaction was stirred at r.t. for 72 h. After addition of water (10 mL), the precipitate was collected by filtration. In an ultrasonic bath, the residue was washed successively with H<sub>2</sub>O, THF, hexane, ethyl acetate, MeOH and CH<sub>2</sub>Cl<sub>2</sub>. After each washing process, the solid was separated from the solvent by centrifugation. The product was obtained as a yellow solid (1.58 g, 86%).

<sup>1</sup>H NMR (500 MHz, CDCl<sub>3</sub>, r.t., ppm): δ = 8.11 (s, 4H), 7.87 (s, 4H), 6.79 (s, 16H), 2.35 (s, 24H), 2.00 (s, 48H).

<sup>13</sup>C{<sup>1</sup>H} NMR (125 MHz, CDCl<sub>3</sub>, r.t., ppm): δ = 141.5, 140.9, 140.0, 138.7, 133.8, 132.7, 130.6, 129.4, 128.4, 23.7, 21.4 (one C not observed, likely that attached to B).

<sup>11</sup>B{<sup>1</sup>H} SSNMR (128 MHz, r.t., ppm): δ = 72.7.

HRMS (APCI<sup>+</sup>): *m/z* calcd. for [M+H]<sup>+</sup> 1245.7957; found: [M+H]<sup>+</sup> 1245.7983 (|Δ| = 2.09 ppm).

**Elem. anal. calcd.** (%) for C<sub>92</sub>H<sub>96</sub>B<sub>4</sub> C 88.75, H 7.77; found: C 87.80, H 7.92. As is common for related organo-Bmes<sub>2</sub> compounds, the carbon analysis of (Bmes<sub>2</sub>)<sub>4</sub>-Per is 0.95% below the calculated value, while the hydrogen analysis is satisfactory. This has been described previously due to the formation of boron carbide.<sup>[75,167,332]</sup>

**(Br)<sub>4</sub>-Per (2-4)**

Under aerobic conditions, CuBr<sub>2</sub> (710 mg, 3.17 mmol), (Bpin)<sub>4</sub>-Per (**2-1**) (200 mg, 0.26 mmol), MeOH (5 mL), THF (5 mL) and H<sub>2</sub>O (5 mL) were added to a 20 mL microwave vial. The vial was sealed and heated to 95 °C for 20 h in a microwave reactor. Reaction progress was monitored by HRMS and revealed that the reaction was not finished, hence another portion of CuBr<sub>2</sub> (710 mg, 3.17 mmol) was added and the reaction mixture was heated at 95 °C for another 20 h. The precipitate was collected by centrifugation and washed with H<sub>2</sub>O, MeOH, EDTA (0.1 M) and THF. The solubility of (Br)<sub>4</sub>-Per is too low to obtain NMR spectra in solution. However, the solubility was enough to obtain absorption and emission spectra. Hence, this product was used as a crude (568 mg) without further purification for the following Buchwald-Hartwig amination reaction. A small part was further purified by Kugelrohr sublimation at 250 °C (0.001 mbar) to afford the title compound as an analytically pure red solid. The yield loss during the Kugelrohr sublimation of (Br)<sub>4</sub>-Per was so large that using the crude product for the following reaction gave higher overall yields.

<sup>13</sup>C{<sup>1</sup>H} SSNMR (100 MHz, r.t., ppm) δ = 134.8, 129.6, 127.6, 124.3, 118.0.

HRMS (ASAP<sup>+</sup>): *m/z* calcd for [M+H]<sup>+</sup>: 568.7385; found [M+H]<sup>+</sup> 568.7363 (|Δ| = 3.87 ppm).

Elem. anal. calcd. (%) for C<sub>20</sub>H<sub>8</sub>Br<sub>4</sub> C 42.30, H 1.42; found: C 42.47, H 1.56.

**(DPA)<sub>4</sub>-Per (2-5)**

Under an argon atmosphere, crude (Br)<sub>4</sub>-Per (2-4) (568 mg, 1.00 mmol), bis(4-methoxyphenyl)amine (1.15 g, 5.00 mmol), Pd<sub>2</sub>(dba)<sub>3</sub>·CHCl<sub>3</sub> (20.7 mg, 0.02 mmol), sPhos (16.4 mg, 0.04 mmol), KO<sup>t</sup>Bu (0.56 g, 5.00 mmol) and toluene were added to a Young's tube, which was then sealed. The reaction mixture was stirred at 110 °C for 5 d, until reaction monitoring indicated that the reaction was complete. After cooling to room temperature, water was added, and the organic layer was extracted with CH<sub>2</sub>Cl<sub>2</sub> (3 x 200 mL). The combined organic extracts were washed with brine and dried over Na<sub>2</sub>SO<sub>4</sub>. After removing the solvent under reduced pressure, the crude product was purified by flash chromatography (silica, cyclohexane/CH<sub>2</sub>Cl<sub>2</sub> first 1:4 then gradually increased to 0:1). (DPA)<sub>4</sub>-Per was obtained as an orange-red solid (220 mg, 189 μmol, 19% yield over 2 steps starting from 2-1).

<sup>1</sup>H NMR (500 MHz, CD<sub>2</sub>Cl<sub>2</sub>, r.t., ppm): δ = 7.33 (d, *J* = 2.1 Hz, 4H), 7.01-6.99 (m, 16H), 6.80-6.77 (m, 16H), 6.63 (d, *J* = 2.1 Hz, 4H), 3.78 (s, 24H).

<sup>13</sup>C{<sup>1</sup>H} NMR (125 MHz, CD<sub>2</sub>Cl<sub>2</sub>, r.t., ppm): δ = 156.5, 147.7, 140.9, 137.5, 131.6, 127.0, 120.1, 115.1, 115.0, 114.0, 55.8.

<sup>15</sup>N NMR (500 MHz, CD<sub>2</sub>Cl<sub>2</sub>, r.t., ppm): δ = -286.3.

HRMS (APCI<sup>+</sup>): *m/z* calcd. for [M+H]<sup>+</sup>: 1161.4797; found [M+H]<sup>+</sup> 1161.4781 (|Δ| = 1.38 ppm).

**Pyrene-4,5-dione (3-1)**

In a round bottom flask pyrene (10.0 g, 49.4 mmol) and  $\text{RuCl}_3 \cdot x \text{H}_2\text{O}$  (987 mg, 4.74 mmol) were dissolved in 200 mL MeCN.  $\text{NaIO}_4$  (42.3 g, 198 mmol, 4.00 eq) was dissolved in 250 mL of hot water and carefully added to the pyrene solution. Another 200 mL of  $\text{CH}_2\text{Cl}_2$  were added and the reaction mixture was vigorously stirred for 18 h at r.t. After filtration of the suspension using Celite®, the filtrate was extracted with  $\text{CH}_2\text{Cl}_2$  (3 x 100 mL) and the combined organic phases were washed with saturated aqueous  $\text{Na}_2\text{S}_2\text{O}_3$  and  $\text{H}_2\text{O}$  and then dried over  $\text{Na}_2\text{SO}_4$ . After removing the solvent under reduced pressure, the product was obtained as a dark orange solid (7.56 g, 66%).

The spectroscopic data match those reported previously.<sup>[237,240,319,320]</sup>

$^1\text{H NMR}$  (200 MHz,  $\text{CDCl}_3$ , r.t., ppm):  $\delta$  = 8.51 (dd,  $J$  = 7.4 Hz,  $J$  = 1.3 Hz, 2H), 8.19 (dd,  $J$  = 8.08 Hz,  $J$  = 1.36 Hz, 2H), 7.87 (s, 2H), 7.77 (t,  $J$  = 7.73 Hz, 2H).

**Pyrene-4,5-di(ethyleneglycol)ketal (3-2)**

Pyrene-4,5-dione (**3-1**) (4.92 g, 21.2 mmol) was suspended in 200 mL toluene and ethylene glycol (148 mL, 2.65 mol, 125 eq) and *p*-toluenesulfonic acid (1.81 g, 9.53 mmol) were added. The reaction mixture was refluxed at 125 °C for 20 h. Toluene was removed under reduced pressure and 400 mL of water. The crude product was isolated by filtration, washed with water and further purified by flash chromatography (silica, cyclohexane/ethyl acetate 9:1). The product was isolated as a white solid (3.46 g, 51%). The spectroscopic data match those reported previously.<sup>[333]</sup>

<sup>1</sup>H NMR (500 MHz, CD<sub>2</sub>Cl<sub>2</sub>, r.t., ppm): δ = 7.98 (dd, *J* = 7.4 Hz, *J* = 1.2 Hz, 2 H), 7.97 (dd, *J* = 8.0 Hz, *J* = 1.2 Hz, 2 H), 7.82 (s, 2 H), 7.73 (dd, *J* = 8.0 Hz, *J* = 7.4 Hz, 2 H), 4.29 (br, 4 H), 3.75 (br, 4 H).

<sup>13</sup>C{<sup>1</sup>H} NMR (125 MHz, CD<sub>2</sub>Cl<sub>2</sub>, r.t., ppm): δ = 133.5, 131.8, 129.2, 127.6, 127.1, 126.9, 124.6, 93.9, 62.3.

HRMS (ASAP<sup>+</sup>): *m/z* calcd for [M+H]<sup>+</sup>: 321.1121; found: [M+H]<sup>+</sup> 321.1115 (|Δ| = 1.87 ppm).

Elem. anal. calcd. (%) for C<sub>20</sub>H<sub>16</sub>O<sub>4</sub> C 74.99, H 5.03; found: C 74.90, H 5.08.

**2,7-Bis(Bpin)-4,5-di(ethyleneglycol)ketal-pyrene (3-3)**

In an argon-filled glovebox, a Young's tube was filled with pyrene-4,5-di(ethyleneglycol)ketal (**3-2**) (2.91 g, 9.08 mmol), B<sub>2</sub>pin<sub>2</sub> (4.61 g, 18.2 mmol), [Ir(OMe)COD]<sub>2</sub> (301 mg, 0.45 mmol), dtbpy (260 mg, 0.91 mmol) and 50 mL of MTBE. Afterwards, the Young's tube was sealed, and the reaction mixture was stirred at 80 °C for 20 h. After cooling to room temperature, the crude product was passed through a pad of silica using toluene as the eluent. The solvent was removed under reduced pressure and the crude product was further purified *via* flash chromatography (silica, cyclohexane/ethyl acetate 95:5). The product was obtained as a white solid (4.58 g, 88%).

<sup>1</sup>H NMR (300 MHz, CD<sub>2</sub>Cl<sub>2</sub>, r.t., ppm): δ = 8.40 (d, *J* = 1.2 Hz, 2H), 8.28 (d, *J* = 1.2 Hz, 2H), 7.85 (s, 2H), 4.33-4.28 (m, 4H), 3.76-3.71 (m, 4H), 1.41 (s, 24H).

<sup>13</sup>C{<sup>1</sup>H} NMR (75 MHz, CD<sub>2</sub>Cl<sub>2</sub>, r.t., ppm): δ = 136.6, 133.0, 131.6, 129.7, 128.6, 127.4, 94.0, 84.6, 62.3, 25.2 (one C not observed, likely that attached to B).

<sup>11</sup>B{<sup>1</sup>H} NMR (96 MHz, CD<sub>2</sub>Cl<sub>2</sub>, r.t., ppm): δ = 31.5.

HRMS (ASAP<sup>+</sup>): *m/z* calcd. for [M+H]<sup>+</sup> 573.2826; found: [M+H]<sup>+</sup> 573.2799 (|Δ| = 4.71 ppm).

Elem. anal. calcd. (%) for C<sub>32</sub>H<sub>38</sub>B<sub>2</sub>O<sub>8</sub> C 67.16, H 6.69; found: C 66.89, H 6.97.

**2,7-Bis(bromo)-4,5-di(ethyleneglycol)ketal-pyrene (3-4)**

The compound 2,7-bis(Bpin)-4,5-di(ethyleneglycol)ketal-pyrene (**3-3**) (4.58 g, 7.99 mmol) was diluted in 100 mL THF and heated to 50 °C. Afterwards, 80 mL of MeOH was added and the reaction temperature was elevated to 90 °C. A solution of CuBr<sub>2</sub> (8.90 g, 40.0 mmol) in 80 mL of H<sub>2</sub>O was slowly added to this reaction mixture *via* a dropping funnel. The reaction mixture was stirred at 90 °C for 96 h and an orange solid precipitated. The precipitate was isolated by filtration and washed with water and EDTA (0.1 M) solution. The crude product was further purified *via* flash chromatography (silica, hexane/ethyl acetate 4:1) to give a white solid (1.02 g, 27%).

<sup>1</sup>H NMR (500 MHz, CDCl<sub>3</sub>, r.t., ppm): δ = 8.08 (s, 4H), 7.71 (s, 2H), 4.32 (br, 4H), 3.78 (br, 4H).

<sup>13</sup>C{<sup>1</sup>H} NMR (125 MHz, CDCl<sub>3</sub>, r.t., ppm): δ = 135.0, 133.1, 131.5, 127.9, 127.1, 125.1, 121.9, 93.2, 62.1.

HRMS (APCI<sup>+</sup>): *m/z* calcd. for [M+H]<sup>+</sup> 476.9332; found: [M+H]<sup>+</sup> 476.9330 (|Δ| = 0.42 ppm).

**2,7-Bis(DPA)-4,5-di(ethyleneglycol)ketal-pyrene (3-5)**

In an argon-filled glovebox, a Young's tube was filled with 2,7-bis(bromo)-4,5-di(ethyleneglycol)ketal-pyrene (**3-4**) (3.00 g, 6.27 mmol), bis(4-methoxyphenyl)amine (3.02 g, 13.2 mmol), Pd<sub>2</sub>(dba)<sub>3</sub>·CHCl<sub>3</sub> (130 mg, 126 μmol), xPhos (120 mg, 251 μmol), KO<sup>t</sup>Bu (2.11 g, 18.8 mmol) and toluene (200 mL), which was then sealed. Afterwards, the reaction mixture was stirred at 115 °C for 15 h. The solvent was removed under reduced pressure and the crude product was further purified by flash chromatography (silica-NH, cyclohexane/CH<sub>2</sub>Cl<sub>2</sub> 4:1 → 1:1). Product (**3-5**) was obtained as a yellow solid (2.83 g, 58%).

<sup>1</sup>H NMR (300 MHz, CD<sub>2</sub>Cl<sub>2</sub>, r.t., ppm): δ = 7.49 (d, *J* = 2.4 Hz, 2H), 7.31 (s, 2H), 7.24 (d, *J* = 2.4 Hz, 2H), 7.14-7.09 (m, 8H), 6.90-6.86 (m, 8H), 4.11 (br, 4H), 3.80 (s, 12H), 3.65 (br, 8H).

<sup>13</sup>C{<sup>1</sup>H} NMR (75 MHz, CD<sub>2</sub>Cl<sub>2</sub>, r.t., ppm): δ = 156.6, 147.6, 141.3, 133.3, 132.0, 127.0, 126.8, 121.3, 119.2, 118.0, 115.1, 93.9, 62.1, 55.9.

<sup>15</sup>N NMR (300 MHz, CD<sub>2</sub>Cl<sub>2</sub>, r.t., ppm): -285.8.

HRMS (APCI<sup>+</sup>): *m/z* calcd. for [M+H]<sup>+</sup> 775.3014; found: 775.3000 [M+H]<sup>+</sup> (|Δ| = 1.80 ppm).

Elem. anal. calcd. (%) for C<sub>48</sub>H<sub>42</sub>N<sub>2</sub>O<sub>8</sub> C 74.40, H 5.46, N 3.62; found: C 74.00, H 6.07, N 3.34.

**2,7-Bis(DPA)-4,5-dione (3-6)**

In a round bottom flask, 2,7-bis(DPA)-4,5-di(ethyleneglycol)ketal-pyrene (**3-5**) (500mg, 645  $\mu\text{mol}$ ) was suspended in water (10 mL). Then, TFA (60 mL) was added dropwise and the reaction mixture was stirred at room temperature for 15 h. Afterwards, the solution was neutralized with an aqueous solution of  $\text{NaHCO}_3$  and extracted with ethyl acetate. The organic phases were dried over  $\text{NaSO}_4$ , the resulting crude product was washed with methanol and the solvents were removed under reduced pressure. The product 2,7-bis(DPA)-4,5-dione (**3-6**) was obtained as a dark green solid (360 mg, 81%).

$^1\text{H NMR}$  (300 MHz,  $\text{CD}_2\text{Cl}_2$ , r.t., ppm):  $\delta$  = 7.88 (d,  $J$  = 2.5 Hz, 2H), 7.43 (d,  $J$  = 2.5 Hz, 2H), 7.39 (s, 2H), 7.15-7.10 (m, 8H), 6.93-6.88 (m, 8H), 3.82 (s, 12H).

$^{13}\text{C}\{^1\text{H}\}$  NMR (75 MHz,  $\text{CD}_2\text{Cl}_2$ , r.t., ppm):  $\delta$  = 181.1, 157.2, 148.1, 140.2, 132.9, 130.3, 127.5, 127.2, 123.5, 123.1, 122.7, 115.4, 55.9.

$^{15}\text{N NMR}$  (300 MHz,  $\text{CD}_2\text{Cl}_2$ , r.t., ppm): -284.9.

**HRMS** (ASAP<sup>+</sup>):  $m/z$  calcd. for  $[\text{M}+\text{H}]^+$  687.2417; found 687.2479  $[\text{M}+\text{H}]^+$  ( $|\Delta|$  = 9.02 ppm).

**Elem. anal.** calcd.(%) for  $\text{C}_{44}\text{H}_{34}\text{N}_2\text{O}_6$  C 76.95, H 4.99, N 4.08; found: C 77.00, H 4.96, N 4.25.

**2,7-Bis(DPA)-4,5-azaacene-CN (3-7)**

In a round bottom flask, 2,7-bis(DPA)-4,5-dione (**3-6**) (200 mg, 291  $\mu\text{mol}$ ), 2,3-diaminomaleonitrile (188 mg, 1.74 mmol), ethanol (35 mL) and acetic acid (35 mL) were stirred at 80 °C for 15 h. Afterwards, the solution was neutralized with an aqueous solution of  $\text{NaHCO}_3$ . The precipitate was collected *via* filtration and washed with water and ethanol. Product (**3-7**) was obtained as a black solid (134 mg, 60%).

$^1\text{H NMR}$  (300 MHz,  $\text{CD}_2\text{Cl}_2$ , r.t., ppm):  $\delta$  = 8.74 (d,  $J$  = 2.4 Hz, 2H), 7.80 (d,  $J$  = 2.4 Hz, 2H), 7.67 (s, 2H), 7.21-7.16 (m, 8H), 6.93-6.88 (m, 8H), 3.83 (s, 12H).

$^{13}\text{C}\{^1\text{H}\}$  NMR (75 MHz,  $\text{CD}_2\text{Cl}_2$ , r.t., ppm):  $\delta$  = 157.0, 148.2, 143.9, 140.9, 132.0, 130.1, 127.7, 127.1, 126.9, 122.8, 121.8, 117.5, 115.4, 114.4, 55.9.

**HRMS** (APCI<sup>+</sup>):  $m/z$  calcd. for 759.2714  $[\text{M}+\text{H}]^+$ ; found: 759.2699  $[\text{M}+\text{H}]^+$  ( $|\Delta|$  = 1.98 ppm).

**Elem. anal. calcd.**(%) for  $\text{C}_{48}\text{H}_{34}\text{N}_6\text{O}_4$  C 75.98, H 4.52, N 11.08; found: C 75.73, H 4.74, N 10.73

**2,7-Bis(DPA)-4,5-azaacene-Ph (3-8)**

In a round bottom flask, 2,7-bis(DPA)-4,5-dione (**3-6**) (200 mg, 291  $\mu\text{mol}$ ), 1,2-diamino-benzene (189 mg, 1.74 mmol), ethanol (35 mL) and acetic acid (35 mL) were stirred at 80 °C for 15 h. Afterwards, the solution was neutralized with an aqueous solution of  $\text{NaHCO}_3$ . The precipitate was collected *via* filtration and washed with water and ethanol. Product (**3-8**) was obtained as a red solid (120 mg, 54%).

$^1\text{H NMR}$  (500 MHz,  $\text{CDCl}_3$ , r.t., ppm):  $\delta = 9.17$  (d,  $J = 2.4$ , 2H), 8.25–8.20 (m, 2H), 7.79–7.74 (m, 2H), 7.69 (d,  $J = 2.4$  Hz, 2H), 7.65 (s, 2H), 7.24–7.17 (m, 8H), 9.94–6.86 (m, 8H), 3.84 (s, 12H).

$^{13}\text{C NMR}$  (125 MHz,  $\text{CDCl}_3$ , r.t., ppm):  $\delta = 156.0, 147.2, 143.4, 142.3, 141.6, 132.0, 130.0, 129.7, 129.6, 127.1, 126.5, 121.6, 121.3, 118.1, 115.0, 55.7$ .

**HRMS** (APCI<sup>+</sup>):  $m/z$  calcd. for 759.2966  $[\text{M}+\text{H}]^+$ ; found: 759.2963  $[\text{M}+\text{H}]^+$  ( $|\Delta| = 0.40$  ppm).

**Elem. anal. calcd.**(%) for  $\text{C}_{50}\text{H}_{38}\text{N}_4\text{O}_4$  C 79.14, H 5.05, N 7.38; found: C 78.82, H 5.07, N 7.53.

**2,7-Bis(azido)-4,5-di(ethyleneglycol)ketal-pyrene (3-4')**

Compound **3-3** (6.62 g, 11.6 mmol),  $\text{NaN}_3$  (2.26 g, 34.8 mmol) and  $\text{Cu}(\text{OAc})_2$  (232 mg, 1.16 mmol) were suspended in MeOH (400 mL) and stirred on a preheated oil bath at 55 °C for 48 h. The green precipitate was filtered and washed with EDTA solution, water and MeOH. The crude product was purified *via* column chromatography (silica, hexane/ethyl acetate 4:1) giving the product **3-4'** as a pale yellow solid (2.58 g, 55%).

$^1\text{H}$  NMR (200 MHz,  $\text{CD}_2\text{Cl}_2$ , r.t., ppm):  $\delta$  = 7.75 (s, 2H), 7.64 (d,  $J$  = 2.3 Hz, 2H), 7.56 (d,  $J$  = 2.3 Hz, 2H), 4.32-4.24 (m, 4H), 3.76-3.68 (m, 4H).

$^{13}\text{C}\{^1\text{H}\}$  NMR (125 MHz,  $\text{CD}_2\text{Cl}_2$ , r.t., ppm):  $\delta$  = 139.7, 135.6, 132.7, 127.5, 124.0, 118.0, 116.8, 93.5, 62.3.

$^{15}\text{N}$  NMR (500 MHz,  $\text{CD}_2\text{Cl}_2$ , r.t., ppm):  $\delta$  = -288.1.

HRMS (ASAP<sup>+</sup>):  $m/z$  calcd. for 403.1149  $[\text{M}+\text{H}]^+$ ; found: 403.1145  $[\text{M}+\text{H}]^+$  ( $|\Delta|$  = 0.99 ppm).

**2,7-Bis(amino)-4,5-di(ethyleneglycol)ketal-pyrene (3-5')**

To a Schlenk flask, **3-4'** (1.03 g, 2.56 mmol) and Pd/C (10% Pd on C, 37.6 mg) were added. After the addition of MeOH (200 mL), the reaction mixture was frozen in liquid N<sub>2</sub>. Successively, the flask was evacuated and flushed with an excess of hydrogen and evacuated again. The procedure was repeated two more times and, after the last hydrogen flush was performed, the reaction mixture was thawed and stirred at r.t. for 16 h. CH<sub>2</sub>Cl<sub>2</sub> was added to the crude product and the suspension was then filtered. Afterwards, the solvent was removed under reduced pressure and the crude product was purified *via* column chromatography (silica, hexane/ethyl acetate 3:7). The final product **3-5'** was obtained as a pale yellow solid (440 mg, 49%).

<sup>1</sup>H NMR (300 MHz, CD<sub>3</sub>CN, r.t., ppm): δ = 7.47 (s, 2H), 7.25 (d, *J* = 2.3 Hz, 2H), 7.00 (d, *J* = 2.3 Hz, 2H), 4.41 (s, 4H), 4.20-4.15 (m, 4H), 3.69 (br, 4H).

<sup>13</sup>C{<sup>1</sup>H} NMR (75 MHz, CD<sub>3</sub>CN, r.t., ppm): δ = 147.0, 134.0, 132.3, 126.8, 120.2, 114.8, 111.2, 94.6, 62.6.

<sup>15</sup>N NMR (300 MHz, CD<sub>3</sub>CN, r.t., ppm): δ = -324.1.

HRMS (ASAP<sup>+</sup>): *m/z* calcd. for 351.1339 [M+H]<sup>+</sup>; found: 351.1324 [M+H]<sup>+</sup> (|Δ| = 4.27 ppm).

Elem. anal. calcd. (%) for C<sub>20</sub>H<sub>18</sub>N<sub>2</sub>O<sub>4</sub> C 68.56, H 5.18, N 8.00; found: C 68.51, H 5.18, N 7.26.

**2,7-Bis(amino)-*N*<sup>2</sup>,*N*<sup>2</sup>,*N*<sup>7</sup>,*N*<sup>7</sup>-tetrakis(3-methylbut-2-en-1-yl)-4,5-di(ethyleneglycol)ketal-pyrene (3-6')**

To a Young's tube, derivative **3-5'** (686 mg, 1.96 mmol), K<sub>2</sub>CO<sub>3</sub> (1.35 g, 9.80 mmol), molecular sieves (4 Å, 0.50 g) and 1-chloro-3-methylbut-2-ene (927 μL, 8.23 mmol) were suspended in MeCN (60 mL). The tube was sealed and the reaction mixture was stirred at 80 °C in an oil bath for 48 h. After cooling to r.t., the precipitate was collected by filtration and washed with ethyl acetate. The solvent was removed from the filtrate under reduced pressure and the remaining brown oil was purified by column chromatography (silica, hexane/ethyl acetate 96:4), which yielded product **3-6'** as a yellow solid (518 mg, 42%).

<sup>1</sup>H NMR 500 MHz, CD<sub>2</sub>Cl<sub>2</sub>, r.t., ppm): δ = 7.49 (s, 2H), 7.38 (s, 2H), 7.00 (s, 2H), 5.30 (m, 4H), 4.22 (br, 4H), 4.03 (d, *J* = 6.1 Hz, 8H), 3.74 (br, 4H), 1.79 (s, 12H), 1.76 (s, 12H).

<sup>13</sup>C{<sup>1</sup>H} NMR (125 MHz, CD<sub>2</sub>Cl<sub>2</sub>, r.t., ppm): δ = 147.6, 134.8, 132.6, 131.7, 126.8, 122.1, 118.6, 112.9, 110.1, 94.5, 62.3, 49.1, 25.9, 18.1.

HRMS (ASAP<sup>+</sup>): *m/z* calcd. for 623.3843 [M+H]<sup>+</sup>; found 623.3839 [M+H]<sup>+</sup> (|Δ| = 0.64 ppm).

**Pyrene-4,5,9,10-tetra(ethyleneglycol)ketal (3-10)**

In a round bottom flask fitted with a reflux condenser, pyrene-4,5,9,10-tetraone (**3-9**) (3.12 g, 11.9 mmol, 1.00 eq) was suspended in toluene (400 mL) followed by the addition of ethylene glycol (166 mL, 2.96 mol) and *p*-toluenesulfonic acid (2.04 g, 10.7 mmol). The reaction mixture was refluxed at 125 °C for 20 h. Toluene was removed under reduced pressure and 400 mL of water. The crude product was isolated by filtration, washed with water and further purified by flash chromatography (silica, toluene/CH<sub>2</sub>Cl<sub>2</sub>/NEt<sub>3</sub> 1:1:0.1) to give the title compound as a white solid (3.46 g, 67%).

<sup>1</sup>H NMR (500 MHz, CD<sub>2</sub>Cl<sub>2</sub>, r.t., ppm): δ = 7.75 (d, *J* = 7.7 Hz, 4 H), 7.51 (t, *J* = 7.7 Hz, 2 H), 4.18 (br, 8 H), 3.65 (br, 8 H).

<sup>13</sup>C{<sup>1</sup>H} NMR (125 MHz, CD<sub>2</sub>Cl<sub>2</sub>, r.t., ppm): δ = 133.4, 129.8, 129.1, 127.6, 92.8, 62.3.

HRMS (ASAP<sup>+</sup>): *m/z* calcd. for [M+H]<sup>+</sup> 439.1387; found [M+H]<sup>+</sup>: 439.1365 (|Δ| = 5.00 ppm).

Elem. anal. calcd. (%) for C<sub>24</sub>H<sub>22</sub>O<sub>8</sub> C 65.75, H 5.06; found: C 65.88, H 5.25.

**2,7-Bis(Bpin)-4,5,9,10-tetra(ethyleneglycol)ketal-pyrene (3-11)**

In an argon-filled glovebox, pyrene-4,5,9,10-tetra(ethyleneglycol)ketal (**3-10**) (4.21 g, 9.60 mmol), B<sub>2</sub>pin<sub>2</sub> (5.35 g, 21.1 mmol), [Ir(OMe)COD]<sub>2</sub> (318 mg, 480 μmol, 0.05 eq), dtbpy (275 mg, 960 μmol) and 40 mL THF were added to a Young's tube. After the tube was sealed and taken out of the glovebox, the reaction mixture was heated at 70 °C for 18 h. After cooling to room temperature, the mixture was passed through a pad of silica using CH<sub>2</sub>Cl<sub>2</sub>/NEt<sub>3</sub> (95:5). The solvent was removed under reduced pressure and the crude product was purified by dissolving it in CH<sub>2</sub>Cl<sub>2</sub> and precipitating it with hexane (4.17 g, 63%).

<sup>1</sup>H NMR (300 MHz, CD<sub>2</sub>Cl<sub>2</sub>, r.t., ppm): δ = 8.11 (s, 4H), 4.21 (br, 8 H), 3.65 (br, 8 H), 1.36 (s, 24 H).

<sup>13</sup>C{<sup>1</sup>H} NMR (75 MHz, CD<sub>2</sub>Cl<sub>2</sub>, r.t., ppm): δ = 133.7, 132.9, 131.4, 92.9, 84.5, 62.0, 25.1 (one C not observed, likely that attached to B).

<sup>11</sup>B{<sup>1</sup>H} NMR (96 MHz, CD<sub>2</sub>Cl<sub>2</sub>, r.t., ppm): δ = 30.6.

HRMS (ASAP<sup>+</sup>): *m/z* calcd. for [M+H]<sup>+</sup> 691.3092; found [M+H]<sup>+</sup>: 691.3065 (|Δ| = 3.91 ppm).

Elem. anal. calcd. (%) for C<sub>36</sub>H<sub>44</sub>B<sub>2</sub>O<sub>12</sub> C 62.63, H 6.42; found: C 62.39, H 6.58.

**2,7-Bis(azido)-4,5,9,10-tetra(ethyleneglycol)ketal-pyrene (3-12)**

Compound **3-II** (4.17 g, 6.04 mmol), NaN<sub>3</sub> (1.18 g, 18.1 mmol) and Cu(OAc)<sub>2</sub> (121 mg, 604 μmol) were suspended in MeOH (700 mL) and stirred at 55 °C for 48 h. The green precipitate was filtered and washed with an EDTA (0.1 M) solution, water and MeOH. The crude product was purified *via* column chromatography (silica, hexane/EtOAc 3:1) giving the desired compound as a pale yellow solid (1.67 g, 53%).

<sup>1</sup>H NMR (200 MHz, CD<sub>2</sub>Cl<sub>2</sub>, r.t., ppm): δ = 7.41 (s, 4 H), 4.20 (br, 8 H), 3.66 (br, 8 H).

<sup>13</sup>C{<sup>1</sup>H} NMR (125 MHz, CD<sub>2</sub>Cl<sub>2</sub>, r.t., ppm): δ = 141.8, 135.3, 125.5, 118.2, 92.5, 62.0.

<sup>15</sup>N NMR (500 MHz, CD<sub>2</sub>Cl<sub>2</sub>, r.t., ppm): δ = -287.0.

HRMS (ASAP<sup>+</sup>): *m/z* calcd. for 521.1415 [M+H]<sup>+</sup>; found: 521.1415 [M+H]<sup>+</sup> (|Δ| = 0.00 ppm).

### General Procedure for the Borylation of 4-Quinolones with the dtbpy ligand

In an argon-filled glovebox, [Ir(OMe)COD]<sub>2</sub> (1.5 mol%), dtbpy (3 mol%), B<sub>2</sub>pin<sub>2</sub> (1 mmol), the corresponding quinolone (1 mmol), and 10 mL of THF were added to a sealable cylindrical microwave vial. The vial was sealed with a crimp top septum cap, taken out of the glovebox and the reaction mixture was stirred in a metal heating block at the respective temperature and stated time. Afterwards, the reaction was cooled to room temperature and volatiles were removed under reduced pressure to afford the crude product.

### General Procedure for the Borylation of 4-Quinolones with the Si-SMAP ligand

In an argon-filled glovebox, Si-SMAP (2.50 μmol), [Ir(OMe)COD]<sub>2</sub> (1.25 μmol), B<sub>2</sub>pin<sub>2</sub> (1 mmol) and 5 mL of THF were added to a sealable cylindrical microwave vial and the mixture was stirred for 1 min. Then, the corresponding quinolone (1 mmol) was added, the flask was sealed with a crimp top septum cap, taken out of the glovebox and the reaction mixture was stirred in a metal heating block at the respective temperature and stated time. Afterwards, the reaction was cooled to room temperature and volatiles were removed under reduced pressure to afford the crude product.

#### Quinolone 4-1-A

<sup>1</sup>H NMR (500 MHz, CDCl<sub>3</sub>, r.t., ppm): δ = 8.43 (dd, *J* = 7.9 Hz, 0.5 Hz, 1H), 7.96 (s, 1H), 7.77 (dd, *J* = 7.9, 0.5 Hz, 1H), 6.29 (s, 1H), 3.81 (s, 3H), 2.50 (d, *J* = 0.5 Hz, 3H).

<sup>13</sup>C NMR (125 MHz, CDCl<sub>3</sub>, r.t., ppm): δ = 177.9, 151.5, 141.3, 129.2, 128.5, 126.0, 122.1, 112.2, 84.6, 34.7, 24.8, 22.5 (one C not observed, likely that attached to B).

<sup>11</sup>B NMR (160 MHz, CDCl<sub>3</sub>, r.t., ppm): δ = 31.0.

HRMS (ASAP<sup>+</sup>): *m/z* calcd. for [M+H]<sup>+</sup> 299.1802, found 299.1795 [M+H]<sup>+</sup> (|Δ| = 2.34 ppm).

#### Quinolone 4-1-B

<sup>1</sup>H NMR (500 MHz, CDCl<sub>3</sub>, r.t., ppm): δ = 8.93 (dd, *J* = 1.7 Hz, 0.5 Hz, 1H), 8.03 (dd, *J* = 8.7, 1.7 Hz, 1H), 7.45 (d, *J* = 8.7, 1H), 6.27 (s, 1H), 3.74 (s, 3H), 2.48 (d, *J* = 0.5 Hz, 3H).

<sup>13</sup>C NMR (125 MHz, CDCl<sub>3</sub>, r.t., ppm): δ = 178.1, 151.2, 143.8, 137.9, 134.8, 125.9, 114.7, 112.6, 84.2, 34.5, 25.1, 22.4 (one C not observed, likely that attached to B).

<sup>11</sup>B NMR (160 MHz, CDCl<sub>3</sub>, r.t., ppm):  $\delta = 31.0$ .

HRMS (ASAP<sup>+</sup>): *m/z* calcd. for [M+H]<sup>+</sup> 299.1802, found 299.1795 [M+H]<sup>+</sup> ( $|\Delta| = 2.34$  ppm).

#### Quinolone 4-3

<sup>1</sup>H NMR (500 MHz, THF-*d*<sub>8</sub>, r.t.):  $\delta = 8.23$  (d, *J* = 7.9 Hz, 1H), 7.60 (d, *J* = 7.9 Hz, 1H), 7.51-7.48 (m, 1H), 7.22-7.13 (m, 1H), 6.04 (s, 1H), 2.38 (s, 3H).

<sup>13</sup>C NMR (125 MHz, THF-*d*<sub>8</sub>, r.t., ppm):  $\delta = 178.7, 151.0, 142.0, 132.1, 126.5, 126.3, 123.6, 119.1, 109.7, 82.4, 25.2, 20.25$ .

<sup>11</sup>B NMR (160 MHz, THF-*d*<sub>8</sub>, r.t., ppm):  $\delta = 34.7$ .

HRMS (ASAP<sup>+</sup>): *m/z* calcd. for [M+H]<sup>+</sup> 285.1645, found 285.1645 [M+H]<sup>+</sup> ( $|\Delta| = 0.00$  ppm).

#### Quinolone 4-4-A

<sup>1</sup>H NMR (200 MHz, CDCl<sub>3</sub>, r.t., ppm):  $\delta = 8.30$  (d, *J* = 8.0 Hz, 1H), 8.03 (s, 1H), 7.67 (d, *J* = 8.0 Hz, 1H), 6.20 (s, 1H), 2.43 (s, 3H).

<sup>11</sup>B NMR (160 MHz, CDCl<sub>3</sub>, r.t., ppm):  $\delta = 34.7$ .

HRMS (ASAP<sup>+</sup>): *m/z* calcd. for [M+H]<sup>+</sup> 410.2534, found 410.2531 [M+H]<sup>+</sup> ( $|\Delta| = 7.30$  ppm).

#### Quinolone 4-4-B

<sup>1</sup>H NMR (200 MHz, CDCl<sub>3</sub>, r.t., ppm):  $\delta = 8.82$  (s, 1H), 7.89 (d, *J* = 8.4 Hz, 1H), 7.59 (d, *J* = 8.4 Hz, 1H), 6.20 (s, 1H), 2.41 (s, 3H).

<sup>11</sup>B NMR (160 MHz, CDCl<sub>3</sub>, r.t., ppm):  $\delta = 34.7$ .

HRMS (ASAP<sup>+</sup>): *m/z* calcd. for [M+H]<sup>+</sup> 410.2534, found 410.2531 [M+H]<sup>+</sup> ( $|\Delta| = 7.30$  ppm).

#### Quinolone 4-9-A

<sup>1</sup>H NMR (300 MHz, CDCl<sub>3</sub>, r.t., ppm):  $\delta = 8.08$  (dd, *J* = 7.9, 1.0 Hz, 1H), 7.98 (s, 1H), 7.69 (dd, *J* = 7.9, 1.0 Hz, 1H), 3.48 (s, 3H), 2.49 (s, 3H).

#### Quinolone 4-9-B

<sup>1</sup>H NMR (300 MHz, CDCl<sub>3</sub>, r.t., ppm):  $\delta = 8.59$  (dd, *J* = 1.5, 0.6 Hz, 1H), 7.98 (dd, *J* = 8.1, 1.5 Hz, 1H), 7.46 (dd, *J* = 8.1, 1.5 Hz, 1H), 3.48 (s, 3H), 2.49 (s, 3H).

**Quinolone 4-10**

<sup>1</sup>H NMR (500 MHz, CD<sub>3</sub>OD, r.t., ppm):  $\delta$  = 8.34 (dd,  $J$  = 8.1, 1.5 Hz, 1H), 8.11 (dd,  $J$  = 7.0, 1.5 Hz, 1H), 7.41 (d,  $J$  = 7.0 Hz, 1H), 6.21 (s, 1H), 2.51 (s, 3H).

<sup>13</sup>C NMR (64 MHz, CD<sub>3</sub>OD, r.t., ppm):  $\delta$  = 30.9

## 6.11 X-Ray

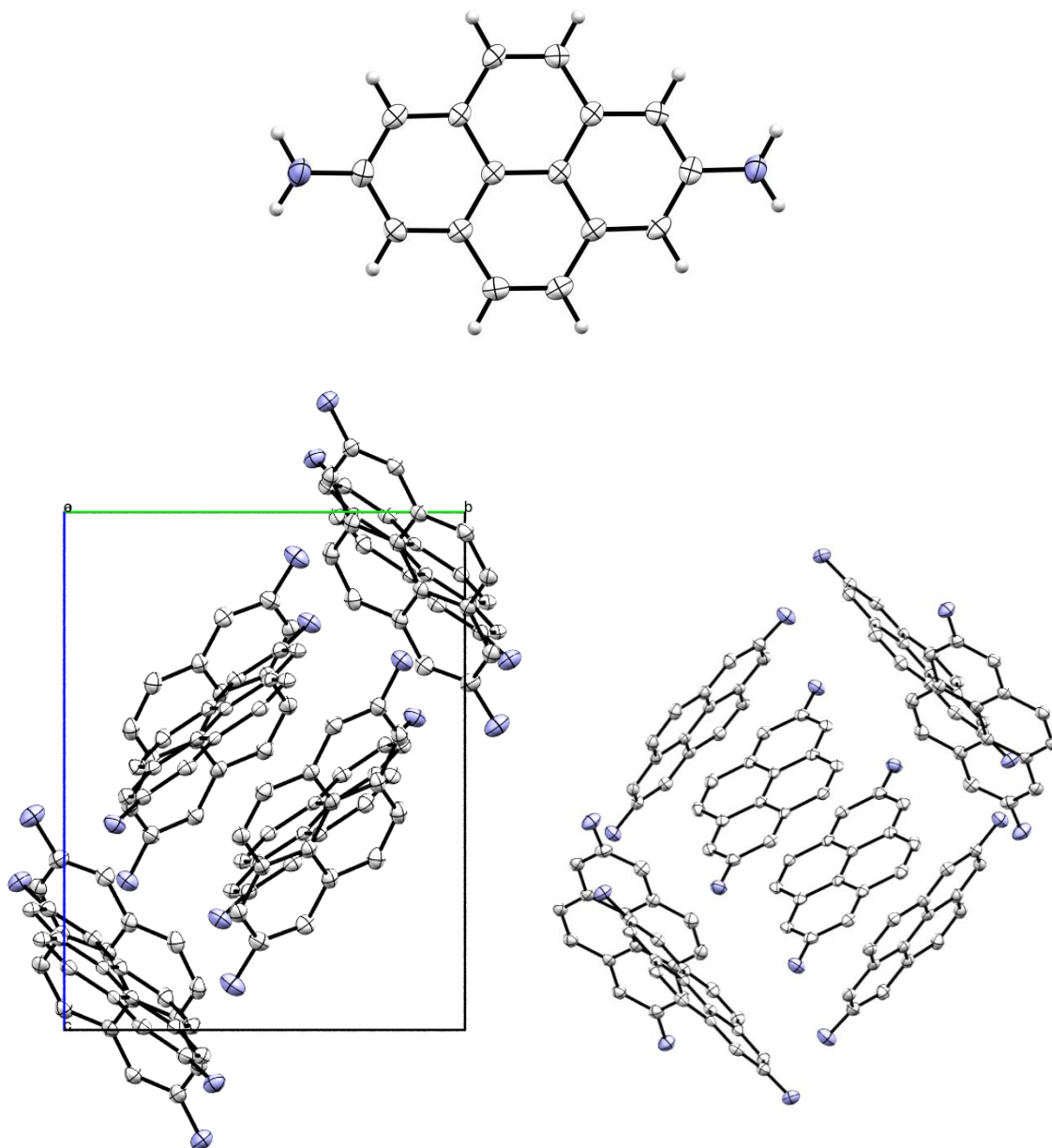


**Figure 6-1.** Molecular structure of **1-1** in the solid state at 100 K (top). Nitrogen atoms are colored blue. The crystal structure contains two independent molecules in the asymmetric unit with C–N bond lengths of 1.383(3) and 1.397(3) Å in one molecule and 1.409(3) Å for both C–N bonds in the other molecule. Projection of the crystal packing along the crystallographic *a*-axis (left) is shown with H atoms omitted for clarity. Compound **1-1** crystallizes in a sandwich-herringbone packing wherein the herringbone is made up of sandwich-like diads with both edge-to-face and offset face-to-face interactions of  $\pi$ - $\pi$  stacked molecules that have an interplanar distance of  $X = 3.32$ - $3.39$  Å.

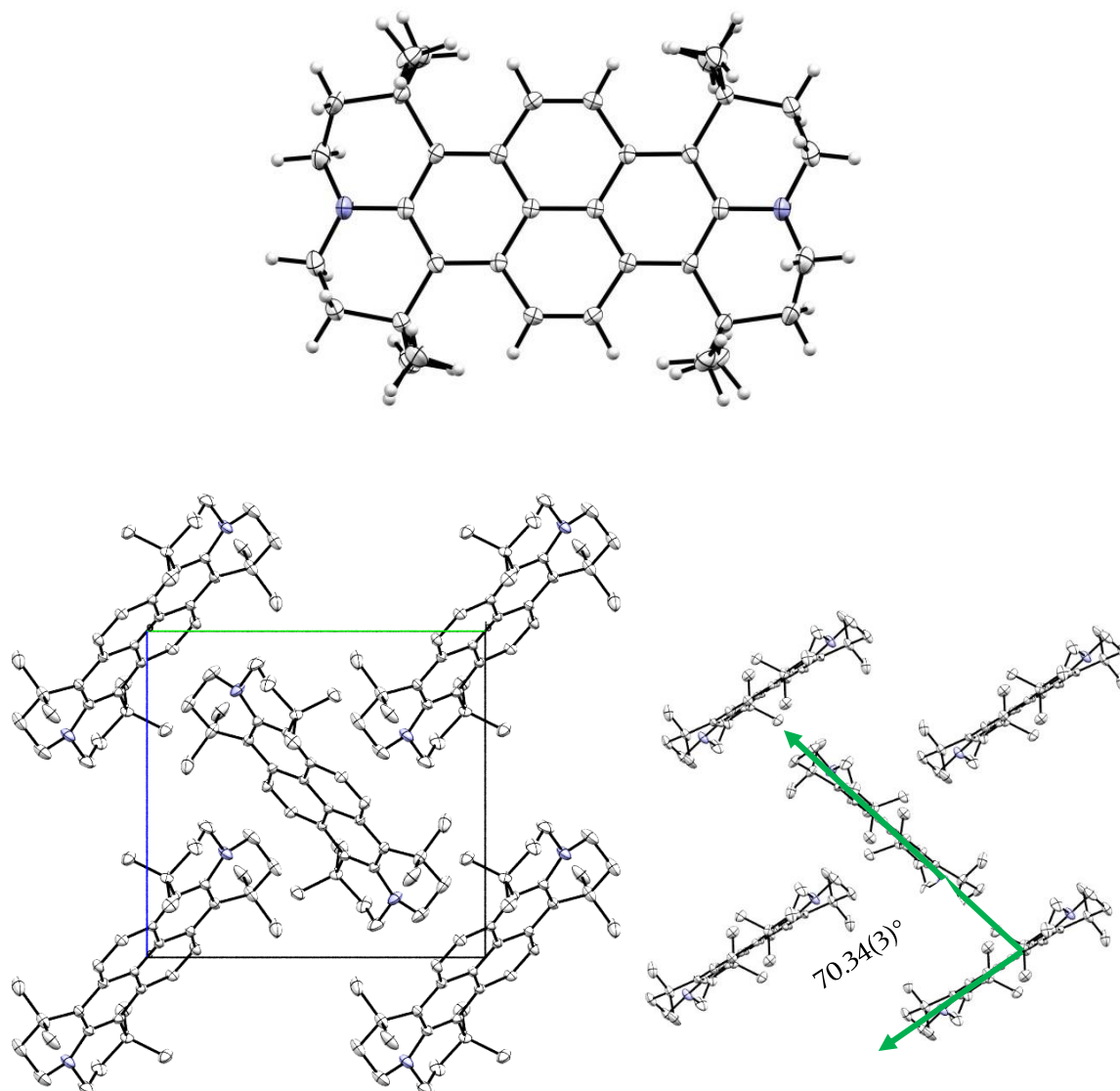


**Figure 6-2.** Molecular structure of **1-4** in the solid state at 100 K (top). Nitrogen atoms are colored blue. The molecule lies on an inversion center. The bond length between the nitrogen of the julolidine moiety and the pyrene carbon atom is 1.4044(16) Å. The crystal packing viewed down the crystallographic *a*-axis is shown with H atoms omitted for clarity. The molecules are arranged in a herringbone motif with edge-to-face stacking. The interplanar angle between the pyrene moieties is 70.34(3)°.

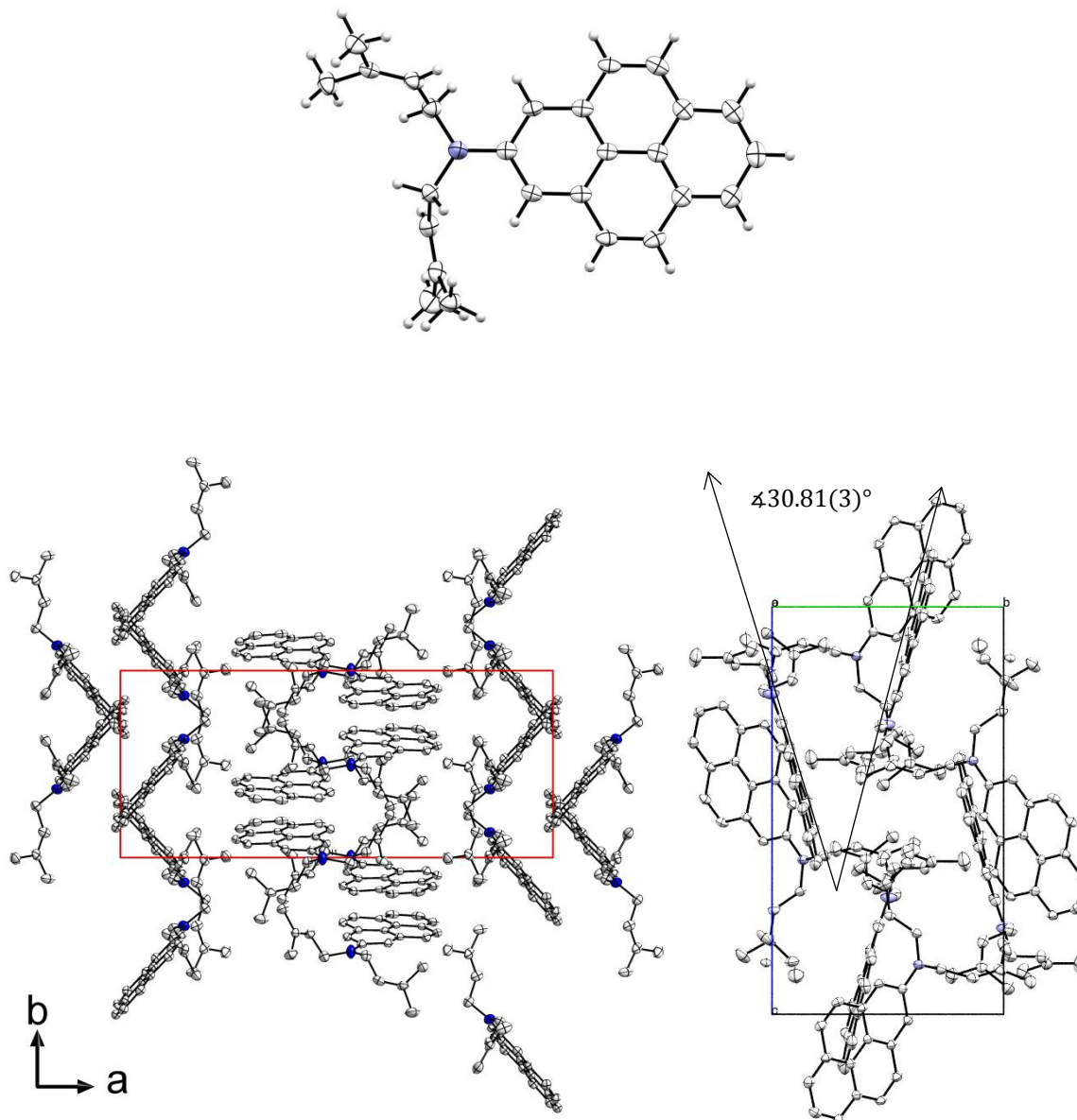


**Figure 6-3.** Molecular structure of **1-6** in the solid state at 100 K (top). The nitrogen atom is colored blue. The C–N bond lengths between the amine and pyrene moiety are 1.380(19) Å and 1.379(2) Å, respectively, in the two independent molecules in the asymmetric unit. Crystal packing diagrams viewed down the crystallographic *a*-axis (bottom left) and *b*-axis (bottom right) are shown, with H atoms omitted for clarity. Symmetry-independent molecules are arranged in bulky double-sheet-like motifs alternating along the *a* axis (bottom left). While symmetry-equivalent molecules in the central motif form a head-to-tail arrangement with an angle between them of  $30.81(3)^\circ$  (bottom right), the marginal motif is made up of a zig-zag-like arrangement of the other, symmetry-independent molecule. Due to the steric demand of the donor ligands, there are no obvious  $\pi$ - $\pi$ -interactions present.

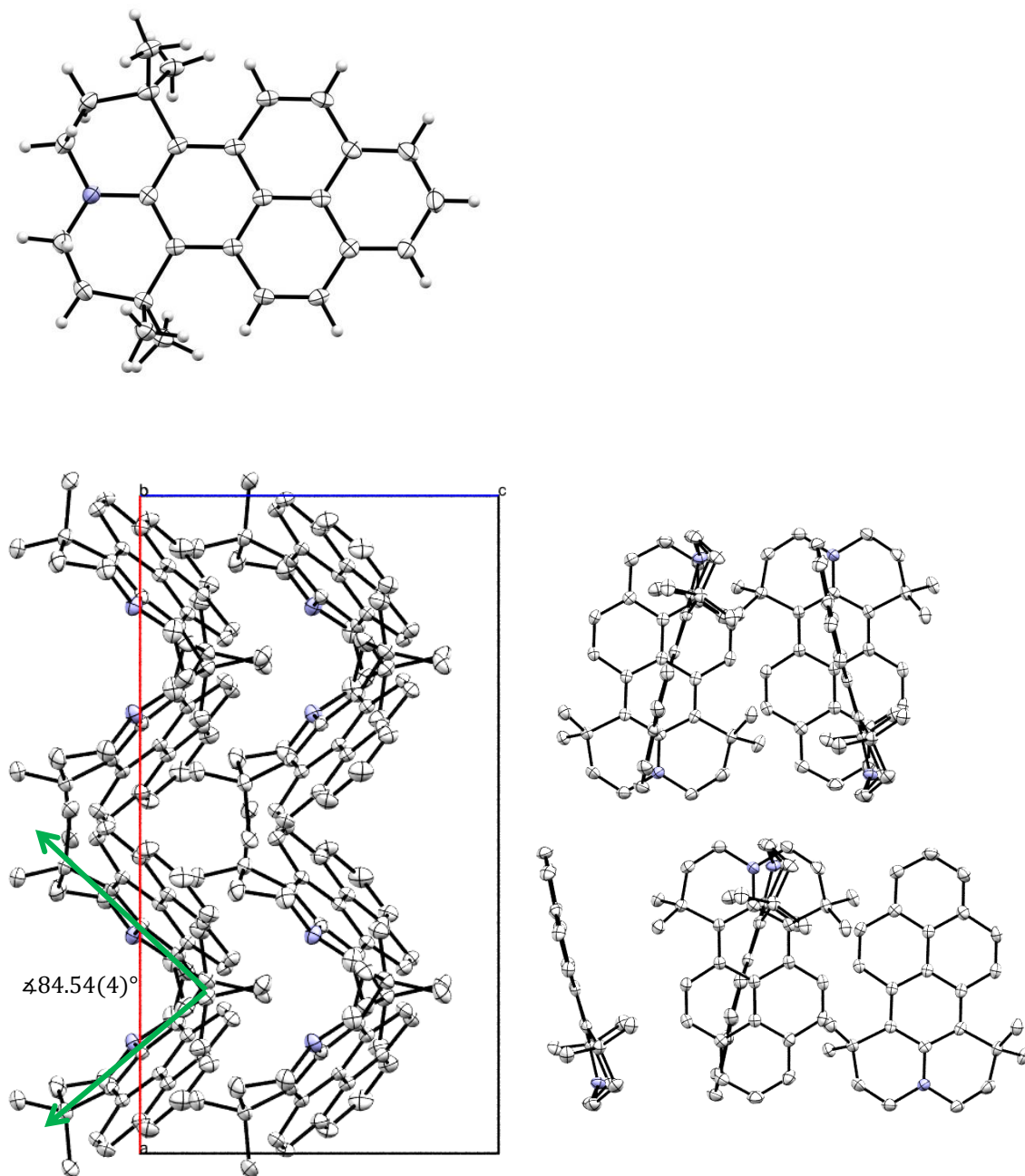


**Figure 6-4.** Molecular structure of **1-8** in the solid state at 100 K (top). The nitrogen atom is colored blue. The C–N bond length between the nitrogen of the julolidine moiety and the pyrene carbon atom is 1.404(3) Å. Crystal packing viewed down the crystallographic *b*-axis is shown (bottom left), with H atoms omitted for clarity. The molecules form a herringbone type motif with an interplanar angle of 84.54(4)° between the pyrene moieties.

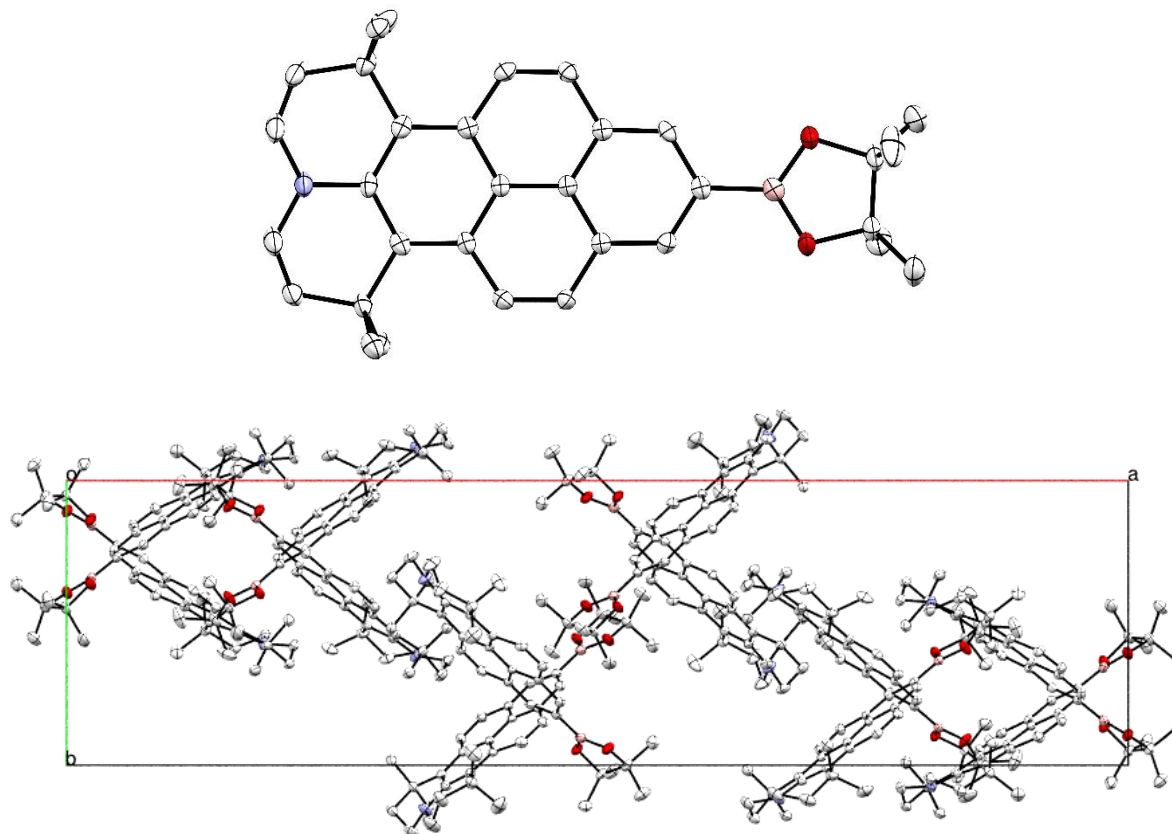


**Figure 6-5.** Molecular structure of **1-9** in the solid state at 100 K (top). There are three independent molecules of **1-9** and three benzenes in the asymmetric unit. The C–N bond length (julolidine to pyrene) is 1.398(3), 1.403(3) and 1.402(3) Å, respectively, and the C–B bond length is 1.552(3), 1.557(3) and 1.557(3) Å, respectively. Crystal packing viewed down the crystallographic *c*-axis is shown (bottom), with H atoms and co-crystallized solvent (benzene) omitted for clarity. The molecules arrange in a herringbone motif.

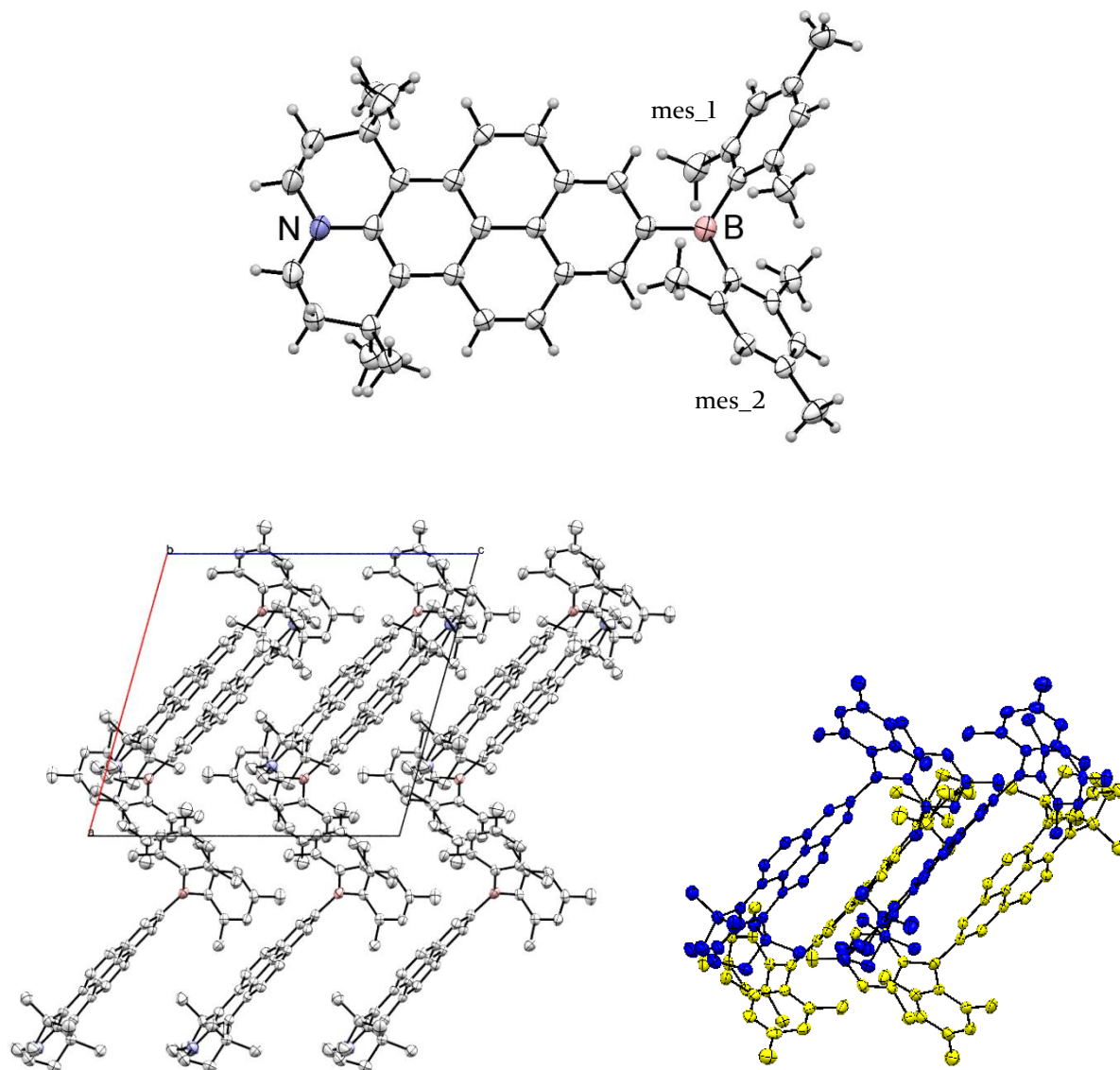


**Figure 6-6.** Molecular structure of **1-11** in the solid state at 100 K (top). The C–N bond length is 1.390(3) Å. The C–B bond length between the B(mes)<sub>2</sub> and pyrene moiety is 1.562(4) Å. The two mesityl moieties at the boron atom are twisted with respect to the pyrene core (plane defined by 16 C atoms of pyrene) by 68.43(7)° (mes\_1) and 68.60(7)° (mes\_2) (planes defined by 9 C atoms of each mesityl moiety). Crystal packing viewed down the *b*-axis is shown with H atoms omitted for clarity. The molecules arrange with their pyrene cores in a roughly parallel, slightly  $\gamma$ -like tilted fashion. Laterally neighbouring molecules are oriented in a head-to-tail fashion. Due to the steric demand of the acceptor ligands, there are no obvious  $\pi$ - $\pi$ -interactions present.

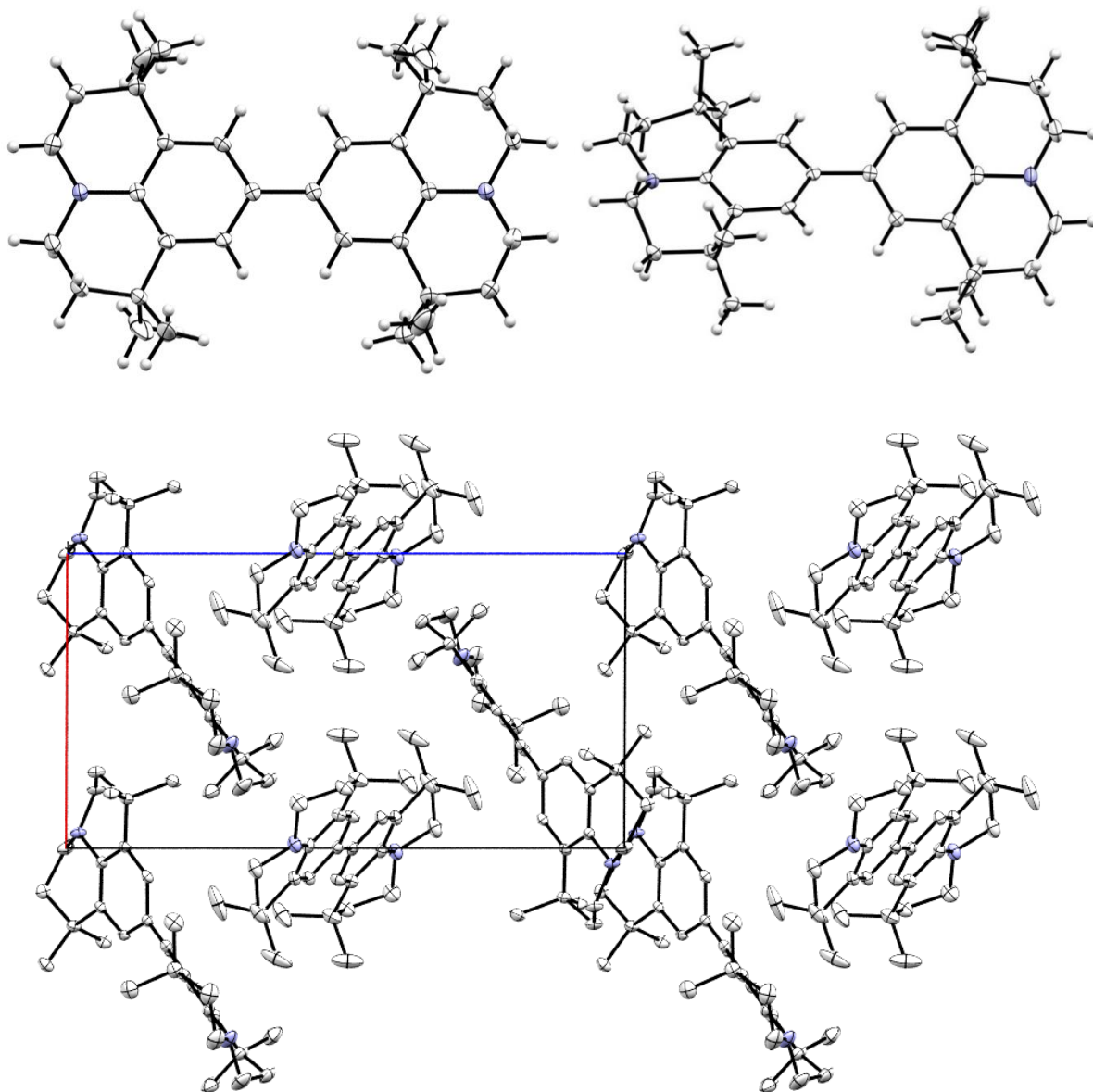


**Figure 6-7.** Molecular structure of **1-14** in the solid state at 100 K (top). Nitrogen atoms are colored blue. The asymmetric unit contains two independent molecules, one of which lies on an inversion center and thus, the aryl rings are coplanar. In the twisted molecule, the dihedral angle is  $43.97(4)^\circ$ . Both the planar and twisted molecules are edge-to-face stacked in a way similar to a herringbone-type motif. Crystal packing viewed down the crystallographic *b*-axis is shown with H atoms omitted for clarity. The central C–C bond length between the julolidine moieties (C7\_1–C8\_1 and C6\_2–C6\_2') is  $1.487(2)$  Å and  $1.494(3)$  Å, respectively, which is significantly longer than the central (analogous) C–C-bond (C7–C7') in **1-4** ( $1.449(2)$  Å).

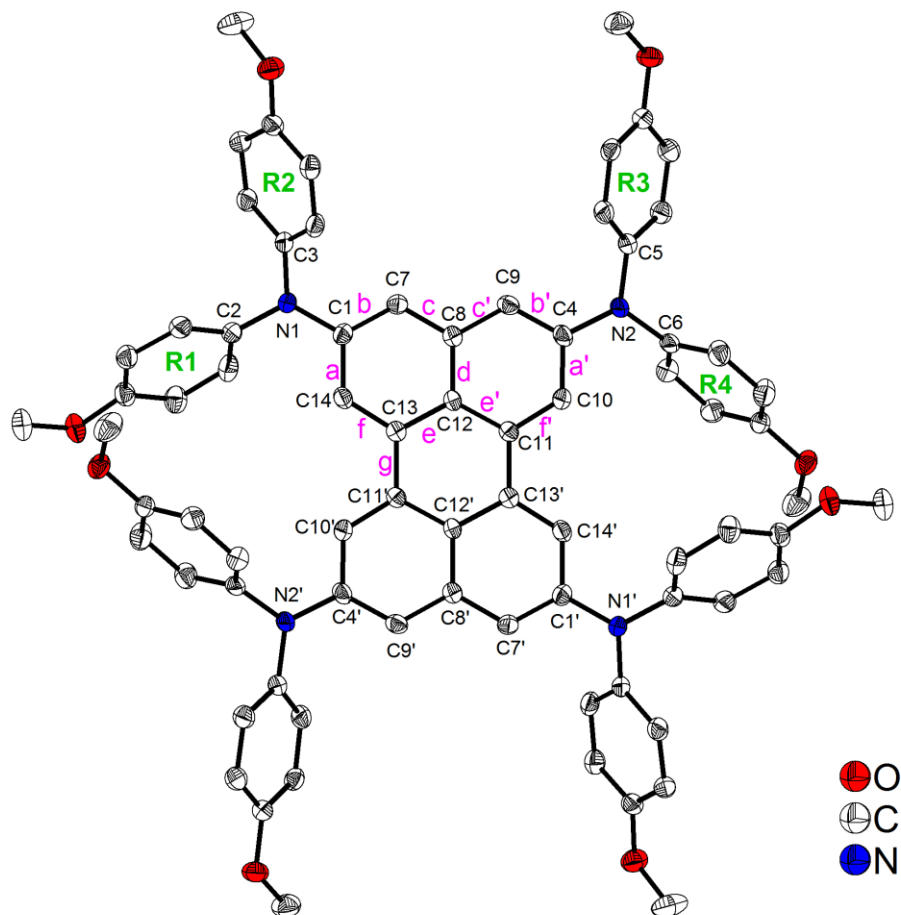


**Figure 6-8.** Solid state molecular structure of **(DPA)<sub>4</sub>-Per** from single-crystal X-ray diffraction at 100 K. Atomic displacement ellipsoids are drawn at the 50% probability level, and hydrogen atoms are omitted for clarity. Terminal aryl rings bonded to nitrogen are labelled R1 and R2 if bonded to N1 and R3 and R4 if bonded to N2, respectively.

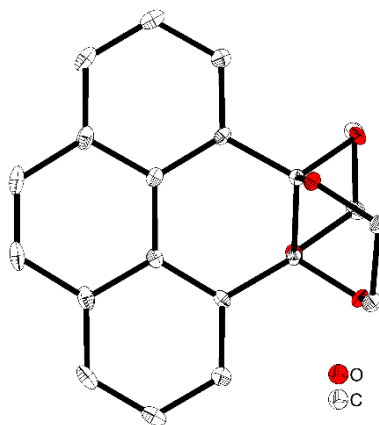


**Figure 6-9.** Solid state molecular structure of compound **3-2** from single-crystal X-ray diffraction at 100 K. Atomic displacement ellipsoids are drawn at the 50% probability level, and hydrogen atoms are omitted for clarity. The molecule has 2-fold rotational symmetry.

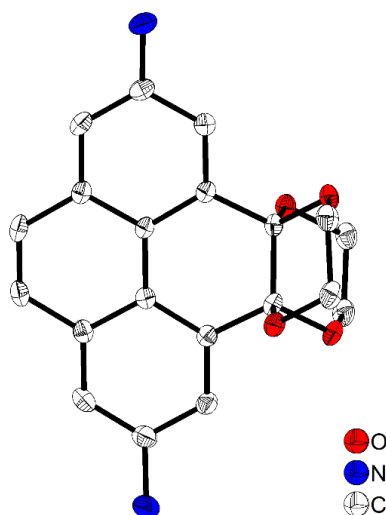


**Figure 6-10.** Solid state molecular structure of compound **3-5'** from single-crystal X-ray diffraction at 100 K. Atomic displacement ellipsoids are drawn at the 50% probability level, and hydrogen atoms are omitted for clarity.

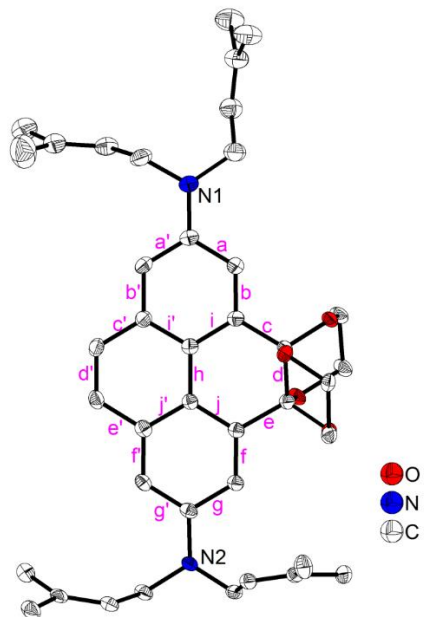


**Figure 6-11.** Solid state molecular structure of compound **3-6'** from single-crystal X-ray diffraction at 100 K. Atomic displacement ellipsoids are drawn at the 50% probability level, and hydrogen atoms are omitted for clarity. The two alkyl chains bonded to the N1 nitrogen atom are disordered and only the major parts with an occupancy of 89% are shown here.

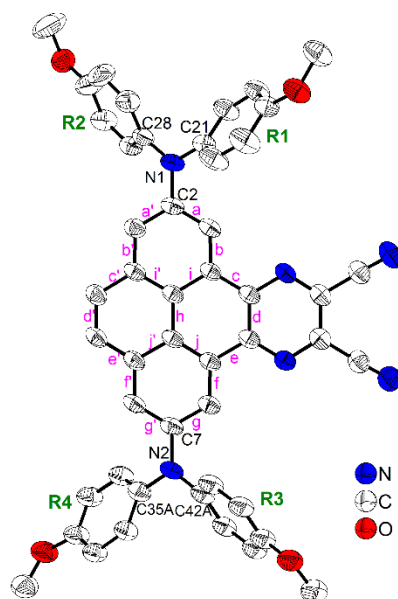


**Figure 6-12.** Solid state molecular structure of compound **3-7** from single-crystal X-ray diffraction at 100 K. Atomic displacement ellipsoids are drawn at the 50% probability level. Hydrogen atoms and the disordered tetrahydrofuran solvent molecule are omitted for clarity. The phenylmethoxy groups are strongly disordered and only the parts with the highest occupancies are shown. Terminal aryl rings bonded to nitrogen are labelled R1 and R2 if bonded to N1 and R3 and R4 if bonded to N2, respectively.

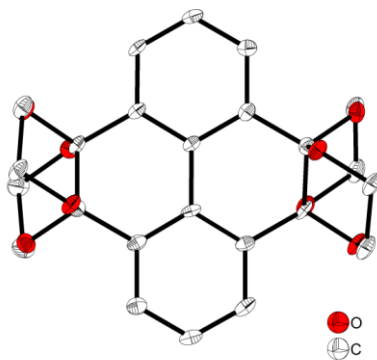


**Figure 6-13.** Solid state molecular structure of compound **3-10** from single-crystal X-ray diffraction at 100 K. Atomic displacement ellipsoids are drawn at the 50% probability level, and hydrogen atoms are omitted for clarity.

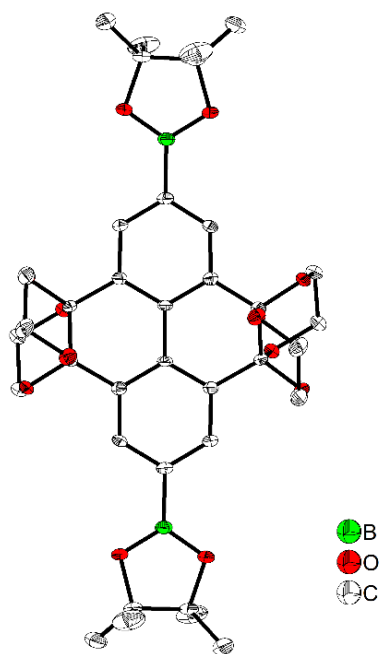


**Figure 6-14.** Solid state molecular structure of compound **3-11** from single-crystal X-ray diffraction at 100 K. Atomic displacement ellipsoids are drawn at the 50% probability level. Hydrogen atoms and the water molecule are omitted for clarity. The molecule has 2-fold rotational symmetry.

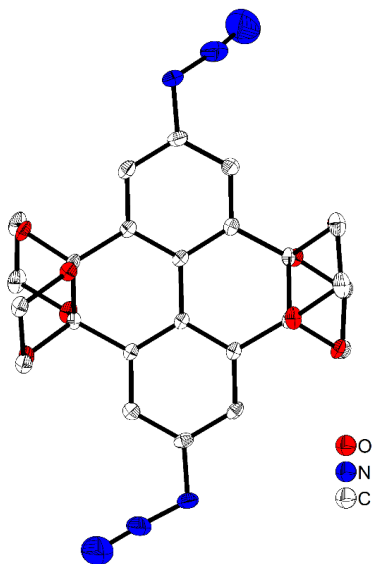


**Figure 6-15.** Solid state molecular structure of compound **3-12** from single-crystal X-ray diffraction at 100 K. Atomic displacement ellipsoids are drawn at the 50% probability level, and hydrogen atoms are omitted for clarity.

**Table 6-1:** Single-crystal X-ray diffraction data and structure refinements of compounds **1-1**, **1-4**, **1-6** and **1-8**.

<b>Compound</b>	<b>1-1</b>	<b>1-4</b>	<b>1-6</b>	<b>1-8</b>
CCDC	1542751	1542754	1542756	1542752
Formula	C <sub>16</sub> H <sub>12</sub> N <sub>2</sub>	C <sub>36</sub> H <sub>44</sub> N <sub>2</sub>	C <sub>26</sub> H <sub>27</sub> N	C <sub>26</sub> H <sub>27</sub> N
$\rho_x$ /g cm <sup>-3</sup>	1.431	1.214	1.171	1.243
Crystal size/mm <sup>3</sup>	0.02×0.31×0.43	0.3×0.35×0.4	0.16×0.39×0.44	0.09×0.19×0.28
$\mu$ /mm <sup>-1</sup>	0.086	0.070	0.067	0.071
$M_r$ /g·mol <sup>-1</sup>	232.28	504.73	353.48	353.48
$T$ /K	100	100	100	100
Crystal system	monoclinic	monoclinic	monoclinic	orthorhombic
Space group	<i>P2<sub>1</sub>/c</i>	<i>P2<sub>1</sub>/c</i>	<i>P2<sub>1</sub>/c</i>	<i>Iba2</i>
$a$ /Å	15.835(3)	9.621(4)	23.016(11)	17.670(9)
$b$ /Å	10.2601(17)	12.201(5)	9.948(6)	22.240(12)
$c$ /Å	13.855(2)	12.490(6)	17.514(9)	9.611(4)
$\alpha$ /°	90	90	90	90
$\beta$ /°	106.632(5)	109.623(19)	90.92(2)	90
$\gamma$ /°	90	90	90	90
$V$ /Å <sup>3</sup>	2156.9(6)	1381.0(10)	4009 (4)	3777(3)
$Z$	8	2	8	8
$\theta_{max}$ /°	26.212	25.997	26.020	26.012
Unique refls.	4289	2707	7894	3565
Parameters	357	176	525	248
$wR_2$ (all data)	0.1275	0.1223	0.1065	0.0835
$R_1$ [ $I > 2\sigma(I)$ ]	0.0461	0.0438	0.0406	0.0327

**Table 6-2.** Single-crystal X-ray diffraction data and structure refinements of compounds **1-9**, **1-11** and **1-14**.

Compound	<b>1-9</b>	<b>1-11</b>	<b>1-14</b>
CCDC	1542757	1542755	1542753
Formula	C <sub>32</sub> H <sub>38</sub> BNO <sub>2</sub> , C <sub>6</sub> H <sub>6</sub>	C <sub>44</sub> H <sub>48</sub> BN	C <sub>32</sub> H <sub>44</sub> N <sub>2</sub>
$\rho_x$ /g cm <sup>-3</sup>	1.180	1.217	1.129
Crystal size/mm <sup>3</sup>	0.13×0.28×0.38	0.28×0.50×0.64	0.31×0.35×0.38
$\mu$ /mm <sup>-1</sup>	0.071	0.069	0.065
$M_r$ /g·mol <sup>-1</sup>	557.55	601.64	465.69
$T$ /K	100	100	100
Crystal system	monoclinic	monoclinic	triclinic
Space group	<i>P</i> 2 <sub>1</sub> / <i>c</i>	<i>P</i> 2 <sub>1</sub> / <i>c</i>	<i>P</i> $\bar{1}$
<i>a</i> /Å	44.991(15)	13.861(14)	9.7465(3)
<i>b</i> /Å	11.896(5)	16.716(16)	12.8492(4)
<i>c</i> /Å	17.822(86)	14.710(15)	17.3321(5)
$\alpha$ /°	90	90	84.250(1)
$\beta$ /°	99.182(13)	105.62(3)	88.172(1)
$\gamma$ /°	90	90	68.950(1)
<i>V</i> /Å <sup>3</sup>	9416(6)	3283(6)	2015.52(11)
<i>Z</i>	12	4	3
$\theta_{max}$ /°	26.020	26.022	25.997
Unique refls.	18534	6458	7898
Parameters	1269	425	502
<i>wR</i> <sub>2</sub> (all data)	0.1427	0.1482	0.1114
<i>R</i> <sub>1</sub> [ <i>I</i> >2σ( <i>I</i> )]	0.0568	0.0535	0.0438

**Table 6-3.** Single-crystal X-ray diffraction data and structure refinement of **(DPA)<sub>4</sub>-Per**.

Compound	(DPA) <sub>4</sub> -Per
CCDC	1881912
Formula	C <sub>76</sub> H <sub>64</sub> N <sub>4</sub> O <sub>8</sub>
$\rho_x$ /g cm <sup>-3</sup>	1.305
<i>F</i> (000)	1224
Crystal size/mm <sup>3</sup>	0.132×0.302×0.39
Crystal color, habit	orange plate
$\mu$ /mm <sup>-1</sup>	0.085
<i>M<sub>r</sub></i> /g·mol <sup>-1</sup>	1161.31
<i>T</i> /K	100
$\lambda$ /Å, radiation	0.71073, MoK $\alpha$
Crystal system	monoclinic
Space group	<i>P</i> 2 <sub>1</sub> / <i>n</i>
<i>a</i> /Å	14.025(7)
<i>b</i> /Å	11.576(7)
<i>c</i> /Å	18.285(9)
$\alpha$ /°	90
$\beta$ /°	95.45(2)
$\gamma$ /°	90
<i>V</i> /Å <sup>3</sup>	2955(3)
<i>Z</i>	2
$\theta_{max}$ /°	26.511
Reflections collected	23828
Unique refls.	6104
Parameters	401
GooF on <i>F</i> <sup>2</sup>	1.016
<i>R</i> <sub>1</sub> [ <i>I</i> >2 $\sigma$ ( <i>I</i> )]	0.0470
<i>wR</i> <sub>2</sub> (all data)	0.1182
Max./min. residual electron density/e·Å <sup>-3</sup>	0.271/-0.214

**Table 6-4.** Single-crystal X-ray diffraction data and structure refinement of **3-2**, **3-5'** and **3-6'**.

Compound	3-2	3-5'	3-6'
CCDC	1917153	1917154	1917155
Formula	C <sub>20</sub> H <sub>16</sub> O <sub>4</sub>	C <sub>20</sub> H <sub>18</sub> N <sub>2</sub> O <sub>4</sub>	C <sub>40</sub> H <sub>50</sub> N <sub>2</sub> O <sub>4</sub>
$\rho_x$ /g cm <sup>-3</sup>	1.488	1.446	1.233
<i>F</i> (000)	336	736	672
Crystal size/mm <sup>3</sup>	0.36×0.36×0.37	0.09×0.27×0.47	0.24×0.39×0.47
Crystal color, habit	colorless needle	yellow plate	yellow plate
$\mu$ /mm <sup>-1</sup>	0.104	0.102	0.079
<i>M<sub>r</sub></i> /g·mol <sup>-1</sup>	320.33	350.36	622.82
<i>T</i> /K	100(2)	100(2)	100(2)
$\lambda$ /Å, radiation	0.71073, MoK $\alpha$	0.71073, MoK $\alpha$	0.71073, MoK $\alpha$
Crystal system	orthorhombic	monoclinic	Triclinic
Space group	<i>P</i> 2 <sub>1</sub> 2 <sub>1</sub> 2	<i>C</i> <i>c</i>	<i>P</i> $\bar{1}$
<i>a</i> /Å	9.6450(8)	9.522(3)	8.987(4)
<i>b</i> /Å	7.7838(6)	15.842(4)	9.778(4)
<i>c</i> /Å	9.5226(8)	10.804(3)	19.688(8)
$\alpha$ /°	90	90	76.792(16)
$\beta$ /°	90	99.100(17)	88.80(3)
$\gamma$ /°	90	90	84.95(2)
<i>V</i> /Å <sup>3</sup>	714.91(10)	1609.4(8)	1677.8(13)
<i>Z</i>	2	4	2
$\theta_{max}$ /°	29.977	28.989	25.086
Reflections collected	8187	24616	34999
Unique refls.	2030	3662	5964
Parameters / restraints	109 / 0	251 / 2	443 / 11
GooF on <i>F</i> <sup>2</sup>	1.051	1.025	1.049
<i>R<sub>I</sub></i> [ <i>I</i> >2 $\sigma$ ( <i>I</i> )]	0.0356	0.0405	0.0525
<i>wR</i> <sub>2</sub> (all data)	0.0907	0.0990	0.1442
Max./min. residual electron density/e·Å <sup>-3</sup>	0.341/-0.236	0.378/-0.280	0.296/-0.308

**Table 6-5.** Single-crystal X-ray diffraction data and structure refinement of **3-7**, **3-10**, and **3-11**.

<b>Compound</b>	<b>3-7</b>	<b>3-10</b>	<b>3-11</b>
CCDC	1917156	1917157	1917158
Formula	C <sub>48</sub> H <sub>34</sub> N <sub>6</sub> O <sub>4</sub> ·C <sub>4</sub> H <sub>8</sub> O	C <sub>24</sub> H <sub>22</sub> O <sub>8</sub>	C <sub>36</sub> H <sub>44</sub> B <sub>2</sub> O <sub>12</sub> ·0.333(H <sub>2</sub> O)
$\rho_x$ /g cm <sup>-3</sup>	1.323	1.475	1.358
<i>F</i> (000)	1744	1840	1108
Crystal size/mm <sup>3</sup>	0.26×0.27×0.39	0.22×0.24×0.48	0.32×0.34×0.40
Crystal color, habit	black block	colorless needle	colorless block
$\mu$ /mm <sup>-1</sup>	0.087	0.111	0.101
<i>M<sub>r</sub></i> /g·mol <sup>-1</sup>	830.91	438.41	696.33
<i>T</i> /K	100(2)	100(2)	100(2)
$\lambda$ /Å, radiation	0.71073, MoK $\alpha$	0.71073, MoK $\alpha$	0.71073, MoK $\alpha$
Crystal system	monoclinic	orthorhombic	Trigonal
Space group	<i>P</i> 2 <sub>1</sub> / <i>n</i>	<i>Pbca</i>	<i>P</i> 3 <sub>1</sub> 21
<i>a</i> /Å	12.476(4)	18.248(9)	10.091(4)
<i>b</i> /Å	17.608(7)	11.425(6)	10.091(4)
<i>c</i> /Å	19.153(8)	18.943(10)	28.958(13)
$\alpha$ /°	90	90	90
$\beta$ /°	97.469(8)	90	90
$\gamma$ /°	90	90	120
<i>V</i> /Å <sup>3</sup>	4172(3)	3949(4)	2554(2)
<i>Z</i>	4	8	3
$\theta_{max}$ /°	26.444	26.332	27.469
Reflections collected	42125	32701	47551
Unique refls.	8553	4025	3901
Parameters / restraints	676 / 530	289 / 0	238 / 3
GooF on <i>F</i> <sup>2</sup>	1.043	1.011	1.097
<i>R<sub>I</sub></i> [ <i>I</i> >2 $\sigma$ ( <i>I</i> )]	0.0727	0.0561	0.0435
<i>wR</i> <sub>2</sub> (all data)	0.2059	0.1434	0.1157
Max./min. residual electron density/e·Å <sup>-3</sup>	0.395/-0.340	0.327/-0.332	0.599/-0.193

**Table 6-6.** Single-crystal X-ray diffraction data and structure refinement of **3-12**.

<b>Compound</b>	<b>3-12</b>
CCDC	1917159
Formula	C <sub>24</sub> H <sub>20</sub> N <sub>6</sub> O <sub>8</sub>
$\rho_x$ /g cm <sup>-3</sup>	1.565
$F(000)$	2160
Crystal size/mm <sup>3</sup>	0.16×0.37×0.76
Crystal color, habit	yellow plate
$\mu$ /mm <sup>-1</sup>	0.121
$M_r$ /g·mol <sup>-1</sup>	520.46
$T$ /K	100(2)
$\lambda$ /Å, radiation	0.71073, MoK $\alpha$
Crystal system	orthorhombic
Space group	<i>Pbca</i>
$a$ /Å	11.599(2)
$b$ /Å	19.104(15)
$c$ /Å	19.942(18)
$\alpha$ /°	90
$\beta$ /°	90
$\gamma$ /°	90
$V$ /Å <sup>3</sup>	4419(5)
$Z$	8
$\theta_{max}$ /°	27.995
Reflections collected	21413
Unique refls.	5185
Parameters / restraints	343 / 0
GooF on $F^2$	1.040
$R_I$ [ $I > 2\sigma(I)$ ]	0.0603
$wR_2$ (all data)	0.1831
Max./min. residual electron density/e·Å <sup>-3</sup>	0.523/-0.775

## 6.12 DFT and TD-DFT Calculations

**Table 6-7.** Lowest energy singlet electronic transitions of **1-4** (TD-DFT CAM-B3LYP/6-31 G(d), gas phase).

FC-S <sub>n</sub>	E / eV	λ / nm	f	major contributions (> 10%)
1	3.16	392.15	0.088	H→L (90%)
2	3.62	342.93	0.425	H-1→L (90%)
3	4.15	298.42	0.000	H-2→L (84%)
4	4.74	261.79	1.519	H→L+1 (85%)
5	4.77	260.06	0.249	H-1→L+1 (88%)
6	4.77	260.05	0.000	H-3→L (29%), H-1→L+2 (69%)
7	5.01	247.36	0.000	H→L+2 (88%)
8	5.12	242.40	0.000	H-3→L (63%), H-1→L+2 (28%)

**Table 6-8.** Lowest energy singlet electronic transitions of **1-8** (TD-DFT CAM-B3LYP/6-31 G(d), gas phase).

FC-S <sub>n</sub>	E / eV	λ / nm	f	major contributions (> 10%)
1	3.46	358.17	0.053	H-1→L+1 (12%), H→L (84%)
2	3.80	326.46	0.303	H-1→L (87%), H→L+1 (12%)
3	4.58	270.79	0.121	H-2→L (21%), H-1→L+1 (60%)
4	4.83	256.63	0.002	H-2→L (35%), H-1→L+2 (54%)
5	4.93	251.40	1.149	H-1→L (12%), H→L+1 (82%)
6	5.02	246.78	0.138	H-2→L (33%), H-1→L+1 (19%), H-1→L+2 (36%)
7	5.24	236.57	0.000	H→L+2 (82%)
8	5.48	226.12	0.028	H-3→L (55%), H→L+3 (30%)

**Table 6-9.** Lowest energy singlet electronic transitions of **1-11** (TD-DFT CAM-B3LYP/6-31 G(d), gas phase).

FC-S <sub>n</sub>	E / eV	λ / nm	f	major contributions (> 10%)
1	3.37	368.36	0.008	H-1→L (35%), H→L+1 (55%)

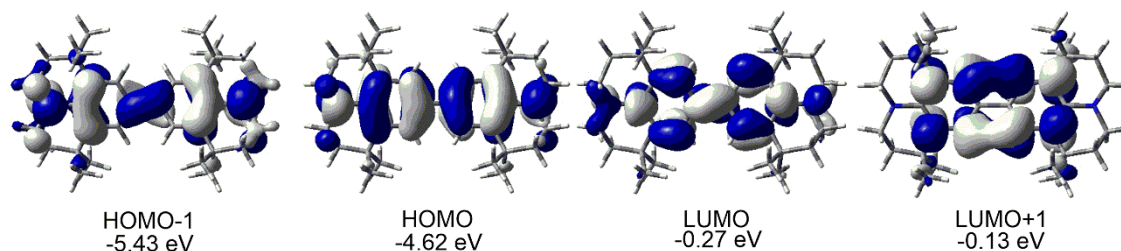
---

2	3.67	337.58	0.020	H-1→L+1 (58%), H→L (32%)
3	3.90	317.96	0.122	H-1→L (54%), H→L+1 (38%)
4	4.08	303.80	1.589	H-3→L (27%), H-1→L+1 (30%), H→L (34%)
5	4.10	302.49	0.137	H-2→L (90%)
6	4.50	275.80	0.338	H-4→L (11%), H-3→L (56%), H→L (15%)
7	4.60	269.48	0.023	H-5→L (80%)
8	4.61	269.24	0.045	H-4→L (70%)

---

**Table 6-10.** Lowest energy singlet electronic transitions of **1-14** (TD-DFT CAM-B3LYP/6-31 G(d), gas phase).

FC-S <sub>n</sub>	E / eV	λ / nm	f	major contributions (> 10%)
1	4.44	279.47	0.013	H-1→L+2 (13%), H→L+1 (77%)
2	4.52	274.31	0.870	H→L (93%)
3	4.56	272.01	0.081	H-3→L (10%), H-1→L+1 (17%)
4	5.40	229.60	0.000	H-1→L (67%), H→L+3 (18%)
5	5.94	208.65	0.001	H-4→L+2 (74%), H-1→L+1 (74%), H→L+2 (20%)
6	5.98	207.29	0.004	H-2→L (18%), H-1→L+2 (56%), H→L+1 (20%)
7	6.14	202.01	0.043	H-2→L (63%), H-1→L+2 (26%)
8	6.18	200.68	0.000	H-1→L (27%), H→L+3 (57%)

**Figure 6-16.** Depiction of the HOMO-1, HOMO, LUMO and LUMO+1 of **1-14** at the optimized geometry (DFT-B3LYP/6-31 G(d)).**Table 6-11.** Lowest energy singlet electronic transitions of pyrene (TD-DFT CAM-B3LYP/6-31 G(d), gas phase).

FC-S <sub>n</sub>	E / eV	λ / nm	f	major contributions (> 10%)
1	3.99	310.76	0.000	H-1→L (47%), H→L+1 (51%)
2	4.02	308.63	0.324	H→L (90%), H-1→L+1 (10%)
3	4.90	253.13	0.000	H→L+2 (89%), H-2→L (9%)
4	5.10	243.24	0.000	H-2→L (86%)
5	5.11	242.52	0.414	H-1→L (51%), H→L+1 (48%)

---

6	5.66	219.05	0.000	H-1→L+2 (38%), H-2→L+1 (29%), H-3→L (15%), H→L+3 (16%)
7	5.78	214.45	0.969	H-1→L+1 (84%), H→L (10%)
8	6.18	205.27	0.000	H→L+3 (72%), H-1→L+2 (20%)

---

**Table 6-12.** Lowest energy singlet electronic transitions of **1-4<sup>+</sup>** (TD-DFT) at the density functional level, using ublyp with 35% exact-exchange admixture, a SVP basis set and a polarizable continuum model accounting for solvent effects.

FC-S <sub>n</sub>	E / eV	λ / nm	f	major contributions (> 10%)
1	0.76	1639.94	0.000	β-H-1→β-L (99%)
2	0.92	1348.94	0.421	β-H→β-L (92%)
3	2.05	605.72	0.008	α-H-1→α-L (42%), β-H-1→L+1 (35%)
4	2.67	466.14	0.019	β-H-2→β-L (86%)
5	2.72	455.90	0.037	α-H→α-L (50%), β-H-3→β-L (44%)
6	2.82	438.97	0.042	β-H-3→β-L (50%), α-H→α-L (45%)
7	3.08	402.36	0.000	β-H→β-L+1 (83%)
8	3.26	380.90	0.000	β-H-4→β-L (83%)

**Table 6-13.** Lowest energy singlet electronic transitions of **1-14<sup>+</sup>** (TD-DFT) at the density functional level, using ublyp with 35% exact-exchange admixture, a SVP basis set and a polarizable continuum model accounting for solvent effects.

FC-S <sub>n</sub>	E / eV	λ / nm	f	major contributions (> 10%)
1	1.28	965.52	0.631	β-H→β-L (96%)
2	2.42	512.11	0.003	β-H-1→β-L (96%)
3	2.58	481.09	0.000	β-H-2→β-L (965%)
4	3.09	401.75	0.666	α-H→α-L (83%)
5	3.24	382.38	0.000	β-H-3→β-L (74%)
6	3.78	328.18	0.002	α-H→β-L+1 (90%)
7	3.81	325.46	0.000	β-H→β-L+2 (45%), α-H-1→α-L (13%), α-H→α-L+3 (11%)
8	4.11	301.77	0.029	α-H→α-L+2 (52%), β-H→β-L+2 (30%), α-H-1→β-L+1 (13%)

**Table 6-14.** TD-DFT results (CAM-B3LYP/6-31G (d,p)) for the five vertical transitions of perylene, (Bmes<sub>2</sub>)<sub>4</sub>-Per and (DPA)<sub>4</sub>-Per.

	FC-S <sub>n</sub>	E / eV	λ /nm	f	major contributions (> 10%)
<b>Perylene</b>	S <sub>1</sub>	3.21	387	0.446	H→L (99%)
	S <sub>2</sub>	4.06	305	0.000	H→L+1 (58%), H-1→L (33%)
	S <sub>3</sub>	4.34	285	0.004	H-2→L (52%), H→L+3 (38%)
	S <sub>4</sub>	4.45	278	0.000	H→L+2 (42%), H-4→L (24%), H-1→L (23%)
	S <sub>5</sub>	4.88	254	0.000	H→L+2 (52%), H-4→L (30%), H→L+1 (13%)
<b>(Bmes<sub>2</sub>)<sub>4</sub>-Per</b>	S <sub>1</sub>	3.03	410	0.367	H→L (96%)
	S <sub>2</sub>	3.21	386	0.000	H→L+1 (87%)
	S <sub>3</sub>	3.54	350	0.212	H→L+3 (79%)
	S <sub>4</sub>	3.64	340	0.000	H→L+2 (92%)
	S <sub>5</sub>	4.01	310	0.055	H-4→L+1 (21%), H-2→L (20%), H-1→L+2 (21%), H-3→L+3 (16%)
<b>(DPA)<sub>4</sub>-Per</b>	S <sub>1</sub>	3.00	413	0.318	H→L (91%)
	S <sub>2</sub>	3.11	398	0.017	H-1→L (76%)
	S <sub>3</sub>	3.30	376	0.281	H-2→L (74%)
	S <sub>4</sub>	3.48	356	0.005	H-3→L (77%)
	S <sub>5</sub>	3.92	316	0.294	H-4→L (78%)

**Table 6-15.** TD-DFT results (CAM-B3LYP/6-31 G(d)) for the five vertical transitions of **7** and **8**.

	FC-S <sub>n</sub>	E / eV	λ /nm	f	major contributions (> 10%)
<b>3-7</b>	S <sub>1</sub>	2.69	461	0.071	H→L (90%)
	S <sub>2</sub>	2.76	449	0.047	H→L+1 (84%)
	S <sub>3</sub>	3.40	365	0.059	H-1→L (66%), H-2→L (18%)
	S <sub>4</sub>	3.43	361	0.005	H-1→L+1 (79%)
	S <sub>5</sub>	3.57	348	0.167	H-2→L (72%), H-1→L (20%)
<b>3-8</b>	S <sub>1</sub>	2.93	423	0.120	H→L (90%)
	S <sub>2</sub>	3.19	398	0.006	H→L+1 (66%), H-2→L (12%)
	S <sub>3</sub>	3.63	342	0.390	H-2→L (75%), H→L+1 (15%)
	S <sub>4</sub>	3.64	341	0.002	H-8→L (90%)
	S <sub>5</sub>	3.76	330	0.000	H-1→L (82%)

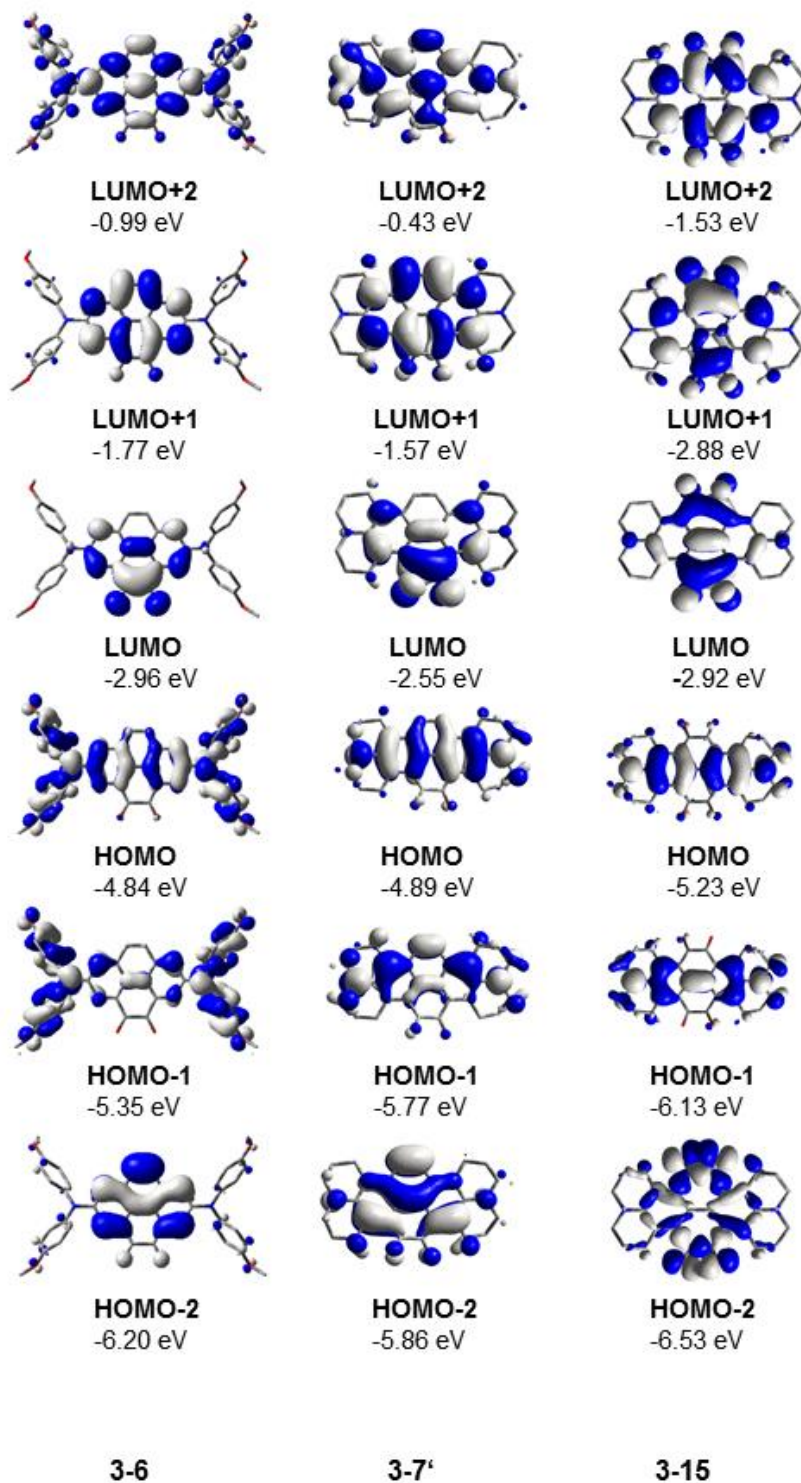


Figure 6-17. Orbital depictions of the compounds 3-6, 3-7' and 3-15 using B3LYP/6-31 G (d).



# References



## 7 References

- [1] J. Merz, J. Fink, A. Friedrich, I. Krummenacher, H. H. Al Mamari, S. Lorenzen, M. Haehnel, A. Eichhorn, M. Moos, M. Holzappel, H. Braunschweig, C. Lambert, A. Steffen, L. Ji, T. B. Marder, *Chem. Eur. J.* **2017**, *23*, 13164.
- [2] T. M. Figueira-Duarte, K. Müllen, *Chem. Rev.* **2011**, *11*, 7260.
- [3] A. Laurent, *Ann. Chim. Phys* **1837**, *66*, 136.
- [4] J. T. K. Kalyanasunaram, *J. Am. Chem. Soc.* **1977**, *99*, 2039.
- [5] W.-L. Jia, T. McCormick, Q.-D. Liu, H. Fukutani, M. Motala, R.-Y. Wang, Y. Tao, S. Wang, *J. Mater. Chem.* **2004**, *14*, 3344.
- [6] J. B. Birks, M. D. Lumb, I. H. Munro, *Proc. R. Soc. Lond. A Math. Phys. Eng. Sci.* **1964**, *280*, 289.
- [7] R. H. Templer, S. J. Castle, A. R. Curran, G. Rumbles, D. R. Klug, *Faraday Discuss.* **1998**, *111*, 41.
- [8] M. R. Pokhrel, S. H. Bossmann, *J. Phys. Chem. B* **2000**, *104*, 2215.
- [9] Y. Fujiwara, Y. Amao, *Sens. Actuator B Chem.* **2003**, *89*, 58.
- [10] E. D. Lee, T. C. Werner, W. R. Seitz, *Anal. Chem.* **1987**, *59*, 279.
- [11] C. C. Nagel, J. G. Bentsen, M. Yafuso, US Patent 5,498,549, **1996**.
- [12] T. Aoyagi, H. Ikeda, A. Ueno, *Bull. Chem. Soc. Jpn.* **2001**, *74*, 157.
- [13] H. Ikeda, M. Nakamura, N. Ise, N. Oguma, A. Nakamura, T. Ikeda, F. Toda, A. Ueno, *J. Am. Chem. Soc.* **1996**, *118*, 10980.
- [14] A. Ueno, I. Suzuki, T. Osa, *Anal. Chem.* **1990**, *62*, 2461.
- [15] B. Valeur, *Coord. Chem. Rev.* **2000**, *205*, 3.
- [16] J.-S. Yang, C.-S. Lin, C.-Y. Hwang, *Org. Lett.* **2001**, *3*, 889.
- [17] R.-H. Yang, W.-H. Chan, A. W. M. Lee, P.-F. Xia, H.-K. Zhang, K.'A. Li, *J. Am. Chem. Soc.* **2003**, *125*, 2884.
- [18] B. Bodenant, F. Fages, M.-H. Delville, *J. Am. Chem. Soc.* **1998**, *120*, 7511.

- [19] W. M. Vaughn, G. Weber, *Biochemistry* **1970**, *9*, 464.
- [20] A.-C. Ribou, J. Vigo, J.-M. Salmon, *Photochem. and Photobiol.* **2004**, *80*, 274.
- [21] a) T. Noda, Y. Shirota, *J. Am. Chem. Soc.* **1998**, *120*, 9714; b) M. Kinoshita, Y. Shirota, *Chem. Lett.* **2001**, *30*, 614.
- [22] O. Kwon, S. Barlow, S. A. Odom, L. Beverina, N. J. Thompson, E. Zojer, J.-L. Bredas, S. R. Marder, *J. Phys. Chem.* **2005**, *109*, 9346.
- [23] C. D. Entwistle, T. B. Marder, *Angew. Chem. Int. Ed.* **2002**, *41*, 2927.
- [24] C. D. Entwistle, T. B. Marder, *Chem. Mater.* **2004**, *16*, 4574.
- [25] L. Ji, S. Griesbeck, T. B. Marder, *Chem. Sci.* **2017**, *8*, 846.
- [26] A. Wakamiya, S. Yamaguchi, *Bull. Chem. Soc. Jpn.* **2015**, *88*, 1357.
- [27] Y. Ren, F. Jäkle, *Dalton Trans.* **2016**, *45*, 13996.
- [28] S. Yamaguchi, A. Wakamiya, *Pure Appl. Chem.* **2006**, *78*, 1413.
- [29] F. Jäkle, *Coord. Chem. Rev.* **2006**, *250*, 1107.
- [30] S.-Y. Li, Z.-B. Sun, C.-H. Zhao, *Inorg. Chem.* **2017**, *56*, 8705.
- [31] A. G. Crawford, A. D. Dwyer, Z. Liu, A. Steffen, A. Beeby, L.-O. Pålsson, D. J. Tozer, T. B. Marder, *J. Am. Chem. Soc.* **2011**, *133*, 13349.
- [32] D. N. Coventry, A. S. Batsanov, A. E. Goeta, J. A. K. Howard, T. B. Marder, R. N. Perutz, *Chem. Commun.* **2005**, 2172.
- [33] M. Ottonelli, M. Piccardo, D. Duce, S. Thea, G. Dellepiane, *J. Phys. Chem.* **2012**, *116*, 611.
- [34] J. M. Casas-Solvas, J. D. Howgego, A. P. Davis, *Org. Biomol. Chem.* **2014**, *12*, 212.
- [35] X. Feng, J.-Y. Hu, C. Redshaw, T. Yamato, *Chem. Eur. J.* **2016**, *22*, 11898.
- [36] H. Ju, K. Wang, J. Zhang, H. Geng, Z. Liu, G. Zhang, Y. Zhao, D. Zhang, *Chem. Mater.* **2017**, *29*, 3580.
- [37] Y. Niko, S. Sasaki, K. Narushima, D. K. Sharma, M. Vacha, G.-i. Konishi, *J. Org. Chem.* **2015**, *80*, 10794.
- [38] L. Zöphel, V. Enkelmann, K. Müllen, *Org. Lett.* **2013**, *15*, 804.

- [39] S.-S. Li, K.-J. Jiang, C.-C. Yu, J.-H. Huang, L.-M. Yang, Y.-L. Song, *New J. Chem.* **2014**, *38*, 4404.
- [40] The Stokes shift is defined as the energy difference between the 0-0 transitions of the absorption and the emission. However, as the first transition is broad, the band maxima of the absorption and emission have been used to determine the Stokes shift throughout the thesis. Consequently, the term "apparent Stokes shift" is used.
- [41] L. Zöphel, D. Beckmann, V. Enkelmann, D. Chercka, R. Rieger, K. Müllen, *Chem. Commun.* **2011**, *47*, 6960.
- [42] A. S. Batsanov, J. A. K. Howard, D. Albesa-Jové, J. C. Collings, Z. Liu, I. A. I. Mkhaliid, M.-H. Thibault, T. B. Marder, *Cryst. Growth Des.* **2012**, *12*, 2794.
- [43] I. A. I. Mkhaliid, J. H. Barnard, T. B. Marder, J. M. Murphy, J. F. Hartwig, *Chem. Rev.* **2010**, *110*, 890.
- [44] L. Ji, K. Fucke, S. K. Bose, T. B. Marder, *J. Org. Chem.* **2015**, *80*, 661.
- [45] D. Hall (Ed.) *Boronic acids: Preparation and Applications in Organic Synthesis, Medicine and Materials*, Wiley-VCH, 2nd edition, Weinheim, **2011**.
- [46] A. G. Crawford, Z. Liu, I. A. I. Mkhaliid, M.-H. Thibault, N. Schwarz, G. Alcaraz, A. Steffen, J. C. Collings, A. S. Batsanov, J. A. K. Howard, T. B. Marder, *Chem. Eur. J.* **2012**, *18*, 5022.
- [47] L. Ji, A. Lorbach, R. M. Edkins, T. B. Marder, *J. Org. Chem.* **2015**, *80*, 5658.
- [48] A. Yagi, G. Venkataramana, Y. Segawa, K. Itami, *Chem. Commun.* **2014**, *50*, 957.
- [49] K. Oniwa, H. Kikuchi, H. Shimotani, S. Ikeda, N. Asao, Y. Yamamoto, K. Tanigaki, T. Jin, *Chem. Commun.* **2016**, *52*, 4800.
- [50] D. Chercka, S.-J. Yoo, M. Baumgarten, J.-J. Kim, K. Müllen, *J. Mater. Chem. C* **2014**, *2*, 9083.
- [51] J.-Y. Hu, Y.-J. Pu, G. Nakata, S. Kawata, H. Sasabe, J. Kido, *Chem. Commun.* **2012**, *48*, 8434.
- [52] X. Zhan, J. Zhang, S. Tang, Y. Lin, M. Zhao, J. Yang, H.-L. Zhang, Q. Peng, G. Yu, Z. Li, *Chem. Commun.* **2015**, *51*, 7156.
- [53] L. Zou, X.-Y. Wang, K. Shi, J.-Y. Wang, J. Pei, *Org. Lett.* **2013**, *15*, 4378.
- [54] H. Chen, X. Hu, S.-C. Ng, *J. Polym. Sci. A Polym. Chem.* **2010**, *48*, 5562.

- [55] C. Wanninger-Weiß, H.-A. Wagenknecht, *Eur. J. Org. Chem.* **2008**, 2008, 64.
- [56] S. N. Keller, N. L. Veltri, T. C. Sutherland, *Org. Lett.* **2013**, 15, 4798.
- [57] C. Lambert, J. Ehbets, D. Rausch, M. Steeger, *J. Org. Chem.* **2012**, 77, 6147.
- [58] D. S. Yang, K. H. Kim, M. J. Cho, J.-I. Jin, D. H. Choi, *J. Polym. Sci. A Polym. Chem.* **2013**, 51, 1457.
- [59] W. Yang, J. H.S.K. Monteiro, A. de Bettencourt-Dias, W. A. Chalifoux, *Can. J. Chem.* **2017**, 95, 341.
- [60] Y. Shibuya, Y. Itoh, T. Aida, *Chem. Asian J.* **2017**, 12, 811.
- [61] A.-C. Bédard, A. Vlassova, A. C. Hernandez-Perez, A. Bessette, G. S. Hanan, M. A. Heuft, S. K. Collins, *Chem. Eur. J.* **2013**, 19, 16295.
- [62] S. Zhang, X. Qiao, Y. Chen, Y. Wang, R. M. Edkins, Z. Liu, H. Li, Q. Fang, *Org. Lett.* **2014**, 16, 342.
- [63] L. Ji, R. M. Edkins, A. Lorbach, I. Krummenacher, C. Bruckner, A. Eichhorn, H. Braunschweig, B. Engels, P. J. Low, T. B. Marder, *J. Am. Chem. Soc.* **2015**, 137, 6750.
- [64] R. Kurata, K. Kaneda, A. Ito, *Org. Lett.* **2017**, 19, 392.
- [65] B. R. Kaafarani, A.'a. O. El-Ballouli, R. Trattnig, A. Fonari, S. Sax, B. Wex, C. Risko, R. S. Khnayzer, S. Barlow, D. Patra, T. V. Timofeeva, E. J. W. List, J.-L. Brédas, S. R. Marder, *J. Mater. Chem. C* **2013**, 1, 1638.
- [66] B. R. Kaafarani, C. Risko, T. H. El-Assaad, A.'a. O. El-Ballouli, S. R. Marder, S. Barlow, *J. Phys. Chem. C* **2016**, 120, 3156.
- [67] R. Kurata, A. Ito, M. Gon, K. Tanaka, Y. Chujo, *J. Org. Chem.* **2017**, 82, 5111.
- [68] It is worth mentioning that Michl and co-workers found<sup>[69,70]</sup> additional symmetry-forbidden transitions beyond  $S_3$  by MCD spectroscopy, and mention the possible existence of further low-lying states of the same kind. Indeed, there is a forbidden transition with 0 or nearly 0 oscillator strength between the observed  $S_2 \leftarrow S_0$  and  $S_3 \leftarrow S_0$  transitions, which was noted by Marder and co-workers previously.<sup>[31]</sup> However, in the discussion, only the transitions which are actually observed are numbered.
- [69] E. W. Thulstrup, J. W. Downing, J. Michl, *Chem. Phys.* **1977**, 23, 307.

- [70] F. W. Langkilde, E. W. Thulstrup, J. Michl, *J. Chem. Phys.* **1983**, *78*, 3372.
- [71] F. Jäkle, *Chem. Rev.* **2010**, *110*, 3985.
- [72] S.-B. Zhao, P. Wucher, Z. M. Hudson, T. M. McCormick, X.-Y. Liu, S. Wang, X.-D. Feng, Z.-H. Lu, *Organometallics* **2008**, *27*, 6446.
- [73] a) D. Reitzenstein, C. Lambert, *Macromolecules* **2009**, *42*, 773; b) R. Stahl, C. Lambert, C. Kaiser, R. Wortmann, R. Jakober, *Chem. Eur. J.* **2006**, *12*, 2358; c) Z. Yuan, N. J. Taylor, T. B. Marder, I. D. Williams, S. K. Kurtz, L.-T. Cheng, *J. Chem. Soc., Chem. Commun.* **1990**, 23, 1489; d) Z. Yuan, C. D. Entwistle, J. C. Collings, D. Albesa-Jové, A. S. Batsanov, J. A. K. Howard, N. J. Taylor, H. M. Kaiser, D. E. Kaufmann, S.-Y. Poon, W.-Y. Wong, C. Jardin, S. Fathallah, A. Boucekkine, J.-F. Halet, T. B. Marder, *Chem. Eur. J.* **2006**, *12*, 2758; e) Z. Yuan, N. J. Taylor, Y. Sun, T. B. Marder, I. D. Williams, C. Lap-Tak, *J. Organomet. Chem.* **1993**, *449*, 27; f) N. S. Makarov, S. Mukhopadhyay, K. Yesudas, J.-L. Brédas, J. W. Perry, A. Pron, M. Kivala, K. Müllen, *J. Phys. Chem. A* **2012**, *116*, 3781; g) M. Lequan, R. M. Lequan, K. C. Ching, M. Barzoukas, A. Fort, H. Lahoucine, G. Bravic, D. Chasseau, J. Gaultier, *J. Mater. Chem.* **1992**, *2*, 719; h) C. Branger, M. Lequan, R. M. Lequan, M. Barzoukas, A. Fort, *J. Mater. Chem.* **1996**, *6*, 555; i) Z.-q. Liu, Q. Fang, D. Wang, G. Xue, W.-t. Yu, Z.-s. Shao, M.-h. Jiang, *Chem. Commun.* **2002**, 248, 2900; j) L. Weber, D. Eickhoff, T. B. Marder, M. A. Fox, P. J. Low, A. D. Dwyer, D. J. Tozer, S. Schwedler, A. Brockhinke, H.-G. Stammler, B. Neumann, *Chem. Eur. J.* **2012**, *18*, 1369.
- [74] Z. Zhang, R. M. Edkins, J. Nitsch, K. Fucke, A. Eichhorn, A. Steffen, Y. Wang, T. B. Marder, *Chem. Eur. J.* **2015**, *21*, 177.
- [75] J. C. Collings, S.-Y. Poon, C. Le Droumaguet, M. Charlot, C. Katan, L.-O. Pålsson, A. Beeby, J. A. Mosely, H. M. Kaiser, D. Kaufmann, W.-Y. Wong, M. Blanchard-Desce, T. B. Marder, *Chem. Eur. J.* **2009**, *15*, 198.
- [76] a) J. He, F. Guo, X. Li, W. Wu, J. Yang, J. Hua, *Chem. Eur. J.* **2012**, *18*, 7903; b) S. Hwang, J. H. Lee, C. Park, H. Lee, C. Kim, C. Park, M.-H. Lee, W. Lee, J. Park, K. Kim, N.-G. Park, C. Kim, *Chem. Commun.* **2007**, 46, 4887; c) Q. Chai, W. Li, J. Liu, Z. Geng, H. Tian, W.-H. Zhu, *Sci. Rep.* **2015**, *5*, 11330; d) H.-H. Chou, Y.-C. Chen, H.-J. Huang, T.-H. Lee, J. T. Lin, C. Tsai, K. Chen, *J. Mater. Chem.* **2012**, *22*, 10929; e) M. Liang, J. Chen, *Chem. Soc. Rev.* **2013**, *42*, 3453; f) H. Yan, P. Lee, N. R. Armstrong, A. Graham, G. A. Evmenenko, P.

- Dutta, T. J. Marks, *J. Am. Chem. Soc.* **2005**, *127*, 3172; g) C. Teng, X. Yang, C. Yang, S. Li, M. Cheng, A. Hagfeldt, L. Sun, *J. Phys. Chem. C* **2010**, *114*, 9101; h) T. Iwanaga, M. Ogawa, T. Yamauchi, S. Toyota, *J. Org. Chem.* **2016**, *81*, 4076; i) Y. Zhang, C. Zuniga, S.-J. Kim, D. Cai, S. Barlow, S. Salman, V. Coropceanu, J.-L. Brédas, B. Kippelen, S. Marder, *Chem. Mater.* **2011**, *23*, 4002.
- [77] C. Wang, J. Li, S. Cai, Z. Ning, D. Zhao, Q. Zhang, J.-H. Su, *Dyes Pigment.* **2012**, *94*, 40.
- [78] L. L. Estrella, M. P. Balanay, D. H. Kim, *J. Chem. Phys. A* **2016**, *120*, 5917.
- [79] G. Pinkus, *Ber. Dtsch. Chem. Ges.* **1892**, *25*, 2798.
- [80] B. Balaganesan, S.-W. Wen, C. H. Chen, *Tetrahedron Lett.* **2003**, *44*, 145.
- [81] K.-H. Lee, Y.-K. Kim, S.-S. Yoon, *Bull. Korean Chem. Soc.* **2012**, *33*, 3433.
- [82] Z. E. X. Dance, M. J. Ahrens, A. M. Vega, A. B. Ricks, D. W. McCamant, M. A. Ratner, M. R. Wasielewski, *J. Am. Chem. Soc.* **2008**, *130*, 830.
- [83] R. Kurata, K. Tanaka, A. Ito, *J. Org. Chem.* **2016**, *81*, 137.
- [84] S. Voth, J. W. Hollett, J. A. McCubbin, *J. Org. Chem.* **2015**, *80*, 2545.
- [85] R. Bolton, *J. Chem. Soc.* **1964**, 4637.
- [86] a) M. Bukowska, R. G. Harvey, *Polycyclic Aromat. Compd.* **1992**, *2*, 223; b) M. Foroozesh, G. Primrose, Z. Guo, L. C. Bell, W. L. Alworth, F. P. Guengerich, *Chem. Res. Toxicol.* **1997**, *10*, 91.
- [87] D. M. Connor, S. D. Allen, D. M. Collard, C. L. Liotta, D. A. Schiraldi, *J. Org. Chem.* **1999**, *64*, 6888.
- [88] E. F. Plaza-Medina, W. Rodríguez-Córdoba, J. Peon, *J. Phys. Chem. B* **2011**, *115*, 9782.
- [89] V. V. Filichev, I. V. Astakhova, A. D. Malakhov, V. A. Korshun, E. B. Pedersen, *Chem. Eur. J.* **2008**, *14*, 9968.
- [90] S. Darses, J.-P. Genet, *Chem. Rev.* **2008**, *108*, 288.
- [91] G. A. Molander, R. Figueroa, *Aldrichim. Acta* **2005**, 49.

- [92] Z. Zhang, R. M. Edkins, M. Haehnel, M. Wehner, A. Eichhorn, L. Mailänder, M. Meier, J. Brand, F. Brede, K. Müller-Buschbaum, H. Braunschweig, T. B. Marder, *Chem. Sci.* **2015**, *6*, 5922.
- [93] K. Schickedanz, T. Trageser, M. Bolte, H.-W. Lerner, M. Wagner, *Chem. Commun.* **2015**, *51*, 15808.
- [94] K. Schickedanz, J. Radtke, M. Bolte, H.-W. Lerner, M. Wagner, *J. Am. Chem. Soc.* **2017**, *139*, 2842.
- [95] E. Clar, *Polycyclic Hydrocarbons. Volume I*, Springer, Berlin, **1964**.
- [96] a) M. P. Johansson, J. Olsen, *J. Chem. Theory Comput.* **2008**, *4*, 1460; b) J. C. Collings, P. S. Smith, D. S. Yufit, A. S. Batsanov, J. A. K. Howard, T. B. Marder, *Cryst. Eng. Comm.* **2004**, *6*, 25.
- [97] L. Weber, V. Werner, M. A. Fox, T. B. Marder, S. Schwedler, A. Brockhinke, H.-G. Stammler, B. Neumann, *Dalton Trans.* **2009**, 1339.
- [98] S. J. Strickler, R. A. Berg, *J. Chem. Phys.* **1962**, *37*, 814.
- [99] A. Heckmann, C. Lambert, *Angew. Chem. Int. Ed.* **2012**, *51*, 326.
- [100] H.-J. Nie, C.-J. Yao, J.-Y. Shao, J. Yao, Y.-W. Zhong, *Chem. Eur. J.* **2014**, *20*, 17454.
- [101] P. Zanello, *Inorganic Electrochemistry: Theory, Practice and Applications*, Royal Society of Chemistry, Cambridge, **2003**.
- [102] M. Steeger, C. Lambert, *Chem. Eur. J.* **2012**, *18*, 11937.
- [103] C. Lambert, G. Nöll, *J. Am. Chem. Soc.* **1999**, *121*, 8434.
- [104] R. F. Winter, *Organometallics* **2014**, *33*, 4517.
- [105] P. Hapiot, L. D. Kispert, V. V. Konovalov, J.-M. Savéant, *J. Am. Chem. Soc.* **2001**, *123*, 6669.
- [106] B. S. Brunshwig, N. Sutin, *Coord. Chem. Rev.* **1999**, *187*, 233.
- [107] B. S. Brunshwig, C. Creutz, N. Sutin, *Chem. Soc. Rev.* **2002**, *31*, 168.
- [108] R. J. Cave, M. D. Newton, *Chem. Phys. Lett.* **1996**, *249*, 15.
- [109] R. J. Cave, M. D. Newton, *J. Chem. Phys. A* **1997**, *106*, 9213.

- [110] M. Renz, K. Theilacker, C. Lambert, M. Kaupp, *J. Am. Chem. Soc.* **2009**, *131*, 16292.
- [111] a) H. Ito, K. Ozaki, K. Itami, *Angew. Chem. Int. Ed.* **2017**, *56*, 11144; b) J. Wu, W. Pisula, K. Müllen, *Chem. Rev.* **2007**, *107*, 718.
- [112] a) H. Zollinger, *Color Chemistry: Syntheses, Properties, and Applications of Organic Dyes and Pigments*, Wiley-VCH, Weinheim, **2003**; b) W. Herbst, G. Wilker, K. Hunger, *Industrial Organic Pigments: Production, Properties, Applications*, Wiley-VCH, Weinheim, **2004**.
- [113] N. G. Connelly, W. E. Geiger, *Chem. Rev.* **1996**, *96*, 877.
- [114] a) K. Peneva, G. Mihov, F. Nolde, S. Rocha, J.-i. Hotta, K. Braeckmans, J. Hofkens, H. Uji-i, A. Herrmann, K. Müllen, *Angew. Chem. Int. Ed.* **2008**, *47*, 3372; b) X. Zhang, S. Rehm, M. M. Safont-Sempere, F. Würthner, *Nat. Chem.* **2009**, *1*, 623; c) T. Weil, T. Vosch, J. Hofkens, K. Peneva, K. Müllen, *Angew. Chem. Int. Ed.* **2010**, *49*, 9068; d) S. Bhosale, A. L. Sisson, P. Talukdar, A. Fürstenberg, N. Banerji, E. Vauthey, G. Bollot, J. Mareda, C. Röger, F. Würthner, N. Sakai, S. Matile, *Science* **2006**, *313*, 84; e) D. Görl, X. Zhang, F. Würthner, *Angew. Chem. Int. Ed.* **2012**, *51*, 6328.
- [115] C. Li, H. Wonneberger, *Adv. Mater.* **2012**, *24*, 613.
- [116] F. Würthner, *Chem. Commun.* **2004**, *14*, 1564.
- [117] a) F. Würthner, C. R. Saha-Möller, B. Fimmel, S. Ogi, P. Leowanawat, D. Schmidt, *Chem. Rev.* **2016**, *116*, 962; b) H. Langhals, *Helv. Chim. Acta* **2005**, *88*, 1309; c) L. Chen, C. Li, K. Müllen, *J. Mater. Chem. C* **2014**, *2*, 1938; d) G. Li, Y. Zhao, J. Li, J. Cao, J. Zhu, X. W. Sun, Q. Zhang, *J. Org. Chem.* **2015**, *80*, 196; e) Z. Chen, U. Baumeister, C. Tschierske, F. Würthner, *Chem. Eur. J.* **2007**, *13*, 450.
- [118] a) C. W. Struijk, A. B. Sieval, J. E. J. Dakhorst, M. van Dijk, P. Kimkes, R. B. M. Koehorst, H. Donker, T. J. Schaafsma, S. J. Picken, A. M. van de Craats, J. M. Warman, H. Zuilhof, E. J. R. Sudhölter, *J. Am. Chem. Soc.* **2000**, *122*, 11057; b) C. D. Dimitrakopoulos, P. R. L. Malenfant, *Adv. Mater.* **2002**, *14*, 99.
- [119] I. B. Berlman, *Handbook of Fluorescence Spectra of Aromatic Molecules*, Academic Press, New York, **1971**.

- [120] a) D. M. Donaldson, J. M. Robertson, J. G. White, *Proc. R. Soc. Lond. A Math. Phys. Eng. Sci.* **1953**, 220, 311; b) H. Shiba, G. Hazato, *Bull. Chem. Soc. Jpn.* **1949**, 22, 92.
- [121] Z. Chen, C. S. Wannere, C. Corminboeuf, R. Puchta, P. v. R. Schleyer, *Chem. Rev.* **2005**, 105, 3842.
- [122] A. Ranganathan, G. U. Kulkarni, *CCDC 215338. Experimental Crystal Structure Determination*, Cambridge Crystallographic Data Centre, **2004**.
- [123] M. Botoshansky, F. H. Herbstein, M. Kapon, *Helv. Chim. Acta* **2003**, 86, 1113.
- [124] A. Camerman, J. Trotter, *Proc. Royal Soc. A* **1964**, 279, 129.
- [125] T. M. Krygowski, A. Ciesielski, B. Swirska, P. Leszczynski, *Pol. J. Chem.* **1994**, 2097.
- [126] F. H. Allen, O. Kennard, D. G. Watson, L. Brammer, G. Orpen, R. Taylor, *J. Chem. Soc., Perkin Trans.* **1987**, S1-S19.
- [127] A. Ranganathan, G. U. Kulkarni, *Proc. Indian Acad. Sci. (Chem. Sci.)* **2003**, 115, 637.
- [128] J. T. Markiewicz, F. Wudl, *ACS Appl. Mater. Interfaces* **2015**, 7, 28063.
- [129] J. R. Platt, *J. Chem. Phys.* **1949**, 17, 484.
- [130] a) J. Tanaka, *Bull. Chem. Soc. Jpn.* **1963**, 36, 1237; b) Y. Tanizaki, T. Yoshinaga, H. Hiratsuka, *Spectrochim. Acta A* **1978**, 34, 205.
- [131] J. R. Lakowicz, *Principles of Fluorescence Spectroscopy*, Springer, New York, **2010**.
- [132] H. Langhals, J. Karolin, L. B.-Å. Johansson, *Faraday Trans.* **1998**, 94, 2919.
- [133] B. S. Jensen, V. D. Parker, *J. Am. Chem. Soc.* **1975**, 97, 5211.
- [134] C. E. Crespo-Hernandez, D. M. Close, L. Gorb, J. Leszczynski, *J. Phys. Chem. B* **2007**, 111, 5386.
- [135] M. Montalti, S. L. Murov, *Handbook of Photochemistry*, Taylor & Francis, Boca Raton, **2006**.
- [136] a) T. C. Werner, J. Chang, D. M. Hercules, *J. Am. Chem. Soc.* **1970**, 92, 5560; b) E. S. Pysh, N. C. Yang, *J. Am. Chem. Soc.* **1963**, 85, 2124.
- [137] J. Salbeck, H. Kunkely, H. Langhals, R. W. Saalfrank, J. Daub, *Chimia* **1989**, 43, 6.
- [138] Y. Zagranyski, L. Chen, D. Jansch, T. Gessner, C. Li, K. Müllen, *Org. Lett.* **2014**, 16, 2814.

- [139] Y. Li, Y. Hong, J. Guo, X. Huang, H. Wei, J. Zhou, T. Qiu, J. Wu, Z. Zeng, *Org. Lett.* **2017**, *19*, 5094.
- [140] a) S. Nakazono, Y. Imazaki, H. Yoo, J. Yang, T. Sasamori, N. Tokitoh, T. Cédric, H. Kageyama, D. Kim, H. Shinokubo, A. Osuka, *Chem. Eur. J.* **2009**, *15*, 7530; b) T. Teraoka, S. Hiroto, H. Shinokubo, *Org. Lett.* **2011**, *13*, 2532.
- [141] S. Ikeda, N. Aratani, A. Osuka, *Chem. Commun.* **2012**, *48*, 4317.
- [142] L. D. Tran, J. Ma, A. G. Wong-Foy, A. J. Matzger, *Chem. Eur. J.* **2016**, *22*, 5509.
- [143] H. Banda, D. Damien, K. Nagarajan, A. Raj, M. Hariharan, M. M. Shaijumon, *Adv. Energy Mater.* **2017**, *7*, 1701316.
- [144] P. J. Low, M. A. J. Paterson, H. Puschmann, A. E. Goeta, J. A. K. Howard, C. Lambert, J. C. Cherryman, D. R. Tackley, S. Leeming, B. Brown, *Chem. Eur. J.* **2004**, *10*, 83.
- [145] V. Bulvic, G. Gu, P. E. Burrows, S. R. Forrest, M. E. Thompson, *Nature* **1996**, *380*, 29.
- [146] N. Tamoto, C. Adachi, K. Nagai, *Chem. Mater.* **1997**, *9*, 1077.
- [147] E. Bellmann, S. E. Shaheen, S. Thayumanavan, S. Barlow, R. H. Grubbs, S. R. Marder, B. Kippelen, N. Peyghambarian, *Chem. Mater.* **1998**, *10*, 1668.
- [148] M. C. Harris, S. L. Buchwald, *J. Org. Chem.* **2000**, *65*, 5327.
- [149] U. Mitschke, P. Bäuerle, *J. Mater. Chem.* **2000**, *10*, 1471.
- [150] P. M. Borsenberger, D. S. Weiss, *Organic Photoreceptors for Xerography*, Marcel Dekker, New York, **1998**.
- [151] M. Stolka, J. F. Yanus, D. M. Pai, *J. Phys. Chem.* **1984**, *88*, 4707.
- [152] P. M. Borsenberger, D. S. Weiss, *Organic Photoreceptors for Imaging Systems*, Dekker, New York, **1993**.
- [153] M. Thelakkat, R. Fink, F. Haubner, H.-W. Schmidt, *Macromol. Symp.* **1998**, *125*, 157.
- [154] M. Thelakkat, *Macromol. Mater. Eng.* **2002**, *287*, 442.
- [155] C. W. Tang, *Appl. Phys. Lett.* **1986**, *48*, 183.
- [156] C. W. Tang, S. A. VanSlyke, *Appl. Phys. Lett.* **1987**, *51*, 913.
- [157] E. S. Kolb, R. A. Gaudiana, P. G. Mehta, *Macromolecules* **1996**, *29*, 2359.

- [158] H. Fujikawa, S. Tokito, Y. Taga, *Synth. Met.* **1997**, *91*, 161.
- [159] C. Giebeler, H. Antoniadis, D. D. C. Bradley, Y. Shirota, *Appl. Phys. Lett.* **1998**, *72*, 2448.
- [160] M. Redecker, D. D. C. Bradley, M. Inbasekaran, W. W. Wu, E. P. Woo, *Adv. Mater.* **1999**, *11*, 241.
- [161] T. Braig, D. C. Müller, M. Groß, K. Meerholz, O. Nuyken, *Macromol. Rapid Commun.* **2000**, *21*, 583.
- [162] W. E. Moerner, S. M. Silence, *Chem. Rev.* **1994**, *94*, 127.
- [163] S. Dapperheld, E. Steckhan, K.-H. G. Brinkhaus, T. Esch, *Chem. Ber.* **1991**, 2557.
- [164] S. Amthor, B. Noller, C. Lambert, *Chem. Phys.* **2005**, *316*, 141.
- [165] a) T. Noda, Y. Shirota, *J. Am. Chem. Soc.* **1998**, *120*, 9714; b) Y. S. M. Kinoshita, *Chem. Lett.* **2001**, *30*, 614.
- [166] a) S. Y. A. Wakamiya, *Bull. Chem. Soc. Jpn.* **2015**, *88*, 1357; b) A. W. S. Yamaguchi, *Pure Appl. Chem.* **2006**, *78*, 1413; c) S. Griesbeck, M. Ferger, C. Czernetzi, C. Wang, R. Bertermann, A. Friedrich, M. Haehnel, D. Sieh, M. Taki, S. Yamaguchi, T. B. Marder, *Chem. Eur. J.* **2019**; d) S. Griesbeck, E. Michail, C. Wang, H. Ogasawara, S. Lorenzen, L. Gerstner, T. Zang, J. Nitsch, Y. Sato, R. Bertermann, M. Taki, C. Lambert, S. Yamaguchi, T. B. Marder, *Chem. Sci.* **2019**, *41*, 2927.
- [167] S. Griesbeck, Z. Zhang, M. Gutmann, T. Lühmann, R. M. Edkins, G. Clermont, A. N. Lazar, M. Haehnel, K. Edkins, A. Eichhorn, M. Blanchard-Desce, L. Meinel, T. B. Marder, *Chem. Eur. J.* **2016**, *22*, 14701.
- [168] a) S. Yamaguchi, T. Shirasaka, K. Tamao, *Org. Lett.* **2000**, *2*, 4129; b) N. Matsumi, K. Naka, Y. Chujo, *J. Am. Chem. Soc.* **1998**, *120*, 5112; c) N. Matsumi, K. Naka, Y. Chujo, *J. Am. Chem. Soc.* **1998**, *120*, 10776.
- [169] a) C. D. Entwistle, T. B. Marder, *Angew. Chem. Int. Ed.* **2002**, *41*, 2927; b) H. C. Brown, V. H. Dodson, *J. Am. Chem. Soc.* **1957**, *79*, 2302.
- [170] Z. Zhang, R. M. Edkins, M. Haehnel, M. Wehner, A. Eichhorn, L. Mailänder, M. Meier, J. Brand, F. Brede, K. Müller-Buschbaum, H. Braunschweig, T. B. Marder, *Chem. Sci.* **2015**, *6*, 5922.

- [171] Z. Zhou, A. Wakamiya, T. Kushida, S. Yamaguchi, *J. Am. Chem. Soc.* **2012**, *134*, 4529.
- [172] G. A. Molander, R. Figueroa, *Aldrichimica Acta* **2005**, *38*, 49.
- [173] a) G. Berionni, B. Maji, P. Knochel, H. Mayr, *Chem. Sci.* **2012**, *3*, 878; b) A. J. J. Lennox, *Organotrifluoroborate Preparation, Coupling and Hydrolysis*, Springer, Heidelberg, **2013**; c) S. E. Denmark (Ed.) *Cross-coupling Reactions of Organotrifluoroborate Salts. In: Organic Reactions*; Vol. 79, John Wiley & Sons, Inc, Hoboken, **2013**.
- [174] A. D. Ainley, F. Challenger, *J. Chem. Soc.* **1930**, 2171.
- [175] A. L. S. Thompson, G. W. Kabalka, M. R. Akula, J. W. Huffman, *Synthesis* **2005**, *36*, 547.
- [176] C. Näther, H. Bock, Z. Havlas, T. Hauck, *Organometallics* **1998**, *17*, 4707.
- [177] M. Bolte, *CCDC 1546182. Experimental Crystal Structure Determination*, Cambridge Crystallographic Data Centre, **2017**.
- [178] F. Würthner, *Pure Appl. Chem.* **2006**, *78*, 2341.
- [179] a) M. A. Spackman, P. G. Byrom, *Chem. Phys. Lett.* **1997**, *267*, 215; b) J. J. McKinnon, A. S. Mitchell, M. A. Spackman, *Chem. Eur. J.* **1998**, *4*, 2136; c) J. J. McKinnon, M. A. Spackman, A. S. Mitchell, *Acta Crystallogr.* **2004**, *B60*, 627; d) M. A. Spackman, D. Jayatilaka, *CrystEngComm* **2009**, *11*, 19.
- [180] a) M. A. Spackman, J. J. McKinnon, *CrystEngComm* **2002**, *4*, 378; b) A. Parkin, G. Barr, W. Dong, C. J. Gilmore, D. Jayatilaka, J. J. McKinnon, M. A. Spackman, C. C. Wilson, *CrystEngComm* **2007**, *9*, 648; c) J. J. McKinnon, D. Jayatilaka, M. A. Spackman, *Chem. Commun.* **2007**, 267, 3814.
- [181] C. Huang, S. Barlow, S. R. Marder, *J. Org. Chem.* **2011**, *76*, 2386.
- [182] We note, that Zeng and co-workers<sup>[139]</sup> do not list their extinction coefficients. Therefore, we estimated them from their Figure 1.
- [183] É. Torres, M. N. Berberan-Santos, M. J. Brites, *Dyes Pigment.* **2015**, *112*, 298.
- [184] We note that we also measured the emission of (Br)<sub>4</sub>-Per in CH<sub>2</sub>Cl<sub>2</sub> for full comparison with the brominated derivative from Zheng and co-workers as they only give photophysical results in CH<sub>2</sub>Cl<sub>2</sub> (see Appendix, Figure 8-112).

- [185] a) M.-J. Lin, Á. J. Jiménez, C. Burschka, F. Würthner, *Chem. Commun.* **2012**, 48, 12050; b) F. Schlosser, V. Stepanenko, F. Würthner, *Chem. Commun.* **2010**, 46, 8350.
- [186] M. Zander, H. Dreeskamp, E. Koch, *Z. Naturforsch. A* **1974**, 29.
- [187] H. Dreeskamp, E. Koch, M. Zander, *Chem. Phys. Lett.* **1975**, 31, 251.
- [188] K. Nagarajan, A. R. Mallia, V. S. Reddy, M. Hariharan, *J. Phys. Chem. C* **2016**, 120, 8443.
- [189] S. K. M. Nalluri, J. Zhou, T. Cheng, Z. Liu, M. T. Nguyen, T. Chen, H. A. Patel, M. D. Krzyaniak, W. A. Goddard, M. R. Wasielewski, J. F. Stoddart, *J. Am. Chem. Soc.* **2019**, 141, 1290.
- [190] H. Dreeskamp, A. Läufer, M. Zander, *Z. Naturforsch. A* **1983**, 38.
- [191] J. Zhao, W. Wu, J. Sun, S. Guo, *Chem. Soc. Rev.* **2013**, 42, 5323.
- [192] H. Xiang, J. Cheng, X. Ma, X. Zhou, J. J. Chruma, *Chem. Soc. Rev.* **2013**, 42, 6128.
- [193] A. Gut, Ł. Łapok, D. Drelinkiewicz, T. Pędziński, B. Marciniak, M. Nowakowska, *Chem. Asian J.* **2018**, 13, 55.
- [194] Q. Zhao, F. Li, C. Huang, *Chem. Soc. Rev.* **2010**, 39, 3007.
- [195] Y. Feng, J. Cheng, L. Zhou, X. Zhou, H. Xiang, *Analyst* **2012**, 137, 4885.
- [196] J.-P. Fouassier, F. Morlet-Savary, J. Lalevée, X. Allonas, C. Ley, *Materials* **2010**, 3, 5130.
- [197] M. L. Marin, L. Santos-Juanes, A. Arques, A. M. Amat, M. A. Miranda, *Chem. Rev.* **2012**, 112, 1710.
- [198] N. Noto, T. Koike, M. Akita, *Chem. Sci.* **2017**, 8, 6375.
- [199] N. Noto, Y. Tanaka, T. Koike, M. Akita, *ACS Catal.* **2018**, 8, 9408.
- [200] I. Ghosh, T. Ghosh, J. I. Bardagi, B. König, *Science* **2014**, 346, 725.
- [201] a) T. N. Singh-Rachford, F. N. Castellano, *Coord. Chem. Rev.* **2010**, 254, 2560; b) J. Zhao, S. Ji, H. Guo, *RSC Adv.* **2011**, 1, 937.
- [202] a) M. R. Detty, S. L. Gibson, S. J. Wagner, *J. Med. Chem.* **2004**, 47, 3897; b) L. Sobotta, P. Skupin-Mrugalska, J. Mielcarek, T. Goslinski, J. Balzarini, *Mini-Rev. Med. Chem.* **2015**, 15, 503.
- [203] W. E. Ford, P. V. Kamat, *J. Phys. Chem.* **1987**, 91, 6373.

- [204] A. J. Tilley, R. D. Pensack, T. S. Lee, B. Djukic, G. D. Scholes, D. S. Seferos, *J. Phys. Chem. C* **2014**, *118*, 9996.
- [205] M. T. Vagnini, A. L. Smeigh, J. D. Blakemore, S. W. Eaton, N. D. Schley, F. D'Souza, R. H. Crabtree, G. W. Brudvig, D. T. Co, M. R. Wasielewski, *Proc. Natl. Acad. Sci. USA* **2012**, *109*, 15651.
- [206] M. Schulze, A. Steffen, F. Würthner, *Angew. Chem. Int. Ed.* **2015**, *127*, 1590.
- [207] A. A. Rachford, S. Goeb, F. N. Castellano, *J. Am. Chem. Soc.* **2008**, *130*, 2766.
- [208] H. Weissman, E. Shirman, T. Ben-Moshe, R. Cohen, G. Leitus, L. J. W. Shimon, B. Rybtchinski, *Inorg. Chem.* **2007**, *46*, 4790.
- [209] a) B. Ventura, H. Langhals, B. Böck, L. Flamigni, *Chem. Commun.* **2012**, *48*, 4226; b) L. Flamigni, A. Zanelli, H. Langhals, B. Böck, *J. Phys. Chem. A* **2012**, *116*, 1503.
- [210] E. Oliveros, S. H. Bossmann, S. Nonell, C. Martí, G. Heit, G. Tröscher, A. Neuner, C. Martínez, A. M. Braun, *New J. Chem.* **1999**, *23*, 85.
- [211] C. Schweitzer, R. Schmidt, *Chem. Rev.* **2003**, *103*, 1685.
- [212] A. A. Abdel-Shafi, F. Wilkinson, *J. Phys. Chem. A* **2000**, *104*, 5747.
- [213] A. J. McLean, D. J. McGarvey, T. G. Truscott, *J. Chem. Soc. Faraday Trans.* **1990**, *86*, 3075.
- [214] J. D. Harris, M. J. Moran, I. Aprahamian, *Proc. Natl. Acad. Sci. USA* **2018**, *115*, 9414.
- [215] A. B. Buades, V. Sanchez Arderiu, D. Olid-Britos, C. Viñas, R. Sillanpää, M. Haukka, X. Fontrodona, M. Paradinas, C. Ocal, F. Teixidor, *J. Am. Chem. Soc.* **2018**, *140*, 2957.
- [216] M. Frasconi, I. R. Fernando, Y. Wu, Z. Liu, W.-G. Liu, S. M. Dyar, G. Barin, M. R. Wasielewski, W. A. Goddard, J. F. Stoddart, *J. Am. Chem. Soc.* **2015**, *137*, 11057.
- [217] J. Kübel, R. Schroot, M. Wächtler, U. S. Schubert, B. Dietzek, M. Jäger, *J. Phys. Chem. C* **2015**, *119*, 4742.
- [218] Y.-M. Tian, X.-N. Guo, M. W. Kuntze-Fechner, I. Krummenacher, H. Braunschweig, U. Radius, A. Steffen, T. B. Marder, *J. Am. Chem. Soc.* **2018**, *140*, 17612-17623.
- [219] a) L. Ramaley, M. S. Krause, *Anal. Chem.* **1969**, 1362; b) G. C. Barker, I. L. Jenkins, *Analyst* **1952**, *77*, 685.

- [220] I. Raabe, K. Wagner, K. Guttsche, M. Wang, M. Grätzel, G. Santiso-Quiñones, I. Krossing, *Chem. Eur. J.* **2009**, *15*, 1966.
- [221] F. Barrière, W. E. Geiger, *J. Am. Chem. Soc.* **2006**, *128*, 3980.
- [222] a) Y. Fan, K. Ziabrev, S. Zhang, B. Lin, S. Barlow, S. R. Marder, *ACS Omega* **2017**, *2*, 377; b) W. Jiang, C. Xiao, L. Hao, Z. Wang, H. Ceymann, C. Lambert, S. Di Motta, F. Negri, *Chem. Eur. J.* **2012**, *18*, 6764; c) W. Jiang, L. Ye, X. Li, C. Xiao, F. Tan, W. Zhao, J. Hou, Z. Wang, *Chem. Commun.* **2014**, *50*, 1024; d) H. Horinouchi, H. Sakai, Y. Araki, T. Sakanoue, T. Takenobu, T. Wada, N. V. Tkachenko, T. Hasobe, *Chem. Eur. J.* **2016**, *22*, 9631.
- [223] L. Echegoyen, L. E. Echegoyen, *Acc. Chem. Res.* **1998**, *31*, 593.
- [224] a) M. Takase, V. Enkelmann, D. Sebastiani, M. Baumgarten, K. Müllen, *Angew. Chem. Int. Ed.* **2007**, *46*, 5524; b) K. Oki, M. Takase, S. Mori, A. Shiotari, Y. Sugimoto, K. Ohara, T. Okujima, H. Uno, *J. Am. Chem. Soc.* **2018**, *140*, 10430.
- [225] Y. Shibano, T. Umeyama, Y. Matano, N. V. Tkachenko, H. Lemmetyinen, H. Imahori, *Org. Lett.* **2006**, *8*, 4425.
- [226] M. J. G. Peach, P. Benfield, T. Helgaker, D. J. Tozer, *J. Chem. Phys.* **2008**, *128*, 44118.
- [227] J. Duhamel, *Langmuir* **2012**, *28*, 6527.
- [228] a) D. Kim, R. Amos, M. Gauthier, J. Duhamel, *Langmuir* **2018**, *34*, 8611; b) F. M. Winnik, *Chem. Rev.* **1993**, *93*, 587.
- [229] a) N. Balsukuri, N. J. Boruah, P. E. Kesavan, I. Gupta, *New J. Chem.* **2018**, *42*, 5875; b) L. Yuan, W. Lin, S. Zhao, W. Gao, B. Chen, L. He, S. Zhu, *J. Am. Chem. Soc.* **2012**, *134*, 13510; c) L. Yuan, W. Lin, K. Zheng, L. He, W. Huang, *Chem. Soc. Rev.* **2013**, *42*, 622.
- [230] R. Liu, H. Ran, Z. Zhao, X. Yang, J. Zhang, L. Chen, H. Sun, J.-Y. Hu, *ACS Omega* **2018**, *3*, 5866.
- [231] S. N. Keller, A. D. Bromby, T. C. Sutherland, *Eur. J. Org. Chem.* **2017**, *2017*, 3980.
- [232] a) U. H. F. Bunz, *Acc. Chem. Res.* **2015**, *48*, 1676; b) U. H. F. Bunz, J. U. Engelhart, B. D. Lindner, M. Schaffroth, *Angew. Chem. Int. Ed.* **2013**, *52*, 3810; c) A. H. Endres, M. Schaffroth, F. Paulus, H. Reiss, H. Wadepohl, F. Rominger, R. Krämer, U. H. F. Bunz, *J. Am. Chem. Soc.* **2016**, *138*, 1792; d) M. Ganschow, S. Koser, S. Hahn, F. Rominger, J.

- Freudenberg, U. H. F. Bunz, *Chem. Eur. J.* **2017**, *23*, 4415; e) P.-Y. Gu, Z. Wang, Q. Zhang, *J. Mater. Chem. B* **2016**, *4*, 7060; f) P.-Y. Gu, Z. Wang, G. Liu, H. Yao, Z. Wang, Y. Li, J. Zhu, S. Li, Q. Zhang, *Chem. Mater.* **2017**, *29*, 4172; g) B.-L. Hu, C. An, M. Wagner, G. Ivanova, A. Ivanova, M. Baumgarten, *J. Am. Chem. Soc.* **2019**, *141*, 5130; h) L. Ji, A. Friedrich, I. Krummenacher, A. Eichhorn, H. Braunschweig, M. Moos, S. Hahn, F. L. Geyer, O. Tverskoy, J. Han, C. Lambert, A. Dreuw, T. B. Marder, U. H. F. Bunz, *J. Am. Chem. Soc.* **2017**, *139*, 15968; i) V. Lami, D. Leibold, P. Fassel, Y. J. Hofstetter, D. Becker-Koch, P. Biegger, F. Paulus, P. E. Hopkinson, M. Adams, U. H. F. Bunz, S. Huettner, I. Howard, A. A. Bakulin, Y. Vaynzof, *Photovoltaic Devices Solar RRL* **2017**, *1*, 1700053; j) D. Leibold, V. Lami, Y. J. Hofstetter, D. Becker - Koch, A. Weu, P. Biegger, F. Paulus, U. H.F. Bunz, P. E. Hopkinson, A. A. Bakulin, Y. Vaynzof, *Org. Electron.* **2018**, *57*, 285; k) Q. Miao, *Adv. Mater.* **2014**, *26*, 5541; l) X. Xu, Y. Yao, B. Shan, X. Gu, D. Liu, J. Liu, J. Xu, N. Zhao, W. Hu, Q. Miao, *Adv. Mater.* **2016**, *28*, 5276; m) Y.-D. Zhang, Y. Wu, Y. Xu, Q. Wang, K. Liu, J.-W. Chen, J.-J. Cao, C. Zhang, H. Fu, H.-L. Zhang, *J. Am. Chem. Soc.* **2016**, *138*, 6739.
- [233] A. Mateo-Alonso, *Chem. Soc. Rev.* **2014**, *43*, 6311.
- [234] a) C.-Z. Wang, X. Feng, M. R. J. Elsegood, T. G. Warwick, S. J. Teat, C. Redshaw, Y.-S. Bi, T. Yamato, *Asian J. Org. Chem.* **2019**, *8*, 155; b) Z.-H. Wu, W.-J. Sun, H.-H. Tian, Z.-F. Yu, R.-X. Guo, X. Shao, H.-L. Zhang, *Adv. Electron. Mater.* **2019**, *5*, 1800598.
- [235] R. García, M. Melle-Franco, A. Mateo-Alonso, *Chem. Commun.* **2015**, *51*, 8037.
- [236] P. K. Sahoo, C. Giri, T. S. Haldar, R. Puttreddy, K. Rissanen, P. Mal, *Eur. J. Org. Chem.* **2016**, *2016*, 1283.
- [237] J. Hu, D. Zhang, F. W. Harris, *J. Org. Chem.* **2005**, *70*, 707.
- [238] F. G. Oberender, J. A. Dixon, *J. Org. Chem.* **1959**, *24*, 1226.
- [239] a) E. Nowicka, T. J. Clarke, M. Sankar, R. L. Jenkins, D. W. Knight, S. Golunski, G. J. Hutchings, D. J. Willock, M. Francisco, S. H. Taylor, *Chem. Eur. J.* **2018**, *24*, 655; b) E. Nowicka, N. W. Hickey, M. Sankar, R. L. Jenkins, D. W. Knight, D. J. Willock, G. J. Hutchings, M. Francisco, S. H. Taylor, *Chem. Eur. J.* **2018**, *24*, 12359.
- [240] J. C. Walsh, K.-L. M. Williams, D. Lungerich, G. J. Bodwell, *Eur. J. Org. Chem.* **2016**, *2016*, 5933.

- [241] S. More, R. Bhosale, S. Choudhary, A. Mateo-Alonso, *Org. Lett.* **2012**, *14*, 4170.
- [242] S.-i. Kawano, M. Baumgarten, D. Chercka, V. Enkelmann, K. Müllen, *Chem. Commun.* **2013**, *49*, 5058.
- [243] J. Ryu, K. Shin, S. H. Park, J. Y. Kim, S. Chang, *Angew. Chem. Int. Ed.* **2012**, *51*, 9904.
- [244] S. More, R. Bhosale, A. Mateo-Alonso, *Chem. Eur. J.* **2014**, *20*, 10626.
- [245] E. Clar (Ed.) *Polycyclic Hydrocarbons*, Springer, Berlin, **1964**.
- [246] G. R. Desiraju, A. Gavezzotti, *J. Chem. Soc., Chem. Commun.* **1989**, 621.
- [247] We note that dione **3-6** does not have a pyrene core, however for simplification reasons we kept the numbering as they are in pyrene derivatives.
- [248] a) R. Englman, J. Jortner, *Mol. Phys.* **1970**, *18*, 145; b) K. F. Freed, J. Jortner, *J. Chem. Phys.* **1970**, *52*, 6272; c) M. Bixon, J. Jortner, J. Cortes, H. Heitele, M. E. Michel-Beyerle, *J. Phys. Chem.* **1994**, *98*, 7289.
- [249] L. Ji, I. Krummenacher, A. Friedrich, A. Lorbach, M. Haehnel, K. Edkins, H. Braunschweig, T. B. Marder, *J. Org. Chem.* **2018**, *83*, 3599.
- [250] We note that we assumed the extinction coefficients from the given absorption spectra (Figure 1) as they are not given.
- [251] a) F. Kakiuchi, S. Murai (Eds.) *Top. Organomet. Chem.*, Vol. 3, Springer, Berlin, **1999**; b) P. H. Dixneuf, H. Doucet (Eds.) *Top. Organomet. Chem.*, Vol. 56, Springer, Cham, **2016**.
- [252] J. A. Labinger, J. E. Bercaw, *Nature* **2002**, *417*, 507.
- [253] a) E. Fernández, A. Whiting (Eds.) *Top. Organomet. Chem.*, Springer, Cham, **2015**; b) A. Pelter, K. Smith, H. C. Brown, *Borane Reagents*, Academic Press, London, **1988**; c) D. S. Matteson, *Stereodirected Synthesis with Organoboranes*, Springer, Berlin, **1995**.
- [254] a) A. Suzuki, in: F. Diederich, P.J. Stang (Eds.) (Ed.) *Metal-catalyzed cross-coupling reactions*, Wiley-VCH, Weinheim, **1999**; b) N. Miyaura in *Advances in Metal-Organic Chemistry*, Vol. 6 (Ed.: N. Miyaura, in: L.S. Liebeskind (Ed.)), JAI Press, Greenwich, Conn., **1998**, pp. 187–243; c) N. Miyaura, A. Suzuki, *Chem. Rev.* **1995**, *95*, 2457.
- [255] a) A. H. Soloway, W. Tjarks, B. A. Barnum, F.-G. Rong, R. F. Barth, I. M. Codogni, J. G. Wilson, *Chem. Rev.* **1998**, *98*, 1515; b) A. Michaelis, P. Becker, *Ber. Dtsch. Chem. Ges.*

- 1882**, *15*, 180; c) P. C. Trippier, C. McGuigan, *Med. Chem. Commun.* **2010**, *1*, 183; d) B. C. Das, P. Thapa, R. Karki, C. Schinke, S. Das, S. Kambhampati, S. K. Banerjee, P. van Veldhuizen, A. Verma, L. M. Weiss, T. Evans, *Future Med. Chem.* **2013**, *5*, 653.
- [256] T. Ishiyama, M. Murata, N. Miyaura, *J. Org. Chem.* **1995**, *60*, 7508.
- [257] a) K. Huang, D.-G. Yu, S.-F. Zheng, Z.-H. Wu, Z.-J. Shi, *Chem. Eur. J.* **2011**, *17*, 786; b) M. Murata, T. Sambommatsu, T. Oda, S. Watanabe, Y. Masuda, *Heterocycles* **2010**, *80*, 213; c) P. Leowanawat, A.-M. Resmerita, C. Moldoveanu, C. Liu, N. Zhang, D. A. Wilson, L. M. Hoang, B. M. Rosen, V. Percec, *J. Org. Chem.* **2010**, *75*, 7822; d) C. Moldoveanu, D. A. Wilson, C. J. Wilson, P. Leowanawat, A.-M. Resmerita, C. Liu, B. M. Rosen, V. Percec, *J. Org. Chem.* **2010**, *75*, 5438; e) C. Moldoveanu, D. A. Wilson, C. J. Wilson, P. Corcoran, B. M. Rosen, V. Percec, *Org. Lett.* **2009**, *11*, 4974; f) D. A. Wilson, C. J. Wilson, C. Moldoveanu, A.-M. Resmerita, P. Corcoran, L. M. Hoang, B. M. Rosen, V. Percec, *J. Am. Chem. Soc.* **2010**, *132*, 1800; g) T. Yamamoto, T. Morita, J. Takagi, T. Yamakawa, *Org. Lett.* **2011**, *13*, 5766.
- [258] a) Y. Nagashima, R. Takita, K. Yoshida, K. Hirano, M. Uchiyama, *J. Am. Chem. Soc.* **2013**, *135*, 18730; b) S. K. Bose, T. B. Marder, *Org. Lett.* **2014**, *16*, 4562.
- [259] a) C. Kleeberg, L. Dang, Z. Lin, T. B. Marder, *Angew. Chem. Int. Ed.* **2009**, *48*, 5350; b) W. Zhu, D. Ma, *Org. Lett.* **2006**, *8*, 261.
- [260] P. K. Verma, S. Mandal, K. Geetharani, *ACS Catal.* **2018**, *8*, 4049.
- [261] W. K. Chow, O. Y. Yuen, P. Y. Choy, C. M. So, C. P. Lau, W. T. Wong, F. Y. Kwong, *RSC Adv.* **2013**, *3*, 12518.
- [262] T. Ishiyama, J. Takagi, K. Ishida, N. Miyaura, N. R. Anastasi, J. F. Hartwig, *J. Am. Chem. Soc.* **2002**, *124*, 390.
- [263] D. W. Robbins, J. F. Hartwig, *Angew. Chem. Int. Ed.* **2013**, *125*, 967.
- [264] R. E. Maleczka, Jr., F. Shi, D. Holmes, M. R. Smith III, *J. Am. Chem. Soc.* **2003**, *125*, 7792.
- [265] H. H. Hodgson, J. S. Wignall, *J. Chem. Soc.* **1926**, 2077.
- [266] P. Nguyen, H. P. Blom, S. A. Westcott, N. J. Taylor, T. B. Marder, *J. Am. Chem. Soc.* **1993**, *115*, 9329.
- [267] C. N. Iverson, M. R. Smith III, *J. Am. Chem. Soc.* **1999**, *121*, 7696.

- [268] J.-Y. Cho, C. N. Iverson, M. R. Smith III, *J. Am. Chem. Soc.* **2000**, *122*, 12868.
- [269] M. K. Tse, J.-Y. Cho, M. R. Smith III, *Org. Lett.* **2001**, *3*, 2831.
- [270] a) H. Chen, S. Schlecht, T. C. Semple, J. F. Hartwig, *Science* **2000**, *287*, 1995; b) S. Shimada, A. S. Batsanov, J. A. K. Howard, T. B. Marder, *Angew. Chem. Int. Ed.* **2001**, *40*, 2168.
- [271] K. Kawamura, J. F. Hartwig, *J. Am. Chem. Soc.* **2001**, *123*, 8422.
- [272] J.-Y. Cho, M. K. Tse, D. Holmes, R. E. Maleczka, Jr., M. R. Smith III, *Science* **2002**, *295*, 305.
- [273] H. Tajuddin, P. Harrisson, B. Bitterlich, J. C. Collings, N. Sim, A. S. Batsanov, M. S. Cheung, S. Kawamorita, A. C. Maxwell, L. Shukla, J. Morris, Z. Lin, T. B. Marder, P. G. Steel, *Chem. Sci.* **2012**, *3*, 3505.
- [274] T. Ishiyama, J. Takagi, J. F. Hartwig, N. Miyaura, *Angew. Chem. Int. Ed.* **2002**, *41*, 3056.
- [275] T. M. Boller, J. M. Murphy, M. Hapke, T. Ishiyama, N. Miyaura, J. F. Hartwig, *J. Am. Chem. Soc.* **2005**, *127*, 14263.
- [276] H. Tamura, H. Yamazaki, H. Sato, S. Sakaki, *J. Am. Chem. Soc.* **2003**, *125*, 16114.
- [277] N. Miyaura, *Bull. Chem. Soc. Jpn.* **2008**, *81*, 1535.
- [278] I. A. I. Mkhaliid, D. N. Coventry, D. Albesa-Jove, A. S. Batsanov, J. A. K. Howard, R. N. Perutz, T. B. Marder, *Angew. Chem. Int. Ed.* **2006**, *45*, 489.
- [279] A. Ros, R. Fernández, J. M. Lassaletta, *Chem. Soc. Rev.* **2014**, *43*, 3229.
- [280] S. Kawamorita, H. Ohmiya, K. Hara, A. Fukuoka, M. Sawamura, *J. Am. Chem. Soc.* **2009**, *131*, 5058.
- [281] A. Ochida, K. Hara, H. Ito, M. Sawamura, *Org. Lett.* **2003**, *5*, 2671.
- [282] a) T. Ishiyama, H. Isou, T. Kikuchi, N. Miyaura, *Chem. Commun.* **2010**, *46*, 159; b) K. Yamazaki, S. Kawamorita, H. Ohmiya, M. Sawamura, *Org. Lett.* **2010**, *12*, 3978.
- [283] A. Ochida, S. Ito, T. Miyahara, H. Ito, M. Sawamura, *Chem. Lett.* **2006**, *35*, 294.
- [284] M. R. Smith III, R. Bisht, C. Haldar, G. Pandey, J. E. Dannatt, B. Ghaffari, R. E. Maleczka, B. Chattopadhyay, *ACS Catal.* **2018**, *8*, 6216.

- [285] T. A. Boebel, J. F. Hartwig, *J. Am. Chem. Soc.* **2008**, *130*, 7534.
- [286] H. Taube, F. A. Posey, *J. Am. Chem. Soc.* **1953**, *75*, 1463.
- [287] a) H. L. Li, Y. Kuninobu, M. Kanai, *Angew. Chem. Int. Ed.* **2017**, *56*, 1495; b) H.-L. Li, M. Kanai, Y. Kuninobu, *Org. Lett.* **2017**, *19*, 5944.
- [288] a) H. J. Davis, G. R. Genov, R. J. Phipps, *Angew. Chem. Int. Ed.* **2017**, *56*, 13351; b) P. C. Roosen, V. A. Kallepalli, B. Chattopadhyay, D. A. Singleton, R. E. Maleczka, M. R. Smith III, *J. Am. Chem. Soc.* **2012**, *134*, 11350; c) S. M. Preshlock, D. L. Plattner, P. E. Maligres, S. W. Krska, R. E. Maleczka, M. R. Smith III, *Angew. Chem. Int. Ed.* **2013**, *52*, 12915.
- [289] B. Chattopadhyay, J. E. Dannatt, I. L. Andujar-De Sanctis, K. A. Gore, R. E. Maleczka, D. A. Singleton, M. R. Smith III, *J. Am. Chem. Soc.* **2017**, *139*, 7864.
- [290] a) T. Ishiyama, Y. Nobuta, J. F. Hartwig, N. Miyaura, *Chem. Commun.* **2003**, 2924; b) T. Ishiyama, J. Takagi, Y. Yonekawa, J. F. Hartwig, N. Miyaura, *Adv. Synth. Catal.* **2003**, *345*, 1103.
- [291] J. Takagi, K. Sato, J. F. Hartwig, T. Ishiyama, N. Miyaura, *Tetrahedron Lett.* **2002**, *43*, 5649.
- [292] S. A. Sadler, H. Tajuddin, I. A. I. Mkhaliid, A. S. Batsanov, D. Albesa-Jove, M. S. Cheung, A. C. Maxwell, L. Shukla, B. Roberts, D. C. Blakemore, Z. Lin, T. B. Marder, P. G. Steel, *Org. Biomol. Chem.* **2014**, *12*, 7318.
- [293] P. Harrisson, J. Morris, T. B. Marder, P. G. Steel, *Org. Lett.* **2009**, *11*, 3586.
- [294] a) G. A. Chotana, M. A. Rak, M. R. Smith III, *J. Am. Chem. Soc.* **2005**, *127*, 10539; b) B. A. Vanchura, S. M. Preshlock, P. C. Roosen, V. A. Kallepalli, R. J. Staples, R. E. Maleczka, Jr., D. A. Singleton, M. R. Smith III, *Chem. Commun.* **2010**, *46*, 7724.
- [295] G. Barbieri, R. Benassi, P. Lazzeretti, L. Schenetti, F. Taddei, *Org. Magn. Reson.* **1975**, *7*, 451.
- [296] W. F. Lo, H. M. Kaiser, A. Spannenberg, M. Beller, M. K. Tse, *Tetrahedron Lett.* **2007**, *48*, 371.
- [297] S. Kawamorita, H. Ohmiya, M. Sawamura, *J. Org. Chem.* **2010**, *75*, 3855.

- [298] S. Konishi, S. Kawamorita, T. Iwai, P. G. Steel, T. B. Marder, M. Sawamura, *Chem. Asian J.* **2014**, *9*, 434.
- [299] Y. Zhang, J. Gao, W. Li, H. Lee, B. Z. Lu, C. H. Senanayake, *J. Org. Chem.* **2011**, *76*, 6394.
- [300] M. I. Andersson, A. P. MacGowan, *J. Antimicrob. Chemother.* **2003**, *51 Suppl 1*, 1.
- [301] S. Heeb, M. P. Fletcher, S. R. Chhabra, S. P. Diggle, P. Williams, M. Cámara, *FEMS Microbiol. Rev.* **2011**, *35*, 247.
- [302] C. Torres-Fuentes, E. Pastor-Cavada, R. Cano, D. Kandil, R. Shanahan, R. Juan, H. Shaban, G. P. McGlacken, H. Schellekens, *Int. J. Mol. Sci.* **2018**, *19*.
- [303] B. Suh, B. Lorber, *Med. Clin. North Am.* **1995**, *79*, 869.
- [304] a) G. Arar, T. Gözler, M. Bashir, M. Shamma, *J. Nat. Prod.* **1985**, *48*, 642; b) J. P. Michael, *Nat. Prod. Rep.* **2008**, *25*, 166.
- [305] G. Y. Leshner, E. J. Froelich, M. D. Gruett, J. H. Bailey, R. P. Brundage, *J. Med. Chem.* **1962**, *5*, 1063.
- [306] V. T. Andriole, *The Quinolones*, Elsevier Science, New York, **2000**.
- [307] L. R. Peterson, *Clin. Infect. Dis.* **2001**, *33*, 180-186.
- [308] J. M. Domagala, *J. Antimicrob. Chemother.* **1994**, *33*, 685.
- [309] a) M. Conrad, L. Limpach, *Ber. Dtsch. Chem. Ges.* **1887**, *20*, 944; b) M. Conrad, L. Limpach, *Ber. Dtsch. Chem. Ges.* **1891**, *24*, 2990; c) R. H. Reitsema, *Chem. Rev.* **1948**, *43*, 43; d) J.-C. Brouet, S. Gu, N. P. Peet, J. D. Williams, *Synth. Commun.* **2009**, *39*, 5193.
- [310] a) St. Niementowski, *Ber. Dtsch. Chem. Ges.* **1894**, *27*, 1394; b) F.-R. Alexandre, A. Berecibar, T. Besson, *Tetrahedron Lett.* **2002**, *43*, 3911.
- [311] R. Camps, *Ber. Dtsch. Chem. Ges.* **1899**, *32*, 3228.
- [312] C. P. Jones, K. W. Anderson, S. L. Buchwald, *J. Org. Chem.* **2007**, *72*, 7968.
- [313] P. Shi, L. Wang, K. Chen, J. Wang, J. Zhu, *Org. Lett.* **2017**, *19*, 2418.
- [314] S. Rádl, I. Obadalová, *Collect. Czech. Chem. Commun.* **2004**, *69*, 822.
- [315] P. Harrisson, J. Morris, P. G. Steel, T. B. Marder, *Synlett* **2009**, *1*, 147.
- [316] J. Hirano, K. Hamase, K. Zaitso, *Tetrahedron* **2006**, *62*, 10065.

- [317] R. Uson, L. A. Oro, J. A. Cabeza, H. E. Bryndza, M. P. Stepro in *Kirschner (Hg.) 1985 – Inorg. Synth.*, pp. 126–130.
- [318] S. S. Zaleskiy, V. P. Ananikov, *Organometallics* **2012**, *31*, 2302.
- [319] P. Dansette, D. M. Jerina, *J. Am. Chem. Soc.* **1974**, *96*, 1224.
- [320] E. R. R. Young, R. L. Funk, *J. Org. Chem.* **1998**, *63*, 9995.
- [321] G. M. Sheldrick, *Acta Crystallogr.* **2015**, *A71*, 3.
- [322] G. M. Sheldrick, *Acta Crystallogr.* **2008**, *A64*, 112.
- [323] K. B. H. Putz, *Diamond, Crystal and Molecular Structure Visualization*, Crystal Impact H. Putz & K. Brandenburg GbR, Bonn (Germany), **2017**.
- [324] C. F. Macrae, I. J. Bruno, J. A. Chisholm, P. R. Edgington, P. McCabe, E. Pidcock, L. Rodriguez-Monge, R. Taylor, J. van de Streek, P. A. Wood, *J. Appl. Crystallogr.* **2008**, *41*, 466.
- [325] O. V. Dolomanov, L. J. Bourhis, R. J. Gildea, J. A. K. Howard, H. Puschmann, *J. Appl. Crystallogr.* **2009**, *42*, 339.
- [326] Gaussian 09, Revision E.01, M. J. Frisch, G. W. Trucks, H. B. Schlegel, G. E. Scuseria, M. A. Robb, J. R. Cheeseman, G. Scalmani, V. Barone, B. Mennucci, G. A. Petersson, H. Nakatsuji, M. Caricato, X. Li, H. P. Hratchian, A. F. Izmaylov, J. Bloino, G. Zheng, J. L. Sonnenberg, M. Hada, M. Ehara, K. Toyota, R. Fukuda, J. Hasegawa, M. Ishida, T. Nakajima, Y. Honda, O. Kitao, H. Nakai, T. Vreven, J. A. Montgomery, Jr., J. E. Peralta, F. Ogliaro, M. Bearpark, J. J. Heyd, E. Brothers, K. N. Kudin, V. N. Staroverov, R. Kobayashi, J. Normand, K. Raghavachari, A. Rendell, J. C. Burant, S. S. Iyengar, J. Tomasi, M. Cossi, N. Rega, J. M. Millam, M. Klene, J. E. Knox, J. B. Cross, V. Bakken, C. Adamo, J. Jaramillo, R. Gomperts, R. E. Stratmann, O. Yazyev, A. J. Austin, R. Cammi, C. Pomelli, J. W. Ochterski, R. L. Martin, K. Morokuma, V. G. Zakrzewski, G. A. Voth, P. Salvador, J. J. Dannenberg, S. Dapprich, A. D. Daniels, Ö. Farkas, J. B. Foresman, J. V. Ortiz, J. Cioslowski, and D. J. Fox, *Gaussian, Inc., Wallingford CT 2009*.
- [327] a) A. D. Becke, *J. Chem. Phys.* **1993**, *98*, 5648; b) C. Lee, W. Yang, R. G. Parr, *Phys. Rev. B* **1988**, *37*, 785; c) P. J. Stephens, F. J. Devlin, C. F. Chabalowski, M. J. Frisch, *J. Phys. Chem.* **1994**, *98*, 11623.

- [328] a) G. A. Petersson, M. A. Al-Laham, *J. Chem. Phys.* **1991**, *94*, 6081; b) G.A. Petersson, A. Bennett, T. G. Tensfeldt, M. A. Al-Laham, W. A. Shirley, *J. Chem. Phys.* **1988**, 2193.
- [329] T. Yanai, D. P. Tew, N. C. Handy, *Chem. Phys. Lett.* **2004**, *393*, 51.
- [330] M. Kaupp, M. Renz, M. Parthey, M. Stolte, F. Würthner, C. Lambert, *Phys. Chem. Chem. Phys.* **2011**, *13*, 16973.
- [331] a) T. Yang, Y. Huang, B. P. Cho, *Chem. Res. Toxicol.* **2006**, *19*, 242; b) P. Šoustek, M. Michl, N. Almonasy, O. Machalický, M. Dvořák, A. Lyčka, *Dyes Pigment.* **2008**, *78*, 139.
- [332] S.-F. Liu, Q. Wu, H. L. Schmider, H. Aziz, N.-X. Hu, Z. Popović, S. Wang, *J. Am. Chem. Soc.* **2000**, *122*, 3671.
- [333] R. García, S. More, M. Melle-Franco, A. Mateo-Alonso, *Org. Lett.* **2014**, *16*, 6096.



# Appendix



## 8 Appendix

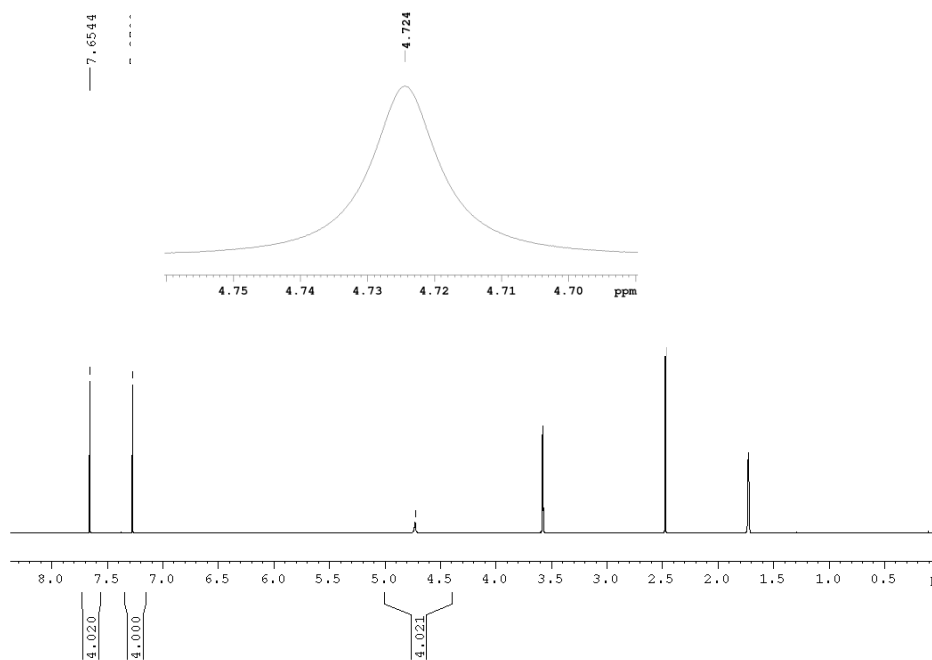


Figure 8-1.  $^1\text{H}$  NMR spectrum of **1-1** in  $\text{THF-}d_8$  at 500 MHz.

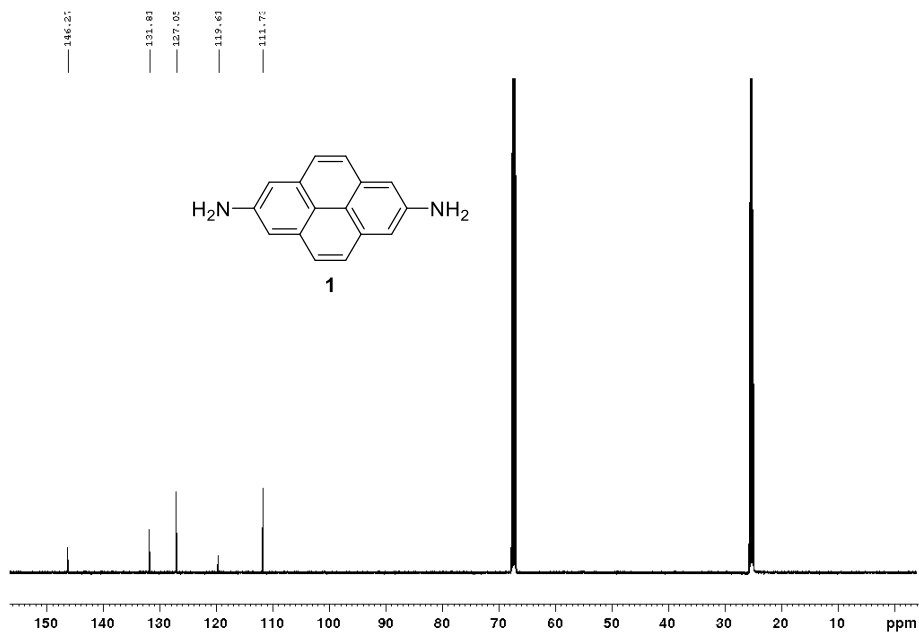


Figure 8-2.  $^{13}\text{C}\{^1\text{H}\}$  NMR spectrum of **1-1** in  $\text{THF-}d_8$  at 75 MHz.

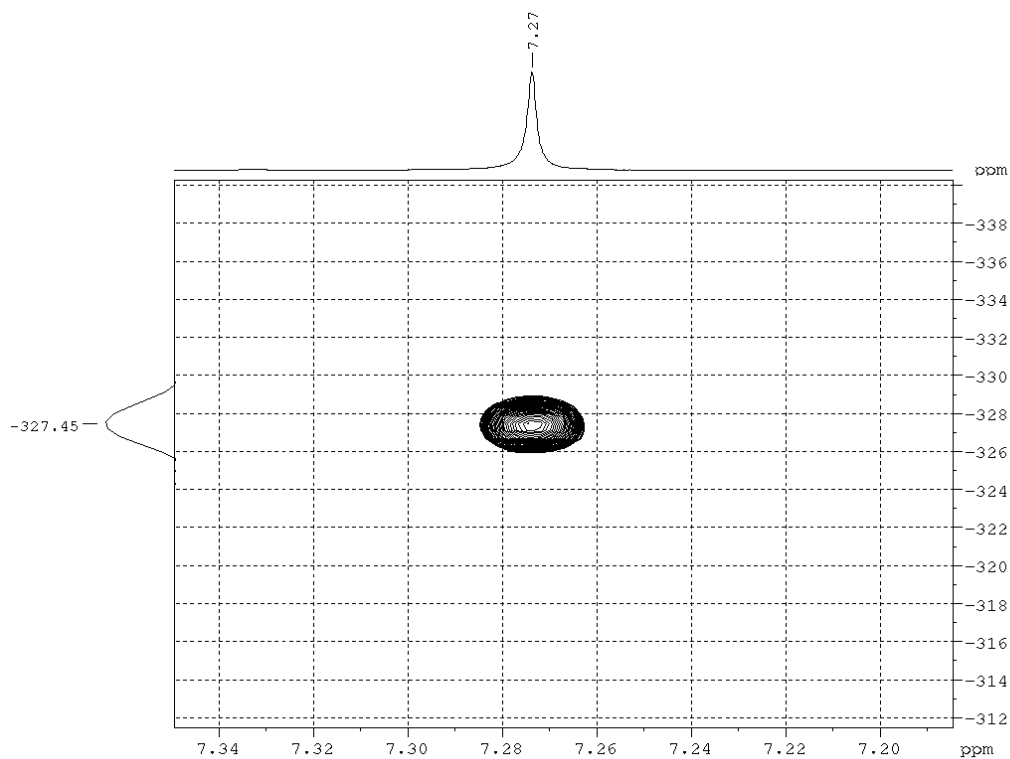


Figure 8-3.  $^{15}\text{N}$ ,  $^1\text{H}$  HMBC NMR spectrum of **1-1** in  $\text{THF-}d_8$  at 300 MHz.

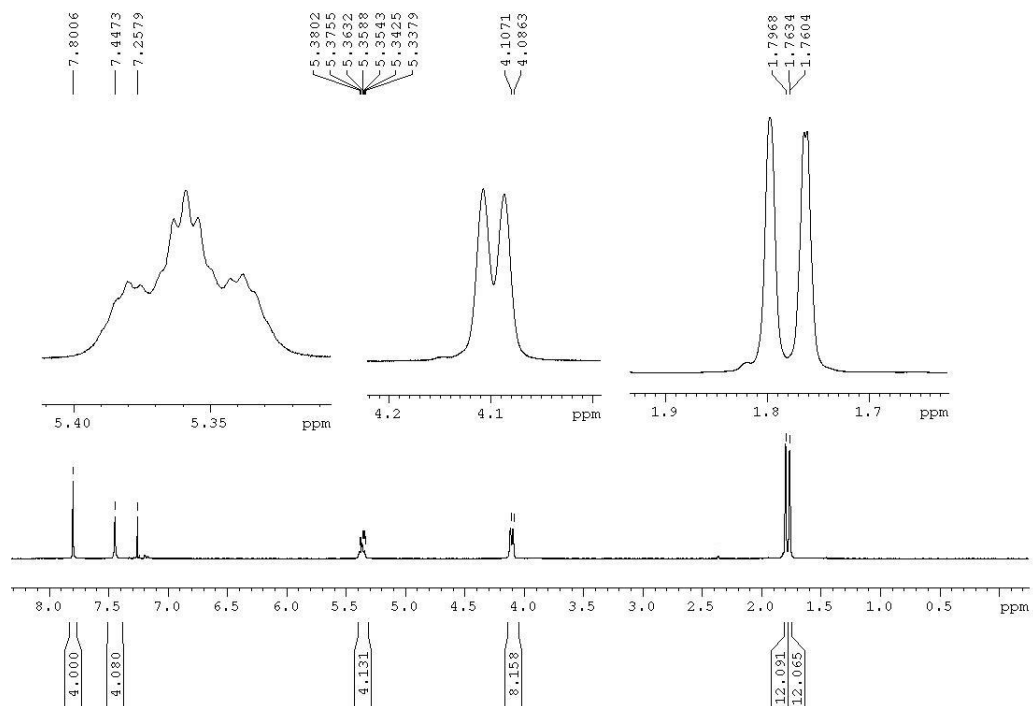


Figure 8-4.  $^1\text{H}$  NMR spectrum of **1-2** in  $\text{CDCl}_3$  at 300 MHz.

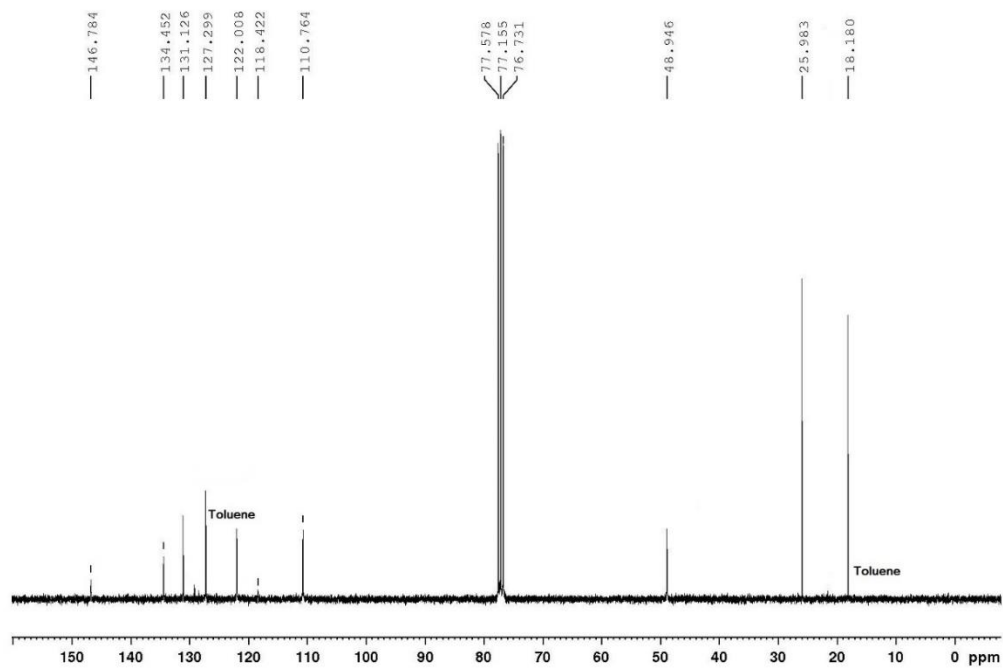


Figure 8-5.  $^{13}\text{C}\{^1\text{H}\}$  NMR spectrum of 1-2 in  $\text{CDCl}_3$  at 75 MHz.

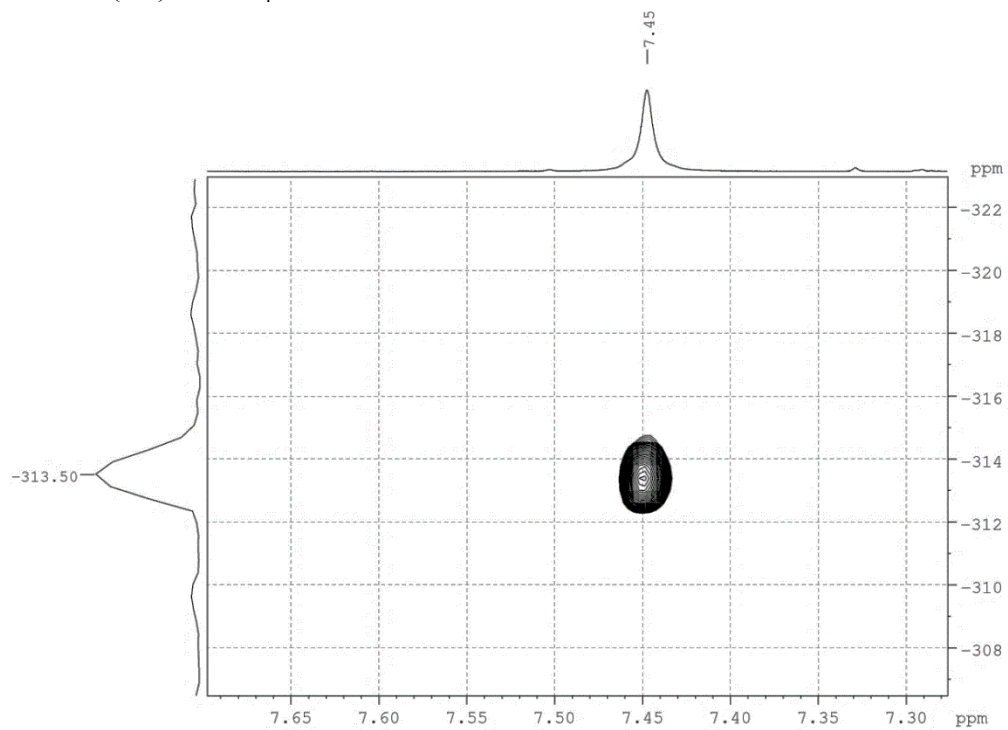


Figure 8-6.  $^{15}\text{N}$ ,  $^1\text{H}$  HMBC NMR spectrum of 1-2 in  $\text{CDCl}_3$  at 300 MHz.

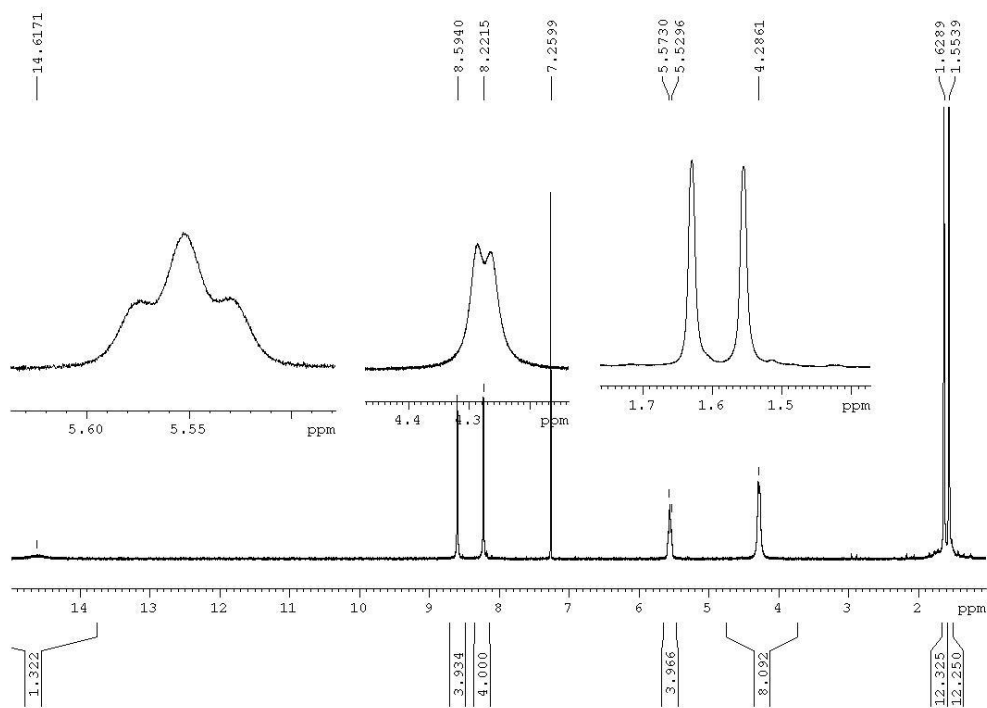


Figure 8-7.  $^1\text{H}$  NMR spectrum of **1-3** in  $\text{CDCl}_3$  at 300 MHz.

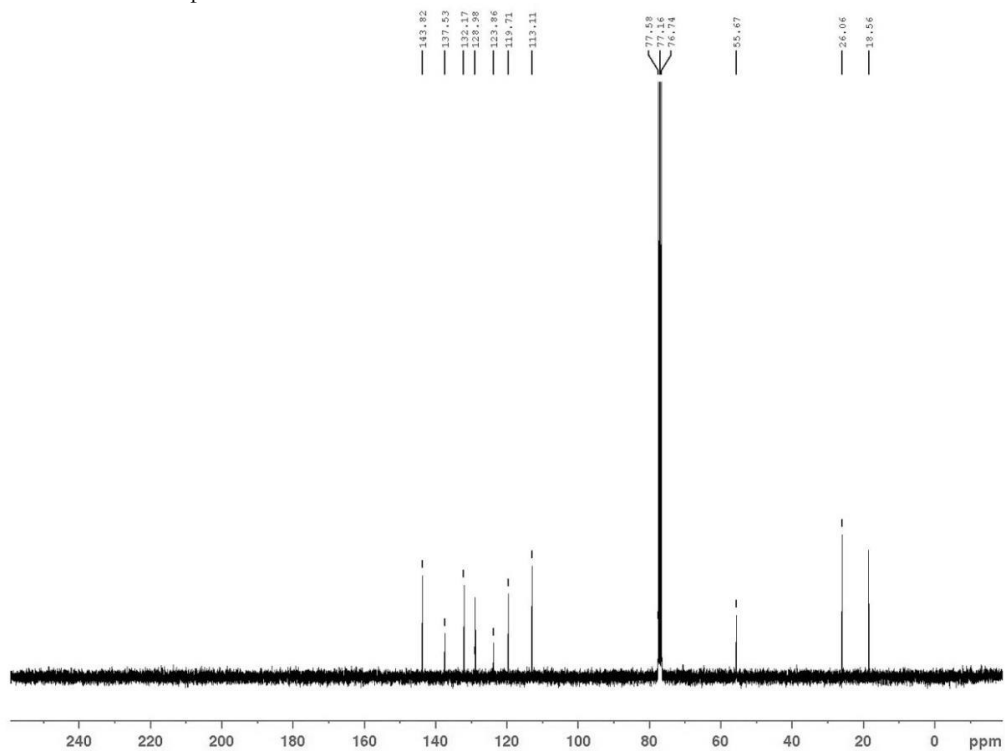


Figure 8-8.  $^{13}\text{C}\{^1\text{H}\}$  NMR spectrum of **1-3** in  $\text{CDCl}_3$  at 75 MHz.

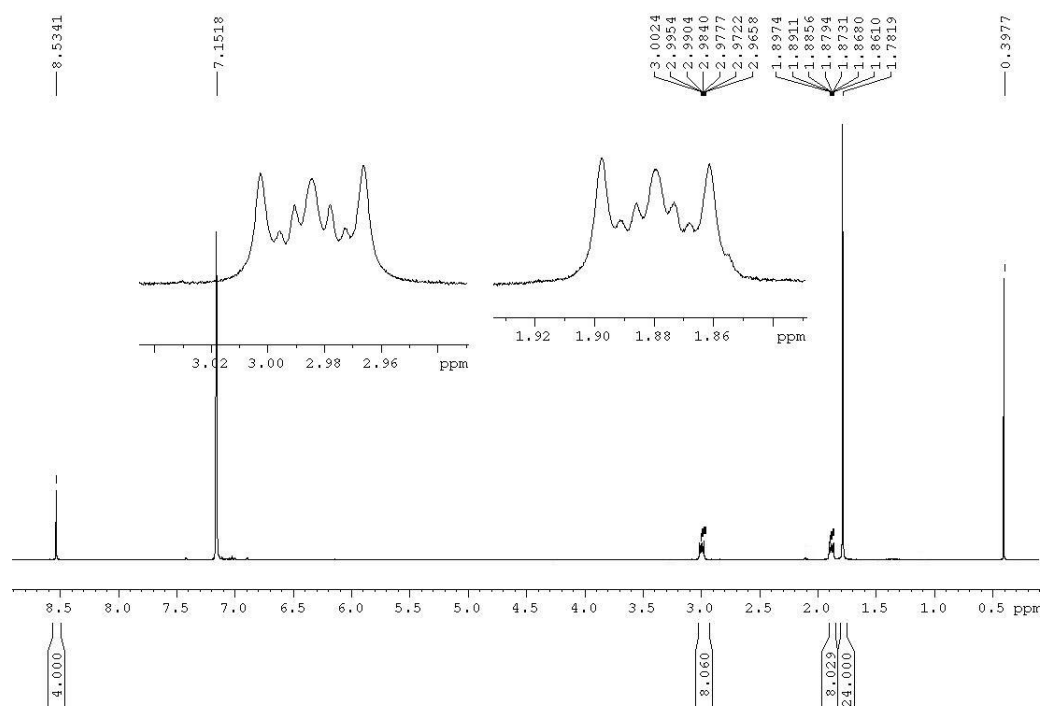


Figure 8-9.  $^1\text{H}$  NMR spectrum of 1-4 in benzene- $d_6$  at 300 MHz.

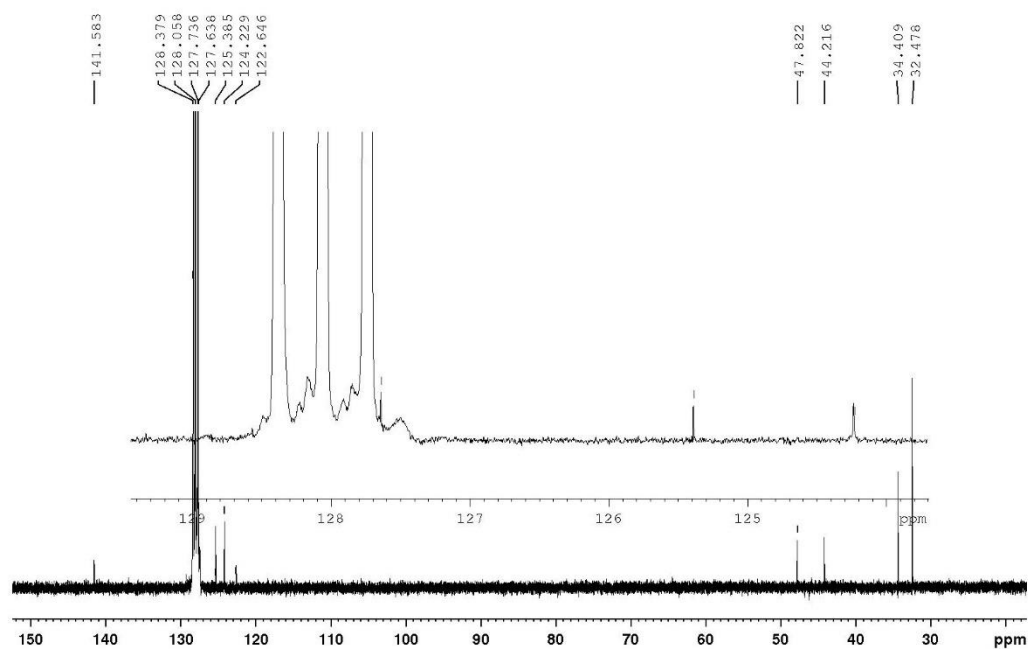


Figure 8-10.  $^{13}\text{C}\{^1\text{H}\}$  NMR spectrum of 1-4 in benzene- $d_6$  at 125 MHz.

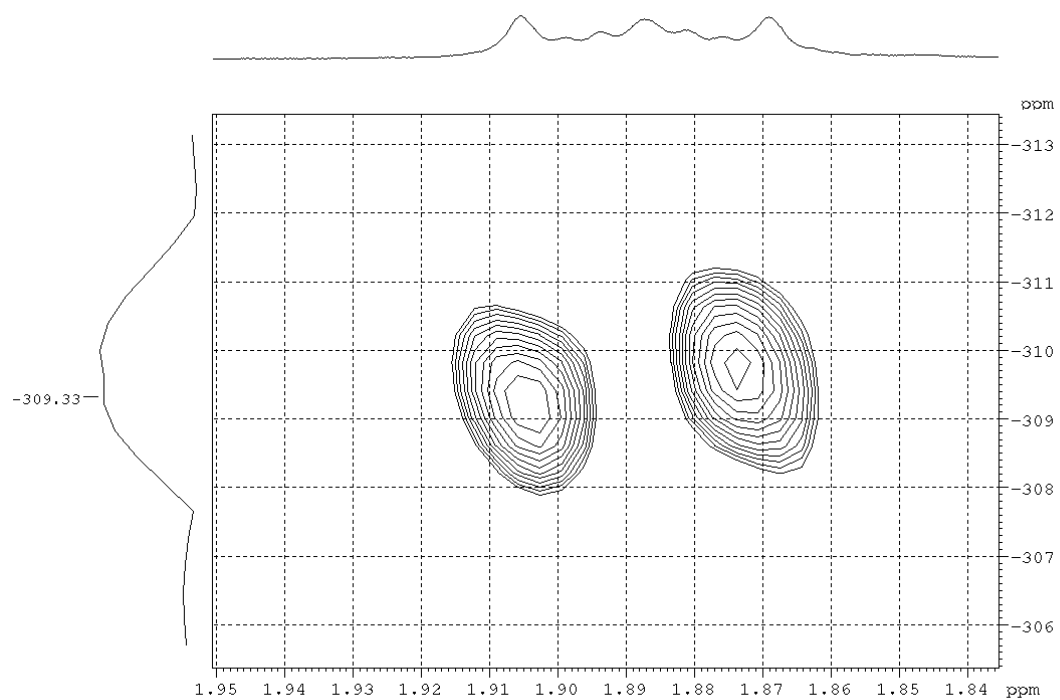


Figure 8-11.  $^{15}\text{N}$ ,  $^1\text{H}$  HMBC NMR spectrum of **1-4** in benzene- $d_6$  at 300 MHz.

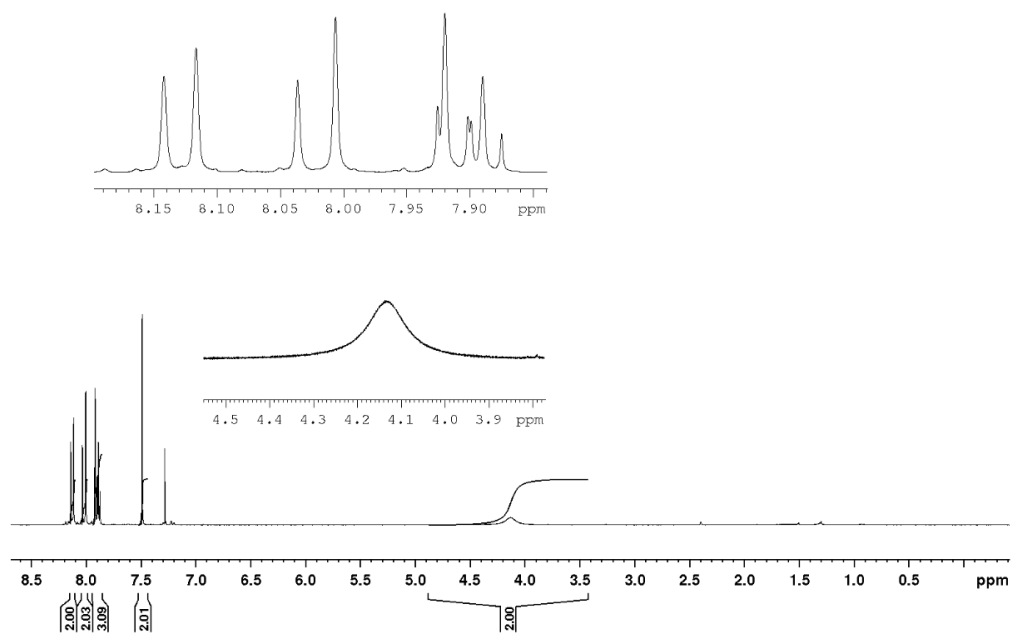


Figure 8-12.  $^1\text{H}$  NMR spectrum of **1-5** in benzene- $d_6$  at 300 MHz.



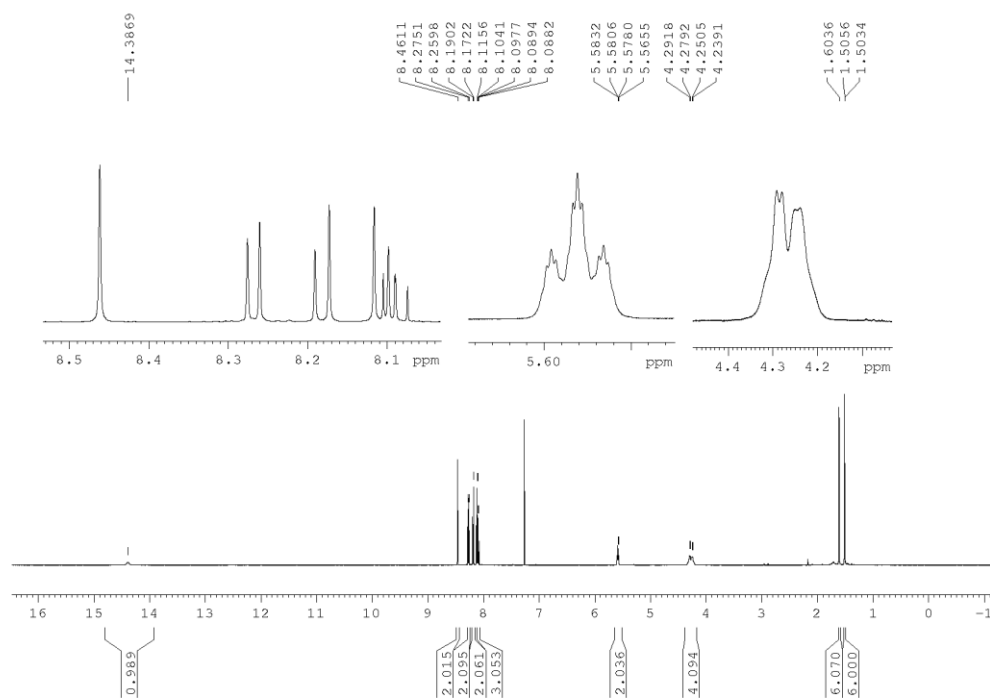


Figure 8-15. <sup>1</sup>H NMR spectrum of 1-7 in CDCl<sub>3</sub> at 500 MHz.

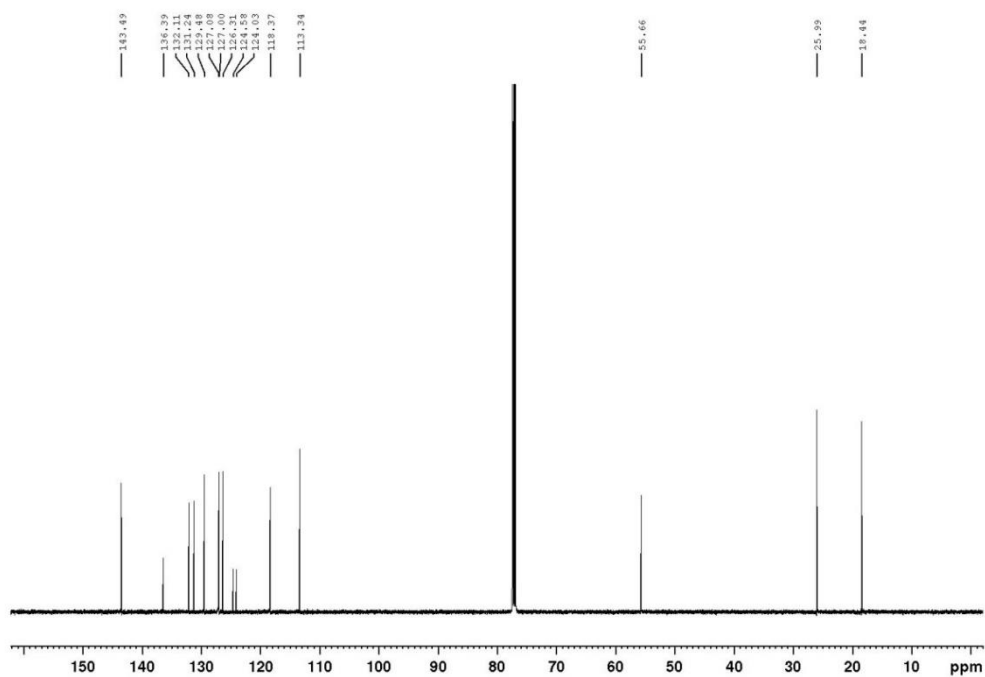


Figure 8-16. <sup>13</sup>C{<sup>1</sup>H} NMR spectrum of 1-7 in CDCl<sub>3</sub> at 125 MHz.

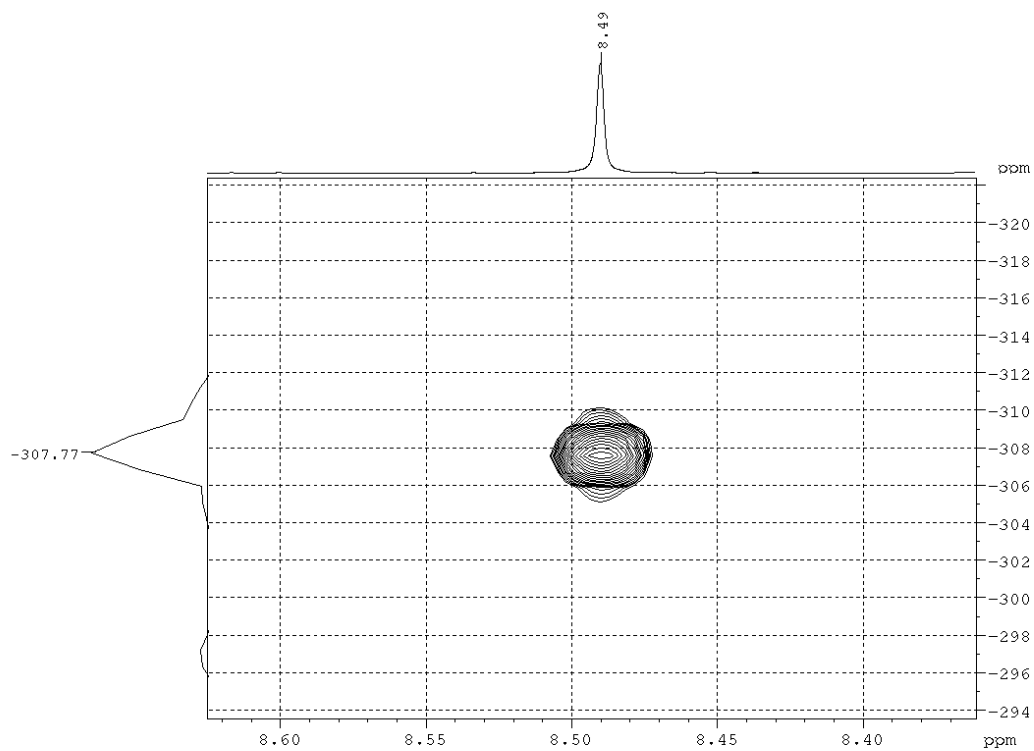


Figure 8-17.  $^{15}\text{N}$ ,  $^1\text{H}$  HMBC NMR spectrum of **1-7** in  $\text{CDCl}_3$  at 500 MHz.

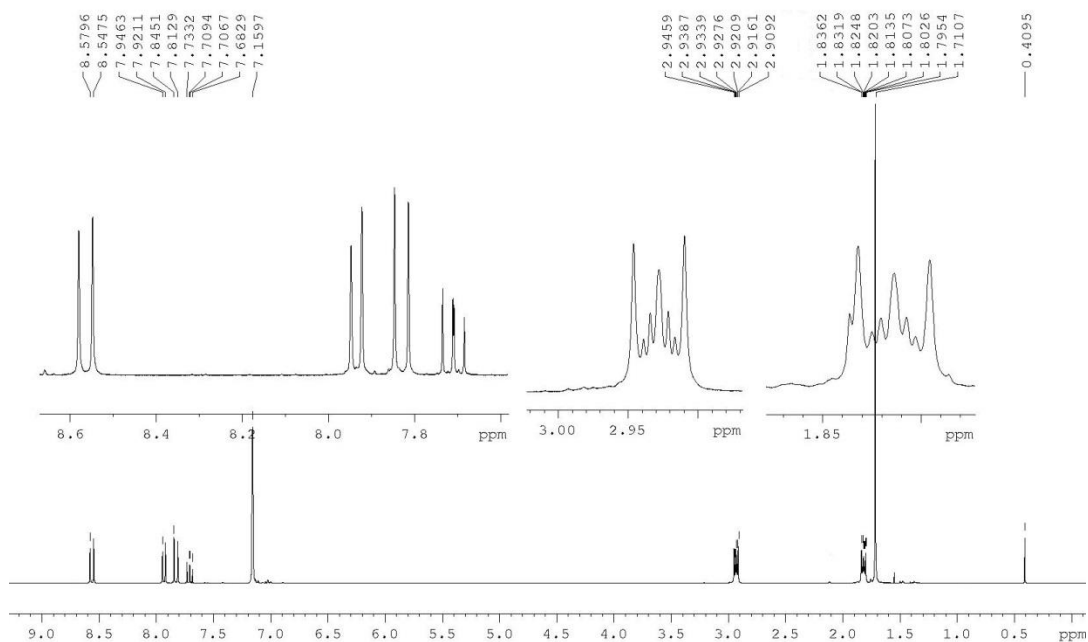


Figure 8-18.  $^1\text{H}$  NMR spectrum of **1-8** in  $\text{benzene-}d_6$  at 300 MHz.

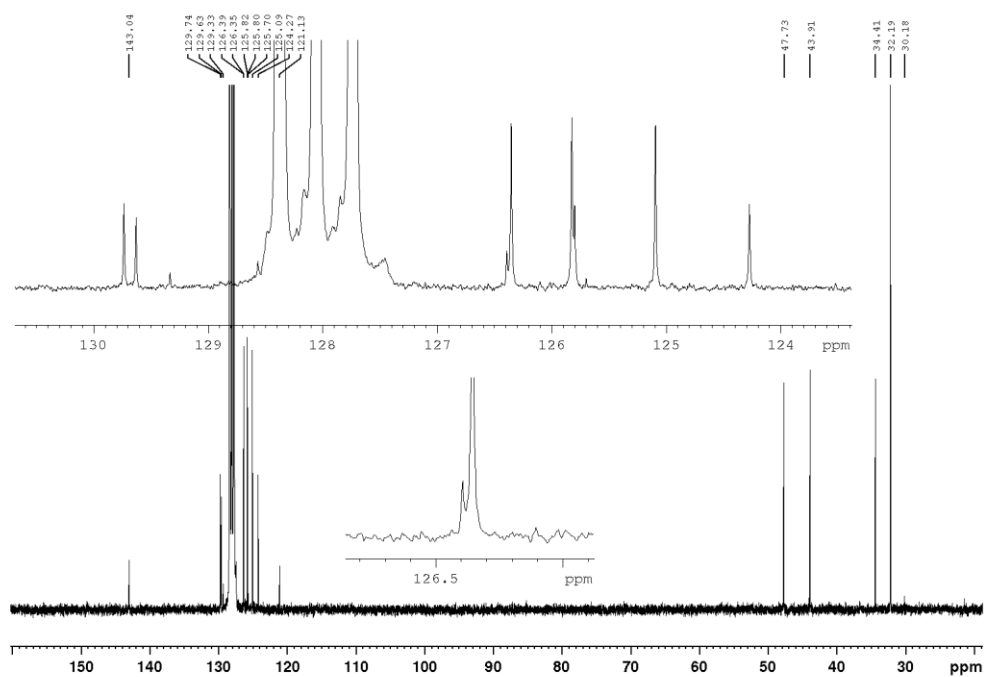


Figure 8-19.  $^{13}\text{C}\{^1\text{H}\}$  NMR spectrum of 1-8 in benzene- $d_6$  at 75 MHz.

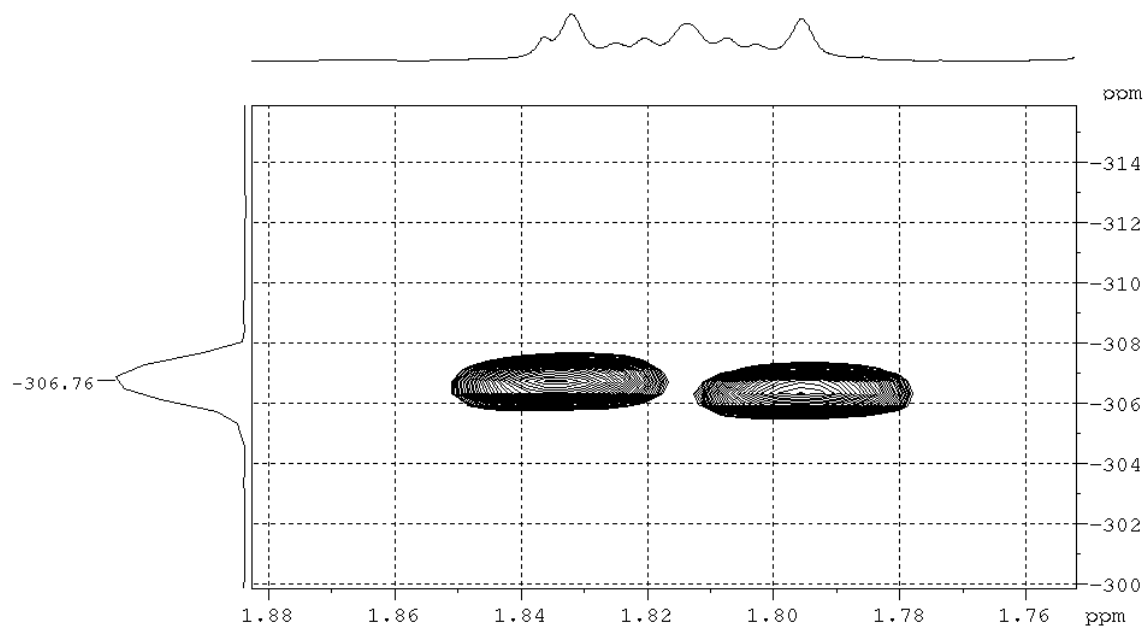


Figure 8-20.  $^{15}\text{N}, ^1\text{H}$  HMBC NMR spectrum of 1-8 in benzene- $d_6$  at 300 MHz.

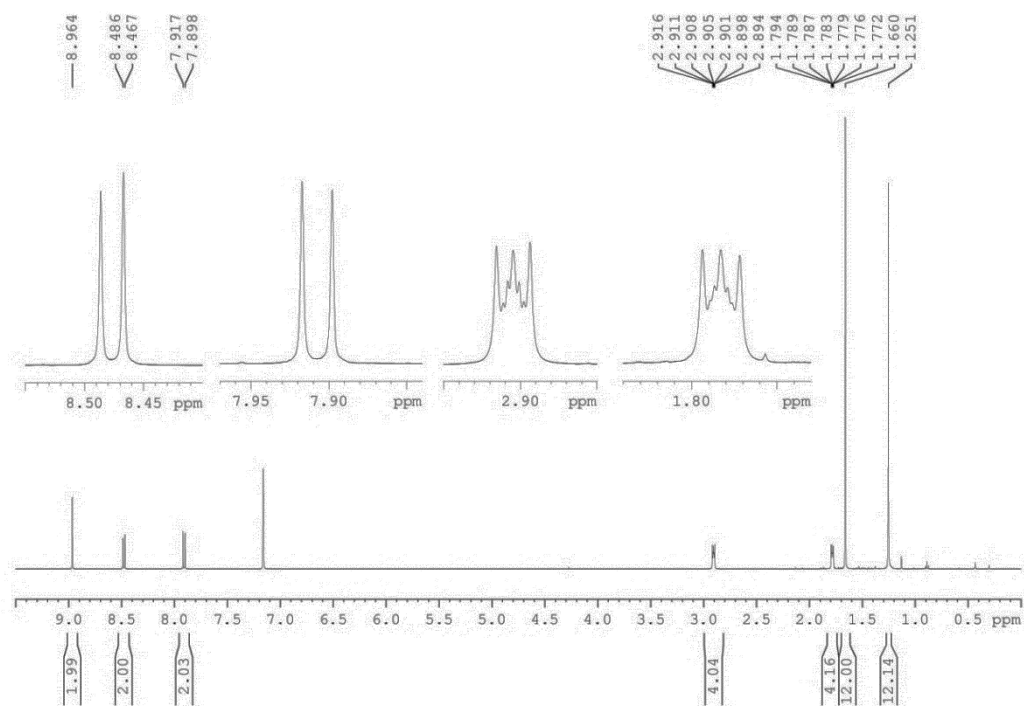


Figure 8-21.  $^1\text{H}$  NMR spectrum of **1-9** in benzene- $d_6$  at 500 MHz.

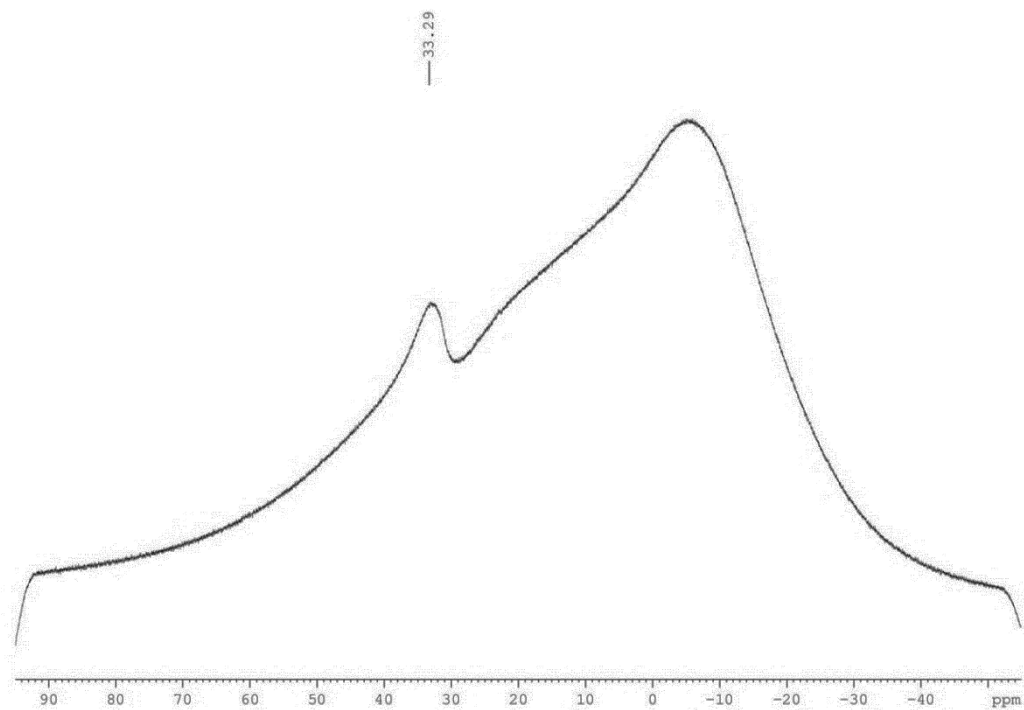


Figure 8-22.  $^{11}\text{B}\{^1\text{H}\}$  NMR spectrum of **1-9** in benzene- $d_6$  at 160 MHz.

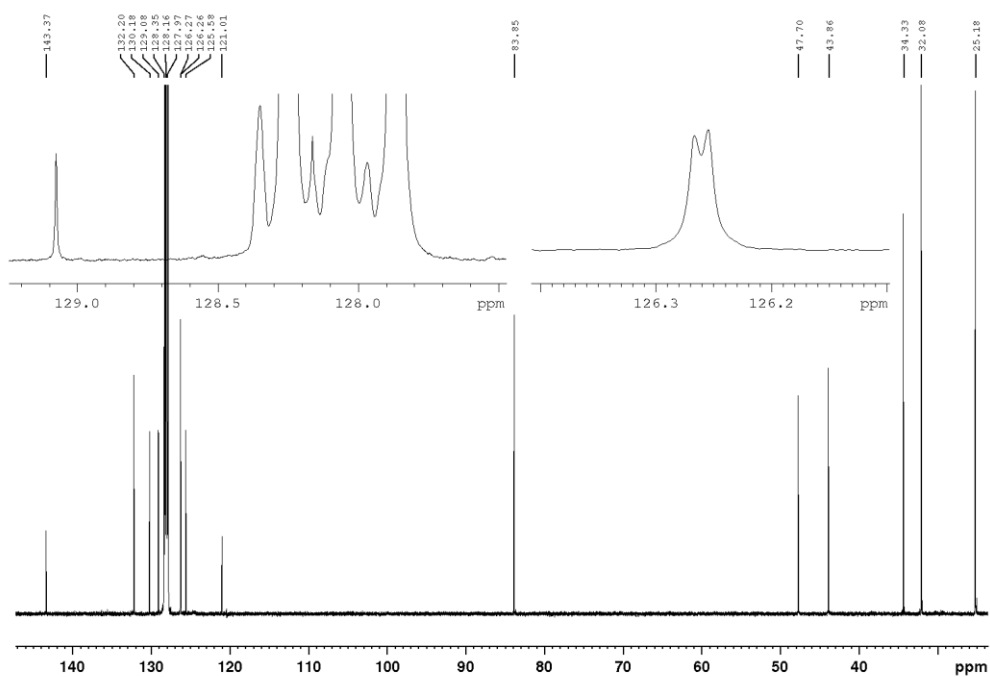


Figure 8-23.  $^{13}\text{C}\{^1\text{H}\}$  NMR spectrum of **1-9** in benzene- $d_6$  at 125 MHz.

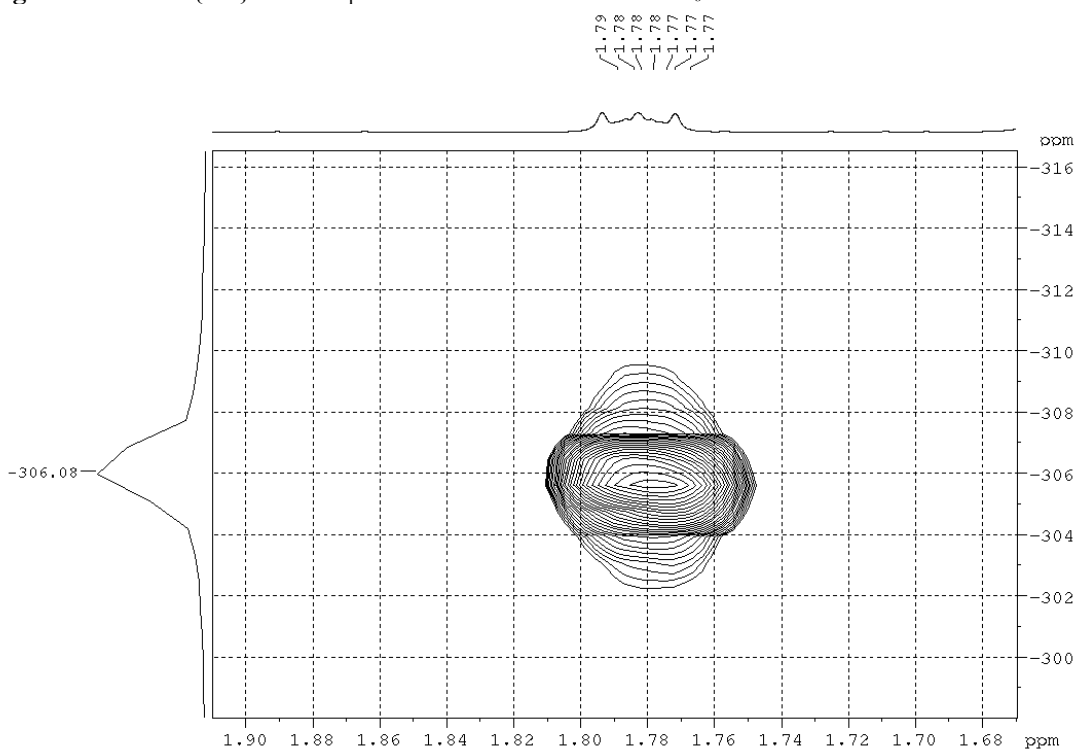
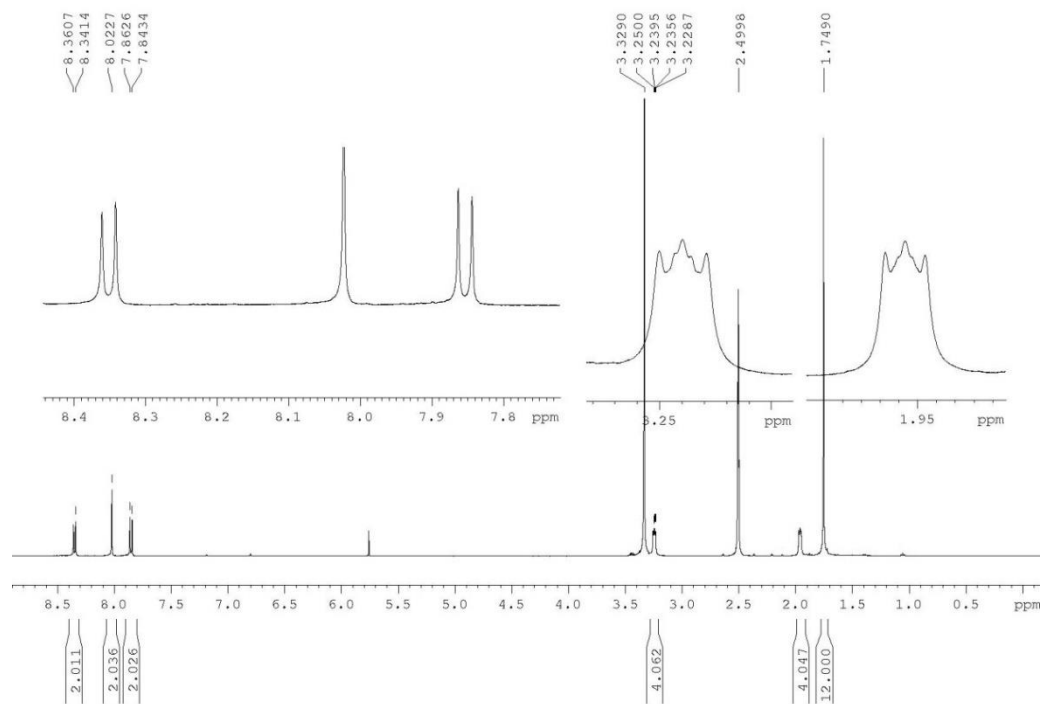
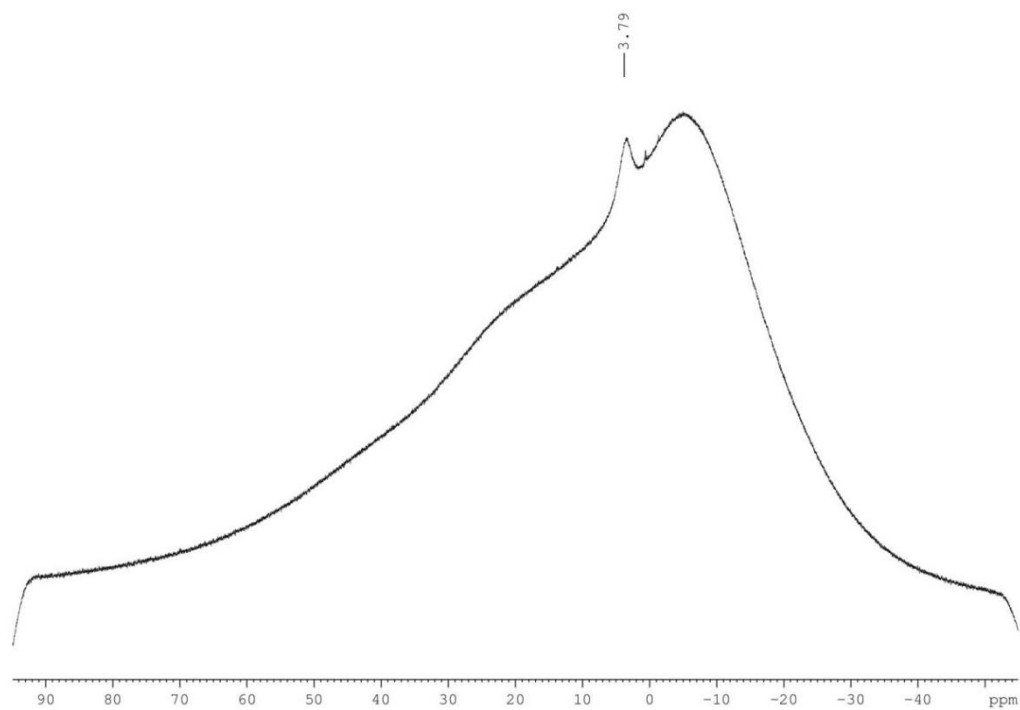


Figure 8-24.  $^{15}\text{N}$ ,  $^1\text{H}$  HMBC NMR spectrum of **1-9** in benzene- $d_6$  at 500 MHz.



**Figure 8-25.**  $^1\text{H}$  NMR spectrum of **1-10** in  $\text{DMSO-}d_6$  at 500 MHz.



**Figure 8-26.**  $^{11}\text{B}\{^1\text{H}\}$  NMR spectrum of **1-10** in  $\text{DMSO-}d_6$  at 160 MHz.

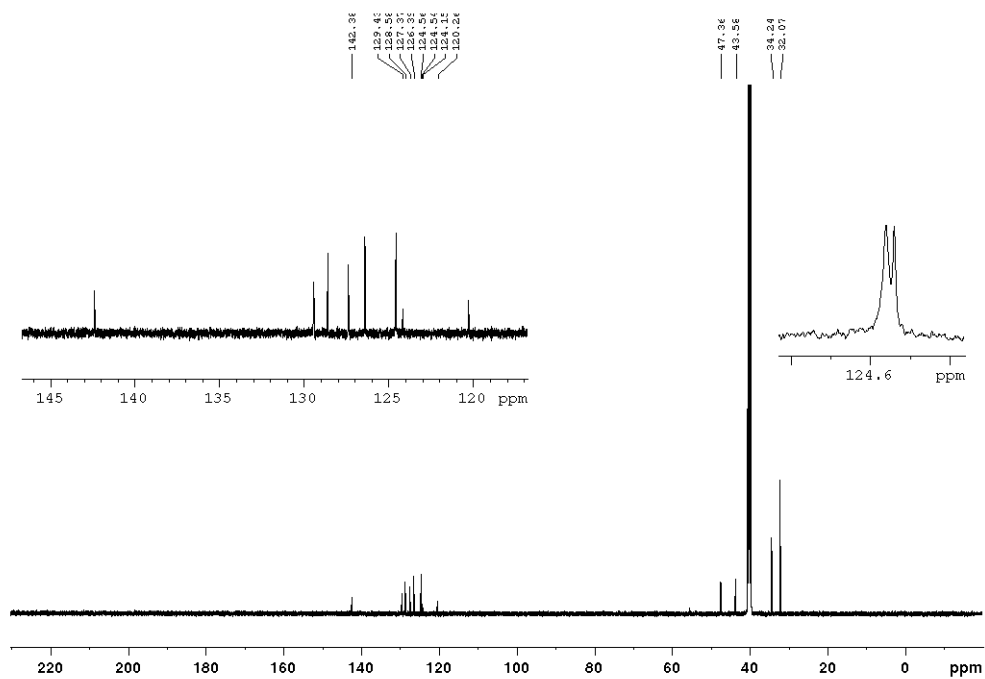


Figure 8-27.  $^{13}\text{C}\{^1\text{H}\}$  NMR spectrum of **1-10** in  $\text{DMSO-}d_6$  at 125 MHz.

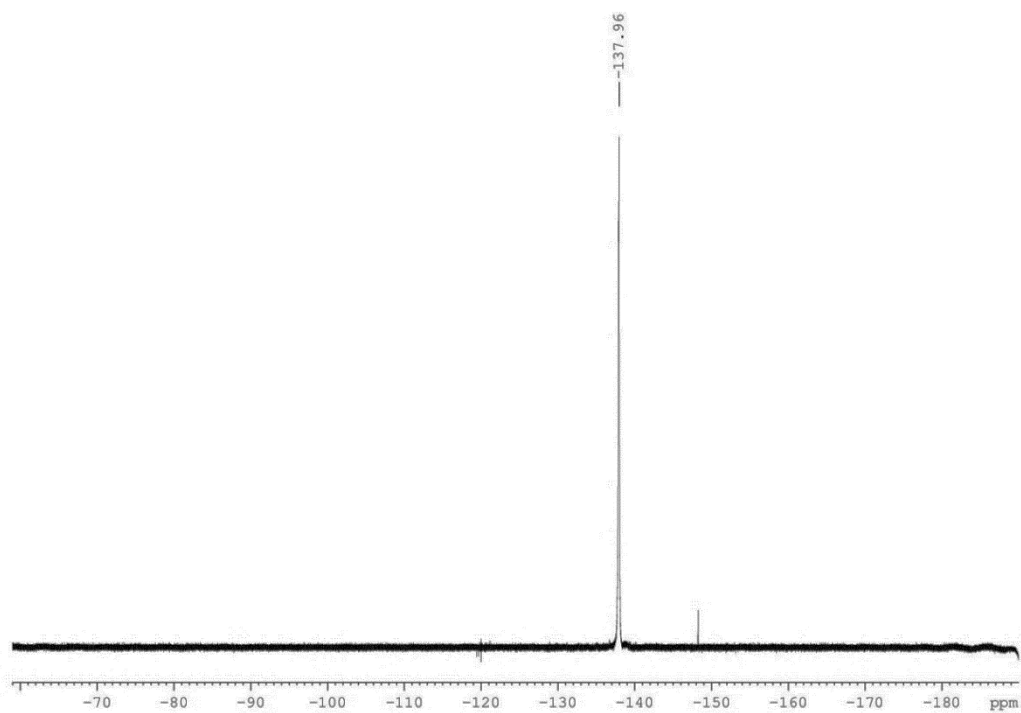


Figure 8-28.  $^{19}\text{F}\{^1\text{H}\}$  NMR spectrum of **1-10** in  $\text{DMSO-}d_6$  at 470 MHz.

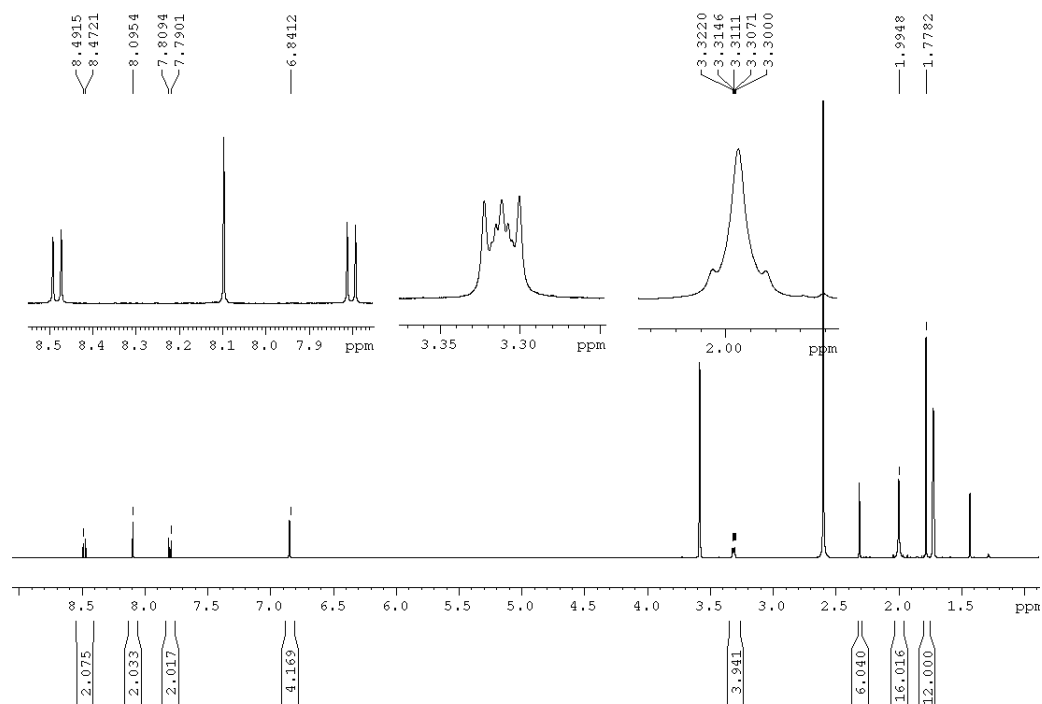


Figure 8-29. <sup>1</sup>H NMR spectrum of **1-11** in THF-*d*<sub>8</sub> at 500 MHz.

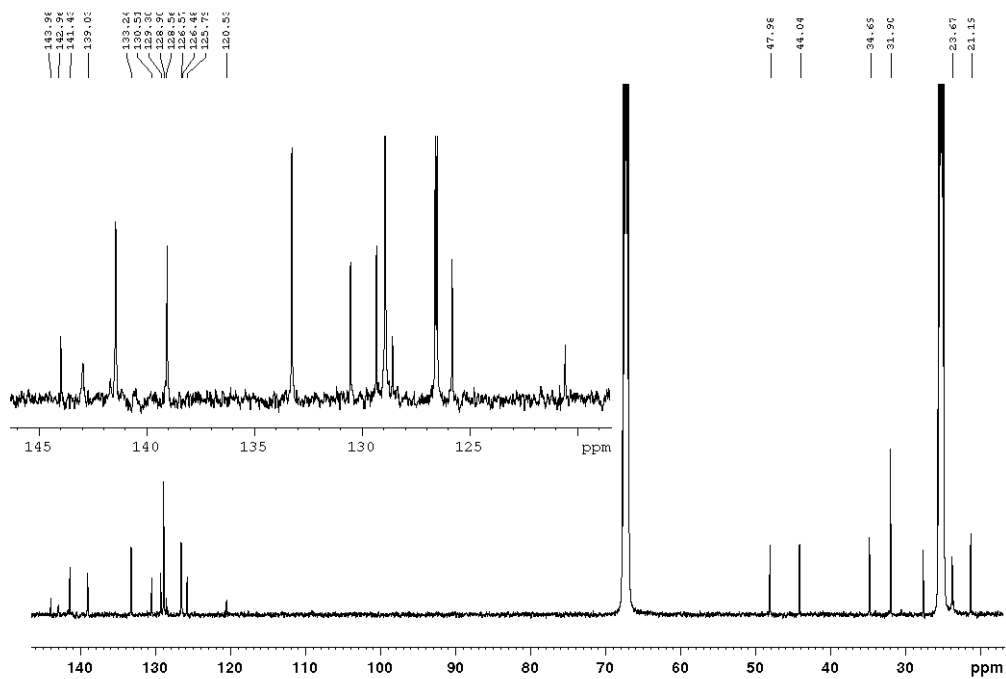


Figure 8-30. <sup>13</sup>C{<sup>1</sup>H} NMR spectrum of **1-11** in THF-*d*<sub>8</sub> at 125 MHz.

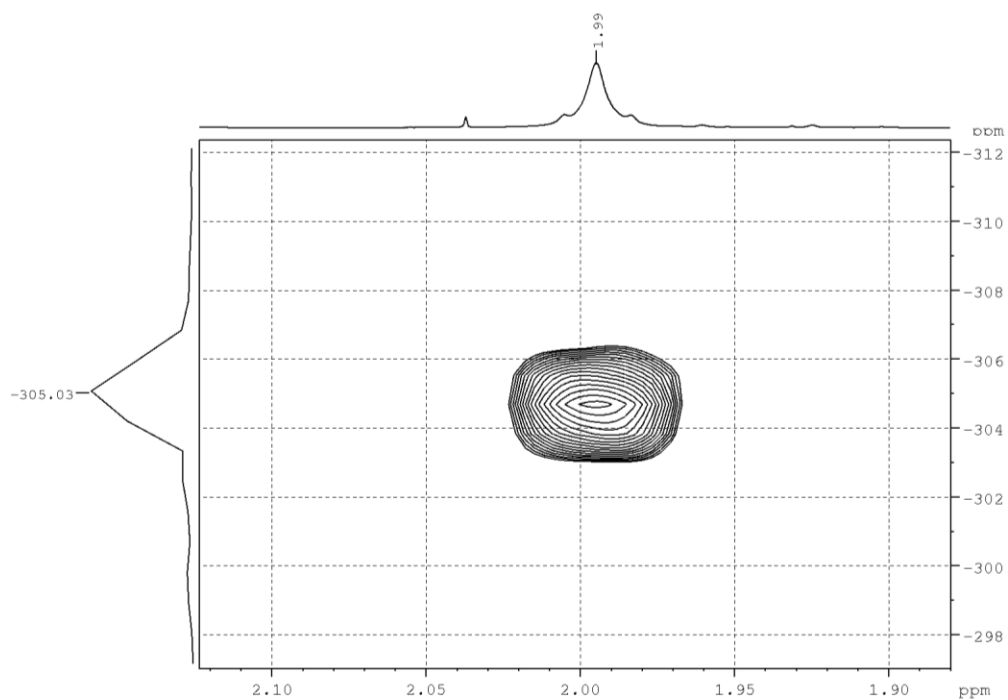


Figure 8-31.  $^{15}\text{N}$ ,  $^1\text{H}$  HMBC NMR spectrum of **1-11** in  $\text{THF-}d_8$  at 500 MHz.

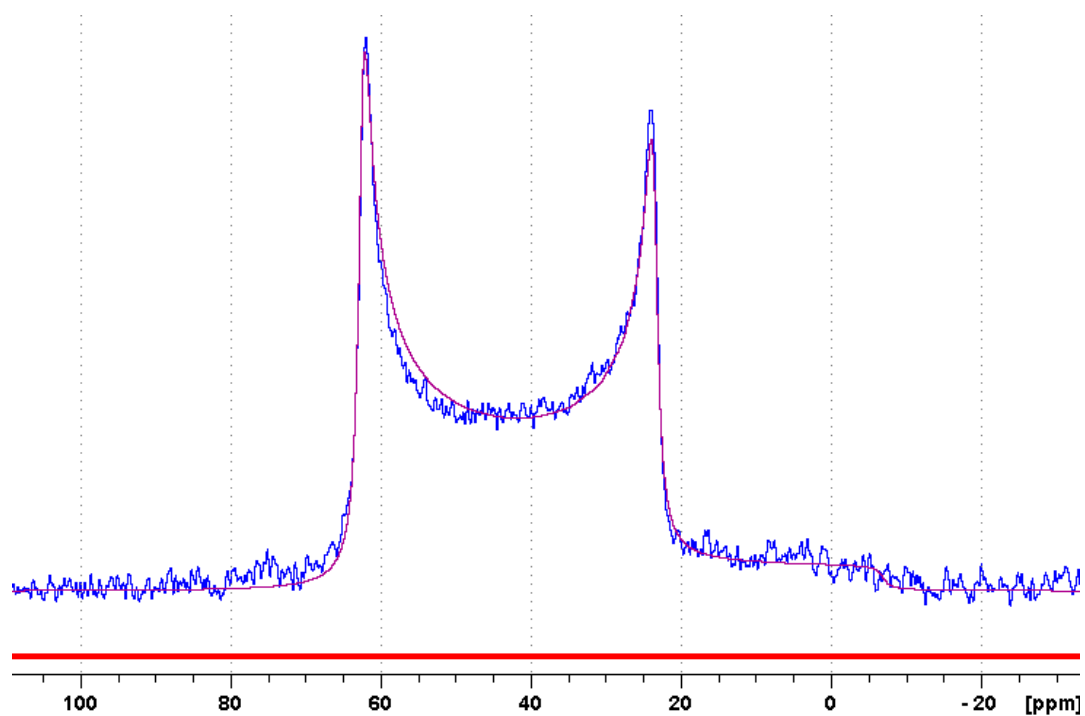


Figure 8-32. Observed (blue) and simulated (red) solid state  $^{11}\text{B}\{^1\text{H}\}$  NMR spectrum of **1-11** at 128 MHz. The isotropic chemical shift ( $\delta_{\text{iso}}$ ) is 74.3 ppm, quadrupolar coupling constant  $C_Q = 4.63$  MHz, quadrupolar asymmetry parameter  $\eta_{\text{Quad}} = 0.0$ .

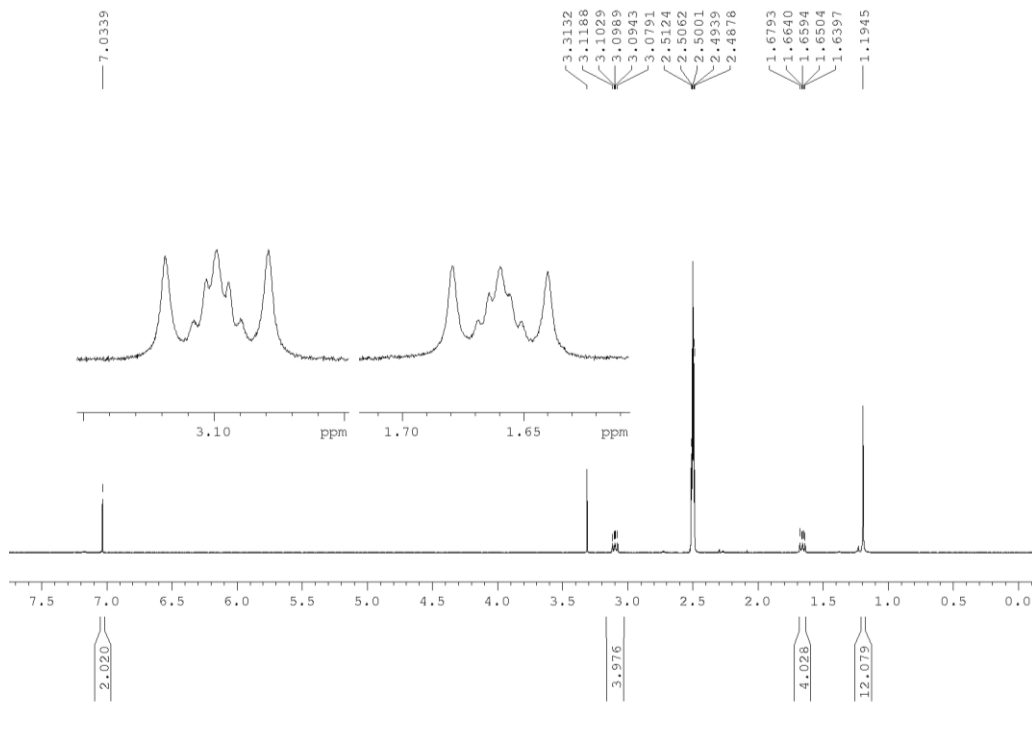


Figure 8-33.  $^1\text{H}$  NMR spectrum of **1-13** in  $\text{DMSO-}d_6$  at 300 MHz.

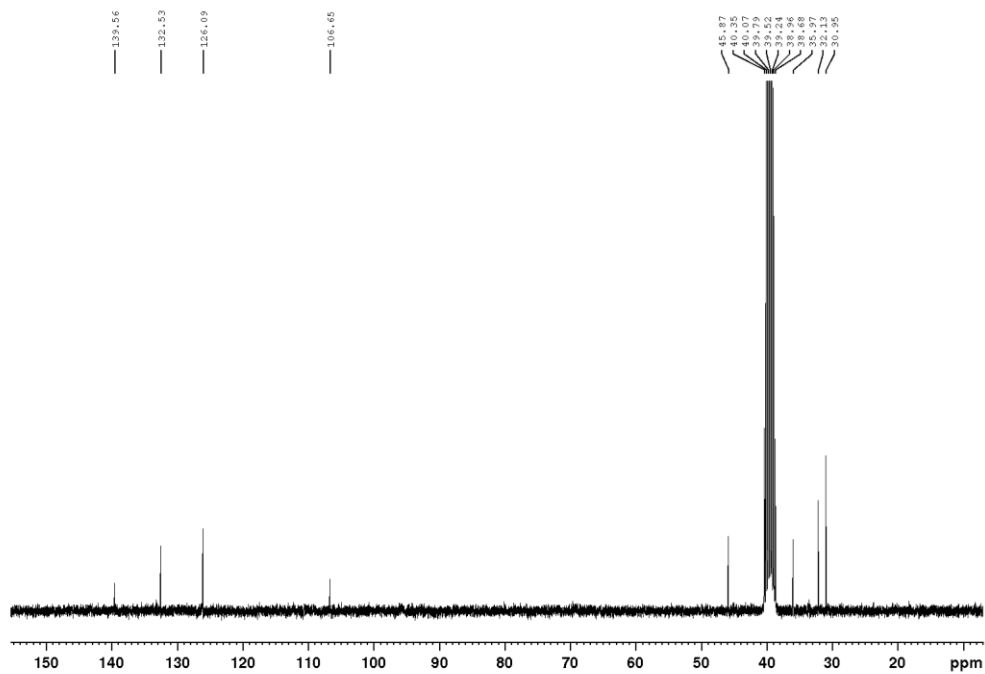


Figure 8-34.  $^{13}\text{C}\{^1\text{H}\}$  NMR spectrum of **1-13** in  $\text{DMSO-}d_6$  at 75 MHz.

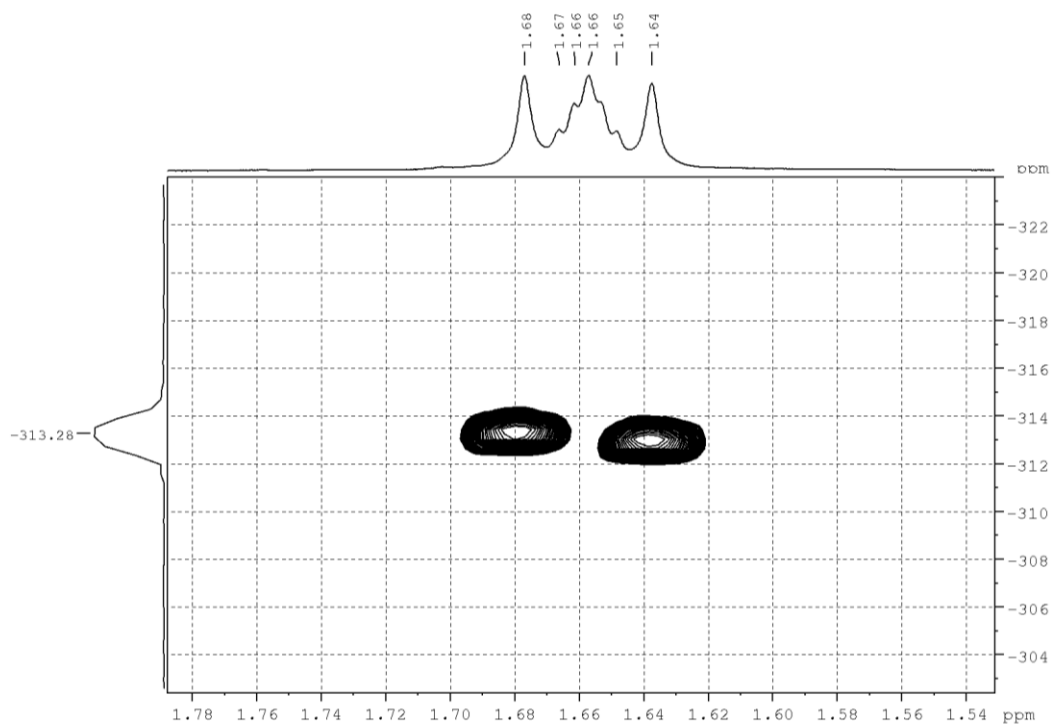


Figure 8-35.  $^{15}\text{N}$ ,  $^1\text{H}$  HMBC NMR spectrum of **1-13** in  $\text{DMSO-}d_6$  at 300 MHz.

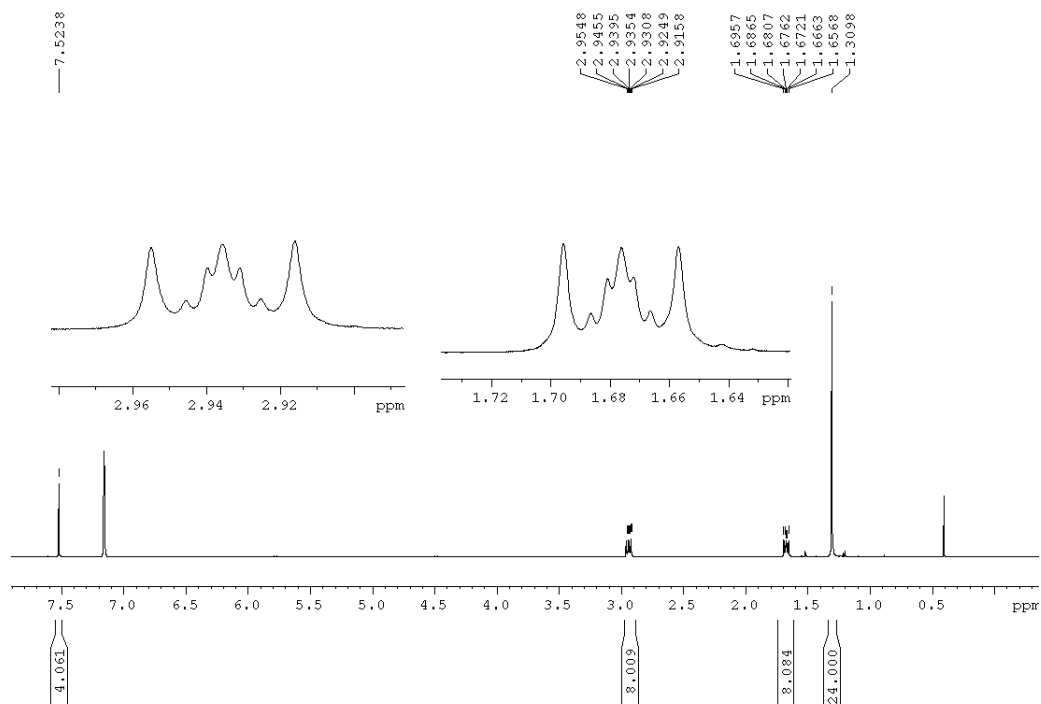


Figure 8-36.  $^1\text{H}$  NMR spectrum of **1-14** in  $\text{benzene-}d_6$  at 300 MHz.

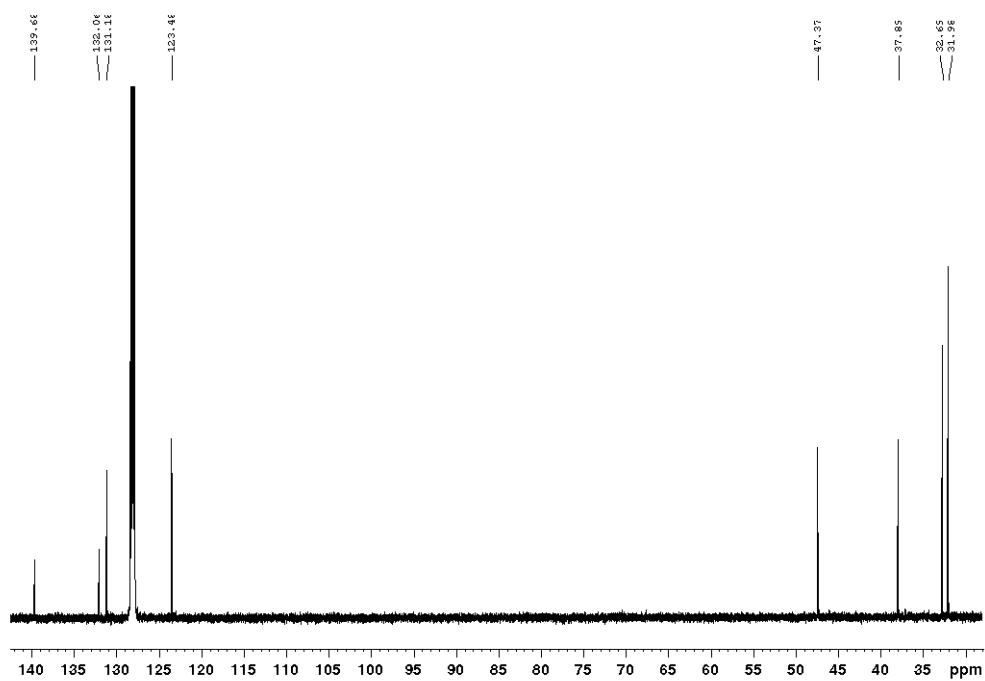


Figure 8-37.  $^{13}\text{C}\{^1\text{H}\}$  NMR spectrum of 1-14 in benzene- $d_6$  at 125 MHz.

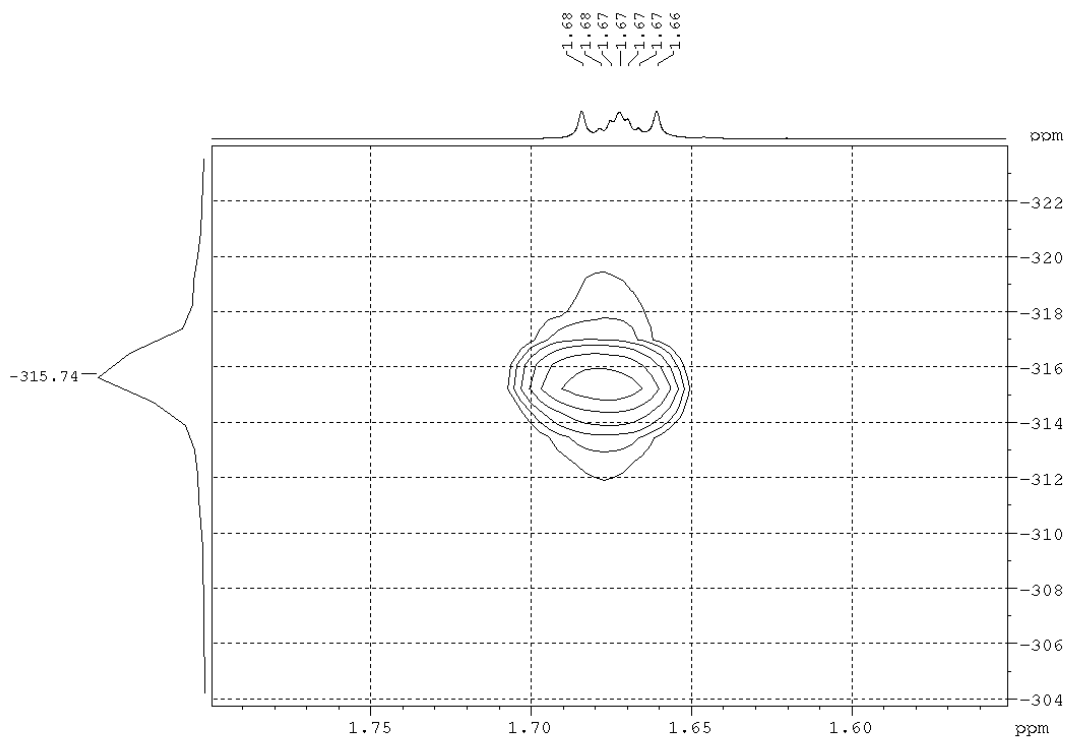


Figure 8-38.  $^{15}\text{N}$ ,  $^1\text{H}$  HMBC NMR spectrum of 1-14 in benzene- $d_6$  at 500 MHz.

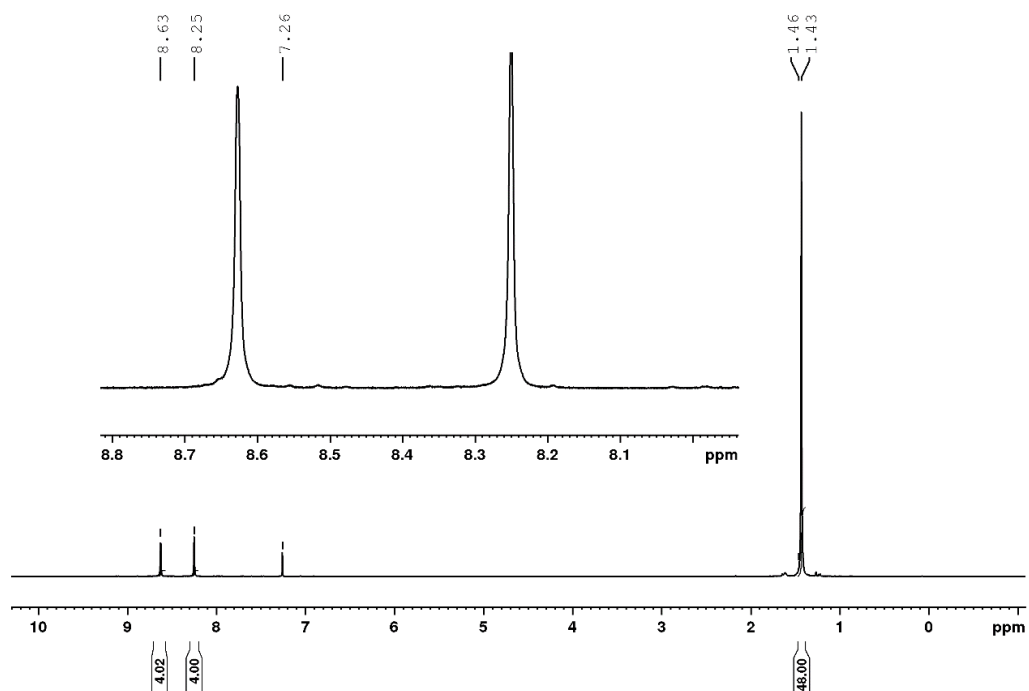


Figure 8-39.  $^1\text{H}$  NMR spectrum of  $(\text{Bpin})_4\text{-Per}$  in  $\text{CDCl}_3$  at 300 MHz.

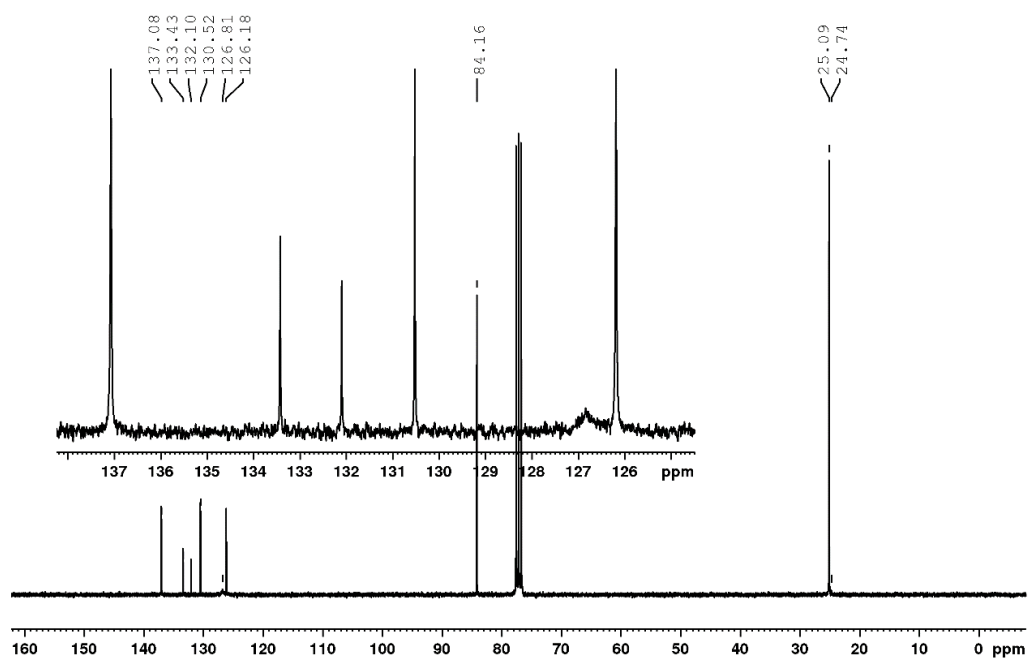


Figure 8-40.  $^{13}\text{C}\{^1\text{H}\}$  NMR spectrum of  $(\text{Bpin})_4\text{-Per}$  in  $\text{CDCl}_3$  at 75 MHz.

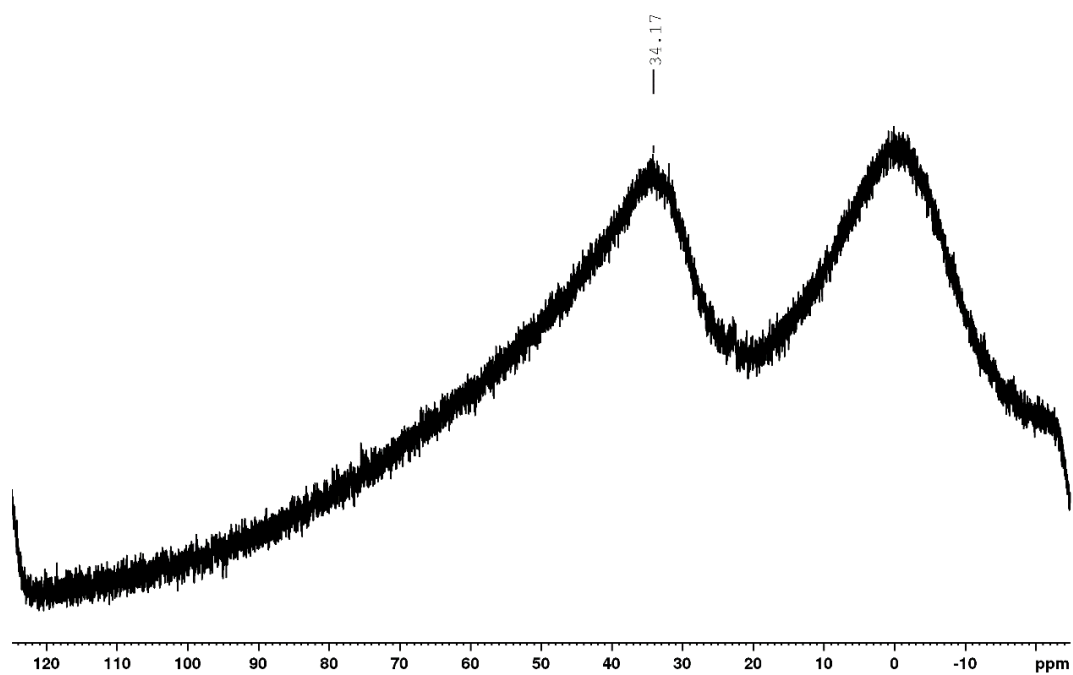


Figure 8-41.  $^{11}\text{B}\{^1\text{H}\}$  NMR spectrum of  $(\text{Bpin})_4\text{-Per}$  in  $\text{CDCl}_3$  at 75 MHz.

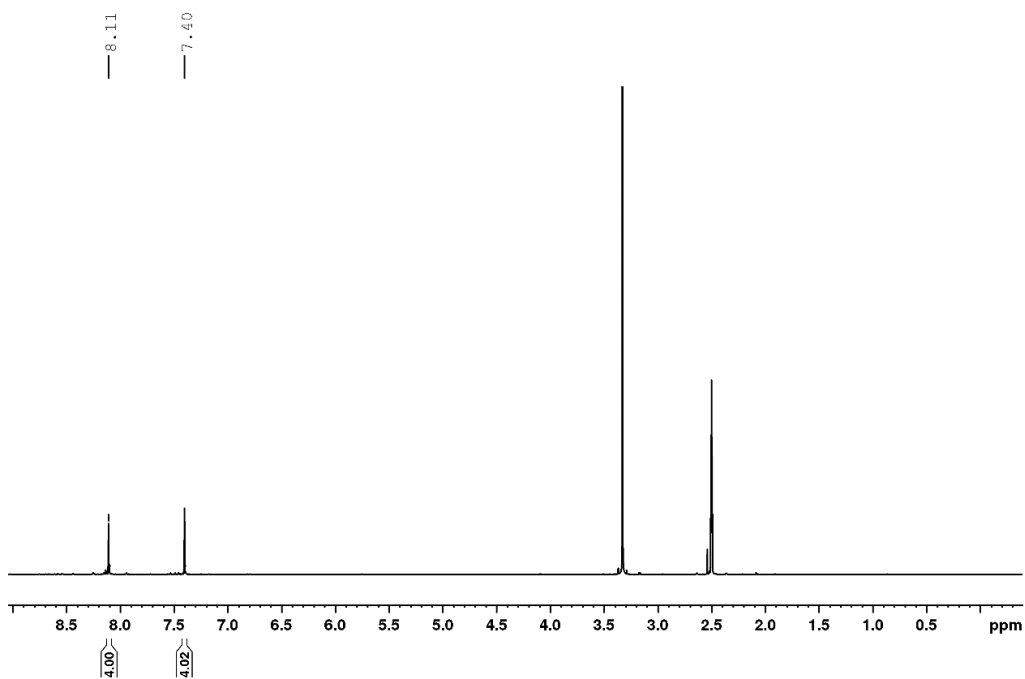


Figure 8-42.  $^1\text{H}$  NMR spectrum of  $(\text{BF}_3\text{K})_4\text{-Per}$  in  $\text{DMSO}-d_6$  at 500 MHz.

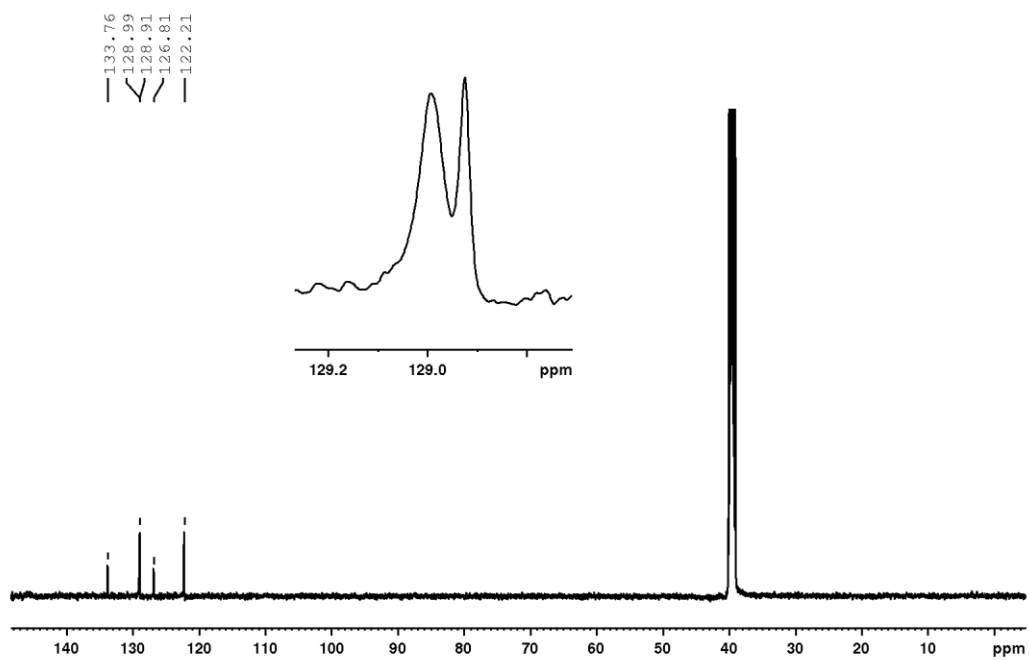


Figure 8-43.  $^{13}\text{C}\{^1\text{H}\}$  NMR spectrum of  $(\text{BF}_3\text{K})_4\text{-Per}$  in  $\text{DMSO-}d_6$  at 125 MHz.

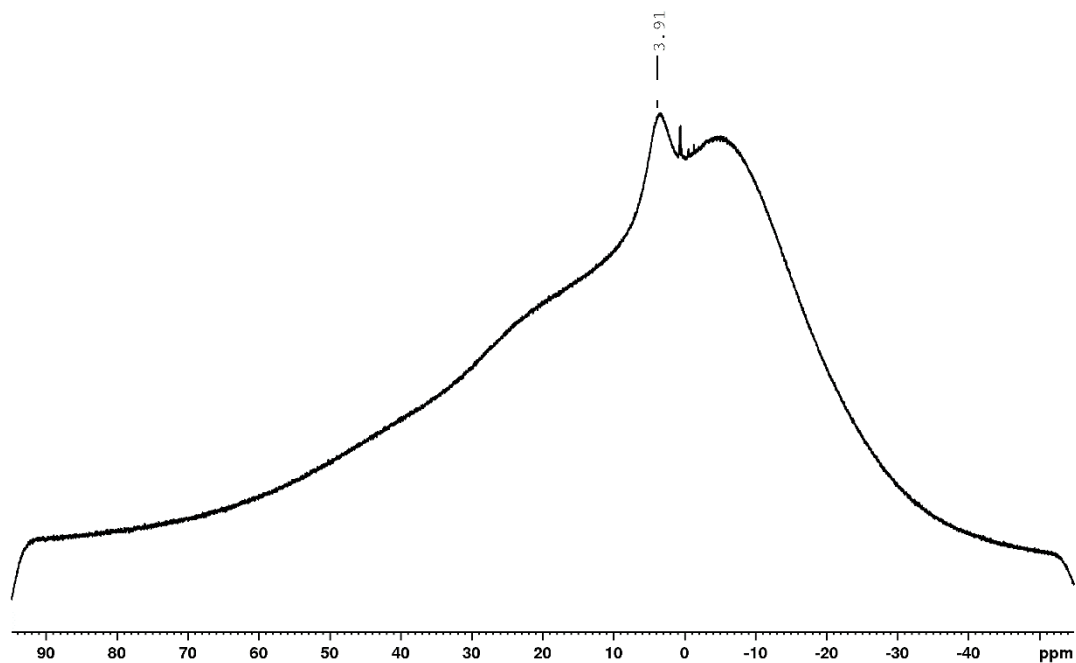


Figure 8-44.  $^{11}\text{B}\{^1\text{H}\}$  NMR spectrum of  $(\text{BF}_3\text{K})_4\text{-Per}$  in  $\text{DMSO-}d_6$  at 160 MHz.

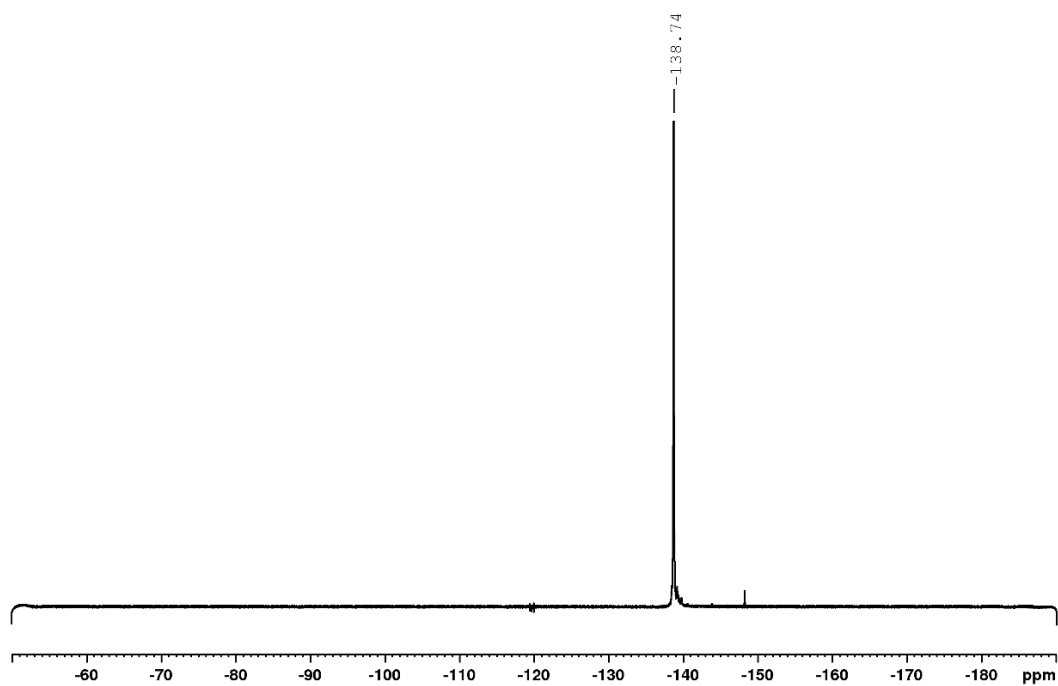


Figure 8-45.  $^{19}\text{F}\{^1\text{H}\}$  NMR spectrum of  $(\text{BF}_3\text{K})_4\text{-Per}$  in  $\text{DMSO-}d_6$  at 470 MHz.

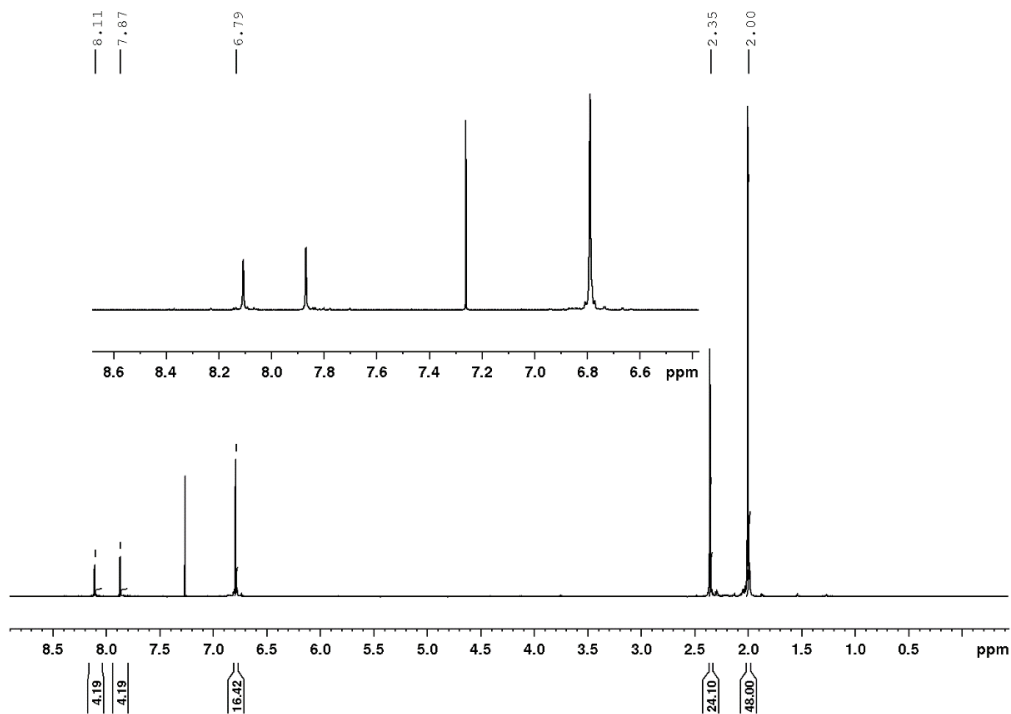
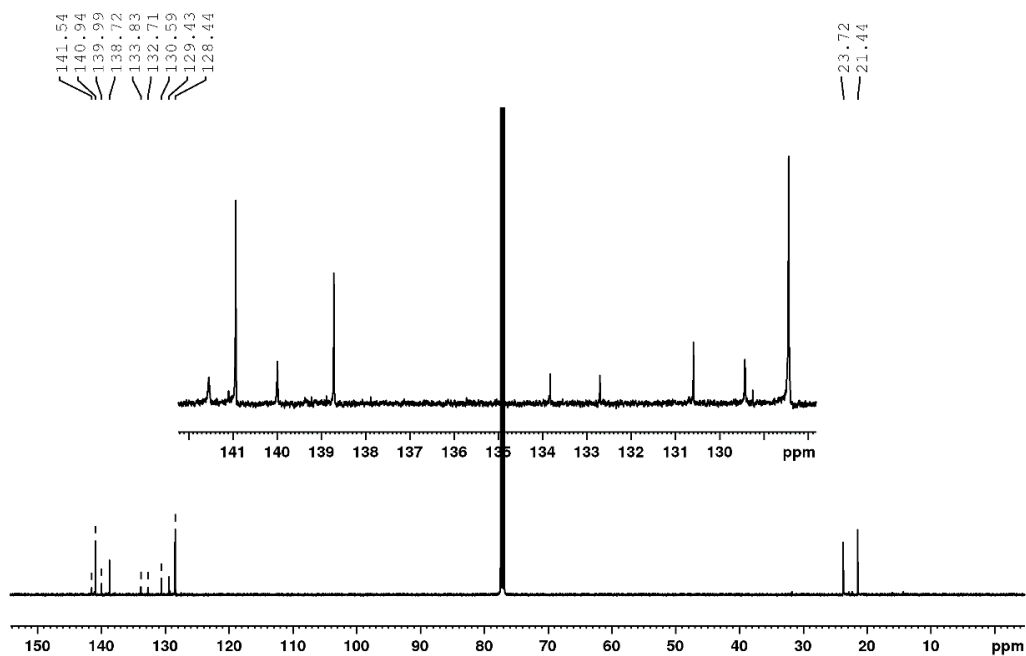
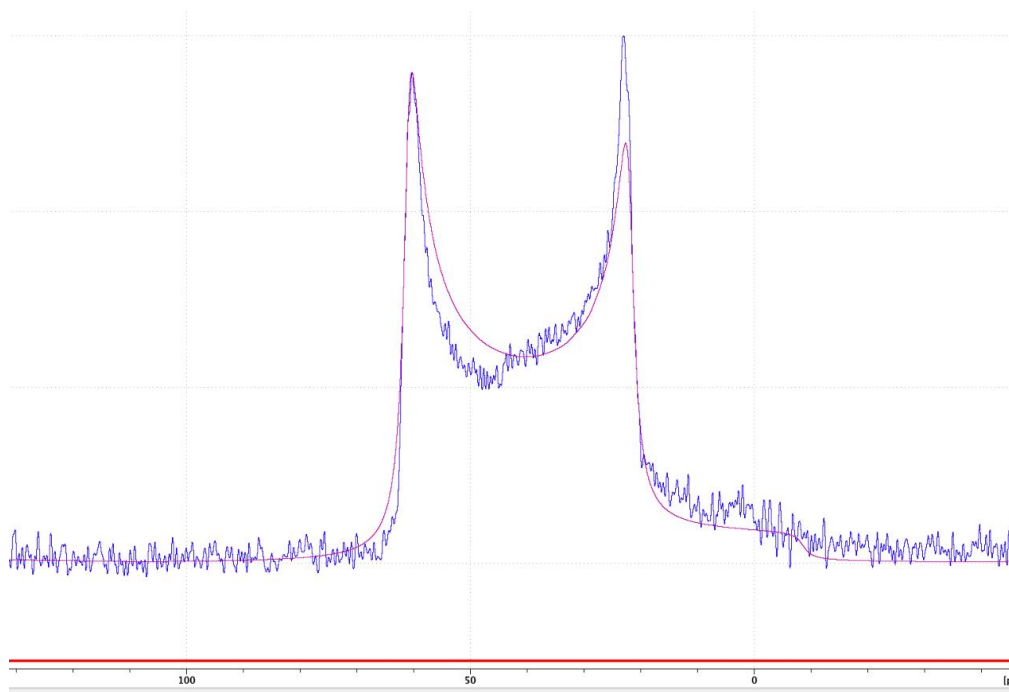


Figure 8-46.  $^1\text{H}$  NMR spectrum of  $(\text{Bmes}_2)_4\text{-Per}$  in  $\text{CDCl}_3$  at 500 MHz.



**Figure 8-47.**  $^{13}\text{C}\{^1\text{H}\}$  NMR spectrum of **(Bmes<sub>2</sub>)<sub>4</sub>-Per** in  $\text{CDCl}_3$  at 125 MHz.



**Figure 8-48.** Observed (blue) and simulated (red) solid state  $^{11}\text{B}\{^1\text{H}\}$  NMR spectrum of **(Bmes<sub>2</sub>)<sub>4</sub>-Per** at 128 MHz. The isotropic chemical shift ( $\delta_{\text{iso}}$ ) is 72.7 ppm, quadrupolar coupling constant  $C_Q = 4.63$  MHz, quadrupolar asymmetry parameter  $\eta_{\text{Quad}} = 0.0$ .

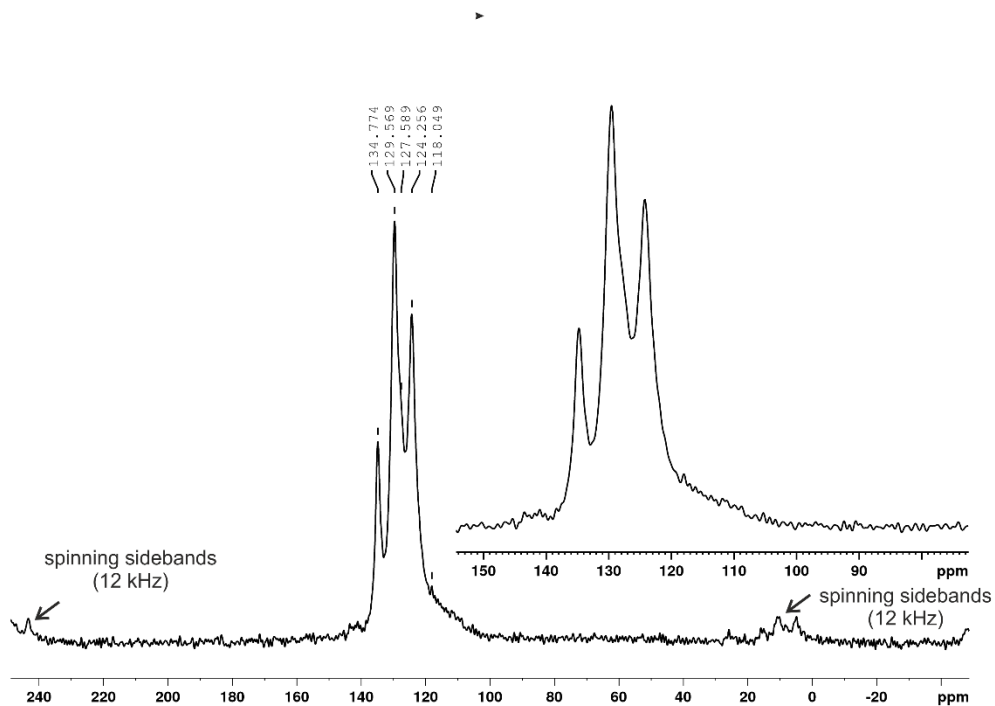


Figure 8-49. Solid state  $^{13}\text{C}\{^1\text{H}\}$ -CP spectrum of **(Br)<sub>4</sub>-Per** at 100 MHz. Measured at 12 kHz rotation.

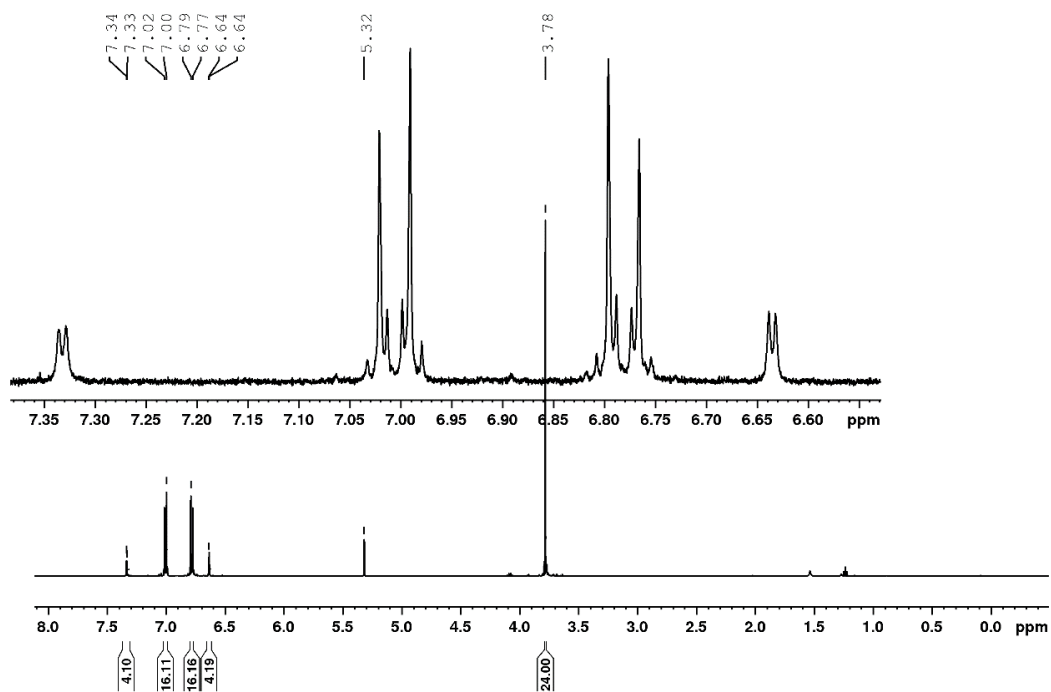


Figure 8-50.  $^1\text{H}$  NMR spectrum of **(DPA)<sub>4</sub>-Per** in  $\text{CD}_2\text{Cl}_2$  at 500 MHz.

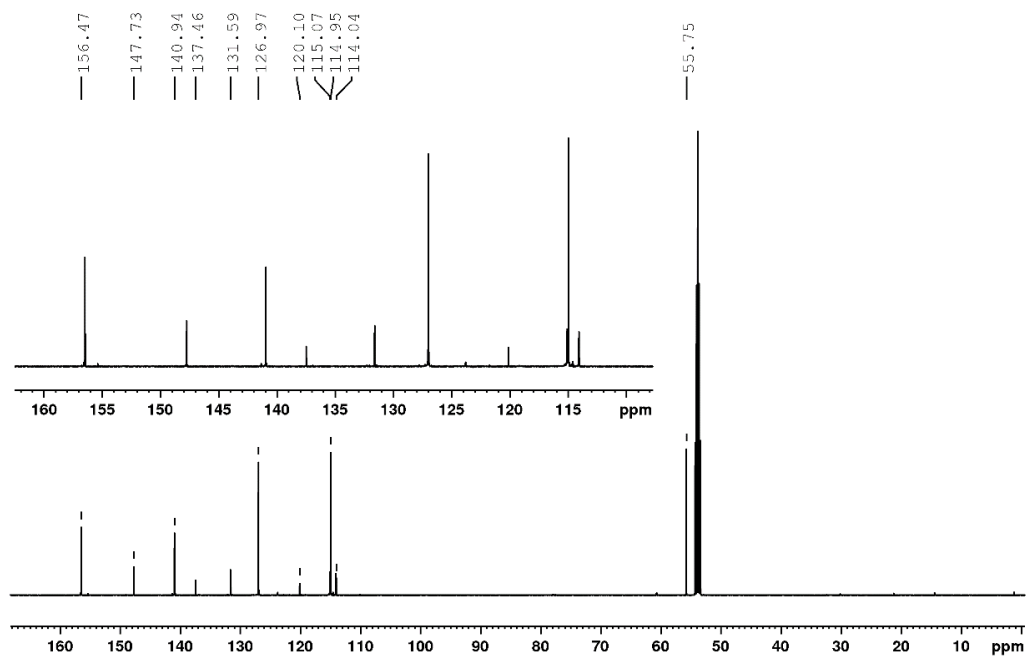


Figure 8-51.  $^{13}\text{C}\{^1\text{H}\}$  NMR spectrum of  $(\text{DPA})_4\text{-Per}$  in  $\text{CD}_2\text{Cl}_2$  at 125 MHz.

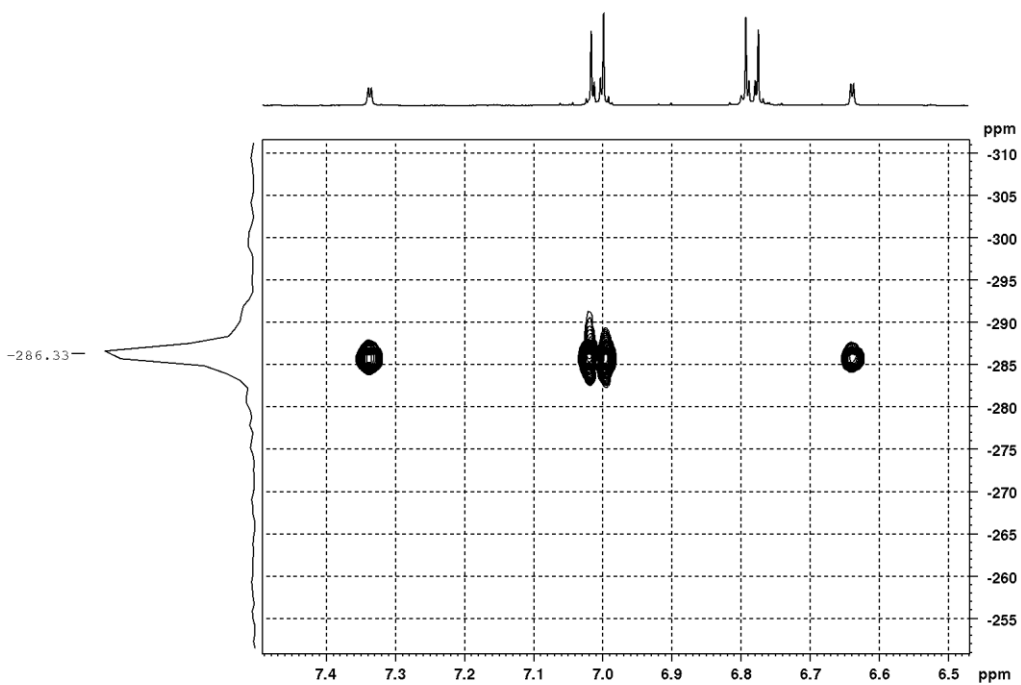


Figure 8-52.  $^{15}\text{N}, ^1\text{H}$  HMBC NMR spectrum of  $(\text{DPA})_4\text{-Per}$  in  $\text{CD}_2\text{Cl}_2$  at 500 MHz.

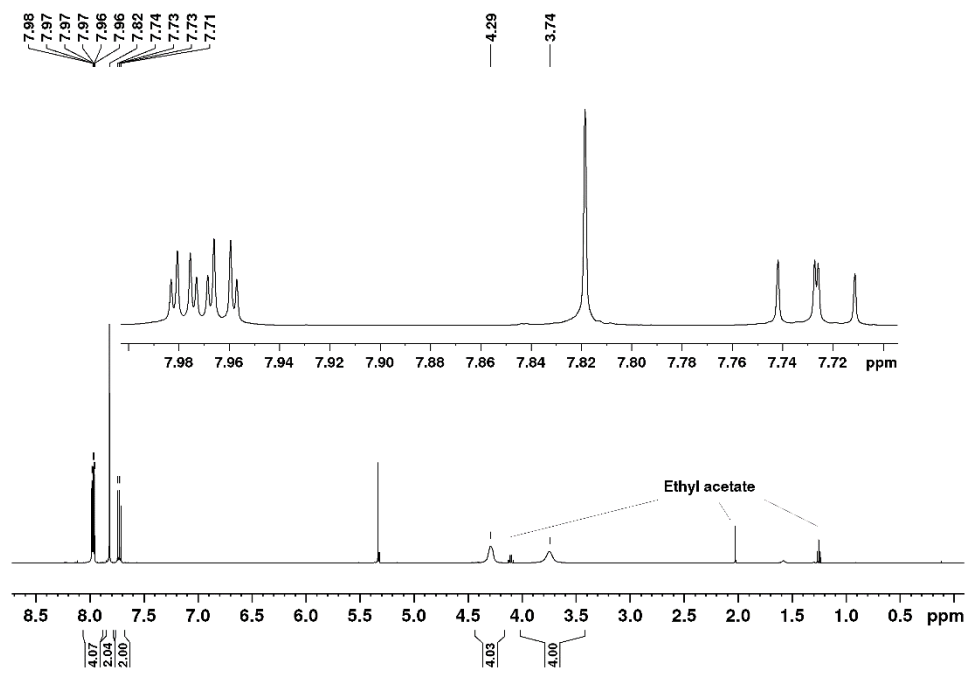


Figure 8-53.  $^1\text{H}$  NMR spectrum of compound 3-2 recorded in  $\text{CD}_2\text{Cl}_2$  at 500 MHz.

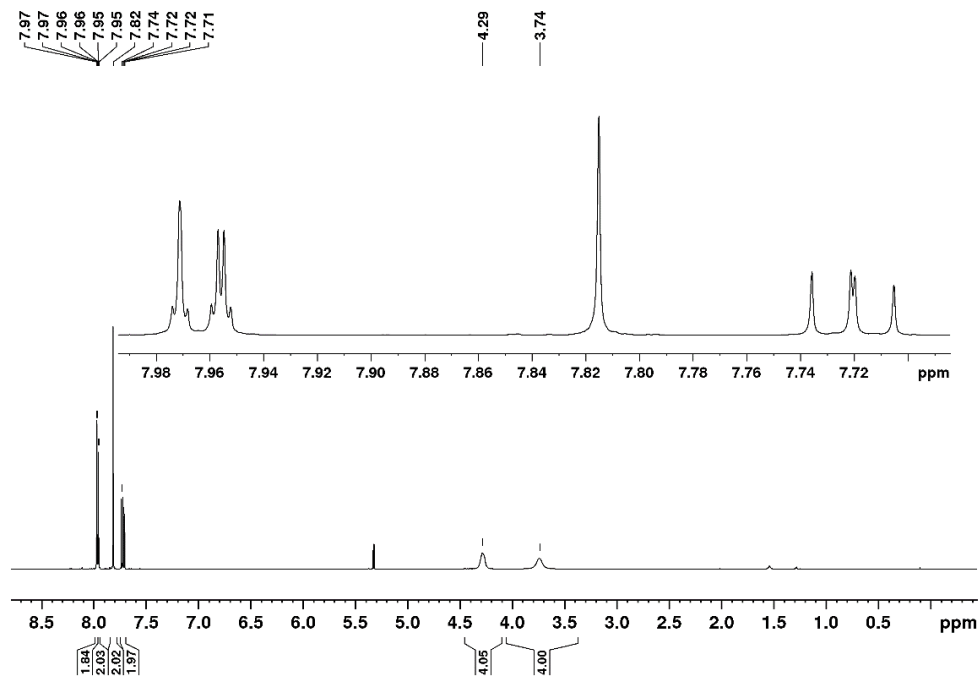


Figure 8-54.  $^1\text{H}$  NMR spectrum of compound 3-2 recorded in  $\text{CD}_2\text{Cl}_2$  at 500 MHz.

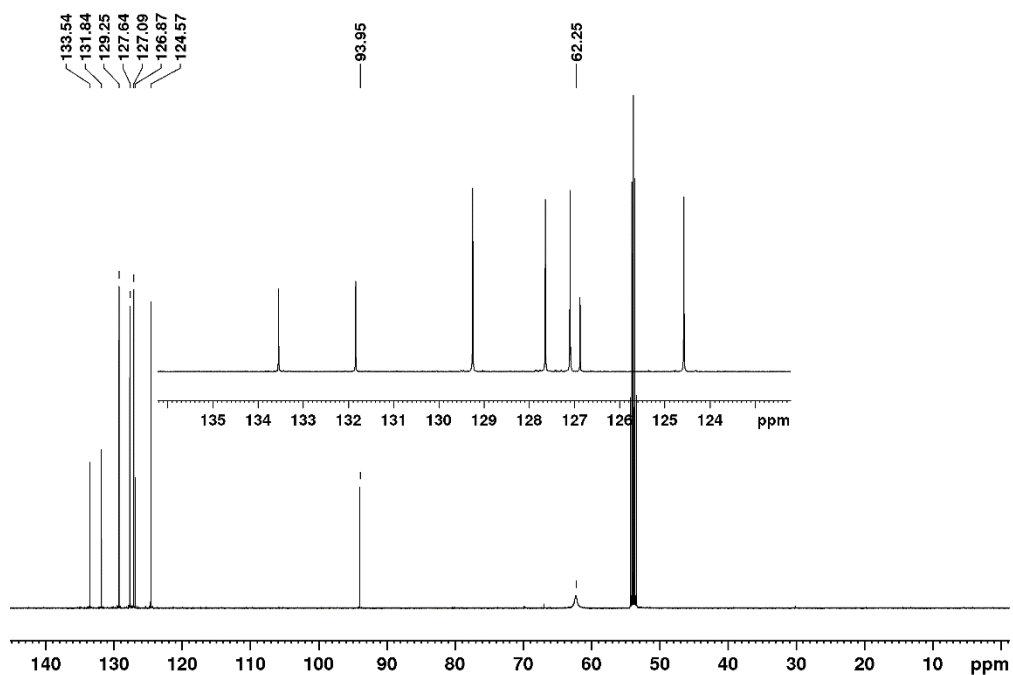


Figure 8-55.  $^{13}\text{C}\{^1\text{H}\}$  NMR spectrum of compound 3-2 recorded in  $\text{CD}_2\text{Cl}_2$  at 125 MHz.

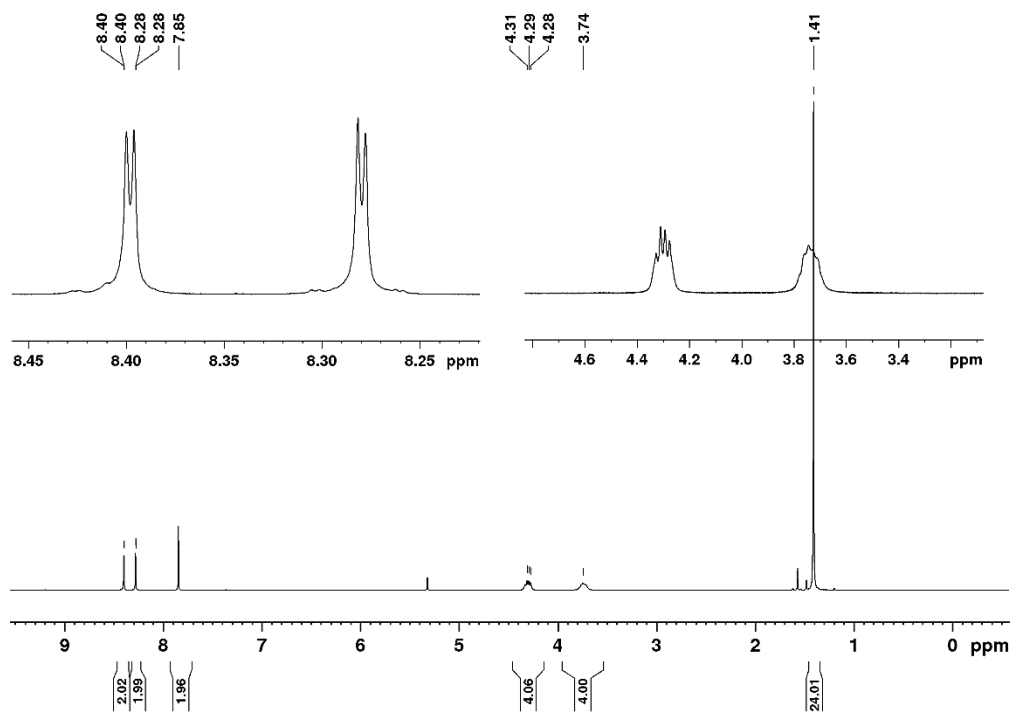


Figure 8-56.  $^1\text{H}$  NMR spectrum of compound 3-3 recorded in  $\text{CD}_2\text{Cl}_2$  at 300 MHz.

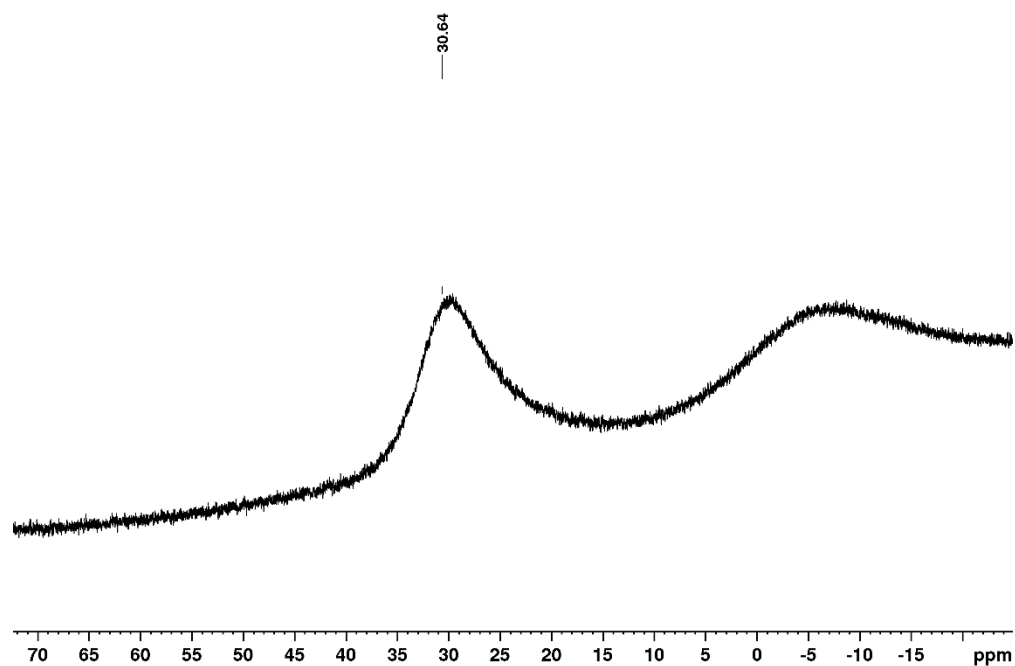


Figure 8-57.  $^{11}\text{B}\{^1\text{H}\}$  NMR spectrum of compound 3-3 recorded in  $\text{CD}_2\text{Cl}_2$  at 96 MHz.

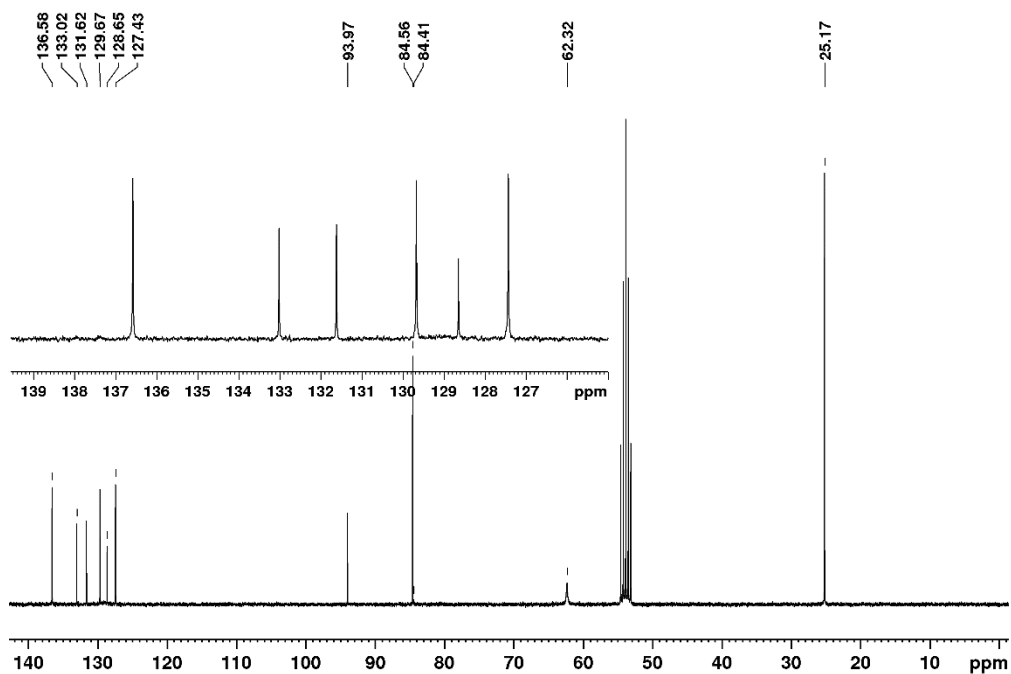


Figure 8-58.  $^{13}\text{C}\{^1\text{H}\}$  NMR spectrum of compound 3-3 recorded in  $\text{CD}_2\text{Cl}_2$  at 75 MHz.

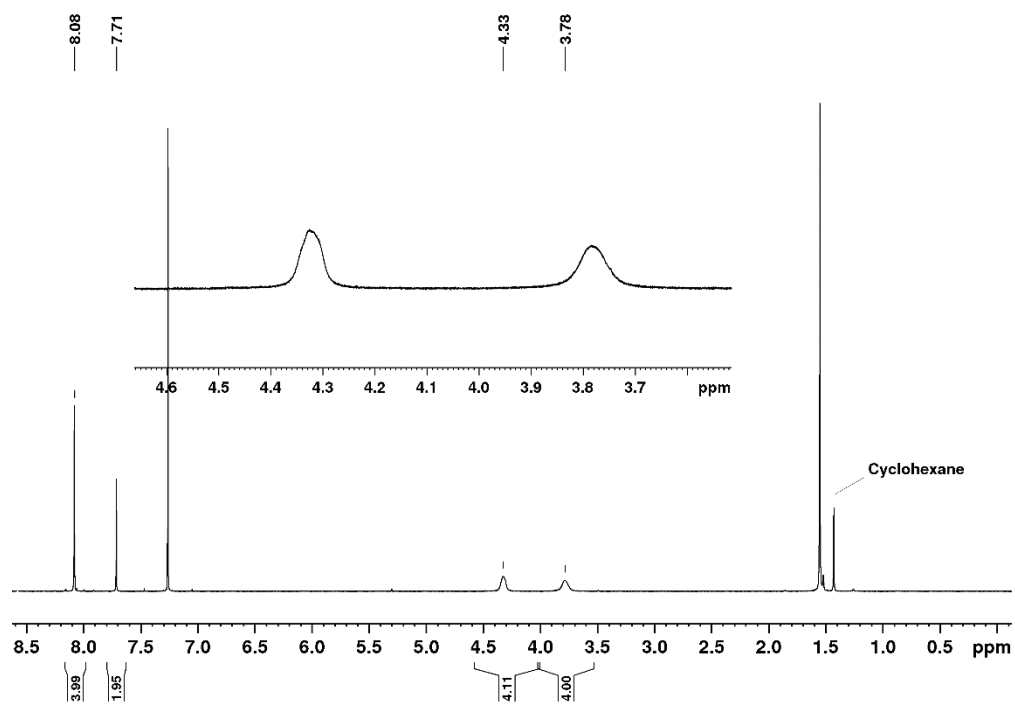


Figure 8-59.  $^1\text{H}$  NMR spectrum of compound 3-4 recorded in  $\text{CDCl}_3$  at 500 MHz.

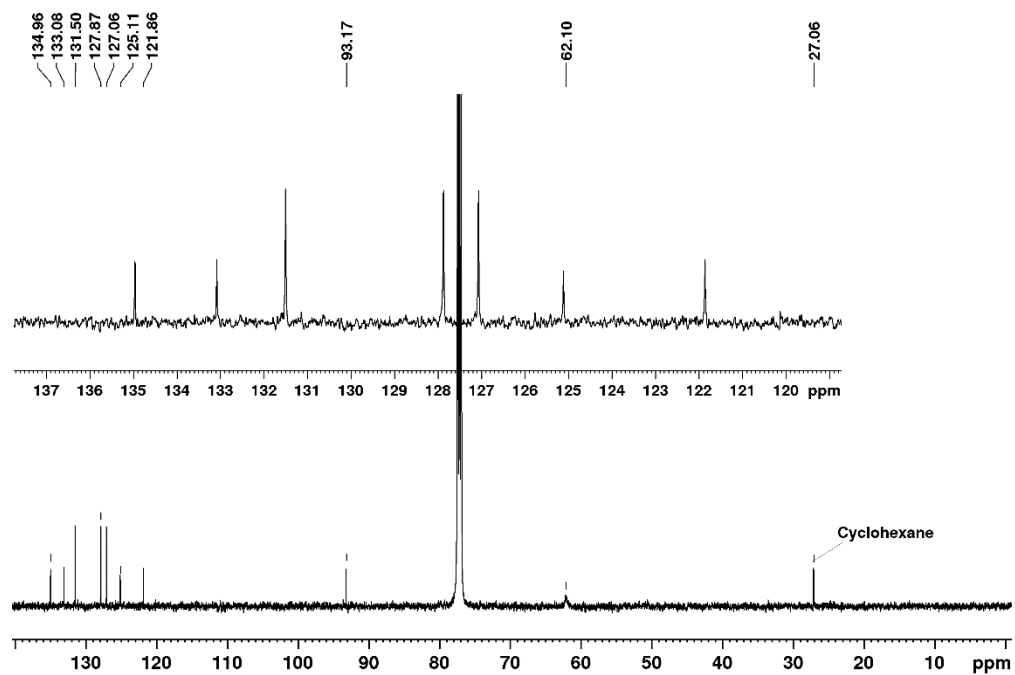


Figure 8-60.  $^{13}\text{C}\{^1\text{H}\}$  NMR spectrum of compound 3-4 recorded in  $\text{CD}_2\text{Cl}_2$  at 125 MHz.

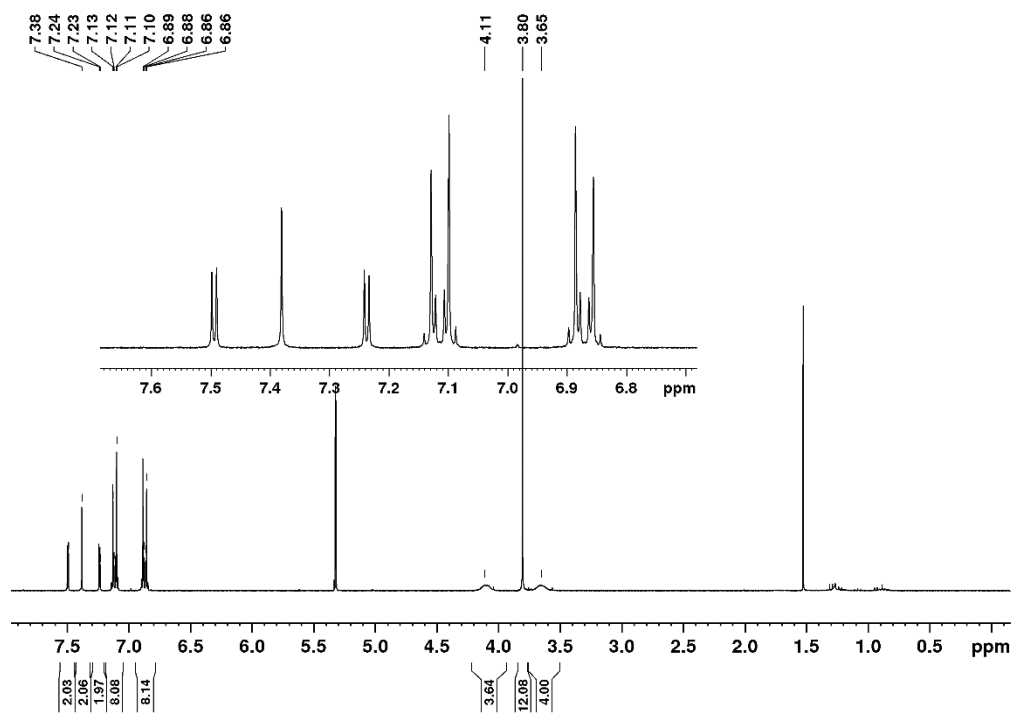


Figure 8-61. <sup>1</sup>H NMR spectrum of compound 3-5 recorded in CD<sub>2</sub>Cl<sub>2</sub> at 500 MHz.

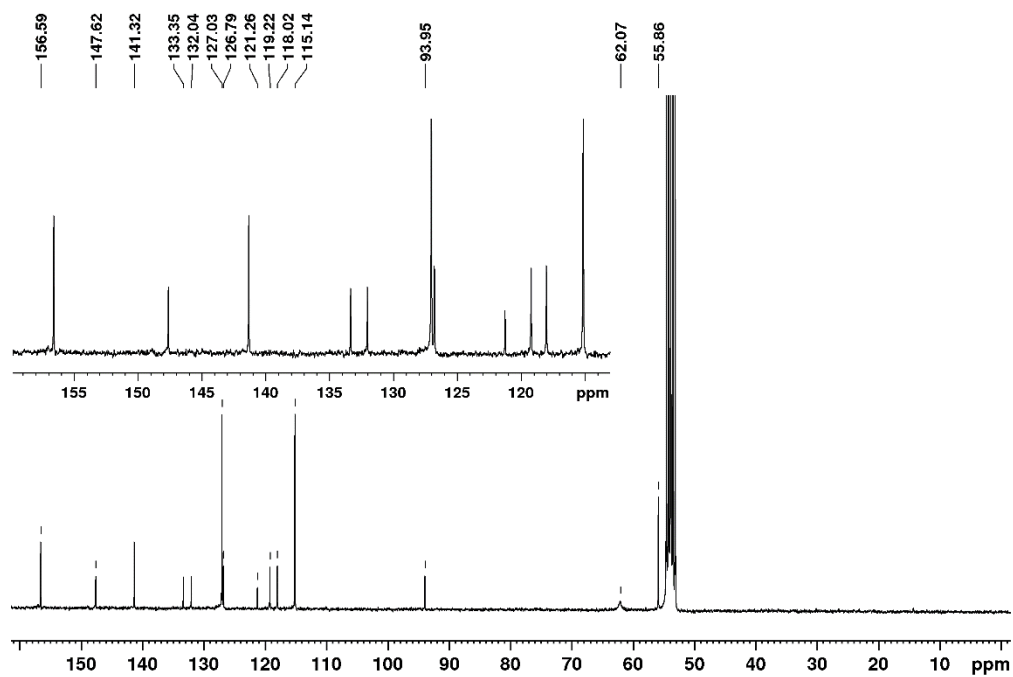


Figure 8-62. <sup>13</sup>C{<sup>1</sup>H} NMR spectrum of compound 3-5 recorded in CD<sub>2</sub>Cl<sub>2</sub> at 125 MHz.

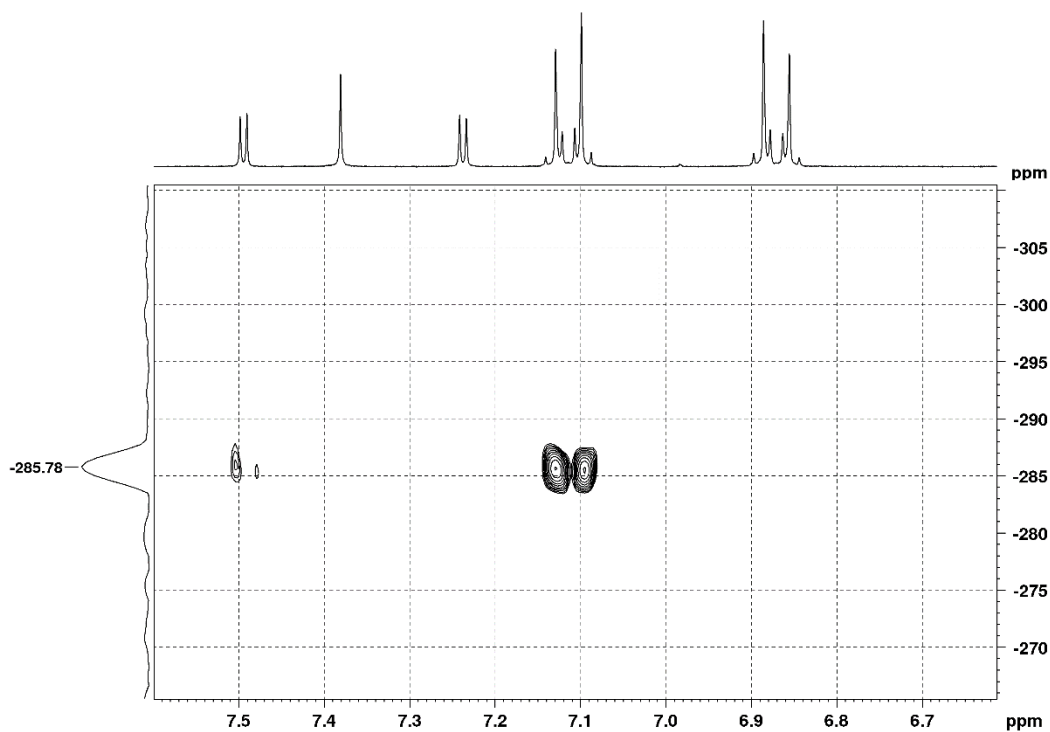


Figure 8-63.  $^{15}\text{N}$   $^1\text{H}$  HMBC NMR spectrum of compound **3-5** recorded in  $\text{CD}_2\text{Cl}_2$  at 500 MHz.

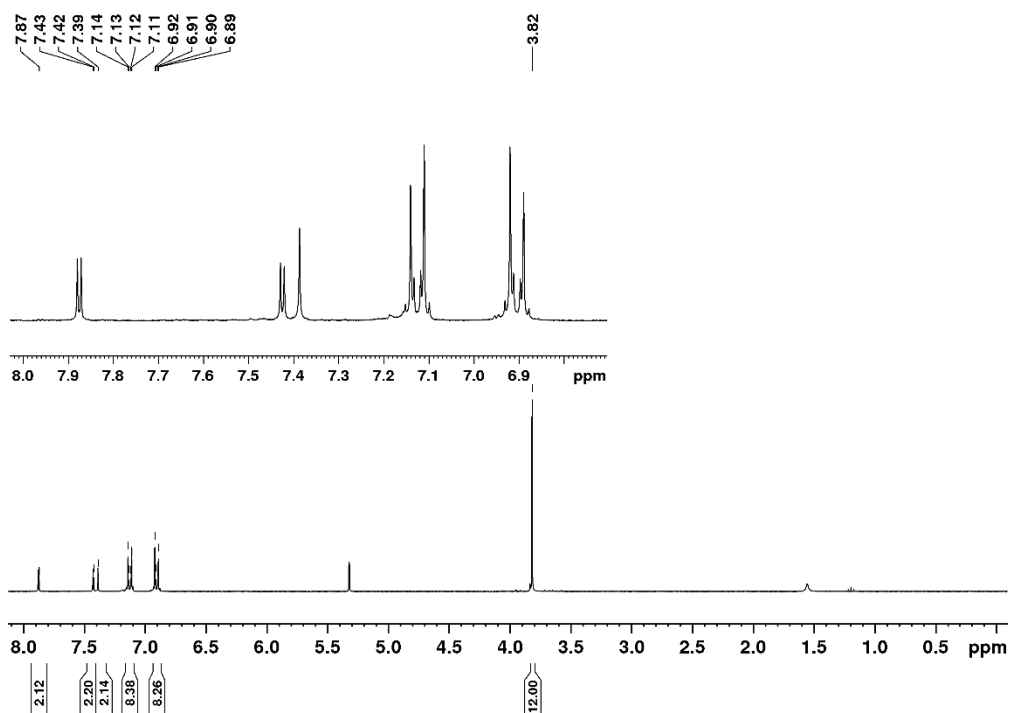


Figure 8-64.  $^1\text{H}$  NMR spectrum of compound **3-6** recorded in  $\text{CD}_2\text{Cl}_2$  at 500 MHz.

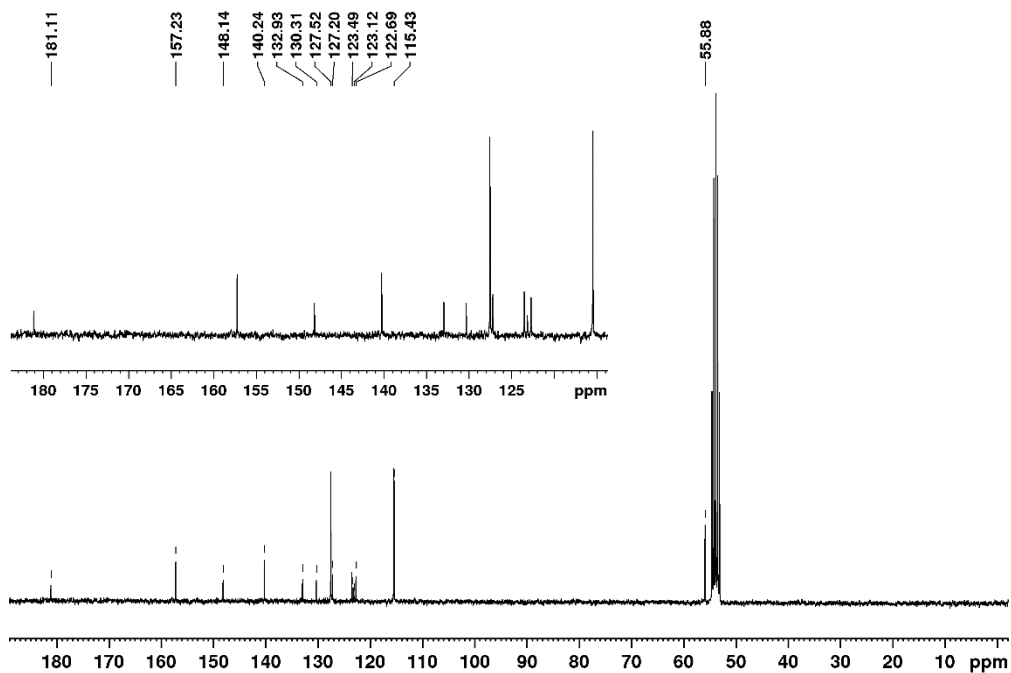


Figure 8-65.  $^{13}\text{C}\{^1\text{H}\}$  NMR spectrum of compound 3-6 recorded in  $\text{CD}_2\text{Cl}_2$  at 125 MHz.

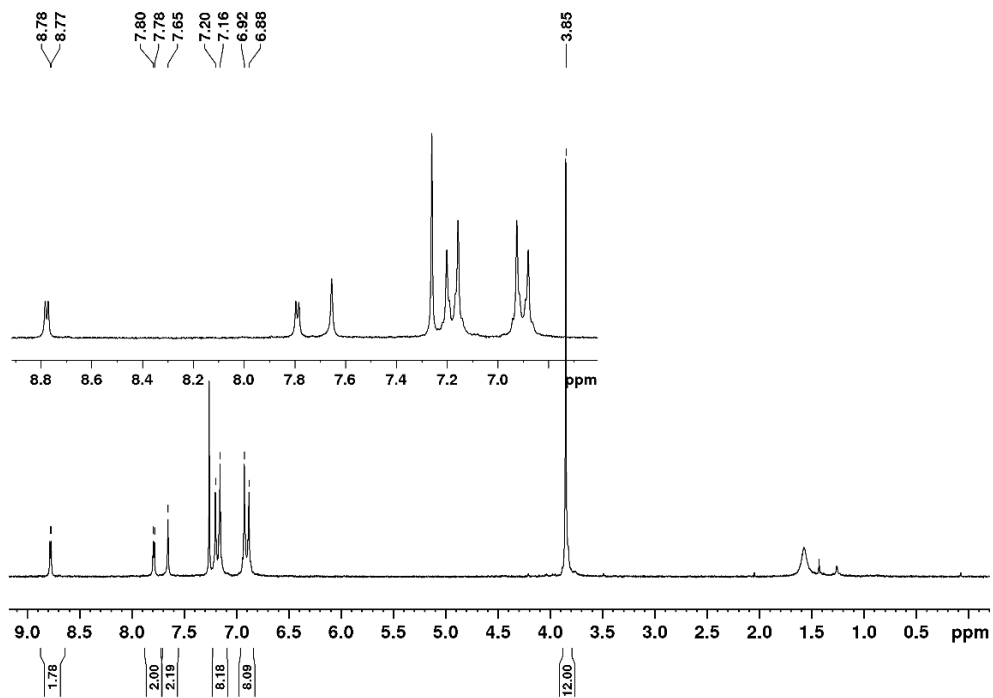


Figure 8-66.  $^1\text{H}$  NMR spectrum of compound 3-7 recorded in  $\text{CDCl}_3$  at 200 MHz.

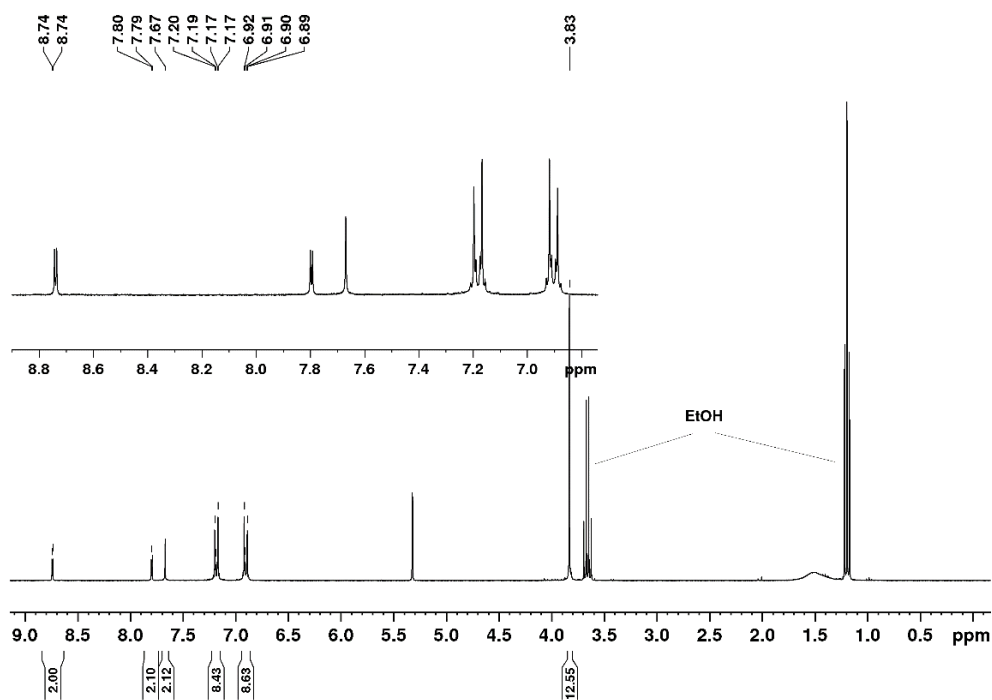


Figure 8-67. <sup>1</sup>H NMR spectrum of compound 3-7 recorded in CD<sub>2</sub>Cl<sub>2</sub> at 300 MHz.

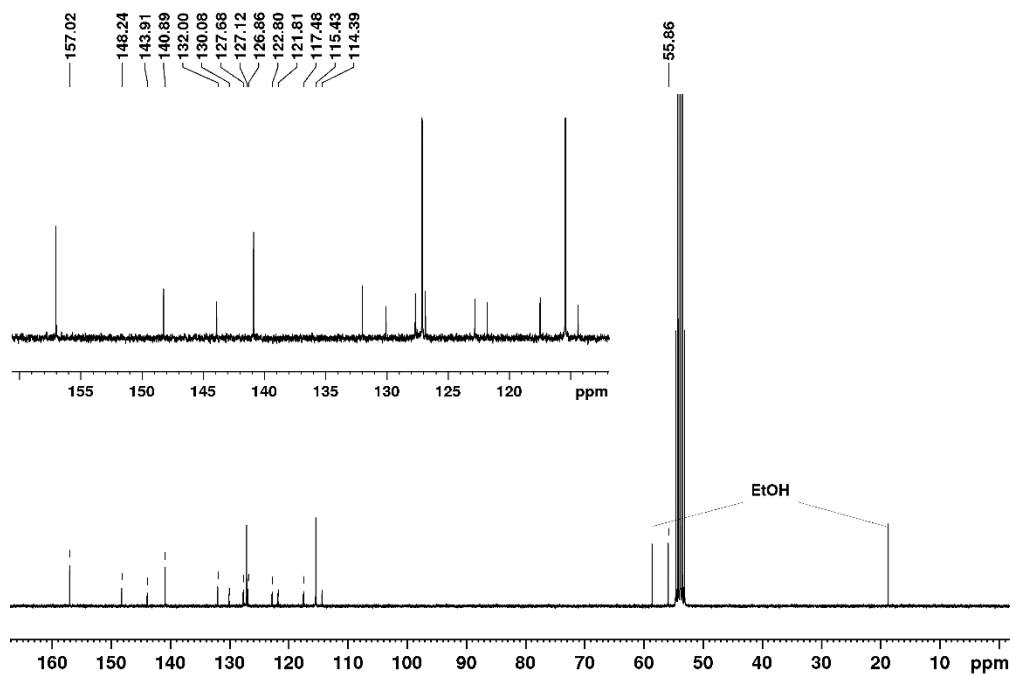


Figure 8-68. <sup>13</sup>C{<sup>1</sup>H} NMR spectrum of compound 3-7 recorded in CD<sub>2</sub>Cl<sub>2</sub> at 75 MHz.

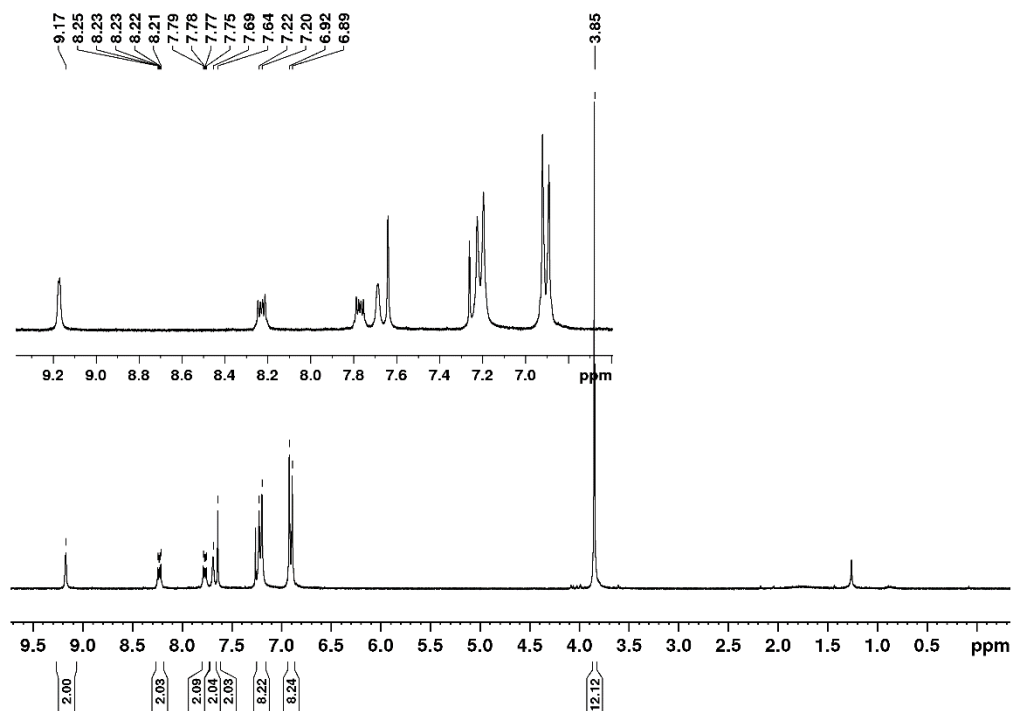


Figure 8-69. <sup>1</sup>H NMR spectrum of compound 3-8 recorded in CDCl<sub>3</sub> at 300 MHz.

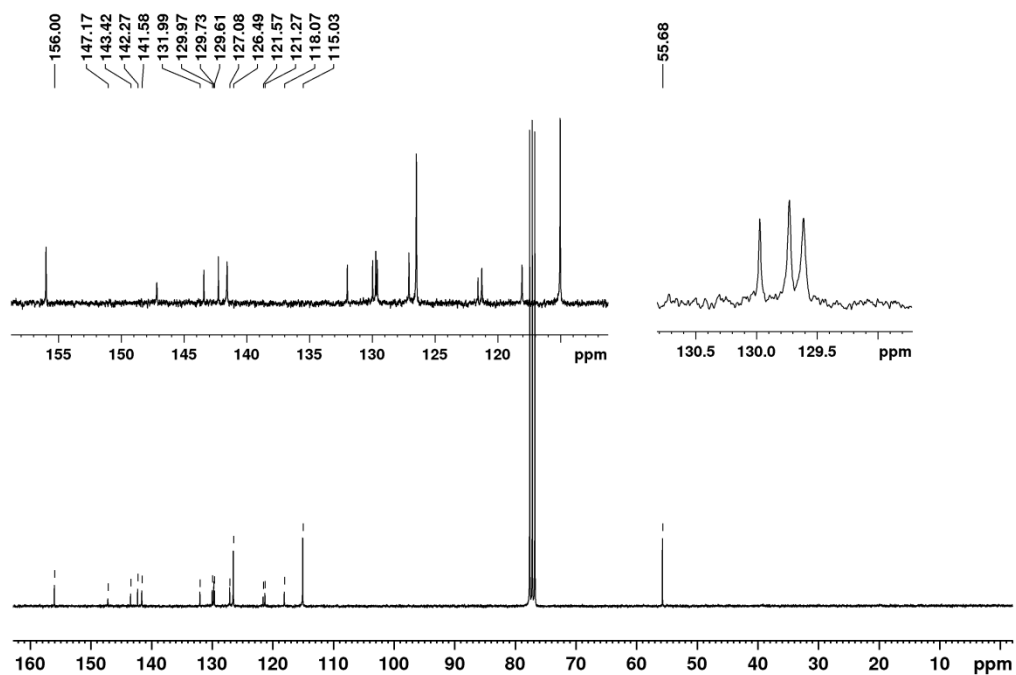


Figure 8-70. <sup>13</sup>C{<sup>1</sup>H} NMR spectrum of compound 3-8 recorded in CDCl<sub>3</sub> at 75 MHz.

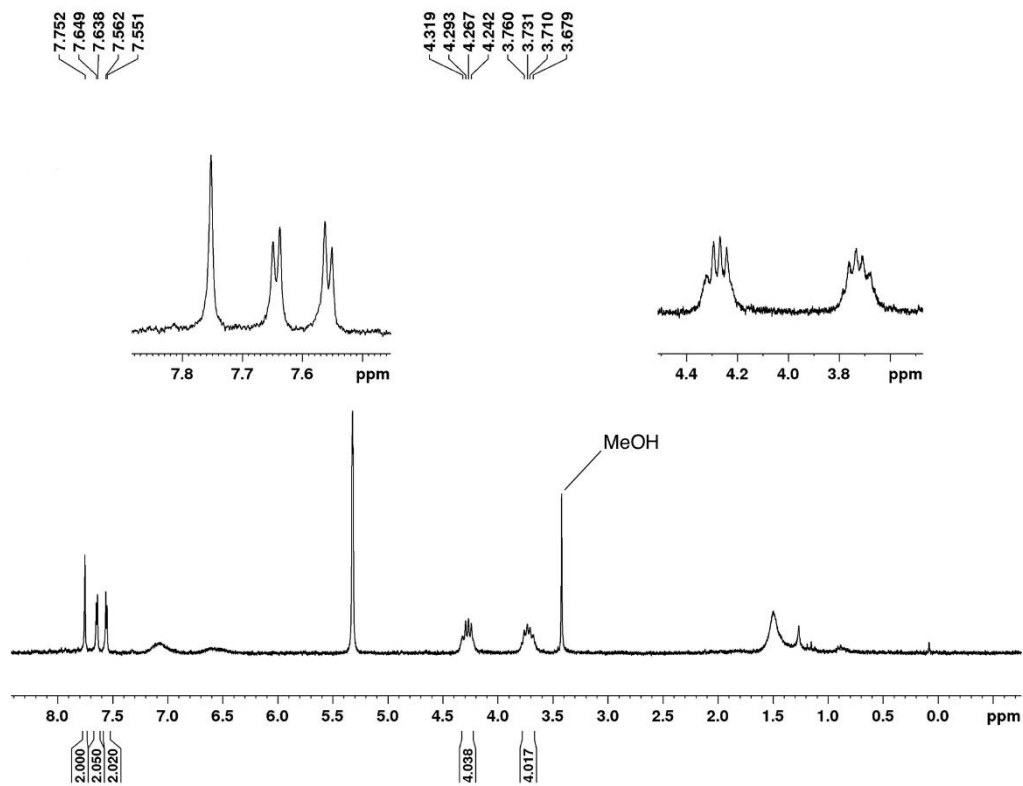


Figure 8-71. <sup>1</sup>H NMR spectrum of compound 3-4' recorded in CD<sub>2</sub>Cl<sub>2</sub> at 300 MHz.

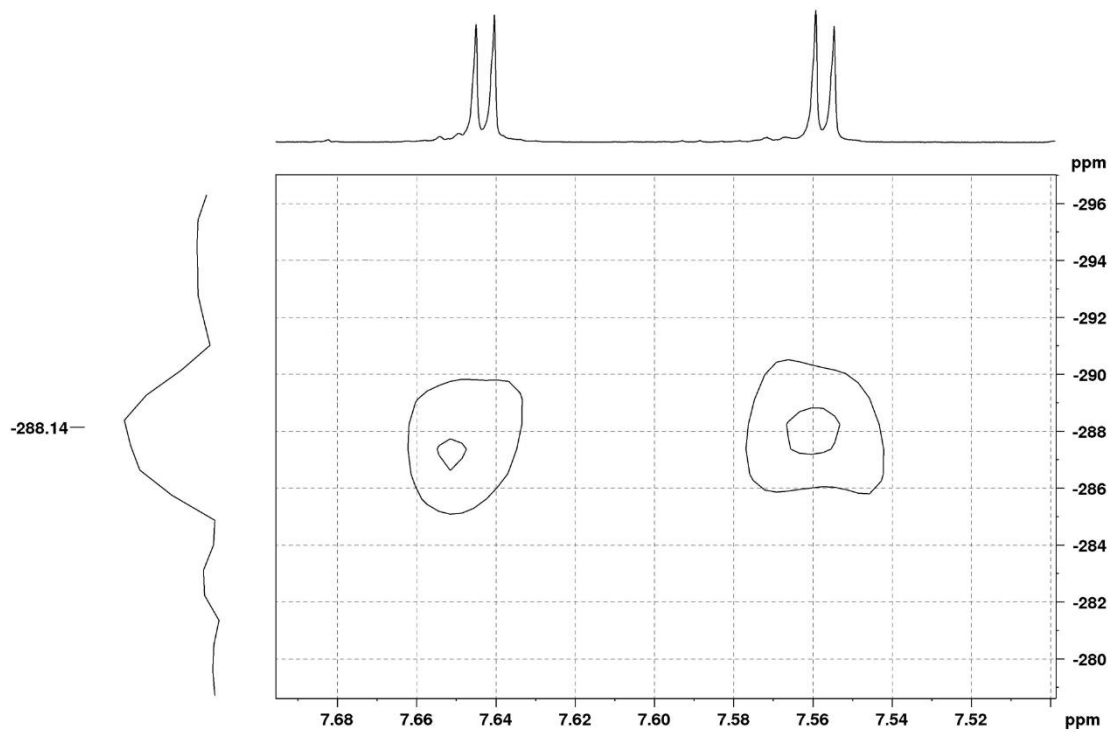


Figure 8-72. <sup>15</sup>N <sup>1</sup>H HMBC NMR spectrum of compound 3-4' recorded in CD<sub>2</sub>Cl<sub>2</sub> at 500 MHz.

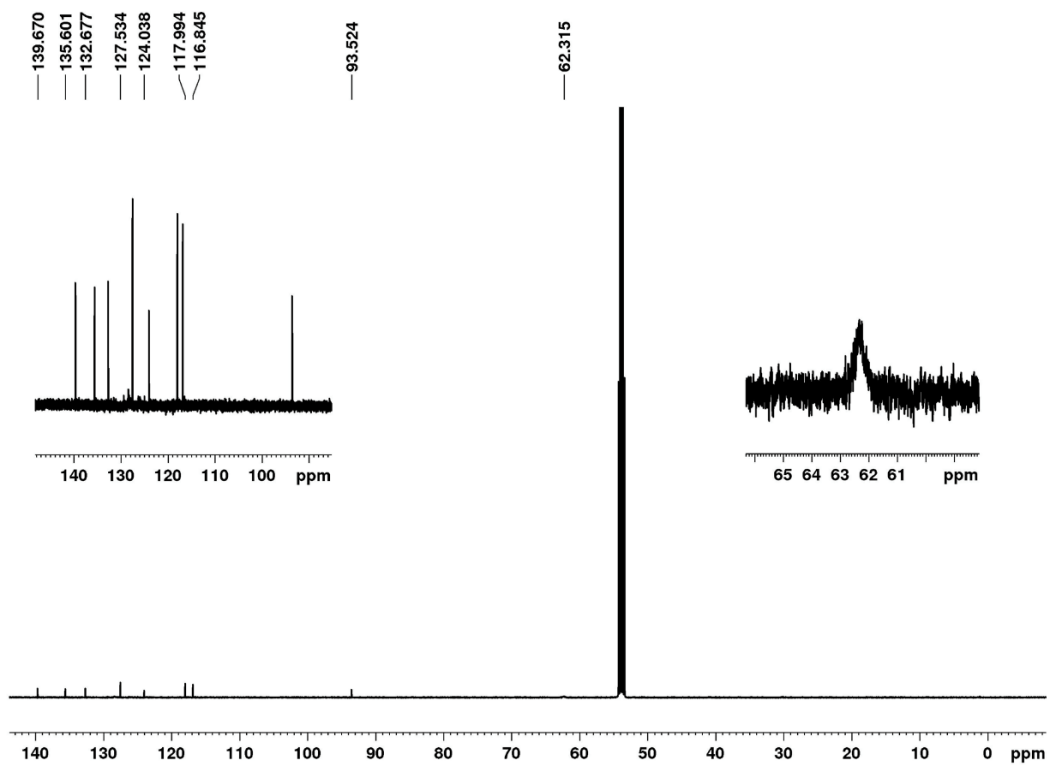


Figure 8-73.  $^{13}\text{C}\{^1\text{H}\}$  NMR spectrum of compound 3-4' recorded in  $\text{CD}_2\text{Cl}_2$  at 75 MHz.

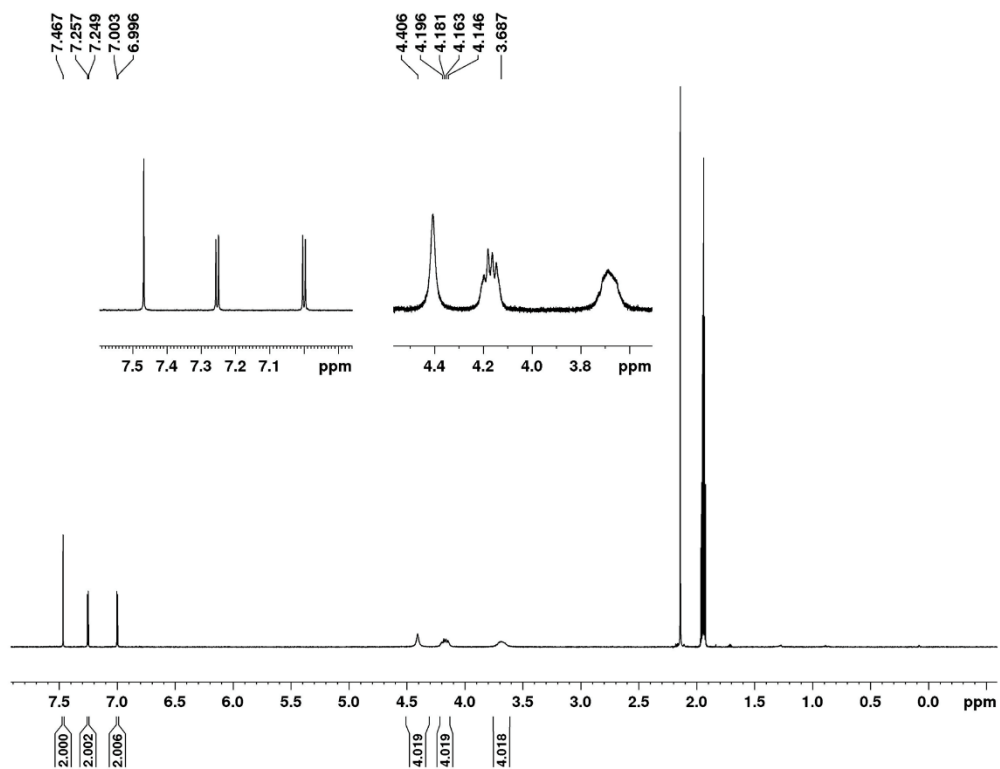


Figure 8-74.  $^1\text{H}$  NMR spectrum of compound 3-5' recorded in  $\text{CD}_3\text{CN}$  at 300 MHz.

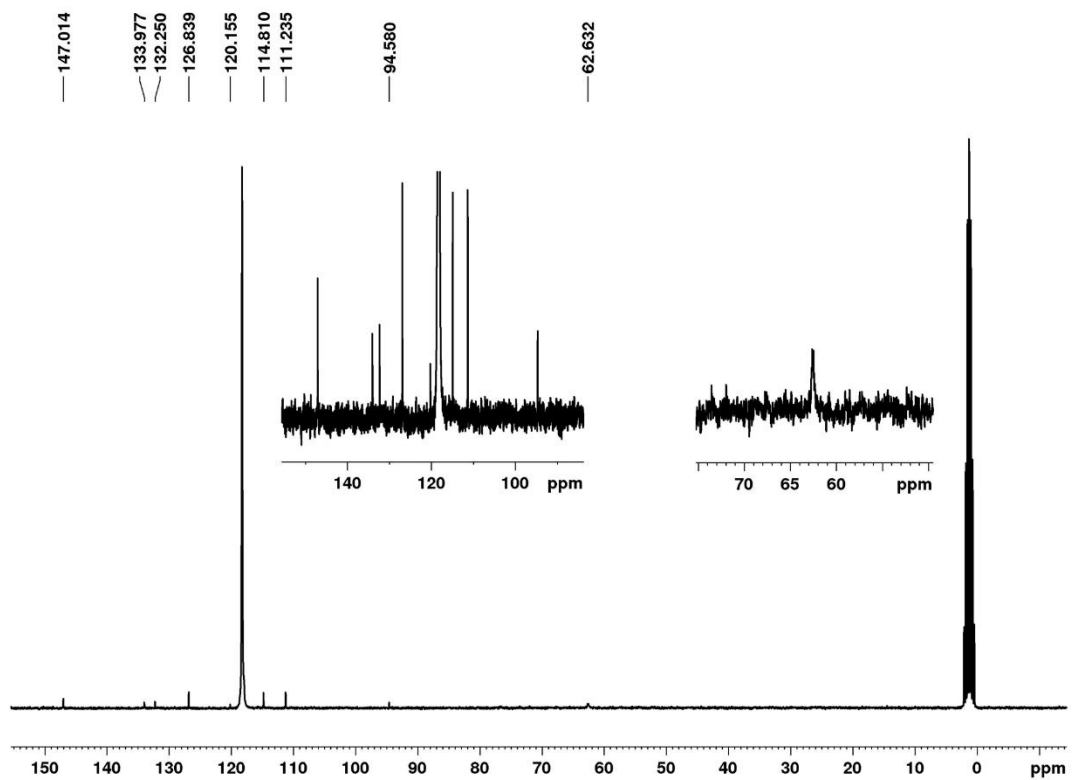


Figure 8-75.  $^{13}\text{C}\{^1\text{H}\}$  NMR spectrum of compound 3-5' recorded in  $\text{CD}_3\text{CN}$  at 75 MHz.

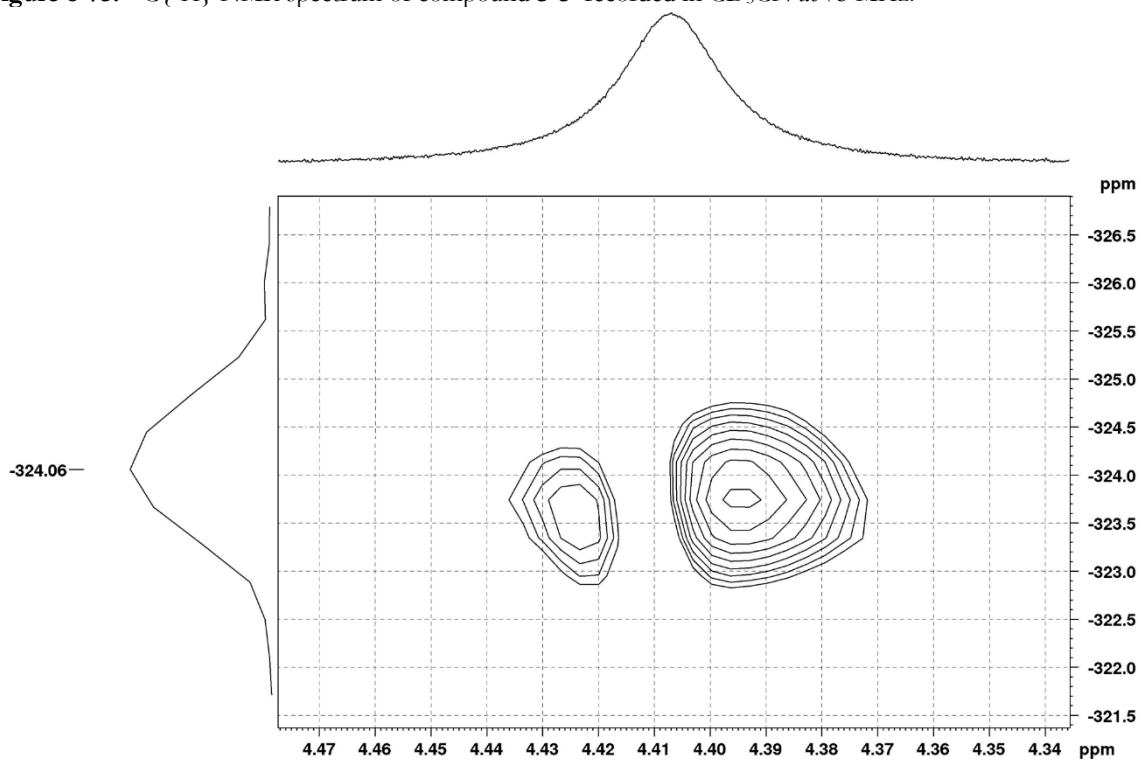


Figure 8-76.  $^{15}\text{N}\ ^1\text{H}$  HMBC NMR spectrum of compound 3-5' recorded in  $\text{CD}_3\text{CN}$  at 300 MHz.

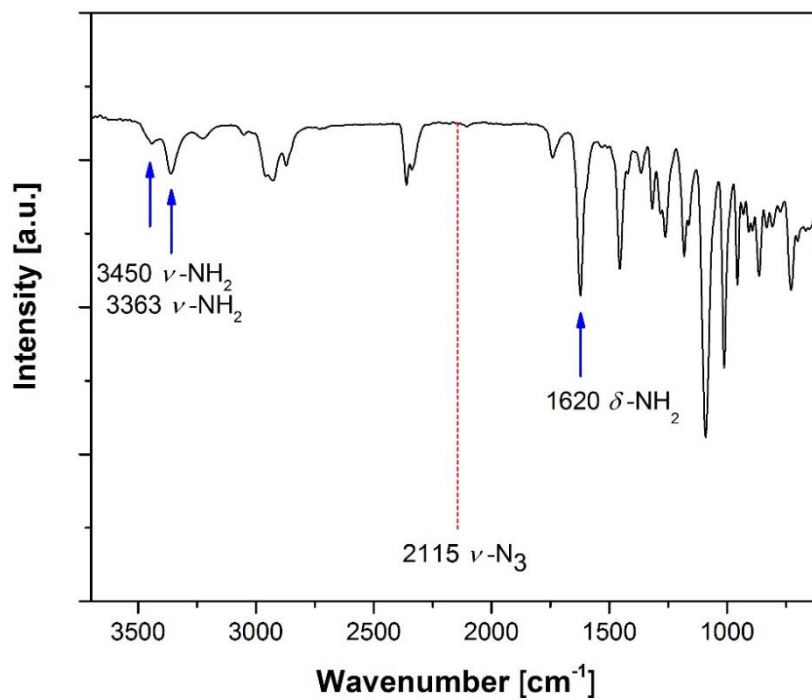


Figure 8-77. FTIR spectrum of the crude reaction mixture of compound 3-5'.

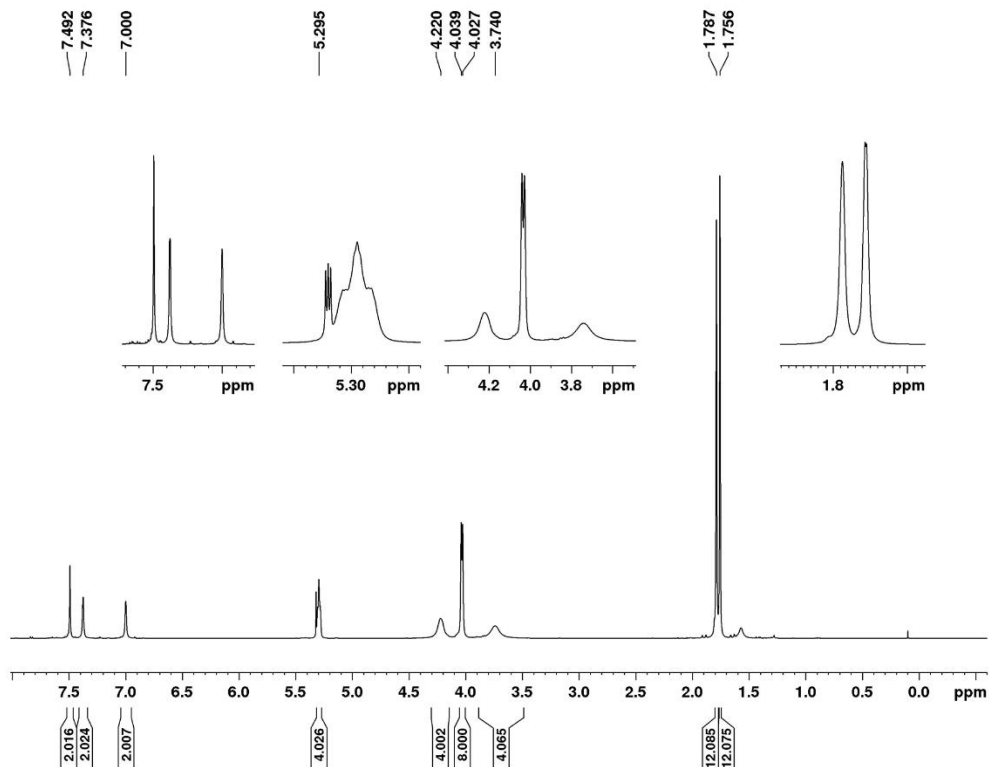


Figure 8-78. <sup>1</sup>H NMR spectrum of compound 3-6' recorded in CD<sub>2</sub>Cl<sub>2</sub> at 500 MHz.

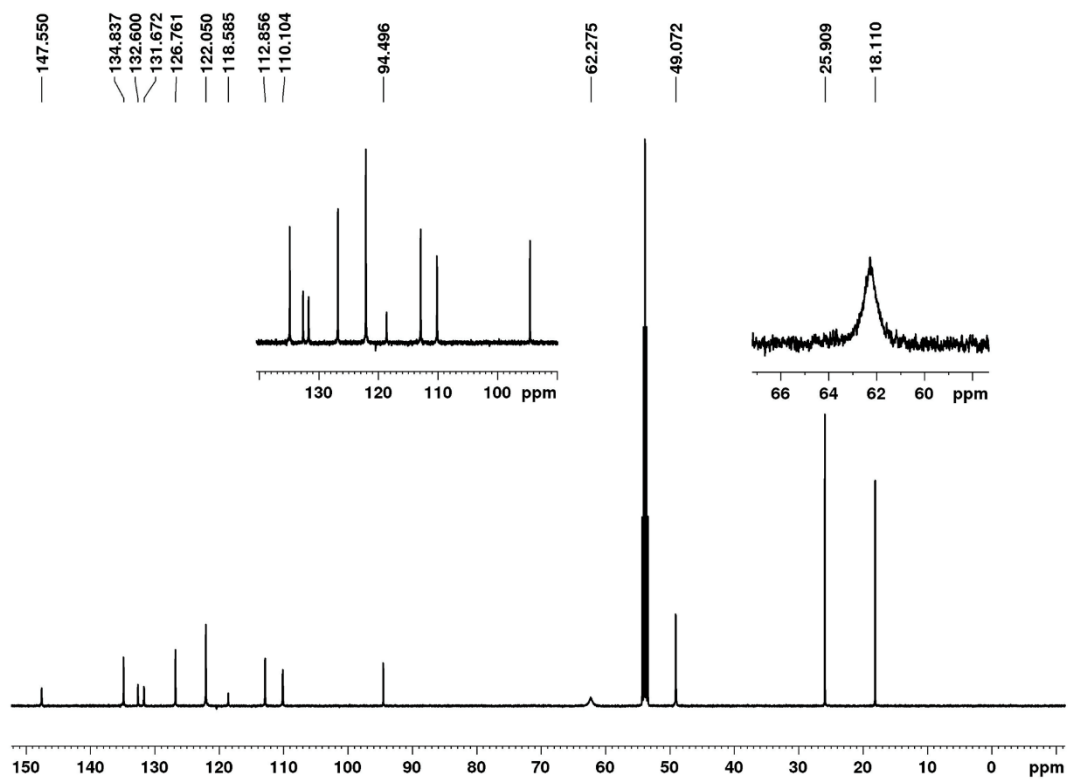


Figure 8-79.  $^{13}\text{C}\{^1\text{H}\}$  NMR spectrum of compound **3-6'** recorded in  $\text{CD}_2\text{Cl}_2$  at 125 MHz.

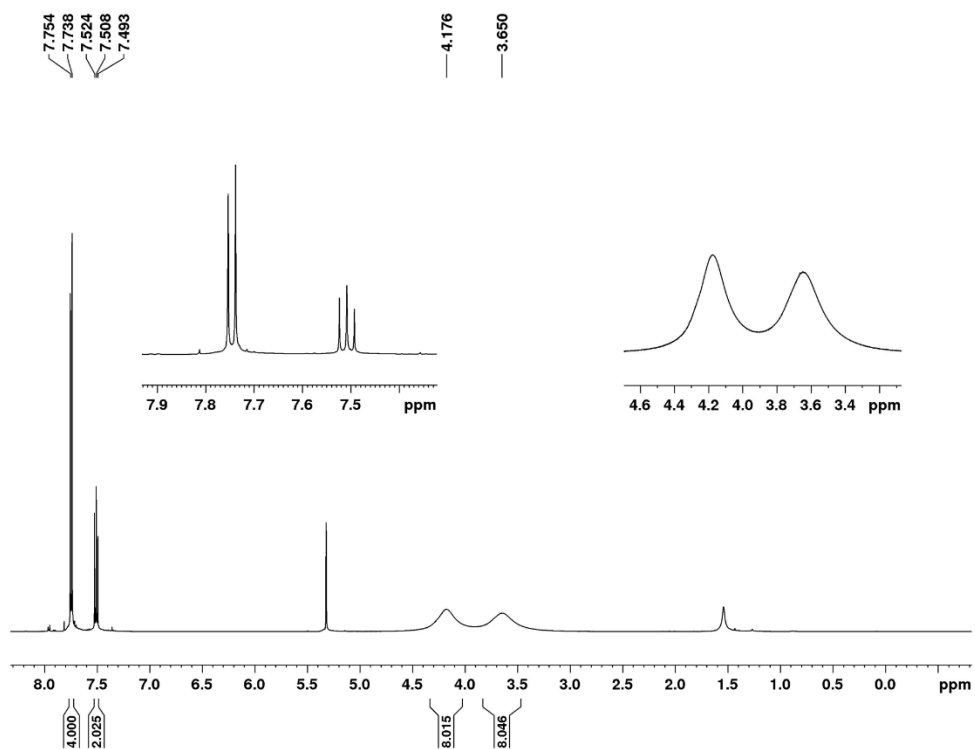


Figure 8-80.  $^1\text{H}$  NMR spectrum of compound **3-10** recorded in  $\text{CD}_2\text{Cl}_2$  at 500 MHz.

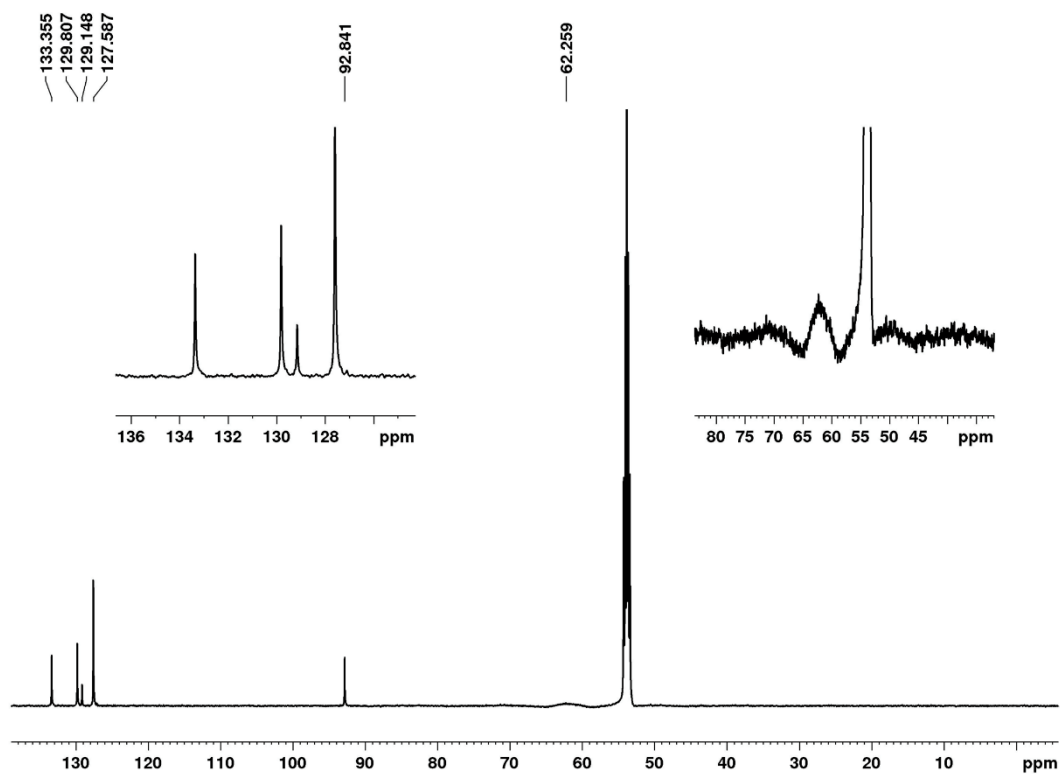


Figure 8-81.  $^{13}\text{C}\{^1\text{H}\}$  NMR spectrum of compound 3-10 recorded in  $\text{CD}_2\text{Cl}_2$  at 125 MHz.

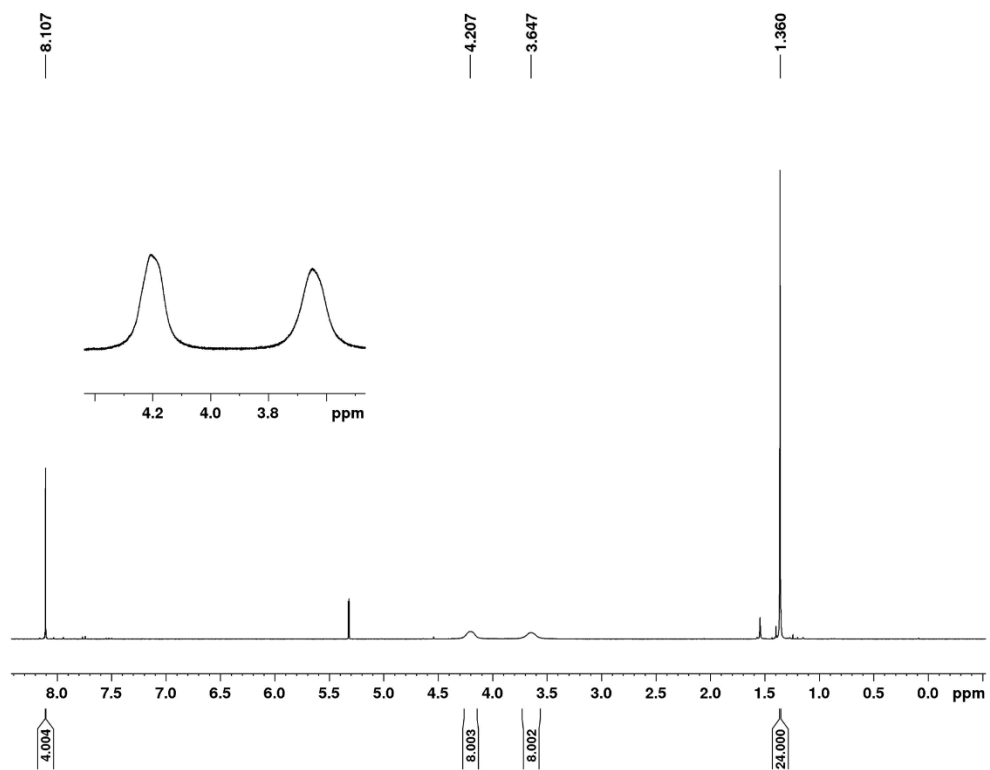


Figure 8-82.  $^1\text{H}$  NMR spectrum of compound 3-11 recorded in  $\text{CD}_2\text{Cl}_2$  at 300 MHz.

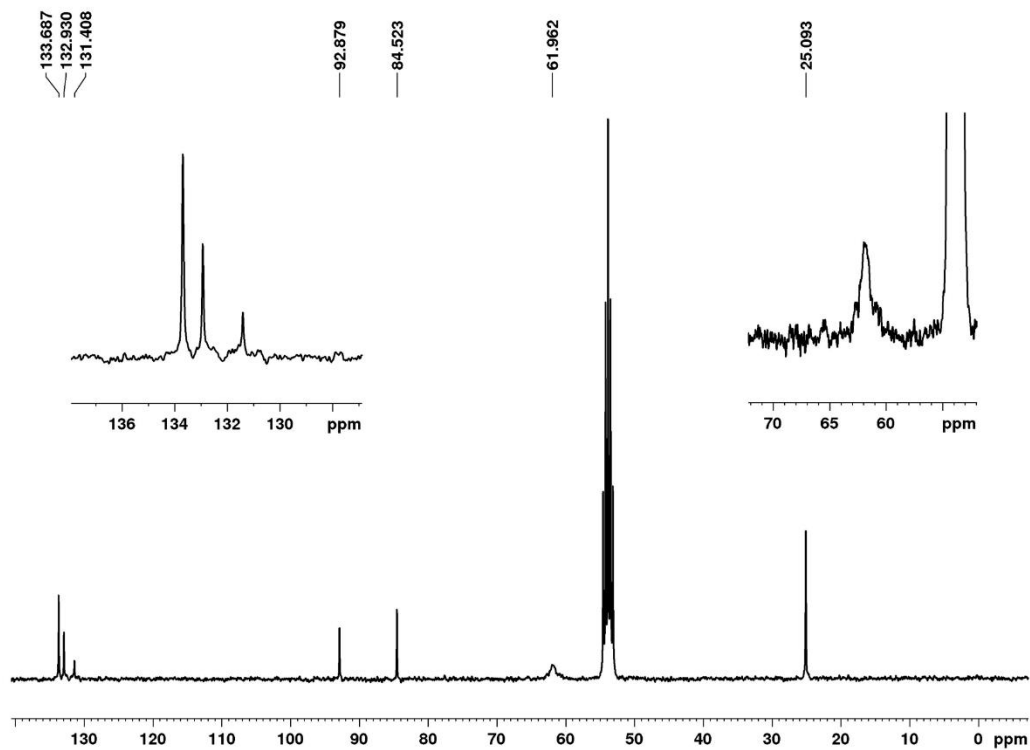


Figure 8-83.  $^{13}\text{C}\{^1\text{H}\}$  NMR spectrum of compound 3-11 recorded in  $\text{CD}_2\text{Cl}_2$  at 75 MHz.

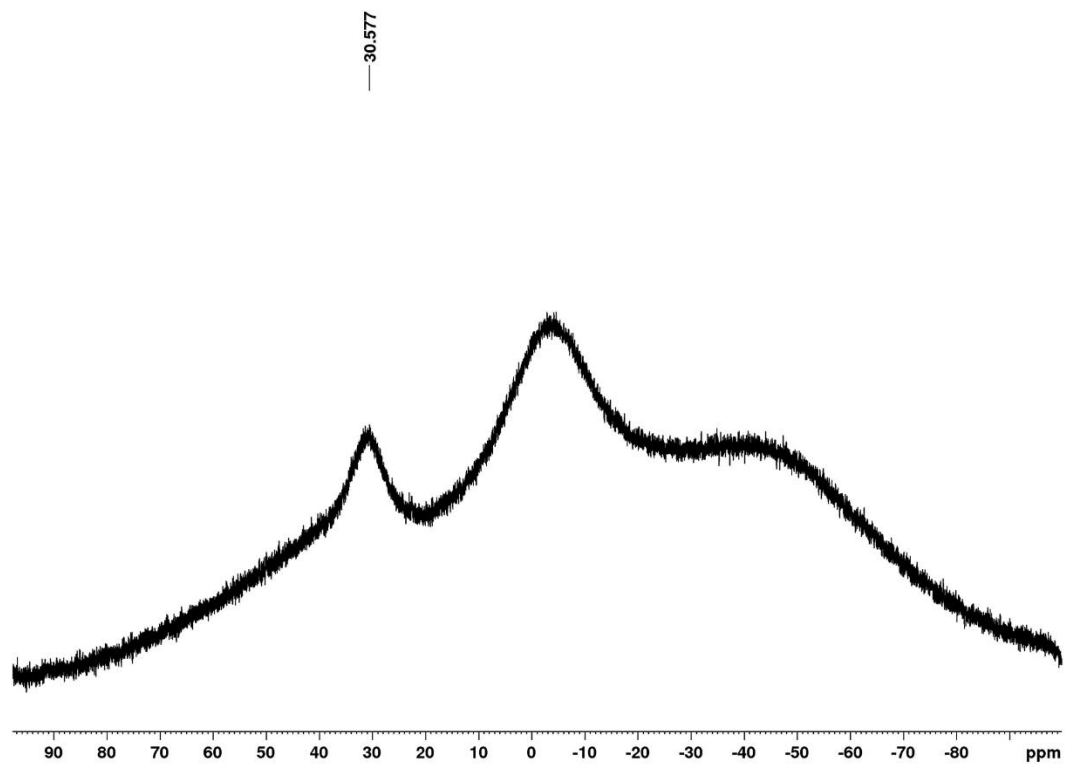


Figure 8-84.  $^{13}\text{B}$  NMR spectrum of compound 3-11 recorded in  $\text{CD}_2\text{Cl}_2$  at 96 MHz.

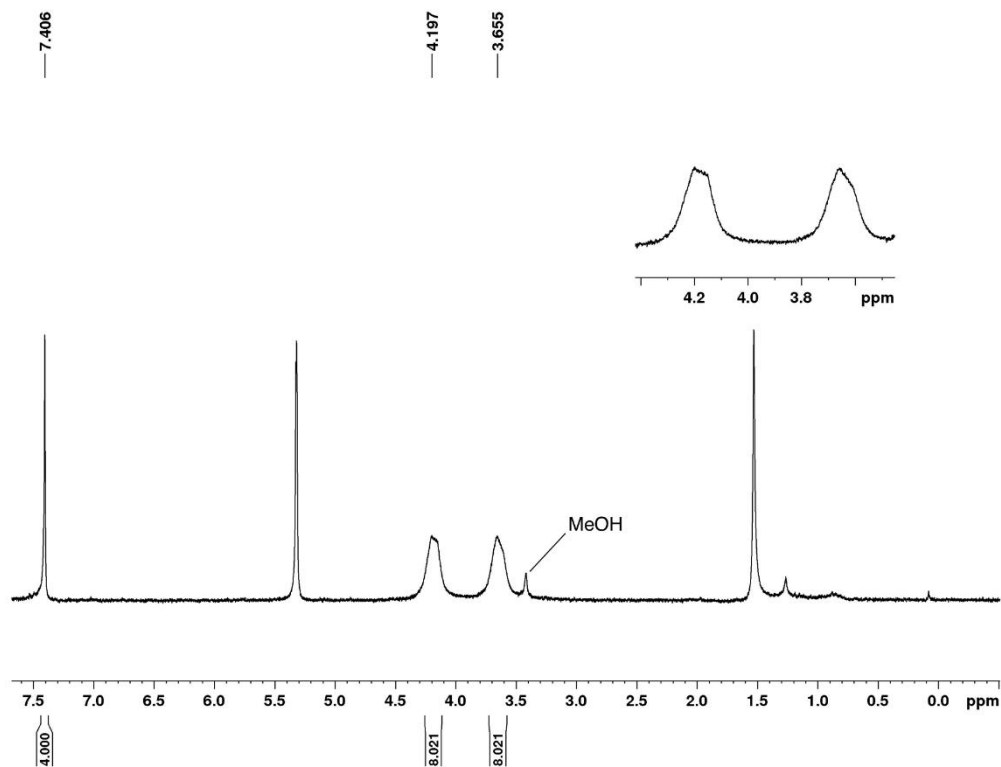


Figure 8-85.  $^1\text{H}$  NMR spectrum of compound 3-12 recorded in  $\text{CD}_2\text{Cl}_2$  at 300 MHz.

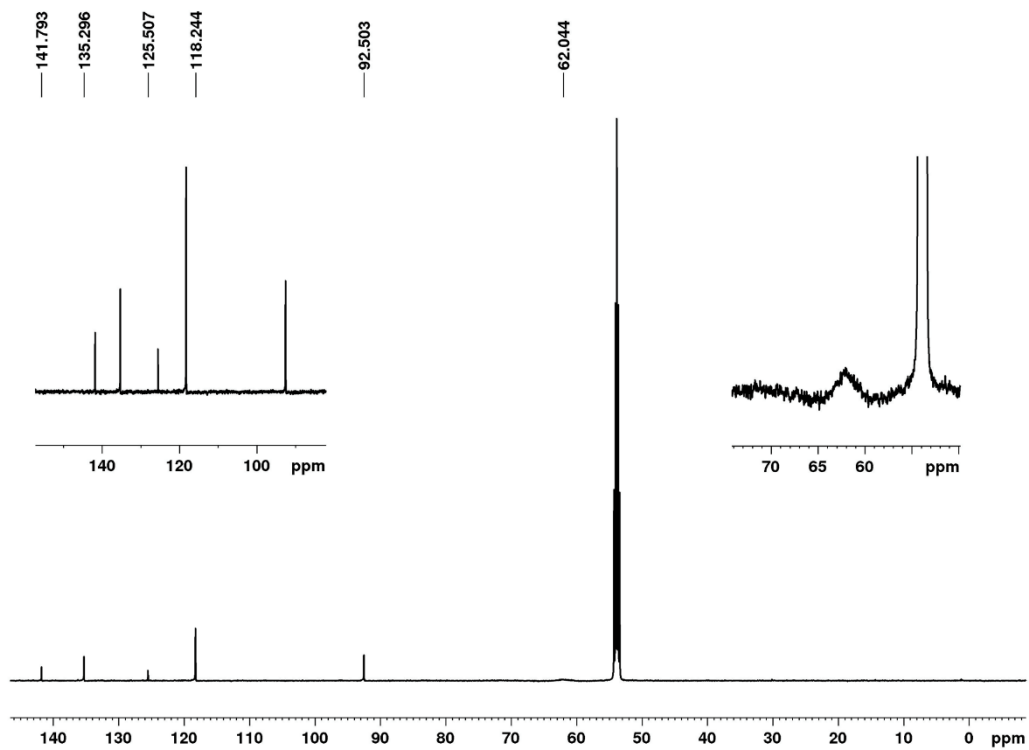


Figure 8-86.  $^{13}\text{C}\{^1\text{H}\}$  NMR spectrum of compound 3-12 recorded in  $\text{CD}_2\text{Cl}_2$  at 75 MHz.

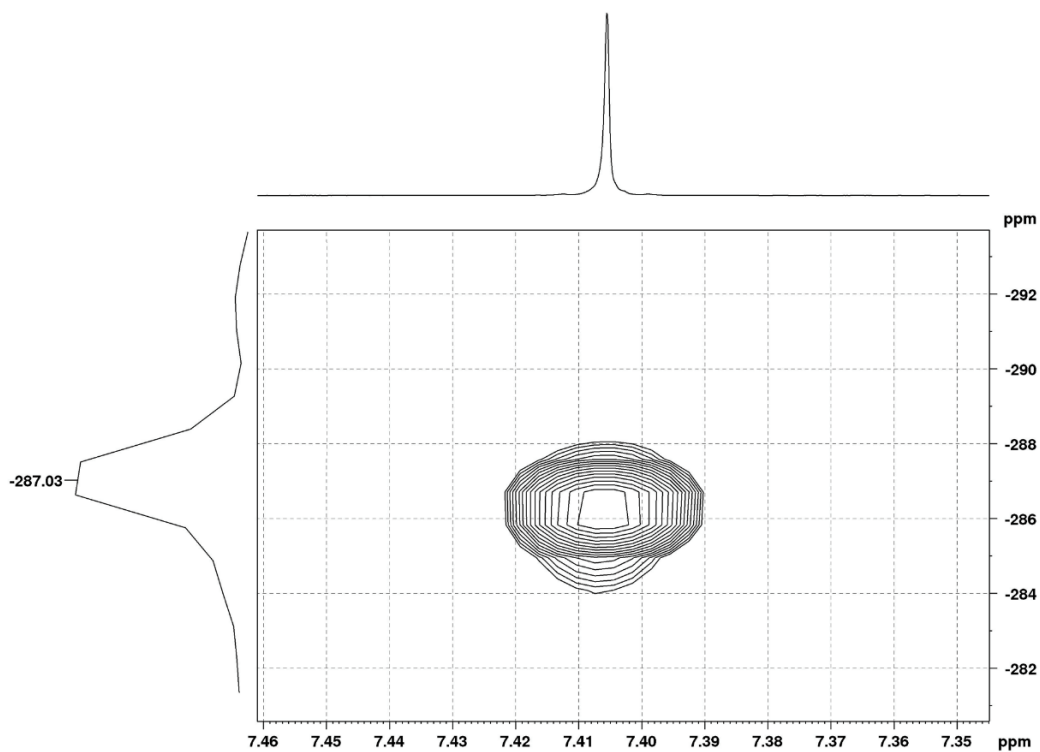


Figure 8-87.  $^{15}\text{N}$ ,  $^1\text{H}$  HMBC NMR spectrum of compound **3-12** recorded in  $\text{CD}_2\text{Cl}_2$  at 300 MHz.

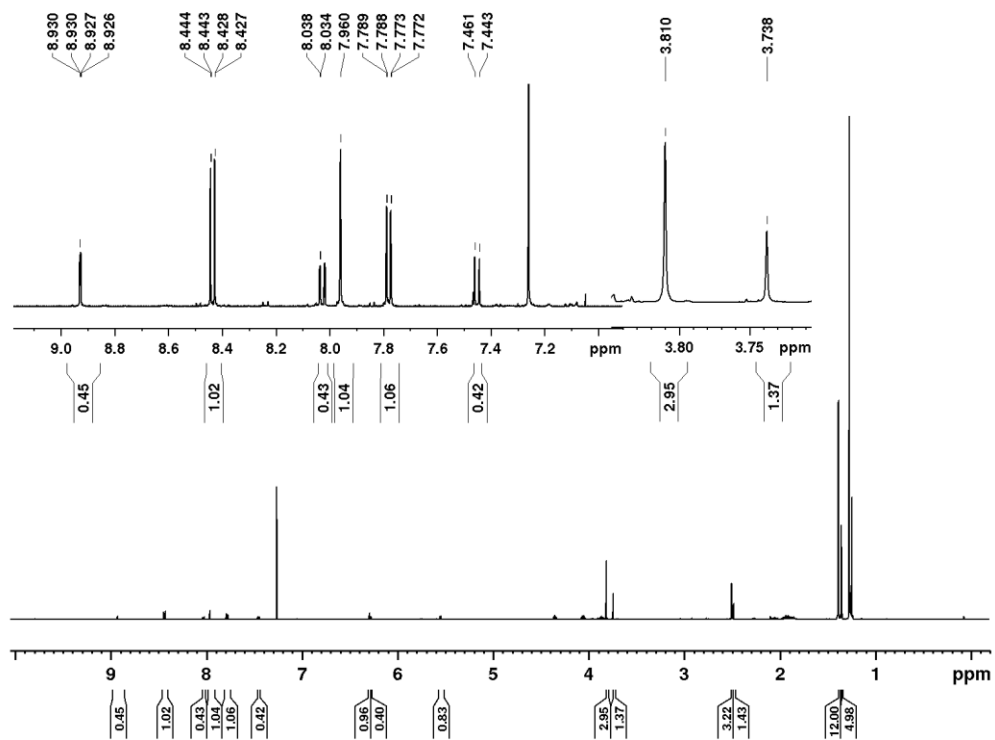


Figure 8-88.  $^1\text{H}$  NMR spectrum of compound **4-1** recorded in  $\text{CDCl}_3$  at 500 MHz.

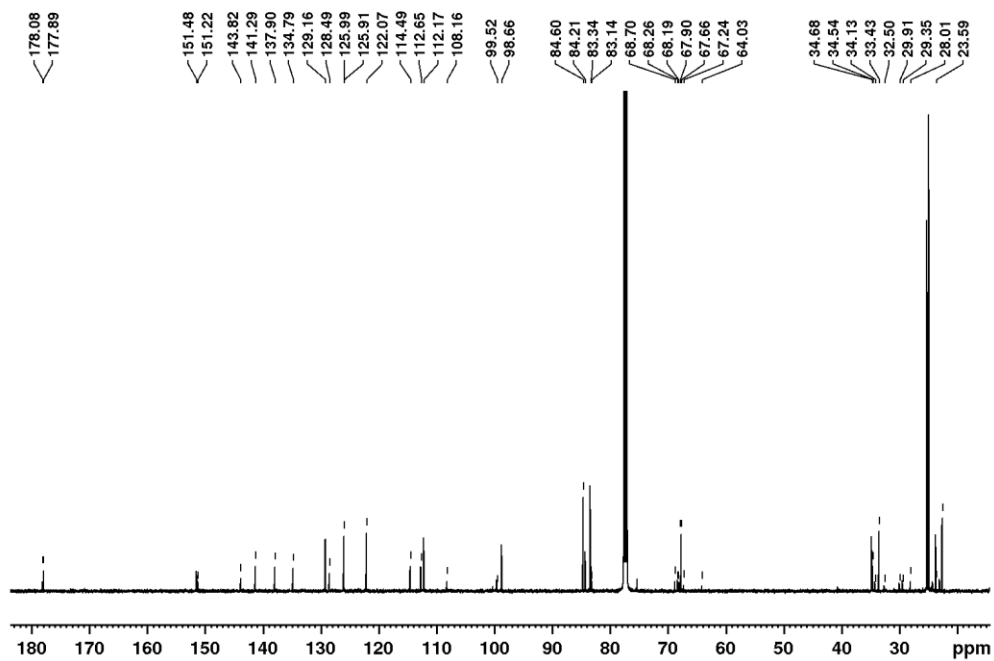


Figure 8-89.  $^{13}\text{C}$  NMR spectrum of compound 4-1 recorded in  $\text{CDCl}_3$  at 125 MHz.

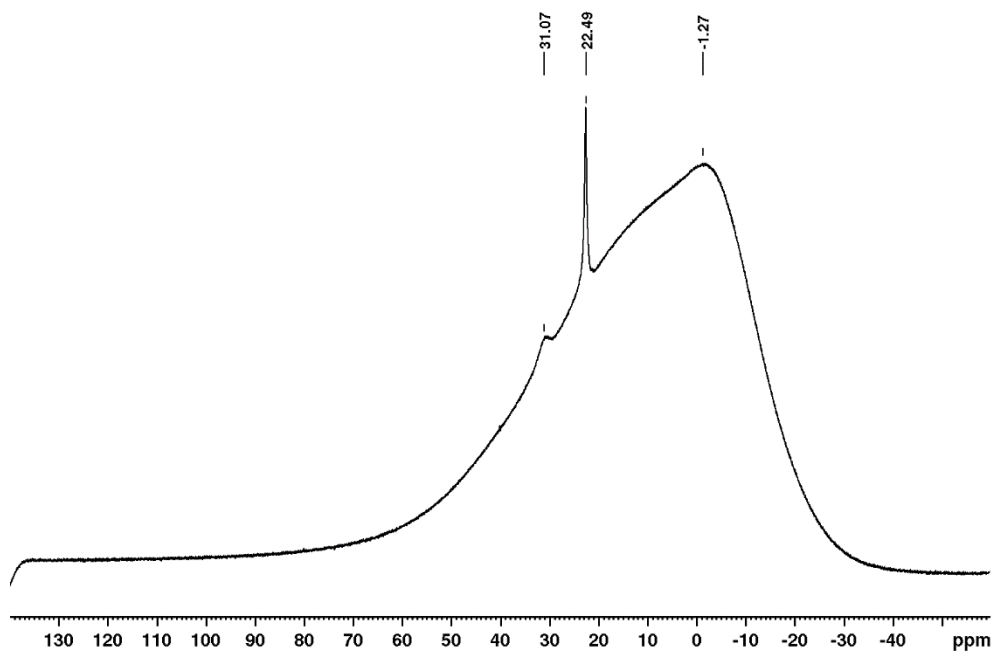


Figure 8-90.  $^{11}\text{B}$  NMR spectrum of compound 4-1 recorded in  $\text{CDCl}_3$  at 160 MHz.

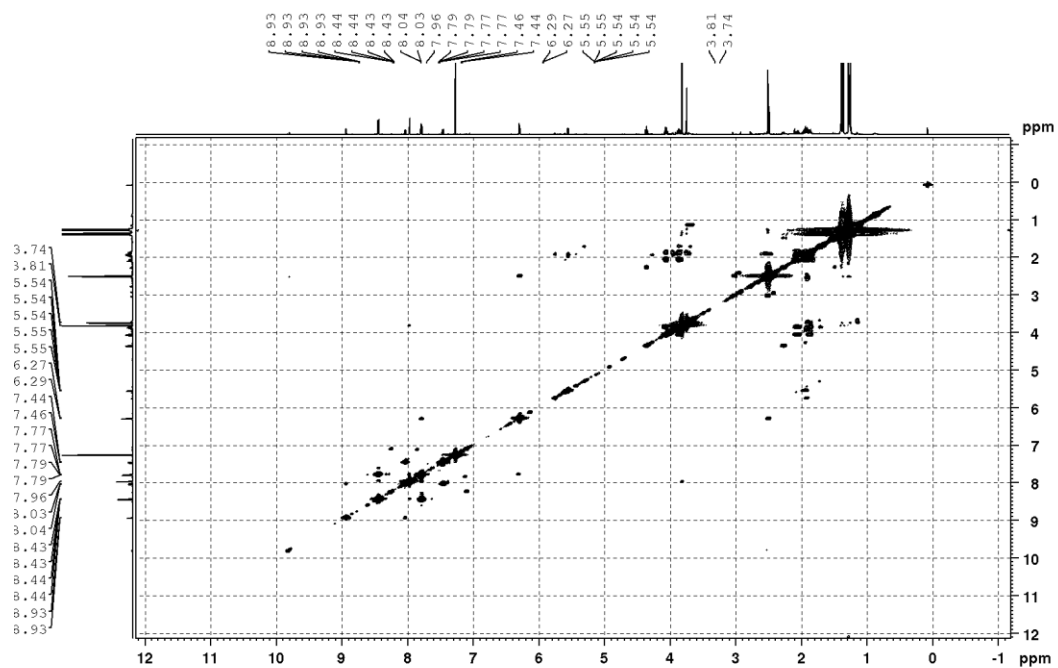


Figure 8-91. <sup>1</sup>H, <sup>1</sup>H COSY NMR spectrum of compound 4-1 recorded in CDCl<sub>3</sub> at 500 MHz.

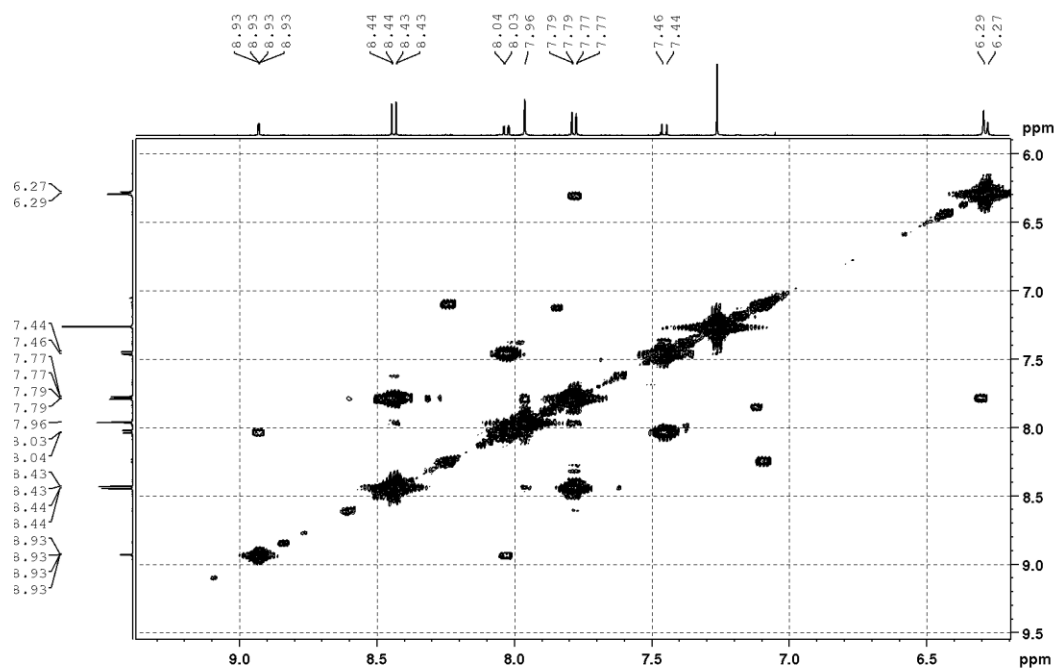


Figure 8-92. <sup>1</sup>H, <sup>1</sup>H COSY NMR spectrum of compound 4-1 recorded in CDCl<sub>3</sub> at 500 MHz.

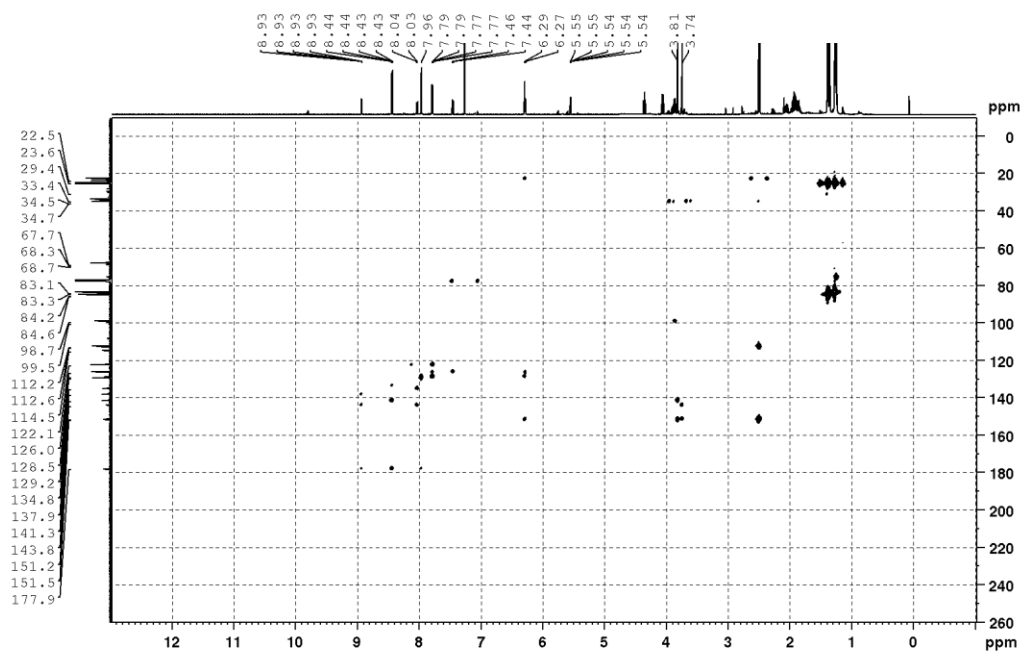


Figure 8-93.  $^1\text{H}$ ,  $^{13}\text{C}$  HMBC NMR spectrum of compound 4-1 recorded in  $\text{CDCl}_3$  at 500 and 125 MHz.

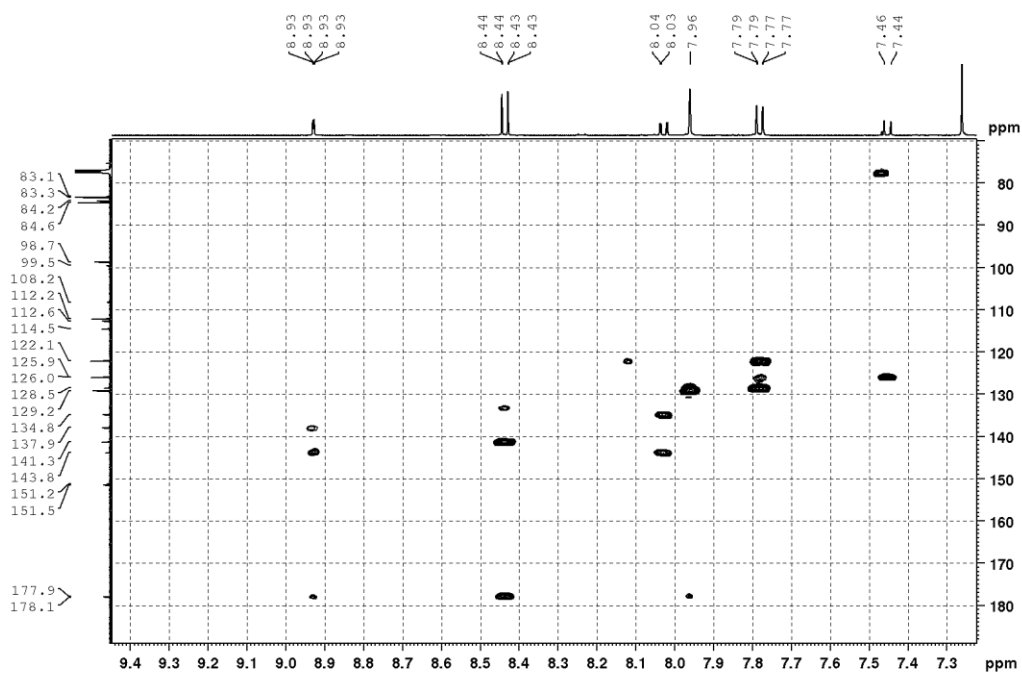


Figure 8-94.  $^1\text{H}$ ,  $^{13}\text{C}$  HMBC NMR spectrum of compound 4-1 recorded in  $\text{CDCl}_3$  at 500 and 125 MHz.

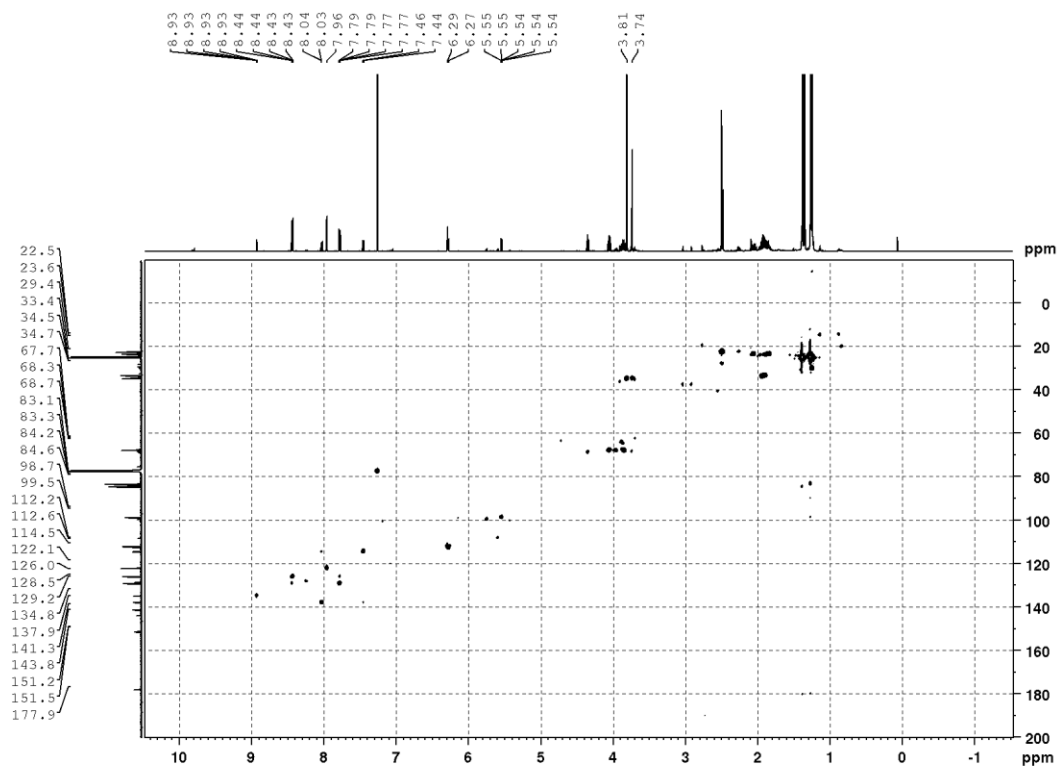


Figure 8-94.  $^1\text{H}$ ,  $^{13}\text{C}$  HSQC NMR spectrum of compound 4-1 recorded in  $\text{CDCl}_3$  at 500 and 125 MHz.

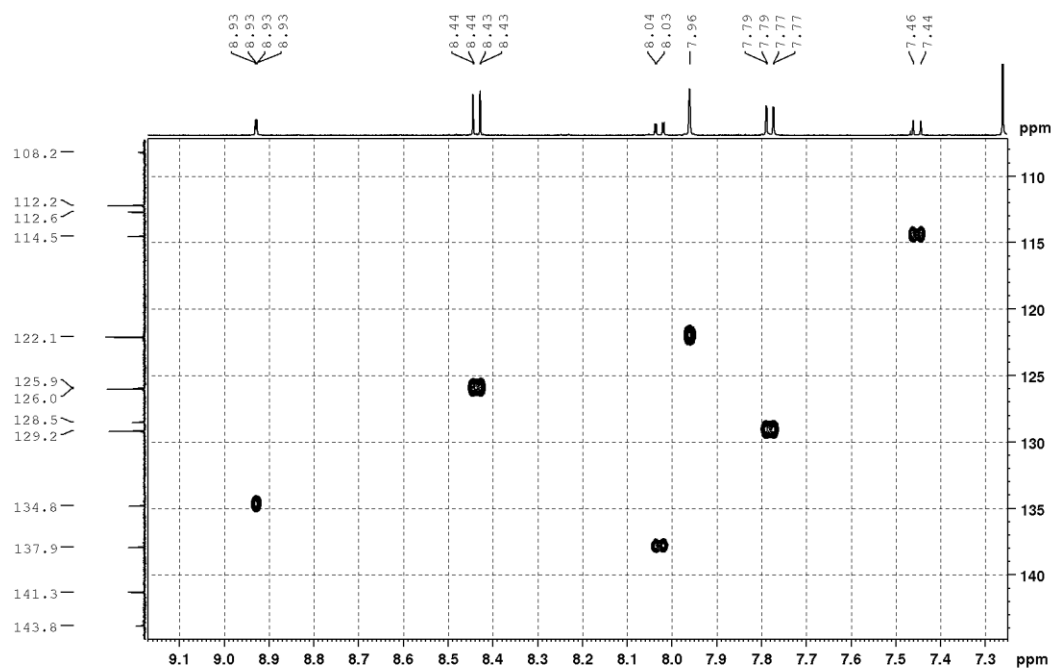


Figure 8-95.  $^1\text{H}$ ,  $^{13}\text{C}$  HSQC NMR spectrum of compound 4-1 recorded in  $\text{CDCl}_3$  at 500 and 125 MHz.

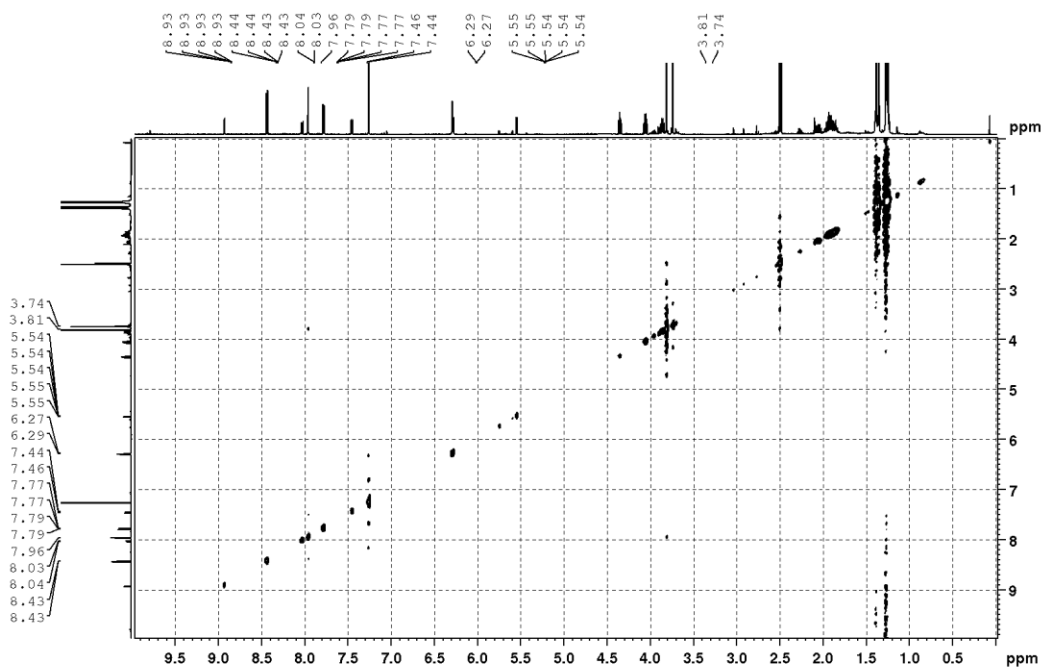


Figure 8-96.  $^1\text{H}$ ,  $^1\text{H}$  NOESY NMR spectrum of compound **4-1** recorded in  $\text{CDCl}_3$  at 500 MHz.

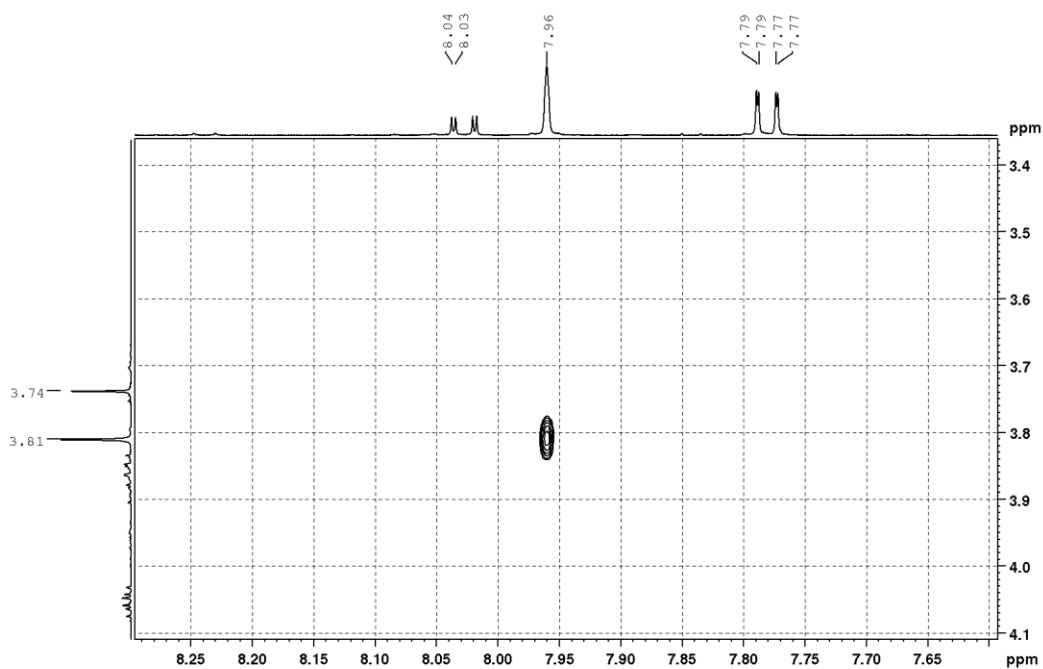


Figure 8-97.  $^1\text{H}$ ,  $^1\text{H}$  NOESY NMR spectrum of compound **4-1** recorded in  $\text{CDCl}_3$  at 500 MHz.

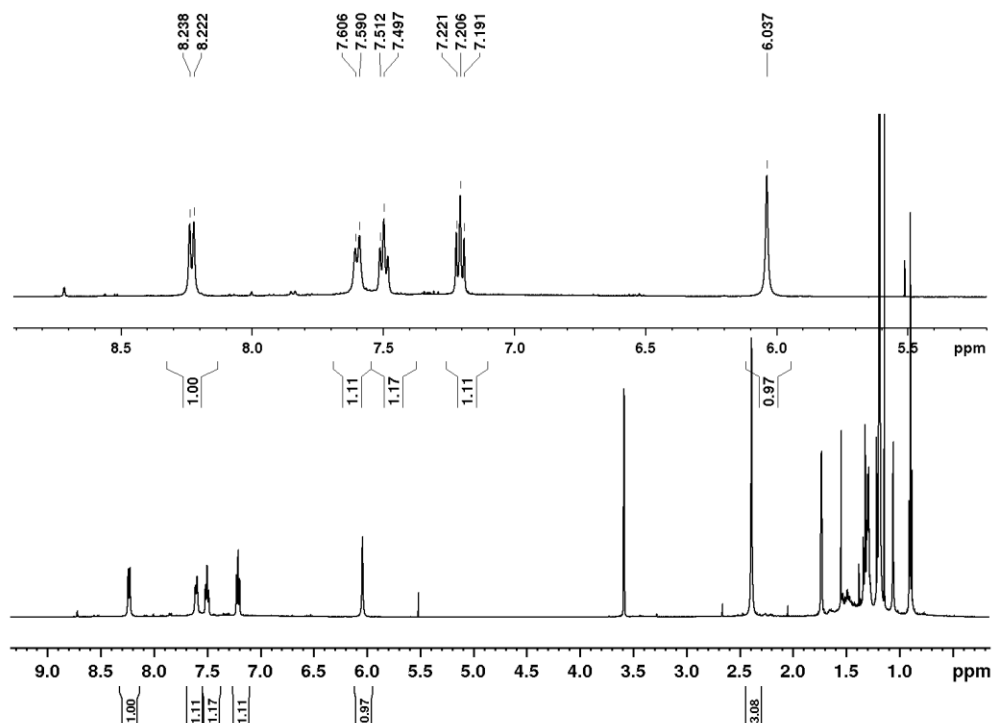


Figure 8-98. <sup>1</sup>H NMR spectrum of compound 4-3 recorded in THF-*d*<sub>8</sub> at 500 MHz.

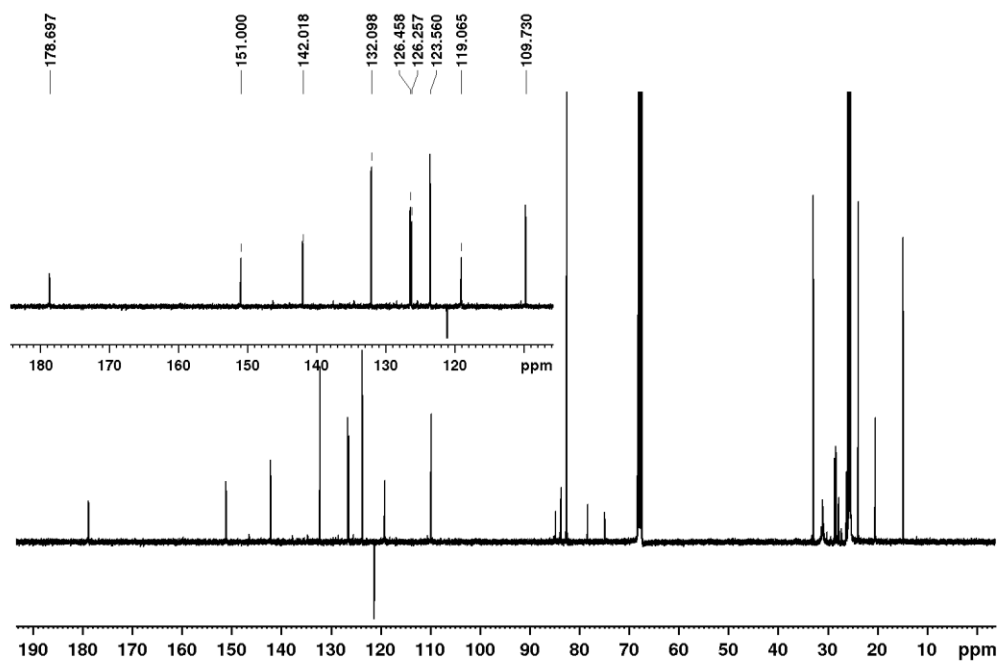


Figure 8-99. <sup>13</sup>C NMR spectrum of compound 4-3 recorded in THF-*d*<sub>8</sub> at 125 MHz.

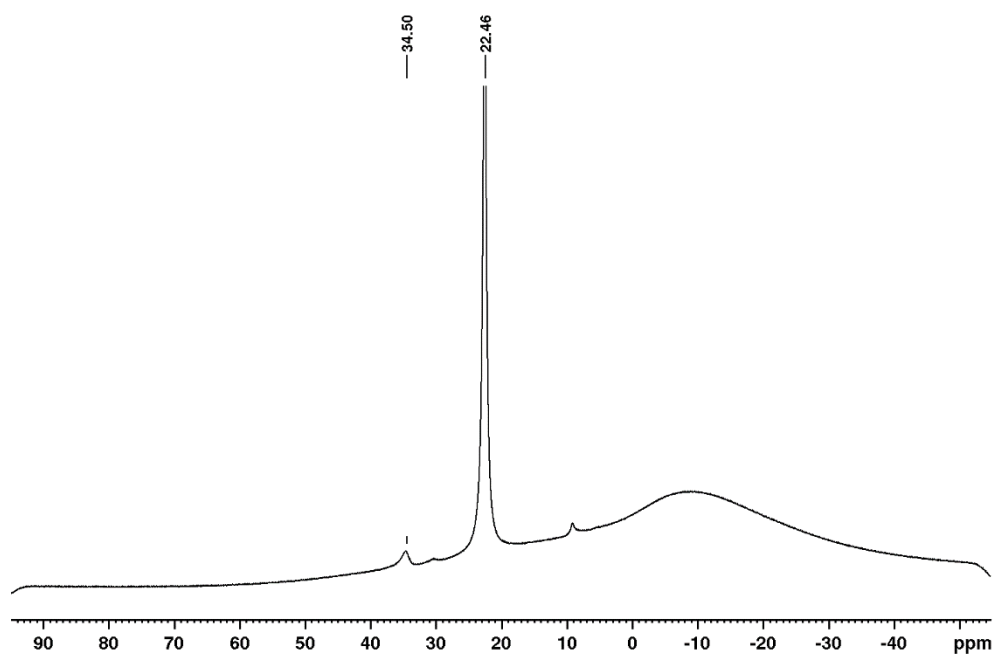


Figure 8-100.  $^{11}\text{B}$  NMR spectrum of compound 4-3 recorded in  $\text{THF-}d_8$  at 160 MHz.

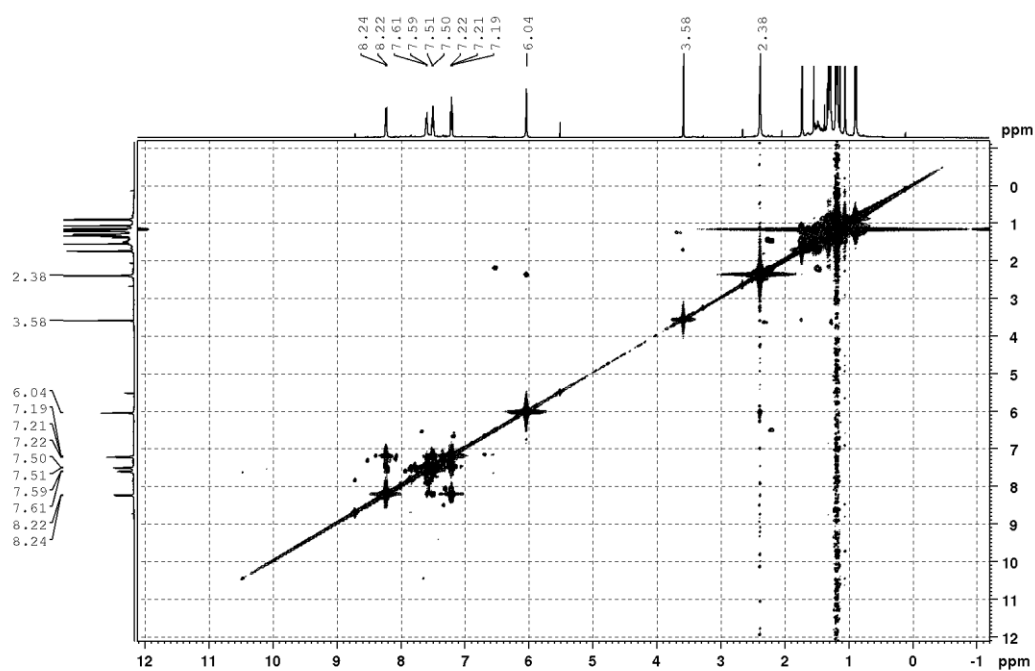


Figure 8-101.  $^1\text{H}$ ,  $^1\text{H}$  COSY NMR spectrum of compound 4-3 recorded in  $\text{THF-}d_8$  at 500 MHz.

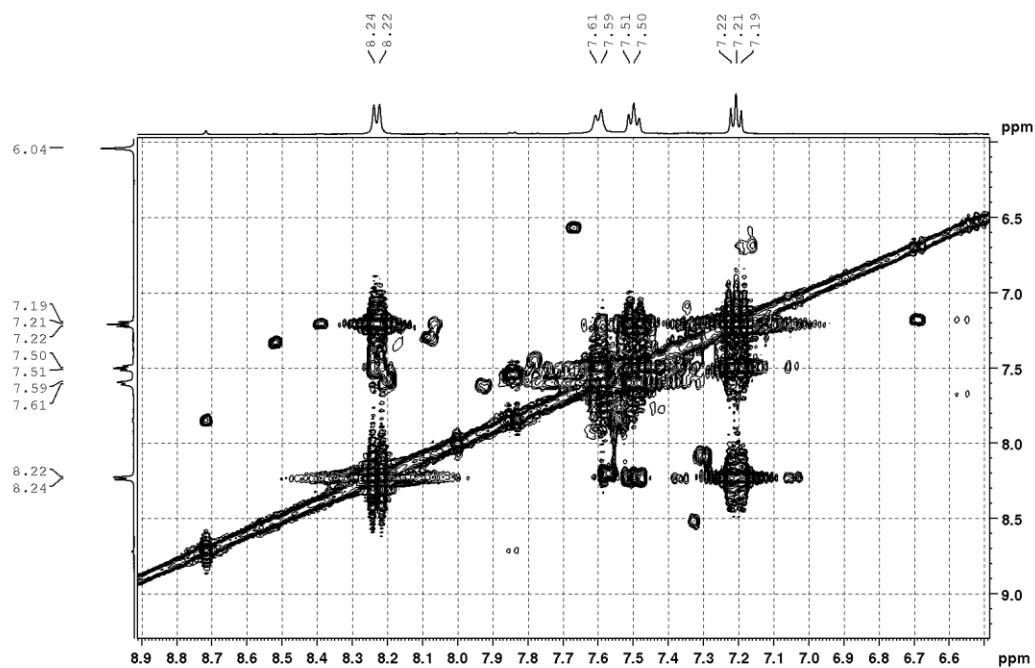


Figure 8-102.  $^1\text{H}$ ,  $^1\text{H}$  COSY NMR spectrum of compound 4-3 recorded in  $\text{THF-}d_8$  at 500 MHz.

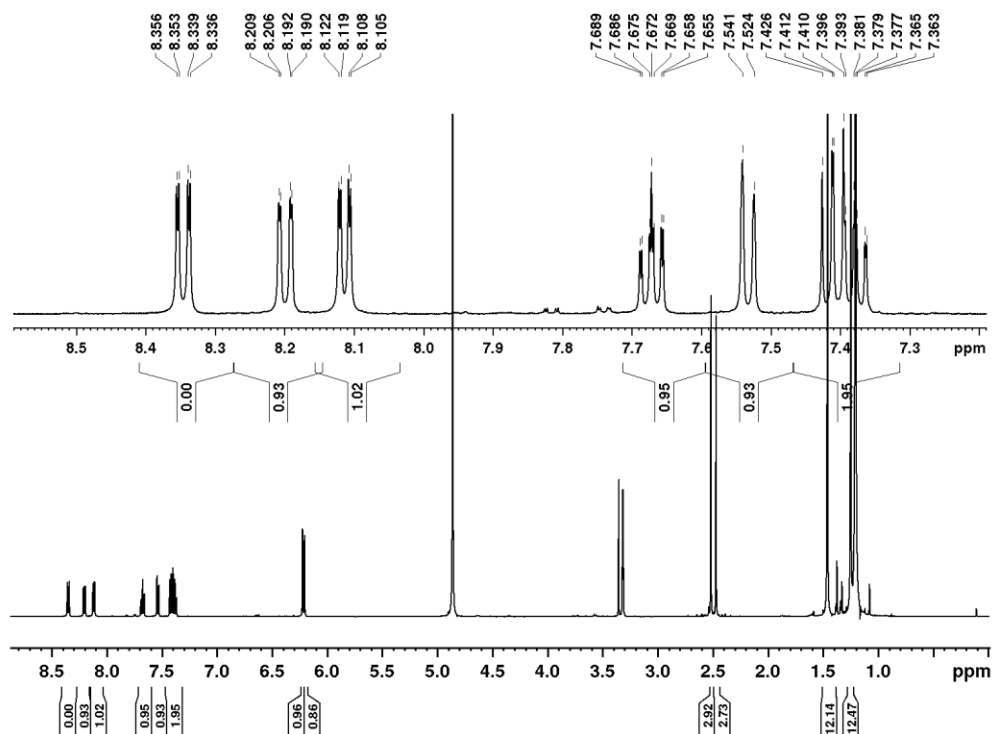


Figure 8-103.  $^1\text{H}$  NMR spectrum of compound 4-10 recorded in  $\text{CD}_3\text{OD}$  at 500 MHz.

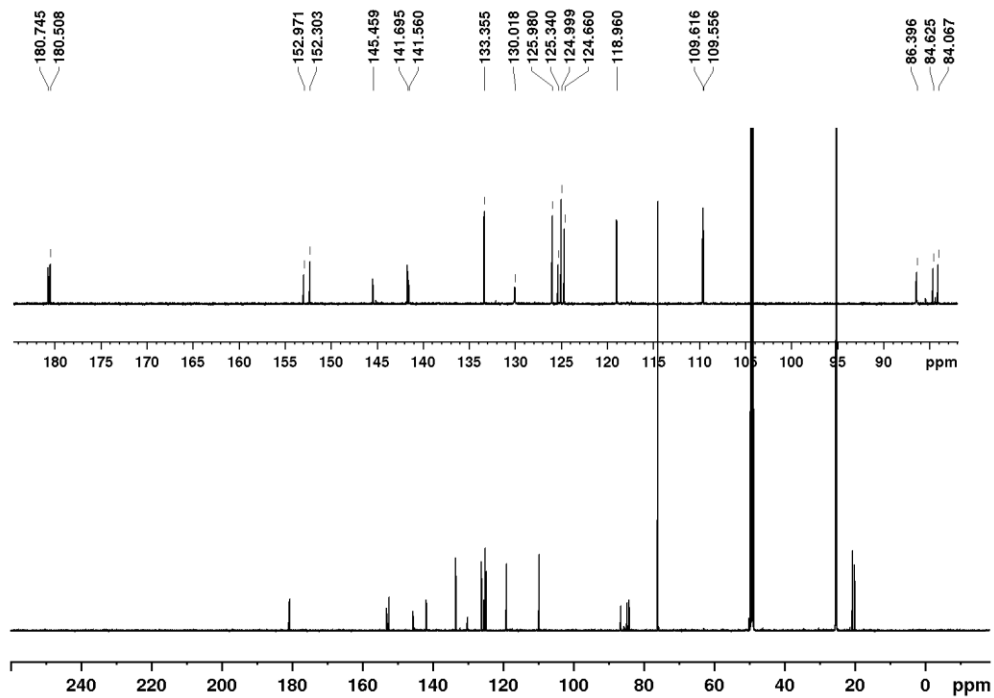


Figure 8-104. <sup>13</sup>C NMR spectrum of compound 4-10 recorded in CD<sub>3</sub>OD at 125 MHz.

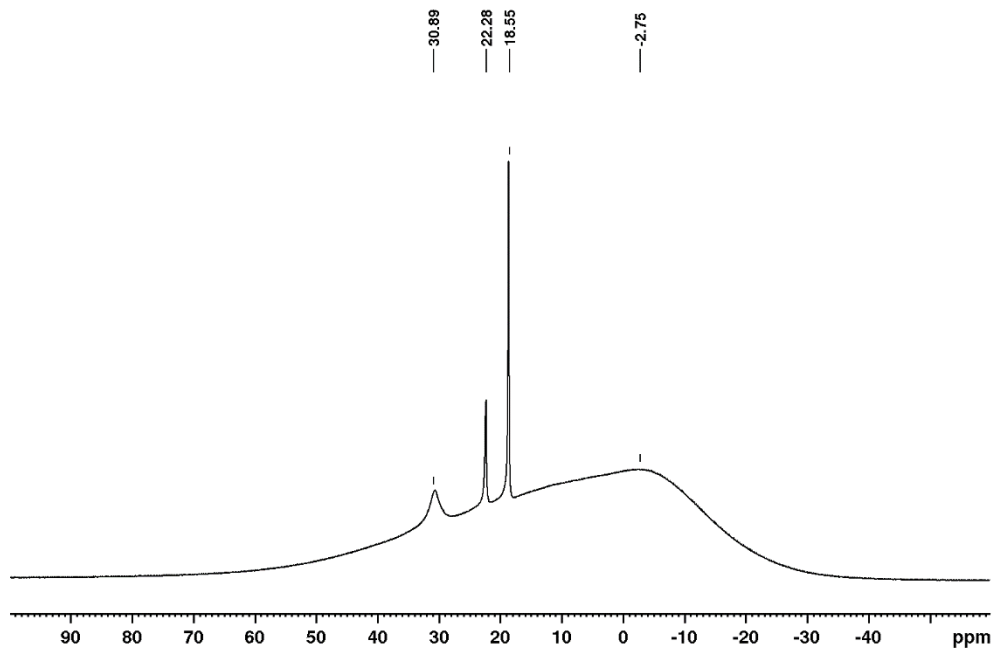


Figure 8-105. <sup>11</sup>B NMR spectrum of compound 4-10 recorded in CD<sub>3</sub>OD at 160 MHz.

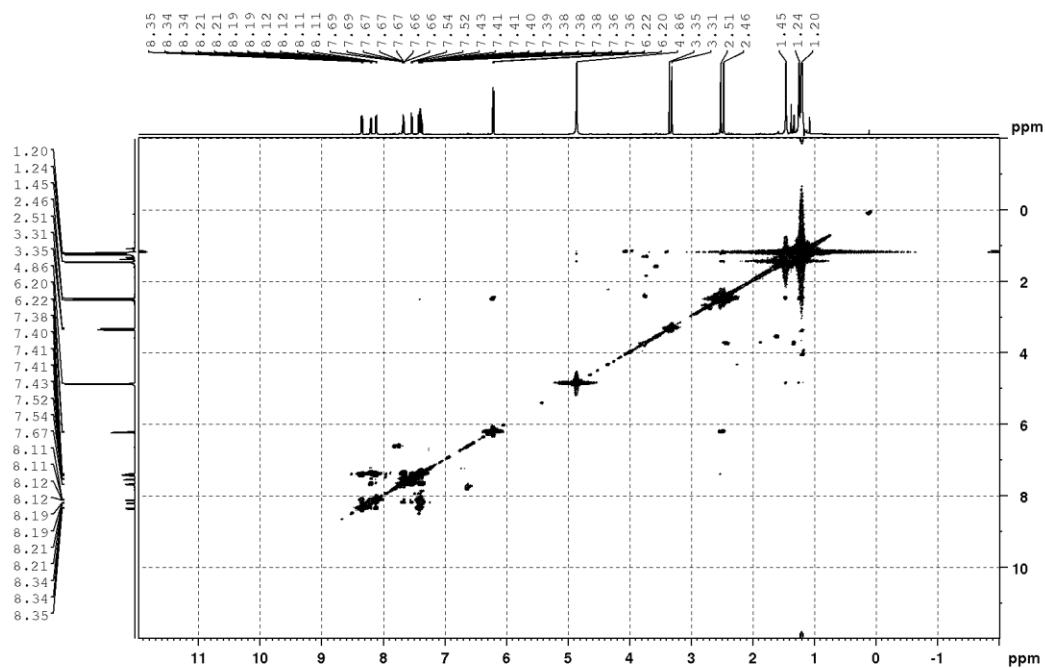


Figure 8-106. <sup>1</sup>H, <sup>1</sup>H COSY NMR spectrum of compound 4-10 recorded in CD<sub>3</sub>OD at 500 MHz.

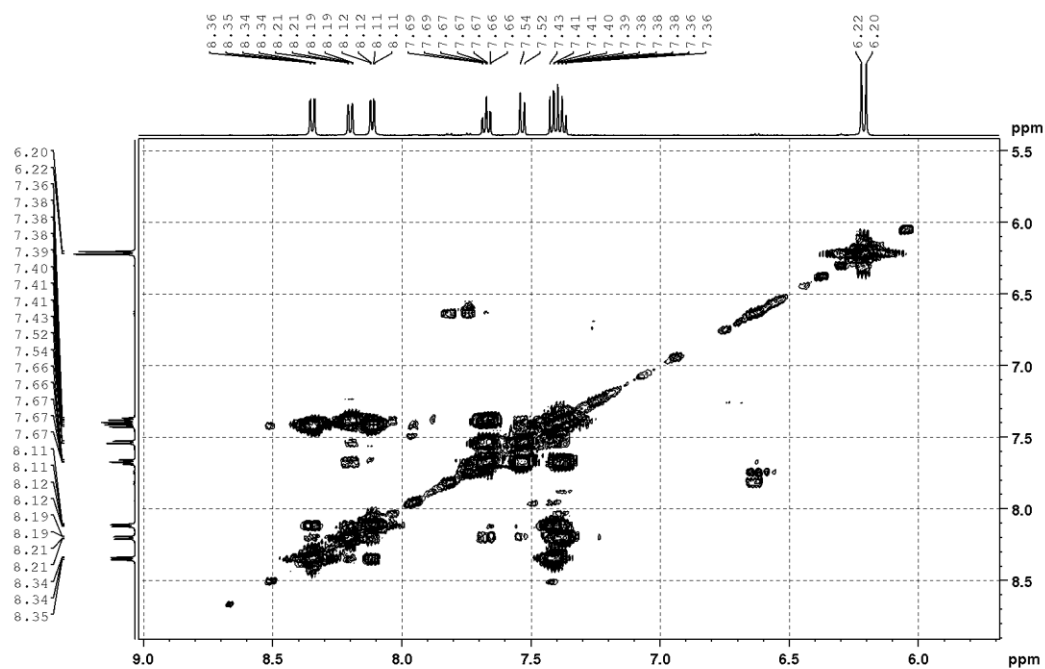


Figure 8-107. <sup>1</sup>H, <sup>1</sup>H COSY NMR spectrum of compound 4-10 recorded in CD<sub>3</sub>OD at 500 MHz.

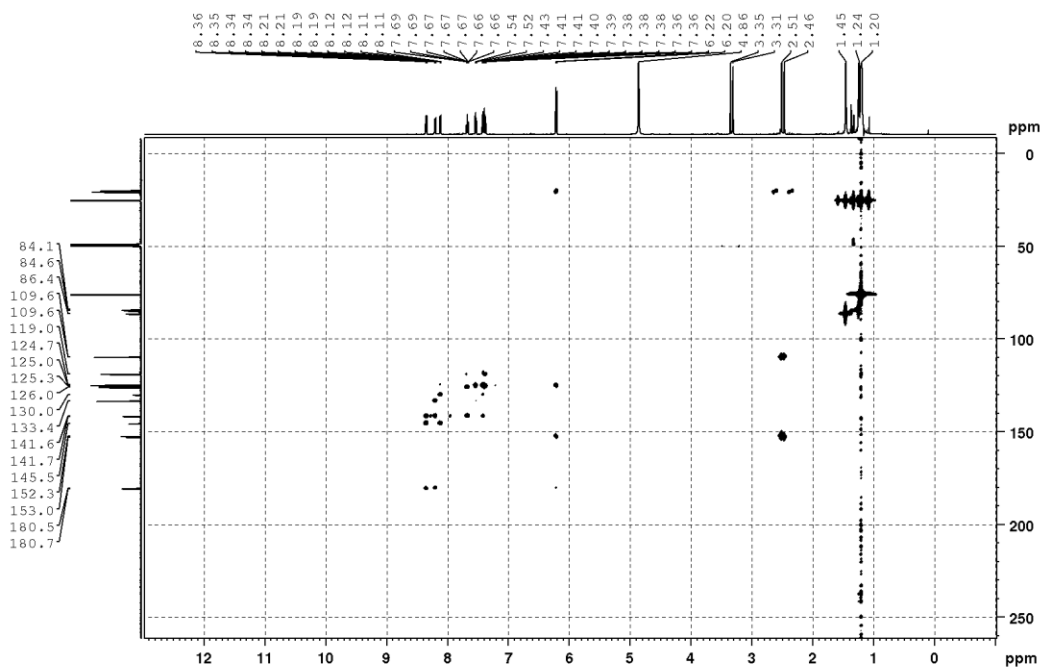


Figure 8-108.  $^1\text{H}$ ,  $^{13}\text{C}$  HMBC NMR spectrum of compound **4-10** recorded in  $\text{CD}_3\text{OD}$  at 500 and 125 MHz.

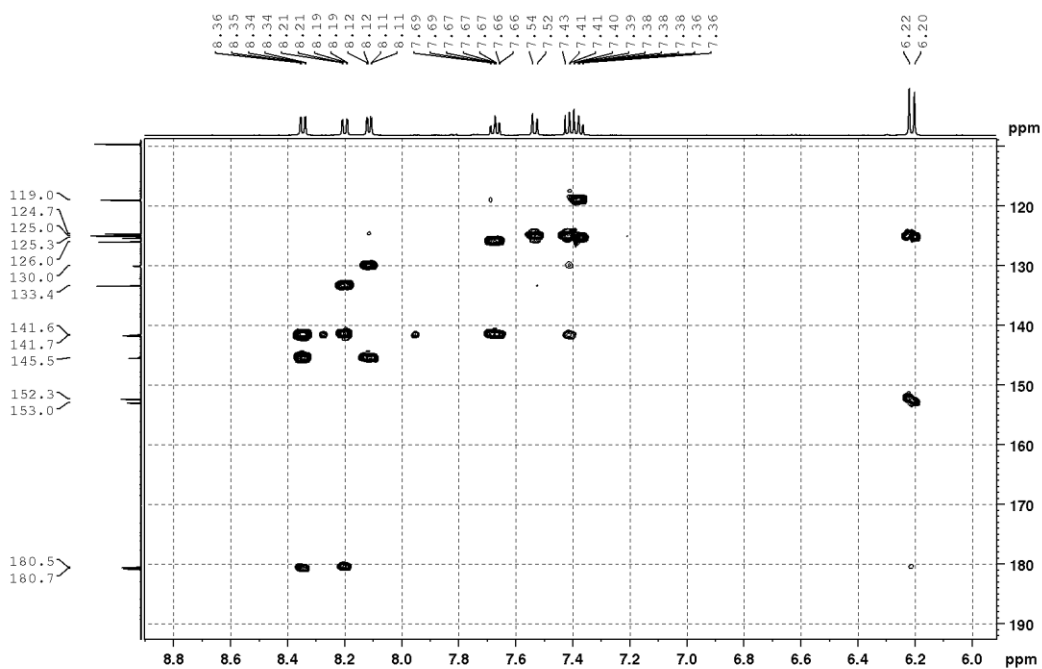


Figure 8-109.  $^1\text{H}$ ,  $^{13}\text{C}$  HMBC NMR spectrum of compound **4-10** recorded in  $\text{CD}_3\text{OD}$  at 500 and 125 MHz.

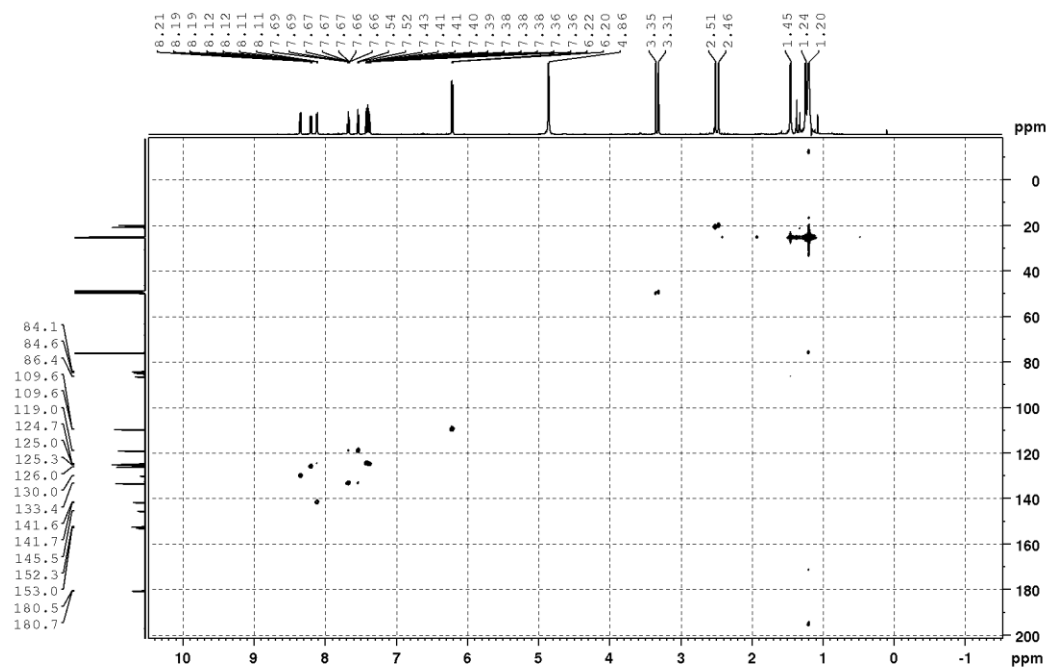


Figure 8-110.  $^1\text{H}$ ,  $^{13}\text{C}$  HSQC NMR spectrum of compound 4-10 recorded in  $\text{CD}_3\text{OD}$  at 500 and 125 MHz.

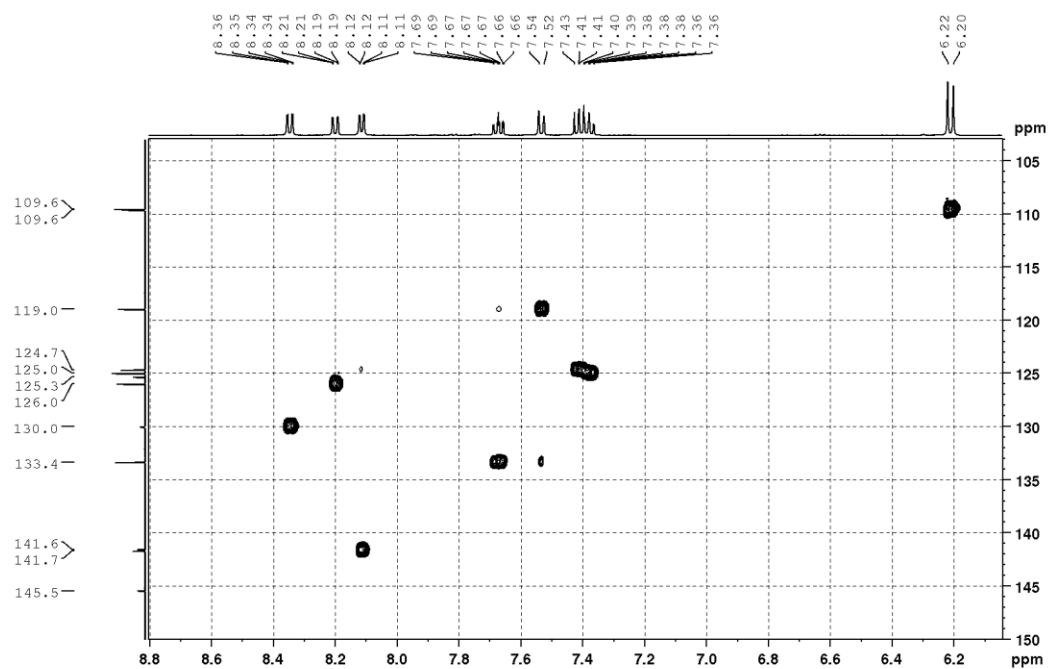


Figure 8-111.  $^1\text{H}$ ,  $^{13}\text{C}$  HSQC NMR spectrum of compound 4-10 recorded in  $\text{CD}_3\text{OD}$  at 500 and 125 MHz.

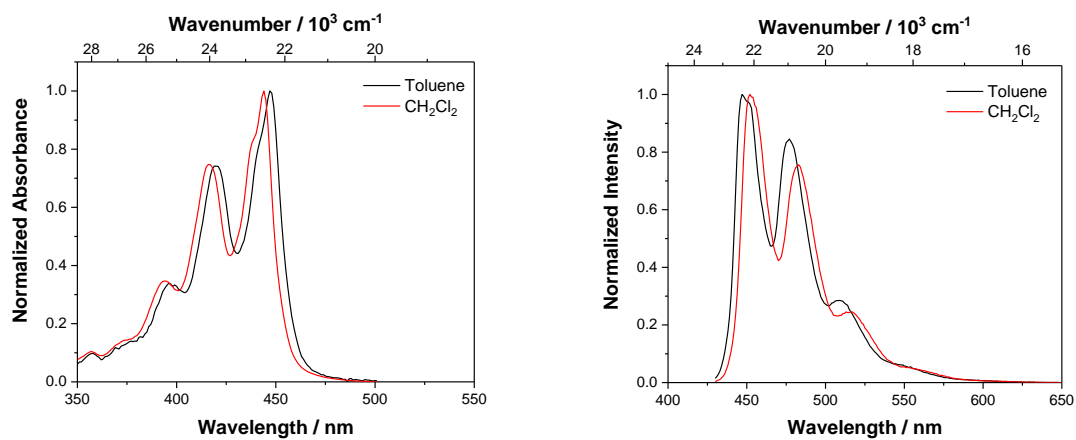


Figure 8-112. Left: absorption spectra; right: emission spectra of **(Br)<sub>4</sub>-Per** in toluene and CH<sub>2</sub>Cl<sub>2</sub>.

**Cartesian Coordinates****Compound I-4 (B3LYP/6-31G (d), S<sub>0</sub>)**Total energy: -946 358.79 kcal mol<sup>-1</sup>

Dipole moment: 0.0001 D

N	-4.980862	-0.000012	-0.138340	H	-3.952713	-4.178944	1.634010
C	-3.581447	0.000000	-0.015610	H	-3.369414	-2.664703	2.349851
C	-2.881535	-1.240730	0.056008	H	-2.250494	-3.733251	1.508632
C	-1.463146	-1.225918	0.041773	N	4.980810	0.000000	0.138428
C	-0.724625	0.000006	0.015966	C	3.581407	0.000000	0.015588
C	-1.463150	1.225927	0.041823	C	2.881510	1.240745	-0.056021
C	-2.881542	1.240735	0.055997	C	1.463111	1.225937	-0.041806
C	-0.677723	2.427099	0.023818	C	0.724592	0.000007	-0.016029
H	-1.156499	3.390121	0.032797	C	1.463106	-1.225925	-0.041893
C	0.677661	2.427102	-0.023642	C	2.881503	-1.240736	-0.056086
H	1.156418	3.390137	-0.032506	C	0.677663	-2.427095	-0.023816
C	-3.649697	2.583201	0.189391	H	1.156422	-3.390123	-0.032730
C	-3.472441	3.480307	-1.063923	C	-0.677721	-2.427090	0.023667
H	-4.000000	3.046593	-1.919992	H	-1.156503	-3.390114	0.032606
H	-2.435506	3.613082	-1.371427	C	3.649681	-2.583194	-0.189521
H	-3.902460	4.472057	-0.872029	C	3.472428	-3.480370	1.063744
C	-3.264645	3.336163	1.490020	H	3.999995	-3.046709	1.919836
H	-3.952940	4.179075	1.633666	H	2.435493	-3.613152	1.371246
H	-2.250656	3.733632	1.508343	H	3.902442	-4.472111	0.871795
H	-3.369400	2.665015	2.349693	C	3.264739	-3.336103	-1.490220
C	-5.167551	2.338180	0.327717	H	3.953106	-4.178953	-1.633888
H	-5.413879	2.055941	1.358510	H	2.250787	-3.733659	-1.508617
H	-5.700412	3.270657	0.105269	H	3.369481	-2.664897	-2.349850
C	-5.627379	1.219594	-0.575010	C	5.167527	-2.338147	-0.327783
H	-6.709683	1.075261	-0.492256	H	5.413881	-2.055839	-1.358551
H	-5.407389	1.438342	-1.636342	H	5.700386	-3.270636	-0.105379
C	-5.627332	-1.219658	-0.574968	C	5.627312	-1.219629	0.575042
H	-5.407264	-1.438468	-1.636266	H	6.709618	-1.075287	0.492331
H	-6.709643	-1.075341	-0.492288	H	5.407289	-1.438456	1.636351
C	-5.167523	-2.338187	0.327850	C	5.627259	1.219612	0.575171
H	-5.700388	-3.270672	0.105473	H	5.407091	1.438392	1.636455
H	-5.413861	-2.055870	1.358620	H	6.709575	1.075278	0.492590
C	-3.649664	-2.583206	0.189532	C	5.167560	2.338170	-0.327659
C	-3.472416	-3.480487	-1.063657	H	5.700424	3.270637	-0.105198
H	-3.902378	-4.472222	-0.871583	H	5.413987	2.055885	-1.358415
H	-2.435498	-3.613287	-1.371216	C	3.649700	2.583212	-0.189454
H	-4.000037	-3.046932	-1.919766	C	3.472465	3.480449	1.063771
C	-3.264540	-3.335949	1.490259	H	3.902397	4.472202	0.871724
				H	2.435562	3.613202	1.371392
				H	4.000139	3.046871	1.919838
				C	3.264760	3.336015	-1.490202
				H	3.952985	4.178988	-1.633838
				H	3.369731	2.664790	-2.349799
				H	2.250730	3.733342	-1.508712

**Compound I-8 (B3LYP/6-31G (d), S<sub>0</sub>)**Total energy: -666 407.85 kcal mol<sup>-1</sup>

Dipole moment: 2.54 D

N	3.048537	-0.000065	-0.171453
C	3.704873	-1.221017	-0.590826
H	4.785456	-1.069236	-0.502374
H	3.493532	-1.450635	-1.651095
C	3.245978	-2.333834	0.319278
H	3.485203	-2.042464	1.349187
H	3.784275	-3.265442	0.107072
C	1.730658	-2.585608	0.173338
C	1.562815	-3.487739	-1.077613
H	0.528049	-3.625898	-1.389983
H	1.995232	-4.477024	-0.879549
H	2.092700	-3.055899	-1.933091
C	1.338851	-3.334357	1.474191
H	1.438949	-2.660926	2.332604
H	2.026199	-4.176792	1.623874
H	0.324810	-3.731793	1.487996
C	0.957305	-1.247420	0.031586
C	-0.459996	-1.238425	0.015132
C	-1.253000	-2.447932	-0.003140
H	-0.767093	-3.407522	-0.005213
C	-2.611843	-2.444140	-0.041642
H	-3.155935	-3.385694	-0.064419
C	-3.351374	-1.223081	-0.058580
C	-4.755351	-1.204966	-0.090256
H	-5.291852	-2.150871	-0.100920
C	-5.454930	0.000044	-0.106615
H	-6.541236	0.000054	-0.130644
C	-4.755326	1.205043	-0.090424
H	-5.291810	2.150956	-0.101245
C	-3.351353	1.223136	-0.058729
C	-2.616176	0.000023	-0.044021
C	-1.180139	0.000005	-0.012340
C	-0.459974	1.238424	0.015106
C	-1.252953	2.447938	-0.003304
H	-0.767013	3.407499	-0.005424
C	-2.611793	2.444183	-0.041893
H	-3.155857	3.385749	-0.064812
C	0.957321	1.247431	0.031627
C	1.652759	0.000000	-0.042841
C	3.705103	1.220926	-0.590330
H	3.494238	1.450772	-1.650647
H	4.785649	1.069080	-0.501458

C	3.245945	2.333607	0.319792
H	3.784441	3.265181	0.107933
H	3.484738	2.042049	1.349752
C	1.730724	2.585591	0.173376
C	1.563252	3.487498	-1.077761
H	1.996443	4.476522	-0.880057
H	0.528480	3.626360	-1.389816
H	2.092554	3.055057	-1.933288
C	1.338729	3.334732	1.473937
H	1.438113	2.661428	2.332522
H	0.324891	3.732725	1.487260
H	2.026444	4.176847	1.623730

**Compound I-II (B3LYP/6-31G (d), S<sub>0</sub>)**Total energy: -1 120 467.16 kcal mol<sup>-1</sup>

Dipole moment: 3.58 D

C	-1.966348	0.001879	-0.004971
C	-1.233677	1.151777	0.335159
C	0.166146	1.166495	0.363781
C	0.903800	-0.003864	0.010441
C	0.165286	-1.172218	-0.347760
C	-1.234689	-1.151339	-0.335935
C	0.904823	2.334949	0.723924
C	2.337312	-0.006937	0.018827
C	3.057589	1.174554	0.394417
C	2.263794	2.334414	0.740518
C	4.473849	1.184188	0.391040
C	5.167211	0.014374	-0.055184
C	4.472883	-1.205927	-0.332945
C	3.056653	-1.198424	-0.325652
C	2.262047	-2.354266	-0.683110
C	0.903106	-2.344003	-0.698784
H	0.355476	-3.238889	-0.985552
H	2.747788	-3.269673	-0.971122
H	0.357848	3.238633	0.983039
H	-1.767958	2.064580	0.590815
H	-1.769852	-2.062499	-0.595549
H	2.750176	3.255561	1.008398
C	5.250915	2.426149	0.903168
C	5.249026	-2.524133	-0.594579
C	4.880076	2.764683	2.370895
H	3.867400	3.139252	2.514283
H	4.991155	1.871622	2.995801
H	5.571549	3.528946	2.748057

C	5.064981	3.651595	-0.029653	H	-4.759897	-0.708317	-2.548457
H	4.025417	3.871501	-0.271264	C	-3.019310	-1.794431	2.386596
H	5.502611	4.542192	0.439545	H	-3.273695	-2.267698	3.341268
H	5.579532	3.487921	-0.982300	H	-2.009435	-2.120872	2.111891
C	4.875243	-3.619608	0.438192	H	-2.961924	-0.715152	2.551693
H	4.984717	-3.223286	1.453748	C	-6.430818	-5.104908	0.771140
H	3.862367	-4.009842	0.347677	H	-7.464789	-5.043898	0.413024
H	5.566098	-4.465402	0.329419	H	-5.939230	-5.911554	0.210301
C	5.065253	-3.026603	-2.050647	H	-6.451666	-5.404073	1.824679
H	5.503560	-4.027678	-2.153442	C	-2.988490	1.802636	-2.406290
H	4.026101	-3.076286	-2.374898	H	-2.935681	0.723261	-2.572449
H	5.580287	-2.361891	-2.752083	H	-3.230277	2.278760	-3.362813
N	6.557652	0.059592	-0.205849	H	-1.979631	2.122744	-2.120632
C	6.765451	-2.317342	-0.399899	C	-6.400908	5.127759	-0.822606
H	7.302554	-3.146958	-0.875103	H	-6.406977	5.429310	-1.875645
H	7.016618	-2.330809	0.667656	H	-7.439671	5.069971	-0.478046
C	7.212072	-0.989322	-0.960389	H	-5.913578	5.931242	-0.253576
H	6.990051	-0.908975	-2.039826	C	-5.655782	0.968812	1.899066
H	8.293131	-0.863327	-0.842877	H	-6.120415	0.018648	1.616091
C	7.211925	1.350854	-0.255288	H	-4.781068	0.723579	2.511629
H	8.293043	1.180965	-0.229305	H	-6.360127	1.515963	2.534234
H	6.987945	1.881130	-1.198469				
C	6.767657	2.146804	0.947390				
H	7.021178	1.567458	1.843497				
H	7.304484	3.101033	1.009453				
B	-3.523912	0.005011	-0.012654				
C	-4.287636	1.363036	-0.231277				
C	-5.285160	1.791212	0.682307				
C	-4.010754	2.183690	-1.352886				
C	-5.948219	3.004910	0.479052				
C	-4.717817	3.377183	-1.540089				
C	-5.681770	3.814674	-0.629438				
H	-6.701306	3.322228	1.198728				
H	-4.510587	3.979618	-2.423325				
C	-4.295346	-1.349768	0.198807				
C	-5.286023	-1.773821	-0.724092				
C	-4.032862	-2.171264	1.323285				
C	-5.956443	-2.984457	-0.526807				
C	-4.746980	-3.361535	1.504050				
C	-5.704154	-3.795041	0.584394				
H	-6.704089	-3.298635	-1.253498				
H	-4.550894	-3.964545	2.389436				
C	-5.641491	-0.950030	-1.944424				
H	-6.341830	-1.494366	-2.586410				
H	-6.105048	0.002000	-1.665967				

<b>Compound I-14 (B3LYP/6-31G (d), S<sub>0</sub>)</b>			
Total energy: -850 702.77 kcal mol <sup>-1</sup>			
Dipole moment: 0.20 D			
N	4.989960	0.013827	0.112329
C	3.585149	0.018126	0.082000
C	2.876209	1.190474	-0.295923
C	1.482231	1.160453	-0.322849
H	0.948142	2.044711	-0.656016
C	0.739181	0.026429	0.022652
C	1.460159	-1.106216	0.416062
H	0.906947	-1.989641	0.718707
C	2.853768	-1.140206	0.460659
C	3.592186	2.479127	-0.722655
C	2.986214	3.713298	-0.023087
H	3.579083	4.605555	-0.261534
H	2.983756	3.582802	1.064826
H	1.957854	3.907858	-0.343638
C	3.457578	2.661435	-2.251294
H	3.943421	3.593071	-2.570636
H	2.403641	2.706915	-2.545598
H	3.914177	1.829721	-2.797803
C	5.079952	2.404176	-0.332651
H	5.637631	3.192114	-0.854300



**Compound I-4<sup>+</sup> (UBLYP/SVP, S<sub>0</sub>)**Total energy: -944 826.75 kcal mol<sup>-1</sup>

Dipole moment: 27.2 D

C	-6.902950	2.860523	0.053987
C	-6.884763	1.462130	0.014714
C	-5.652037	0.712183	0.032349
C	-4.417527	1.450217	0.148068
C	-4.390410	2.848329	0.191013
C	-5.636738	3.559396	0.002504
C	-8.093861	0.683436	-0.080497
C	-8.095242	-0.660330	-0.174517
C	-6.890100	-1.450240	-0.144288
C	-5.655629	-0.712343	-0.027594
C	-4.422980	-1.462355	-0.009122
C	-3.214068	-0.683756	0.089233
C	-3.212636	0.660095	0.182148
C	-6.917080	-2.848201	-0.191442
C	-5.670996	-3.559866	-0.003455
C	-4.404717	-2.860737	-0.050413
N	-5.691881	-4.891781	0.254028
C	-4.475463	-5.629594	0.546182
C	-3.380869	-5.150327	-0.367141
C	-3.075247	-3.658263	-0.153265
C	-8.233643	-3.632654	-0.444443
C	-7.916888	-5.125406	-0.635363
C	-6.938566	-5.623775	0.392296
C	-3.073518	3.633492	0.440306
C	-3.388929	5.127684	0.622589
C	-4.368968	5.619955	-0.406477
N	-5.616078	4.890344	-0.259638
C	-6.833061	5.628582	-0.548315
C	-7.925003	5.150845	0.368973
C	-8.231891	3.658601	0.158212
C	-2.395568	3.213904	1.766580
C	-2.091819	3.520571	-0.749753
C	-9.214838	-3.526797	0.746644
C	-8.912677	-3.206552	-1.768088
C	-2.252309	-3.246802	-1.397374
C	-2.229404	-3.552574	1.137769
C	-9.052292	3.249531	1.404775
C	-9.080581	3.550974	-1.130757
H	-9.052181	1.174667	-0.104118
H	-2.252603	1.142284	0.260864
H	-4.208333	-5.511666	1.607594
H	-4.681212	-6.691654	0.386172

H	-2.467599	-5.733901	-0.202547
H	-3.695673	-5.328556	-1.404210
H	-7.486206	-5.297018	-1.631165
H	-8.847452	-5.702320	-0.582149
H	-6.721978	-6.685092	0.241166
H	-7.326226	-5.519003	1.417417
H	-2.458050	5.703584	0.564102
H	-3.817747	5.306049	1.617999
H	-3.983911	5.506870	-1.431689
H	-4.583899	6.682608	-0.262794
H	-6.626181	6.690673	-0.389811
H	-7.103755	5.510085	-1.608775
H	-7.607044	5.330387	1.404859
H	-8.838516	5.734566	0.206285
H	-1.591673	3.925865	1.993983
H	-1.950050	2.217639	1.758322
H	-3.116770	3.250833	2.592529
H	-1.822852	2.492692	-1.002146
H	-2.514486	3.967616	-1.657075
H	-1.165732	4.059600	-0.511219
H	-10.140110	-4.066463	0.506349
H	-9.485547	-2.500464	1.003487
H	-8.790860	-3.976816	1.651879
H	-8.191737	-3.237662	-2.594508
H	-9.715535	-3.918472	-1.999246
H	-9.359809	-2.211092	-1.753995
H	-1.808269	-2.251302	-1.344713
H	-1.429805	-3.961587	-1.529590
H	-2.876780	-3.287215	-2.298561
H	-1.287987	-4.100877	1.002875
H	-1.979844	-2.527055	1.418003
H	-2.754098	-3.994359	1.993093
H	-9.496747	2.254075	1.354722
H	-9.874314	3.964771	1.537522
H	-8.425900	3.291266	2.304563
H	-10.021167	4.100494	-0.995039
H	-8.557306	3.990331	-1.988203
H	-9.331734	2.525053	-1.408097

**Compound I-14<sup>+</sup> (UBLYP/SVP, S<sub>0</sub>)**Total energy: -899 318.11 kcal mol<sup>-1</sup>

Dipole moment: 16.8 D

C	-6.162645	-1.528288	0.465742
C	-4.807322	-1.299661	0.466417
C	-4.218127	-0.092539	0.011065



C	2.881794	-2.421270	0.000013	C	1.231166	3.567854	0.005249
C	-3.571327	-1.231757	-0.000001	C	2.439141	-2.893025	-0.009276
C	0.737074	1.248462	-0.000001	C	2.423644	1.477418	-0.006328
C	1.437291	-0.000012	-0.000002	C	-2.423412	1.477304	0.010682
C	0.737083	-1.248499	0.000005	C	-2.438938	2.892913	0.016415
C	2.871147	0.000008	-0.000006	C	-1.231016	3.567798	0.014281
C	3.571330	-1.231759	0.000000	H	-3.382359	-0.973422	-0.008286
C	-2.881789	-2.421273	-0.000014	H	-1.215870	-4.654211	-0.015162
C	1.476194	-2.426126	0.000018	H	3.382608	-0.973471	-0.003299
C	1.476138	2.426109	0.000001	H	1.216050	-4.654220	-0.016496
C	2.881733	2.421290	-0.000006	H	1.216011	4.654215	0.008336
C	3.571298	1.231790	-0.000010	H	3.382590	0.973503	-0.011279
H	-3.416808	3.365822	0.000007	H	-3.382335	0.973338	0.014100
H	-0.971928	3.384539	-0.000003	H	-1.215888	4.654159	0.017487
H	-4.657190	1.216550	0.000013	C	-5.264528	5.379895	-0.138985
H	-0.972024	-3.384570	-0.000029	C	-6.017806	4.045593	0.213979
H	3.416892	-3.365789	0.000020	O	-3.877784	5.028898	0.120525
H	-4.657217	-1.216503	0.000001	O	-5.005704	3.039259	-0.061123
H	4.657220	-1.216497	-0.000004	C	-5.634782	6.576882	0.727495
H	-3.416894	-3.365788	-0.000025	H	-5.048565	7.447262	0.421060
H	0.972032	-3.384573	0.000032	H	-6.695225	6.823202	0.613024
H	0.971923	3.384537	0.000006	H	-5.431133	6.385817	1.781853
H	3.416809	3.365821	-0.000006	C	-5.354714	5.747063	-1.622909
H	4.657188	1.216556	-0.000016	H	-6.356883	6.091928	-1.892359

**Compound (Bpin)<sub>4</sub>-Per**(B3LYP/6-31G (d,p), S<sub>0</sub>)Total energy: -1 513 850 kcal mol<sup>-1</sup>

Dipole moment: 0.0015 D

C	-2.438937	-2.892983	-0.012328	H	-4.643679	6.550317	-1.831251
C	-2.423420	-1.477370	-0.007758	H	-5.097366	4.893440	-2.255396
C	-1.249129	-0.737654	-0.004034	C	-7.243129	3.751280	-0.641960
C	0.000122	-1.436258	-0.007337	H	-7.683843	2.798698	-0.336197
C	0.000103	-2.870130	-0.011264	H	-7.999287	4.532668	-0.515629
C	-1.231002	-3.567848	-0.013311	H	-6.984985	3.680814	-1.699341
C	1.249382	-0.737645	-0.006651	C	-6.363920	3.924627	1.700769
C	2.423661	-1.477397	-0.006514	H	-7.174072	4.602991	1.982526
C	2.439111	2.893041	-0.001716	H	-6.682128	2.899571	1.906144
C	1.231196	-3.567862	-0.012612	H	-5.493636	4.141334	2.325695
C	-1.249129	0.737612	0.002484	O	5.005374	3.039657	-0.095008
C	0.000114	1.436237	0.001852	C	5.262867	5.380085	-0.184838
C	1.249375	0.737652	-0.004305	O	3.877648	-5.030021	0.076225
C	0.000087	2.870102	0.007823	C	5.264318	-5.379012	-0.186415
				C	6.017879	-4.048012	0.178196
				O	-5.005374	-3.039484	0.075356
				C	-6.018538	-4.045856	-0.195659
				C	-5.263685	-5.380157	0.153955
				O	3.877993	5.029722	0.085231
				O	-3.878064	-5.029010	-0.111292
				O	5.005941	-3.039064	-0.087654

C	6.018975	4.047499	0.168663
C	6.375407	3.933163	1.653551
H	6.695665	2.909176	1.861120
H	7.187136	4.613130	1.926767
H	5.509357	4.152114	2.283558
C	7.238448	3.749850	-0.694444
H	7.995219	4.531991	-0.576696
H	7.681535	2.798664	-0.387786
H	6.973011	3.674704	-1.749677
C	5.638392	6.580794	0.674204
H	6.697949	6.827038	0.551661
H	5.049803	7.449669	0.368050
H	5.441817	6.394060	1.730685
C	6.364323	-3.940438	1.665960
H	7.174313	-4.621534	1.941516
H	6.682990	-2.917368	1.880376
H	5.494087	-4.162407	2.289111
C	5.634354	-6.583598	0.669575
H	5.047873	-7.451115	0.355625
H	6.694715	-6.829199	0.552835
H	5.430884	-6.401671	1.725592
C	7.243086	-3.746260	-0.675324
H	7.683884	-2.796392	-0.361369
H	7.999218	-4.528786	-0.556021
H	6.984744	-3.666387	-1.731972
C	5.354407	-5.733201	-1.673479
H	6.356483	-6.075987	-1.945904
H	4.643131	-6.534384	-1.888839
H	5.097334	-4.874003	-2.298476
C	-5.637466	-6.577041	-0.711155
H	-5.049919	-7.447424	-0.407288
H	-6.697404	-6.823453	-0.592293
H	-5.438245	-6.385805	-1.766332
C	-6.370908	-3.924684	-1.680961
H	-7.182188	-4.603067	-1.959408
H	-6.690061	-2.899622	-1.884836
H	-5.503247	-4.141223	-2.309582
C	-7.240279	-3.751802	0.665467
H	-7.682399	-2.799231	0.361703
H	-7.996862	-4.533270	0.542211
H	-6.977692	-3.681459	1.721759
C	-5.347639	-5.747572	1.638184
H	-6.348653	-6.092534	1.911775
H	-4.635684	-6.550805	1.843429
H	-5.087684	-4.894040	2.269725

C	5.343153	5.741132	-1.670832
H	4.630532	6.543339	-1.877780
H	6.343429	6.085121	-1.948314
H	5.081877	4.884842	-2.298076
B	-3.782784	3.661001	0.025154
B	3.782828	3.661414	-0.004011
B	3.782895	-3.661328	-0.007343
B	-3.782773	-3.661128	-0.015959

**Compound (Br)<sub>4</sub>-Per**(B3LYP/6-31G (d,p), S<sub>0</sub>)Total energy: -6 936 347.82 kcal mol<sup>-1</sup>

Dipole moment: 0 D

C	-2.870519	-2.405753	-0.000006
C	-1.467131	-2.428014	-0.000005
C	-0.736740	-1.247265	-0.000001
C	-1.434915	0.000002	0.000000
C	-2.866741	-0.000001	0.000000
C	-3.574357	-1.227674	-0.000003
C	-0.736743	1.247272	0.000001
C	-1.467143	2.428017	0.000006
C	2.870526	2.405754	-0.000006
C	-3.574363	1.227667	0.000003
C	0.736742	-1.247264	0.000001
C	1.434914	0.000004	0.000000
C	0.736741	1.247273	-0.000001
C	2.866740	0.000003	0.000000
C	3.574361	1.227673	-0.000003
C	-2.870530	2.405750	0.000007
C	1.467139	2.428019	-0.000005
C	1.467135	-2.428012	0.000004
C	2.870522	-2.405749	0.000005
C	3.574359	-1.227669	0.000003
H	-0.976278	-3.390972	-0.000007
H	-4.657739	-1.224680	-0.000003
H	-0.976297	3.390978	0.000009
H	-4.657745	1.224669	0.000004
H	4.657743	1.224676	-0.000003
H	0.976292	3.390979	-0.000008
H	0.976283	-3.390971	0.000006
H	4.657740	-1.224674	0.000003
Br	3.802752	-4.070220	0.000009
Br	3.802759	4.070223	-0.000011

Br	-3.802766	4.070218	0.000012	C	6.093884	1.540831	-2.377191
Br	-3.802746	-4.070226	-0.000010	C	7.250881	1.353954	-1.615324
				H	8.189659	1.805788	0.261044
				H	6.039104	1.106467	-3.374764
<b>Compound (Bmes<sub>2</sub>)<sub>4</sub>-Per</b>				C	3.921449	5.102863	0.537794
(DFT B3LYP/6-31G (d,p), S <sub>0</sub> )				C	4.477303	6.142156	-0.252994
Total energy: -2 299 118.34 kcal mol <sup>-1</sup>				C	3.468777	5.421869	1.842006
Dipole moment: 0.00028 D				C	4.538959	7.445772	0.246404
				C	3.576286	6.733190	2.319637
				C	4.094002	7.764575	1.533609
C	2.447730	2.893775	0.017218	H	4.955966	8.232420	-0.380423
C	2.418076	1.475385	0.013540	H	3.249142	6.953125	3.334758
C	1.244958	0.738065	0.007485	C	-3.929081	5.097092	-0.536653
C	-0.001316	1.437479	-0.000417	C	-4.486511	6.134548	0.255268
C	-0.002563	2.872403	0.000026	C	-3.476236	5.418401	-1.840294
C	1.232973	3.567376	0.017815	C	-4.549687	7.438797	-0.242469
C	-1.246351	0.735853	-0.008789	C	-3.585273	6.730133	-2.316252
C	-2.420781	1.471105	-0.014849	C	-4.104641	7.759855	-1.529015
C	-2.447693	-2.894699	0.016406	H	-4.967937	8.224091	0.385205
C	-1.239315	3.565179	-0.017393	H	-3.258050	6.951803	-3.330986
C	1.246288	-0.736701	-0.008571	C	5.061574	-2.855193	0.607760
C	0.001276	-1.438348	-0.000861	C	6.242131	-2.686212	-0.156769
C	-1.245012	-0.738936	0.006935	C	5.006367	-2.259397	1.894547
C	0.002592	-2.873284	-0.000840	C	7.303652	-1.928149	0.350386
C	-1.232928	-3.568278	0.016770	C	6.096408	-1.530917	2.377492
C	-2.452911	2.889449	-0.017616	C	7.253325	-1.342213	1.615932
C	-2.418106	-1.476296	0.012806	H	8.193259	-1.792449	-0.260230
C	2.420734	-1.471914	-0.014261	H	6.040694	-1.096650	3.375055
C	2.452925	-2.890249	-0.017656	C	-5.056853	-2.864621	-0.607031
C	1.239375	-3.566031	-0.018230	C	-6.236844	-2.697134	0.158679
H	3.373864	0.965004	0.008162	C	-5.003927	-2.269343	-1.894151
H	1.216825	4.655292	0.025918	C	-7.300088	-1.940967	-0.347692
H	-3.375683	0.959048	-0.010142	C	-6.095659	-1.542887	-2.376316
H	-1.225098	4.653121	-0.024689	C	-7.252054	-1.355613	-1.613597
H	-1.216771	-4.656193	0.024749	H	-8.189197	-1.806337	0.263876
H	-3.373923	-0.965954	0.007468	H	-6.041690	-1.109016	-3.374144
H	3.375606	-0.959827	-0.008738	C	-3.921163	-5.103656	0.538347
H	1.225197	-4.653978	-0.025987	C	-4.477863	-6.143077	-0.251595
B	3.826397	-3.633003	0.019017	C	-3.467537	-5.422326	1.842379
B	3.819863	3.639082	-0.019174	C	-4.539401	-7.446543	0.248320
B	-3.826145	3.632678	0.018508	C	-3.574940	-6.733419	2.320527
B	-3.819817	-3.640015	-0.019092	C	-4.093460	-7.765003	1.535219
C	5.056493	2.863514	-0.607771	H	-4.957097	-8.233310	-0.377884
C	6.237161	2.696481	0.157047	H	-3.247093	-6.953057	3.335496
C	5.002562	2.267613	-1.894546	C	-5.062696	2.855403	0.604954
C	7.299979	1.940050	-0.349788				

C	-5.009446	2.257043	1.890619	H	4.149197	9.212019	3.142092
C	-6.243201	2.690106	-0.160608	H	5.063339	9.693613	1.699320
C	-6.101119	1.529508	2.371431	C	5.001756	5.882890	-1.649822
C	-7.306433	1.933145	0.344467	H	5.855112	5.197316	-1.637821
C	-7.257993	1.344674	1.608949	H	4.241172	5.430605	-2.296416
H	-6.046739	1.093060	3.368114	H	5.321564	6.817502	-2.121950
H	-8.195943	1.800303	-0.266934	C	3.798565	-2.399242	2.800637
C	3.930966	-5.096636	-0.537803	H	3.065000	-1.605565	2.614356
C	4.489019	-6.134701	0.252972	H	3.274520	-3.348719	2.661779
C	3.479050	-5.416619	-1.842097	H	4.098985	-2.332226	3.851982
C	4.553542	-7.438200	-0.246462	C	8.412260	-0.544101	2.160204
C	3.589465	-6.727653	-2.319740	H	8.088889	0.452288	2.484469
C	4.109359	-7.757949	-1.533660	H	8.861625	-1.039034	3.030824
H	4.972208	-8.223953	0.380370	H	9.196641	-0.416141	1.407301
H	3.262895	-6.948272	-3.334904	C	6.385742	-3.281256	-1.541962
C	6.379478	3.291919	1.542202	H	6.312920	-4.373195	-1.523158
H	7.347214	3.024751	1.979165	H	5.606137	-2.921894	-2.223974
H	6.304690	4.383725	1.523258	H	7.353066	-3.012301	-1.978743
H	5.600410	2.931245	2.224135	C	-5.011437	5.872714	1.651451
C	3.794788	2.405537	-2.800968	H	-4.251663	5.417781	2.297095
H	3.062552	1.610550	-2.615055	H	-5.330043	6.806653	2.125731
H	3.269070	3.354083	-2.662077	H	-5.865802	5.188388	1.637674
H	4.095640	2.339249	-3.852236	C	-2.906616	4.376451	-2.784317
C	8.411159	0.557559	-2.159248	H	-1.825078	4.258808	-2.648300
H	8.089546	-0.439713	-2.482552	H	-3.348560	3.387246	-2.638490
H	8.859325	1.052570	-3.030436	H	-3.079183	4.670914	-3.825328
H	9.195996	0.431694	-1.406465	C	-4.169961	9.178231	-2.040944
C	-5.003537	-5.884220	-1.648038	H	-3.299589	9.757937	-1.704611
H	-5.857191	-5.199018	-1.635413	H	-4.180630	9.208370	-3.135777
H	-4.243695	-5.431697	-2.295314	H	-5.064926	9.694886	-1.676094
H	-5.323338	-6.819030	-2.119781	C	5.013023	-5.874336	1.649767
C	-2.898901	-4.378247	2.784644	H	5.865929	-5.188188	1.637506
H	-3.070528	-4.671533	3.826142	H	4.252078	-5.422217	2.296019
H	-1.817608	-4.259227	2.647924	H	5.333430	-6.808480	2.122421
H	-3.342382	-3.389905	2.637688	C	4.176576	-9.175585	-2.047384
C	-4.157341	-9.182600	2.049477	H	5.077229	-9.688392	-1.691101
H	-3.290764	-9.764378	1.707010	H	3.312080	-9.759655	-1.703574
H	-4.159556	-9.211294	3.144383	H	4.177539	-9.204742	-3.142275
H	-5.056102	-9.698085	1.692306	C	2.909103	-4.373927	-2.785103
C	2.900994	4.377989	2.784997	H	3.351469	-3.384958	-2.638914
H	3.344834	3.389764	2.638297	H	3.080987	-4.667783	-3.826392
H	3.072926	4.671813	3.826292	H	1.827693	-4.256026	-2.648374
H	1.819695	4.258443	2.648785	C	-3.796713	-2.407591	-2.801256
C	4.158517	9.182361	2.047274	H	-3.063431	-1.613729	-2.614700
H	3.298331	9.767659	1.694887	H	-3.272070	-3.356948	-2.663696

H	-4.097905	-2.339716	-3.852319	C	2.333807	-1.616159	-0.023567
C	-6.377990	-3.291646	1.544350	C	2.265055	-3.016689	0.168631
H	-6.303295	-4.383470	1.526095	C	1.031650	-3.604866	0.411074
H	-5.598287	-2.930547	2.225335	H	3.424277	0.755826	0.104550
H	-7.345309	-3.024068	1.981982	H	1.502342	4.500095	-0.701494
C	-8.412791	-0.559562	-2.157042	H	-3.290517	1.173276	0.112866
H	-8.091193	0.437021	-2.482458	H	-0.930724	4.647192	-0.720691
H	-8.862551	-1.055815	-3.026709	H	-1.482379	-4.534949	0.589465
H	-9.196410	-0.432094	-1.403266	H	-3.421966	-0.751025	0.164650
C	-3.802284	2.393195	2.798155	H	3.293204	-1.178657	-0.260021
H	-4.104142	2.326372	3.849104	H	0.957844	-4.675042	0.562506
H	-3.070588	1.597682	2.612351	N	-3.434404	3.759302	-0.347003
H	-3.275575	3.341350	2.660451	N	-3.869682	-3.289410	0.389992
C	-6.385154	3.288254	-1.544644	N	3.435972	-3.792809	0.079728
H	-6.312988	4.380200	-1.523168	N	3.869537	3.329369	-0.291274
H	-5.604435	2.931035	-2.226457	C	3.359924	-5.165931	-0.291488
H	-7.351757	3.019804	-1.983336	C	4.023913	-6.136189	0.473042
C	-8.419559	0.549241	2.151530	C	2.652019	-5.570106	-1.425280
H	-8.096943	-0.443282	2.488026	C	3.981994	-7.473589	0.108349
H	-8.876932	1.051749	3.013662	H	4.579276	-5.825626	1.351475
H	-9.197749	0.412711	1.393736	C	2.584861	-6.915993	-1.787304

**Compound (DPA)<sub>4</sub>-Per**(B3LYP/6-31G (d,p), S<sub>0</sub>)Total energy: -2 356 809.05 kcal mol<sup>-1</sup>

Dipole moment: 2.6740 D

C	2.609538	2.701189	-0.314511	H	2.136821	-4.825039	-2.021529
C	2.515458	1.305665	-0.094121	C	3.256188	-7.875482	-1.021607
C	1.295888	0.649248	-0.099173	H	4.492802	-8.231483	0.692226
C	0.093345	1.407027	-0.211474	H	2.021612	-7.197783	-2.668120
C	0.178151	2.819097	-0.425347	C	4.729621	-3.225737	0.236651
C	1.449194	3.433271	-0.520535	C	5.748896	-3.560580	-0.658404
C	-1.189500	0.806017	-0.056952	C	5.027167	-2.350789	1.295097
C	-2.320060	1.605117	-0.078765	C	7.044017	-3.072858	-0.491971
C	-2.581262	-2.703954	0.391166	H	5.529006	-4.227027	-1.484873
C	-1.008515	3.583645	-0.528607	C	6.307077	-1.835598	1.447988
C	1.207298	-0.813313	0.049501	H	4.247195	-2.079454	1.997908
C	-0.074237	-1.416393	0.216702	C	7.332803	-2.212196	0.570830
C	-1.276716	-0.649888	0.151733	H	7.809859	-3.364762	-1.198956
C	-0.154672	-2.834898	0.392241	H	6.543078	-1.161835	2.264274
C	-1.424860	-3.457028	0.486123	O	3.265130	-9.215163	-1.288847
C	-2.249398	2.996013	-0.329105	C	2.538444	-9.667695	-2.418356
C	-2.494107	-1.300757	0.242641	H	2.667329	-10.750336	-2.447413
				H	1.469763	-9.432788	-2.332320
				H	2.924821	-9.232762	-3.349156
				C	3.976227	4.707075	0.053924
				C	4.721766	5.577166	-0.754776
				C	3.366290	5.213201	1.203731
				C	4.853809	6.916120	-0.418074
				H	5.201330	5.187338	-1.646143

C	3.473776	6.563520	1.538102	C	-4.820049	-2.803364	-0.549039
H	2.788631	4.546046	1.833975	C	-6.142074	-2.550017	-0.174851
C	4.224394	7.422137	0.727633	C	-4.431526	-2.543051	-1.873023
H	5.428236	7.596892	-1.036805	C	-7.065700	-2.051190	-1.094832
H	2.982032	6.926309	2.432009	H	-6.447982	-2.742079	0.848060
C	5.075799	2.606555	-0.494399	C	-5.336603	-2.026147	-2.786312
C	6.169688	2.828819	0.346032	H	-3.407877	-2.738680	-2.172080
C	5.214268	1.683978	-1.545263	C	-6.662099	-1.779765	-2.406167
C	7.386316	2.182944	0.132645	H	-8.077351	-1.842495	-0.772071
H	6.072094	3.530770	1.166581	H	-5.043232	-1.816580	-3.809272
C	6.413149	1.012884	-1.743774	O	8.578516	-1.716590	0.843852
H	4.374673	1.498643	-2.206033	O	-7.468393	-1.260387	-3.380932
C	7.517430	1.275436	-0.922270	O	-5.096943	-7.833843	3.416122
H	8.214491	2.390533	0.797905	O	4.401910	8.756045	0.964254
H	6.526069	0.301030	-2.554014	O	8.679317	0.625929	-1.239513
C	-3.415640	5.139194	0.000907	O	-8.381014	1.163798	-0.723614
C	-4.140819	6.056101	-0.761646	O	-3.414326	9.162490	1.110735
C	-2.713482	5.601794	1.125482	C	-8.854951	-1.124136	-3.093438
C	-4.177440	7.408729	-0.419832	H	-9.022786	-0.378906	-2.310775
H	-4.689803	5.701975	-1.627643	H	-9.319903	-0.790364	-4.022302
C	-2.726641	6.947402	1.460126	H	-9.293065	-2.085413	-2.795368
H	-2.150008	4.897094	1.726658	C	-4.596707	-7.990865	4.731429
C	-3.460943	7.862182	0.692124	H	-4.949329	-7.192733	5.397914
H	-4.752395	8.092566	-1.031654	H	-4.975816	-8.949451	5.088382
H	-2.185255	7.315019	2.325125	H	-3.499043	-8.007717	4.748692
C	-4.706253	3.125046	-0.442688	C	3.771564	9.313317	2.104606
C	-5.673733	3.340560	0.540515	H	4.135770	8.855129	3.033246
C	-5.009085	2.266085	-1.511653	H	4.026735	10.373751	2.103761
C	-6.917906	2.713472	0.473686	H	2.680462	9.203679	2.057560
H	-5.448943	4.005406	1.367291	C	9.838312	0.993124	-0.508989
C	-6.236332	1.620406	-1.577172	H	9.750242	0.706183	0.545093
H	-4.263624	2.093387	-2.280298	H	10.668009	0.449782	-0.962578
C	-7.197156	1.840764	-0.581052	H	10.031248	2.070740	-0.581420
H	-7.645004	2.901080	1.253783	C	-9.351763	1.304015	0.299068
H	-6.473292	0.948546	-2.393868	H	-10.190183	0.668230	0.010576
C	-4.161198	-4.432092	1.171253	H	-8.963699	0.973157	1.270485
C	-4.963013	-5.467681	0.662874	H	-9.700583	2.340670	0.387316
C	-3.665635	-4.551215	2.474225	C	-4.133638	10.123170	0.357432
C	-5.263179	-6.577246	1.439619	H	-3.965836	11.081972	0.849601
H	-5.352716	-5.391903	-0.345873	H	-3.771711	10.179612	-0.677261
C	-3.944066	-5.675903	3.250614	H	-5.209663	9.906163	0.346511
H	-3.047399	-3.758927	2.881059	C	9.651365	-2.214342	0.060672
C	-4.752373	-6.695672	2.738219	H	9.556564	-1.902629	-0.985639
H	-5.883342	-7.378264	1.051779	H	10.560521	-1.785722	0.483907
H	-3.537414	-5.735063	4.252604	H	9.710183	-3.308626	0.114075

**Compound 3-6** (B3LYP/6-31G (d), S<sub>0</sub>)Total energy: -1 413 365.49 kcal mol<sup>-1</sup>

Dipole moment: 5.67 D

				H	8.373691	-2.941772	-0.206638
				H	5.753278	-2.679356	-3.610165
				C	-5.694094	1.200291	-0.558103
				C	-6.741427	1.822709	0.139833
				C	-5.390736	1.640284	-1.849166
				C	-7.465492	2.854526	-0.443474
				H	-6.988298	1.483317	1.141052
				C	-6.099331	2.692383	-2.435913
				H	-4.587737	1.160812	-2.400947
				C	-7.146491	3.301981	-1.734039
				H	-8.278281	3.337746	0.089861
				H	-5.834925	3.010544	-3.437659
				C	-5.691108	-0.905163	0.692742
				C	-6.790774	-1.501645	0.072100
				C	-5.326134	-1.330938	1.980386
				C	-7.524103	-2.502019	0.715810
				H	-7.082058	-1.176025	-0.921878
				C	-6.035110	-2.339848	2.618419
				H	-4.477078	-0.869717	2.475618
				C	-7.142569	-2.931354	1.992584
				H	-8.373691	-2.941773	0.206642
				H	-5.753276	-2.679354	3.610168
				O	7.780610	-3.906962	-2.705888
				O	7.909754	4.328950	2.216400
				O	-7.909756	4.328948	-2.216398
				O	-7.780609	-3.906961	2.705893
				C	-8.890174	-4.559102	2.105545
				H	-8.597329	-5.068962	1.178409
				H	-9.231772	-5.295858	2.834132
				H	-9.701719	-3.850353	1.893494
				C	-7.634341	4.811878	-3.523164
				H	-7.773675	4.024897	-4.276034
				H	-8.350374	5.615814	-3.700227
				H	-6.613004	5.208957	-3.593828
				C	7.634338	4.811880	3.523165
				H	8.350371	5.615816	3.700228
				H	6.613001	5.208959	3.593828
				H	7.773671	4.024899	4.276036
				C	8.890174	-4.559103	-2.105540
				H	8.597330	-5.068962	-1.178403
				H	9.231773	-5.295860	-2.834125
				H	9.701720	-3.850353	-1.893489
				O	1.367557	-3.498078	-0.024739
				O	-1.367556	-3.498078	0.024737
				C	0.778099	-2.430967	-0.011328
C	2.834596	1.317362	-0.030721				
C	1.426442	1.318621	-0.007523				
C	0.718271	0.085263	-0.006354				
C	1.470528	-1.119752	-0.018019				
C	2.857877	-1.095911	-0.021801				
C	3.564506	0.127173	-0.032281				
C	-0.718271	0.085263	0.006348				
C	-1.426442	1.318620	0.007519				
C	-2.834596	1.317362	0.030718				
C	-3.564505	0.127172	0.032280				
C	-2.857876	-1.095912	0.021798				
C	-1.470527	-1.119753	0.018013				
C	0.681256	2.548074	-0.002708				
C	-0.681256	2.548074	0.002704				
H	3.359603	2.267402	-0.042970				
H	3.392116	-2.039322	-0.013768				
H	-3.359604	2.267402	0.042969				
H	-3.392115	-2.039322	0.013764				
H	1.231937	3.485441	-0.005545				
H	-1.231938	3.485440	0.005543				
N	4.968828	0.130296	-0.035780				
N	-4.968828	0.130295	0.035780				
C	5.694094	1.200292	0.558103				
C	6.741427	1.822709	-0.139832				
C	5.390734	1.640286	1.849165				
C	7.465492	2.854527	0.443475				
H	6.988300	1.483317	-1.141050				
C	6.099328	2.692385	2.435913				
H	4.587735	1.160814	2.400947				
C	7.146489	3.301982	1.734041				
H	8.278281	3.337747	-0.089859				
H	5.834922	3.010546	3.437659				
C	5.691109	-0.905162	-0.692741				
C	6.790775	-1.501644	-0.072098				
C	5.326135	-1.330939	-1.980385				
C	7.524104	-2.502019	-0.715807				
H	7.082058	-1.176023	0.921880				
C	6.035111	-2.339850	-2.618416				
H	4.477079	-0.869718	-2.475617				
C	7.142570	-2.931355	-1.992581				

C	-0.778098	-2.430968	0.011318	C	-6.133834	-3.269528	2.349086
				H	-4.574545	-1.787096	2.311983
				C	-7.208972	-3.836947	1.654852
<b>Compound 3-7</b> (DFT B3LYP/6-31G (d), S <sub>0</sub> )				H	-8.364416	-3.815632	-0.154581
Total energy: -1 551 680.98 kcal mol <sup>-1</sup>				H	-5.867681	-3.606376	3.344238
Dipole moment: 8.86 D				C	-5.660230	0.358668	-0.724950
				C	-6.703542	0.995445	-0.051152
				C	-5.325434	0.787480	-2.019443
				C	-7.410899	2.042715	-0.648746
C	-2.829821	-1.918064	-0.067476	H	-6.971097	0.666230	0.948388
C	-1.429549	-1.929195	-0.025910	C	-6.007987	1.840145	-2.613147
C	-0.713490	-0.695635	-0.014908	H	-4.518662	0.293552	-2.552693
C	-1.454430	0.519424	-0.035644	C	-7.058515	2.475313	-1.932677
C	-2.848319	0.501581	-0.056014	H	-8.216726	2.515071	-0.099347
C	-3.552878	-0.715527	-0.077744	H	-5.750550	2.182868	-3.610418
C	0.713489	-0.695635	0.014906	C	5.702242	-1.772220	-0.480944
C	1.429547	-1.929196	0.025910	C	6.778996	-2.352248	0.209211
C	2.829819	-1.918066	0.067475	C	5.398160	-2.234761	-1.763951
C	3.552877	-0.715529	0.077740	C	7.529259	-3.365324	-0.372908
C	2.848318	0.501579	0.056010	H	7.027133	-1.993992	1.203539
C	1.454430	0.519423	0.035641	C	6.133848	-3.269522	-2.349088
C	0.715786	1.772521	0.018093	H	4.574556	-1.787094	-2.311989
C	-0.715786	1.772522	-0.018095	C	7.208985	-3.836940	-1.654851
C	-0.680825	-3.158456	-0.011997	H	8.364422	-3.815625	0.154586
C	0.680822	-3.158457	0.011999	H	5.867700	-3.606369	-3.344242
N	1.397210	2.928756	0.036267	C	5.660226	0.358669	0.724950
C	0.709111	4.067278	0.018384	C	6.703537	0.995447	0.051153
C	-0.709109	4.067279	-0.018397	C	5.325424	0.787481	2.019441
N	-1.397209	2.928757	-0.036272	C	7.410891	2.042720	0.648748
C	-1.453708	5.297117	-0.037052	H	6.971095	0.666233	-0.948386
N	-2.044573	6.297900	-0.050136	C	6.007973	1.840147	2.613146
C	1.453710	5.297116	0.037057	H	4.518652	0.293552	2.552689
N	2.044576	6.297899	0.050146	C	7.058502	2.475318	1.932678
H	-3.364508	-2.862273	-0.092327	H	8.216717	2.515077	0.099352
H	-3.385098	1.441926	-0.055642	H	5.750533	2.182871	3.610416
H	3.364506	-2.862275	0.092328	O	-7.672811	3.493389	-2.603885
H	3.385098	1.441924	0.055638	O	-7.999585	-4.843319	2.136015
H	-1.230860	-4.096094	-0.022304	O	7.999603	-4.843309	-2.136013
H	1.230857	-4.096094	0.022308	O	7.672794	3.493396	2.603888
N	-4.955297	-0.719227	-0.115426	C	8.711335	4.203040	1.943048
N	4.955296	-0.719228	0.115424	H	8.344273	4.677802	1.023980
C	-5.702240	-1.772221	0.480943	H	9.038551	4.971606	2.644706
C	-6.778994	-2.352251	-0.209210	H	9.554981	3.542149	1.703970
C	-5.398151	-2.234764	1.763948	C	7.725519	-5.347817	-3.434972
C	-7.529252	-3.365330	0.372911	H	7.830149	-4.563938	-4.196621
H	-7.027135	-1.993995	-1.203536				

H	8.465766	-6.129294	-3.612818
H	6.717185	-5.779116	-3.489846
C	-7.725495	-5.347827	3.434972
H	-8.465741	-6.129307	3.612820
H	-6.717161	-5.779124	3.489843
H	-7.830126	-4.563949	4.196623
C	-8.711352	4.203031	-1.943043
H	-8.344287	4.677795	-1.023976
H	-9.038571	4.971596	-2.644701
H	-9.554996	3.542139	-1.703962

**Compound 3-8** (DFT B3LYP/6-31G (d), S<sub>0</sub>)Total energy: -1 532 391.68 kcal mol<sup>-1</sup>

Dipole moment: 0.040 D

C	2.832040	-1.942374	0.064264
C	1.429154	-1.949741	0.024396
C	0.715647	-0.715651	0.013784
C	1.452895	0.499075	0.030944
C	2.844868	0.476542	0.045242
C	3.548984	-0.741466	0.068313
C	-0.715647	-0.715651	-0.013779
C	-1.429155	-1.949741	-0.024391
C	-2.832040	-1.942374	-0.064262
C	-3.548984	-0.741466	-0.068313
C	-2.844868	0.476543	-0.045240
C	-1.452895	0.499075	-0.030939
C	-0.722101	1.768918	-0.016463
C	0.722102	1.768917	0.016479
C	0.681091	-3.178344	0.011380
C	-0.681091	-3.178344	-0.011375
N	-1.408040	2.904543	-0.035200
N	1.408041	2.904543	0.035196
H	3.366363	-2.887088	0.087522
H	3.380621	1.417664	0.039752
H	-3.366364	-2.887087	-0.087522
H	-3.380621	1.417664	-0.039749
H	1.231261	-4.116191	0.021191
H	-1.231261	-4.116191	-0.021187
N	4.958146	-0.743979	0.093046
N	-4.958146	-0.743979	-0.093048
C	5.689489	-1.773503	-0.558077
C	6.768346	-2.397294	0.090133

C	5.360948	-2.178704	-1.854678
C	7.497938	-3.392964	-0.546286
H	7.033856	-2.087703	1.096251
C	6.075336	-3.195787	-2.494554
H	4.531926	-1.701270	-2.368068
C	7.153718	-3.804776	-1.842224
H	8.333646	-3.876771	-0.050048
H	5.788735	-3.487765	-3.498238
C	5.668815	0.291843	0.757021
C	6.780066	0.889525	0.157271
C	5.278006	0.724673	2.035517
C	7.499417	1.893737	0.812098
H	7.093088	0.561671	-0.829218
C	5.972461	1.737325	2.683131
H	4.418534	0.265772	2.514184
C	7.091866	2.327991	2.078276
H	8.359291	2.331243	0.318201
H	5.670541	2.078937	3.668387
C	-5.689489	-1.773503	0.558077
C	-6.768345	-2.397295	-0.090133
C	-5.360948	-2.178702	1.854678
C	-7.497937	-3.392965	0.546287
H	-7.033855	-2.087706	-1.096252
C	-6.075336	-3.195785	2.494555
H	-4.531926	-1.701267	2.368067
C	-7.153717	-3.804775	1.842226
H	-8.333645	-3.876772	0.050049
H	-5.788735	-3.487761	3.498240
C	-5.668816	0.291843	-0.757024
C	-6.780066	0.889524	-0.157273
C	-5.278007	0.724671	-2.035520
C	-7.499418	1.893736	-0.812101
H	-7.093088	0.561671	0.829216
C	-5.972463	1.737323	-2.683134
H	-4.418535	0.265770	-2.514186
C	-7.091867	2.327989	-2.078280
H	-8.359292	2.331242	-0.318204
H	-5.670542	2.078934	-3.668391
O	7.714535	3.309356	2.801424
O	7.925216	-4.799838	-2.378734
O	-7.925215	-4.799837	2.378737
O	-7.714537	3.309353	-2.801428
C	-8.848484	3.942612	-2.229247
H	-8.589987	4.450713	-1.290628
H	-9.180031	4.679543	-2.962540

H	-9.656241	3.222038	-2.043582	H	-6.014852	1.365506	0.838377
C	-7.620157	-5.247957	3.690694	C	-3.593460	-2.739114	0.209935
H	-7.720862	-4.435721	4.422823	H	-3.801929	-3.188579	-0.773585
H	-8.346135	-6.031269	3.914281	H	-2.985366	-3.461822	0.759632
H	-6.605043	-5.663555	3.743926	C	-4.905761	-2.520719	0.961150
C	7.620158	-5.247960	-3.690691	H	-5.473698	-3.454749	1.036916
H	8.346137	-6.031272	-3.914277	H	-4.687939	-2.181104	1.981762
H	6.605044	-5.663559	-3.743922	C	-5.738919	-1.473688	0.242929
H	7.720862	-4.435725	-4.422821	H	-6.133601	-1.886356	-0.701647
C	8.848482	3.942614	2.229242	H	-6.606575	-1.199753	0.857304
H	8.589986	4.450715	1.290623	C	-5.062864	1.973928	-1.006258
H	9.180028	4.679546	2.962535	H	-4.957977	1.585306	-2.027976
H	9.656240	3.222041	2.043579	H	-5.655455	2.893765	-1.063734
C	0.716766	4.066508	0.019061	C	-3.686055	2.272688	-0.421040
C	-0.716764	4.066508	-0.019102	H	-3.787601	2.844100	0.513697
C	1.413445	5.305155	0.039919	H	-3.130524	2.928673	-1.089306
C	0.711056	6.488771	0.020472	N	-4.976984	-0.260978	-0.023405
H	1.243049	7.436024	0.036288	C	3.560137	-2.754901	-0.326578
C	-0.711058	6.488771	-0.020432	H	3.464155	-3.345103	0.597081
C	-1.413444	5.305155	-0.039936	H	3.057355	-3.334624	-1.108917
H	-1.243051	7.436025	-0.036215	C	5.037149	-2.608167	-0.687775
H	-2.498563	5.278977	-0.071388	H	5.563095	-3.557862	-0.536990

**Compound 3-7'** (DFT B3LYP/6-31G (d), S<sub>0</sub>)Total energy: 840 420.97 kcal mol<sup>-1</sup>

Dipole moment: 6.17 D

C	3.589001	-0.226993	-0.039250	H	5.143481	-2.333274	-1.744269
C	2.893298	1.013508	0.115421	C	5.661224	-1.513136	0.160576
C	1.490853	1.016925	0.149561	H	6.720448	-1.385380	-0.085685
C	0.726215	-0.178685	0.021456	H	5.601907	-1.781006	1.233136
C	1.436718	-1.403722	-0.086317	C	5.738080	0.928587	0.320306
C	2.856688	-1.422032	-0.145124	H	6.770923	0.802739	-0.022679
C	0.742804	2.257857	0.411730	H	5.765814	1.012441	1.423673
C	-0.724298	-0.174753	0.013366	C	5.109737	2.172642	-0.279475
C	-1.488474	1.030574	-0.056951	H	5.688609	3.061667	-0.004876
C	-0.750915	2.308842	0.014782	H	5.129064	2.087994	-1.373574
C	-2.889226	1.009243	-0.167606	C	3.676606	2.307469	0.225479
C	-3.586679	-0.236046	-0.042371	H	3.156392	3.107075	-0.307304
C	-2.850063	-1.430913	0.051412	H	3.682947	2.631458	1.274044
C	-1.432250	-1.407607	0.011056	N	4.991481	-0.248548	-0.099546
C	-5.780140	0.944600	-0.155812	O	1.214666	3.259653	0.931596
H	-6.733876	0.660408	-0.617778	O	-1.227272	3.422070	-0.164204
				C	-0.676215	-2.625104	-0.052091
				H	-1.193780	-3.576120	-0.084590
				C	0.683193	-2.622958	-0.120030
				H	1.200052	-3.572461	-0.186086

**Compound 3-15** (DFT B3LYP/6-31 G(d), S<sub>0</sub>)Total energy: 933 187.216 kcal mol<sup>-1</sup>

Dipole moment: 0.40 D

				H	2.484296	1.611247	2.360114
				H	3.701815	0.569904	3.144896
				H	4.691910	-2.174423	-1.446917
				H	5.022870	-0.462066	-1.075525
				H	2.484338	-1.611245	-2.360128
				H	3.701861	-0.569884	-3.144880
				H	-2.484319	-1.611219	2.360141
				H	-3.701837	-0.569850	3.144892
				H	-4.691904	-2.174395	1.446947
				H	-5.022856	-0.462039	1.075541
				H	-2.484364	1.611220	-2.360146
				H	-3.701880	0.569837	-3.144878
				H	-4.691942	2.174375	-1.446924
				H	-5.022867	0.462017	-1.075503
C	1.198576	2.835616	-0.169622				
C	1.199512	1.442576	-0.170455				
C	0.000003	0.734996	-0.000004				
C	-1.199505	1.442580	0.170434				
C	-1.198567	2.835620	0.169575				
C	0.000005	3.533112	-0.000030				
C	0.000003	-0.734995	0.000003				
C	1.199511	-1.442578	0.170447				
C	1.198576	-2.835617	0.169599				
C	0.000005	-3.533111	-0.000001				
C	-1.198568	-2.835618	-0.169597				
C	-1.199506	-1.442578	-0.170442				
C	-2.474627	-0.654070	-0.418361				
C	-2.474624	0.654073	0.418364				
C	2.474632	0.654066	-0.418369				
C	2.474629	-0.654068	0.418371				
O	-3.632879	1.432879	0.122468				
O	-3.632878	-1.432875	-0.122459				
O	3.632880	1.432880	-0.122470				
O	3.632879	-1.432883	0.122478				
O	2.494229	0.372584	-1.799320				
O	2.494220	-0.372587	1.799323				
O	-2.494214	0.372606	1.799318				
O	-2.494230	-0.372603	-1.799316				
C	4.235746	1.221444	1.160822				
C	3.209805	0.804752	2.195889				
C	4.235764	-1.221435	-1.160802				
C	3.209836	-0.804745	-2.195884				
C	-3.209818	-0.804721	2.195895				
C	-4.235753	-1.221412	1.160821				
C	-3.209852	0.804713	-2.195888				
C	-4.235775	1.221400	-1.160801				
H	2.136819	3.362741	-0.304936				
H	-2.136810	3.362748	0.304881				
H	0.000006	4.619618	-0.000041				
H	2.136819	-3.362742	0.304909				
H	0.000005	-4.619617	-0.000005				
H	-2.136810	-3.362745	-0.304904				
H	4.691882	2.174436	1.446939				
H	5.022858	0.462079	1.075561				

**Permission of Wiley-VCH****Pyrene MO Shuffle Controlling Excited State and Redox Properties by Changing the Nature of the Frontier Orbitals**

This Agreement between Universität Würzburg -- Julia Merz ("You") and John Wiley and Sons ("John Wiley and Sons") consists of your license details and the terms and conditions provided by John Wiley and Sons and Copyright Clearance Center.

License Number	4598181386794
License date	May 29, 2019
Licensed Content Publisher	John Wiley and Sons
Licensed Content Publication	Chemistry - A European Journal
Licensed Content Title	Pyrene Molecular Orbital Shuffle—Controlling Excited State and Redox Properties by Changing the Nature of the Frontier Orbitals
Licensed Content Author	Julia Merz, Julian Fink, Alexandra Friedrich, et al
Licensed Content Date	Aug 21, 2017
Licensed Content Volume	23
Licensed Content Issue	53
Licensed Content Pages	17
Type of use	Dissertation/Thesis
Requestor type	Author of this Wiley article
Format	Print and electronic
Portion	Full article
Will you be translating?	No
Title of your thesis / dissertation	C-H BORYLATION: A ROUTE TO NOVEL PYRENES AND PERYLENES AND THE INVESTIGATION OF THEIR EXCITED STATES AND REDOX PROPERTIES
Expected completion date	Jul 2019
Expected size (number of pages)	200
Requestor Location	Universität Würzburg Am Hubland 97074 Würzburg

Würzburg, Bayern 97074  
Germany  
Attn: Universität Würzburg  
Publisher Tax ID EU826007151  
Total 0.00 EUR  
Terms and Conditions  
**TERMS AND CONDITIONS**

This copyrighted material is owned by or exclusively licensed to John Wiley & Sons, Inc. or one of its group companies (each a "Wiley Company") or handled on behalf of a society with which a Wiley Company has exclusive publishing rights in relation to a particular work (collectively "WILEY"). By clicking "accept" in connection with completing this licensing transaction, you agree that the following terms and conditions apply to this transaction (along with the billing and payment terms and conditions established by the Copyright Clearance Center Inc., ("CCC's Billing and Payment terms and conditions"), at the time that you opened your RightsLink account (these are available at any time at <http://myaccount.copyright.com>).

### Terms and Conditions

- The materials you have requested permission to reproduce or reuse (the "Wiley Materials") are protected by copyright.
- You are hereby granted a personal, non-exclusive, non-sub licensable (on a stand-alone basis), non-transferable, worldwide, limited license to reproduce the Wiley Materials for the purpose specified in the licensing process. This license, **and any CONTENT (PDF or image file) purchased as part of your order**, is for a one-time use only and limited to any maximum distribution number specified in the license. The first instance of republication or reuse granted by this license must be completed within two years of the date of the grant of this license (although copies prepared before the end date may be distributed thereafter). The Wiley Materials shall not be used in any other manner or for any other purpose, beyond what is granted in the license. Permission is granted subject to an appropriate acknowledgement given to the author, title of the material/book/journal and the publisher. You shall also duplicate the copyright notice that appears in the Wiley publication in your use of the Wiley Material. Permission is also granted on the understanding that nowhere in the text is a previously published source acknowledged for all or part of this Wiley Material. Any third party content is expressly excluded from this permission.
- With respect to the Wiley Materials, all rights are reserved. Except as expressly granted by the terms of the license, no part of the Wiley Materials may be copied, modified, adapted (except for minor reformatting required by the new Publication), translated, reproduced, transferred or distributed, in any form or by any means, and no derivative works may be made based on the Wiley Materials without the prior permission of the respective copyright owner. **For STM Signatory Publishers**

**clearing permission under the terms of the STM Permissions Guidelines only, the terms of the license are extended to include subsequent editions and for editions in other languages, provided such editions are for the work as a whole in situ and does not involve the separate exploitation of the permitted figures or extracts,** You may not alter, remove or suppress in any manner any copyright, trademark or other notices displayed by the Wiley Materials. You may not license, rent, sell, loan, lease, pledge, offer as security, transfer or assign the Wiley Materials on a stand-alone basis, or any of the rights granted to you hereunder to any other person.

- The Wiley Materials and all of the intellectual property rights therein shall at all times remain the exclusive property of John Wiley & Sons Inc, the Wiley Companies, or their respective licensors, and your interest therein is only that of having possession of and the right to reproduce the Wiley Materials pursuant to Section 2 herein during the continuance of this Agreement. You agree that you own no right, title or interest in or to the Wiley Materials or any of the intellectual property rights therein. You shall have no rights hereunder other than the license as provided for above in Section 2. No right, license or interest to any trademark, trade name, service mark or other branding ("Marks") of WILEY or its licensors is granted hereunder, and you agree that you shall not assert any such right, license or interest with respect thereto
- NEITHER WILEY NOR ITS LICENSORS MAKES ANY WARRANTY OR REPRESENTATION OF ANY KIND TO YOU OR ANY THIRD PARTY, EXPRESS, IMPLIED OR STATUTORY, WITH RESPECT TO THE MATERIALS OR THE ACCURACY OF ANY INFORMATION CONTAINED IN THE MATERIALS, INCLUDING, WITHOUT LIMITATION, ANY IMPLIED WARRANTY OF MERCHANTABILITY, ACCURACY, SATISFACTORY QUALITY, FITNESS FOR A PARTICULAR PURPOSE, USABILITY, INTEGRATION OR NON-INFRINGEMENT AND ALL SUCH WARRANTIES ARE HEREBY EXCLUDED BY WILEY AND ITS LICENSORS AND WAIVED BY YOU.
- WILEY shall have the right to terminate this Agreement immediately upon breach of this Agreement by you.
- You shall indemnify, defend and hold harmless WILEY, its Licensors and their respective directors, officers, agents and employees, from and against any actual or threatened claims, demands, causes of action or proceedings arising from any breach of this Agreement by you.
- IN NO EVENT SHALL WILEY OR ITS LICENSORS BE LIABLE TO YOU OR ANY OTHER PARTY OR ANY OTHER PERSON OR ENTITY FOR ANY SPECIAL, CONSEQUENTIAL, INCIDENTAL, INDIRECT, EXEMPLARY OR PUNITIVE DAMAGES, HOWEVER CAUSED, ARISING OUT OF OR IN CONNECTION WITH THE DOWNLOADING, PROVISIONING, VIEWING OR USE OF THE MATERIALS REGARDLESS OF THE FORM OF ACTION, WHETHER FOR BREACH OF CONTRACT, BREACH OF WARRANTY, TORT, NEGLIGENCE, INFRINGEMENT OR OTHERWISE (INCLUDING, WITHOUT LIMITATION, DAMAGES BASED ON LOSS OF PROFITS, DATA, FILES, USE, BUSINESS OPPORTUNITY OR CLAIMS OF THIRD

PARTIES), AND WHETHER OR NOT THE PARTY HAS BEEN ADVISED OF THE POSSIBILITY OF SUCH DAMAGES. THIS LIMITATION SHALL APPLY NOTWITHSTANDING ANY FAILURE OF ESSENTIAL PURPOSE OF ANY LIMITED REMEDY PROVIDED HEREIN.

- Should any provision of this Agreement be held by a court of competent jurisdiction to be illegal, invalid, or unenforceable, that provision shall be deemed amended to achieve as nearly as possible the same economic effect as the original provision, and the legality, validity and enforceability of the remaining provisions of this Agreement shall not be affected or impaired thereby.
- The failure of either party to enforce any term or condition of this Agreement shall not constitute a waiver of either party's right to enforce each and every term and condition of this Agreement. No breach under this agreement shall be deemed waived or excused by either party unless such waiver or consent is in writing signed by the party granting such waiver or consent. The waiver by or consent of a party to a breach of any provision of this Agreement shall not operate or be construed as a waiver of or consent to any other or subsequent breach by such other party.
- This Agreement may not be assigned (including by operation of law or otherwise) by you without WILEY's prior written consent.
- Any fee required for this permission shall be non-refundable after thirty (30) days from receipt by the CCC.
- These terms and conditions together with CCC's Billing and Payment terms and conditions (which are incorporated herein) form the entire agreement between you and WILEY concerning this licensing transaction and (in the absence of fraud) supersedes all prior agreements and representations of the parties, oral or written. This Agreement may not be amended except in writing signed by both parties. This Agreement shall be binding upon and inure to the benefit of the parties' successors, legal representatives, and authorized assigns.
- In the event of any conflict between your obligations established by these terms and conditions and those established by CCC's Billing and Payment terms and conditions, these terms and conditions shall prevail.
- WILEY expressly reserves all rights not specifically granted in the combination of (i) the license details provided by you and accepted in the course of this licensing transaction, (ii) these terms and conditions and (iii) CCC's Billing and Payment terms and conditions.
- This Agreement will be void if the Type of Use, Format, Circulation, or Requestor Type was misrepresented during the licensing process.
- This Agreement shall be governed by and construed in accordance with the laws of the State of New York, USA, without regards to such state's conflict of law rules. Any legal action, suit or proceeding arising out of or relating to these Terms and Conditions or the breach thereof shall be instituted in a court of competent

jurisdiction in New York County in the State of New York in the United States of America and each party hereby consents and submits to the personal jurisdiction of such court, waives any objection to venue in such court and consents to service of process by registered or certified mail, return receipt requested, at the last known address of such party.

## **WILEY OPEN ACCESS TERMS AND CONDITIONS**

Wiley Publishes Open Access Articles in fully Open Access Journals and in Subscription journals offering Online Open. Although most of the fully Open Access journals publish open access articles under the terms of the Creative Commons Attribution (CC BY) License only, the subscription journals and a few of the Open Access Journals offer a choice of Creative Commons Licenses. The license type is clearly identified on the article.

### **The Creative Commons Attribution License**

The Creative Commons Attribution License (CC-BY) allows users to copy, distribute and transmit an article, adapt the article and make commercial use of the article. The CC-BY license permits commercial and non-

### **Creative Commons Attribution Non-Commercial License**

The Creative Commons Attribution Non-Commercial (CC-BY-NC) License permits use, distribution and reproduction in any medium, provided the original work is properly cited and is not used for commercial purposes.(see below)

### **Creative Commons Attribution-Non-Commercial-NoDerivs License**

The Creative Commons Attribution Non-Commercial-NoDerivs License (CC-BY-NC-ND) permits use, distribution and reproduction in any medium, provided the original work is properly cited, is not used for commercial purposes and no modifications or adaptations are made. (see below)

### **Use by commercial "for-profit" organizations**

Use of Wiley Open Access articles for commercial, promotional, or marketing purposes requires further explicit permission from Wiley and will be subject to a fee.

Further details can be found on Wiley Online Library  
<http://olabout.wiley.com/WileyCDA/Section/id-410895.html>

### **Other Terms and Conditions:**

**v1.10 Last updated September 2015**

**Questions? [customercare@copyright.com](mailto:customercare@copyright.com) or +1-855-239-3415 (toll free in the US) or +1-978-646-2777.**



## **Affidavit**

I hereby confirm that my theses entitled “*C-H Borylation: A Route to Novel Pyrenes and Perylenes and the Investigation of their Excited States and Redox Properties*” is the result of my own work. I did not receive any help or support from commercial consultants. All sources and/or materials applied are listed and specified in the thesis. Furthermore, I confirm that this thesis has not yet been submitted as part of another examination process neither in identical nor similar form.

Würzburg, 03.06.2019

---

Signature

## **Eidesstaatliche Erklärung**

Hiermit erkläre ich an Eides statt, die Dissertation „*C-H Borylation: A Route to Novel Pyrenes and Perylenes and the Investigation of their Excited States and Redox Properties*” eigenständig, d.h. insbesondere selbstständig und ohne Hilfe eines kommerziellen Promotionsberaters angefertigt und keinen anderen als die von mir angegebenen Quellen und Hilfsmittel verwendet zu haben. Ich erkläre außerdem, dass die Dissertation weder in gleicher noch ähnlicher Form bereits in einem anderen Prüfungsverfahren vorgelegen hat.

Würzburg, 03.06.2019

---

Unterschrift